ENGINEERING SERVICE CENTER
Port Hueneme, California 93043-4370

CONTRACT REPORT

CR-NAVFAC ESC-EV-1201

Development of a Protocol and a Screening Tool for the Selection of DNAPL Source Area Remediation

By

Carmen A. Lebrón (NAVFAC ESC)

Dr. David Major (Geosyntec Consultants, Inc.)

Dr. Julie Konzuk (Geosyntec Consultants, Inc.)

Dr. Bernard H. Kueper (Queen's University)

Dr. Jason Gerhard (University of Edinburgh)

January 2012

REPORT DOCUMENTATION PAGE

Form Approved
OMB No. 0704-0188

PLEASE DO NOT RETURN YOUR FORM TO THE ABOVE ORGANIZATION.

1. REPORT DATE *(DD-MM-YYYY)*	2. REPORT TYPE	3. DATES COVERED *(From - To)*
02-23-2012	Contract Report	2004-2011

4. TITLE AND SUBTITLE

FINAL REPORT: Development of a Protocol and a Screening Tool for Selection of DNAPL Source Area Remediation

5a. CONTRACT NUMBER

N47408-04-C-7515

5b. GRANT NUMBER

5c. PROGRAM ELEMENT NUMBER

6. AUTHOR(S)

Carmen A. Lebrón (NAVFAC ESC)
Dr. David Major (Geosyntec Consultants, Inc.)
Dr. Julie Konzuk (Geosyntec Consultants, Inc.)
Dr. Bernard H. Kueper (Queen's University)
Dr. Jason Gerhard (University of Edinburgh)

5d. PROJECT NUMBER

ESTCP Project ER0424

5e. TASK NUMBER

5f. WORK UNIT NUMBER

7. PERFORMING ORGANIZATION NAME(S) AND ADDRESS(ES)

NAVFAC ESC: 1100 23rd Ave. Port Hueneme, CA 93043
Geosyntec Consultants: 130 Research Lane, Suite 2, Guelph, Ontario N1G 5G3 Canada
Queen's University: Kingston, Ontario, Canada. K7L 3N6

8. PERFORMING ORGANIZATION REPORT NUMBER

CR-NAVFAC ESC-EV-1201

9. SPONSORING/MONITORING AGENCY NAME(S) AND ADDRESS(ES)

Environmental Security Technology Certification Program (ESTCP)
901 North Stuart Street, Suite 303 Arlington, VA 22203
Phone (703) 696-2127 | Fax (703) 696-2114

10. SPONSOR/MONITOR'S ACRONYM(S)

ESTCP

11. SPONSOR/MONITOR'S REPORT NUMBER(S)

ESTCP ER0424 Final Report

12. DISTRIBUTION/AVAILABILITY STATEMENT

DISTRIBUTION A: APPROVED FOR PUBLIC RELEASE; DISTRIBUTION IS UNLIMITED

13. SUPPLEMENTARY NOTES

14. ABSTRACT

ESTCP project ER-200424's main goal was to address this data gap and assist environmental remediation practitioners in evaluating and selecting appropriate remedial technologies (given particular site conditions and performance goals). More importantly, given that the U.S. Department of Defense (DoD) is moving rapidly towards achieving Response Complete (RC) at 95% of Installation Restoration Program (IRP) sites by 2021, the information and screening tool developed as part of this project can be utilized to evaluate existing remedial systems. For those sites where remedies are not meeting established remedial action objectives, the screening tool can assist in determining whether there is a realistic expectation of meeting the remedial action objectives for a given site and technology. The screening tool also can provide an assessment of

15. SUBJECT TERMS

DNAPL source zone remediation, bioremediation, chemical oxidation, technology performance, mass removed, achieving remedial goals, case studies database, thermal treatment, technology selection tool, source area remediation, protocol source area remediation.

16. SECURITY CLASSIFICATION OF:			17. LIMITATION OF ABSTRACT	18. NUMBER OF PAGES	19a. NAME OF RESPONSIBLE PERSON
a. REPORT	b. ABSTRACT	c. THIS PAGE		594	Carmen A. Lebron
					19b. TELEPHONE NUMBER *(Include area code)* 805-982-1616

DISCLAIMER

Several remedial technologies are represented in DNAPL TEST. NAVFAC ESC does not endorse the use of any specific technology nor vendor. The information pertaining to the technologies performance was collected from various sources including conference proceedings, ESTCP reports, consultant's reports, government documents, peer-reviewed journal articles, theses, and vendor publications. The source of the information is made available to the DNAPL TEST user in the citations. Additionally, numerical modeling of remediation technologies was completed to supplement available field and laboratory data, and to quantify other metrics difficult to quantify in a field setting. NAVFAC ESC does not necessarily endorse the use of any modeling or simulations software programs used in this exercise.

The Data Quality Rankings (DQRs) in the DNAPL TEST are provided to the user as a means to express the completeness of the data set from the various literature sources. However, a high DQR should not be misconstrued as an endorsement to a specific journal, conference, website, or vendor publication.

Furthermore, the user of the DNAPL TEST software should be aware that results of the analysis do not constitute a prediction of how a technology will perform under the specified conditions. At the heart of the DNAPL TEST are the results of 200+ case studies, including over 80 modeling simulations. However, past performance and modeling simulations do not guarantee future performance. DNAPL architecture, the site's biogeochemical conditions and geology/hydrogeology will determine technology performance. DNAPL TEST is to be used only as a guide for technology selection and cannot replace appropriate site-specific evaluations based on engineering judgment. ESTCP, NAVFAC ESC, Geosyntec Consultants, Queen's University, and the University of Edinburgh are not liable for misuse of the information contained in, or output by, the DNAPL TEST software. Moreover, NAVFAC ESC does not endorse Geosyntec Consultants, Queen's University, the University of Edinburgh, nor any of the participating entities in this effort.

Environmental Security Technology Certification Program (ESTCP)

FINAL REPORT

Development of a Protocol and a Screening Tool for Selection of DNAPL Source Area Remediation

Lead Organization:
Naval Facilities Engineering Service Center (NFESC)
1100 23rd Ave.
Port Hueneme, CA 93043

Prepared for

ESTCP Support Office
1155 Herndon Parkway
Suite 900
Herndon, VA 20170

By

NAVFAC ESC, Geosyntec Consultants, Queen's University and University of Edinburgh
December 2011

EXECUTIVE SUMMARY

Multiple technologies have been developed and applied over the past few decades for remediation of chlorinated solvents in the subsurface. The remediation of solvents in the form of dense nonaqueous phase liquids (DNAPLs) is particularly challenging. Factors such as geology, geochemistry, hydrogeology, the composition and distribution of the DNAPL, as well as the presence and absence of other contaminants, play a role in technology selection and performance. To date, despite a multitude of reviews on several individual technologies, no comprehensive studies have been completed that illustrate which technologies generally work best under specific site conditions and desired remedial outcomes/goals.

ESTCP project ER-200424's main goal was to address this data gap and assist environmental remediation practitioners in evaluating and selecting appropriate remedial technologies (given particular site conditions and performance goals). More importantly, given that the U.S. Department of Defense (DoD) is moving rapidly towards achieving Response Complete (RC) at 95% of Installation Restoration Program (IRP) sites by 2021, the information and screening tool developed as part of this project can be utilized to evaluate existing remedial systems. For those sites where remedies are not meeting established remedial action objectives, the screening tool can assist in determining whether there is a realistic expectation of meeting the remedial action objectives for a given site and technology. The screening tool also can provide an assessment of alternative technologies to consider that may offer a higher likelihood of success.

Information on site characteristic parameters and remedial performance data was collected for a range of site characteristics and remedial technologies and compiled into a database as part of the effort. To supplement this dataset, numerical modeling simulations were conducted on template sites having frequently encountered site characteristics. A software interface was then constructed to allow for a user-friendly means of evaluating the case study information on a site-by-site basis. Recognizing that each site is unique and that performance goals and regulatory constraints will vary from site to site, the DNAPL Technology Evaluation Screening Tool (DNAPL TEST) enables the user to select and constrain their analysis to focus on those performance goals, remedial technologies, and site characteristics of interest.

The remedial technologies evaluated in DNAPL TEST include *in situ* chemical oxidation (ISCO), thermal technologies [including thermal conductive heating (TCH), steam flooding, electrical resistive heating (ERH) and microwave heating, surfactant flushing (also known as surfactant enhanced aquifer remediation, or SEAR) and/or co-solvent flushing, hydraulic displacement (HD), enhanced *in situ* bioremediation (EISB), and chemical reduction with zero-valent iron (ZVI). For these technologies, DNAPL TEST provides a summary of observed remedial performance for a number of performance metrics, including decrease in the DNAPL mass in the subsurface, decrease in VOC concentrations in soil and groundwater, achievement of MCLs in groundwater, rebound in groundwater concentrations after termination of treatment, duration of treatment, achievement of remedial goals (including achieving desired reductions in DNAPL mass, groundwater and soil concentrations, and contaminant mass discharge and/or flux,

as well as achievement of site closure or reduction of groundwater concentrations to below MCLs), and unit treatment cost.

Field and laboratory cases studies were collected from various sources including conference proceedings, ESTCP reports, consultant's reports, government documents, peer-reviewed journal articles, theses, and vendor publications. Additionally, as part of the tool development, numerical modeling of remediation technologies was completed to supplement available field and laboratory data, and to quantifiy other metrics difficult to quantify in a field setting. Template sites were create for simulations in unconsolidated media, fractured rock, and fractured clay, and the four remedial technologies that were simulated and included in DNAPL TEST are anaerobic EISB, ISCO (using permanganate as an oxidant), HD, and SEAR. Modeling was performed using the numerical code DNAPL3D-RX and the process included sensitivity studies to evaluate the influence of site parameters (e.g. DNAPL type and release volume, fracture aperture, matrix porosity, fraction of organic carbon, fracture spacing, bedrock type, bulk density, matrix tortuosity, hydraulic conductivity, and heterogeneity) on the performance of each remedial technology.

DNAPL TEST allows the user to customize their analysis to meet their own objective by providing two options. With the General Analysis, the user can query the database of case studies for general performance information by refining their search to include specific technologies, case study type, data quality rankings, and site characteristics. The tool will generate reports of average and select individual performance data from case studies matching the search criteria. With the Site Specific Analysis, the user can input characteristics of the site of interest and specify other search criteria (e.g., specify data quality rankings and case study types to be included, geologies, DNAPL types, etc.). DNAPL TEST then searches for case studies with statistically similar site characteristics for performance metrics where correlations between technology performance and site characteristics were observed. The Site Specific Analysis output reports provide more details of case-study specific performance as well as average and min/max performance trends. Output reports also are provided on an individual performance metric basis as well as technology specific basis.

The basis of the Site Specific Analysis is a statistical evaluation that identified and quantified correlations between site parameters and performance metrics. This evaluation was completed in a two-step process. In the first step, a series of correlation tests were conducted to identify linear associations between a given site parameter and a given technology performance metric. A five percent (%) level of significance was used as the criteria for statistically significant linear correlations. In the second step, site parameter – performance metric pairs that showed a statistically significant correlation were analyzed using simple linear regression methods. Regression quantifies the sensitivity of the technology performance to each site parameter, and also was used to calculate a range of site parameters values given a particular technology performance value *via* a 95% confidence interval. A total of nine pairs for all technologies were found to have statistically significant correlations. For EISB, reduction in DNAPL mass correlated to hydraulic conductivity. For SEAR, reduction in DNAPL mass was correlated to the

areal extent of the DNAPL zone, pre-remediation DNAPL mass, and the volume of the DNAPL zone. For thermal (steam), treatment duration was correlated to the volume of the DNAPL zone, and for thermal (resistive), reduction in DNAPL mass was correlated to the area and volume of the DNAPL zone, and treatment duration was correlated to the pre-remediation DNAPL mass and electrode spacing.

Observations on technology performance can be made based on the modeling results and field case study data collection completed to date. Some of these are summarized below.

- **Reductions in Groundwater Concentrations:** None of the site characteristic or technology implementation parameters that were evaluated as part of the statistical analysis were found to have a statistical correlation with reductions in groundwater concentrations, however, there does appear to be a relationship between the amount of DNAPL mass removed from the subsurface during treatment and reduction in groundwater concentration. This relationship appears to be independent of treatment technology.
- **DNAPL Mass Removal:** Near complete mass removal has been achieved with all technologies with the exception of hydraulic displacement. In field studies, the highest DNAPL mass removal was observed in thermal treatment case studies (94% to 96%) and the median mass removed for anaerobic EISB, ISCO, SEAR, and co-solvent flushing ranged from 64% to 81%. If modeling cases are included, for each technology the range of percent DNAPL mass removal increases, but the median value decreases. This is likely due to the different remedial time frames used in the modeling case studies.
- **Matrix Diffusion:** Modeling results demonstrated that in fractured rock environments, with an older DNAPL release, matrix diffusion (diffusion of DNAPL into lower permeability media) has a substantial influence on the distribution of DNAPL mass. If degradation of DNAPL within the lower permeability matrix is limited, back-diffusion of contaminant mass out of the matrix will sustain groundwater concentrations for long periods of time.
- **DNAPL Properties:** The solubility of the DNAPL was observed to influence the resulting net benefit of implementing more aggressive DNAPL treatment technologies over other approaches primarily on dissolution of the DNAPL as the DNAPL mass reduction mechanism. For more soluble DNAPLs such as trichloroethene (TCE), dissolution of the DNAPL is a significant component of the DNAPL mass removal and incorporating other degradation or mass removal mechanisms (*e.g.,* oxidation, biodegradation, enhanced dissolution) may only result in relatively small incremental increases in DNAPL mass removal.
- **Precipitate Formation:** Through the modeling sensitivity analysis, it was observed that the formation of a manganese dioxide rind (resulting in encapsulation of DNAPL pools and flow bypassing around DNAPL areas) significantly increased the time required to remove TCE DNAPL in ISCO applications using permanganate as the oxidant. This evaluation is specific to permanganate treatment and the corresponding

manganese dioxide rind formation; however, it is anticipated that similar results may be observed with other technologies that result in the formation of a precipitate or result in permeability reductions. The influence of the precipitate formation on DNAPL treatment is anticipated to be particularly pronounced where the precipitate forms within close proximity of the DNAPL phase, as occurs when permanganate reacts with the DNAPL.

DNAPL TEST has been designed to be updated in the future to reflect new data. As new field, laboratory, or modeling case studies become available, they can be added to the database. When sufficient new case studies have been added, the statistical analysis can be conducted again to refine statistical relationships.

TABLE OF CONTENTS

LIST OF TABLES

LIST OF FIGURES

LIST OF APPENDICES

LIST OF ABBREVIATIONS

%	percent
µg/L	micrograms per liter
1,1,1-TCA	1,1,1-trichloroethane
2D	two dimensional
3D	three dimensional
cDCE	*cis*-1,2-dichloroethene
CMC	critical micelle concentration
cm/s	centimeters per second
DNAPL	Dense, Non-Aqueous Phase Liquid
DNAPL TEST	DNAPL Technology Evaluation Screening Tool
DoD	Department of Defense
DQR	data quality rankings
EISB	enhanced *in situ* bioremediation
EPA SITE	Environmental Protection Agency Superfund Innovative Technology Evaluation
ERH	electrical resistive heating
ESTCP	Environmental Security Technology Certification Program
f_{oc}	fraction of organic carbon
FRAC	fractured media
ft	feet
gal	US gallons
HD	hydraulic displacement
ISCO	*in situ* chemical oxidation
K	hydraulic conductivity
kg	killograms
m	meters
m^2	square meters
m^3	cubic meters
MCL	maximum contaminant level
mg/L	milligrams per liter
MIN/MAX	minimum / maximum
MnO_2	manganese dioxide
NFESC	Naval Facilities Engineering Service Center
O&M	operation and maintenance
P&T	pump and treat
PCE	tetrachloroethene
QA/QC	quality assurance / quality control
R^2	coefficient of determination
RPMs	remedial program managers
RX	porous media
SEAR	surfactant enhanced aquifer remediation

TCE	trichloroethene
TCH	thermal conductive heating
tDCE	*trans*-1,2-dichloroethene
USEPA	United States Environmental Protection Agency
VOCs	volatile organic compounds
ZVI	zero valent iron

1. INTRODUCTION

This Final Report provides a summary of the scope of work and findings of the Environmental Security Technology Certification Program (ESTCP) project ER-200424, *Development of a Dense, Non-Aqueous Phase Liquid (DNAPL) Remediation Technology Screening Tool*. The report is structured as follows:

- Section 1: Introduction - Includes background information, a discussion of the objectives and regulatory drivers that influence the project scope;
- Section 2: Technology – Includes a description of the technology (i.e., DNAPL TEST), an overview of the screening tool developments, and a discussion of advantages and limitations of the screening tool;
- Section 3: Performance Objectives;
- Section 4: Site Description;
- Section 5: Test Design;
- Section 6: Technology Performance Assessment;
- Section 7: Cost Assessment;
- Section 8: Implementation Issues; and
- Section 9: References.

1.1 Background

Multiple technologies have been developed and applied over the past few decades for remediation of chlorinated solvents in the subsurface. The remediation of solvents in the form of DNAPLs is particularly challenging. Factors such as geology, geochemistry, hydrogeology, the composition and distribution of the DNAPL, as well as the presence and absence of other contaminants, play a role in technology selection and performance. To date, despite a multitude of reviews on several individual technologies, no comprehensive studies have been completed that illustrate which technologies generally work best under specific site conditions and desired remedial outcomes/goals.

This project's main goal was to address this data gap and assist environmental remediation practitioners in evaluating and selecting appropriate remedial technologies (given particular site conditions and performance goals). More importantly, given that the U.S. Department of Defense (DoD) is moving rapidly towards achieving Response Complete (RC) at 95% of Installation Restoration Program (IRP) sites by 2021, the information and screening tool developed as part of this project can be utilized to evaluate existing remedial systems. For those sites where remedies are not meeting established remedial action objectives, the screening tool can assist in determining whether there is a realistic expectation of meeting the remedial action objectives for a given site and technology. The screening tool also can provide an assessment of alternative technologies to consider that may offer a higher likelihood of success.

Information on site characteristic parameters and remedial performance data was collected for a range of site characteristics and remedial technologies and compiled into a database. To supplement this dataset, numerical modeling simulations were conducted on template sites having frequently encountered site characteristics. A software interface was then constructed to allow for a user-friendly means of evaluating the case study information on a site-by-site basis. Recognizing that each site is unique and that performance goals and regulatory constraints will vary from site to site, the DNAPL Technology Evaluation Screening Tool (DNAPL TEST) enables the user to select and constrain their analysis to focus on those performance goals, remedial technologies, and site characteristics of interest.

1.2 Objective of the Demonstration

The primary objective of the project was to develop a user-friendly screening tool that can be utilized by decision makers [*e.g.*, site owners, United States Department of Defense (DoD) remedial program managers (RPMs), regulators, and site consultants] during the remedial technology selection or evaluation process to:

i) Evaluate potential technology performance at a particular site;

ii) Evaluate potential technology performance in different geological strata at a complex site;

iii) Aid in the selection of feasible technologies for a particular site based on desired performance metrics; and

iv) Reduce the uncertainty of estimating and predicting remedial outcomes and implementation costs at DNAPL source zone sites.

1.3 Regulatory Drivers

This project focused on the remediation of chlorinated ethenes. The United States Environmental Protection Agency (USEPA) maximum contaminant level (MCL) for tetrachloroethene (PCE) and trichloroethene (TCE) in drinking waters is 5 micrograms per liter (µg/L). This concentration is considerably less than the concentrations present in groundwater at many sites throughout the United States. The MCLs for vinyl chloride, *cis*-1,2-dichloroethene (cDCE), and *trans*-1,2-dichloroethene (tDCE) are 2 µg/L,70 µg/L, and 100 µg/L, respectively.

A number of DoD sites have volatile organic compounds (VOCs) present as DNAPLs that will act as long-term sources of VOCs to groundwater. Although it is uncertain how many sites still contain a DNAPL source area, many contain chlorinated hydrocarbons at significant concentrations in soil and groundwater. Due to the slow dissolution of VOCs from residual or pooled DNAPL, as well as the slow diffusive release of VOCs from low permeability materials (i.e. back-diffusion), conventional treatments often serve solely as

containment technologies and require long operational periods to remove significant amounts of DNAPL and VOC mass. Therefore, this project's deliverables promote the use of more effective technologies in remediating DNAPL source areas and meeting these regulations.

2. TECHNOLOGY

This section provides a description of DNAPL TEST (Section 2.1), a summary of the development of the screening tool (Section 2.2) and the advantages and limitations of the screening tool (Section 2.3).

2.1 Technology Description

DNAPL TEST is a user-friendly, Microsoft Access™ -based screening tool that is intended to be used to: (*i*) aid in the selection of technologies based on desired performance metrics (*ii*) evaluate potential technology performance; and (*iii*) reduce the uncertainty of estimating and predicting remedial outcomes and implementation costs at DNAPL source zone sites. The tool focuses on remediation of chlorinated solvent DNAPL sources only.

The components of DNAPL TEST and the software development process are illustrated in **Figure 2-1**. The basis of the screening tool is a database of information derived from case studies of field implementation of various remedial technologies, supported by numerical modeling of targeted technologies to address data gaps, and laboratory studies to provide information on fundamental processes impacting technology performance. Information from field and laboratory case studies was collected as discussed in Section 2.2.1 through reviewing the available literature (including on-line databases, peer-reviewed journals, conference proceedings, guidance documents, consultant reports, *etc*.). A list of case studies included in DNAPL TEST and the associated reference information is provided in **Appendix B**. The remedial technologies evaluated in DNAPL TEST include:

- *In situ* chemical oxidation (ISCO);
- Thermal technologies [including thermal conductive heating (TCH), steam flooding, electrical resistive heating (ERH) and microwave heating];
- Surfactant flushing (also known as surfactant enhanced aquifer remediation, or SEAR) and/or co-solvent flushing;
- Hydraulic displacement (HD, sometimes referred to as waterflooding);
- Enhanced *in situ* bioremediation (EISB); and
- Chemical reduction with zero-valent iron (ZVI).

Numerical modeling of five remedial technologies (anaerobic EISB, ISCO using permanganate, SEAR, hydraulic displacement, and pump and treat [P&T]) was conducted as discussed in Section 2.2.2 on a select number of representative template sites to provide information that is difficult and costly to collect in the field in a timely manner (*e.g.,* long-term impacts, estimates of mass removal, post-treatment changes in DNAPL architecture, sensitivity of technology performance to site characteristics, *etc*.).

DNAPL TEST provides a summary of observed remedial performance for a number of performance metrics, including:

i) Decrease in the DNAPL mass remaining in the subsurface;

ii) Decrease in VOC concentrations in groundwater;

iii) Reduction of VOC concentrations in soil;

iv) Achievement of MCLs in groundwater;

v) Occurrence of rebound in groundwater concentrations after termination of treatment;

vi) Duration of treatment;

vii) Achievement of remedial goals (including achieving desired reductions in DNAPL mass, groundwater and soil concentrations, and contaminant mass discharge and/or flux, as well as achievement of site closure or reduction of groundwater concentrations to below MCLs); and

viii) Unit treatment cost.

Information provided includes technology performance statistics (e.g., average performance, standard deviation, range in performance), and data quality information (e.g., total number of case studies and average data quality rankings for the case studies included in the analysis). Development of data quality rankings is described in Section 2.2.3.2.

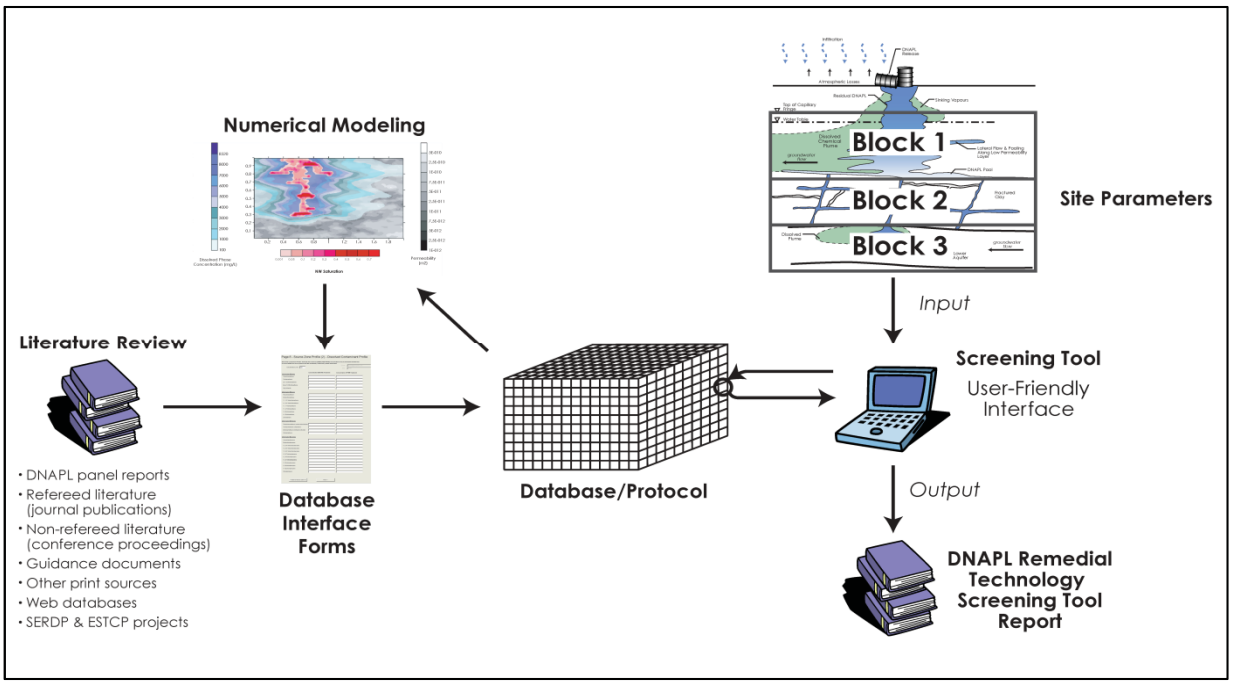

Figure 2-1. Components of DNAPL TEST development process.

2.2 Technology Development

Sections 2.2.1 to 2.2.3 provide an overview of the development of DNAPL TEST, focusing on field case study collection (Section 2.2.1), the numerical modeling completed to supplement the field case studies (Section 2.2.2), and development of DNAPL TEST code (Section 2.2.3).

2.2.1 Collection of Field and Laboratory Case Studies

The screening tool software interfaces with a database that contains raw data from 216 DNAPL remediation case studies. Case studies entered into the database include 129 field and laboratory studies, as well as 87 modeling studies. In order for any case study to be entered into the database, it must have met the following five criteria:

- Information on at least one performance metric (e.g. mass removal, concentration reduction, cost, treatment duration, etc.) was available.
- Chlorinated solvent DNAPL was present within the treatment zone.
- The DNAPL remedial technology used was specified in the document.
- The components of the DNAPL were specified (e.g. PCE, TCE, 1,1,1-trichloroethane [1,1,1-TCA]); and

- Site characterization data (e.g. hydraulic conductivity, geology/lithology, concentration data) was available.

Once studies were determined to meet the requirements for inclusion in DNAPL TEST, they were entered into the database using a set of database interface forms following a defined protocol (i.e., a set procedure to extract and analyze data from case studies), to ensure consistency between entries.

The majority of field and laboratory case studies in the database were collected from a review of publicly available literature, which included both peer-reviewed and grey literature, online databases, guidance documents, consultant reports, and Environmental Protection Agency Superfund Innovative Technology Evaluation (EPA SITE) reports. A limited number of case study results were provided under a confidential basis, and references for these sites are not available. **Appendix B** provides a comprehensive listing of the case studies compiled and included in DNAPL TEST database. **Figure 2-2** provides the breakdown of case studies contained within DNAPL TEST by case study type, reference source and DNAPL remediation technology.

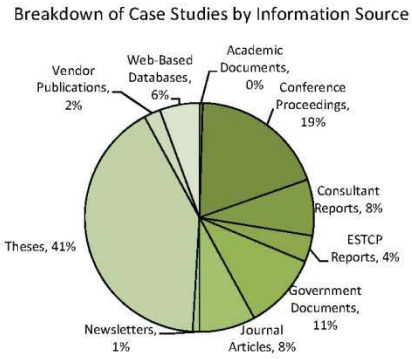

Information Source	Case Studies	Percent
Academic Documents	1	0%
Conference Proceedings	41	19%
Consultant Reports	17	8%
ESTCP Reports	8	4%
Government Documents	23	11%
Journal Articles	17	8%
Newsletters	2	1%
Theses	88	41%
Vendor Publications	5	2%
Web-Based Databases	12	6%

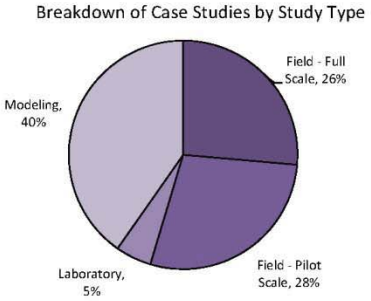

Type of Study	Case Studies	Percent
Field - Full Scale	57	26%
Field - Pilot Scale	61	28%
Laboratory	11	5%
Modeling	87	40%

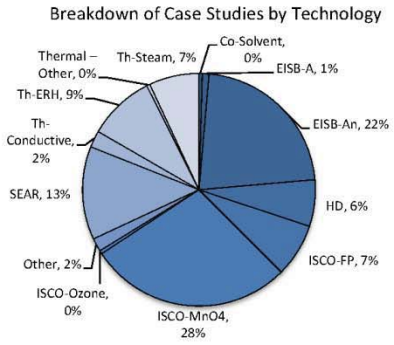

Technology	Case Studies	Percent
Co-Solvent	1	0%
EISB-A	2	1%
EISB-An	48	22%
HD	14	6%
ISCO-FP	16	7%
ISCO-MnO4	61	28%
ISCO-Ozone	1	0%
Other	4	2%
SEAR	28	13%
Th-Conductive	5	2%
Th-ERH	20	9%
Thermal – Other	1	0%
Th-Steam	15	7%

Figure 2-2. Breakdown of the case studies included in DNAPL TEST by reference source, case study type, and technology**.**

2.2.2 Development of Modeling Case Studies

Modeling of remediation technologies was completed to provide additional information with regards to long-term performance and other metrics that are difficult to quantify in a field setting (e.g., DNAPL mass destruction, post-treatment groundwater concentration reductions, etc.). Five remedial technologies were simulated in both unconsolidated and consolidated media, including anaerobic EISB, ISCO using permanganate, HD (unconsolidated media only), SEAR, and P&T (unconsolidated media only). As discussed below, the modeling process included sensitivity studies to evaluate the influence of key processes and site parameters on the performance of each remedial technology. Pump and treat was primarily simulated to provide a baseline comparison for the *in situ* remediation technologies, and these simulations were therefore not included in the screening tool.

2.2.2.1 Modeling Overview

The numerical modeling of the remediation of the template sites was performed using the numerical code DNAPL3D-RX. This model has been extensively tested, validated, and employed for DNAPL field scale studies (e.g., Kueper and Gerhard, 1995; Gerhard et al., 1998; Gerhard et al., 2001; Gerhard and Kueper, 2003a, 2003b, 2003c; Grant et al., 2006, 2007; Grant and Gerhard, 2007a, 2007b; Mundle et al., 2007; West et al., 2008; West and Kueper, 2010). In this work, the model was employed to examine the sensitivity of DNAPL source zone remediation to a variety of key site characteristics (e.g., mean and variance of intrinsic permeability for unconsolidated media, fractured rock type for consolidated media, DNAPL type) and remedial system design parameters (e.g., concentration/duration of injected remedial fluid, pulsed injection strategies, applied gradient for hydraulic displacement). In order to complete the maximum number of sensitivity simulations, the unconsolidated media simulations were conducted in three-dimensions while the computationally more expensive fractured rock simulations were conducted in two-dimensions. This latter assumption is considered conservative insofar as it minimizes bypassing of the injected remedial fluids around the DNAPL source zone and thereby provides the best chance of remediation technology success in fractured rock.

In this work, a four-stage modeling process was employed to recognize that the history of DNAPL scenarios is often complex (e.g., most often remediation is attempted several years to decades after the initial DNAPL release). The first stage contained two parts: (1) a near-surface release of DNAPL below the water table was simulated, followed by (2) the DNAPL source was terminated and DNAPL redistribution was simulated until the DNAPL had come to rest in an equilibrium distribution of residual (i.e., immobile blobs and ganglia) and pools (i.e., potentially mobile, continuous distributions). This period lasted on the order of 1 to 10 years depending on the DNAPL type, size of release, and site characteristics.

The second stage simulated the "aging" of the DNAPL scenario. For a subset of the unconsolidated media simulations, DNAPL dissolution and removal of DNAPL pools through pre-remediation hydraulic displacement was simulated prior to initiation of the remedial technology to simulate "aged" sources that have predominantly residual DNAPL. For all of the consolidated media (*i.e.,* fractured rock/clay) simulations, a 20-year aging period was simulated during which a natural hydraulic gradient was applied; this permitted DNAPL mass reduction as well as VOC mass diffusion into the matrix. These first and second stages were simulated for each different template site scenario (e.g., granite, sandstone, etc.) and the end-point of the second stage (i.e., the aged DNAPL site) was used as input for the many different remediation simulations.

The third stage simulated the remedial activities, using a numerical code that incorporates both non-reactive (*i.e.,* dissolution, sorption, desorption, diffusion) and reactive (*e.g.,* biodegradation, oxidation) transport processes, including processes specific to each technology (*e.g.,* dechlorination for enhanced biodegradation, manganese dioxide precipitation for oxidant flushing, and micelle formation for surfactant flushing). **Table 2-1** below provides a summary of the specific processes included in modeling of each technology in each type of porous media. It is noted that some of the second-order processes (e.g., permeability reductions due to manganese dioxide in ISCO and due to biomass growth in EISB) were not included in the fractured rock simulations because they would have unfairly reduced technology performance in the two-dimensional domain employed. The treatment period typically lasted on the order of one to several years with sensitivity simulations exploring the influence of treatment design parameters such as amendment concentration/duration.

The fourth stage involved simulating a post-remediation period on the order of 5 to 20 years. In the consolidated media simulations, forward/back diffusion of mass and injected fluids between the fractures and matrix occurred during this stage. DNAPL mass, groundwater concentrations and VOC mass flux were monitored throughout this period. For most technologies, a 'no treatment' case was included to distinguish the influence of the remedial approach from natural dissolution/diffusion effects.

	Pump and Treat	ISCO	EISB	Hydraulic Displacement	SEAR
Processes Common to Both Unconsolidated and Consolidated Media Simulations	• Not applicable (pump and treat not simulated for consolidated media)	• Physical attenuation mechanisms as with pump and treat • Reaction of permanganate with both organic carbon in the soil/rock and contaminant • Species-specific diffusion rates	• Physical attenuation mechanisms as with pump and treat • Biodegradation of TCE and PCE to ethene	• Not applicable (HD not simulated for consolidated media)	• Physical attenuation mechanisms as with pump and treat • Formation of surfactant micelles • Enhanced dissolution of the DNAPL where micelle concentrations exceed critical levels
Processes Simulated in Unconsolidated Media Runs Only	• Physical attenuation mechanisms including DNAPL dissolution, sorption, diffusion, dispersion, dilution, etc.	• Manganese dioxide precipitate formation, resulting pore clogging and reductions in permeability	• Biomass growth and decay • Pore clogging due to biomass growth and related reduction in permeability • Competition for hydrogen with non-dechlorinating biomass	• Physical attenuation mechanisms as with pump and treat • DNAPL redistribution and recovery due to induced hydraulic gradients	• Not applicable (SEAR simulated using similar processes for both media types)

Table 2-1. Physical processes incorporated into numerical modeling for each remedial technology.

2.2.2.2 Development and Validation of the Numerical Model

The development and validation of all the numerical codes employed in this study followed essentially the same steps, including:

i) A comprehensive literature review to evaluate the relevant processes that occur during DNAPL remediation using the specified technology;

ii) Development of the code and verification that it is error-free through comparison to analytical solutions (where available) and thorough rigorous testing;

iii) Validation of the numerical approach through direct comparison to well-characterized laboratory experiments conducted under controlled conditions (where available); and

iv) Publication of simulation results in peer-reviewed journals, graduate student theses, and conference proceedings.

The results of the above have been published in several peer-reviewed journal articles, including Mundle et al. (2007), West et al. (2008), and West and Kueper (2010) and in student theses, including Mundle (2007), and Pang (2010), based upon which several additional manuscripts are in preparation for submission to peer-reviewed journals.

The numerical code was developed to simulate both DNAPL migration and reactive transport processes (in both unconsolidated and consolidated media), as described in Sections 2.2.2.3 and 2.2.2.4 respectively. Details on the model development, verification,validation, and testing processes are provided in **Appendices C** (unconsolidated media) **and D** (consolidated media).

2.2.2.3 DNAPL Migration Code

The existing DNAPL migration numerical code (DNAPL3D) has been developed and extensively tested and peer reviewed over the past 15 years by researchers at Queen's University and the University of Edinburgh (Kueper and Frind, 1991a,b; Kueper and Gerhard, 1995; Gerhard *et al.,* 1998, 2001; Gerhard and Kueper, 2003a,b,c; Gerhard *et al*., 2007; Grant *et al*., 2006, 2007; Grant and Gerhard, 2007a,b). The first version of the fractured media code was developed in 1991 (Kueper and McWhorter, 1991) and numerous revisions to the code have taken place since that time. The numerical code was developed to incorporate all relevant parameters that govern migration of two phases (DNAPL and groundwater) through the subsurface, including relevant fluid parameters (*e.g.,* density, viscosity, interfacial tension) and the relative permeability – saturation – capillary pressure constitutive relationships that govern two-phase (nonwetting- and wetting-phase) fluid migration pathways and rates. For porous media, spatially variable soil parameters (*e.g.,* permeability, displacement pressure, fraction organic carbon) are incorporated. For fractured media, fracture spacing can be assigned from any distribution as can fracture-specific hydraulic apertures and constitutive relationships (*i.e.,* capillary pressure and relative permeability). Fracture entry pressures are scaled according to DNAPL-water interfacial tension and the code is capable of simulating the formation of both residual and pooled DNAPL in fractures. DNAPL3D is capable of simulating DNAPL migration in one-, two-, and three-dimensions in porous media (*i.e.,* unconsolidated deposits) and in one- and two-dimensions for fractured media. Extensive model validation has been undertaken for a variety of scenarios, including DNAPL infiltration and redistribution in two-dimensional, heterogeneous porous media (Grant et al., 2007).

2.2.2.4 Reactive Transport Code

DNAPL3D has been coupled with RT3D (a publicly available, peer-reviewed reactive transport code) to allow simulation of remedial technologies such as EISB, ISCO and SEAR. The coupled code is referred to as DNAPL3D-RX (porous media) and DNAPL3D-RX-FRAC (fractured media). The fractured media code (DNAPL3D-RX-FRAC) was also modified to incorporate an adaptive gridding routine; this step was necessary to preserve the accuracy of predictions of DNAPL migration and diffusion into the rock matrix while minimizing computational expense in order to perform field scale simulations (see **Appendix D** for details).

Dissolved phase fate and transport incorporated into the numerical code include the following processes:

- Dissolution of the DNAPL according a mass transfer routine selected by the user from a range of published models;
- Diffusion of the dissolved phase into and out of low permeability zones, including the incorporation of compound-specific diffusion coefficients;
- Sorption/desorption of the dissolved phase onto/from the soil/bedrock; and
- Degradation of the dissolved phase.

Of these four processes, diffusion and sorption/desorption are incorporated into the unconsolidated media numerical code through calculation of a local retardation factor including a diffusive transport term and allowing for spatial variability of the soil organic carbon content. RT3D has been modified such that DNAPL3D-RX and DNAPL3D-RX-FRAC can accommodate compound specific diffusion coefficients. This will allow, for example, an oxidant such as permanganate to diffuse through a manganese dioxide rind at a different rate than TCE will diffuse out. The consolidated media code employs this local retardation term for sorption but model diffusion separately via a highly resolved numerical grid in the matrix adjacent to fractures, ensuring that forward/back diffusion as well as diffusive mass storage are accurately and independently simulated. The numerical codes also have the ability to accommodate cross-correlated permeability – fraction organic carbon (f_{oc}) fields and to track f_{oc} as it varies in space and time (e.g., as organic carbon is consumed by permanganate, thus reducing local sorption capacity).

A total of six empirical equilibrium and non-equilibrium mass transfer equations from published literature were incorporated into the model (Miller et al., 1990; Powers et al., 1992; Powers et al., 1994; Imhoff et al., 1993; Saba and Illangasekare, 2000; Nambi and Powers, 2003) as well as a non-empirical model based upon fluid-fluid interfacial area (Grant and Gerhard, 2007a,b). When utilizing models to simulate the dissolution observed in experimental work, it is difficult to predict *a priori* whether to use an

equilibrium or non-equilibrium approach, and which (if any) of the numerous published non-equilibrium approaches is most representative. Each of these empirical equations is best suited to one particular set of conditions (*e.g.,* range of DNAPL saturation, type of porous medium). For each remedial technology, the mass transfer routine most appropriate for the template site conditions is employed. In some cases (e.g., SEAR in fractured rock) the mass transfer routine was varied as a sensitivity parameter.

Reactive transport processes specific to each remedial technology incorporated into the numerical code as appropriate are outlined in more detail below:

Hydraulic Displacement

Processes that have been included in the numerical model for the hydraulic displacement simulations (unconsolidated media only) include the following:

i) Transient infiltration of various types of DNAPL into a spatially correlated, random hydraulic conductivity field. The random hydraulic conductivity field follows a log-normal distribution and is characterized by a mean hydraulic conductivity, the variance of hydraulic conductivity, and spatial correlation lengths (assuming an exponential autocorrelation function). Simulations have focused on horizontally bedded media with horizontal correlation lengths greater than vertical correlation lengths.

ii) Redistribution of the DNAPL to residual and pools following cessation of 'source on' (i.e., DNAPL release to surface) conditions. The relative percentage of residual to pools (*i.e.,* ganglia to pool ratio) is governed by the DNAPL density, the DNAPL-water interfacial tension, and the degree of porous media heterogeneity incorporated into the hydraulic conductivity field.

iii) Mobilization and recovery of the DNAPL *via* hydraulic displacement through the incorporation of groundwater injection and recovery wells. Hydraulic displacement is continued until all recoverable DNAPL is removed *via* the extraction wells.

iv) Simulation of DNAPL dissolution (plume formation) both before and after hydraulic displacement to assess the impacts of the technology on post remediation plume concentrations and mass flux.

More details on the numerical code development and simulation results for hydraulic displacement are included in **Appendix C.1.**

Chemical Oxidation using Permanganate

Processes that have been included in the numerical models (both unconsolidated and consolidated media) for the chemical oxidation simulations include the following:

- Compound-specific, concentration-dependent reaction rates of the chlorinated solvents with permanganate;
- Formation of manganese dioxide (MnO_2) rind as a reaction byproduct, and the associated depletion in permanganate available for remediation;
- Permeability reductions caused by the clogging of soil pores with the MnO_2 precipitate (unconsolidated media simulations only);
- Destruction of organic matter due to reaction with permanganate and the associated local reduction of sorption capacity;
- Diffusion of both dissolved phase contaminants and permanganate through the MnO_2 rind (unconsolidated media) and forward/backwards between fractures/matrix (consolidated media), with compound-specific diffusion coefficients; and
- Equilibrium and non-equilibrium dissolution of the DNAPL phase using published mass transfer routines. Equilibrium mass transfer is being used for the field-scale simulations to keep run times reasonable and to better identify the potential beneficial impact of oxidation on DNAPL mass depletion rates.

The development and calibration of the ISCO reactive transport code is described in more detail in **Appendix C**.2 (porous media simulations), **Appendix D**.1 (fractured clay simulations) and both **Appendices D.2** and **D.3** (fractured rock simulations).

Bioremediation

As outlined in **Table 2-1**, bioremediation was handled differently in the unconsolidated and consolidated porous media simulations. The latter employed a simpler conceptual model because the primary factors dictating bioremediation success in fractured rock are considered to be associated with delivery issues (i.e., of the organic substrate and amendments to the source zone), diffusive transport of VOCs and amendments, and ability of microorganisms to achieve degradation in the rock matrix. The following process were included and evaluated in the numerical models:

- Sequential dechlorination of PCE and TCE to DCE, VC, and ethene, with all parent and daughter products exhibiting individual transport, sorption, and diffusion parameters (unconsolidated and consolidated media).

- Biomass growth kinetics, including growth and decay of biomass linked to electron donor and acceptor availability, and potential impact to soil permeability (unconsolidated media only);

- First-order degradation kinetics in the presence of both electron donor and microbial community, where the organic substrate can diffusive into the rock and the ability of microorganisms to penetrate the rock matrix was a sensitivity parameter (consolidated media only);

- Fate and transport of the electron donor including: consumption of donor as it is transported away from the point of injection; and temporal changes in consumption rate as a function of supply and demand (unconsolidated and consolidated media).

The development and testing of the bioremediation reactive transport code is described in more detail in **Appendix C.4** (unconsolidated media simulations) and **Appendices D.2** and **D.4** (consolidated media simulations).

Surfactant Flooding

With respect to surfactant flushing, the following processes were represented in all template site simulations:

- Micellar solubilization of the DNAPL at surfactant concentrations greater than the critical micelle concentration (CMC);

- Surfactant diffusion into rock matrix and extramicellular encapsulation of dissolved phase VOC when diffused surfactant concentrations exceed the CMC (consolidated media only);

- Conservation of mass between injected surfactant and monomers and micelles in the subsurface and independent transport/diffusion of VOCs, monomers and micelles;

- Sorption of the surfactant.

- Equilibrium mass transfer between DNAPL and water and DNAPL and micelles was assumed in all template sites, except an empirically derived rate-limited expression for DNAPL solubilization in fractured rock (Dickson and Thomson, 2003) was included in the consolidated media model and tested as a sensitivity parameter.

The numerical code and results for the surfactant flooding simulations are described in more detail in **Appendix C.5** (porous media simulations) and **Appendices D.1** and **D.4** (fractured media simulations).

Treatment Trains

For the unconsolidated media simulations, the use of treatment trains was evaluated through comparing changes in remedial performance when ISCO, EISB and SEAR are applied both before and after the use of hydraulic displacement (which tends to "smear" the DNAPL pools such that the majority of the mass remaining is in the form of residual, with higher interfacial areas available for dissolution).

2.2.2.5 Template Site Development and Remediation Simulations

Site characteristic parameters that were evaluated as part of the sensitivity study for the unconsolidated and consolidated media are listed in **Table 2-2** to **Table 2-4** below. In each table, Site characteristic parameters that were varied are shown in bold font. These included the degree of soil heterogeneity, DNAPL density and solubility, soil permeability, and DNAPL release volume in unconsolidated simulations, and average fracture aperture, DNAPL density, matrix porosity, and fraction organic carbon within the matrix in fractured clay simulations, and fracture spacing and aperture, and rock matrix bulk density, porosity, f_{oc}, and tortuosity in fractured rock simulations.

Template Site	DNAPL Type	DNAPL Release Volume	Mean Hydraulic Conductivity	Soil Heterogeneity (variance ln K)
Low Heterogeneity	TCE	7.57 m^3 (2000 gallons)	$1.0x10^{-3}$ cm/s	**ln K = 1**
Low K	TCE	7.57 m^3 (2000 gallons)	**$1.0x10^{-4}$ cm/s**	ln K = 2
Low DNAPL Volume	TCE	**1.89 m^3 (500 gallons)**	$1.0x10^{-3}$ cm/s	ln K = 2
DNAPL Type 2 (lower density)	**1,1,1-TCA**	7.57 m^3 (2000 gallons)	$1.0x10^{-3}$ cm/s	ln K = 2
Base Case	**TCE**	**7.57 m^3 (2000 gallons)**	**$1.0x10^{-3}$ cm/s**	**ln K = 2**
DNAPL Type 3 (high density)	**PCE**	7.57 m^3 (2000 gallons)	$1.0x10^{-3}$ cm/s	ln K = 2
High DNAPL Volume	TCE	**3.79 m^3 (5000 gallons)**	$1.0x10^{-3}$ cm/s	ln K = 2
High K	TCE	7.57 m^3 (2000 gallons)	**$1.0x10^{-2}$ cm/s**	ln K = 2
High Heterogeneity	TCE	7.57 m^3 (2000 gallons)	$1.0x10^{-3}$ cm/s	**ln K = 4**

Table 2-2. Template site parameters for unconsolidated media simulations.

Template Site	DNAPL Type	Fracture Aperture	Matrix Porosity	Fraction Organic Carbon	Fracture Spacing
Low Organic Carbon	TCE	75 μm	30%	**0.0015**	1.0 m
Low Matrix Porosity	TCE	75 μm	**15%**	0.003	1.0 m
Low Fracture Aperture	TCE	**37.5 μm**	30%	0.003	1.0 m
Low Density DNAPL	**1,1,1-TCA**	75 μm	30%	0.003	1.0 m
Base Case	**TCE**	75 μm	**30%**	**0.003**	1.0 m
High Density DNAPL	**PCE**	75 μm	30%	0.003	1.0 m
High Fracture Aperture	TCE	**150 μm**	30%	0.003	1.0 m
High Matrix Porosity	TCE	75 μm	**45%**	0.003	1.0 m
High Organic Carbon	TCE	75 μm	30%	**0.006**	1.0 m

Table 2-3. Template site parameters for fractured clay simulations.

Template Site	DNAPL Type	Bedrock Type	Fracture Spacing (m)	Bulk Density (g/cm^3)	Matrix Porosity (%)	f_{oc}	Matrix Tortuosity	Fracture Aperture (μm)
Bedrock 2	TCE	**Shale**	**1.0 (h) x 4.0 (v)**	**2.619**	**3**	**0.009**	**0.10**	**150 (50-250)**
Base Case	**TCE**	**Sandstone**	**1.0 (h) x 6.0 (v)**	**2.490**	**7.7**	**0.005**	**0.20**	**125 (25-230)**
Higher Density DNAPL	**PCE**	Sandstone	1.0 (h) x 6.0 (v)	2.490	7.7	0.005	0.20	125 (25-230)
Bedrock 3	TCE	**Granite**	**2.0 (h) x 2.0 (v)**	**2.697**	**0.1**	**0.0005**	**0.05**	**300 (100-500)**

Table 2-4. Template site parameters for fractured rock simulations.

2.2.2.5.1 Porous Media

Table 2-2 lists the template sites used for the porous media numerical simulations. Each porous media template site has dimensions 20 meters (m;65.6 feet [ft]) by 20 m (65.6 ft) by 5 m (16.4 ft) high. In cases where the site of interest is larger than this, the simulation

results can be scaled up. The water table is located at the top of the domain, and constant head boundaries are assigned to opposite ends to create horizontal flow conditions. The side boundaries and bottom boundary are assigned no-flow conditions for the DNAPL. For some of the remediation simulations (*e.g.,* ISCO), the template site domain was reduced in size along lines of symmetry to allow simulations to be completed in a reasonable time frame. In such cases, the results will be scaled up to match those of the full template site size prior to entering into the protocol database.

The base case for the analysis was a TCE DNAPL release (7.57 cubic meters [m^3]; 2000 US gallons) sufficient to form DNAPL pools as well as residual DNAPL in soil with an average hydraulic conductivity (K) of 1.0 x 10^{-3} centimeters per second (cm/s) and moderate variability in hydraulic conductivity (variance ln K = 2). **Table 2-1** lists the parameters associated with the other template sites. The collection of template sites is intended to span a reasonable range in average hydraulic conductivity, DNAPL release volume, and degree of heterogeneity. In addition, the template sites include use of TCE, PCE and 1,1,1-TCA as the DNAPL of interest.

2.2.2.5.2 Fractured Media

With respect to fractured media, both fractured rock and fractured clay were examined. The emphasis of the fractured clay simulations was the application of ISCO and a study of the effects of concentration rebound. For the fractured rock simulations, template sites were developed to provide a basis for follow-on simulation of ISCO, EISB and SEAR technologies.

The fractured clay simulations adopted parallel, equally spaced fractures in a two-dimensional domain. **Table 2-3** summarizes the parameters that describe each fractured clay template site. The presented numerical simulations are based on a two-dimensional (2D) fracture-matrix system in which the results can be scaled up using symmetry to represent a larger, three-dimensional (3D) parallel fractured system subject to unidirectional groundwater flow. In order to manage computational run times, lines of symmetry were located along the center of the fractures and the matrix blocks so that the modeled domain consisted of a half fracture and a half matrix block. **Figure 2-3** illustrates how the modeled domain is scaled up to represent a 3D template site 15 m long in the direction of groundwater flow, 20 m wide orthogonal to the direction of groundwater flow, and 5 m high. The modeled domain is a 2D vertical slice of the 3D domain. It should be noted that although the presented domain incorporates horizontal fractures, the results are directly applicable to a set of vertical fractures having the same hydraulic characteristics (i.e., aperture, spacing and applied hydraulic gradient) as the modeled horizontal fractures since diffusion is independent of orientation. The source zone emplaced within the fracture is 5 m long, 20 m wide, and is initially assigned a specified non-wetting phase (DNAPL) saturation. Constant head boundaries were applied to the upgradient and downgradient ends of the domain, producing unidirectional

groundwater flow in the fracture subject to advection and longitudinal dispersion. Longitudinal and vertical transverse (2D) diffusion are permitted in the matrix.

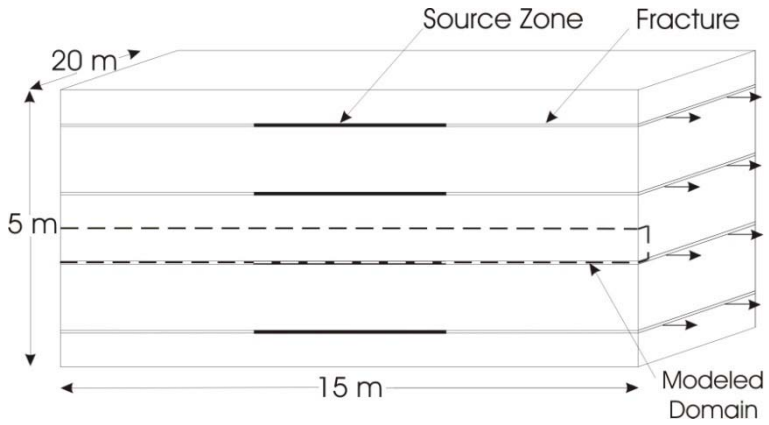

Figure 2-2 Model domain and scaled up system (Mundle et al., 2007).

Table 2-4 lists the template sites that are being used for the ISCO, EISB and SEAR fractured rock numerical simulations at the field scale. **Figure 2-4** presents the distribution of intrinsic permeability for the three domains, illustrating the distribution of horizontal and vertical fractures. In each case, the mean aperture is at the midpoint of the range specified in the table. The collection of template sites is intended to span a reasonable range in fracture aperture mean, fracture aperture range, fracture spacing, matrix porosity, matrix fraction organic carbon, and matrix permeability. Each fractured rock template site has dimensions 20 m (65.6 ft) long by 5 m (16.4 ft) high and unit depth.

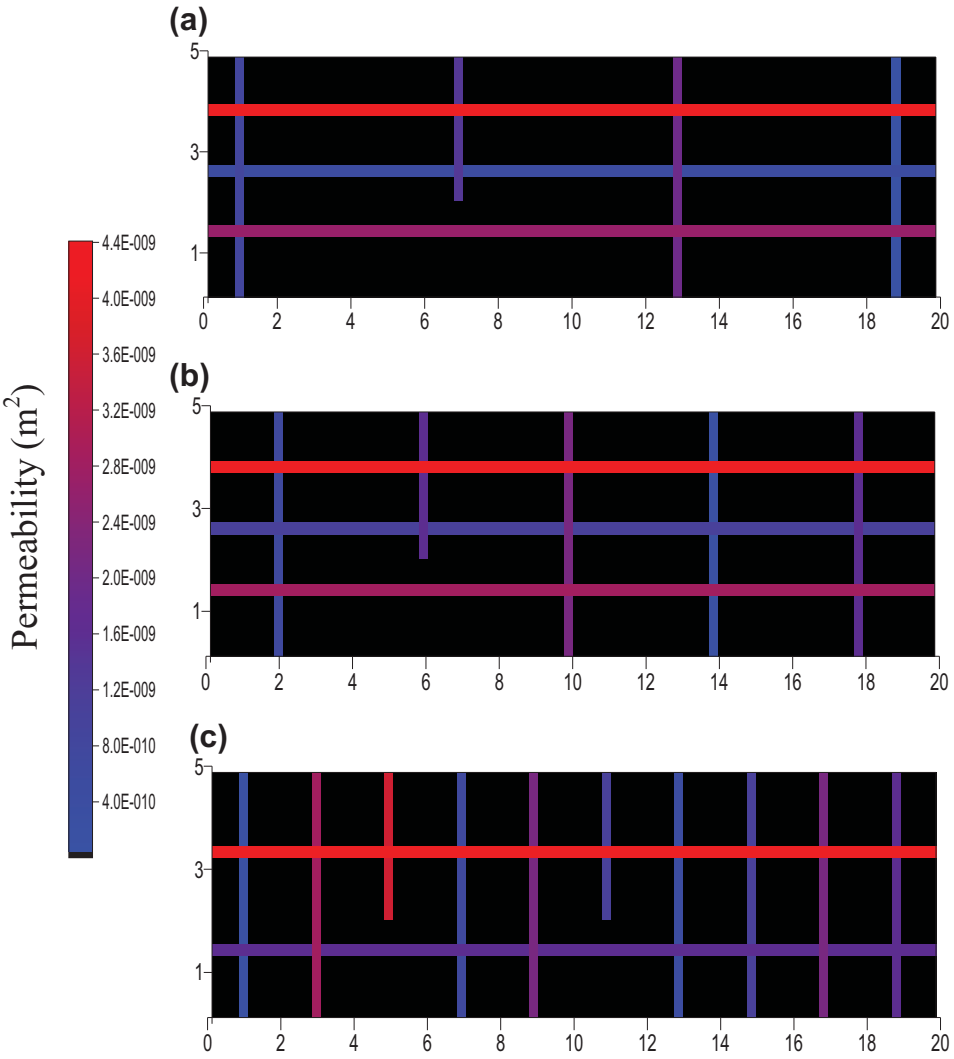

Figure 2-3. Distribution of permeability for the field scale fractured rock domains: (a) sandstone, (b) shale, and (c) granite. Colour corresponds to fracture permeability according to the scale bar provided; matrix permeability is uniform (black). Note that fracture apertures are exaggerated for visual purposes.

In cases where the site of interest is larger than this, the simulation results can be scaled up. Each template site includes a DNAPL release sufficient to form pooled and residual DNAPL in fractures followed by a period of 'aging' providing sufficient time for TCE diffusion into the rock (with an average matrix permeability of 1.05×10^{-15} square meters [m^2]). The water table is located at the top of the domain, and constant head boundaries are assigned to opposite ends to create horizontal flow conditions.

Remedial fluids are injected at the upgradient boundary at the start of the treatment period. Each study provided suites of sensitivity simulations to key treatment parameters. **Tables 2-5, 2-6**, and **2-7**, provide the sensitivity simulations conducted in fractured rock for ISCO, EISB, and

SEAR, respectively. In each study, a 'no treatment' simulation was also conducted for comparison purposes.

Run No.	DNAPL Type	Rock Type	$KMnO_4$ Concentration (mg/L)	$KMnO_4$ Injection Strategy
1 (Base Case)	TCE	Sandstone	2500	Continuous Injection for 2 Years
2	TCE	Sandstone	5000	Continuous Injection for 1 Year
3	TCE	Sandstone	1250	Continuous Injection for 4 Years
4	TCE	Sandstone	2500	3 Months On 3 Months Off for 4 Years
5	TCE	Sandstone	2500	6 Months On 3 Months Off for 4 Years
6	TCE	Sandstone	2500	12 Months On 12 Months Off for 4 Years
7	TCE	Shale	2500	Continuous Injection for 2 Years
8	TCE	Granite	2500	Continuous Injection for 2 Years
9	PCE	Sandstone	2500	Continuous Injection for 2 Years
10	TCE	Sandstone	0	No Treatment

Table 2-5. Field Scale ISCO Fractured Rock Simulations

Run No.	DNAPL Type	Rock Type	Lactate Concentration (mg/L)	Dechlorination Rate	Lactate Injection Strategy	Bioremediation Location
1 (Base Case)	TCE	Sandstone	2000	Mean	Continuous Injection for 2 Years	Fractures + Matrix
2	TCE	Sandstone	2000	Mean	Continuous Injection for 2 Years	Fractures Only
3	TCE	Sandstone	2000	Mean x 10	Continuous Injection for 2 Years	Fractures + Matrix
4	TCE	Sandstone	2000	Mean x 0.10	Continuous Injection for 2 Years	Fractures + Matrix
5	TCE	Sandstone	2000	Mean	3 Months on 3 Months Off for 4 Years	Fractures + Matrix
6	TCE	Sandstone	2000	Mean	6 Months on 6 Months Off for 4 Years	Fractures + Matrix
7	TCE	Sandstone	2000	Mean	12 Months on 12 Months Off for 4 Years	Fractures + Matrix
8	TCE	Sandstone	1000	Mean	Continuous Injection for 4 Years	Fractures + Matrix
9	TCE	Sandstone	4000	Mean	Continuous Injection for 1 Year	Fractures + Matrix
10	TCE	Shale	2000	Mean	Continuous Injection for 2 Years	Fractures + Matrix
11	TCE	Granite	2000	Mean	Continuous Injection for 2 Years	Fractures + Matrix
12	PCE	Sandstone	2000	Mean	Continuous Injection for 2 Years	Fractures + Matrix
13	TCE	Sandstone	0	Mean	No Treatment	Fractures + Matrix

Table 2-6. Field Scale EISB Fractured Rock Simulations

Run No.	DNAPL Type	Rock Type	Surfactant Concentration (mg/L)	Degree of Matrix Loading	Mass Transfer Assumption
1 (Base Case)	TCE	Sandstone	40000	20 Years Aging	Equilibrium
2	TCE	Sandstone	20000	20 Years Aging	Equilibrium
3	TCE	Sandstone	60000	20 Years Aging	Equilibrium
4	PCE	Sandstone	40000	20 Years Aging	Equilibrium
5	TCE	Shale	40000	20 Years Aging	Equilibrium
6	TCE	Granite	40000	20 Years Aging	Equilibrium
7	TCE	Sandstone	40000	0 Years Aging	Equilibrium
8	TCE	Sandstone	40000	5 Years Aging	Equilibrium
9	TCE	Sandstone	40000	10 Years Aging	Equilibrium
10	TCE	Sandstone	40000	20 Years Aging	Rate Limited
11	TCE	Sandstone	0.0	20 Years Aging	Equilibrium

Table 2-7. Field Scale SEAR Fractured Rock Simulations

Assuming a two-dimensional domain for the fractured rock simulations is conservative since it reduces the potential for the injected remedial fluids to bypass the source zone and thus provides the best opportunity for remediation success. Full details of the fractured rock simulations are presented in **Appendix D.2** (model development and testing), **Appendix D.3** (ISCO), **Appendix D.4** (EISB), **Appendix D.5** (SEAR), and **Appendix D.6** (notation definition and full references).

2.2.3 Screening Tool Development

Sections 2.2.3.1 to 2.2.3.3 provide an overview of the programming of DNAPL TEST, focusing on an overview of the screening tool structure (Section 2.2.3.1), calculation of case study data quality rankings (Section 2.2.3.2), and formulation of the site specific analysis case study selection protocol (Section 2.2.3.3).

2.2.3.1 Screening Tool Structure

DNAPL TEST was developed to allow the user to customize their analysis to meet their own unique goals and objectives. The user is provided with two options:

- The General Analysis option, in which the user can query the database of case studies for general performance information. In this option, the user can refine their search to include specific technologies, case study type, data quality rankings, and site characteristics, and the tool will generate reports of average and select individual performance data from case studies matching the search criteria.

- The Site Specific Analysis option, in which the user is given the opportunity to tailor their analysis to provide performance information from case studies with specific characteristics. Using this alternative, the user is asked to input characteristics of the site of interest and specify other search criteria (e.g., specify data quality rankings and case study types to be included, geologies, DNAPL types, etc.). DNAPL TEST then searches for case studies with statistically similar site characteristics (i.e., case studies with site characteristics that are anticipated to have similar technology performance) for performance metrics where correlations between technology performance and site characteristics were observed (see Section 2.2.3.2 for more details). For performance metrics where correlations were not observed, case studies that meet the user-specified search criteria are included in the analysis. The Site Specific Analysis output reports provide more details of case-study specific performance as well as average and min/max performance trends. Output reports are also provided on an individual performance metric basis as well as technology specific basis.

2.2.3.2 Development of Data Quality Rankings

Data Quality Rankings (DQRs) were designed to provide DNAPL TEST users an assessment of the relative quality of the data upon which their analyses are based. They are not to be interpreted as a judgment on the quality of the modeling, field, or laboratory work described in each case study, as this would require a detailed evaluation of the technical aspects of each case study and more detailed information than typically available. Rather the DQRs have been developed to use certain key indicators to provide an assessment of the quality of each case study, based on readily available information.

There are some limitations to this approach. For example, some well-implemented case studies may have been assigned lower DQRs in DNAPL TEST if detailed reports could not be obtained by the project team and insufficient information was available to develop a full assessment of the DQR. The converse situation may also occur, with a poorly implemented program being assigned a higher DQR if more information was available describing the implementation or if the remediation program was implemented more recently.

While such ratings cannot be developed with complete objectivity, efforts were made to minimize subjectivity by automating the DQR calculation. The DQR calculation reflects the following five criteria:

- A – Quality of the information source;
- B – Age of the study;
- C – Type and density of DNAPL assessment methods and locations;
- D – The methodology used and amount of information available for pre-treatment performance monitoring; and
- E – The methodology used and amount of information available for post-treatment performance monitoring.

Case studies receive an integer ranking between 1 and 3 (three being highest) for each of these criteria (criteria ranking assignment described below), and the DQR is their weighted average calculated as follows:

$$DQR = 0.1A + 0.2B + 0.2C + 0.25D + 0.25E$$

The average was weighted according to the following rationale:

- A: Information sources vary in reputability (e.g., a peer-reviewed journal article *versus* a technology vendor's project description). However, this criterion does not weigh as highly as other criteria that reflect the completeness of the data record.
- B: Older studies were ranked lower than more recent studies to account for improved technology application resulting from lessons learned from previous technology applications and ongoing technology developments.
- C: The density of sampling and methods used to characterize the DNAPL are an important subset of site characterization activities.
- D and E: The completeness of site characterization and monitoring (e.g., hydrogeological parameters, area or volume treated, and assessment of performance metrics, particularly DNAPL mass removal), both before and after treatment, are the most important indicators of data quality.

For use in DNAPL TEST, DQRs were considered low if the value was ≤1.8 out of 3.0, medium if the DQR ranged from >1.8 to <2.4, and high if the value is ≥2.4. **Appendix E** provides additional details on each of the criterion, and how the rankings were assigned.

The average DQR as well as the number of studies included in the analysis is shown on the bottom left corner of General Analysis input screens. This information is automatically updated as the user changes selection criteria.

Users can output a Data Quality Rating Summary for the case studies included in their analysis in Step 5 of the General Analysis or Step 6 of the Site Specific Analysis. **Appendix B** of this report provides the DQR for all of the case studies included in DNAPL TEST version 2.0.

2.2.3.3 Site-Selection Protocol Development

A statistical correlation analysis between site characteristics and technology performance was completed with the following objectives in mind:

- Identify correlation between various site parameters and remedial performance and assess the relative influence that specific site parameters have on technology performance; and
- Develop a protocol for the Site Specific Analysis to provide a basis for DNAPL TEST to find and extract case studies from the database that are anticipated to have statistically similar technology performance as that of the user's site.

The following sections summarize the methodology used to perform the statistical analysis and the results of the analysis (Section 2.2.3.3.1), and describe how the statistical results were used to develop the site selection protocol that is the basis of the Site Specific Analysis (Section 2.2.3.3.2).

2.2.3.3.1 Statistical Analysis

The identification and quantification of correlations between site parameters and performance metrics was completed in two steps:

i) A series of correlation tests were conducted to identify linear associations between a given site parameter and a given technology performance metric. A five percent (%) level of significance was used as the criteria for statistically significant linear correlations; and

ii) Site parameter – performance metric pairs that showed a statistically significant correlation were analyzed using simple linear regression methods. Regression quantifies the sensitivity of the technology performance to each site parameter, and was also used to calculate a range of site parameters values given a particular technology performance value *via* a 95% confidence interval.

The majority of the case studies did not report information for the complete list of site parameters and performance metrics evaluated, which resulted in limited information available for many performance metric – site parameter pair datasets. A total of nine pairs for all technologies were found to have statistically significant correlations, including two performance metrics: removal of DNAPL mass (EISB, ERH, and SEAR only) and treatment duration (thermal resistive heating and steam flushing only). Five site parameters, specifically areal extent of the DNAPL zone, electrode spacing, hydraulic conductivity, pre-remediation DNAPL mass, and volume of the DNAPL zone were correlated with these two performance metrics, as summarized in **Table 2-8** below. Coefficient of determination (R^2) values for the regression model ranged from 0.44 to 0.99, indicating a relatively good to an almost perfect fit, respectively. **Appendix F**

provides a detailed summary of the statistical procedure that was followed, the data considered, and the resulting correlations that were observed.

Technology	Media Type	Performance Metric (Dependent Variable)	Input Parameter (Independent Variable)	R^2
EISB	Unconsolidated	Reduction in DNAPL mass	Hydraulic conductivity	0.44
SEAR	Both	Reduction in DNAPL mass	Areal extent of DNAPL zone	0.69
SEAR	Both	Reduction in DNAPL mass	Pre-remediation DNAPL mass	0.51
SEAR	Both	Reduction in DNAPL mass	Volume of DNAPL zone	0.93
Thermal - resistive	Both	Reduction in DNAPL mass	Areal extent of DNAPL zone	0.82
Thermal - resistive	Both	Reduction in DNAPL mass	Volume of DNAPL zone	0.87
Thermal - resistive	Both	Treatment Duration	Pre-remediation DNAPL mass	0.88
Thermal - resistive	Both	Treatment Duration	Electrode spacing	0.59
Thermal - steam	Both	Treatment Duration	Volume of DNAPL zone	0.99

Table 2-8. Summary of correlations observed between performance metric and site parameter pairs.

The correlated site parameter – performance metric pairs listed in **Table 2-8** were further analyzed *via* regression techniques to quantify intervals of site parameter values that would correspond to a statistically significant similar level of performance for each performance metric. The results of this analysis are summarized in

Table 2-9 below, and these provide the basis for the case study selection protocol described in Section 2.2.3.3.2. The R^2 values for the regression model ranged from 0.51 to 0.99, again representing a reasonably good to an almost perfect fit of the data to the model.

2.2.3.3.2 Development of the Case Study Selection Protocol for the Site Specific Analysis

DNAPL TEST has been developed to allow for the use of "statistical filters" where correlations between technology performance and site parameters have been identified, and to allow for the use of "non-statistical filters" where correlations do not exist. As discussed in Section 2.2.3.3.1 above, statistical correlations between performance metrics and site characteristics were observed for only select technologies and for select performance metrics. For these performance metric-site correlation pairs, the statistical correlations govern the selection of case studies, such that case studies included in the DNAPL TEST output are those that are statistically more likely to have similar performance to the User's site. For the remainder of the technology – performance pairs (*e.g.,* reductions in groundwater concentrations, ISCO technologies, *etc.*), there is no ability to predict technology performance based on site parameters; however, it is

Technology	Media Type	Performance Metric (Independent Variable)	Input Parameter (Dependent Variable)	Regression Coefficients		R^2	95% Confidence Interval	Units
				Intercept (SE)	Slope (SE)			
EISB	Unconsolidated	Reduction in DNAPL mass	Hydraulic conductivity	-10.5 (1.51)	1.22 (0.38)	0.98	*/÷ 1.58 [3]	cm/s
SEAR	Both	Reduction in DNAPL mass	Areal extent of DNAPL zone	206 (17.5)	-1.86 (0.25)	0.69	+/- 22	m^2
SEAR	Both	Reduction in DNAPL mass	Preremediation DNAPL mass	3,260 (439)	-33.1 (6.32)	0.51	+/- 553	kg
SEAR	Both	Reduction in DNAPL mass	Volume of DNAPL zone	1,000 (40.1)	-9.89 (0.59)	0.93	+/- 54	m^3
Thermal - resistive	Both	Reduction in DNAPL mass	Areal extent of DNAPL zone	4,370 (675)	-41.1 (8.55)	0.81	+/- 889	m^2
Thermal - resistive	Both	Reduction in DNAPL mass	Volume of DNAPL zone	38,600 (5,090)	-363 (68.0)	0.87	+/- 8,380	m^3
Thermal - resistive	Both	Treatment Duration	Electrode spacing	2.75 (0.83)	0.09 (0.02)	0.59	*/÷ 2.17 [3]	kg
Thermal - resistive	Both	Treatment Duration	Preremediation DNAPL mass	-2.83 (1.83)	3.42 (0.56)	0.68	+/- 1.06	m
Thermal - steam	Both	Treatment Duration	Volume of DNAPL zone	-27,500 (10,300)	1,760 (104)	0.99	+/- 25,200	m^3

Notes:

[1] All estimates of the slope parameter were statistically significant at the 5% level of significance (i.e., p-value < 0.05).

[2] 95% confidence intervals give the range of the expected upper and lower limits for a performance metric, given a specific input parameter value.

[3] Log-transformed data was used to fit the model; therefore, the effect of the independent variable is multiplicative rather than additive.

Acronyms:

R^2 - coefficient of determination
SE - standard error
kg - kilograms
m - meters
m^2 - squared meters
m^3 - cubic meters
cm/s - centimeters per siemen

Table 2-9. Summary of confidence intervals identified for site parameter - performance metric pairs.

recognized that the user may still wish to refine their analysis using specific ranges for particular site parameters; hence the incorporation of "non-statistical filters".

The case study selection process for the Site Specific Analysis follows the protocol described below:

- **Where a correlation exists between a site parameter and a technology performance metric**: the statistical filter is preferentially used to select case studies to include in the analysis. Sites included in the analysis are those with parameter values that fall within the range dictated by the confidence intervals calculated in the second regression analysis. Case studies with no information on that site parameter will not be included in the analysis. For cases where more than one site parameter exhibits a correlation to the performance metric (*e.g.,* DNAPL mass removal for thermal resistive heating), the Site Specific Analysis will include all sites that have site parameters that fall within the range calculated from the second regression analysis (*i.e.,* the selection criteria is an OR statement, and the inclusion of sites is additive).

- **Where no correlation exists between a site parameter and a technology performance metric:** user-specified, non-statistical filter ranges are preferentially used to select applicable case studies. The case studies included in the analysis must meet all non-statistical criteria (*i.e.,* the selection process is an AND criteria, and all site parameters must fall within all ranges specified by the user or they are excluded from the analysis). Case studies with no data for any of the site parameters with specified ranges will not be included in the analysis. Where no non-statistical filters are specified by the user, then all case studies containing data for that performance metric is included in the output to the user.

2.3 Advantages and Limitations of the Technology

Advantages offered by the screening tool include the following:

- The screening tool allows users to easily and quickly access performance information on a large number of case studies;
- The filtering capabilities built into the tool allow for customized analyses, such that the output presents only performance information from case studies relevant to the particular site or case study profile under evaluation;
- The data can be filtered according to data quality, to restrict output to only those case studies categorized of being "higher quality", although this will reduce the amount of information presented in the output;
- The screening tool allows users to access the results of laboratory and modeling studies along with documented field studies, or conversely, to filter out modeling studies and/or field studies to focus on only a subset of case studies;

- Users may modify filtering criteria input to the screening tool to conduct sensitivity analyses. Such sensitivity analyses could help to streamline site data collection activities to better refine those site parameters that govern the performance of the selected remedial technology; and
- Case study reference details are provided to the user, which allows them to follow up with a more detailed assessment of the case study performance, if so desired.

Some of the limitations of the screening tool include the following:

- Chlorinated solvent DNAPL remediation case studies have been collected from multiple sources and incorporated into the screening tool database. These case studies were obtained from a wide range of sources (on-line databases such as CLU-in.org, peer-reviewed journal papers, conference proceedings, *etc.*); as such the level of information provided and peer-review on information provided varies widely.
- Field case studies representing a range of "implementation quality" have been collected, including technologies that were applied under less optimal or ideal or controlled conditions.
- Field-scale numerical simulations of remediation were used to provide additional information that was incorporated into the database for parameters that are often difficult to quantify under field conditions (*e.g.,* DNAPL mass removal; see Section 2.2.2). Multiple modeling runs were completed per template site to evaluate the sensitivity of technology performance to individual site or technology characteristics. For these types of parameters (*e.g.,* DNAPL mass removal), the output may be dominated by modeling results.
- The case study selection protocol developed for the Site Specific Analysis was developed using a dataset that was limited by incomplete information for field case studies and multiple modeling case studies developed using similar site parameters, which sometimes resulted in a dataset biased towards those particular site parameters. As described in **Appendix F**, several quality assurance/quality control (QA/QC) measures were undertaken to minimize to the extent possible the influence of biased and small datasets in the regression analysis to avoid artificially influencing case study selection in the Site Specific Analysis.

Extensive efforts have been made over the past 15 years to validate DNAPL-3D used for the simulations and to ensuring that critical functions and site characteristics have been incorporated into the model so that “typical” performance of each simulated technology is captured in the model results. The development and validation of the numerical code followed the steps below:

i) A comprehensive literature review to evaluate the relevant processes that occur during DNAPL remediation using the specified technology;
ii) Development of the code and verification that it is error-free through comparison to analytical solutions (where available) and thorough testing;

iii) Validation of the numerical approach through direct comparison to well-characterized laboratory experiments conducted under controlled conditions (where available); and

iv) Publication of simulation results in peer-reviewed journals, graduate student theses, and conference proceedings.

However, the user should be aware that models by their nature require the incorporation of simplifying assumptions, finite domain sizes, controlled boundary conditions, and other approximations of system conditions that contain more complexity in reality. Specific examples of limitations of the modeling completed for incorporation into DNAPL TEST include the following:

i) Naturally occurring biological attenuation, a process that may occur at many sites to varying degrees, was not incorporated into the numerical modeling. Natural biological attenuation would further enhance concentration and mass reductions beyond that simulated due to active remediation efforts. As a result, concentration and mass reductions simulated should be considered conservative, and more representative of sites in which natural attenuation is not occurring or is occurring very slowly, or where the remedial application interferes with the natural attenuation by modifying the geochemistry (e.g., redox, pH, temperature) to conditions not favorable to biological attenuation;

ii) For the EISB simulations, the role of the biomass itself in sustaining elevated levels of bioactivity beyond termination of active treatment was not simulated. Biomass decay and its use by dechlorinating bacteria as a secondary electron donor source has been well documented (e.g., Adamson and Newell, 2009) to result in sustained reductions in concentrations and little to no rebound for extended periods of time beyond the end of active EISB treatment. For the numerical modeling simulations conducted for DNAPL TEST, rebound was observed immediately upon consumption of the amended lactate, which is inconsistent with field observations (e.g., McGuire et al., 2006). To avoid inconsistencies with field observations, the rebound behavior for the EISB simulations was not incorporated into the DNAPL TEST database;

iii) For the SEAR simulations, biodegradation of the surfactant and resulting micelle breakage was not simulated. As a result, elevated contaminant concentrations were observed for a period of time (months to years) beyond the end of surfactant injection as the surfactant was flushed from the model domain and enhanced dissolution of DNAPL continued. Many surfactants are biodegradable, which results in faster reductions of the surfactant concentrations post injection. SEAR treatment often includes flushing of one or more pore volume flushes of water alone through the treatment area after termination of the SEAR flush to maximize contaminant recovery. To reflect more representative "post-treatment" concentrations, the end of treatment concentrations were taken approximately 12 months after termination of surfactant injection when the majority of the surfactant had been flushed from the domain.

iv) For the fractured rock simulations, it is unknown whether biodegradation can be stimulated within the rock matrix. Pore size limitations may physically prevent the migration of the bacteria into the matrix itself; however, limited research has been conducted to date to demonstrate the extent that biodegradation can be physically stimulated in the rock matrix. For these simulations, matrix biodegradation was assumed, and in one case, biodegradation was assumed to occur only in the fractures. Due to the idealized assumptions representing end-points of the spectrum of behavior and the uncertainty as to which scenario is most representative of actual field behavior, the EISB fractured rock simulations were not included in the DNAPL TEST database. However the full suite of ESIB fractured rock simulation results, including a sensitivity to the presence of biodegradation in the fractures or in the fractures and matrix, is presented in **Appendix D.4**.

In an effort to minimize bias created through incorporation of case studies representing "non-typical" or "non-optimal" field scenarios or poor quality case studies, technology performance is reported as average or median performance of multiple sites. Ranges in performance (minimum/maximum) are provided to give the user information on potential variation in performance observed at other sites. The user is also provided with performance on a case study by case study basis, as well as reference sources (where publicly available) if additional information on particular case studies is desired. Other options available to the user include the ability to filter case studies retained in the analysis by study type (field study, modeling simulation, etc.) and data quality rankings (see Section 2.2.3.2 for details), which provide a measure of the quality of information available on a case study.

3. PERFORMANCE OBJECTIVES

Specific performance objectives for the screening tool development are summarized in **Table 3-1** below and consist of one quantitative and two qualitative performance objectives. The first two objectives listed in **Table 3-1** pertain to the screening tool itself, and require development of a screening tool that is easy to use and provides output that is accurate and relevant to the user. To ensure that these performance objectives were met, the following actions were taken:

Beta testing of the tool was completed partway through development. Multiple reviewers both from within the DoD, ESTCP, industry, and USEPA were contacted and asked to review the beta version of the screening tool and provide specific feedback, which included targeted questions regarding ease of use, errors encountered, and relevance of information included in the screening tool output. Feedback was also solicited for suggestions for improvement. In general, reviewers provided positive feedback with regards to the ease of use of the screening tool and only minor comments were received. A summary of the beta version review comments and how these were addressed in the final version of the screening tool is provided in Section 5.5.

Upon completion of the screening tool programming, a detailed verification of the screening tool code was undertaken to verify that appropriate case studies were included in the output as dictated by the case study selection protocol and filtering criteria, and that the information included in output reports accurately reflected the information included in the case study database. Section 6.1 provides a summary of the various checks completed and the result of the verification process.

The third performance objective listed in **Table 3-1** specifically addresses Demonstration Objective *iv*): "Reduce the uncertainty of estimating and predicting remedial outcomes and implementation costs at DNAPL source zone sites" (Section 1.2). By improving our understanding of the relative influence of various factors on DNAPL remediation technology performance, we can reduce the uncertainty of estimating and predicting remedial outcomes. As described in Section 2.2.2.5, this performance objective was addressed through completing: (*i*) a sensitivity study as part of the numerical modeling exercise; and (*ii*) statistical correlation analyses of both field and modeling case studies to investigate the relative influence that site parameters have on technology performance. Section 6.2 provides a discussion of the findings of this evaluation.

Performance Objective	Data Requirements	Success Criteria	Results
Quantitative Performance Objectives			
DNAPL TEST should accurately select case studies according to the site selection protocol and accurately output information included in the selected database.	Verification of screening tool code and output.	Output accurately reports technology performance data and includes appropriate case studies.	Data verification confirmed that reports generated from the tool were appropriate (See Section 6.1 and Appendix G).
Qualitative Performance Objectives			
Ease of use of the screening tool and information reported relevant and of interest to users.	Beta testing - Feedback from peer reviewers on ease of use of the screening tool.	Screening tool should be easy to use, and output should be of interest and relevant to users.	Beta testing was conducted and changes were made to the tool based on user comments to improve ease of use. A summary of the comments from beta test reviewers is provided in Table 5-1.
Evaluation of factors that influence DNAPL remediation technology performance.	Sensitivity study completed as part of the numerical modeling exercise and statistical correlation analysis between site parameters and technology performance.	Identification of factors that influence technology performance.	Sensitivity analysis during modeling allowed for evaluation of factors influencing technology performance. See Section 6.2 for a discussion of the DNAPL remediation technology performance assessment.

Table 3-1. Screening Tool Performance Objectives

4. SITE DESCRIPTION

Although the technology developed and demonstrated during this project was not demonstrated at specific sites, DNAPL TEST development relied on information compiled from a large number of field sites in the general domain and simulations dealing with contaminated sites. Information on the field and numerically simulated sites is presented in Sections 2.2.1 and 2.2.2, respectively, and is summarized below.

4.1 Site Location and History

The field case study sites that are in DNAPL TEST are predominantly located in the United States, with 29 individual states represented. Additionally, there is one site in Asia, one site in Canada, and three sites in Europe.

4.2 Site Geology/Hydrogeology

There is a wide range of geological and hydrogeological settings represented by the field case studies available in DNAPL TEST. Sites include have varying unconsolidated media such as clays, sands and gravels with hydraulic conductivities ranging from $3x10^{-12}$ to 0.2 cm/s, as well as consolidated media such as sedimentary limestone, sandstone, and shale, igneous basalts and granites, and metamorphous rock.

For the modeling sites, three general geologies are represented: porous media, fractured clay, and fractured bedrock. For each of these geological settings, a 'base case' site was created, and site characteristic parameters were varied as part of a sensitivity analysis. Geological/hydrogeological site characteristic parameters that were varied included heterogeneity and permeability in unconsolidated simulations, fracture aperture, matrix porosity, and f_{oc} in fractured clay simulations, and fracture spacing and aperture, rock matrix bulk density, porosity, f_{oc}, and tortuosity in fractured rock simulations.

In the porous media modeling template sites, each site had dimensions 20 m (65.6 ft) by 20 m (65.6 ft) by 5 m (16.4 ft) high. The water table is located at the top of the domain, and constant head boundaries were assigned to opposite ends to create horizontal flow conditions. The side boundaries and bottom boundary were assigned no-flow conditions for the DNAPL. For some of the remediation simulations (*e.g.,* ISCO), the template site domain was reduced. The base case for the porous media analysis was a TCE DNAPL release (7.57 m^3; 2000 US gallons [gal]) sufficient to form DNAPL pools as well as residual DNAPL in soil with an average K of 1.0 x 10^{-3} cm/s and moderate variability in hydraulic conductivity (variance ln K = 2). Table 2.1 lists the parameters associated with the other template sites. The collection of template sites is intended to span a reasonable range in average hydraulic conductivity, and degree of heterogeneity.

The fractured clay modeling template sites had parallel, equally spaced fractures in a two-dimensional domain. **Table 2-3** summarizes the parameters that describe each fractured clay

template site. The presented numerical simulations are based on a 2D fracture-matrix system which is scaled up to represent a 3D template site 15 m long in the direction of groundwater flow, 20 m wide orthogonal to the direction of groundwater flow, and 5 m high. The modeled domain is a 2D vertical slice of the 3D domain. It should be noted that although the presented domain incorporates horizontal fractures, the results are directly applicable to a set of vertical fractures having the same hydraulic characteristics (i.e., aperture, spacing and applied hydraulic gradient) as the modeled horizontal fractures since diffusion is independent of orientation. Constant head boundaries were applied to the upgradient and downgradient ends of the domain, producing unidirectional groundwater flow in the fracture subject to advection and longitudinal dispersion.

The fractured rock modeling template sites each have dimensions 20 m (65.6 ft) long by 5 m (16.4 ft) high and unit depth. The collection of template sites is intended to span a reasonable range in fracture aperture mean, fracture aperture range, fracture spacing, matrix porosity, matrix fraction organic carbon, and matrix permeability. The water table is located at the top of the domain, and constant head boundaries are assigned to opposite ends to create horizontal flow conditions.

4.3 Contaminant Distribution

In the field sites the areal extent of DNAPL ranges from 10 to almost 40,000 m^2 with the maximum depth of DNAPL at sites between 4 and 100 m. The volume of DNAPL at the sites ranges from less than 1 to over 100,000 m^3.

For the modeling sites sensitivity analysis was conducted by varying the type of DNAPL from the Base Case (i.e., altering the DNAPL density and solubility) in each of the porous media, fractured clay, and fractured bedrock sites. DNAPL types included PCE, TCE, and 1,1,1-TCA in each of these media. In the porous media template sites only, the volume of DNAPL release was also varied, and the template sites included released of 500 gal, 2000 gal, and 5000 gal of DNAPL. For the fractured rock sites, the DNAPL release was followed by a period of “aging’ providing sufficient time for TCE diffusion into the rock.

5. TEST DESIGN

There was no test conducted as part of the scope of this project, thus this section is not relevant. Discussion of the development of DNAPL TEST is provided in Section 2.2.

5.1 Treatability or Laboratory Study Results

Eleven laboratory case studies are included in DNAPL TEST. These are column studies that evaluated a range of technologies, including ISCO, EISB, steam injection, and thermal treatment.

5.2 Field Testing

A *beta* version of the screening tool (focusing on thermal technologies only for the Site Specific Analysis) was developed and in 2008 was peer-reviewed by several people from outside of the development team (including DoD, USEPA, and ESTCP personnel. *Beta* testers were asked to spend time analyzing sites using the tool, and provide feedback on the tool with respect to four performance criteria: ease of use, relevancy of reported information, accuracy, and reliability. Suggestions for improvements in each of these areas and overall were requested. All of the *beta*-tester comments were fully reviewed and implemented or addressed as appropriate. **Table 5-1** below summarizes the beta comments and actions taken.

Comment	Action
Problems running on a Mac or Windows ME	Incompatibility between MS Access and MAC
More transparency on how metrics were defined (e.g. how 'achieving MCLs' was defined)	Addressed in final user's manual and final report for project
Discussion on costs and limitations was not consistent between the technologies	Due to parity in level of information available at time of beta release - Addressed for final version
Greater detail on statistical analysis as Appendix (e.g. types of tests run, p-values, coefficients)	Added to the final User's Manual
Consider running statistical analyses on the field studies alone	This was done
Add page numbers and bookmarks to the User's Manual	Added to the final User's Manual
Manual negative about ISCO use	Manual described results of modeling, which indicated some limitations of ISCO. Not intended to be negative.
Expand report window	Can manually expand, will look into whether maximizing an option
Add ability to screen based on heterogeneity to General Analysis section	Has been added to DNAPL Test

Table 5-1. Beta-tester comments and resulting actions

6. TECHNOLOGY PERFORMANCE ASSESSMENT

6.1 Verification of DNAPL TEST Software Code

Verification of the DNAPL TEST software code was conducted through completion of a site-specific technology performance analysis for two well-characterized sites at which remediation has been completed. The characteristics of the case studies identified for the screening tool analysis were compared to the filtering criteria and confirmed to be appropriate for inclusion in the analysis. Validation of the General Analysis search function was also verified with site characteristics compared to filter criteria. Finally, cross-checking of output statistics to actual case study data confirmed that the statistics were being calculated correctly. Details on the verification process and results are included in **Appendix G**.

6.2 DNAPL Technology Performance Evaluation

General observations on trends in technology performance are discussed in further detail below. This information was developed from an analysis of general trends seen from the field case studies and supplemented with additional information gleaned from the results of the numerical modeling simulations.

6.2.1 Reductions in Groundwater Concentrations

The influence of various site characteristics and technology implementation parameters on achievable reductions in groundwater concentrations for each DNAPL remediation technology was evaluated as part of the numerical modeling studies and the statistical correlation evaluations. As discussed in Section 2.2.3.3.1, of the site characteristic and technology implementation parameters that were evaluated statistically, none were found to statistically correlate to reductions in groundwater concentrations. Similar observations were seen from the numerical modeling exercise, with the exception of the duration of treatment (i.e., longer treatment durations generally resulted in greater reductions in groundwater concentrations). Longer treatment durations in the modeling also generally resulted in greater removal of DNAPL mass.

The graph below (**Figure 6-1**) illustrates the correlation between the reduction of mass in the system at the start of remediation and groundwater concentration reductions. The data included in this plot includes both results observed in field case studies (open symbols) as well as in the numerical modeling studies (closed symbols). Groundwater concentrations correspond to concentrations observed at the termination of treatment, and do not reflect rebound post-treatment (if any). Overall there appears to be an approximate 1:1 correlation between the amount of DNAPL mass that is removed from the subsurface and the corresponding reductions in groundwater concentrations that result (with some deviations as discussed below). This overall relationship between DNAPL mass and groundwater concentration reductions is generally independent of remedial approach, which suggests that the greatest influence on

remedial performance from a groundwater concentration reduction perspective is the degree of DNAPL mass removal. Therefore, as a rule of thumb, if 50% groundwater concentration reductions are the remedial goal, it is likely that removal of approximately 50% of the DNAPL mass will be required. Similarly, if achievement of maximum contaminant levels (MCLs) is desired (typically representing >99% reduction in groundwater concentrations), then >99% removal of the DNAPL mass is likely going to be required.

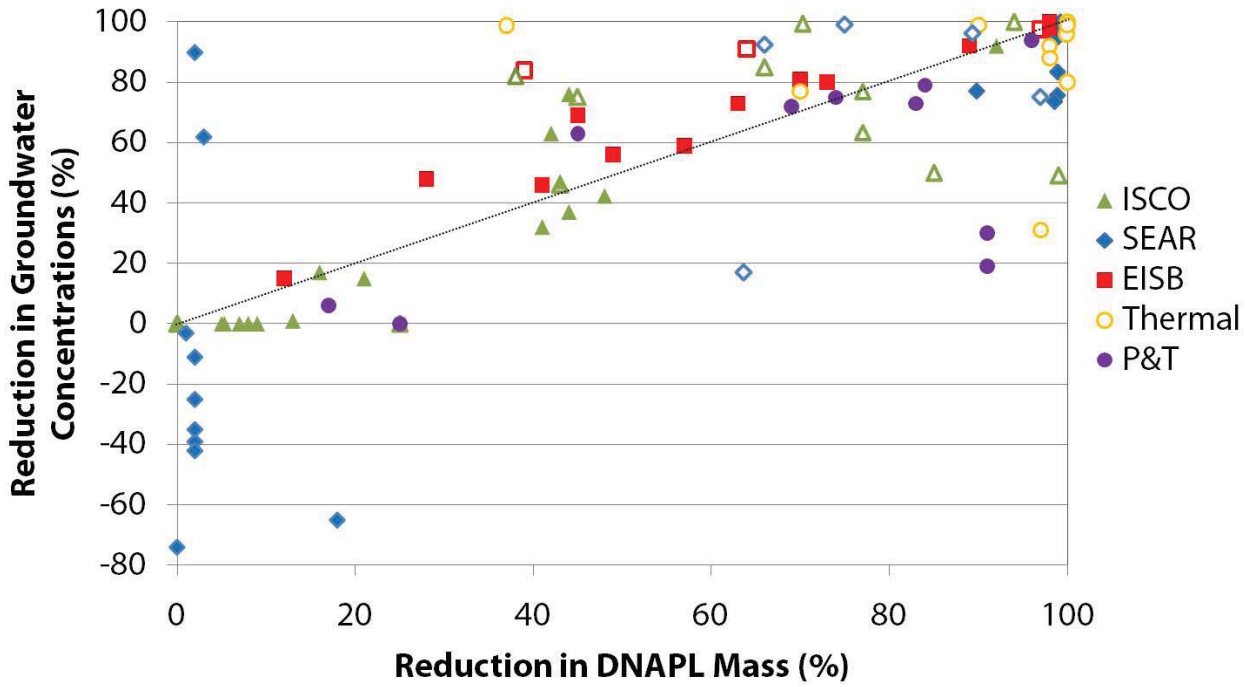

Figure 6-1. Relationship between reduction of mass in the system at the start of remediation and groundwater concentrations reductions by remedial technology.

Slight deviations from the above behavior are evident for a couple of technologies. For example, for EISB, the resulting DNAPL removal – groundwater concentration reduction pairs consistently plot above the 1:1 line, indicating that the groundwater concentration reduction achieved with EISB is consistently greater than the corresponding reduction in DNAPL mass removal, even after treatment is terminated. As a result, slightly less DNAPL mass removal is required for EISB to achieve similar results as would be observed with ISCO, for example. This can be explained by ongoing natural attenuation processes that have been enhanced by implementation of EISB and are sustained after treatment by cycling of biomass as electron donor as it decays (Adamson and Newell, 2009).

Another example of slight deviation from this behavior is the consistent plotting of groundwater concentration reduction – DNAPL removal pairs for pump and treat below the 1:1 line. This behavior suggests that greater reductions in DNAPL removal are required for pump and treat to achieve similar reductions in groundwater concentrations. Thermal case studies tend to cluster at the upper range of the reduction in DNAPL mass and groundwater concentrations (*i.e.,* typically

>90-99% mass removal and corresponding reductions in groundwater concentrations are achieved), due to the fact that thermal technologies are very effective at achieving near complete mass removal, when designed appropriately and the treatment zone encompasses the entire DNAPL zone.

At sites where ISCO has been applied, the groundwater concentration reduction – DNAPL mass removal pairs plot consistently on both sides of the 1:1 line, indicating that a reasonable predictor for groundwater concentration reductions would be the reduction in DNAPL mass for ISCO technologies. Conversely, the variability in the position of groundwater concentration reduction – DNAPL mass removal pairs for sites where SEAR has been applied varies widely on both sides of the 1:1 line. It should be noted that the variability at the low end of the DNAPL removal range occurs in the modeling studies, and may be an artifact of the modeling assumptions.

6.2.2 DNAPL Mass Removal

Table 6-1 provides a summary of DNAPL mass removal achieved for the various technologies for field case studies only and for both field and modeling studies for technologies where modeling was completed (shown in brackets). As seen in **Table 6-1** near complete removal of the DNAPL mass has been achieved by the majority of the technologies; the one exception being hydraulic displacement, which relies upon mobilization of the DNAPL phase as the primary DNAPL removal mechanism. Capillary forces acting upon the DNAPL phase effectively traps smaller blobs and ganglia of residual DNAPL, and enhancement of pressure gradients to levels high enough to mobilize residual DNAPL is unlikely to be achievable. Therefore, hydraulic displacement can only achieve partial removal of the DNAPL, but may be (i) a cost-effective means of stabilizing a source zone (i.e., eliminating the potential for future pool mobilization to deeper depths), (ii) a cost-effective means of removing large quantities of DNAPL mass, and (iii) a pre-treatment step as it results in an increase in the DNAPL surface area to volume ratio which is beneficial for mass-transfer driven remedial technologies.

As seen by the median % DNAPL mass removal in **Table 6-1** thermal technologies typically achieve high levels of DNAPL mass removal (94% to 96%). Median removals for the remaining technologies including anaerobic EISB, ISCO, SEAR and co-solvent flushing ranged from 64% to 81% for the field case studies. When modeling case studies are included, the ranges are larger and the medians tend to be lower; however, this is more likely due to the fact that treatment duration during the modeling was varied to evaluate sensitivity of remedial performance, rather than treatment being terminated as a result of achieving desired performance levels as is more typical for field applications.

Technology	No. of Studies	Median % DNAPL Mass Removal	Range in % DNAPL Mass Removal
Aerobic EISB	1	39%	--
Anaerobic EISB	3 (15)	64% (63%)	48% to 97% (12% to 98%)
Hydraulic Displacement	0 (13)	(31%)	(9% to 45%)
ISCO – Fenton's Reagent	4	68%	38% to 99%
ISCO – Permanganate	5 (19)	77% (44%)	70% to 99% (1% to 100%)
SEAR	2 (27)	81% (72%)	66% to 98% (0% to 99%)
Co-solvent Flushing	1	64%	--
Thermal – TCH	2	NA	NA
Thermal – ERH	15	94%	37% to 98%
Thermal – Steam	9	96%	79% to 100%

Table 6-1. Summary of DNAPL mass removal achieved with the various technologies for field case studies only and where modeling studies are also included (shown in brackets).

6.2.3 Influence of Matrix Diffusion

The potential influence of matrix diffusion into lower permeability media and the resulting influence of back-diffusion on remedial performance were investigated as part of the sensitivity study for the numerical modeling. The numerical modeling included simulations of ISCO (permanganate) treatment of TCE and PCE diffused into fractured clay, and EISB, ISCO and SEAR treatment of TCE diffused into fractured rock matrices of various porosities (*i.e.,* ranges typical for shale, granite and sandstone) and fraction organic carbon content (which governs the level of influence that sorption/desorption mechanisms dictate contaminant behavior within the matrix).

Through incorporating various fate and transport processes into the numerical model (*e.g.,* sorption/desorption of TCE onto organic matter within the matrix, degradation of amendments both within the fractures and matrix, constituent-specific forward- and back-diffusion into and out of the matrix, *etc.*), the following was demonstrated:

- The significance of matrix diffusion in a particular fractured rock environment will have a substantial influence on the distribution of DNAPL and VOC mass at the start of remediation, particularly if the DNAPL release is not recent. Fractured rock types that exhibit higher matrix porosity, higher fracture density, lower mean fracture apertures (contributing to lower groundwater velocities) and/or higher matrix fraction organic carbon (e.g., sandstone and shale) may exhibit a much higher fraction of VOC mass present in the matrix. Large amounts of sorbed and aqueous VOCs in the matrix may correspond to a decrease in DNAPL mass present, particularly if the DNAPL release is not recent. In many simulations in this work, more than 97% of the DNAPL released was present as sorbed VOC mass in the matrix at the end of the site aging stage. In contrast, factors contribute to a significant amount of DNAPL remaining in the fractures (DNAPL

release is recent, matrix diffusion is low, DNAPL type has low solubility, etc) then groundwater flow rates through the source zone may be low, impacting delivery of amendment. The impact of any treatment must be considered in the context of the distribution of DNAPL and VOC mass prior to treatment application.

- For sites where degradation/transformation of the contaminant phase within the lower permeability matrix is limited, back-diffusion of contaminant mass from the matrix will sustain groundwater concentrations for long periods of time. This can occur, for example, due to pore size restrictions on the ability of microorganisms to penetrate the matrix, or natural organic matter in the matrix consuming permanganate during forward diffusion, or amendments with high reactivity that react and degrade faster than they can diffuse very far into matrix. As a result, treatment primarily occurs within the fracture network and treatment of contaminant mass contained within the matrix is limited to the rate it can back-diffuse into the matrices and thus very slow. Moreover, it can be difficult to maintain amendment in the advection-dominated fractures for a long enough period to effectively address contaminant mass via back diffusion. Due to the majority of the contaminant mass being unavailable in such cases, *in situ* treatment is unlikely to have a substantial net benefit in terms of reducing treatment durations over containment approaches like pump and treat. Reduction in overall treatment costs over pump and treat may be achieved if an approach with lower operation and maintenance (O&M) costs is used (*e.g.,* EISB). This scenario (*i.e.,* insubstantial matrix treatment) can occur at sites with a very tight matrix (e.g., granite) or with sites exhibiting high VOC mass loading in the matrix but limited ability for diffused amendment to be effective in the matrix (SEAR, possibly EISB) or with sites dominated by large horizontal apertures (such that mean residence time for amendment in the source zone is low) or with treatment approaches that depend on advective flushing of the contaminant mass for *ex situ* treatment (*e.g.,* pump and treat) or those that require the use of amendments that do not persist for very long in the subsurface (*e.g.,* oxidants).

- Where degradation/transformation can occur within the lower permeability matrix, and thus treatment effectiveness is less influenced by back-diffusion to the fractures, *in situ* treatment times are likely to be shorter than flushing technologies such as pump and treat, and post-treatment rebound of groundwater concentrations will be less likely to occur. This scenario (i.e., substantial matrix treatment) is expected to occur for sites where significant VOC mass is stored in the matrix (e.g., sandstone) and the amendment can penetrate and react effectively in the matrix (e.g., ISCO in a low-f_{oc} matrix, possible EISB). Note that this latter example assumes that significant rates of biodegradation can be attained and sustained within the matrix; there is little data currently available to quantify such rates.

- Where significant amounts of DNAPL have accumulated and remain in fractures, then treatment approaches that depend on advective flushing may provide significant benefit

in DNAPL mass reduction. This scenario may apply for sites that have a tight matrix (e.g., granite) and for technologies that directly target DNAPL (e.g., SEAR).

- Where DNAPL has accumulated in dead-end fractures, DNAPL removal may again be limited for technologies, such as SEAR, that rely on delivery of the amendment directly to the NAPL phase.

The maximum rebound of concentrations in the fracture can occur years after termination of treatment, which has implications with respect to designing and interpreting the results of performance monitoring programs. The limitations of diffusion also imply that complete mass removal is not going to be achievable in a reasonable time frame in fractured clay or rock environments, and that partial mass removal to target reductions in groundwater concentrations and mass flux may be a more appropriate remedial goal.

6.2.4 DNAPL Properties

The solubility of the DNAPL was observed to influence the resulting net benefit of implementing more aggressive DNAPL treatment technologies over other approaches such as monitored natural attenuation or pump and treat that rely primarily on dissolution of the DNAPL as the DNAPL mass reduction mechanism. For more soluble DNAPLs such as TCE, dissolution of the DNAPL is a significant component of the DNAPL mass removal and incorporating other degradation or mass removal mechanisms (*e.g.,* oxidation, biodegradation, enhanced dissolution) may only result in relatively small incremental increases in DNAPL mass removal. However, introducing other mass removal mechanisms can potentially result in more significant enhancements over dissolution alone for lower solubility DNAPLs such as PCE.

6.2.5 Impact of Precipitate Formation on Technology Performance

The impact of precipitate formation on treatment performance for ISCO applications using permanganate as the oxidant was investigated as part of the numerical modeling sensitivity study. The formation of manganese dioxide rind specific to permanganate injections can result in encapsulation of the DNAPL (particularly pools) and flow bypassing around DNAPL areas (Conrad *et al.,* 2002). Once the rind forms around the DNAPL, the rate at which permanganate can contact the DNAPL becomes diffusion limited, and the rate of DNAPL mass removal slows significantly as a result. Ongoing diffusion of dissolved contaminant phase through the rind occurs as well, and rebound of concentrations post-treatment is common as a result.

Table 6-2 illustrates the results of the numerical modeling sensitivity study (West et al., 2008) where 3 kg of TCE DNAPL were assumed to be evenly distributed throughout a 1 m^3 volume of homogeneous sand. The simulation continued until all TCE mass was removed from the domain for several scenarios, including:

- Dissolution of the DNAPL only;

- Dissolution of the DNAPL for 10 years, then either: (*i*) 1 year permanganate amendment followed by dissolution only; (*ii*) 2 years permanganate amendment followed by dissolution only; and (*iii*) continuous treatment with permanganate until all of the TCE mass had been degraded. To illustrate the impact of rind formation on treatment performance, two sets of runs were completed, one with rind formation and the second without rind formation.

As seen in **Table 6-2** the formation of the rind significantly increased the time required to remove the TCE DNAPL (14 years) when compared to the scenario with no rind being formed (8 years). Where only partial treatment with permanganate was completed, the encapsulation of the remaining DNAPL phase resulted in a longer persistence of TCE (25 years) than if no treatment had been completed (20 years).

Scenario	DNAPL Lifespan
Dissolution only	20 yrs
1 yr treatment with permanganate with rind, followed by dissolution	25 yrs
2 yr treatment with permanganate with rind, followed by dissolution	25 yrs
Continuous treatment with permanganate without rind formation	7 yrs
Continuous treatment with permanganate with rind formation	14 yrs

Table 6-2. Results of the sensitivity study completed to investigate the potential influence of manganese dioxide rind formation during permanganate treatment (West et al., 2008).

The influence of the manganese dioxide rind formation in consolidated media environments will vary, depending on where the rind forms. Rind formation and the associated permeability reductions in fractures is anticipated to have a much larger influence on technology performance than formation of the manganese dioxide rind in the matrix, where contact with the contaminant is already diffusion-limited. Similar behavior as seen in the numerical modeling sensitivity study has been observed at the field scale; a prime example being the Watervliet Arsenal site (Goldstein et al., 2004).

The above examples are specific to permanganate treatment and the corresponding manganese dioxide rind formation; however, it is anticipated that similar results may be observed with other technologies that result in the formation of a precipitate or result in permeability reductions. The influence of the precipitate formation on DNAPL treatment is anticipated to be particularly pronounced where the precipitate forms within close proximity of the DNAPL phase, as occurs when permanganate reacts with the DNAPL.

6.3 Benefits of Partial DNAPL Mass Removal

Figure 6-2 illustrates near- and long-term groundwater concentration reductions, DNAPL mass removal, and reduction in contaminant mass flux from the source area for four different partial DNAPL treatment scenarios based on the base case modeling scenario (*i.e.,* TCE DNAPL source, moderate heterogeneity and permeability, etc. as described in Section 2.2.2), including:

i) Treatment with ISCO (permanganate) or EISB for approximately 2 years only;

ii) Treatment with ISCO or EISB for approximately 2 years followed by monitored natural attenuation (MNA), assuming physical attenuation mechanisms only (e.g., DNAPL dissolution, dispersion, sorption, etc., no biological attenuation);

iii) Continuous treatment with ISCO or EISB for 10 years; and

iv) Continuous treatment with ISCO or EISB for 30 and 20 years respectively.

As seen in **Figure 6-2**, ongoing treatment results in increasing groundwater concentrations reductions, removal of DNAPL mass and reduction in mass flux from the downgradient source zone boundary for both ISCO and EISB. Interestingly, the results achieved with 2.3 years of ISCO implementation followed by 7.7 of MNA were not much less than those achieved with 10 years of active treatment. The benefit achieved with ongoing treatment appears to be less for ISCO than for EISB particularly, for example, the further removal of DNAPL mass. This trend reflects the impact that the formation of the manganese dioxide rind has on the DNAPL removal efficiency when using permanganate, as discussed in Section 6.2.5. Similarly, continuing ISCO treatment beyond 10 years to 30 years has little to no net benefit in reducing groundwater concentrations at the downgradient source boundary for the site conditions evaluated.

In comparison, EISB appears to have some net benefit for continuing treatment, although again the difference between 2.5 yrs of active treatment followed by 7.5 years of MNA and 10 years of

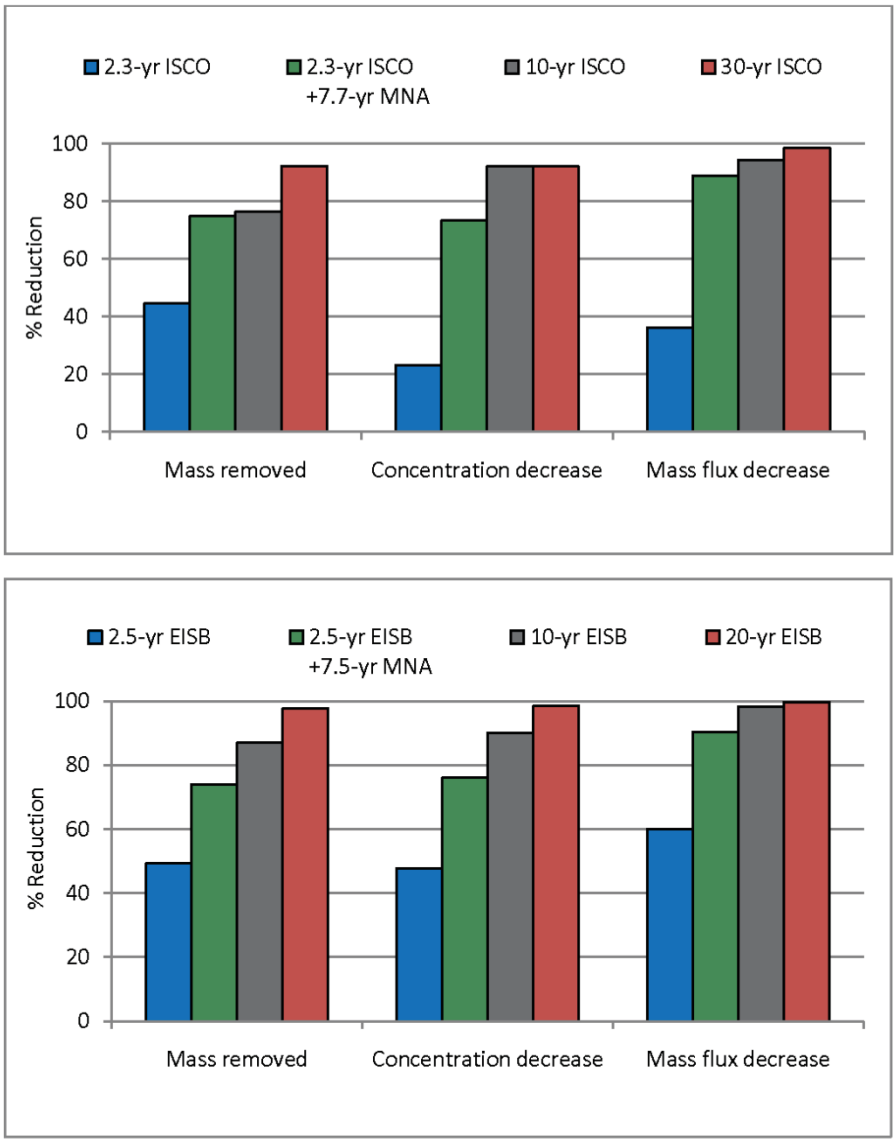

Figure 6-2. Comparison of technology performance with partial mass removal compared to near-complete treatment for ISCO and EISB approaches.

active treatment may not be substantial enough to justify the added costs of an additional 7.5 years of treatment.

Please note that the trends presented in **Figure 6-2** may only be relevant to DNAPLs with higher solubilities only (*e.g.,* TCE), where dissolution has a greater influence on the rate of DNAPL removal than would be observed with a lower solubility DNAPL such as PCE. For PCE sites, ongoing treatment is likely to have correspondingly greater benefit than would be observed for partial mass removal followed by MNA.

6.4 Post-Treatment Rebound of Groundwater Concentrations

Table 6-3 summarizes post-treatment rebound of groundwater concentrations observed at field sites included in the screening tool database. Rebound was defined as a significant (*i.e.,* >20%) increase in groundwater concentrations after treatment was terminated, in comparison to concentrations observed at the end of active treatment. Technologies not included in **Table 6-3** did not have any case studies reporting rebound behavior in the screening tool database.

As seen in **Table 6-3** rebound was not observed at any of the thermal sites, and was observed at only a small proportion (23%) of the anaerobic EISB sites. The lack of rebound at thermal sites is due to the high proportion of DNAPL mass removed, while at EISB sites, rebound is suppressed due to ongoing bioactivity for a period of time upon termination of active treatment due to the biomass using decaying biomass as a nutrient source (Adamson and Newell). In comparison, rebound was observed at the majority of ISCO and SEAR sites (>67%), where partial DNAPL mass removal is typically achieved and treatment effectively terminates once amendment injection is terminated. In general, fractured rock sites saw concentration rebound due to back diffusion of contaminants stored in the matrix after the fractures have been flushed/cleaned. The back-diffusion, and thus the concentration rebound, is more significant for scenarios with a higher proportion of the VOC mass stored in the matrix (e.g., longer time since DNAPL release, higher solubility DNAPL, higher matrix porosity, higher fracture density, lower mean apertures, higher matrix foc). This rebound behavior is consistent with observations reported in an independent study completed by McGuire *et al*. (2006).

Technology	Site Observing Rebound Post-Treatment	Percentage of Sites with Rebound
Anaerobic EISB	3 of 13 sites	23%
ISCO – Fenton's Reagent	5 of 7 sites	71%
ISCO – Permanganate	8 of 11 sites	73%
ISCO – Ozone	1 of 1 sites	100%
SEAR	2 of 3 sites	67%
Thermal – ERH	0 of 9 sites	0%
Thermal – SEAR	0 of 3 sites	0%

Table 6-3. Summary of post-treatment groundwater concentration rebound behavior observed at field sites.

6.5 Treatment Costs

Limited cost data was available for the case studies collected in DNAPL TEST, as case-study specific costs are rarely discussed in publicly available literature sources. **Table 6-4** below presents a summary of the costs available, presented as costs per unit volume of the treatment zone. Costs are normalized by volume in an effort to provide comparable values between both large and small remedial implementations. It should be recognized that, although unit costs

reduce some of the variability in costs related to treatment scale, they can still be skewed in cases where the treatment volume size is small. For example, the ISCO – permanganate application that had a unit cost of \$60,000 per m^3 in **Table 6-4** below was a 1 m^3, highly instrumented research demonstration that is not representative of larger scale costs.

As seen in **Table 6-4**, median unit costs for EISB, ISCO, and thermal technologies are of similar order of magnitude (\$100 to \$270/m^3) with similar ranges in unit costs as well (\$9 to \$770/m^3). Costs for co-solvent flushing and SEAR for the case studies included in the screening tool database are an order of magnitude higher, although a limited number of case studies for these technologies were available with cost data, and the range in costs may not therefore be representative of costs for all sites.

Technology	No. of Case Studies Reporting Costs	Median Unit Cost (\$/m^3)	Range in Unit Costs (\$/m^3)
Aerobic EISB	1	\$100	--
Anaerobic EISB	4	\$270	\$9 - \$630
ISCO – Fenton's Reagent	4	\$260	\$51 - \$770
ISCO – Permanganate	5	\$240	\$35 - \$60,000
SEAR	3	\$8,200	\$5,500 - \$41,000
Co-solvent Flushing	1	\$23,000	--
Thermal - ECH	2	\$270	\$150 - \$380
Thermal – ERH	11	\$170	\$42 - \$720
Thermal - Steam	4	\$170	\$18 - \$390

Table 6-4. Breakdown of unit costs by treatment technology.

7. COST ASSESSMENT

The costs to operate DNAPL Test are very low. The tool is available for free download at http://projects.geosyntec.com/DNAPL/dnapltest.aspx and will also be available from the ESTCP website in the near future. The time required to run an analysis on the tool is approximately 10-20 minutes.

8. IMPLEMENTATION ISSUES

8.1 Limitation of DNAPL TEST

Limitations of DNAPL TEST are discussed above in Section 2.3.

8.2 Effective Use of DNAPL TEST

Given the limitations of the information incorporated into DNAPL TEST, this tool is most effectively used as a preliminary screening for technology selection or as a screening for possible performance limitations for a remedy in place. It cannot replace appropriate site-specific evaluations based on engineering judgment.

Specific applications of the screening tool could include the following:

- Assessment of a realistic level of performance for a particular remedial technology given specific site conditions;
- Comparison of potential remedial performance between various technologies for specific site conditions;
- Comparison of potential remedial performance of a particular technology in different geological strata at a complex site; and
- Performance of sensitivity analyses on key site parameters to optimize remedial performance.

DNAPL TEST cannot "predict" technology performance for a particular site, but will provide the user with an anticipated range of performance and the ability to compare performance observed for multiple technologies. This information can be used as the basis for developing realistic remedial end goals, as well as develop a short list of potential technologies for a site.

For users that are interested in obtaining potential technology performance information for a specific site, a Site Specific Analysis will better focus the screening evaluation to include sites that are anticipated to have similar performance. Multiple Site Specific Analyses may be completed for the same site to focus on different areas with different site characteristics. It should be noted that the Site Specific Analysis does require a minimum level of knowledge of conditions at the user's site, which may limit its usefulness for some sites. Guidance for estimating of these parameters is provided within the tool.

For more general analyses of overall performance trends between parameters, and for sites at which key site parameters are unquantified, the General Analysis will be a better option. Modifications to search parameters can easily be changed at any time during the screening process, allowing the user to refine their analysis to better meet their needs. Specific examples illustrating a General and a Site Specific Analysis are provided in the User's Manual, which is accessible at http://projects.geosyntec.com/DNAPL/, to better illustrate how the tool can be effectively used to meet the user's goals.

8.3 Lessons Learned

Lessons learned with regards to DNAPL remediation technology performance and factors that influence performance are discussed in Section 6.2. Lessons learned from development and testing of the tool include the following:

- Because of limited information typically provided in publically available literature sources, case study details are frequently sparse and a complete dataset of performance metrics and site parameters are rarely reported. As such, evaluating correlations between site characteristics and performance metrics is challenging without having a very large dataset of sites available. Although a large dataset of 87 modeling studies, 118 field studies and 11 laboratory studies is available, correlations between many performance metric and site parameter pairs could not be evaluated due to lack of data.

- Finally, there is a need for continued compilation of case studies to maintain and keep the screening tool up-to-date. Technology developments and improvements are ongoing, and technology performance as such can change over time. Also, increasing the dataset of case studies as more DNAPL remediation programs are completed will improve the accuracy of the statistics included in the tool output and allow for expanded evaluation of the influence of site characteristics on DNAPL remediation performance and thus improved prediction of DNAPL remediation performance.

9. REFERENCES

Adamson, D.T., and C.J. Newell. 2009. Support of Source Zone Bioremediation through Endogenous Biomass Decay and Electron Donor Recycling. Bioremediation Journal, 13(1): 29-40.

Conrad, S.H., Glass, R.J., Peplinski, W.J. 2002, Bench-scale visualization of DNAPL remediation processes in analog heterogeneous aquifers: surfactant floods and in situ oxidation using permanganate. *J. Contam. Hydrol.* 58, 13– 49.

Dickson, S.E., Thomson, N.R. 2003, Dissolution of entrapped DNAPLs in variable aperture fractures: experimental data and empirical model, *Environ. Sci. Technol.* 37, 4128-4137, Paper 1D-01.

Gerhard, J. I., Kueper, B. H., and Hecox, G. R. 1998, The Influence of Waterflood Design on the Recovery of Mobile DNAPLs, *Ground Water*, 36 (2), 283-292.

Gerhard, J. I., Kueper, B. H., Hecox, G. R., and Schwarz, E. J. 2001, Site-Specific Design for Dual Phase Recovery and Stabilization of Pooled DNAPL, *Ground Water Monitoring & Remediation*, 21 (2), 71-88.

Gerhard, J. I., and Kueper, B. H. 2003a, Capillary pressure characteristics necessary for simulating DNAPL infiltration, redistribution, and immobilization in saturated porous media, *Water Resources Research*, 39 (8).

Gerhard, J. I., and Kueper, B. H. 2003b, Influence of constitutive model parameters on the predicted migration of DNAPL in heterogeneous porous media, *Water Resources Research*, 39 (10), 1279.

Gerhard, J. I., and Kueper, B. H. 2003c, Relative permeability characteristics necessary for simulating DNAPL infiltration, redistribution, and immobilization in saturated porous media, *Water Resources Research*, 39 (8), 1213.

Gerhard, J. I., Pang, T.W. and Kueper, B. H. 2007, Time scales of DNAPL migration in sandy aquifers examined via numerical simulation, *Ground Water* Vol. 45 (2) pp 147–157.

Grant, G. P., and Gerhard, J. I. 2007a, Simulating the dissolution of a complex dense nonaqueous phase liquid source zone: 1. Model to predict interfacial area, *Water Resources Research*, 43 (12).

Grant, G. P., and Gerhard, J. I. 2007b, Simulating the dissolution of a complex dense nonaqueous phase liquid source zone: 2. Experimental validation of an interfacial areabased mass transfer model, *Water Resources Research*, 43 (12).

Grant, G. P., Gerhard, J. I., and Kueper, B. H. 2007, Multidimensional validation of a numerical model for simulating a DNAPL release in heterogeneous porous media Journal of Contaminant Hydrology 92 109–128

Grant, G. P., Gerhard, J. I., and Kueper, B. H. 2006, Field scale impacts of spatially correlated relative permeability in heterogeneous multiphase systems, *Advances in WaterResources*, 30 (5), 1144-1159.

Imhoff, P.T., P.R. Jaffé and G.F. Pinder. 1993, An experimental study of complete dissolution of a nonaqueous phase liquid in saturated porous media, Water Resour. Res., 30(2): 307-320.

Kueper, B.H. and E.O. Frind. 1991a, Two-phase flow in heterogeneous porous media: 2. Model development. *Water Res. Res.* 27 (6), 1049–1057.

Kueper, B.H., and E.O. Frind. 1991b, Two phase flow in heterogeneous porous media: 2. Model application, *Water Resources Research*, 27(6), 1059-1070.

Kueper, B.H., McWhorter, David B. 1991, Behavior of dense, nonaqueous phase liquids in fractured clay and rock, *Ground Water* Volume 29, Issue 5, Pages 716-728.

Kueper, B.H. and J.I. Gerhard, 1995. Variability of point source infiltration rates for two-phase flow in heterogeneous porous media. Water Resources Research, 31(12): 2971-2980.

Kueper, B.H. and Mundle, K., 2007. Selection of monitoring times to assess remediation performance. Invited paper. Proceedings, Canadian Geotechnical Society Diamond Jubilee Conference, Ottawa, ON. 5 pp.

Miller, C.T., M.M. Poirier-McNeill and A.S. Mayer. 1990, Dissolution of trapped nonaqueous phase liquids: mass transfer characteristics, *Water Resour. Res.*, 26(11): 2783-2796, 1990.

McGuire, T.M., J.M. McDade, and C.J. Newell. 2006. Performance of DNAPL Source Depletion Technologies at 59 Chlorinated Solvent-Impacted Sites. Groundwater Monitoring and Remediation, 26: 73-84.

Mundle, K., Reynolds, D.A., West, M. and Kueper, B.H., 2007. Concentration rebound following in-situ chemical oxidation in fractured clay. Journal of Ground Water, Vol. 45, No. 6, pp. 692-700.

Mundle, K. Kueper, B.H. and Reynolds, D.A., 2006. Numerical modeling of in-situ chemical oxidation of TCE by potassium permanganate in fractured clay. Proceedings, DNAPL-1, Pittsburgh, PA, September 25 – 28. 10 pp.

Nambi, I.M., and S.E. Powers. 2003, Mass transfer correlations for nonaqueous phase liquid dissolution from regions with high initial saturations, *Water Resources Research,* 39(2), SBH41-SBH411.

Pang, TW, J.I. Gerhard, M. West, and B.H. Kueper, 2007. Numerical Simulation of ISCO to Remediate DNAPL in Fractured Rock, Proceedings of the 2007 U.S. EPA/ NGWA Fractured Rock Conference: State of the Science and Measuring Success in Remediation, pp.133-147.

Pang, TW, 2010., 'Investigations of DNAPL remediation in fractured porous media', PhD Thesis, University of Edinburgh (UK), 445 p. Powers, S. E., Abriola, L. M., and Weber Jr., W. J. 1992, An experimental investigation of nonaqueous phase liquid dissolution in saturated subsurface systems: Steady state mass transfer rates, *Water Resour. Res.*, 28(10), 2691–2706.

Powers, S.E., L.M. Abriola, W.J. Weber Jr., 1994. An experimental investigation of nonaqueous phase liquid dissolution in saturated subsurface systems: Transient mass transfer rates, *Water Resources Research, 30*(2), 321-332.

Richards, A., Kueper, B.H. and Gerhard, J.I., 2005. Hydraulic displacement of DNAPL source zones. Conference proceedings, First International Conference on Challenges in Site Remediation. Chicago, IL, October 23-27, 2005.

Richards, A., Gerhard, J.I. and Kueper, B.H., 2011. Hydraulic Displacement of Dense, Non-Aqueous Phase Liquids. Submitted for publication.

Saba, T., and T.H. Illangasekare. 2000, Effect of groundwater flow dimensionality on mass transfer from entrapped nonaqueous phase liquid contaminants, *Water Resources Research*, 36(4), 971-979.

West, M.R. and Kueper, B.H., 2005. Numerical simulation of chemical oxidation of trichloroethylene with potassium permanganate. Conference proceedings, First International Conference on Challenges in Site Remediation. Chicago, IL, October 23-27, 2005.

West, M., Kueper, B.H. and Gerhard, J.I., 2007. Evaluation of DNAPL source zone removal technologies in porous media and implications for site monitoring. Proceedings, Canadian Geotechnical Society Diamond Jubilee Conference, Ottawa, ON. 5 pp.

West, M. and Kueper, B.H., 2007. Plume detachment and recession times following source treatment in bedded fractured rock. Proceedings, USEPA/ NGWA Fractured Rock Conference: State of the Science and Measuring Success in Remediation, pp. 343-356.

West, M. R., Grant, G. P., Gerhard, J. I., and Kueper, B. H. 2008, The influence of precipitate formation on the chemical oxidation of TCE DNAPL with potassium permanganate, *Advances in Water Resources*, 31 (2), 324-338.

West, M. and Kueper, B.H., 2010. Plume detachment and recession times in fractured rock. Journal of Ground Water, 48(3), pp. 416-426.

West, M.R., Grant, G.P., Gerhard, J.I. and Kueper, B.H., 2008. The Influence of Precipitate Formation on the Chemical Oxidation of TCE DNAPL with Potassium Permanganate. Advances in Water Resources, Vol. 31, pp. 324-338.

APPENDIX A Points of Contact

POINT OF CONTACT Name	ORGANIZATION Name Address	Phone Fax E-mail	Role in Project
Carmen Lebrón	NAVFAC Engineering Services Center	(805) 982-1616 (805) 982-4304 Carmen.lebron@navy.mil	Principal-In-Charge and Project Manager
Dr. David Major	Geosyntec Consultants 130 Research Lane Guelph, ON, Canada N1G 5G3	(519) 822-2230 (529) 822-3151 dmajor@geosyntec.com	Principal-In-Charge, Screening Tool Development
Dr. Bernard Kueper	Department of Civil Engineering 58 University Ave. Ellis Hall Queen's University Kingston, ON, Canada K7L 3N6	(613) 533-6834 (613) 533-2128 kueper@civil.queensu.ca	Principal-In-Charge, Numerical Modeling

APPENDIX B

CASE STUDIES

TABLE B.1
LIST OF CASE STUDIES IN DNAPL TEST

Technology	Site Identifier	DQR	Reference Type	Reference
Cosolvent	141	2.8	Journal	Jawitz JW, Sillan RK, Annable MD, Rao PSC, Warner K. In-Situ Alcohol Flushing of a DNAPL Source Zone at a Dry Cleaner Site. Environmental Science and Technology. 2000, 34: 3722-3729.
		2.8	Government	IRTC DNAPL Team Case Study Summary Report: Sages Dry Cleaners Jacksonville Florida. www.irtcweb.org/Documents//DNAPLs-3
EISB-A	86	1.3	Conference	Lewis RF, Dooley MA, Johnson JC, and Murray WA. 1998. Sequential anaerobic/aerobic biodegradation of chlorinated solvents: Pilot-scale field demonstration. In Proceedings of the First International Conference on Remediation of Chlorinated and Recalcitrant Compounds, pp. 1-7, vol. C1-6: Physical, Chemical, and Thermal Technologies (Editors: Wickramanayake GB and Hinchee RE), Monterey CA, May 18-21.
	155	1.8	Government	U.S. Environmental Protection Agency. September 1998.(EPA 542-R-98-008) Field Applications of In Situ Remediation Technologies, Chemical Oxidation.
		1.8	Government	U.S. DOE, Implementation of Deep Soil Mixing at the Kansas City Plat, Oak Ridge National Laboratory, Grand Junction, CO, February 1997
	19	2.1	ESTCP	Martin J and Sorenson K. Appendix E.1-Case study of enhanced bioremediation of a DNAPL source area: four years of data from Test Area North, INEEL. In: Principles and Practices of Enhanced Anaerobic Bioremediation of Chlorinated Solvents. Parsons, Aug. 2004.
	20	2.5	Government	Environmental Security Technology Certification Program (ESTCP). Alleman B, Place M, Major D. Demonstration of Bioaugmentation at Kelly AFB, TX - Final Report (ER-9914). April 2004.
	25	2.4	Government	Innovative Treatment Remediation Demonstration (Department of Energy). Cost and Performance Report - In situ anaerobic bioremediation Pinellas Northeast Site Largo, Florida. April 1998.
	45	1.7	Web	Farrell, J. Site Profile: Dixie Cleaners. Accessed Nov. 2005. http://www.drycleancoalition.org/profiles/display.cfm?id=21
	57	1.9	Web	Parrett, K. Accessed Sept. 2006. http://www.drycleancoalition.org/profiles/display.cfm?id=55
		1.9	Web	Regenesis, 2004. Case History HX-1: PCE and TCE Remediation at a Dry Cleaning Facility – Portland, OR. www.regenesis.com/library/Case%20Histories/HRC-X/1.%20HRC.Portland%20OR.pdf
	75	1.5	Conference	Smith W. and Morris KA. 2004. In-situ anaerobic reductive dechlorination at a former AS/SVE site. Paper 3C-07 in Proceedings of the Fourth International Conference on Remediation of Chlorinated and Recalcitrant Compounds (Chairs: Gavaskar A and Chen ASC), Monterey CA, May 24-27.
	77	1.5	Conference	Bures GH, Sorenson KS, Jr., Martin JP, and Reinke RF. 2004. Bio-fracing for enhanced in situ bioremediation of chlorinated solvents in low permeability sediments. Paper 3D-21 in Proceedings of the Fourth International Conference on Remediation of Chlorinated and Recalcitrant Compounds (Chairs: Gavaskar A and Chen ASC), Monterey CA, May 24-27.

TABLE B.1
LIST OF CASE STUDIES IN DNAPL TEST

Technology	Site Identifier	DQR	Reference Type	Reference
EISB-An	78	2.4	Conference	Fam SA, Fogel S, Findlay M, and Gaudette M. 2004. Full-scale bioenhancement for anaerobic dechlorination of PCE and cDCE. Paper 3D-17 in Proceedings of the Fourth International Conference on Remediation of Chlorinated and Recalcitrant Compounds (Chairs: Gavaskar A and Chen ASC), Monterey CA, May 24-27.
	79	1.7	Conference	Boulicault KJ, Hinchee RE, Wiedemeier TH, Hoxworth SW, Swingle TP, Carver E, and Haas PE. 2000. Vegoil: A novel approach for stimulating reductive dechlorination. Vol. C2-4 pp. 1-7 in Proceedings of the Second International Conference on Remediation of Chlorinated and Recalcitrant Compounds, Monterey CA, May 22-25.
	80	1.6	Conference	Murray W, Dooley M, and Koenigsberg S. 2000. HRC enhanced bioremediation of chlorinated solvents. Vol C2-4 pp. 287-294 in Proceedings of the Second International Conference on Remediation of Chlorinated and Recalcitrant Compounds, Monterey CA, May 22-25.
	81	1.3	Conference	Schuhmacher TT, Bow WA, Chitwood JP. 2000. A field demonstration showing enhanced reductive dechlorination using polymer injection. Vol. C2-4 pp. 15-22 in Proceedings of the Second International Conference on Remediation of Chlorinated and Recalcitrant Compounds, Monterey CA, May 22-25.
	82	1.5	Conference	Klutz T, Baird A, Maalouf G, McDonnell D, and Sandefur C. 2002. Accelerated bioremediation of trichloroethylene: A comparison between saprolite and crystilline bedrock aquifers. Paper 2C-46 in Proceedings of the Third International Conference on Remediation of Chlorinated and Recalcitrant Compounds Monterey CA, May 20-23.
	83	1.5	Conference	Klutz T, Baird A, Maalouf G, McDonnell D, and Sandefur C. 2002. Accelerated bioremediation of trichloroethylene: A comparison between saprolite and crystilline bedrock aquifers. Paper 2C-46 in Proceedings of the Third International Conference on Remediation of Chlorinated and Recalcitrant Compounds Monterey CA, May 20-23.
	87	1.3	Conference	Lewis RF, Dooley MA, Johnson JC, and Murray WA. 1998. Sequential anaerobic/aerobic biodegradation of chlorinated solvents: Pilot-scale field demonstration. In Proceedings of the First International Conference on Remediation of Chlorinated and Recalcitrant Compounds, pp. 1-7, vol. C1-6: Physical, Chemical, and Thermal Technologies (Editors: Wickramanayake GB and Hinchee RE), Monterey CA, May 18-21.
	90	1.8	Conference	Boyle SL, Dick VB, Ramsdell MN, and Caffoe TM. 2000. Enhanced closure of a TCE site using injectable HRC. Vol. C2-4 pp. 255-262 in Proceedings of the Second International Conference on Remediation of Chlorinated and Recalcitrant Compounds, Monterey CA, May 22-25.
	115	2.1	Web	Cost & Performance Report: In Situ Bioremediation Using Various Additives at Five Drycleaner Sites, Various Locations. 2005. http://www.costperformance.org/pdf/drycleaner_bio.pdf Accessed Mar. 2007
	133	1.7	Consultant	Confidential. Reference not available.
	134	1.9	Vendor	Confidential. Reference not available.

TABLE B.1
LIST OF CASE STUDIES IN DNAPL TEST

Technology	Site Identifier	DQR	Reference Type	Reference
EISB-An	135	1.8	Conference	Newman WA, Barr KD, Pelle RC, Crisman DP. 2003. An improved method for injection of emulsified edible oils. Paper B-19 in Proceedings of the Seventh International In Situ and On-Site Bioremediation Symposium, Orlando, June 2-5.
		1.8	Conference	Newman WA, Barr KD, Pelle RC, Crisman DP. An improved method for injection of emulsified edible oils. Paper D-11 in Proceedings of the Eighth International In Situ and On-Site Bioremediation Symposium, Baltimore, June 6-9.
	136	2.2	Conference	Neumann NP, Mannebach RC, Porter GL. 2005. Bioremediation of a Former Dry-Cleaning Site Using Hydrogen Release Compound. In Proceedings of the Eighth International In Situ and On-Site Bioremediation Symposium, Baltimore, June 6-9.
		2.2	Web	State Coalition for Remediation of Drycleaners - Cypress Village ShppingCenter, Bridgeton Missouri
	137	1.7	Conference	Bennett P, Mackay D, Einarson M, Buscheck T, O'Reilly K, Semprini L, Swinderman M. 2003 Evaluating Lactate Utilization In Situ: Sulfate Reduction versus Dehalorespiration. Paper A-07 in Proceedings of the Seventh International in Situ and On-Site Bioremediation Symposium, Orlando, June 2-5.
	138	2.0	Conference	Nachlas PE, Tesler PG. HRC® Remediation of PCE at a New Jersey Printed Circuits Site. 2003. Paper A-30 in Proceedings of the Seventh International In Situ and On-Site Bioremediation Symposium, Orlando, June 2-5.
	139	2.5	Journal	Adamson DT, McDade JM, Hughes, JB. Inoculation of a DNAPL source zone to initiate reductive dechlorination of PCE. Environmental Science and Technology. 2003, 37: 2525-2533
	140	1.7	Conference	Fiacco RJ, Cho HJ, Leary R, Zoltay V, Lee MD, Rasmussen E, Madera E, Burkhardt L. 2005. Paper M-13 In Proceedings of the Eighth International In Situ and On-Side Bioremediation Symposium, Baltimore, June 6-9.
	145	1.6	Web	Linn, B.; Frearson, G. Site Profile: Classic French Cleaners. Accessed Dec. 2007. http://www.drycleancoalition.org/profiles/display.cfm?id=277
	147	2.0	Journal	Confidential. Reference not available.
	148	2.5	Journal	Lebron, C.A.; McHale T.; Young, R.' Williams, D.; Bogaart, M.G.; Major, D.W.; McMaster, M.L.; Tasker, I.; Akladiss, N. 2007. Pilot-Scale Evaluation Using Bioaugmentation to Enhance PCE Dissolution at Dover AFB National Test Site. Remediation, Spring 2007, pp. 5-17.
	149	2.0	Conference	Burdick, J.; Dols, Pieter, den Dekker, A.; Bareman, M.; Stolzenburg, M. 2003. Enhanced In Situ Bioremediatio of Chlorinated Solvents in Groundwater at a Former Dry-Cleaning Site in The Netherlands. In Proceedings of the 8th International FZK/TNO Conference on Contaminate Soil, Belgium, May 12-16.
	156	1.6	Consultant	Water, Earth Solutions & Technologies, Inc. (W.E.S.T., Inc.) 2003. The Response Action Work Plan (RAWP).
	157	1.4	Consultant	ENSR Consulting & Engineering. August 2001. Hydrogen Release Compound Pilot Test Results, BNSF Former Railyard Choldress, Texas
		1.4	Consultant	Roux Associates, Inc. May 1994. Site Investigation Report, Burlington Northern Railyard Childress, Texas.

TABLE B.1
LIST OF CASE STUDIES IN DNAPL TEST

Technology	Site Identifier	DQR	Reference Type	Reference
EISB-An	158	1.7	Consultant	Dougherty Sprague Enterprises, Inc. Dec. 2003. Revised Affected Property Assessment Report, 3735 Westheimer Road, Houston, Texas, prepared for Craig's Interests
		1.7	Consultant	Dougherty Sprague Enterprises, Inc. January 6, 2000 Letter- Re: Response Action Status Report.
	161	2.9	Thesis	West, M. R. (2009), Mathematical Modelling of DNAPL Source Zone Remediation, Ph.D. thesis, 431 pp, Queen's University, Kingston, Ontario
	165	2.9	Thesis	West, M. R. (2009), Mathematical Modelling of DNAPL Source Zone Remediation, Ph.D. thesis, 431 pp, Queen's University, Kingston, Ontario
	169	2.9	Thesis	West, M. R. (2009), Mathematical Modelling of DNAPL Source Zone Remediation, Ph.D. thesis, 431 pp, Queen's University, Kingston, Ontario
	174	2.7	Thesis	West, M. R. (2009), Mathematical Modelling of DNAPL Source Zone Remediation, Ph.D. thesis, 431 pp, Queen's University, Kingston, Ontario
	175	2.7	Thesis	West, M. R. (2009), Mathematical Modelling of DNAPL Source Zone Remediation, Ph.D. thesis, 431 pp, Queen's University, Kingston, Ontario
	177	2.9	Thesis	West, M. R. (2009), Mathematical Modelling of DNAPL Source Zone Remediation, Ph.D. thesis, 431 pp, Queen's University, Kingston, Ontario
	180	2.9	Thesis	West, M. R. (2009), Mathematical Modelling of DNAPL Source Zone Remediation, Ph.D. thesis, 431 pp, Queen's University, Kingston, Ontario
	184	2.9	Thesis	West, M. R. (2009), Mathematical Modelling of DNAPL Source Zone Remediation, Ph.D. thesis, 431 pp, Queen's University, Kingston, Ontario
	188	2.9	Thesis	West, M. R. (2009), Mathematical Modelling of DNAPL Source Zone Remediation, Ph.D. thesis, 431 pp, Queen's University, Kingston, Ontario
	192	2.9	Thesis	West, M. R. (2009), Mathematical Modelling of DNAPL Source Zone Remediation, Ph.D. thesis, 431 pp, Queen's University, Kingston, Ontario
	196	2.9	Thesis	West, M. R. (2009), Mathematical Modelling of DNAPL Source Zone Remediation, Ph.D. thesis, 431 pp, Queen's University, Kingston, Ontario
	200	2.9	Thesis	West, M. R. (2009), Mathematical Modelling of DNAPL Source Zone Remediation, Ph.D. thesis, 431 pp, Queen's University, Kingston, Ontario
	209	1.9	Consultant	C&E Environmental, LLC. January 26, 2004 Letter- Re: Quarterly Sampling Summary Report.
	210	1.8	Web	Kean J & Lodato M. Feb. 2004. State Coalition for Remediation of Drycleaners: Contemporary Cleaners. Orlando, Florida. Accessed April 2004; www.drycleancoalition.org/profiles/display.cfm?id=15
		1.8	Government	Kean J., Graves D., & Lodato M. Enhanced Reductive Dechlorination and the Relationship Between cis-1,2-DCE and Accumulation and Methanogensis.
		1.8	Consultant	IT Corporation. June 2000. Remedial Action Plan- TablesB-2 &4

TABLE B.1
LIST OF CASE STUDIES IN DNAPL TEST

Technology	Site Identifier	DQR	Reference Type	Reference
EISB-An	210	1.8	Consultant	IT Corporation. May 1998. Contamination Assessment Report, Contemporary Cleaners Site, 4882 South Kirkman Road, Orlando Florida.
	213	1.9	Consultant	Pecevich J., Coloer & Colantonio Inc. 2003. Decision Support For Evaluation of Chlorinated Solvent Source Zone Treatment Survey (GSI case study forms)
	216	1.4	Consultant	Ecosystems Environmental, INC. Dec. 1998. Annual Groundwater Monitoring Report, Oates Park Shopping Center; Carrollton, Texas. Pp 7-9.
		1.4	Consultant	Ecosystems Environmental, INC. Jan. 2004. VCP Site Investigation Report. Oates Park Shopping Center; Carrollton, Texas. Pp 7-9.
	217	2.1	Consultant	Arcadis. July 2003. Decision Support System for Evaluation of Chlorinated Solvent Source Zone Treatment Survey.
HD	65	2.7	Thesis	Richards, A. 2006. Hydraulic Displacement of Dense Non-Aqueous Phase Liquid Source Zones. M.Sc. Thesis, Dept. of Civil Engineering, Queen's University, Kingston, ON.
	66	2.7	Thesis	Richards, A. 2006. Hydraulic Displacement of Dense Non-Aqueous Phase Liquid Source Zones. M.Sc. Thesis, Dept. of Civil Engineering, Queen's University, Kingston, ON.
	67	2.7	Thesis	Richards, A. 2006. Hydraulic Displacement of Dense Non-Aqueous Phase Liquid Source Zones. M.Sc. Thesis, Dept. of Civil Engineering, Queen's University, Kingston, ON.
	68	2.7	Thesis	Richards, A. 2006. Hydraulic Displacement of Dense Non-Aqueous Phase Liquid Source Zones. M.Sc. Thesis, Dept. of Civil Engineering, Queen's University, Kingston, ON.
	69	2.7	Thesis	Richards, A. 2006. Hydraulic Displacement of Dense Non-Aqueous Phase Liquid Source Zones. M.Sc. Thesis, Dept. of Civil Engineering, Queen's University, Kingston, ON.
	70	2.7	Thesis	Richards, A. 2006. Hydraulic Displacement of Dense Non-Aqueous Phase Liquid Source Zones. M.Sc. Thesis, Dept. of Civil Engineering, Queen's University, Kingston, ON.
	71	2.7	Thesis	Richards, A. 2006. Hydraulic Displacement of Dense Non-Aqueous Phase Liquid Source Zones. M.Sc. Thesis, Dept. of Civil Engineering, Queen's University, Kingston, ON.
	72	2.7	Thesis	Richards, A. 2006. Hydraulic Displacement of Dense Non-Aqueous Phase Liquid Source Zones. M.Sc. Thesis, Dept. of Civil Engineering, Queen's University, Kingston, ON.
	73	2.7	Thesis	Richards, A. 2006. Hydraulic Displacement of Dense Non-Aqueous Phase Liquid Source Zones. M.Sc. Thesis, Dept. of Civil Engineering, Queen's University, Kingston, ON.
	74	2.7	Thesis	Richards, A. 2006. Hydraulic Displacement of Dense Non-Aqueous Phase Liquid Source Zones. M.Sc. Thesis, Dept. of Civil Engineering, Queen's University, Kingston, ON.
	84	2.7	Thesis	Richards, A. 2006. Hydraulic Displacement of Dense Non-Aqueous Phase Liquid Source Zones. M.Sc. Thesis, Dept. of Civil Engineering, Queen's University, Kingston, ON.
	88	2.7	Thesis	Richards, A. 2006. Hydraulic Displacement of Dense Non-Aqueous Phase Liquid Source Zones. M.Sc. Thesis, Dept. of Civil Engineering, Queen's University, Kingston, ON.
	89	2.7	Thesis	Richards, A. 2006. Hydraulic Displacement of Dense Non-Aqueous Phase Liquid Source Zones. M.Sc. Thesis, Dept. of Civil Engineering, Queen's University, Kingston, ON.

Table B.1

TABLE B.1
LIST OF CASE STUDIES IN DNAPL TEST

Technology	Site Identifier	DQR	Reference Type	Reference
HD	242	2.4	Thesis	Pang, T. W. (2010), DNAPL Remediation of Fractured Rock Evaluated via Numerical Simulation, Ph.D. thesis, The University of Edinburgh, Edinburgh, Scotland, United Kingdom. March, 2010
ISCO-FP	14	1.9	Conference	Levin R, Kellar E, Wilson J, Ware L, Findley J, and Baehr J. 1998. Full-scale remediation of chlorinated solvents in clay soils by in situ chemical oxidation. In Proceedings of the First International Conference on Remediation of Chlorinated and Recalcitrant Compounds, vol. C1-5: Physical, Chemical, and Thermal Technologies (Editors: Wickramanayake GB and Hinchee RE), Monterey CA, May 18-21.
		1.9	ESTCP	Environmental Security Technology Certification Program (ESTCP). 1999. Technology Status Review: In Situ Oxidation. Nov. 1999.
	23	2.3	Government	Environmental Protection Agency (US EPA). DNAPL Remediation: selected projects approaching regulatory closure. December 2004.
	24	2.0	Government	Confidential. Reference not available.
	29	1.5	Conference	Werner P. 2002. Chemical oxidation of tetrachloroethene contamination in a fractured saprolitic bedrock aquifer. Paper 2C-44 in Proceedings of the Third International Conference on Remediation of Chlorinated and Recalcitrant Compounds Monterey CA, May 20-23.
	33	1.9	Web	FRTR, 2004. In Situ Treatment at Three Dry Cleaner Sites, Various Locations. www.costperformance.org/pdf/20040706_356.pdf
	36	1.9	Journal	Cho HJ, Fiacco RJ Jr. and Daly MH. 2002. Soil vapor extraction and chemical oxidation to remediate chlorinated solvents in fractured crystalline bedrock: pilot study results and lessons learned. Remediation. 12: 35-50.
	37	1.7	Conference	Lisiecki JB and Colvin MD. 2004. Assessment and remediation of TCE DNAPL and adjacent plume. Paper 2A-19 in Proceedings of the Fourth International Conference on Remediation of Chlorinated and Recalcitrant Compounds (Chairs: Gavaskar A and Chen ASC), Monterey CA, May 24-27.
	54	2.0	Government	U.S. Department of Energy. Final Report for Demonstration of In Situ Oxidation of DNAPL using the Geo-Cleanse ® Technology (Report # WSRC-TR-97-00283). September 1997.
		2.0	Conference	Jerome KM, Looney BB, Wilson J. 1998. Field demonstration of in situ fentons destruction of DNAPLs. In Proceedings of the First International Conference on Remediation of Chlorinated and Recalcitrant Compounds (Wickramanayake GB and Hinchee RE, eds.) C1(5) 353-358.
	123	2.4	Web	Accessed Mar. 2007 www.costperformance.org/pdf/oxidation.pdf
	144	1.4	Consultant	Harding Lawson Associates, 2000. Letter to Florida Department of Environmental Protection 30 August 2000, Re: Chemical Oxidation (OxyCat) Pilot Test Report, Beaches Laundry, Florida Department of Environmental Protection (FDEP) ID No. 169602467, Jacksonville Beach, Duval County, Florida
		1.4	Consultant	Harding ESE, 2001. Remedial Alternatives Evaluation, Beaches Laundry and Cleaners, FDEP Facility Identification Number: 169602467.
	146	1.9	Consultant	Confidential. Reference not available.

TABLE B.1
LIST OF CASE STUDIES IN DNAPL TEST

Technology	Site Identifier	DQR	Reference Type	Reference
ISCO-FP	150	1.7	Government	U.S. Army Corps of Engineers, 2000. Summary Report for the In Situ Chemical Oxidation Remediation Pilot Study of the Bedrock Aquifer at the Southeastern (SE) Disposal Area (DA), Letterkenny Army Depot
	151	1.8	Consultant	EA Engineering, Science, and Technology, 2004. Phase II Chemical Oxidation Pilot Study Report, Site 3: Ball Road Landfill and Burn Pits, Naval Support Activity, Mechanicsburg, Pennsylvania. 30 December, 2004.
	152	1.8	Consultant	EA Engineering, Science, and Technology, 2004. Phase I Chemical Oxidation Pilot Study Report, Site 3: Ball Road Landfill and Burn Pits, Naval Support Activity Mechnaicsburg, Pennsylvania. 29 December 2004.
	208	1.9	Consultant	DeHghi, B., Hodges, A., Feng, T.H. Full Scale Application of Fenton's Reagent In Situ Chemical Oxidation.
		1.9	Consultant	CH2M HILL. Semiannual Status Report, January 2006 through June 2006 Former Baron-Blakeslee Facility, Belmont, California. 24 July, 2006.
	214	1.4	Consultant	IVI Environmental, Inc. October 1998. Supplemental Site Investigation Report Response Action WorkPlan. Green Oaks Village Shopping Center, Arlington, Texas. Prepared for: Today Realty Advisors.
		1.4	Consultant	IVI Environmental, Inc. Letter dated: March 7, 2000. Monthly Status Report No. 10; February 2000. To: Smith M., Voluntary Cleanup Section, Remediation Division, Texas Natural Resource Conservation Commission
		1.4	Consultant	IVI Environmental, Inc. Letter dated: September 10, 2001. Monthly Status Report No. 21; May-July 2001. To: Smith M., Voluntary Cleanup Section, Remediation Division, Texas Natural Resource Conservation Commission
		1.4	Consultant	IVI Environmental, Inc. Letter dated: February 28, 2001. Monthly Status Report No. 25; January 2002. To: Smith M., Voluntary Cleanup Section, Remediation Division, Texas Natural Resource Conservation Commission
ISCO-MnO4	26	2.1	Government	Department of Energy. In situ chemical oxidation using potassium permanganate. September 1999.
	28	2.0	Conference	Parker BI, Cherry JA and Al TA. 2002. Passive permanganate remediation of a solvent DNAPL source zone. Paper 2C-05 in Proceedings of the Third International Conference on Remediation of Chlorinated and Recalcitrant Compounds Monterey CA, May 20-23.
	30	1.8	Conference	Werner P. 2002. Chemical oxidation of tetrachloroethene contamination in a fractured saprolitic bedrock aquifer. Paper 2C-44 in Proceedings of the Third International Conference on Remediation of Chlorinated and Recalcitrant Compounds Monterey CA, May 20-23.
	31	2.6	Journal	MacKinnon LK and Thomson NR. 2002. Laboratory-scale in situ chemical oxidation of a perchloroethylene pool using permanganate. Journal of Contaminant Hydrology 56: 49-74.

TABLE B.1
LIST OF CASE STUDIES IN DNAPL TEST

Technology	Site Identifier	DQR	Reference Type	Reference
ISCO-MnO4	34	1.9	Conference	Blicke FW, Richards K, Balba T and Landale B. 2004. Performance evaluation of chemical oxidation treatment of chlorinated groundwater plumes. Paper 2A- 16 in Proceedings of the Fourth International Conference on Remediation of Chlorinated and Recalcitrant Compounds (Chairs: Gavaskar A and Chen ASC), Monterey CA, May 24-27.
	35	2.0	Conference	Drescher E, Gavaskar A, Sass B, Cumming L, Drescher M and Williamson T. 2000. Batch and column testing to evaluate chemical oxidation of DNAPL source zones. In Proceedings of the Second International Conference on Remediation of Chlorinated and Recalcitrant Compounds, Monterey CA, May 22-25.
	38	1.7	Conference	Ladaa T, Tingle A, Kirkpatrick T, Iehn S and Caretti T. 2004. Successful pilot test using USP-grade potassium permanganate. Paper 2A-11 in Proceedings of the Fourth International Conference on Remediation of Chlorinated and Recalcitrant Compounds (Chairs: Gavaskar A and Chen ASC), Monterey CA, May 24-27.
	39	1.5	Conference	Moes M, Peabody C, Siegrist R and Urynowicz M. 2000. Permanganate injection for source zone treatment of TCE DNAPL. Vol. C2-6 in Proceedings of the Second International Conference on Remediation of Chlorinated and Recalcitrant Compounds, Monterey CA, May 22-25.
	40	1.7	Conference	Williams CL. 2002. Degradation of trichloroethene (TCE) in a fractured bedrock aquifer using sodium permanganate. Paper 2C-43 in Proceedings of the Third International Conference on Remediation of Chlorinated and Recalcitrant Compounds Monterey CA, May 20-23.
	42	2.3	Thesis	Hood E. 2000. Permanganate flushing of DNAPL source zones: experimental and numerical investigation. PhD Thesis. Dept. of Civil Engineering, University of Waterloo, Waterloo Ontario
	43	2.3	Government	Fitton, D. 2001 In situ chemical oxidation at Butler Cleaners, Jacksonville, Florida. www.frtr.gov/pdf/abstractsvol5.pdf
	46	2.5	Thesis	Hood E. 2000. Permanganate flushing of DNAPL source zones: experimental and numerical investigation. PhD Thesis. Dept. of Civil Engineering, University of Waterloo, Waterloo Ontario
	50	2.8	Government	Battelle. Demonstration of ISCO Treatment of a DNAPL Source Zone at Launch Complex 34 in Cape Canaveral Air Station: Final Innovative Technology Evaluation Report. October 2002.
		2.8	Consultant	IT Corporation. In Situ Oxidation System Demonstration Test, Final Report, Treatment Cell C, Launch Complex 34 DNAPL Source Oxidation Project, Cape Canaveral, FL. Revision 1, October 2000.
	53	1.9	Journal	Siegrist RL, Lowe KS, Murdoch LC, Case TL, and Pickering DA. 1999. In situ oxidation by fracture emplaced reactive solids. Journal of Environmental Engineering 125: 429-440
	58	2.0	Government	U.S. Environmental Protection Agency. Field Applications of In Situ Remediation Technologies: Chemical Oxidation (Report No. 542R98008) September 1998.
		2.0	Conference	LaChance JC, Reitsma S, McKay D, Baker R. In situ oxidation of trichloroethene using potassium permanganate Part 1. Theory and design. 1998. Vol C1-5 in Proceedings of the First International Conference on Remediation of Chlorinated and Recalcitrant Compounds, Monterey CA, May 18-21.

TABLE B.1
LIST OF CASE STUDIES IN DNAPL TEST

Technology	Site Identifier	DQR	Reference Type	Reference
ISCO-MnO4	58	2.0	Conference	McKay D, Hewitt A, Reitsma S, LaChance J, Baker R. In situ oxidation of trichloroethene using potassium permanganate Part 2. Pilot study. 1998. Vol C1-5 in proceedings of the First International Conference on Remediation of Chlorinated and Recalcitrant Compounds, Monterey CA, May 18-21.
	59	1.9	Academic	Gonullu T and Farquhar G. 1989. Oxidation to Remove TCE from Soil. Dept. of Civil Engineering, University of Waterloo, Waterloo, ON. Accessed Dec. 2005. www.civil.uwaterloo.ca/groundwater/oxlitrev.html
	60	1.9	Web	Navon, D. and Pirnie, M. 2005 www.clu-in.org/fracrock/
	91	2.9	Thesis	Mundle K. 2006. Concentration Rebound Following In Situ Chemical Oxidation in Fractured Clay. M.Sc. Thesis, Dept. of Civil Engineering, Queen's University, Kingston, ON.
	92	2.9	Thesis	Mundle K. 2006. Concentration Rebound Following In Situ Chemical Oxidation in Fractured Clay. M.Sc. Thesis, Dept. of Civil Engineering, Queen's University, Kingston, ON.
	93	2.9	Thesis	Mundle K. 2006. Concentration Rebound Following In Situ Chemical Oxidation in Fractured Clay. M.Sc. Thesis, Dept. of Civil Engineering, Queen's University, Kingston, ON.
	94	2.9	Thesis	Mundle K. 2006. Concentration Rebound Following In Situ Chemical Oxidation in Fractured Clay. M.Sc. Thesis, Dept. of Civil Engineering, Queen's University, Kingston, ON.
	95	2.9	Thesis	Mundle K. 2006. Concentration Rebound Following In Situ Chemical Oxidation in Fractured Clay. M.Sc. Thesis, Dept. of Civil Engineering, Queen's University, Kingston, ON.
	97	2.9	Thesis	Mundle K. 2006. Concentration Rebound Following In Situ Chemical Oxidation in Fractured Clay. M.Sc. Thesis, Dept. of Civil Engineering, Queen's University, Kingston, ON.
	98	2.9	Thesis	Mundle K. 2006. Concentration Rebound Following In Situ Chemical Oxidation in Fractured Clay. M.Sc. Thesis, Dept. of Civil Engineering, Queen's University, Kingston, ON.
	99	2.9	Thesis	Mundle K. 2006. Concentration Rebound Following In Situ Chemical Oxidation in Fractured Clay. M.Sc. Thesis, Dept. of Civil Engineering, Queen's University, Kingston, ON.
	100	2.9	Thesis	Mundle K. 2006. Concentration Rebound Following In Situ Chemical Oxidation in Fractured Clay. M.Sc. Thesis, Dept. of Civil Engineering, Queen's University, Kingston, ON.
	101	2.9	Thesis	Mundle K. 2006. Concentration Rebound Following In Situ Chemical Oxidation in Fractured Clay. M.Sc. Thesis, Dept. of Civil Engineering, Queen's University, Kingston, ON.
	102	2.9	Thesis	Mundle K. 2006. Concentration Rebound Following In Situ Chemical Oxidation in Fractured Clay. M.Sc. Thesis, Dept. of Civil Engineering, Queen's University, Kingston, ON.
	103	2.9	Thesis	Mundle K. 2006. Concentration Rebound Following In Situ Chemical Oxidation in Fractured Clay. M.Sc. Thesis, Dept. of Civil Engineering, Queen's University, Kingston, ON.
	104	2.9	Thesis	Mundle K. 2006. Concentration Rebound Following In Situ Chemical Oxidation in Fractured Clay. M.Sc. Thesis, Dept. of Civil Engineering, Queen's University, Kingston, ON.
	105	2.9	Thesis	Mundle K. 2006. Concentration Rebound Following In Situ Chemical Oxidation in Fractured Clay. M.Sc. Thesis, Dept. of Civil Engineering, Queen's University, Kingston, ON.

Table B.1

TABLE B.1
LIST OF CASE STUDIES IN DNAPL TEST

Technology	Site Identifier	DQR	Reference Type	Reference
ISCO-MnO4	106	2.9	Thesis	Mundle K. 2006. Concentration Rebound Following In Situ Chemical Oxidation in Fractured Clay. M.Sc. Thesis, Dept. of Civil Engineering, Queen's University, Kingston, ON.
	107	2.9	Thesis	Mundle K. 2006. Concentration Rebound Following In Situ Chemical Oxidation in Fractured Clay. M.Sc. Thesis, Dept. of Civil Engineering, Queen's University, Kingston, ON.
	108	2.9	Thesis	Mundle K. 2006. Concentration Rebound Following In Situ Chemical Oxidation in Fractured Clay. M.Sc. Thesis, Dept. of Civil Engineering, Queen's University, Kingston, ON.
	109	2.9	Thesis	Mundle K. 2006. Concentration Rebound Following In Situ Chemical Oxidation in Fractured Clay. M.Sc. Thesis, Dept. of Civil Engineering, Queen's University, Kingston, ON.
	110	2.9	Thesis	Mundle K. 2006. Concentration Rebound Following In Situ Chemical Oxidation in Fractured Clay. M.Sc. Thesis, Dept. of Civil Engineering, Queen's University, Kingston, ON.
	111	2.9	Thesis	Mundle K. 2006. Concentration Rebound Following In Situ Chemical Oxidation in Fractured Clay. M.Sc. Thesis, Dept. of Civil Engineering, Queen's University, Kingston, ON.
	122	1.7	Web	Viellenave JH, Lauer JP, Fontana, JV. Using Risk Based Cleanup Goals for In Situ Chemical Oxidation of PCE in Vadose Zone Soils Under a Voluntary Cleanup Program. http://ipec.utulsa.edu/conf2002/viellenave_lauer_fontana_66.pdf
	122	1.7	Web	Accessed Mar. 2007. http://costperformance.org/pdf/isco_perm.pdf
	143	1.7	Consultant	Shaw Environmental Inc., 2005. Alaric Superfund Site-Tampa, FL. Interim Remedial Action Vital Signs Report V7.0, November 1, 2004 to October 31, 2005.
	159	2.7	Thesis	West, M. R. (2009), Mathematical Modelling of DNAPL Source Zone Remediation, Ph.D. thesis, 431 pp, Queen's University, Kingston, Ontario
	163	2.9	Thesis	West, M. R. (2009), Mathematical Modelling of DNAPL Source Zone Remediation, Ph.D. thesis, 431 pp, Queen's University, Kingston, Ontario
	167	2.9	Thesis	West, M. R. (2009), Mathematical Modelling of DNAPL Source Zone Remediation, Ph.D. thesis, 431 pp, Queen's University, Kingston, Ontario
	171	2.9	Thesis	West, M. R. (2009), Mathematical Modelling of DNAPL Source Zone Remediation, Ph.D. thesis, 431 pp, Queen's University, Kingston, Ontario
	173	2.7	Thesis	West, M. R. (2009), Mathematical Modelling of DNAPL Source Zone Remediation, Ph.D. thesis, 431 pp, Queen's University, Kingston, Ontario
	179	2.9	Thesis	West, M. R. (2009), Mathematical Modelling of DNAPL Source Zone Remediation, Ph.D. thesis, 431 pp, Queen's University, Kingston, Ontario
	182	2.9	Thesis	West, M. R. (2009), Mathematical Modelling of DNAPL Source Zone Remediation, Ph.D. thesis, 431 pp, Queen's University, Kingston, Ontario
	186	2.9	Thesis	West, M. R. (2009), Mathematical Modelling of DNAPL Source Zone Remediation, Ph.D. thesis, 431 pp, Queen's University, Kingston, Ontario

TABLE B.1
LIST OF CASE STUDIES IN DNAPL TEST

Technology	Site Identifier	DQR	Reference Type	Reference
ISCO-MnO4	190	2.9	Thesis	West, M. R. (2009), Mathematical Modelling of DNAPL Source Zone Remediation, Ph.D. thesis, 431 pp, Queen's University, Kingston, Ontario
	198	2.9	Thesis	West, M. R. (2009), Mathematical Modelling of DNAPL Source Zone Remediation, Ph.D. thesis, 431 pp, Queen's University, Kingston, Ontario
	207	2.2	Government	U.S. Environmental Protection Agency, Region 1, Boston Massachusetts. Five-Year Review, Eastern Surplus Company Superfund Site, Meddybemps, Maine. 29 September 2006.
	212	1.7	Consultant	IT Corporation .April 4, 2002. Response Action Progress Report, Former Dry Cleaner Tract, McKinney and Lemmon Avenue East, Dallas, Texas. Prepared for: Mr. Neal Sleeper, Blackburn Central Holdings, L.P.
	212	1.7	Consultant	Pastor, Behling & Wheeler, LLC. .April 7, 2004. Site Investigation Report Addendum, Source Tract, McKinney and Lemmon Avenue East, Dallas, Texas. Prepared for: Blackburn Central Holdings, L.P.
	215	1.8	Government	U.S. Environmental Protection Agency. September 1998.(EPA 542-R-98-008) Field Applications of In Situ Remediation Technologies, Chemical Oxidation.
		1.8	Government	U.S. DOE, Implementation of Deep Soil Mixing at the Kansas City Plat, Oak Ridge National Laboratory, Grand Junction, CO, February 1997
	233	2.7	Thesis	Pang, T. W. (2010), DNAPL Remediation of Fractured Rock Evaluated via Numerical Simulation, Ph.D. thesis, The University of Edinburgh, Edinburgh, Scotland, United Kingdom. March, 2010
	234	2.7	Thesis	Pang, T. W. (2010), DNAPL Remediation of Fractured Rock Evaluated via Numerical Simulation, Ph.D. thesis, The University of Edinburgh, Edinburgh, Scotland, United Kingdom. March, 2010
	235	2.7	Thesis	Pang, T. W. (2010), DNAPL Remediation of Fractured Rock Evaluated via Numerical Simulation, Ph.D. thesis, The University of Edinburgh, Edinburgh, Scotland, United Kingdom. March, 2010
	236	2.7	Thesis	Pang, T. W. (2010), DNAPL Remediation of Fractured Rock Evaluated via Numerical Simulation, Ph.D. thesis, The University of Edinburgh, Edinburgh, Scotland, United Kingdom. March, 2010
	237	2.9	Thesis	Pang, T. W. (2010), DNAPL Remediation of Fractured Rock Evaluated via Numerical Simulation, Ph.D. thesis, The University of Edinburgh, Edinburgh, Scotland, United Kingdom. March, 2010
	238	2.7	Thesis	Pang, T. W. (2010), DNAPL Remediation of Fractured Rock Evaluated via Numerical Simulation, Ph.D. thesis, The University of Edinburgh, Edinburgh, Scotland, United Kingdom. March, 2010
	239	2.7	Thesis	Pang, T. W. (2010), DNAPL Remediation of Fractured Rock Evaluated via Numerical Simulation, Ph.D. thesis, The University of Edinburgh, Edinburgh, Scotland, United Kingdom. March, 2010
	240	2.9	Thesis	Pang, T. W. (2010), DNAPL Remediation of Fractured Rock Evaluated via Numerical Simulation, Ph.D. thesis, The University of Edinburgh, Edinburgh, Scotland, United Kingdom. March, 2010
	241	2.9	Thesis	Pang, T. W. (2010), DNAPL Remediation of Fractured Rock Evaluated via Numerical Simulation, Ph.D. thesis, The University of Edinburgh, Edinburgh, Scotland, United Kingdom. March, 2010
ISCO-Ozone	49	1.7	Web	Kerfoot, W., K-V Associates. Accessed Sept. 2005. www.clu-in.org/products/siteprof/sitedtl.cfm?mid=50

Table B.1

TABLE B.1
LIST OF CASE STUDIES IN DNAPL TEST

Technology	Site Identifier	DQR	Reference Type	Reference
Other	13	2.2	Newsletter	Puls R, Olson M, and Sale T. ZVI-clay soil mixing treats DNAPL source area at 35-foot depth. Technology News and Trends, February 2006. http://www.cluin.org/products/newsltrs/tnandt/view.cfm?issue=0206.cfm#2
	21	3.0	Journal	Quinn J, Geiger C, Clausen C, Brooks K, Coon C, O'Hara S, Krug T, Major D, Yoon WS, Gavaskar A, Holdsworth T. 2005. Field demonstration of DNAPL dehalogenation using emulsified zero-valent iron. Environmental Science and Technology 39: 1309-1318.
	44	2.1	Web	Farrell, J. Site Profile: Butler Cleaners (#2). Accessed Nov. 2005. http://www.drycleancoalition.org/profiles/display.cfm?id=10
	52	1.9	Journal	Siegrist RL, Lowe KS, Murdoch LC, Case TL, and Pickering DA. 1999. In situ oxidation by fracture emplaced reactive solids. Journal of Environmental Engineering 125: 429-440
SEAR	15	2.6	ESTCP	Environmental Security Technology Certification Program (ESTCP). Cost and Performance Report: Surfactant Enhanced DNAPL Removal (CU-9714). Aug. 2001.
	16	2.6	Journal	Childs J, Acosta E, Annable M, Brooks M, Enfield C, Harwell J, Hasegawa M, Knox R, Suresh P, Rao D, Shiau B, Szekeres E and Wood L. 2006. Field demonstration of surfactant-enhanced solubilization of DNAPL at Dover Air Force Base, Delaware. Journal of Contaminant Hydrology 82: 1-22.
	18	1.7	Journal	Londergan J, Meinardus H, Mariner P, Jackson R, Brown C, Dwarakanath V, Pope G, Ginn J and Taffinder S. 2001. DNAPL removal from a heterogeneous alluvial aquifer by surfactant-enhanced aquifer remediation. Groundwater Monitoring and Remediation Fall 2001: 57-67.
	61	1.5	Conference	Drummond CD, Lemke LD, Rathfelder KM, Hahn EJ, and Abriola LM. 2000. Simulation of surfactant-enhanced PCE recovery at a pilot test field site. Vol. C2-2 in Proceedings of the Second International Conference on Remediation of Chlorinated and Recalcitrant Compounds (Wickramanayake G, Gavaskar AR, and Gupta N., eds.). Battelle Press, Columbus, Ohio. pp. 77-84.
	63	2.5	Conference	Holzmer FJ, Pope GA, and Yeh L. 2000. Surfactant-enhanced aquifer remediation of PCE-DNAPL in low-permeability sand. Vol. C2-2 in Proceedings of the Second International Conference on Remediation of Chlorinated and Recalcitrant Compounds (Wickramanayake G, Gavaskar AR, and Gupta N., eds.). Battelle Press, Columbus, Ohio. pp. 187-193.
	76	2.2	Conference	Suchomel EJ and Pennell KD. 2004. Assessment of Contaminant Plume Development Following Surfactant-Based DNAPL Source Zone Treatment. Paper 5C-01 in Proceedings of the Fourth International Conference on Remediation of Chlorinated and Recalcitrant Compounds (Chairs: Gavaskar A and Chen ASC), Monterey CA, May 24-27.
	132	2.7	Government	ITRC DNAPL Team Case Summary Report: Alameda Naval Air Station, Alameda, California. http://www.itrcweb.org/Documents//DNAPLs-3.pdf
	142	2.4	Journal	Martel R; Gelinas PJ; Saumure L. Aquifer washing by micellar solutions: Field test at the Thouin Sand Pit (L'Assomption, Quebec, Canada). Journal of Contaminant Hydrogeology. 1998, 30: 33-48

TABLE B.1
LIST OF CASE STUDIES IN DNAPL TEST

Technology	Site Identifier	DQR	Reference Type	Reference
SEAR	162	2.9	Thesis	West, M. R. (2009), Mathematical Modelling of DNAPL Source Zone Remediation, Ph.D. thesis, 431 pp, Queen's University, Kingston, Ontario
	166	2.9	Thesis	West, M. R. (2009), Mathematical Modelling of DNAPL Source Zone Remediation, Ph.D. thesis, 431 pp, Queen's University, Kingston, Ontario
	170	2.9	Thesis	West, M. R. (2009), Mathematical Modelling of DNAPL Source Zone Remediation, Ph.D. thesis, 431 pp, Queen's University, Kingston, Ontario
	178	2.9	Thesis	West, M. R. (2009), Mathematical Modelling of DNAPL Source Zone Remediation, Ph.D. thesis, 431 pp, Queen's University, Kingston, Ontario
	181	2.9	Thesis	West, M. R. (2009), Mathematical Modelling of DNAPL Source Zone Remediation, Ph.D. thesis, 431 pp, Queen's University, Kingston, Ontario
	185	2.9	Thesis	West, M. R. (2009), Mathematical Modelling of DNAPL Source Zone Remediation, Ph.D. thesis, 431 pp, Queen's University, Kingston, Ontario
	189	2.9	Thesis	West, M. R. (2009), Mathematical Modelling of DNAPL Source Zone Remediation, Ph.D. thesis, 431 pp, Queen's University, Kingston, Ontario
	193	2.9	Thesis	West, M. R. (2009), Mathematical Modelling of DNAPL Source Zone Remediation, Ph.D. thesis, 431 pp, Queen's University, Kingston, Ontario
	197	2.9	Thesis	West, M. R. (2009), Mathematical Modelling of DNAPL Source Zone Remediation, Ph.D. thesis, 431 pp, Queen's University, Kingston, Ontario
	201	2.9	Thesis	West, M. R. (2009), Mathematical Modelling of DNAPL Source Zone Remediation, Ph.D. thesis, 431 pp, Queen's University, Kingston, Ontario
	243	2.9	Thesis	Pang, T. W. (2010), DNAPL Remediation of Fractured Rock Evaluated via Numerical Simulation, Ph.D. thesis, The University of Edinburgh, Edinburgh, Scotland, United Kingdom. March, 2010
	244	2.9	Thesis	Pang, T. W. (2010), DNAPL Remediation of Fractured Rock Evaluated via Numerical Simulation, Ph.D. thesis, The University of Edinburgh, Edinburgh, Scotland, United Kingdom. March, 2010
	245	2.9	Thesis	Pang, T. W. (2010), DNAPL Remediation of Fractured Rock Evaluated via Numerical Simulation, Ph.D. thesis, The University of Edinburgh, Edinburgh, Scotland, United Kingdom. March, 2010
	246	2.9	Thesis	Pang, T. W. (2010), DNAPL Remediation of Fractured Rock Evaluated via Numerical Simulation, Ph.D. thesis, The University of Edinburgh, Edinburgh, Scotland, United Kingdom. March, 2010
	247	2.9	Thesis	Pang, T. W. (2010), DNAPL Remediation of Fractured Rock Evaluated via Numerical Simulation, Ph.D. thesis, The University of Edinburgh, Edinburgh, Scotland, United Kingdom. March, 2010
	248	2.9	Thesis	Pang, T. W. (2010), DNAPL Remediation of Fractured Rock Evaluated via Numerical Simulation, Ph.D. thesis, The University of Edinburgh, Edinburgh, Scotland, United Kingdom. March, 2010
	249	2.9	Thesis	Pang, T. W. (2010), DNAPL Remediation of Fractured Rock Evaluated via Numerical Simulation, Ph.D. thesis, The University of Edinburgh, Edinburgh, Scotland, United Kingdom. March, 2010

TABLE B.1
LIST OF CASE STUDIES IN DNAPL TEST

Technology	Site Identifier	DQR	Reference Type	Reference
SEAR	250	2.9	Thesis	Pang, T. W. (2010), DNAPL Remediation of Fractured Rock Evaluated via Numerical Simulation, Ph.D. thesis, The University of Edinburgh, Edinburgh, Scotland, United Kingdom. March, 2010
	251	2.9	Thesis	Pang, T. W. (2010), DNAPL Remediation of Fractured Rock Evaluated via Numerical Simulation, Ph.D. thesis, The University of Edinburgh, Edinburgh, Scotland, United Kingdom. March, 2010
	252	2.9	Thesis	Pang, T. W. (2010), DNAPL Remediation of Fractured Rock Evaluated via Numerical Simulation, Ph.D. thesis, The University of Edinburgh, Edinburgh, Scotland, United Kingdom. March, 2010
Th-Conductive	5	1.5	Conference	LaChance J, Baker RS, Galligan JP, Bierschenk JM. 2004. Application of "thermal conductive heating/in situ thermal desorption (ISTD)" to the remediation of chlorinated volatile organic compounds in saturated and unsaturated settings. Paper 2B-21 in Proceedings of the Fourth International Conference on Remediation of Chlorinated and Recalcitrant Compounds (Chairs: Gavaskar A and Chen ASC), Monterey CA, May 24-27.
	32	2.5	Conference	Baker RS, Lachance JC, and Heron G. Application of thermal remediation techniques for in-situ treatment of contaminated soil and water. Presented at the NATO Advanced Research Workshop, Athens, Greece, June 2006.
		2.5	Web	Commercial Brownfields Project: Terminal One Tank Farm. www.terratherm.com
	218	2.1	ESTCP	Terratherm case study form - Confidential Midwest
		2.1	Web	Terratherm PDS file - Terra Therm. Confidential Midwest CVOC Site. Www.terratherm.com
	219	1.5	ESTCP	Terratherm case study form - Confidential Plant Portland, IN
		1.5	Vendor	Terratherm PDS file - Commercial ISTD Project Indiane
	220	2.1	ESTCP	Terratherm case study form - South Eastern US
Th-ERH	1	1.8	Conference	Fain S, Holloway C, Heath W, Lundberg WR, Walters G and Ficklen D. 2002. Electrical resistance heating under an active industrial plant. Paper 2G-10 in Proceedings of the Third International Conference on Remediation of Chlorinated and Recalcitrant Compounds, Monterey CA, May 20-23.
	2	1.8	Conference	Scaramuzzo J. 2004. Electrical resistance heating pilot for in-situ VOC remediation. Paper 2B-15 in Proceedings of the Fourth International Conference on Remediation of Chlorinated and Recalcitrant Compounds, Monterey CA, May 24-27.
	3	2.0	Conference	Francis J and Wolf J. 2004. In situ remediation of chlorinated VOCs and BTEX using electrical resistance heating. Paper 2B-19 in Proceedings of the Fourth International Conference on Remediation of Chlorinated and Recalcitrant Compounds (Chairs: Gavaskar A and Chen ASC), Monterey CA, May 24-27.
	8	1.9	Journal	Heron G, Van Zutphen M, Christensen TH and Enfield CG. 1998. Soil heating for enhanced remediation of chlorinated Solvents: a laboratory study on resistive heating and vapour extraction in a silty, low-permeable soil contaminated with trichloroethylene. Environmental Science and Technology 32: 1474-1481.
	17	2.4	Government	U.S. Army Corps of Engineers. Draft-Final East Gate Disposal Yard Thermal Remediation Performance Assessment Report, Area 2, August 2006.

TABLE B.1
LIST OF CASE STUDIES IN DNAPL TEST

Technology	Site Identifier	DQR	Reference Type	Reference
Th-ERH	27	2.2	Newsletter	Hood D and Townsend G. ERH pilot project removes 48 tons of PCA DNAPL within six months. Technology News and Trends, February 2006. http://www.cluin.org/products/newsltrs/tnandt/view.cfm?issue=0206.cfm#3
	47	2.0	Government	U.S. Environmental Protection Agency. In Situ Thermal Treatment of Chlorinated Solvents: Fundamentals and Field Applications (Cost and Performance Report). June 2003.
	47	2.0	Government	US EPA Technology Innovation Office, Cost and Performance Report – Six-Phase Heating (SPH) at a former manufacturing facility Skokie, Illinois, October 1999.
	48	2.8	Consultant	Thermal Remediation Services. Final NAPL Area 1 Completion Report. April 2005. http://extranet.nws.usace.army.mil/extranet/documents/egdy/
	51	2.0	Government	U.S. Environmental Protection Agency. In Situ Thermal Treatment of Chlorinated Solvents: Fundamentals and Field Applications (Cost and Performance Report dated June 2003). March 2004.
	56	2.1	Vendor	Thermal Remediation Services. Project Example - Full Scale Guaranteed Remediation of Tetrachloroethene using Electrical Resistance Heating, Queens, New York. 2006.
	96	1.5	Government	U.S. Environmental Protection Agency. In Situ Thermal Treatment of Chlorinated Solvents: Fundamentals and Field Applications (Cost and Performance Report dated February 2004). March 2004.
	113	2.2	Conference	Demonstration of Resistive Heating Treatment of DNAPL Source Zone at Launch Complex 34 in Cape Canaveral Airforce Station, Florida. Battelle. 2003
	114	2.2	Government	CDM Federal Programs corporation. Final Remedial Action Report for Lasagna™ Phase IIb In-Situ Remediation of Solid Waste Management Unit 91 at the Paducah Gaseous Diffusion Plant. Document Control No. 5132-001-CO-0222. Sept. 2002
	116	2.2	Government	Foster Wheeler Environmental Corporation. Electrical Resistance Heating Pilot Test Final Report Silresim Superfund Site. September 2003. Prepared for the US Army Corps of Engineers.
	117	2.8	Vendor	Thermal Remediation Services Inc.Project Example - Remediation of TCE DNAPL using ERH Under an Operating Industrial Manufacturing Building. Accessed Mar. 2007 http://thermalrs.com/performance/projects/pdfs/TRS-AFP4-073106-ACF.pdf
		2.8	Web	Walters G, Peacock D, Fleming D. Air Force Uses Electrical Resistance Heating for TCE Source Removal and Plume Reduction. Technology News and Trends, December 2004. http://clu-in.org/products/newsltrs/tnandt/view.cfm?issue=1204.cfm#2
		2.8	Consultant	URS Corporation. Final Enlarged Electrical Resistive Heating Application: Construction and Performance Report. 2004.
	118	2.5	Vendor	Shaw Environmental Inc. Field Activities Report DNAPL Source Removal Action: Installation Restoration Site 5, Plume 5-1, Alameda Point, Alameda, California. Document Control Number 9573. 2005.
		2.5	Conference	Gavaskar, A.; Bhargava, Mohit; Condit, W. Final Report: Cost and Performance Review of Electrical Resistance Heating (ERH) for Source Treatment. Battelle, February 2007

TABLE B.1
LIST OF CASE STUDIES IN DNAPL TEST

Technology	Site Identifier	DQR	Reference Type	Reference
Th-ERH	119	2.2	Web	Cost and Performance Report: Electrical Resistive Heating at the Charleston Naval Complex Site Charleston, South Carolina. June 2005 Accessed Mar. 2007. http://costperformance.org/pdf/charleston_061505.pdf
	121	2.4	Conference	Confidential. Reference not available.
	204	1.9	ESTCP	ASU case study form - Delevan Municipal Well
	205	1.7	ESTCP	ASU case study form- Naval Station Site 22
		1.7	Web	Remedial Project Manager News. Spring 2007. In Situ Electric Resistance Heating at Former Dry Cleaning Facility. http://www.thermalrs.com/news/newsView.php?pdf=24
Th-Other	7	2.1	Journal	Kawala Z and Atamanczuk T. 1998. Microwave-enhanced thermal decontamination of soil. Environmental Science and Technology 32: 2602-2607.
Th-Steam	4	1.6	Conference	Stewart LD, Ginn J and Hicken S. 1998. Field demonstrations of thermally enhanced extraction for DNAPL source removal. In Proceedings of the First International Conference on Remediation of Chlorinated and Recalcitrant Compounds, Monterey CA, May 18-21.
	6	1.4	Journal	Sleep BE and McClure PD. 2001. Removal of volatile and semivolatile organic contamination from soil by air and steam flushing. Journal of Contaminant Hydrology 50: 21-40.
	9	2.0	Conference	Keller AA. 1998. Displacement of DNAPLs from fractured media using steam injection. In proceedings of the First International Conference on Remediation of Chlorinated and Recalcitrant Compounds, Monterey CA, May 18-21.
	10	1.8	Conference	Heron G, Carroll S, Crisp G, Sowers HJ, Palmer S, Coleman K and Watts S. 2004. Steam in fractured rock: source removal at Edwards AFB. Paper 2F-04 in Proceedings of the Fourth International Conference on Remediation of Chlorinated and Recalcitrant Compounds (Chairs: Gavaskar A and Chen ASC), Monterey CA, May 24-27.
		1.8	Consultant	Earth Tech, Inc. 2003. Site 61 Treatability Study Report Steam Injection - Northwest Main Base Operable Unit 8 Edwards Air Force Base, California.
	11	1.8	Conference	Farber AM, Trotschler O, Steidinger S, Ochs S, Class H, Koschitzky HP and Bai Y. 2004. CHC remediation of the saturated zone by steam-air injection. Paper 2B-02 in Proceedings of the Fourth International Conference on Remediation of Chlorinated and Recalcitrant Compounds (Chairs: Gavaskar A and Chen ASC), Monterey CA, May 24-27.
	12	2.7	Conference	Juhlin R, Butherus M, Daniel J, Ingle DS, Heron G and McGee B. 2004. In situ thermal NAPL remediation at the Young-Rainey Star Center. Paper 2B-01 in Proceedings of the Fourth International Conference on Remediation of Chlorinated and Recalcitrant Compounds (Chairs: Gavaskar A and Chen ASC), Monterey CA, May 24-27.
		2.7	Conference	Tabor C, Juhlin R, Darr P, Caballero J, Ingle D. 2004. Nonaqueous-phase liquid characterization and post-remediation verification sampling. Paper 1B-03 in Proceedings of the Fourth International Conference on Remediation of Chlorinated and Recalcitrant Compounds (Chairs: Gavaskar A and Chen ASC), Monterey CA, May 24-27.

TABLE B.1
LIST OF CASE STUDIES IN DNAPL TEST

Technology	Site Identifier	DQR	Reference Type	Reference
Th-Steam	12	2.7	Conference	Carroll S, Heron G, Aines R, Newmark R, Gavaskar A, Yoon WS, Greene K. 2004. Single-well steam-enhanced extraction and HPO of chlorinated solvents. Paper 2B-03 in Fourth International Conference on Remediation of Chlorinated and Recalcitrant Compounds (Chairs: Gavaskar A and Chen ASC), Monterey CA, May 24-27.
		2.7	Government	U.S. Environmental Protection Agency. In Situ Thermal Treatment of Chlorinated Solvents: Fundamentals and Field Applications. March 2004.
		2.7	Government	US Department of Energy. Northeast Site Area A NAPL Remediation File Report. September 2003.
	22	2.2	Government	Environmental Protection Agency (US EPA). Davis E, Hoey R, Brandon B, Nalipinski M, Carrol S, Heron G, Novakowski K, Udell K. Steam-enhanced remediation research for DNAPL in fractured rock. August 2005.
	41	1.8	Government	Environmental Protection Agency (US EPA). In situ thermal treatment of chlorinated solvents: fundamentals and field applications (cost and performance report). March 2004.
	55	2.5	Government	U.S. Environmental Protection Agency. In Situ Thermal Treatment of Chlorinated Solvents: Fundamentals and Field Applications (Cost and Performance Report dated June 2003). March 2004.
		2.5	Government	In Situ Thermal-Enhanced Remediation Technologies, Sept. 2003. Prepared for the U.S. DOE.
	85	2.2	Conference	Heron G, LaBrecque D, Beadle D, and Sowers H. 2000. Steam stripping/hydrous pyrolysis oxidation for in-situ remediation of a TCE DNAPL spill. Vol. C2-5 pp. 149-156 in Proceedings of the Second International Conference on Remediation of Chlorinated and Recalcitrant Compounds, Monterey CA, May 22-25.
	112	2.0	Vendor	Integrated Water Resources Inc. In-Situ Thermal Remediation demonstration Project, Launch Complex 34, Cape Canaveral, Florida - Final Report. 2003
		2.0	Conference	Battelle. Performance Evaluation of In-Situ Thermal Remediation System for DNAPL Removal at Launch Complex 34, Cape Canaveral, Florida. 2001
	120	2.1	Journal	Kaslusky SF, Udell KS. 2005. Co-injection of air and steam for the prevention of the downward migration of DNAPLs during steam enhanced extraction: An experimental value of optimum injection ratio predictions. Journal of Contaminant Hydrology. 77: 325-347
	124	2.1	Journal	Kaslusky SF, Udell KS. 2005. Co-injection of air and steam for the prevention of the downward migration of DNAPLs during steam enhanced extraction: An experimental value of optimum injection ratio predictions. Journal of Contaminant Hydrology. 77: 325-347
	203	1.9	ESTCP	ASU case study form - Cape Canaveral_pilot
	206	1.8	Thesis	Kent S. Udell & Lyoyd D. Stewart, Jr. Department of Mechanical Engineering. University of California. 1989. Field Study of In Situ Steam Injection and Vacuum Extraction For Recovery of Volatile Organic Solvents.
		1.8	ESTCP	ASU case study form- Solvent Services

APPENDIX C

UNCONSOLIDATED MEDIA MODELING

Appendix C.1

Hydraulic Displacement Numerical Model Development and Summary of Simulation Results

Abstract

Hydraulic displacement is a mass removal technology suitable for stabilization of a DNAPL source zone, where stabilization is defined as reducing DNAPL saturations and reducing the risk of future pool mobilization. High resolution three-dimensional multiphase flow simulations incorporating a spatially correlated, heterogeneous porous medium illustrate that hydraulic displacement results in an increase in the amount of residual DNAPL present, which in turn results in increased solute concentrations in groundwater, an increase in the rate of DNAPL dissolution, and an increase in solute mass flux. A higher percentage of DNAPL recovery is associated with higher initial DNAPL release volumes, lower density DNAPLs, more heterogeneous porous media, and increased drawdown of groundwater at extraction wells. The fact that higher rates of recovery are associated with more heterogeneous porous media stems from the fact that larger contrasts in permeability provide for a higher proportion of capillary barriers upon which DNAPL pooling and lateral migration can occur. Across all scenarios evaluated in this study, the ganglia to pool (GTP) ratio generally increased from approximately 0.1 to between approximately 0.3 and 0.7 depending on the type of DNAPL, the degree of heterogeneity, and the imposed hydraulic gradient. The volume of DNAPL recovered as a result of implementing hydraulic displacement ranged from between 9.4% and 46.1% of the initial release volume, with the largest percentage recovery associated with 1,1,1 TCA, the least dense of the three DNAPLs considered.

1.0 - Introduction

Dense, non-aqueous phase liquids (DNAPLs) will distribute themselves in the subsurface as both disconnected blobs and ganglia of organic liquid referred to as residual, and in connected distributions referred to as pools. Pooled DNAPL frequently accumulates above capillary barriers, eventually achieving hydrostatic equilibrium with pool thickness typically varying from centimeters to meters (Kueper et al., 2004). Manipulating the hydraulic gradient has the potential to mobilize pooled DNAPL while residual DNAPL remains immobilized by capillary forces. An increase in hydraulic gradient can be implemented through the use of injection and extraction wells, or extraction wells alone, to create a capillary pressure imbalance across the pools resulting in the mobilization of DNAPL towards the extraction wells. Once having reached the well, DNAPL will enter the well screen as a result of both hydraulic gradient induced mobilization and gravity.

The recovery of pooled DNAPL from the subsurface by means of injection/extraction wells is referred to in a variety of ways including hydraulic displacement, waterflooding (Craig, 1971; Willhite, 1986) and dual phase extraction (Gerhard et al., 2001). It can be employed as a remedial option at sites exhibiting pooled DNAPL in order to (1) remove DNAPL mass, and (2) reduce pool heights and saturations so as to reduce the risk of future DNAPL mobilization (referred to as source zone stabilization). Hydraulic displacement can be employed with or without injection wells; the use of injection wells along with extraction wells, however, typically results in steeper hydraulic gradients and therefore faster rates of DNAPL recovery.

Hydraulic displacement was initially employed by the petroleum industry as a secondary recovery procedure (Craig, 1971). More recently, hydraulic displacement has

been applied to DNAPL source zones, in some cases using horizontal wells to address large DNAPL accumulations below the watertable (e.g., Sale and Applegate, 1997; Gerhard et al., 1998). Selection of injection and extraction well placement is influenced by the DNAPL fluid properties, the characteristics of the pool(s) and subsurface geology, and the specific remedial action objectives. Extraction wells placed at the base of a large accumulation of DNAPL tend to experience the largest recovery by taking advantage of gravity drainage. Recovery rates of DNAPL in extraction wells are typically highest at early time and decrease over time due to depletion in pool height and reduction of DNAPL relative permeabilities. Intermittent pumping of extraction wells is an effective means for reducing the amount of contaminated groundwater extracted while maximizing DNAPL yield by allowing DNAPL saturations and relative permeabilities to recover periodically (Gerhard et al., 2001).

DNAPL will dissolve into groundwater prior to, during and following hydraulic displacement operation. Partitioning of components from the DNAPL phase to groundwater has been examined extensively via both experiments and modeling (e.g., Miller et al., 1990; Powers et al., 1992; Powers et al., 1994; Imhoff et al., 1993; Saba and Illangasekare, 2000; Nambi and Powers, 2003; Grant and Gerhard, 2007a,b). At the field scale, pooled DNAPL will dissolve more slowly than residual DNAPL due to reduced relative permeability to water at high DNAPL saturations. This results in groundwater bypassing around DNAPL pools (similar to flow around low permeability lenses), and the low water flux through and adjacent to DNAPL pools limits mass removal (Brusseau *et al.,* 2002; Parker and Park, 2004). Hydraulic displacement is expected to increase the

ganglia-to-pool (GTP) ratio of a source zone and thereby modify the groundwater flow field and thus affect global mass transfer rates.

The objective of this study is to examine the efficacy of hydraulic displacement on the removal of pooled DNAPL from heterogeneous porous media through the use of vertical injection and withdrawal wells. A two-phase numerical flow model was employed to simulate DNAPL infiltration, redistribution, and recovery through hydraulic displacement for a number of scenarios. Specifically, this study examined the sensitivity of source zone mass removal and DNAPL distribution to (i) DNAPL type, (ii) degree of porous media heterogeneity, (iii) release volume, and (iv) hydraulic gradient. To evaluate the effect of hydraulic displacement on mass transfer, dissolution simulations were carried out both before and after hydraulic displacement. Specific metrics that were evaluated in this context included ganglia-to-pool ratio, groundwater concentration, and mass flux changes.

2.0 - Numerical Model

This work employed the three-dimensional two-phase flow reactive transport model DNAPL3D-RX (West et al., 2008). This model was developed for the simulation of DNAPL infiltration and redistribution, mass transfer between the non-aqueous and aqueous phases, and advective–dispersive aqueous phase reactive transport of contaminants in heterogeneous porous media. This was achieved by coupling the migration model DNAPL3D [Gerhard et al., 1998, Gerhard and Kueper, 2003a,b,c] and the dissolved phase reactive multispecies transport model RT3D (version 2.5) (Clement, 1997, 2003; Clement et al., 1998) through a mass transfer module (Grant and Gerhard, 2007a,b).

The model employs a seven-point node-centered finite difference scheme to discretize the three-dimensional multiphase flow equations, formulated in terms of two unknowns P_W and S_W (Kueper and Frind, 1991):

$$\frac{\partial}{\partial x_i}\left[\frac{-k_{i,j}k_{r,W}}{\mu_W}\left(\frac{\partial P_W}{\partial x_j}+\rho_W g\frac{\partial z}{\partial x_j}\right)\right]-\phi\frac{\partial S_W}{\partial t}=0 \qquad (1)$$

$$\frac{\partial}{\partial x_i}\left[\frac{-k_{i,j}k_{r,N}}{\mu_N}\left(\frac{\partial (P_C+P_W)}{\partial x_j}+\rho_N g\frac{\partial z}{\partial x_j}\right)\right]+\phi\frac{\partial S_W}{\partial t}=0 \qquad (2)$$

where $i,j = x, y, z$ and are spatial coordinates, k_{ij} [L^2] is a second order tensor defining the porous medium permeability, $k_{r,W}$ and $k_{r,N}$ are the relative permeabilities of the wetting and non-wetting phases respectively [-], ρ_N is the non-wetting phase density [M/L^3], μ_N is the non-wetting phase viscosity [M/L T], P_C and P_W are the capillary and wetting phase pressures with $P_c = P_W + P_N$ where P_N is the non-wetting phase pressure [M/L T^2], g is the gravitational constant [L/T^2], and S_N [-] is the non-wetting phase saturation with $S_W + S_N = 1$.

The advection-dispersion equation utilized by the multi-component transport model, formulated in terms of the single unknown, C_K, is (Zheng, 1990):

$$\frac{\partial}{\partial t}(\phi C_K)+\frac{\partial}{\partial x_i}(\phi v_{K,j}C_K)-\frac{\partial}{\partial x_i}\left(\phi D_{ij}\frac{\partial C_K}{\partial x_j}\right)=\sum R_n+q_s C_{K,S} \qquad (3)$$

where C_K is the aqueous phase concentration of component K [M/L^3], ΣR_n is a chemical reaction term which can be used to include effects of general biochemical and geochemical reactions (set to zero for this study), $q_s C_{K,s}$ represent the external supply of species K to the α phase through biotic and abiotic transformations with q_s representing the volumetric flow rate per unit volume of aquifer representing fluid sources and sinks [L^3/T], and $v_{K,j}$ is the groundwater velocity calculated according to Darcy's Law (Bear, 1972):

$$v_{K,j} = \frac{q_{K,j}}{\phi} \tag{4}$$

The groundwater velocity is calculated by DNAPL3D as part of the solution to (1) and (2), where it is influenced by DNAPL saturation via the relative wetting phase permeability function, and then is passed to MT3D for solution of (3).

DNAPL3D and MT3D are coupled by a mass transfer routine that permits the user to select one of a variety of published, local, mass transfer expressions. A standard split-operator (SO) approach is used to link the two sub-models, where a DNAPL migration time step is followed by dissolved phase transport performed over the same time period. A source of error proportional to the numerical time step size is introduced in split-operator approaches (Barry et al., 2002). After a dissolution and aqueous phase transport step is solved, the saturation change at every node is updated, and if any single node exceeds a user-specified tolerance then the migration and dissolution steps are rerun with a smaller timestep.

3.0 - Numerical Simulations

DNAPL releases into a heterogeneous porous media domain were simulated prior to performing hydraulic displacement simulations. The model domain spanned 20.0 m in both lateral dimensions (x and z) and 5.0 m in the vertical dimension (y). A nodal spacing of 0.4 m in the x and z directions and 0.05 m in the y direction discretized the domain into 250,000 nodes. Each node was assigned a permeability value using a spatially correlated random field generator (FGEN) (Robin et al., 1993), thereby creating a heterogeneous, horizontally stratified deposit.

Initially, the entire domain was saturated with wetting fluid (water). The four vertical faces of the rectangular domain were assigned boundary conditions that specified (i) constant wetting phase pressures distributed hydrostatically, and (ii) zero non-wetting phase flux which prohibited DNAPL migration outside of the domain. Water pressures specified on the upgradient vertical face were slightly higher than along the downgradient vertical face, such that an ambient hydraulic gradient of 0.001 was achieved in the positive x-direction. The top (water table) and bottom boundaries were assigned zero fluxes for both the non-wetting and wetting phases, except for the DNAPL source location. To simulate a DNAPL release, a 0.4 m x 0.4 m x 0.05 m high non-wetting phase source boundary was specified at the center of the top boundary via a constant wetting phase pressure of 0.0 Pa and a constant non-wetting phase saturation of 0.50.

3.1 – Base Case Simulation

The base case permeability field was log-normally distributed and characterized by a mean ln-k (m^2) of -27.6 and a variance of ln-k of 2.0 (moderate heterogeneity). Correlation lengths of 3.0 m for x and z (7.5 nodes) and 0.2 m for y (4 nodes) were used

to create horizontally stratified deposits with grain sizes ranging from silt to medium sand. All porous medium and fluid properties employed for the base case scenario are listed in Tables 1 and 2. For the base case, the non-wetting fluid properties are characteristic of trichloroethylene (TCE), a common chlorinated solvent DNAPL.

Table 1 – Base case simulation input parameters. See Gerhard and Kueper (2003a,b) for further definition and explanation of model input parameters.

Parameter	Value
Wetting phase density	1000 kg/m^3
Non-wetting phase density	1460 kg/m^3
Wetting phase viscosity	0.001 Pa-s
Non-wetting phase viscosity	0.00057 Pa-s
DNAPL-water interfacial tension	0.020 N/m
Porosity	0.30
Residual wetting phase saturation	0.13
Emergence saturation	0.92
Terminal/Displacement pressure ratio	0.52
Maximum non-wetting phase relative permeability	0.85
Maximum non-wetting phase residual saturation	0.25
Drainage pore size distribution index	2.50
Wetting pore size distribution index	1.25

The base case simulation release involved activating the source boundary condition until 7.57 m^3 (2000 gallons) of DNAPL had entered the domain. The source boundary condition was then eliminated and the infiltrated DNAPL was allowed to redistribute until migration effectively ceased (i.e., approximately 95% occupation of the total number of nodes ultimately invaded) which, for the base case, occurred after

approximately 14 years. This distribution of DNAPL was then utilized as the initial condition for the hydraulic displacement simulation.

Hydraulic displacement was simulated employing a total of six fully penetrating wells: three for water injection in the upgradient portion of the domain and three for the extraction of both DNAPL and water in the downgradient portion of the domain. For the base case, three evenly spaced injection wells were placed 1.0 m away from the upgradient boundary (6.4 m between each outer well and the center well). Similarly, three evenly spaced extraction wells were placed 1.0 m from the downgradient boundary. The well boundary conditions comprised constant, hydrostatically distributed wetting phase pressures and a constant wetting phase saturation equal to 1.0, which dictates instantaneous removal of DNAPL upon entering the well. Drawdown was specified through the wetting phase pressures and was set to 2.0 m for the base case. All hydraulic displacement runs simulated 200 days of source zone treatment, by which time the majority of runs were observed to reach a maximum for cumulative DNAPL volume recovery. DNAPL migration and hydraulic displacement simulations were conducted with the mass transfer routine inactive, which is a reasonable approach for low to moderate solubility DNAPLs given the time scales of interest.

3.2 – Sensitivity Analysis Simulations

Table 2 lists the base case (Run 1) and 12 sensitivity simulations, each one modifying a single parameter from the base case. Runs 2 and 3 varied the volume of DNAPL released to form the source zone, Runs 4 and 5 varied the DNAPL type (see Table 3 for fluid properties), Runs 6 and 7 varied the mean hydraulic conductivity of the

generated permeability field (maintaining the same structure), Runs 8 and 9 varied the variance of the permeability field (maintaining the same structure), Runs 10 and 11 varied the hydraulic gradient (by varying the drawdown) employed during treatment, and Runs 12 and 13 varied the injection and extraction well spacing. Runs 2 – 9 involved re-simulating the DNAPL release and redistribution phase, whereas Runs 10 – 13, looking at modifications to the hydraulic displacement design, utilized the DNAPL distribution from the base case. For each simulation, the parameters evaluated with time included (i) the volume of DNAPL recovered by the extraction wells, (ii) the number of nodes invaded by DNAPL and the fractions exhibiting pooled and residual saturations (i.e., the ganglia-to-pool ratio), and (iii) the distribution of DNAPL saturations.

Table 2 – Schedule of simulations (TCE = trichloroethylene, PCE = tetrachloroethylene, TCA = 1,1,1 trichloroethane)

Run #	DNAPL	Volume (m^3)[1]	Mean K (m/s)	Variance	Well Spacing (m)	Drawdown (m)
1	TCE	7.57	$1x10^{-5}$	2.00	6.4	2.0
2	TCE	1.89	$1x10^{-5}$	2.00	6.4	2.0
3	TCE	18.9	$1x10^{-5}$	2.00	6.4	2.0
4	TCA	7.57	$1x10^{-5}$	2.00	6.4	2.0
5	PCE	7.57	$1x10^{-5}$	2.00	6.4	2.0
6	TCE	7.57	$1x10^{-4}$	2.00	6.4	2.0
7	TCE	7.57	$1x10^{-6}$	2.00	6.4	2.0
8	TCE	7.57	$1x10^{-5}$	1.00	6.4	2.0
9	TCE	7.57	$1x10^{-5}$	4.00	6.4	2.0
10	TCE	7.57	$1x10^{-5}$	2.00	6.4	0.5
11	TCE	7.57	$1x10^{-5}$	2.00	6.4	1.0
12	TCE	7.57	$1x10^{-5}$	2.00	8.0	2.0
13	TCE	7.57	$1x10^{-5}$	2.00	3.6	2.0

1 - 7.57 m^3 = 2000 US gallons, 1.89 m^3 = 500 US gallons, 18.9 m^3 = 5000 US gallons

Table 3 – Fluid properties

Compound	Density (kg/m^3)	Aqueous Solubility (mg/L)	Effective Diffusion Coefficient (m^2/s)	Viscosity (cP)
1,1,1- Trichloroethane	1350	1300	6.4E-10	0.84
Trichloroethylene	1460	1100	6.6E-10	0.57
Tetrachloroethylene	1630	200	6.0E-10	0.89

3.3 – DNAPL Dissolution

A select number of dissolution simulations (one each for TCE, PCE and TCA) were performed to assess changes in aqueous phase concentrations attributable to hydraulic displacement. Local scale mass transfer rate coefficients were predicted by the correlation model of Nambi and Powers (2003):

$$K = \frac{ShD_o}{l_c^2} \tag{5}$$

$$Sh = 37.2 S_n^{1.24} \mathrm{Re}^{0.61} \tag{6}$$

where Sh is the Sherwood number [-], l_c [L] is the median grain size and D_o [L^2/T] is the diffusion coefficient for the contaminant in water, S_n [-] is the non-wetting phase saturation and Re ($\bar{v}\rho_w d_{50}/\mu_w$) is the Reynolds number, calculated by the model at each node at each timestep utilizing:

$$\bar{v} = \frac{q}{\phi Se} \tag{7}$$

where q is the Darcy flux [L/T] solved for at the node, ϕ is the porosity of the medium [-] and *Se* is the effective saturation [-] of the node. Nambi and Powers (2003) was chosen as the most appropriate, published correlation model because it was derived from multi-dimensional experiments characterized with heterogeneous porous media and relatively high initial NAPL saturations.

The effective diffusion coefficient (Table 3) was calculated via $D_{eff} = D_o \tau$ where τ is the tortuosity, assigned a value of 0.7 (consist with medium to fine grained sands) and the median grain size (l_c) was represented by d_{50} = 0.05 cm. Diffusion coefficients are calculated according to Wilke and Change (1955) and Lyman et al. (1982). Dissolution simulations employed the same boundary conditions as the DNAPL infiltration simulations, namely a uniform, ambient hydraulic gradient of 0.001 in positive x and no injection or extraction wells. These runs simulated 10 years of dissolution.

4.0 - Results and Discussion

4.1 - Hydraulic Displacement Simulations

Figures 1 and 2 superimpose on the permeability field the spatial distribution of DNAPL saturations before and after hydraulic displacement, respectively, for the base case simulation. Visual inspection indicates that a substantial number of discrete DNAPL pools with moderate to high saturations are present in the subsurface prior to hydraulic displacement. In contrast, Figure 2 reveals that these pools generally decrease in

saturation following hydraulic displacement (with a few exceptions) and that the remaining DNAPL is spread through a larger portion of the domain.

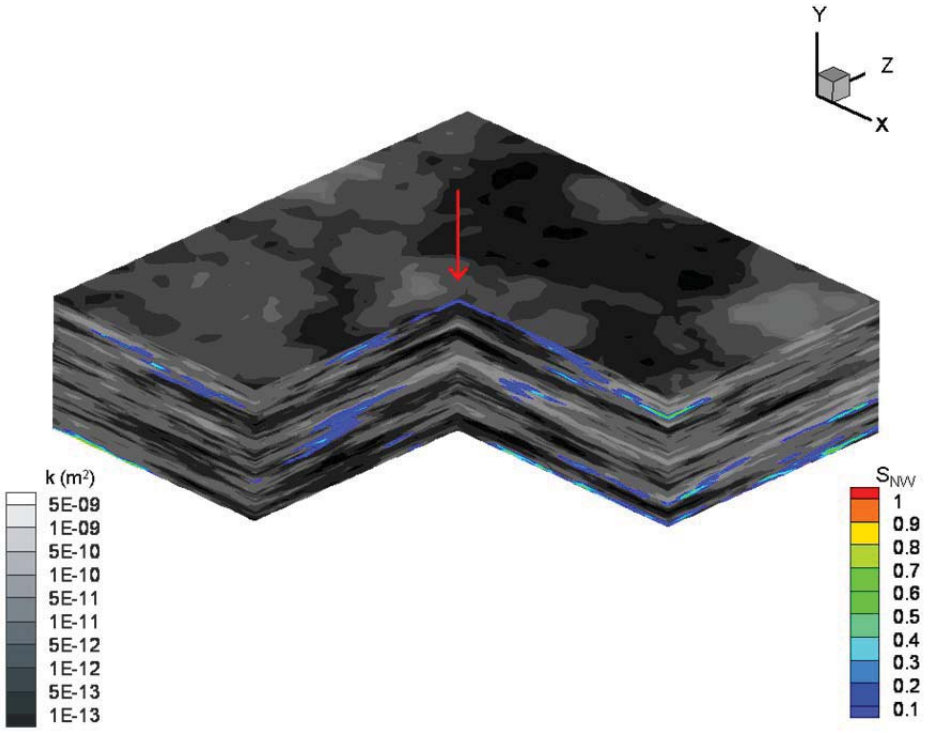

Figure 1 - Base case DNAPL distribution before hydraulic displacement. Grey scale represents hydraulic conductivity field, with darker shades representing lower permeabilities. Color scale represents DNAPL saturation expressed as fraction of pore space.

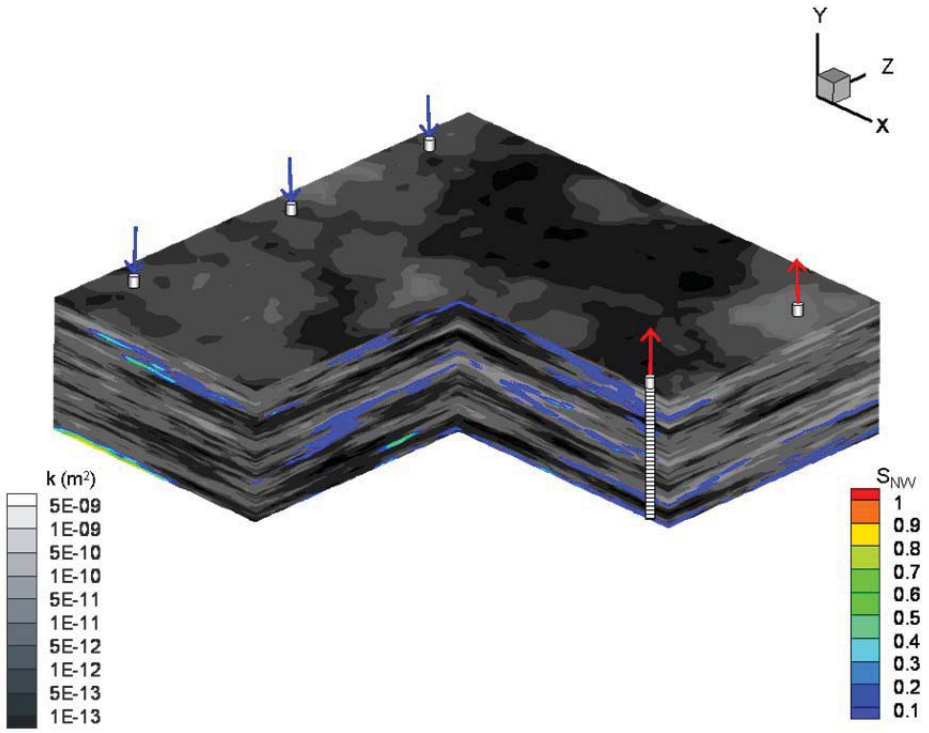

Figure 2 - Base case DNAPL distribution before hydraulic displacement. Grey scale represents hydraulic conductivity field, with darker shades representing lower permeabilities. Color scale represents DNAPL saturation expressed as fraction of pore space.

Figure 3 presents the volume of subsurface invaded by DNAPL (expressed as the percentage of model domain nodes invaded by DNAPL) versus time for the base case scenario. The figure further identifies the fraction of nodes experiencing drainage, experiencing wetting, and existing at residual. In this context, drainage refers to DNAPL displacing water, wetting refers to water displacing DNAPL, and residual refers to locations (i.e., nodes) in which DNAPL continuity is lost. The definition of residual in the model is that capillary pressure for a node has decreased to the terminal pressure, which is the capillary pressure associated with complete residual formation and loss of non-wetting phase continuity (Gerhard and Kueper, 2003a,b); this strict definition of

residual implies that a large fraction of the invaded subsurface may have low DNAPL saturations at late time, but not be classified as residual. All nodes containing DNAPL that are not at residual are referred to as exhibiting pooled DNAPL, denoting their continuity of DNAPL with adjacent nodes and potential for mobilization.

Figure 3 demonstrates that approximately 5.6% of the model domain nodes are occupied by DNAPL at the start of hydraulic displacement (i.e., the end of migration and redistribution) for the base case simulation. Figure 3 further demonstrates that greater than 90% of the DNAPL body is experiencing drainage conditions while the DNAPL source is active; however, once the source is terminated, this fraction steadily decreases to approximately 60% at end of the DNAPL redistribution period. This corresponds to increases in the fractions experiencing wetting and residual, achieving 21% and 7%, respectively, of the subsurface invaded by the DNAPL body at the start of hydraulic displacement. Similar trends in nodal distribution are observed for all simulations with the major difference associated with the time required for complete redistribution of the DNAPL released (ranging from 6 to 34 years, figures not shown). Migration timescale has been demonstrated to be correlated to mean intrinsic permeability, DNAPL release volume, and DNAPL fluid properties (Gerhard et al., 2007).

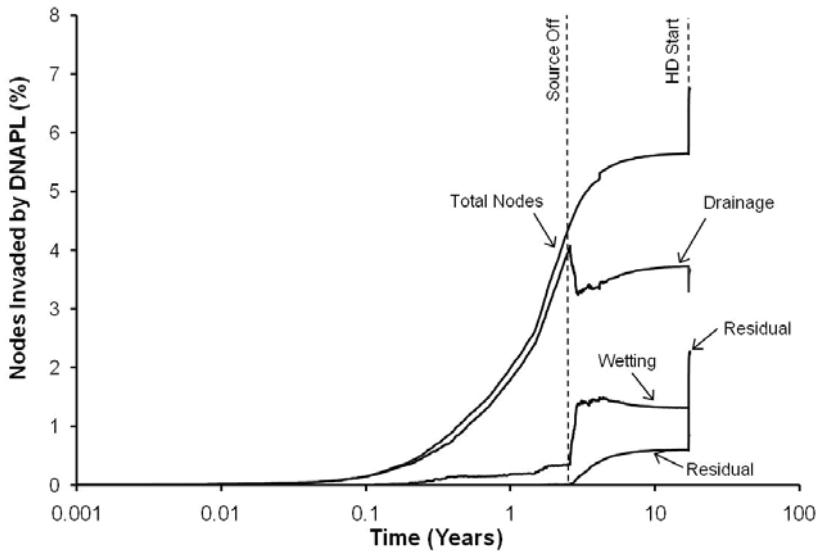

Figure 3 – Base case simulation percentage of model domain nodes invaded by DNAPL (drainage, residual, wetting and total).

The volume of DNAPL recovered by the extraction wells in the base case simulation is 2.37 m^3 (626 gallons) [31% of the initial volume of DNAPL present]. Figure 3 illustrates that hydraulic displacement brings about an increase (from 5.6% to 7%) in the volume of subsurface occupied by DNAPL. Hydraulic displacement brings about an abrupt increase in the amount of residual DNAPL during the 200 day treatment period. This is accompanied by the simultaneous decrease in locations experience wetting, although the magnitude of the decrease does not entirely offset the increase in residual. The total increase in subsurface volume invaded is observed to result from a combination of increased locations on drainage (i.e., DNAPL driven into previously unoccupied pores) and previously occupied pore space driven to residual. This pattern is repeated for all simulations, although the magnitudes of the changes in each case vary (figures not shown).

The DNAPL recovery results for all 13 simulations are presented in Figures 4 - 6, with each curve providing the cumulative DNAPL volume recovered summed over all extraction wells. Characteristic of oil and DNAPL extraction data, all curves exhibit an initial rapid recovery rate that decreases and eventually plateaus over time. This is due to the high relative permeability to DNAPL that exists at the initially high DNAPL saturations, and the rapid decrease in DNAPL permeability as saturations decrease. Figure 4 illustrates that DNAPL recovery rate and final extracted volume is highly sensitive to the original amount released. Moreover, the recovered volume does not increase proportionally to the volume released; only 9.35% of the 1.89 m^3 (500 gallon) TCE release is recovered, compared to 31% of the 7.57 m^3 (2000 gallon) TCE release, and 45% of the 18.9 m^3 (5000 gallon) TCE release (which is an underestimate of the potential total since 200 days of hydraulic displacement was insufficient to reach the recovery plateau in this simulation). It is also observed that the final recovered volume of the lower density DNAPL (TCA) is approximately twice that of the higher density DNAPL (PCE), attributable to the greater ability of lower density DNAPL to form pools above capillary barriers.

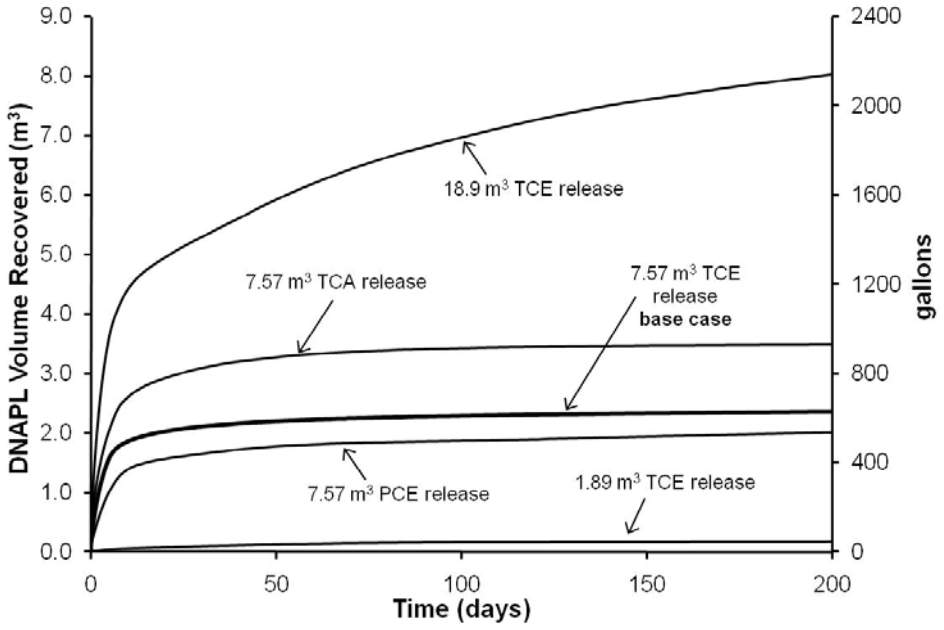

Figure 4 – DNAPL volume recovery comparisons for DNAPL type and initial volume of DNAPL released.

Figure 5 reveals that DNAPL recovery is sensitive to the mean and variance of hydraulic conductivity of the aquifer. Both lower mean hydraulic conductivity and higher variance of permeability correspond to increased final amounts of DNAPL recovered. This contrasts with general expectations that overall higher hydraulic conductivity and smaller variations in hydraulic conductivity (less heterogeneity) typically are considered beneficial for remedial flushing technologies. In the case of hydraulic displacement, however, the technology benefits from overall lower hydraulic conductivity and greater variations in hydraulic conductivity because these conditions provide the capillary barriers capable of supporting pooled DNAPL (higher GTP ratio). A larger proportion of capillary barriers provides for more lateral DNAPL spreading, more formation of pools, the accumulation of higher saturations within pools, and less

vertical plunging of the infiltrating DNAPL prior to application of hydraulic displacement.

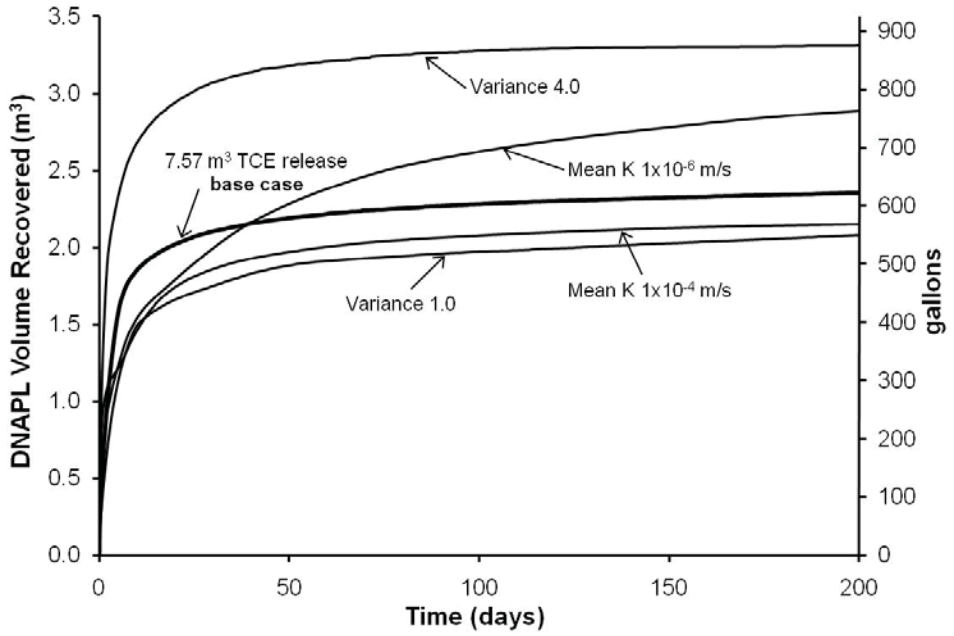

Figure 5 - DNAPL volume recovery comparisons for different mean hydraulic conductivity and degree of heterogeneity (variance).

Figure 6 demonstrates that DNAPL recovery for the base case release scenario is less sensitive to injection/extraction well spacing than to the other parameters investigated. While some early time sensitivity to well spacing is demonstrated, the final recovered volumes are not significantly different. This conclusion may be limited to the scale of this study, however, since it is expected that in the general case, fewer wells would ultimately result in less DNAPL recovery. Figure 6 also demonstrates that decreases in extraction well drawdown resulted in reductions in the DNAPL volume recovered because of the weaker hydraulic gradients that were achieved.

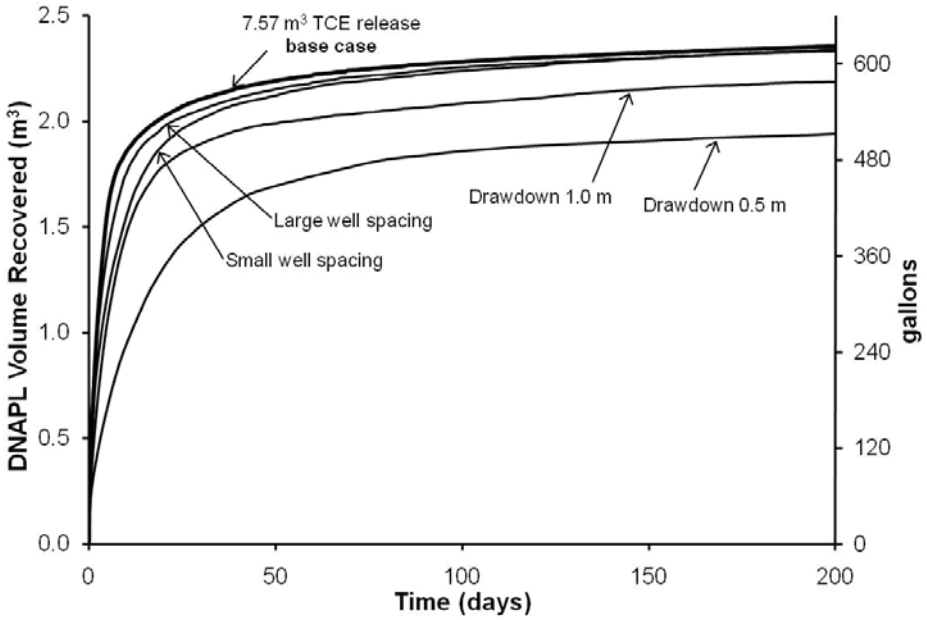

Figure 6 - DNAPL volume recovery comparisons for varying drawdown in recovery wells and well spacing.

Figure 7 presents the distribution of DNAPL saturations as grouped in 10% intervals both before and immediately after hydraulic displacement for the base case simulation. The figure reveals that a significant fraction of the DNAPL is present at high saturations within the domain prior to hydraulic displacement, providing the potential for DNAPL recovery. For the DNAPL volume not extracted, hydraulic displacement clearly decreases the highest saturation regions and shifts the distribution towards low and residual DNAPL saturations present in the domain. Similar shifts in saturation distribution were exhibited in all 13 hydraulic displacement simulations; in summary, those parameters associated with increased lateral spreading during release and increased DNAPL recovery during HD (decreased DNAPL density, increased release volume, decreased mean permeability, and increased variance of permeability) all presented initial

saturation distributions skewed towards the higher saturation bins and substantial reductions in those bins following HD (figures not shown).

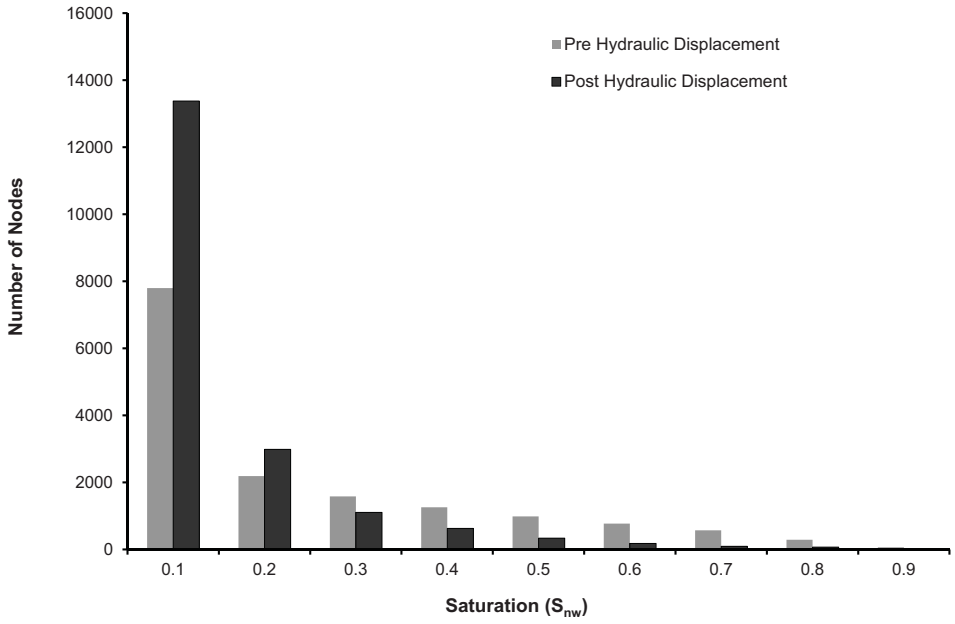

Figure 7 – Base case simulation distribution of nodal DNAPL saturation (fraction of pore space) before and after hydraulic displacement.

Figure 8 presents the pre- and post-hydraulic displacement GTP (ganglia to pool) ratios for all simulations. In all cases, hydraulic displacement results in a substantial increase in the GTP ratio. The greatest increases (GTP ratio between 0.50 and 0.70) are associated with those simulations exhibiting the highest initial DNAPL saturations and largest DNAPL recovery volumes. As mentioned previously, a strict definition of residual is employed; hence, Figure 8 may be biased towards low GTP ratios for 'practical' purposes.

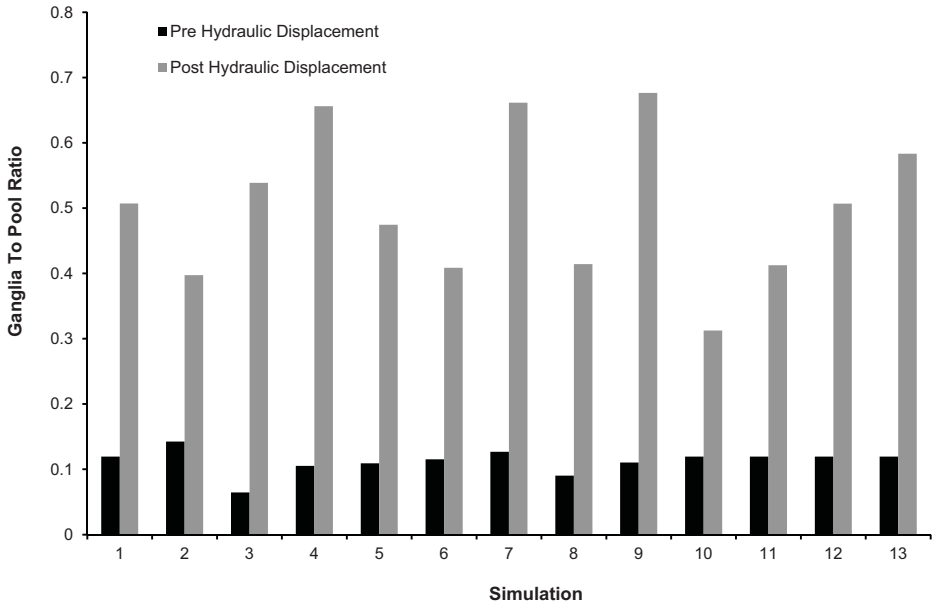

Figure 8 - Ganglia to pool ratio before and after hydraulic displacement.

4.2 - Dissolution Simulations

Figure 9 presents the results of the TCE base case dissolution simulation, both in terms of average concentration and average mass flux at the downgradient (exit) face of the domain. In each case a simulation examining 10 years of plume evolution following 200 days of hydraulic displacement were compared to the same scenario in which no hydraulic displacement was conducted. Figure 9 illustrates that hydraulic displacement causes the concentrations leaving the treatment zone to increase relative to what they would have been if no hydraulic displacement was undertaken (similar results were obtained for PCE and TCA, figures not shown). Consequently, the mass flux leaving the domain is greater post-hydraulic displacement than in the absence of hydraulic displacement. The higher concentrations and mass flux exiting the domain post-

hydraulic displacement are due to the reduced DNAPL saturations (including increased amounts of residual) present in the subsurface. Low and residual DNAPL saturations are predicted to dissolve more quickly into the passing groundwater than higher saturations associated with pooled DNAPL due to the increased groundwater velocities through the lower saturation nodes (associated with increased relative permeability to water). It is likely that the mass flux for the post-hydraulic displacement case will eventually decrease below that of the no hydraulic displacement case and achieve zero sooner due to (i) the redistribution of DNAPL to lower saturations, and (ii) reduced DNAPL mass in the subsurface. The total time required to achieve this condition was not a focus of this study.

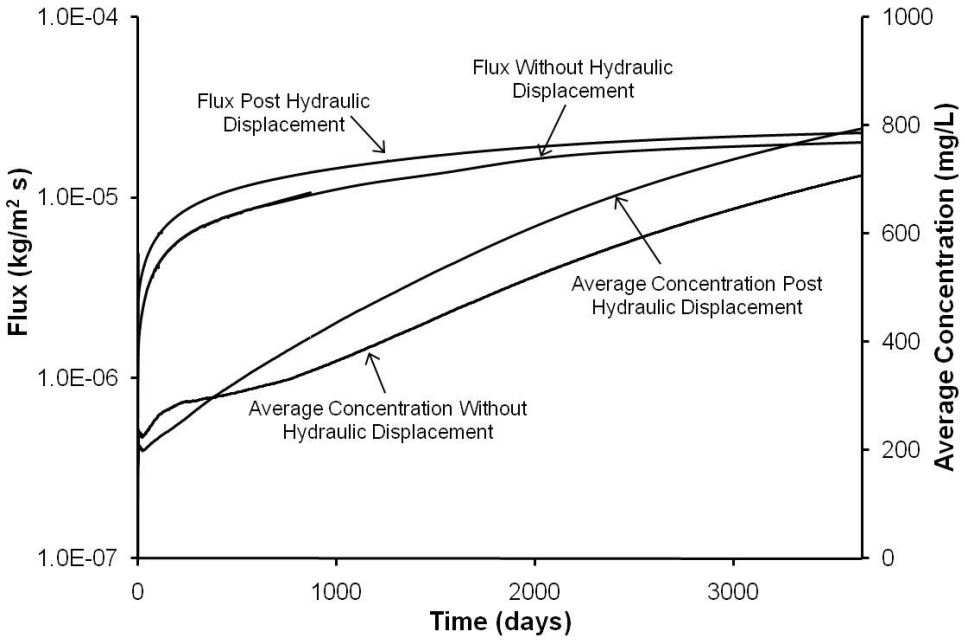

Figure 9 – Base case exit face TCE mass flux (log scale) and average exit face TCE concentration (linear scale) versus time with and without hydraulic displacement.

5.0 - Conclusions

Hydraulic displacement, also referred to as dual phase extraction and waterflooding, is a non-chemical and non-thermal remediation technology suitable for reducing DNAPL saturations and removing DNAPL pools from the subsurface. Because hydraulic displacement results in the depletion of DNAPL pools, it can be viewed as a mass removal technology suitable for stabilization of a DNAPL source zone, where stabilization is defined as reducing DNAPL saturations and reducing the risk of future pool mobilization. Hydraulic displacement involves increasing the hydraulic gradient within a source zone, thereby altering the capillary pressure distribution within pools, bringing about DNAPL mobilization and subsequent recovery at extraction wells.

High resolution numerical simulations illustrate that hydraulic displacement results in an increase in the amount of residual DNAPL present, which in turn results in increased solute concentrations in groundwater, an increase in the rate of DNAPL dissolution, and an increase in solute mass flux. A higher percentage of DNAPL recovery is associated with higher initial DNAPL release volumes, lower density DNAPLs, more heterogeneous porous media, and increased drawdown of groundwater at extraction wells. The fact that higher rates of recovery are associated with more heterogeneous porous media stems from the fact that larger contrasts in permeability provide for a higher proportion of capillary barriers upon which DNAPL pooling and lateral migration can occur. Across all scenarios evaluated in this study, the ganglia to pool (GTP) ratio generally increased from approximately 0.1 to between approximately 0.3 and 0.7 depending on the type of DNAPL, the degree of heterogeneity, and the imposed hydraulic gradient. The volume of DNAPL recovered as a result of implementing hydraulic displacement ranged from between 9.4% and 46.1% with the

largest percentage recovery associated with 1,1,1 TCA, the least dense of the three DNAPLs considered.

Literature Cited

Barry, D. A., H. Prommer, C. T. Miller, P. Engesgaard, A. Brun, and C. Zheng (2002), Modelling the fate of oxidisable organic contaminants in groundwater, *Advances in Water Resources*, 25(8-12), 945-983.

Bear, Jacob. 1972. *Dynamics of Fluids In Porous Media*. American Elsevier Publishing Company, New York.

Brusseau, M. L., Z. Zhang, N. T. Nelson, R. B. Cain, G. R. Tick, and M. Oostrom (2002), Dissolution of Nonuniformly Distributed Immiscible Liquid: Intermediate-Scale Experiments and Mathematical Modeling, *Environmental Science & Technology*, 36(5), 1033-1041.

Clement, T. P., 1997. RT3D - A Modular Computer Code for Simulating Reactive Multispecies Transport in 3-Dimensional Groundwater Systems (Version 1.0), 59 pp, Pacific Northwest National Laboratory, Richland, Washington 99352. PNNL-11720.

Clement, T. P., 2003. RT3D v2.5 Update Document, February, 20 pp, Battelle PNWD, http://bioprocess.pnnl.gov/rt3d.htm.

Clement, T. P., Y. Sun, B. S. Hooker, and J. N. Petersen, 1998. Modeling Multispecies Reactive Transport in Ground Water, Ground Water Monitoring & Remediation, 18(2), 79-92.

Craig, F.F. 1971. *The Reservoir Engineering Aspects of Waterflooding*. Society of Petroleum Engineers of AIME., New York.

Gerhard, J.I. and B.H. Kueper. 2003a. Capillary pressure characteristics necessary for simulating DNAPL infiltration, redistribution, and immobilization in saturated porous media. *Water Resources Research* 39, no. 8, pp. SBH 7-1 – 7-17.

Gerhard, J.I. and B.H. Kueper. 2003b. Influence of constitutive model parameters on the predicted migration of DNAPL in heterogeneous porous media. *Water Resources Research* 39 no. 10, pp. SBH 4-1 – 4-13.

Gerhard, J.I. and B.H Kueper. 2003c. Relative permeability characteristics necessary for simulating DNAPL infiltration, redistribution, and immobilization in saturated porous media. *Water Resources Research* 39 no. 8, pp. SBH 8-1 – SBH 8-16.

Gerhard, J. I., B. H. Kueper, and G. R. Hecox. 1998. The Influence of Waterflood Design on the Recovery of Mobile DNAPLs. *Ground Water* 36 no. 2, pp. 283-292.

Gerhard, J. I., B.H. Kueper, G. R. Hecox, and E. J. Schwarz. 2001. Site-Specific Design for Dual Phase Recovery and Stabilization of Pooled DNAPL. *Groundwater Monitoring and Remediation* 21 no. 2, pg. 71-88.

Grant, G., and J. Gerhard (2007a), Simulating the dissolution of a complex dense nonaqueous phase liquid source zone: 1. Model to predict interfacial area, *Water Resources Research*, 43(12), W12410.

Grant, G., and J. Gerhard (2007b), Simulating the dissolution of a complex dense nonaqueous phase liquid source zone: 2. Experimental validation of an interfacial area-based mass transfer model, *Water Resources Research*, 43, W12409.

Imhoff, P. T., P. R Jaffé and G. F. Pinder. 1993. An experimental study of complete dissolution of a nonaqueous phase liquid in saturated porous media. *Water Resources Research* 30, no. 2, pg. 307-320.

Kueper, B.H., and E.O. Frind. 1991. Two phase flow in heterogeneous porous media: 1. Model development, *Water Resources Research* 27, no. 6, pg. 1049-1057.

Kueper, B.H., G.P. Wealthall, J.W.N. Smith, S.A. Leharne, and D.N. Lerner. 2004. *An illustrated handbook of DNAPL transport and fate in the subsurface.* Environment Agency: Bristol, UK.

Lyman, Warren J., William F. Reehl and David H. Rosenblatt. 1982. *Handbook of Chemical Property Estimation Methods. Environmental Behavior of Organic Chemicals*. McGraw-Hill, New York.

Miller, C. T., M. M. Poirier-McNeill and A. S. Mayer. 1990. Dissolution of Trapped Nonaqueous Phase Liquids: Mass Transfer Characteristics. *Water Resources Research* 26, no. 11, pg. 2783-2796.

Nambi, I. M. and S. E. Powers. 2003. Mass transfer correlations for nonaqueous phase liquid dissolution for regions with high initial saturations. *Water Resources Research* 39, no. 2, pg. 4-1 – 4-11.

Parker, J. C., and E. Park (2004), Modeling field-scale dense nonaqueous phase liquid dissolution kinetics in heterogeneous aquifers, *Water Resources Research*, *40*(W05109), 1-12.

Powers, S. E., L. M. Abriola and W. J. Weber, Jr. 1992. An Experimental Investigation of Nonaqueous Phase Liquid Dissolution in Saturated Subsurface Systems: Steady State Mass Transfer Rates. *Water Resources Research* 28, no. 10, pg. 2691-2705.

Powers, S. E., L. M. Abriola and W. J. Weber, Jr. 1994. An experimental investigation of nonaqueous phase liquid dissolution in saturated subsurface systems: Transient mass transfer rates. *Water Resources Research* 30, no. 2, pg. 321-332.

Robin, M; A. Gutjahr, E. Sudicky, J. Wilson. 1993. *Water Resources Research*, 29, no. 7, pg. 2385-2397

Saba, T. and T.H. Illangasekare. 2000. Effect of groundwater flow dimensionality on mass transfer from entrapped nonaqueous phase liquid contaminants. *Water Resources Research* 36 no. 4, pg. 971-979.

Sale, T. and D.Applegate. 1997. Mobile NAPL Recovery: Conceptual, Field and Mathematical Considerations. *Ground Water* 35, no. 3, pg. 418-426.

West, M. R., G. P. Grant, J. I. Gerhard, and B. H. Kueper, 2008. The influence of precipitate formation on the chemical oxidation of TCE DNAPL with potassium permanganate, *Advances in Water Resources*, 31(2), 324-338.

Wilke, C.R. and P. Chang. 1955. *Correlation of Diffusion Coefficients in Dilute Solutions*. AIChE, 1(2): 264-270.

Willhite, G. Paul. 1986. *Waterflooding*. The Society of Petroleum Engineers, Richardson, Texas.

Zheng, C. (1990), MT3D, A modular three-dimensional transport model for simulation of advection, dispersion and chemical reactions of contaminants in groundwater systems, Report to the U.S. Environmental Protection Agency, Robert S. Kerr Environmental Research Laboratory, Ada, OK., edited.

Appendix C.2

The Influence of Precipitate Formation on the Chemical Oxidation of TCE DNAPL with Potassium Permanganate

Abstract

A three-dimensional two-phase flow model is coupled to a non-linear reactive transport model to study the efficacy of potassium permanganate treatment on dense, non-aqueous phase liquid (DNAPL) source removal in porous media. A linear relationship between the soil permeability (k) and concentration of manganese dioxide precipitate ($[MnO_{2(s)}]$), $k = k_o + S_{rind} [MnO_{2(s)}]$, is utilized to simulate nodal permeability reductions due to precipitate formation. Using published experimental column studies, an S_{rind} = -5.5 x 10^{-16} m^2 L/mg was determined for trichloroethylene (TCE) DNAPL. This S_{rind} was then applied to treatment simulations on three-dimensional TCE DNAPL source zones comprising either DNAPL at residual saturations, or DNAPL at pooled saturations.

DNAPL dissolution without oxidation treatment, simulated using equilibrium and the Nambi and Powers (2003) mass transfer expression, required 31 and 36 years, respectively, to eliminate the residual source zone. For equilibrium dissolution with continuous treatment and no precipitate influence (S_{rind} = 0 m^2 L/mg), the residual source zone was removed after 11 years. However, when considering the precipitate influence (i.e., S_{rind} = -5.5 x 10^{-16} m^2 L/mg), 21 years of treatment were necessary to remove the DNAPL. When considering pulse treatments of 1 and 2 years duration followed by only dissolution, approximately 36 and 38 years, respectively, were required before the source zone was depleted, suggesting that there is no benefit to pulse treatment. Similar trends were observed when allowing 10 years of dissolution prior to treatment initiation. The treatment behaviour of the pooled TCE source, while slightly more efficient than the residual saturation source, was similar.

Based on simulation findings, the precipitate (rind) formation significantly influences DNAPL treatment with permanganate; the most significant reductions in efficacy were observed for single pulse treatments (of 1 and 2 years), which exhibited times to source depletion similar to the case of dissolution without treatment.

1.0 Introduction

A variety of technologies have been proposed for the remediation of sites impacted by dense, non-aqueous phase liquids (DNAPLs). Their effectiveness and the benefits of partial mass removal have been recently examined by a variety of authors including Sale and McWhorter (2001), Saenton et al. (2002), Rao and Jawitz (2003), Seol et al. (2003), and Jawitz et al. (2005). The efficacy of *in situ* DNAPL source zone treatment with chemical oxidation is highly dependent on heterogeneity (Ibaraki and Schwartz, 2001) and the presence of organic materials in the aquifer (Yan and Schwartz, 2000). With respect to chlorinated ethene and potassium permanganate ($KMnO_4$) systems, the reaction products have been found to significantly reduce soil permeability and treatment efficiency (e.g., Schnarr et al., 1998). During fractured rock treatment studies, Tunnicliffe and Thomson (2004) suggested that reaction products formed adjacent to the DNAPL (potentially encapsulating portions of the DNAPL) reduced mass transfer rates. As a result, complete source removal potentially cannot be achieved in a reasonable time with the technology. The goal of this work is to explore some of these issues as they pertain to the treatment of trichlorethene (TCE) with permanganate in porous media.

The modeling of DNAPL-permanganate processes in complex sub-surface domains must incorporate the system specific influences of chemistry, heterogeneity, differential diffusion, and reaction kinetics. The main chemical oxidation approaches, associated chemistry, and practical limitations have recently been reviewed by Seol et al. (2003). For the purpose of this study subsequent discussion is limited to chemical

oxidation of DNAPLs by potassium permanganate. The stoichiometry of chemical oxidation of TCE by potassium permanganate can be described as (Seol et al., 2003; Crimi and Siegrist, 2004):

$$C_2HCl_3 + 2MnO_4^- \Rightarrow 3Cl^- + 2CO_2 + H^+ + 2MnO_{2(s)} \quad (1)$$

One- and two-dimensional laboratory studies have consistently demonstrated the formation of manganese dioxide ($MnO_{2(s)}$) precipitate (or 'rind') and its ability to encapsulate NAPL (MacKinnon and Thomson, 2002; Schnarr et al., 1998; Schroth et al., 2001; Conrad et al., 2002). *In situ* field experiments with chemical oxidation have reported DNAPL mass destruction and post-treatment concentration rebound, but have not provided significant detail with respect to rind formation (Schnarr et al., 1998; Seigrist et al., 1999; Jordana et al., 2005). The rind is sparsely soluble in non-acidic groundwater (Li and Schwartz, 2004a). Li and Schwartz (2004 a,b) investigated the composition and characteristics of the rind and methods to solubilize the precipitate using acidic solutions. While ultimately successful, the dissolution efficiency of the rind was poor, requiring 20 to 45 times more acid than predicted from stoichiometry. The authors suggested that heterogeneity and insufficient contact times lead to flow bypassing and poor sweep efficiency.

In heterogeneous porous media, permeability can vary over several orders of magnitude. As a result, there will be some regions of transport dominated by advection and others by diffusion. The published free water diffusion coefficient (D^o) for TCE is

approximately 40% less than that of MnO_4^- (CRC, 2004). Therefore, all other conditions being equal, the permanganate ions will migrate further than TCE solute for a given time under diffusive transport. Siegrist et al. (1999) and Struse et al. (2002) observed significant diffusive transport of permanganate in low permeability media with hydraulic conductivity less than 10^{-5} cm/s.

Yan and Schwartz (1999) and Huang et al. (2001) experimentally determined second-order rate constants for the oxidation of PCE, TCE, cis-DCE, trans-DCE, and 1,1-DCE in the presence of $KMnO_4$. In other studies, Hood et al. (2000) and Dai and Reitsma (2004), examined PCE degradation kinetics. These studies assumed and demonstrated that the reactions between $KMnO_4$ and chlorinated ethenes are second-order when $KMnO_4$ is always in excess. The assumption of excess $KMnO_4$ may not be valid in subsurface systems with significant dispersion, low $KMnO_4$ injection concentrations, low injection duration, and high rates of $KMnO_4$ consumption. Dai and Reitsma (2004) observed that the reaction rate is highly dependent on permanganate concentrations between 200 mg/L and 5000 mg/L. Hood et al. (2000) found that the reaction rate for PCE decreased for PCE concentrations below 0.5 mg/L and suggested that, in some circumstances, *in situ* treatment times could be greater than those times predicted using published rate constants. Both Yan and Schwartz (1999) and Dai and Reitsma (2004) demonstrated the successful prediction of the second-order constant for TCE and PCE at non-standard temperatures using the Arrhenius equation. This observation is helpful for estimating rate constants appropriate to groundwater systems.

To date, only a few reactive transport models have been developed to examine DNAPL source zone treatment by chemical oxidation. Zhang & Schwartz (2000) conducted simulations that reasonably matched one-dimensional experiments by Schnarr et al. (1998) and three-dimensional field experiments. A key aspect of that modelling work was examining the influence of organic aquifer materials on treatment efficiency. Ibaraki and Schwartz (2001) conducted two-dimensional simulations of a chemical oxidation injection/withdrawal system, with a particular focus on incorporating density-driven treatment characteristics and studying the influence of soil heterogeneity on sweep efficiency.

This study examines the benefits and challenges of TCE source zone remediation by chemical oxidation with potassium permanganate ($KMnO_4$). A numerical model capable of simulating two-phase flow, with NAPL dissolution and non-linear reactive contaminant transport is introduced. Novel model features include multiple species diffusion and the formation of chemical oxidation precipitates (i.e., rind) accompanied by a corresponding reduction in soil permeability within a transient flow field. The model is calibrated to published one-dimensional column experiments. Subsequently, the calibrated model is employed to investigate the influence of MnO_2(s) rind formation on mass transfer from both residual and pooled three-dimensional DNAPL source zones using multiple species advection, dispersion and diffusion. Of particular interest is the influence of rind formation on *in situ* chemical oxidation treatment efficiency. The use of numerical simulation allows the long term performance (i.e., decades) of the technology to be examined in a cost-effective manner.

2.0 Model Formulation

The model developed for this work (DNAPL3D-RX) is a coupling of the three-dimensional two-phase flow model (DNAPL3D) (Gerhard et al., 1998, 2001; Gerhard and Kueper, 2003 a,b,c) and RT3D, a three-dimensional multi-species contaminant transport model with non-linear kinetic reactions (Clement,1997; Clement et al.,1998). This coupling was executed using a split operator approach similar to Grant (2005). Within a time step, DNAPL migration is initially simulated using DNAPL3D. The contaminant solute is then added to the aqueous phase at nodes with DNAPL present via equilibrium or non-equilibrium mass transfer routines. RT3D is then employed within the same time step to simulate advection, dispersion and reactions of the solute. Finally, the phase saturations are updated at the end of the time step in accordance with the amount of mass transferred from the DNAPL to the aqueous phase.

2.1 Multiphase Flow

The governing equations for two phase flow are (Gerhard and Kueper, 2003c):

$$\frac{\partial}{\partial x_i}\left[\frac{k_{ij}k_{r_W}}{\mu_W}\left(\frac{\partial P_W}{\partial x_j}+\rho_W g\frac{\partial z}{\partial x_j}\right)\right]+S_W(\alpha+\theta\beta)\frac{\partial P_W}{\partial t}-\theta\frac{\partial S_W}{\partial t}=0\,,\qquad i,j=x,y,z \tag{2}$$

$$\frac{\partial}{\partial x_i}\left[\frac{k_{ij}k_{r_{NW}}}{\mu_{NW}}\left(\frac{\partial(P_W+P_c)}{\partial x_j}+\rho_{NW}g\frac{\partial z}{\partial x_j}\right)\right]+(1-S_W)(\alpha)\frac{\partial P_W}{\partial t}+\theta\frac{\partial S_W}{\partial t}=0\,,\quad i,j=x,y,z \tag{3}$$

where P is the pressure {M L^{-1} T^{-2}}, P_C is the capillary pressure {M L^{-1} T^{-2}}, k_{ij} is the intrinsic permeability tensor {L^2}, k_r is the relative permeability, μ is the dynamic viscosity {M L^{-1} T^{-1}}, ρ is the fluid density {M L^{-3}}, θ is the porosity, S is the phase saturation, g is gravitational acceleration, α is the porous medium compressibility {M^{-1} L T^2}, β is the wetting phase compressibility { M^{-1} L T^2}, t is time {T}, and x, y, z denote spatial coordinates {L}. The subscripts W and NW specify the wetting and non-wetting phase, respectively. The multiphase flow component of the coupled model employs detailed submodels of capillary pressure and relative permeability, incorporating hysteresis and trapping mechanisms that have been validated against physical experiments in one (Gerhard and Kueper, 2003a,b) and two (Grant et al., 2007a,b) dimensions. It has also been verified against the analytical solution of McWhorter and Sunada (1990) and validated against a two dimensional heterogeneous laboratory experiment for drainage conditions (Kueper and Frind, 1991).

The multiphase flow component of the model permits the accurate simulation of NAPL migration during release, redistribution, and remediation with various technologies. During treatment, the hydraulic gradients can be enhanced relative to natural conditions, and soil properties can be modified to account for reaction byproducts. The multiphase flow simulator is integral to capturing the physics of the NAPL-porous medium system.

2.2 Interphase Mass Transfer

Interphase mass transfer is an important component of the chemical oxidation process. When utilizing models to simulate the dissolution observed in experimental

work, it is difficult to predict *a priori* whether to use an equilibrium or non-equilibrium approach, and which (if any) of the numerous non-equilibrium approaches is most representative. It is often most elucidating to select several appropriate approaches and test them against an experimental dataset. For model calibration purposes, the work presented here considers both equilibrium and non-equilibrium dissolution correlation expressions to the simulation of TCE DNAPL dissolution in a one-dimensional column experiment.

Non-equilibrium behaviour can be attributed to both chemical (e.g., rate-limited dissolution) and physical (e.g., flow bypassing) processes (Sale and McWhorter, 2001). The bulk of work examining rate limited mass transfer has been conducted using one-dimensional column experiments (e.g., Miller et al., 1990; Powers et al., 1992, 1994, 1998; Imhoff et al., 1993; Geller and Hunt, 1993), a limited number of two-dimensional experiments (e.g., Seagren et al., 1999; Saba and Illangesakare, 2000; Nambi and Powers, 2003), and a few three-dimensional field trials (e.g., Rivett and Feenstra, 2005). Due to the complexity of NAPL dissolution, conceptual models have generally not been derived to describe the mechanisms, and the core of research has progressed by developing empirical expressions that capture the general equilibrium/non-equilibrium dissolution behaviour for a particular system. Most models are derived using the steady-state approximation of the thin stagnant film model:

$$\frac{\partial C}{\partial t} = k_{la} a^n (C_s - C) = K_l (C_s - C) \tag{4}$$

where C_s is the thermodynamic equilibrium solubility of the NAPL species in aqueous solution $\{ML^{-3}\}$, C is the average solute concentration in the aqueous solution $\{ML^{-3}\}$, a^n is the specific interfacial area between the NAPL phase and the aqueous phase $\{L^2L^{-3}\}$, t is time $\{T\}$, k_{la} is the average mass transfer coefficient for the NAPL-aqueous phase interface $\{LT^{-1}\}$, and K_l is a lumped kinetic mass transfer coefficient $\{T^{-1}\}$. The mass transfer coefficient K_l is typically related to a dimensionless Sherwood coefficient (*Sh*), which in turn is related to other dimensionless parameters (e.g., Reynolds number, Schmidt number). While these expressions have elucidated system characteristics that are pertinent to the dissolution process, they are not universally applicable, thus limiting their utility to general systems (Mayer and Miller, 1996; Sale, 1998; Zhu and Sykes, 2000; Grant and Gerhard, 2004). The *Sh* is typically correlated to K_l by:

$$Sh = \frac{K_l (d_{50})^2}{D^o} \tag{5}$$

where d_{50} is the mean grain size diameter $\{L\}$ and D^o is the free-water diffusion coefficient $\{L^2T^{-1}\}$. In this work, the correlation expressions by Miller et al. (1990) and Nambi and Powers (2003) are utilized to assess the potential influence of non-equilibrium dissolution on chemical oxidation processes in a one-dimensional column experiment. The flow rates and saturations used in the development of these empirical expressions are representative of the simulations conducted herein; these expressions also provide some contrast with respect to dimensionality given their one- and two-dimensional configurations. The Sherwood correlation expressions by Miller et al. (1990) and Nambi and Powers (2003) are, respectively:

$$Sh = 12 \ \mathrm{Re}^{0.75} \theta_{NW}^{0.6} \ Sc^{0.5} \tag{6}$$

$$Sh = 37.15 \ S_{NW}^{1.24} \mathrm{Re}^{0.61} \tag{7}$$

where Re is the Reynolds number (Re = $d_{50} \rho_W v / \mu_W$), θ_{NW} is the volumetric content of non-wetting phase, S_{NW} is the non-wetting phase saturation, Sc is the Schmidt number ($Sc = \mu_W / (\rho_W D^o)$), d_{50} is the mean particle diameter {L}, v is mean pore velocity {LT^{-1}}, and D^o is the free-water molecular diffusion coefficient {L^2T^{-1}}.

Following each DNAPL migration time-step of DNAPL3D-RX, each of the mass transfer parameters is calculated at nodes with $S_{NW} > 0$. For equilibrium conditions, nodes with NAPL are assumed to have a concentration equal to solubility (C_s), while equations (4) through (7) are utilized for the rate-limited cases. The concentration fields are then passed into RT3D to simulate solute transport. The dissolution and non-reactive transport components of the model have been tested and assessed in two-dimensional heterogeneous porous media experiments (Grant and Gerhard, 2007c, 2007d) for both equilibrium and non-equilibrium mass transfer from complex DNAPL source zones.

2.3 Solute Transport

The governing equation of contaminant transport of the mobile species is (Clement, 1997; and Clement et al., 1998):

$$\frac{\partial(\theta C_m^n)}{\partial t} = \frac{\partial}{\partial x_i}\left(\theta D_{ij}^n \frac{\partial C_m^n}{\partial x_j}\right) - \frac{\partial}{\partial x_i}\left(\theta v_i C_m^n\right) + q_s C_s^n + \sum R_m \;,\; i,j = x,y,z \qquad (8)$$

while the immobile species governing equation is:

$$\frac{\partial(\theta C_{im}^n)}{\partial t} = \sum R_{im} \qquad (9)$$

where D_{ij} is the hydrodynamic dispersion tensor $\{L^2\ T^{-1}\}$, v_i is the average linear groundwater velocity $\{L\ T^{-1}\}$ obtained from the multiphase flow model, q_s is volumetric flux representing sources and/or sinks $\{T^{-1}\}$, R is the rate of all reactions $\{M\ L^{-3}\ T^{-1}\}$, and t is time $\{T\}$. The superscript n denotes the species number, while the subscripts m and im designate mobile and immobile species, respectively. The subscript s denotes a source or a sink. Note that DNAPL3D-RX additionally simulates multiple species diffusion, allowing the inclusion of unique diffusion coefficients for each mobile species (i.e., TCE and MnO_4^-). This feature is not available in RT3D and was added to DNAPL3D-RX to permit the differential diffusion of TCE solute and MnO_4^-.

Using a split-operator approach specific to the simulated transport processes (Clement, 1997; and Clement et al., 1998), the reaction equations of interest for TCE with permanganate are as follows (Zhang and Schwartz, 2000; Randwana, 2001; Mundle et al., 2007):

$$\frac{\partial[TCE]}{\partial t} = \frac{-K_{rxns}[TCE][MnO_4^-]}{R_{TCE}} \tag{10}$$

$$\frac{\partial[MnO_4^-]}{\partial t} = -2K_{rxns}[TCE][MnO_4^-] \tag{11}$$

$$\frac{\partial[Cl^-]}{\partial t} = 3K_{rxns}[TCE][MnO_4^-] \tag{12}$$

$$\frac{\partial[CO_2]}{\partial t} = 2K_{rxns}[TCE][MnO_4^-] \tag{13}$$

$$\frac{\partial[MnO_2]}{\partial t} = 2K_{rxns}[TCE][MnO_4^-] \tag{14}$$

where the square brackets [ ] denote molar concentration, K_{rxns} is the second-order reaction constant between aqueous TCE and MnO_4^- $\{M^{-1}\ L^3\ T^{-1}\}$, and R_{TCE} is the retardation factor for TCE,. For reasons provided later, CO_2 is considered an aqueous species, rather than a gaseous species for this study. The rind is designated as an immobile aqueous species: it undergoes reactions, but does not advect or disperse. It is recognized that this assumption is an approximation in that it may be possible for solid MnO_2 to migrate as a colloidal substance in some porous media systems.Further discussion of the rind behaviour is provided in the following section.

2.4 Representation of Rind Formation

It has been reported that manganese dioxide is transported and deposited as colloids (e.g., Li and Schwartz, 2004a; Randwana, 2001), and that subsequent rind formation has adverse consequences for the successful implementation of chemical oxidation (MacKinnon and Thomson, 2002; Conrad et al., 2002). The modeling of colloidal transport is complex, and particular to the species and porous media properties. The inherit physiochemical characteristics that influence the behavior of the colloids are often captured with macroscopic coefficients and simplified kinetic equations, which are evaluated using laboratory experiments (e.g., Randwana, 2001; Bekhit and Hassan, 2005; Bradford and Bettahar, 2005). In order to apply these approaches to a TCE-permanganate system, the experimental data set must have a detailed record of the influent and effluent TCE, permanganate, and manganese dioxide concentrations. While thorough one-dimensional column experiments have been conducted by some researchers (e.g., Schnarr et al., 1998; Schroth et al., 2001; Huang et al., 2002), the data necessary to calibrate a representative colloidal transport model has not been obtained. However, experimental and modeling work by Randwana (2001) for PCE and permanganate demonstrated that rind formation, and the subsequent degree of permeability reduction, was a function of fluid velocity and greatly exceeded the magnitude predicted using published colloidal transport models: when using 3 cm long sand pack columns with a hydraulic conductivity of 0.008 to 0.013 cm/s, 5 g/L of $KMnO_4$, 61 mg/L of PCE, and a hydraulic gradient of 1.0 (the maximum was 8.0), complete plugging occurred with a period of 4 to 8 days. Given that PCE and permanganate are considerably less reactive than TCE (approximately one order of magnitude), it is anticipated that plugging effects may be more significant for the latter species. Although the PCE and permanganate

concentrations used by Randwana (2001) were representative of field conditions, the hydraulic gradients of 1 to 8 are considered extreme. For the case of much lower hydraulic gradients (0.001 to 0.01) commonly used in the field, and given the degree of uncertainty regarding the related colloidal transport mechanisms, it is reasonable to assume that colloidal transport will be minimal, and that manganese dioxide can be considered as an immobile species for the purposes of modeling. Conrad et al. (2002) conducted two-dimensional visualization TCE-permanganate experiments in heterogeneous porous media using a hydraulic gradient of 0.007; upon inspection, it was visually observed that the bulk of the rind encapsulated the TCE sources zones. Similar deposition behaviour was also visually observed in the two-dimensional experiments by Li and Schwartz (2004b).

The formation of the rind and its influence on the flow field are incorporated into the model by modifying the intrinsic permeability of the porous medium as a function of aqueous rind concentration. A pseudo linear relationship is adopted for each node:

$$k = (k_o) + S_{rind}\,[MnO_2] \tag{15}$$

where k is the nodal permeability at the time of interest, k_o is the original permeability of the node, and S_{rind} is the slope of the assumed linear relationship between k and the MnO_2 concentration. Equation (15) is kinetic; the concentration of MnO_2 is obtained from (14), whose reaction rate and order has been independently determined via laboratory batch experiments (Yan and Schwartz, 1999; Huang et al., 2001). Due to aforementioned

uncertainty regarding MnO_2 colloidal transport, the macroscopic lumped-reaction term S_{rind} is utilized and calibrated to experimental conditions; it is analogous to the implementation of the term K_l in (4) (i.e., Miller et al. (1990) stated that K_l is function of ten different dimensionless parameters, yet it is typically simplified to one or two). Although explained in detail later, S_{rind} is evaluated against a one-dimensional column experiment using: (i) experimental column effluent concentrations, (ii) stoichiometry in (1), (iii) equations (10) to (14), (iv) kinetically modelled MnO_2 concentration, and (v) experimental column pressure head values. S_{rind} is a bulk parameter related to flow characteristics, reaction kinetics, and species concentration, but decoupled from the explicit influence of geochemistry and other influences that have not been ascertained in sufficient detail for discrete model implementation. Hence, (15) implicitly captures the net effect of rind formation by altering the overall permeability.

While the concentrations of aqueous CO_2 are simulated, the permeability reduction due to CO_2 gas formation is not considered in this study; in this sense, the current approach represents a conservative estimate of permeability reduction where the buffering capacity of the system maintains CO_2 as dissolved bicarbonate (HCO_3^-) above neutral pH (Randwana, 2001; Schroth et al., 2001; Drever, 2002). In contrast, unbuffered experiments have yielded relatively more severe clogging due to CO_2 gas formation (Schroth et al., 2001). Hence, CO_2 does not appear in (15). In addition, the porosity is constant throughout the domain and does not change with reducing permeability; although research regarding porosity change due to MnO_2(s) deposition is limited, this

assumption is consistent with the experimental findings of Struse et al. (2002) for low permeability silty-clay media.

2.5 Metrics for Source zone Study

The DNAPL mass removal and the total boundary mass discharge are the two metrics utilized in this study to assess the performance of TCE DNAPL remediation by permanganate. Reductions of mass discharge and/or increases of mass removal are typically desirable when conducting a remediation program. The instantaneous DNAPL mass is calculated using saturations outputted by the two-phase flow model, the non-wetting phase density, and the nodal volume. The total boundary mass discharge (M_{ft}) $\{M\ T^{-1}\}$ is calculated as per Bockelmann et al. (2003), where M_{ft} is the cumulative sum of all instantaneous mass discharges for each boundary node:

$$M_{ft} = \sum_{i=1}^{n} C_i q_i A_i \tag{16}$$

where i denotes an individual node, q is the Darcy flux $\{L\ T^{-1}\}$, and A is the cell area $\{L^2\}$ centered at the node.

2.6 Verification to Analytical Solutions

The DNAPL3D-RX chemical oxidation model was tested against published analytical solutions to verify its accuracy. Analytical solutions used for comparison purposes include: 1) one-dimensional semi-infinite advection and dispersion in homogeneous porous media with sorption and first-order decay (Bear, 1979); 2) one-

dimensional semi-infinite advection and dispersion in homogeneous porous media with steady-state, non-equilibrium mass transfer (Miller et al., 1990); 3) advection, dispersion, linear sorption and first-order decay of a tracer in an infinite one-dimensional column of homogenous porous media (Bear, 1979); 4) two-dimensional advection and dispersion in homogeneous porous media with linear sorption and first-order decay (Batu, 1989); and, 5) one-dimensional diffusion in porous media (Crank, 1975) to evaluate simultaneous multiple species diffusion with different diffusion coefficients. In all cases, numerical model results were in agreement with the analytical solution.

3.0 Model Calibration

One-dimensional column experiments by Schroth et al. (2001) were used to validate and calibrate the model: to date, this is the most useful dataset available for evaluating the influence of rind formation on permeability. Using residual TCE DNAPL, Schroth et al. (2001) conducted one dissolution experiment and two chemical oxidation experiments with potassium permanganate. Experiment 3 (buffered chemical oxidation) by Schroth et al. (2001) was utilized for the calibration, as the influence of CO_2 gas formation on permeability reduction in this experiment was minimal. Note that Experiment 2 (unbuffered treatment) was terminated at approximately 33 hours due to excessive permeability reductions and only a partial data set is available: at 30 hours, the Experiment 2 increase in pressure head due to permeability reduction from CO_2 and rind formation was three orders of magnitude greater than Experiment 3 over the same time.

A schematic of these experiments is provided in Figure 1 and the system and simulation parameters are listed in Table 1. Effluent concentrations were monitored for TCE, chloride (Cl^-), and permanganate (MnO_4^-), and were subsequently used to assess model behaviour. Constant flow conditions were maintained in the column throughout the duration of the experiment. Seven ports were located along the column to monitor TCE saturations and wetting phase pressures. This feature was particularly useful, as Schroth et al. (2001) were interested in assessing permeability reductions due to MnO_2(s) rind formation. These data were utilized to calibrate the slope of the assumed linear relationship (S_{rind}) identified in (15).

Despite the utility and thoroughness of work by Schroth et al. (2001), this dataset does have some shortcomings with respect model calibration. In Experiment 3, the system was buffered with a Na_2HPO_4 solution, which (to some degree) may have yielded stoichiometry somewhat dissimilar to (1). The authors also visually observed a brownish colour to the effluent prior to permanganate breakthrough, which they hypothesized could be due colloidal transport or the reduction of MnO_4^- to Mn_2^+; there also were discrepancies with Cl^- mass balance. That being noted, this is the most complete data set published to date. The authors did not resolve any of the foregoing issues, but did observed a 53% reduction in permeability during chemical oxidation (compared to a 96% reduction in Experiment 2) and a general lack of CO_2 gas formation. Given the uncertainty surrounding geochemistry, but high resolution of the pressure head and effluent data sets, (15) was deemed the most reasonable approach. Again, in light of the

permeability reductions and failure of Experiment 2, the use of Experiment 3 and (15) will yield a highly conservative approximation of the rind formation.

Simulations for only dissolution are presented in Figure 2. These simulations were conducted using equilibrium and the two non-equilibrium expressions (Nambi and Powers, 2003, and Miller et al., 1990) to elucidate the dissolution kinetics of the system. In the absence of treatment (only dissolution – Experiment 1 by Schroth et al., 2001), the expression by Nambi and Powers (2003) was a superior fit to the column effluent data when compared to equilibrium dissolution and the expression by Miller et al. (1990). The latter two expressions over-predicted dissolved phase concentrations, with Miller et al. (1990) and equilibrium yielding nearly identical breakthrough curves.

Measured effluent TCE concentrations (Schroth et al., 2001) were compared to the predicted effluent concentrations of DNAPL3D-RX in Figure 3 for the case of chemical oxidation with a buffered potassium permanganate solution (i.e., Schroth et al., 2001, Experiment 3). In accordance with the experimental methodology of Schroth et al. (2001), the chemical oxidation simulations comprise 87 hours of potassium permanganate injection at a concentration of 790 mg/L. As indicated in Table 1, Schroth et al. (2001) measured an effective TCE solubility of 829 mg/L in the buffered solution.

In an effort to reproduce the data sets, both the reaction constants (K_{rxns}) reported by Yan and Schwartz (1999) and Huang et al., (2001) (0.65 $M^{-1}s^{-1}$ or 0.8 $M^{-1}s^{-1}$, respectively) were employed. It can be observed in Figure 3 that utilizing either K_{rxns} =

0.65 $M^{-1}s^{-1}$ or 0.8 $M^{-1}s^{-1}$, in conjunction with either equilibrium or rate-limited dissolution, produces a range of model outputs. The cases of equilibrium dissolution and rate-limited dissolution with Miller et al. (1990) behave similarly with higher concentrations than Experiment 3 for the bulk of the experiment, but accurately simulating the time to complete TCE removal. The application of Nambi and Powers (2003) accurately reproduces the earlier-time behaviour of Experiment 3, but does not provide a reasonable fit to data at late-time due to excessive tailing. Although the Experiment 3 data demonstrates that the application of chemical oxidation enhances the interphase mass transfer as theoretically proposed by Reitsma and Dai (2001), the associated modelling suggests that correlation expressions developed for dissolution are system specific and potentially not applicable to reactive systems. It is further noted that the one-dimensional expression by Miller et al. (1990), while sufficient for this chemical oxidation experiment, may be inappropriate for two- (and three-) dimensional systems (Saba and Illangasekare, 2000).

Figure 4 plots normalized MnO_4^- effluent concentrations versus time for Experiment 3 (Scroth et al., 2001) and the model. The consumption of MnO_4^- is well-predicted using both K_{rxns} = 0.65 and 0.8 $M^{-1}s^{-1}$ in conjunction with either equilibrium dissolution or rate-limited dissolution utilizing the correlation of Miller et al. (1990) when compared to the experimental data. Whether considering equilibrium dissolution or the correlation expression by Miller et al. (1990), the trend and timing of abrupt break-through is captured. The utilization of the expression by Nambi and Powers (2003) produces a more pronounced sigmoidal shape and excessive tailing. Given the

reasonable match between the equilibrium model results and the experimental data, only equilibrium conditions were considered for all subsequent simulations of the column experiments.

The data set from Experiment 3 was used to test, and subsequently calibrate, the parameter S_{rind} in (15) utilizing K_{rxns} = 0.39 to 0.8 $M^{-1}s^{-1}$ for equilibrium dissolution conditions. The former K_{rxns} value was determined using the Arrhenius equation (Yan and Schwartz, 1999; Dai and Reitsma, 2004). The reaction rate determined by Yan and Schwartz (1999) at 21°C (i.e., K_{rxns} = 0.65 $M^{-1}s^{-1}$) was calculated to be K_{rxns} = 0.39 $M^{-1}s^{-1}$ for 10°C. The Experiment 3 and simulation final wetting phase pressure heads and the observed and predicted changes in wetting phase pressure for each port are plotted in Figure 5 and 6, respectively. To achieve this fit, the model was executed iteratively until the Pearson correlation coefficient (r) between the experimental and model data reached a value of r = 0.99 in Figure 5. These results demonstrate that the application of equation (15) is satisfactory. The selection of S_{rind}, and its influence on the steady-state post-treatment wetting phase pressure field, is seemingly independent of K_{rxns} for the range of values considered (Figure 5): the relative pressure head difference between K_{rxn} = 0.39 to 0.8 $M^{-1}s^{-1}$ ranges from -0.1% to 0.6%. However, the simulated pressure heads are sensitive to the value of S_{rind} as demonstrated by the ± 25% range presented on Figure 5. Note that both Experiment 3 and the model exhibit considerable increases in wetting phase pressure at all seven ports (i.e., approximately 50 to 900 Pa) as shown in Figure 6. Although not presented here, the modeled pressure heads were compared to Experiment #3 at ports T1 (influent end) and T7 (effluent end). The model matched the steady-state

pressure at both ports (Figure 5), but the experimental pressure head increased rapidly with a sigmodial behavior at the inlet port (T1) compared with a much slower, rectilinear model behavior. In other words, the model is kinetically conservative when predicting the rate of permeability reduction.

The model reasonably captures the timing and general behaviour of the Schroth et al. (2001) one-dimensional column TCE experiments for chemical oxidation by potassium permanganate. A range of parameter values for K_{rxns} (i.e., values equal to, or slightly less than, those determined by Yan and Schwartz, 2000, and Huang et al., 2001) and S_{rind} generate representative results, with S_{rind} being independent of the K_{rxns} values tested. When the absence of rind is simulated (S_{rind} = 0 m^2 L/mg), the model produces an excellent match to the pre-treatment Experiment 3 pressure head data. Utilizing S_{rind} = -5.5 x 10^{-16} m^2L/mg for K_{rxns} = 0.39 to 0.80 $M^{-1}s^{-1}$ yields a good match to the experimental pressure head results. It should be noted that when considering (15), the aforementioned S_{rind} value yields an 'apparent' maximum [$MnO_{2(s)}$] of 1854 mg/L. In fact, the model is set up such that [$MnO_{2(s)}$] is unrestricted, but only $MnO_{2(s)}$ concentrations up to 1854 mg/L contribute to the reduction in permeability. The approach identified in (15) produces a good 'average' match to the data for all seven ports.

It is worthwhile summarizing the salient outcomes of the calibration exercise. Equation (15) uses a single lumped parameter (S_{rind}) that relates MnO_2 concentration, wetting phase pressure head, and a chlorinated ethene reaction rate to a corresponding reduction in permeability. Using (15), DNAPL3D-RX was tested against the laboratory Experiment 1

by Schroth et al. (2001). Using a number of different mass transfer routines, the model was able capture the effluent concentrations of the dissolution experiment. More importantly, the model was calibrated to, and successfully captured, the pressure head and concentration behaviour of the buffered TCE-permanganate Experiment 3. Equation (15) is highly conservative in many respects, and can be easily modified for the calibration to, and simulation of, a different data set of sufficient resolution. Although Schroth et al. (2001) encountered several difficulties during Experiment 3, (15) utilizes a single calibration parameter, thus capturing the overall behavior of the system. Notable conservative aspects of the calibration exercise include: (i) Schroth et al. (2001) demonstrated that the unbuffered chemical oxidation of TCE (Experiment 2) yielded pressure head increases approximately 1000-fold greater than the buffered system (Experiment 3); (ii) the rate of pressure increase for the unbuffered Experiment 2 is significantly greater than Experiment 3; (iii) the influence of MnO_2 concentration on modeled permeability is limited to 1854 mg/L; and, (iv) equation (15) employs (1) and (10) through (14), but utilizes the ensemble permeability from Experiment 3.

4.0 Numerical Simulations

The findings from the one-dimensional column simulations were applied to three-dimensional simulations of chemical oxidation of a single TCE source zone. Two cases are considered: (i) a simple block of residual TCE (Figure 7a), and (ii) a finite-volume surface release resulting in a final distribution that includes both pooled and residual TCE DNAPL (Figure 7b). Due to computational demands, the bulk of the simulations are conducted using case (i). The system parameters are listed in Table 1. The case (i)

source zone contained 2.981 kg of TCE DNAPL at a residual non-wetting phase saturation of 20% of pore space, while case (ii) comprises a TCE DNAPL mass of 2.952 kg with non-wetting phase saturations ranging from 1 to 40%. The domain configuration and nodal discretization are identical for both cases; only the shape and degree of saturation of the TCE DNAPL source zone differs.

Case (ii) was generated using a constant saturation point release at the top center of the domain until 2.952 kg of TCE was present. The source was then terminated and the DNAPL was allowed to migrate and redistribute. This resulted in 6.1% of the total nodes invaded by DNAPL (4001 nodes), with 8.2% of invaded nodes (329 nodes) at residual saturations between 1-14%. The remaining 91.8% of invaded nodes (3672 nodes) were at non-residual/pooled saturations. The dissolution and chemical oxidation were initiated only after the DNAPL was hydraulic stable, as depicted in Figure 13.

The simulations were designed with a focus on assessing the influence of rind formation on the efficacy of DNAPL removal and concurrent downstream boundary mass discharges. Although the configurations are idealized, they capture the essential physics of an *in situ* source zone, while neglecting the effects of sorption, heterogeneous soil structure, organic carbon consumption, and non-symmetrical flow in the *x*-*z* plane. Stated otherwise, the simulations have been designed to assess the influence of rind formation in the absence of other, potentially complicating processes. The two-phase flow simulator component of the model resolves local changes in wetting phase relative permeability (i.e., the flow field) due to DNAPL dissolution. The permanganate is introduced by

specifying the entire upstream boundary face as a constant concentration source. To optimize the effectiveness of treatment, a $KMnO_4$ inlet concentration of 5000 mg/L was utilized for all cases. A reaction constant of K_{rxns} = 0.39 $M^{-1}s^{-1}$ was selected for all simulations by utilizing the Arrhenius equation to adjust a K_{rxns} = 0.65 $M^{-1}s^{-1}$ for an assumed groundwater temperature of 10ºC (Yan and Schwartz, 1999 and Dai and Reitsma, 2004), and a S_{rind} = -5.5 x 10^{-16} m^2L/mg was selected based on the calibration presented in the section 3.0. In all cases, equilibrium dissolution is utilized due to nodal dimensions (Miller et al., 1990; Imhoff et al., 1993; Sale and McWhorter, 2001). As a check, dissolution of the residual block using both equilibrium dissolution and the expression of Nambi and Powers (2003) produced similar results, with the latter yielding a small degree of tailing relative to the former.

Three suites of simulations are considered for this work with the objective of assessing the influence of rind formation on DNAPL removal efficacy. Each of these suites comprises a set of similar simulations that are summarized in Table 2. Suites 1 and 2 examine the block of residual TCE (case (i)), while Suite 3 simulates treatment of the surface released TCE DNAPL (pooled and residual, case (ii)). In Suite 1, chemical oxidation with potassium permanganate in the absence of prior dissolution is considered (Simulations 2 through 5 in Table 2). In Suite 2, ten years of dissolution is permitted prior to initiating the treatment to represent remediation of a historical release (Simulations 7 through 10 in Table 2). Note that Simulation 1 (dissolution only) is utilized as the benchmark for treatment efficiency in Suite 1 and 2. In Suite 3, nine years of dissolution is permitted prior to initiating either continuous or one year of treatment on

the surface released TCE. These results are then compared to dissolution in the absence of treatment for the same release.

Details on the influence of rind formation on media tortuosity are sparse in the literature. Struse et al. (2002) conducted a number of treatment studies with TCE and $KMnO_4$ in low permeability soil cores for period of 30 to 60 days and reported no significant change in the soil pore size or apparent tortuosity. Therefore, a global tortuosity value of 0.7 (Bear, 1972) was used for all simulations and combined with the D^o values (Wilke and Chang, 1955) presented in Table 1 to arrive at effective diffusion coefficients.

4.1 Suite 1: Treatment Without Prior Dissolution

Figure 8 presents the TCE mass remaining versus time for the Suite 1 simulations (see Table 2). In the absence of rind formation, it is observed that 11 years of continuous treatment is necessary to completely deplete the source zone (Simulation 2). Treatment efficiency is greatly reduced when including rind formation, as depletion time is extended to approximately 21 years (Simulation 3). Treating the source zone for only brief periods of time does not appear to be beneficial. Treatment periods of only 1 or 2 years extends the source zone life span beyond dissolution alone, with complete depletion times of 36 years and 38 years, respectively (Simulations 4 and 5). The corresponding total boundary mass discharges are plotted in Figure 9. Note that in the absence of rind formation (Simulation 2) the time to achieve negligible mass discharge matches closely the time for DNAPL mass depletion for this simulation (11 years). However, these times are

observed to differ significantly when rind formation is incorporated. For continuous treatment with rind formation (Simulation 3), the total mass discharge becomes negligible after 11 years compared with the 21 years required to deplete the DNAPL. For the case of 2 years pulse oxidation (Simulation 5), the discharge is greatly reduced during treatment; however, once treatment has ceased, the mass discharge substantially rebounds and is only eliminated after 39 years compared with 32 years for dissolution without treatment (Simulation 1).

A visual inspection of Figure 10 illustrates the mechanisms controlling treatment efficacy. This figure is a time sequence for a simulation displaying S_{NW} and k. Once the permanganate treatment is initiated, rind formation ensues at the zones of high TCE solute concentrations. Typically, these zones surround the pools, blobs and ganglia where dissolution is occurring, but extend downstream as well. The rind significantly reduces the permeability of the porous medium, effectively encapsulating the source and resulting in flow bypassing of the dissolving source zone. Transport of dissolved constituents then becomes diffusion limited. If treatment is completely discontinued, the DNAPL is depleted solely by dissolution and diffusion through the rind encapsulation zone into the surrounding flow field. If treatment is continued, the differential diffusion rates between TCE and MnO_4^- favour source depletion as the diffusion coefficient for MnO_4^- is greater than that for TCE. Essentially, the combination of rind and permanganate can behave as an *in situ* diffusive chemical reactor.

4.2 Suite 2: Treatment With Prior Dissolution

Figure 11 presents a plot of TCE mass remaining versus time for treatment initiated after 10 years of dissolution (Suite 2 in Table 2). The trends observed in this figure are similar to Suite 1. In the presence of continuous treatment, 24 years are required for source depletion when considering rind formation (Simulation 7), while the absence of a rind yields a depletion time of 18 years (Simulation 6). Surprisingly, despite a 50% reduction in source mass at the time of chemical oxidation initiation (10 years), a pulse treatment time of 2 years (Simulation 9) extends the time of source depletion several years beyond that of only dissolution (35 years and 31 years, respectively). Similar complications are observed in Figure 12, where the pulse treatments (Simulation 8 and 9) yield tailing of the total boundary mass discharge when compared to only dissolution (Simulation 1). Although the degree of tailing in Suite 2 is less pronounced than Suite 1, the pulse treatment still has adverse consequences.

An examination of the mass balance provides some insight into treatment efficiency in three-dimensional heterogeneous domains. At the end of the two year injection period for Simulation 9, approximately 0.55 kg of TCE DNAPL was removed during chemical oxidation. During this same period 11.87 kg of MnO_4^- was injected, but only 1 kg of MnO_4^- participated in the destruction of TCE. The contrast is more notable for Simulation 7, where after 25 years (15 years of injection), 87.9 kg of MnO_4^- was injected, but only 2.7 kg of MnO_4^- was used in the destruction of the TCE DNAPL. This reduction in treatment efficiency is primarily due to flow bypassing following rind formation and encapsulation of the DNAPL.

4.3 Suite 3: Treatment of Pooled TCE with Prior Dissolution

The influence of chemical oxidation on mass removal from a TCE pool is presented in Figure 13. Although slightly more efficient, the trends in the pooled TCE scenarios are similar to those for the residual block scenarios; one year of treatment (Simulation 12) reduces the source life to approximately 24 years compared with 25 years for only dissolution (Simulation 10). Once initiated, continuous treatment (Simulation 11) for 6 years (elapsed time of 15 years) is required to completely remove the source zone; this represents a 2 to 3 fold reduction in source life span compared to only dissolution, which requires approximately 15 years after the same reference start time (Simulation 10). When examining Figure 13 it is observed that the initial reduction in TCE mass occurs quickly (i.e., 9 to 10 years); however, as the rind forms, the system becomes progressively more diffusion dominated and the rate the mass removal concurrently decreases.

Figure 14 presents the total mass discharge. As with the residual block suites (1 and 2), the 1 year pulse treatment on the pooled TCE (Simulation 12) initially yields a rapid reduction in discharge due to solute consumption and rind formation. However, once treatment is discontinued, significant rebound occurs with discharge values recovering to near non-treatment conditions (i.e., Simulation 10). Approximately 24 and 25 years are required to achieve negligible mass discharge values for the case of 1 year of treatment and only dissolution, respectively. Conversely, continuous treatment (Simulation 11) reduces TCE concentrations to negligible levels for the entire treatment

period. As with the block residual suites, it should be noted that although the mass discharge can be negligible during treatment, substantial DNAPL may remain.

In terms of model output, the 9 years of dissolution prior to treatment reduced the total number of DNAPL invaded nodes from 4001 to 637 and the number of nodes at residual from 329 to 112, thus increasing the residual TCE from 8.2% to 17.6%. Upon completion of the subsequent 12 months of chemical oxidation, 328 nodes remained invaded with only 73 nodes at residual saturations, representing a 35% increase in residual and 52% reduction in non-residual/pooled nodes. Interestingly, a visual inspection of a DNAPL saturation plot time-sequence for Suite 3 (not presented) demonstrated that while there was a significant increase in residual saturations, the TCE pooled on the low permeability lens remained following treatment. Based on these findings, it can be surmised that in complex DNAPL architectures, chemical oxidation will be most effective at destroying residual DNAPL and pooled DNAPL will be recalcitrant once rind encapsulation occurs.

5.0 Conclusions

Three-dimensional numerical simulations of TCE DNAPL overlying a low permeability lens within a higher permeability porous media domain were carried out. The TCE was subjected to both dissolution and chemical oxidation with potassium permanganate. Separate suites of simulations were carried out with the DNAPL distributed at either residual saturation, or a combination of pooled and residual saturations from a surface release of TCE.

Due to computational demands, the bulk of the simulations were conducted with the residual block of TCE. For the case of dissolution without treatment, approximately 32 years elapsed before the 2.981 kg source was completely depleted. In the presence of continuous chemical oxidation, the formation of the MnO_2(s) rind doubled treatment times when compared to the case of no rind. The rind formation resulted in source encapsulation and flow bypassing, and subsequently, the transport of solute from the source zone to the contiguous aqueous phase became diffusion limited. Single pulse treatments of one and two years greatly exacerbated treatment efficiency as the encapsulated DNAPL behaved as a long-term diffusive source. Continuous treatment is beneficial due to the higher diffusion rates for permanganate relative to TCE; the combination of rind and favourable differential diffusion rates permits the encapsulated source zone to behave as a self-contained *in situ* chemical reactor.

The behaviour of pooled TCE was similar to the residual saturation configuration, although the chemical oxidation proved slightly more efficient. In the case of 1 year of treatment initiated after 9 years of dissolution, the 2.952 kg source zone (both pool and residual) was depleted after 24 years, which was similar to the time to depletion for the corresponding dissolution only simulation. Continuous treatment initiated at 9 years completely removed the source zone by approximately 15 years (i.e., 6 years of continuous treatment was required). The mass discharge for continuous treatment exhibited similar trends for both the residual and pooled configurations. Partial treatment initially depleted the TCE solute, but once terminated, substantial concentration / mass

flux rebound occurred. Continuous treatment effectively reduces the TCE solute to negligible concentrations, despite substantial mass remaining in the source zone. It was also observed that non-residual/pooled DNAPL is particularly recalcitrant to chemical oxidation once the rind precipitation encapsulation occurs.

This study suggests the potential importance of the rind formation on treatment efficacy. Chemical oxidation with $KMnO_4$ can potentially exacerbate DNAPL source longevity and the time to achieve maximum allowable concentrations, depending on how it is implemented. In the absence of rind dissolution, results suggest that pulsed (i.e., non-continuous) KMnO4 treatment methodologies are ineffective mass removal strategies for DNAPL source zones. Clearly, a more thorough fundamental understanding of *in situ* chemical oxidation precipitates, and their consequences and benefits is necessary, if both numerical simulators and field treatment programs are to be optimized.

Although the rind formation significantly influences chemical oxidation treatment efficiency and the intended rate of mass destruction, the encapsulation tendency can also be viewed as a potential benefit in certain specific situations. Although not demonstrated directly, this work suggests $KMnO_4$ injection could be utilized to entrap and stabilize pooled (i.e., non-residual) DNAPL that is actively migrating or potentially mobile.

References

Batu, V. (1989) "A generalized two-dimensional analytical solution for hydrodynamic dispersion in bounded media with the first-type condition at the source", *Water Resources Research*, Vol. 25, No. 6, pg. 1125-1132.

Bekhit, H. and Hassan, A. (2005) "Stochastic modeling of colloid-contaminant transport in physically and geochemically heterogeneous porous media", Water Resources Research, 41, W02010, 1-18.

Bear, J. (1972) "Dynamics of Fluids in Porous Media", Dover Publications Inc., pg 111-112.

Bear, J. (1979) "Hydraulics of Groundwater", McGraw-Hill Inc., 1979.

Bockelmann, A., Zamfirescu, D., Ptak, T., Grathwohl, P., and Teutsch, G. (2003) "Quantification of mass fluxes and natural attenuation rates at an industrial site with a limited monitoring network: a case study", Journal of Contaminant Hydrology, 60, 97-121.

Bradford, S. and Bettahar, M. (2006) "Concentration dependent transport of colloids in saturated porous media", Journal of Contaminant Hydrology, 82 (1-2), 99-117.

Clement, T. (1997) “RT3D – A Modular Computer Code for Simulating Reactive Multi-species Transport in 3-Dimensional Groundwater Systems”, Version 1.0, Pacific Northwest National Laboratory, PNNL-11720.

Clement, T., Sun, Y., Hooker, B., and Petersen, J. (1998) “Modeling Multi-species Reactive Transport in Groundwater Aquifers”, Groundwater Monitoring & Remediation, 18 (2): 79-92.

Conrad, S., Glass, R., and Peplinski, W. (2002) “Bench-scale visualization of DNAPL remediation processes in analog heterogeneous aquifers: surfactant floods and in situ oxidation using permanganate”, Journal of Contaminant Hydrology, 58, 13-49.

Crank, J. (1975) “The Mathematics of Diffusion”, Second Edition, Clarendon Press, Oxford, England.

Crimi, M. and Siegrist, R. (2004) “Impact of Reaction Conditions on MnO_2 Genesis during Permanganate Oxidation”, Journal of Environmental Engineering, May, 562-572.

“CRC Handbook of Chemistry and Physics”, Edition 85, Chemical Rubber Company, Cleveland, Ohio, United States of America.

Dai, Q. and Reitsma, S. (2004) “Kinetic Study of Permanganate Oxidation of Tetrachloroethylene at a High pH Under Acidic Conditions”, Remediation, Autumn, 67-79.

Drever, J. (2002) “The Geochemistry of Natural Waters – Surface and Groundwater Environments”, Third Edition, Prentice Hall, New Jersey, pp. 436

Geller, J. and Hunt, J. (1993) “Mass Transfer From Nonaqueous Phase Organic Liquids in Water-Saturated Porous Media”, Water Resources Research, Vol. 29, No. 4, 833-845.

Gerhard, J., Kueper, B. and Hecox, G. (1998) “The Influence of Waterflood Design on the Recovery of Mobile DNAPLs”, Ground Water, Vol. 36, No. 2, 283-292.

Gerhard, J., Kueper, B., Hecox, G. and Schwarz, R. (2001) “Site-Specific Design for Dual Phase Recovery and Stabilization of Pooled DNAPL”, Ground Water Monitoring and Remediation, Spring, 71-88.

Gerhard, J. and Kueper, B. (2003a) “Capillary pressure characteristics necessary for simulating DNAPL infiltration, redistribution, and immobilization in saturated porous media”, Water Resources Research, Vol. 39, No. 8, SBH 7, 1-17.

Gerhard, J. and Kueper, B. (2003b) “Relative permeability characteristics necessary for simulating DNAPL infiltration, redistribution, and immobilization in saturated porous media”, Water Resources Research, Vol. 39, No. 8, SBH 8, 1-16.

Gerhard, J. and Kueper, B. (2003c) “Influence of constitutive model parameters on the predicted migration of DNAPL in heterogeneous porous media”, Water Resources Research, Vol. 39, No. 10, SBH 4, 1-15.

Grant, G. and Gerhard, J. (2004) “Sensitivity of Predicted DNAPL Source Zone Longevity to Mass Transfer Correlation Model”, Geoenvironmental Engineering: Integrated management of groundwater and contaminated land, R.N. Young and H.R. Thomas (eds), Telford Publishing, London, pp. 59-67.

Grant, G. (2005) “The Evolution of Complex DNAPL Releases: Rates of Migration and Dissolution”, Ph.D. Thesis, The University of Edinburgh, Edinburgh, Scotland, United Kingdom. (MIKE: Best not to reference a student thesis unless we absolutely have to – do the journal papers by Gavin not cover the issues we want to reference?)

Grant, G., Gerhard, J, and Kueper, B., (2006a) “Field scale impacts of spatially correlated relative permeability in heterogeneous multiphase systems”, Advances in Water Resources, 30 (5), 1144-1159.

Grant, G., Gerhard, J, and Kueper, B., (2006b) "Multidimensional validation of a numerical model for simulating a DNAPL release in heterogeneous porous media". Journal of Contaminant Hydrology, 92 (1-2), 109-128 .

Grant, G.P. and Gerhard, J.I. (2007c) "Simulating The Dissolution Of A Complex DNAPL Source Zone: 1. Model To Predict Interfacial Area", Water Resources Research, accepted for publication.

Grant, G.P. and Gerhard, J.I. (2007d) "Simulating The Dissolution Of A Complex DNAPL Source Zone: 2. Experimental Validation Of An Interfacial Area-Based Mass Transfer Model", Water Resources Research, Accepted for publication.

Hood, E., Thomson, N., Grossi, D., and Farquhar, G. (2000) "Experimental determination of the kinetic rate law for the oxidation of perchloroethylene by potassium permanganate", Chemosphere, 40, 1383-1388.

Huang, K.-C., Hoag, G., Chheda, P., Woody, B., and Dobbs, G. (2001) "Oxidation of chlorinated ethenes by potassium permanganate: a kinetics study", Journal of Hazardous Materials, B87, 155-169.

Huang, K.-C., Hoag, G., Chheda, P., Woody, B., and Dobbs, G. (2002) "Chemical oxidation of trichloroethene with potassium permanganate in a porous medium", Advances in Environmental Research, 7, 217-229.

Ibaraki, M. and Schwartz, F. (2001) "Influence of Natural Heterogeneity on the Efficiency of Chemical Floods in Sources Zones", Ground Water, Vol. 39, No. 5, 660-666.

Imhoff, P., Jaffé, P., and Pinder, G. (1993) "An experimental study of complete dissolution of a nonaqueous phase liquid in saturated porous media", Water Resources Research, Vol. 30, No. 2, 307-320.

Jawitz, J., Fure, A., Demmy, G., Berglund, S., and Rao, P. (2005) "Groundwater contaminant flux reduction resulting from nonaqueous phase liquid mass reduction", Water Resources Research, Vol. 41, W10408, 1-15.

Kueper, B and Frind, E. (1991) "Two-phase flow in heterogeneous porous media, 1. Model Development", Water Resources Research, Vol. 27, No. 6, pp. 1049-1057.

Jordana, S., Guimera,J., Domenec, J., and Subirana, J. (2005) "*In situ* chemical oxidation test of organic solvents with potassium permanganate", Bringing Groundwater Quality Research to the Watershed Scale (Proceedings of GQ2004, the 4th International Groundwater Quality Conference, Waterloo, Canada, July 2004), IAHS Publication 297, 398-403.

Li, D. and Schwartz, F. (2004a) “DNAPL remediation with in situ chemical oxidation using potassium permanganate. Part I. Mineralogy of Mn oxide and its dissolution in organic acids”, Journal of Contaminant Hydrology, 68, 39-53.

Li, D. and Schwartz, F. (2004b) “DNAPL remediation with in situ chemical oxidation using potassium permanganate. Part II. Increasing removal efficiency by dissolving Mn oxide precipitates”, Journal of Contaminant Hydrology, 68, 39-53.

MacKinnon, L.K. and Thomson, N. (2002) “Laboratory-scale in situ chemical oxidation of a perchloroethylene pool using permanganate”, Journal of Contaminant Hydrology, 49-74.

Mayer, A. and Miller, C. (1996) “The influence of mass transfer characteristics and porous media heterogeneity on nonaqueous phase dissolution”, Water Resources Research, Vol. 32, No. 6, 1551-1567.

McWhorter, D. and Sunada, D. (1990) “Exact integral solutions for two-phase flow”, Water Resources Research, 23, 399-414.

Miller, C., Poirier-McNeill, M., and Mayer, A. (1990) “Dissolution of Trapped Nonaqueous Phase Liquids: Mass Transfer Characteristics”, Water Resources Research, Vol. 26, No. 11, 2783-2796.

Mundle, K., Reynolds, D., West, M., and Kueper, B.K. (2007) "Concentration Rebound Following In Situ Chemical Oxidation in Fractured Clay", Ground Water, accepted for publication. MIKE: I think we have an issue number etc. for this paper – should be able to get it online at either Ground Water, or NGWA, or Blackwell Publishing.

Nambi, I. and Powers, S. (2003) "Mass transfer correlations for nonaqueous phase liquid dissolution from regions with high initial saturations", Water Resources Research, Vol. 39, No. 2, SBH 4, 1-11.

Powers, S., Abriola, L., and Weber, W. (1992) "An experimental investigation of nonaqueous phase liquid dissolution in saturated subsurface systems: Steady state mass transfer rates", Water Resources Research, Vol. 28, No. 10, 2691-2705.

Powers, S., Abriola, L., and Weber, W. (1994) "An experimental investigation of nonaqueous phase liquid dissolution in saturated subsurface systems: Transient mass transfer rates", Water Resources Research, Vol. 30, No. 2, 321-332.

Powers, S., Nambi, I., and Curry, G. (1998) "Non-aqueous phase liquid dissolution in heterogeneous systems: Mechanisms and a local equilibrium modeling approach", Water Resources Research, 3293-3302.

Randhawa, J. (2001) “Manganese Dioxide Induced Permeability Reduction of Porous Media During Permanganate Oxidation of Chlorinated Alkenes”, Thesis – Master of Applied Science, University of Windsor, Windsor, Ontario, Canada. pp. 88

Rao, P. and Jawitz, J. (2003) “Comment on “Sale, T. and McWhorter, D. (2001) “Steady state mass transfer from single-component dense nonaqueous phase liquids in uniform flow fields” by T.C. Sale and D.B. McWhorter”, Water Resources Research, Vol. 39, No. 3, COM 1, 1 -3.

Reddi, L., Ming, X., Hajra, M., and Lee, I. (2000) “Permeability Reduction of Soil Filters due to Physical Clogging”, Journal of Geotechnical and Geoenvironmental Engineering, March, 236-246.

Reitsma, S. and Dai, Q. (2001) “Reaction-enhanced mass transfer and transport from non-aqueous phase liquid source zones”, Journal of Contaminant Hydrology, 49, 49-66.

Rivett, M. and Feenstra, S. (2005) “Dissolution of an Emplaced Source of DNAPL in a Natural Aquifer Setting”, Environmental Science and Technology, 39, 447-455.

Saba, T. and Illangasekare, T. (2000) “Effect of groundwater flow dimensionality on mass transfer from entrapped nonaqueous phase liquid contaminants”, Water Resources Research, Vol. 36, No. 4, 971-979.

Saenton, S., Illangasekare, T., Soga, K. and Saba, T. (2002) “Effects of source zone heterogeneity on surfactant-enhanced NAPL dissolution and resulting remediation end-points”, Journal of Contaminant Hydrology, 59, 27-44.

Sale, T. (1998) “Interphase Mass Transfer From Single Component DNAPLs”, Ph.D. Dissertation, Department of Chemical and Bioresources Engineering, Colorado State University, Fort Collins, Colorado, United States of America.

Sale, T. and McWhorter, D. (2001) “Steady state mass transfer from single-component dense nonaqueous phase liquids in uniform flow fields”, Water Resources Research, Vol.37, No.2, 393-404.

Schnarr, M., Truax, C., Farquhar, G., Hood., E., Gonullu, T., and Stickney, B. (1998) “Laboratory and controlled field experiments using potassium permanganate to remediate trichloroethylene and perchloroethylene DNAPLs in porous media”, Journal of Contaminant Hydrology, 29, 205-224.

Schroth, M., Oostrom, M., Wietsma, T., and Istok, J. (2001) “In-situ oxidation of trichloroethene by permanganate: effects on porous medium hydraulic properties”, Journal of Contaminant Hydrology, 50, 79-98.

Seagren, E., Rittman, B., and Valocchi, A. (1999) “An experimental investigation of NAPL pool dissolution enhancement by flushing”, Journal of Contaminant Hydrology, 37, 111-137.

Seol, Y., Zhang, H., and Schwartz, F. (2003) “A Review of *In Situ* Chemical Oxidation and Heterogeneity”, Environmental & Engineering Geoscience, Vol. IX, No. 1, 37-49.

Siegrist, R.L., Lowe, K.S., Murdoch, L.C., Case, T.L., and Pickering, D.A. (1999) “In Situ Oxidation by Fracture Emplaced Reactive Solids”, Journal of Environmental Engineering, May, 429-440.

Struse, A.M., Siegrist, R.L., Dawson, J.E., Urynowicz, M.A. (2002) “Diffusive Transport of Permanganate during In Situ Oxidation”, Journal of Environmental Engineering, April, 327-334.

Tunnicliffe, B. and Thomson, N. (2004) “Mass removal of chlorinated ethenes from rough-walled fractures using permanganate”, Journal of Contaminant Hydrology, 75, 91-114.

Wilke, C. and Chang, P. (1955) “Correlation of diffusion coefficients in dilute solutions”, American Institute of Chemical Engineers Journal, 1, 264-270.

Yan, E. and Schwartz, F. (1999) “Oxidative degradation and kinetics of chlorinated ethylenes by potassium permanganate”, Journal of Contaminant Hydrology, 37, 343-365.

Yan, E. and Schwartz, F. (2000) “Kinetics and Mechanisms for TCE Oxidation by Permanganate”, Environmental Science and Technology, 30, 2535-2541.

Zhang, H. and Schwartz, F. (2000) “Simulating the in situ oxidative treatment of chlorinated ethylenes by potassium permanganate”, Water Resources Research, Vol. 36, No. 10, pg. 3031-3042.

Zhu, J. and Sykes, J. (2000) “The influence of NAPL dissolution characteristics on field-scale contaminant transport in subsurface”, Journal of Contaminant Hydrology, 41, 133-154.

Table 1 – Simulation parameters

Parameter	**1D column calibration**	**3D source zone simulation**
ρ_W	1000 kg m^{-3}	1000 kg m^{-3}
ρ_{NW}	1460 kg m^{-3}	1460 kg m^{-3}
μ_W	0.001 Pa·s	0.001 Pa·s
μ_{NW}	0.00057 Pa·s	0.00057 Pa·s
α	0 Pa^{-1}	0 Pa^{-1}
β	0 Pa^{-1}	0 Pa^{-1}
d_{50}	0.0005 m (1)	0.0005 m
k_{domain}	1.2 x 10^{-10} m^2 (1)	1.02 x 10^{-12} m^2
k_{lens}	-	1.02 x 10^{-14} m^2
θ	0.34 (1)	0.34
α_x	0.01 m	0.01 m
α_y	0.001 m	0.001 m
α_z	0.0001 m	0.0001 m
τ	0.7 (2)	0.7 (2)
K_{rxns}	Various	0.39 $M^{-1}s^{-1}$ @ 10ºC (3)
S_{NW}	16% (residual) (1)	20% (residual)
S_{rind} (rind slope)	Various	-5.5 x 10^{-16} m^2 L mg^{-1}
Solubility (TCE)	829 mg/L (1)	1100 mg/L
C ($KMnO_4^-$)	790 mg/L (1)	5000 mg/L
D^o_{TCE}	1.0 x 10^{-9} m^2 s^{-1} (4)	1.0 x 10^{-9} m^2 s^{-1} (4)
$D^o_{MnO4^-}$	1.6 x 10^{-9} m^2 s^{-1} (5)	1.6 x 10^{-9} m^2 s^{-1} (5)
$D^o_{Cl^-}$	2.0 x 10^{-9} m^2 s^{-1} (5)	2.0 x 10^{-9} m^2 s^{-1} (5)
R_{TCE}	1.0 (1)	1.0
Q	21.77 ml/min (1)	-
∇h	-	0.005
X	0.95 m (1)	1.0 m
Y	0.045 m	1.0 m
Z	0.045 m	1.0 m
Δx	0.01 m	0.025 m
Δy	0.045 m	0.025 m
Δz	0.045 m	0.025 m
Number of nodes	95	64,000

1 – From Schroth et al., 2001

2 – From Bear, 1972.

3 – Calculated as per Yan and Schwartz, 2000.

4 – Calculated from Wilke & Chang, 1955. Reference temperature is 25ºC.

5 – From CRC Handbook of Chemistry and Physics, 2004.

Table 2 – Descriptions of three-dimensional simulations.

Suite	Simulation No.	Description
1 (residual)	1	Only equilibrium dissolution
	2	Equilibrium dissolution with continuous oxidation; no prior dissolution; no rind formation
	3	Equilibrium dissolution with continuous oxidation; no prior dissolution; rind formation included
	4	Equilibrium dissolution with 1 year of treatment followed by only equilibrium dissolution; rind formation included
	5	Equilibrium dissolution with 2 years of treatment followed by only equilibrium dissolution; rind formation included
2 (residual)	6	10 years of equilibrium dissolution, then continuous treatment; no rind formation
	7	10 years of equilibrium dissolution, then continuous treatment; rind formation included
	8	10 years of equilibrium dissolution, then 1 year of treatment followed by only equilibrium dissolution; rind formation included
	9	10 years of equilibrium dissolution, then 2 years of treatment followed by only equilibrium dissolution; rind formation included
3 (surface release)	10	Only equilibrium dissolution
	11	9 years of equilibrium dissolution, then continuous treatment; rind formation included
	12	9 years of equilibrium dissolution, then 1 year of treatment followed by only equilibrium dissolution; rind formation included

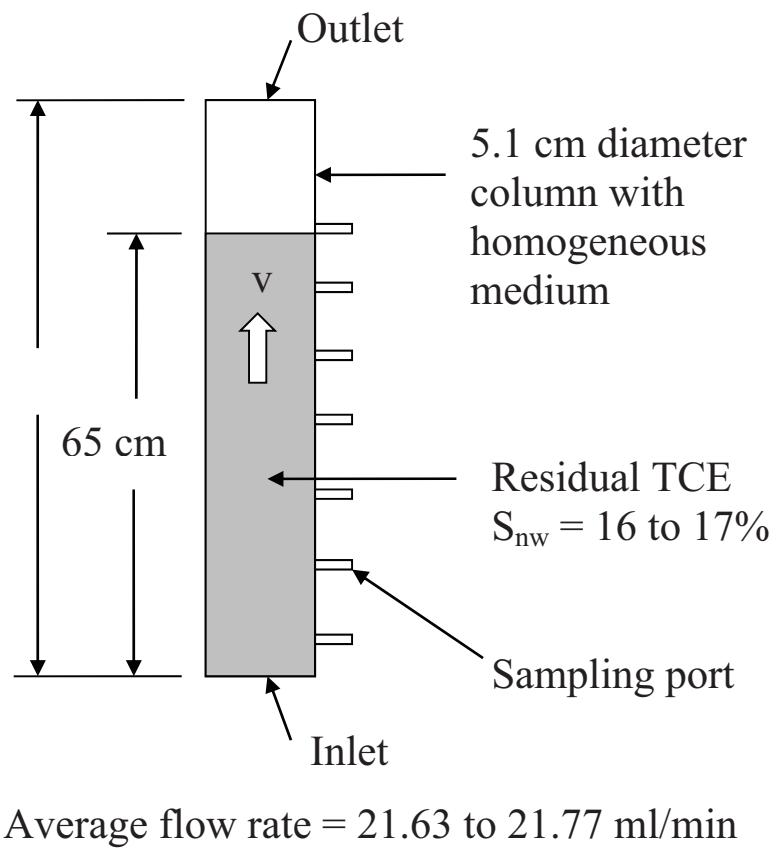

Figure 1 – Experimental setup by Schroth et al. (2001) used to calibrate DNAPL3D-RX.

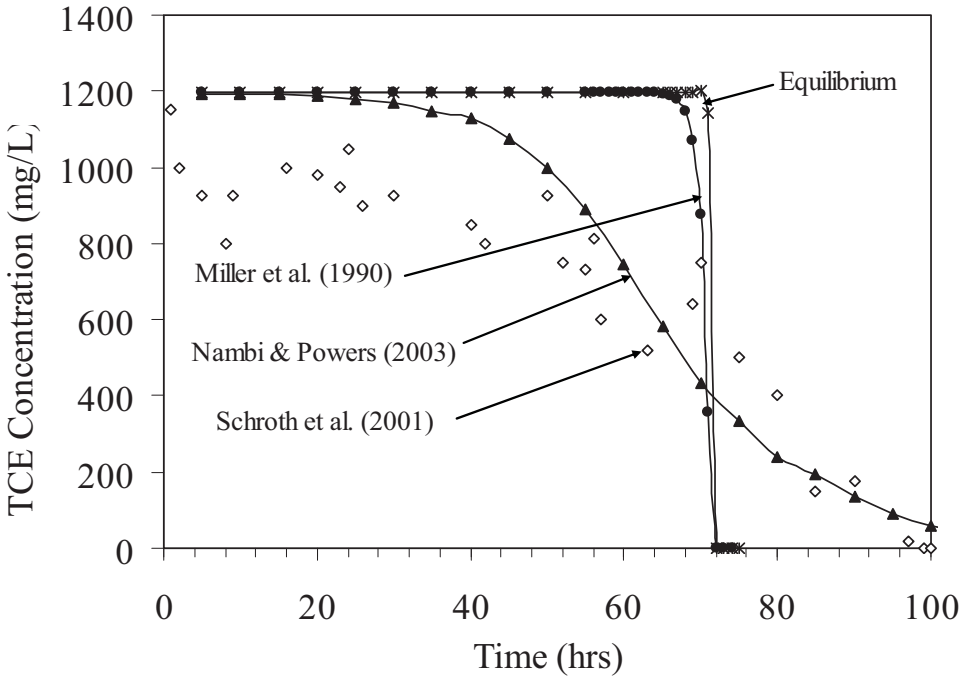

Figure 2 – Comparison of dissolution experiment by Schroth et al. (2001) with numerical model utilizing various mass transfer expressions.

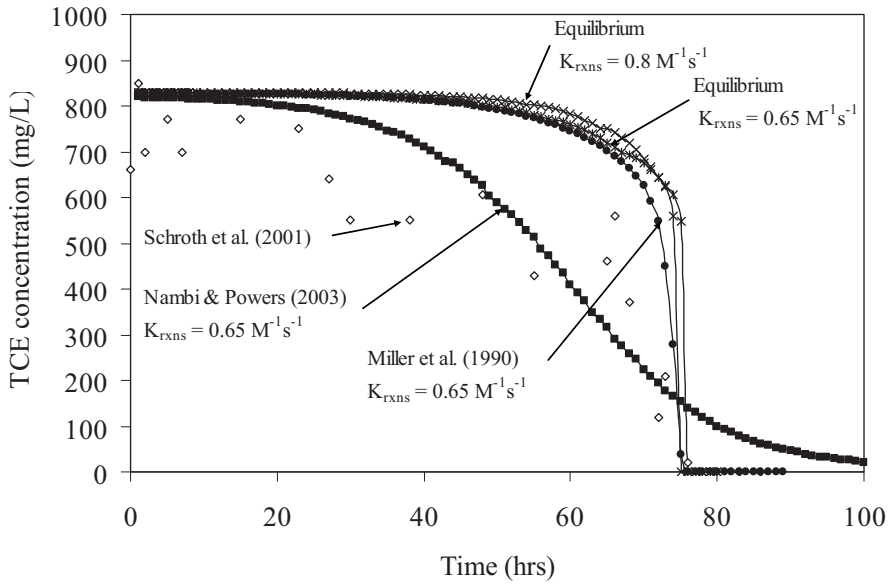

Figure 3 – Comparison of experimental TCE effluent concentrations in the presence of chemical oxidation (Schroth et. al, 2001) with model results for various mass transfer expressions and TCE-$KMnO_4$ reaction rate constants.

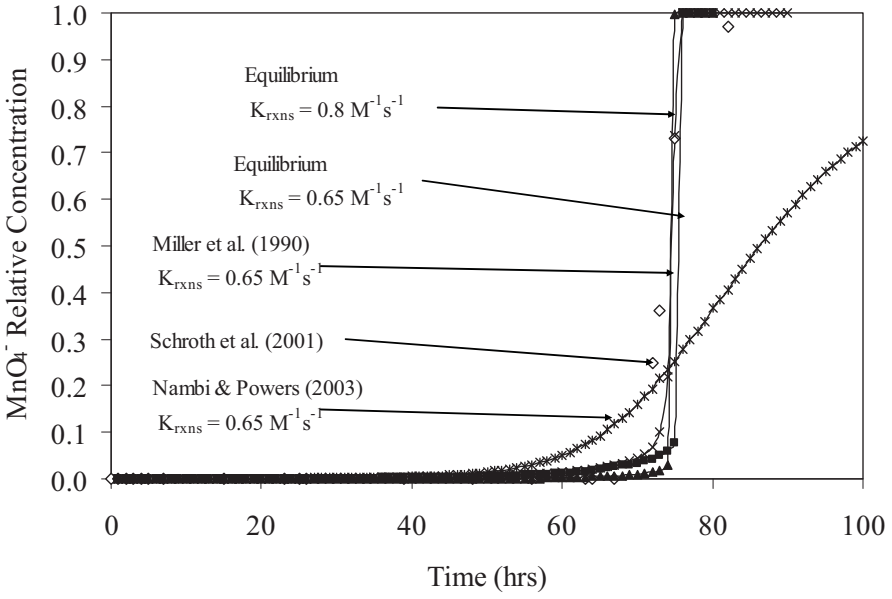

Figure 4 - Comparison of experimental MnO_4^- effluent concentrations (Schroth et. al, 2001) with model results for two TCE-$KMnO_4$ reaction rate constants.

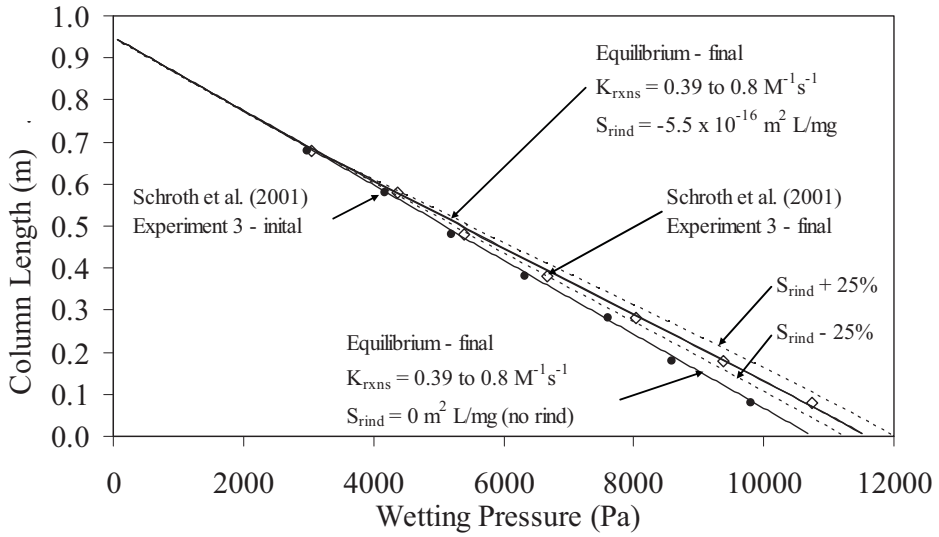

Figure 5 - Comparison of experimental wetting pressures (Schroth et. al, 2001) with model results for two TCE-$KMnO_4$ reaction rate constants and two different S_{rind} values.

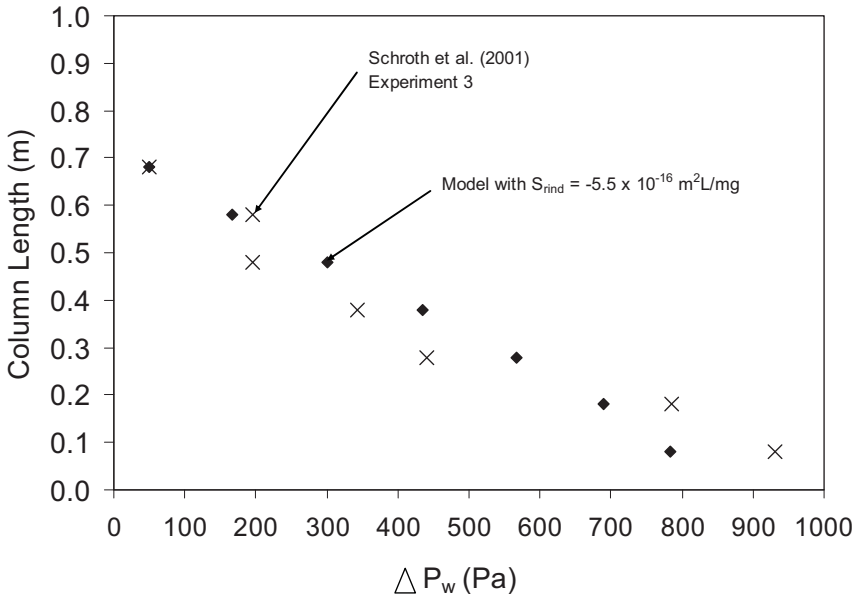

Figure 6 – Comparison between experimental and model pre- and post treatment wetting pressures due to rind formation. The changes in wetting pressure are presented as the difference between initial (pre-treatment) and final (post treatment) measurements.

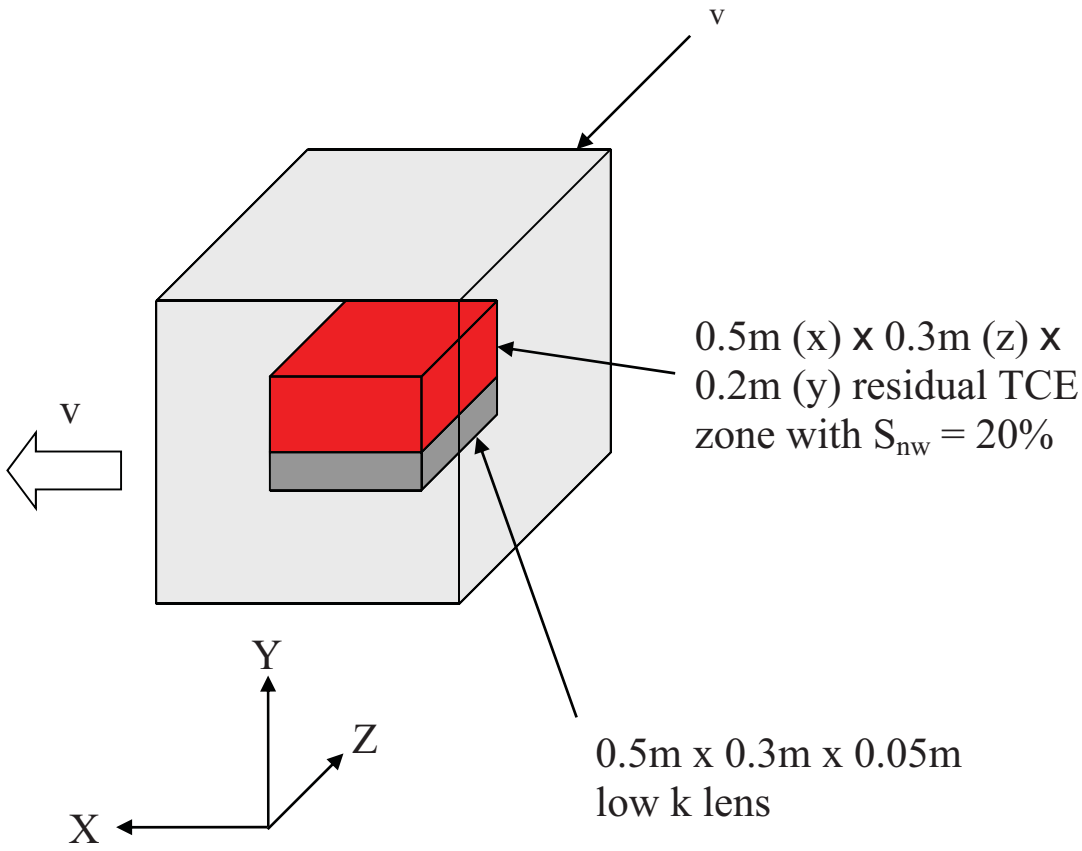

Figure 7a – Configuration of three-dimensional domain used in model simulation of residual TCE source zone dissolution and chemical oxidation.

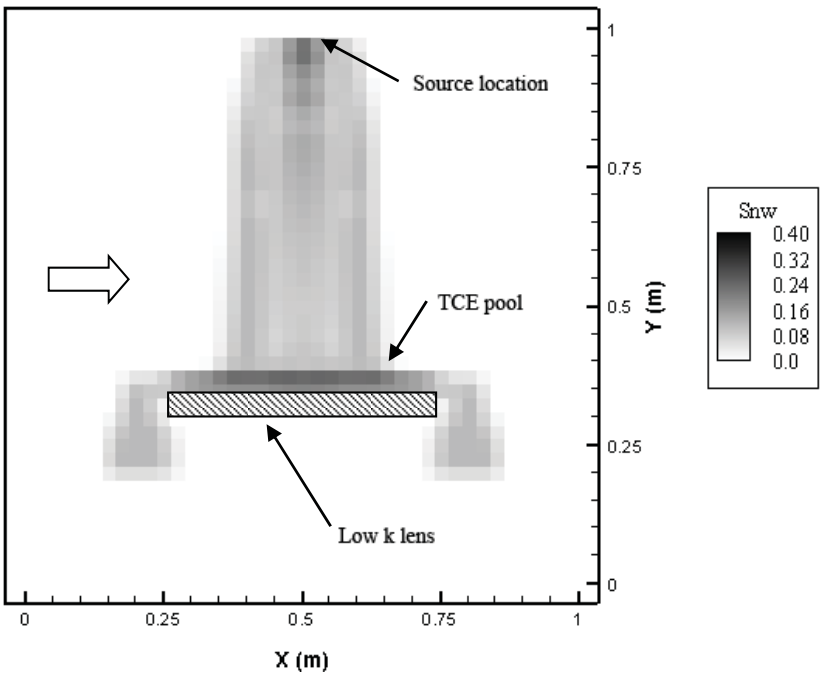

Figure 7b – Cross-section of three-dimensional domain used in model simulation of pooled TCE source zone dissolution and chemical oxidation. TCE saturations range from 1 to 40%. Groundwater flow is from left to right.

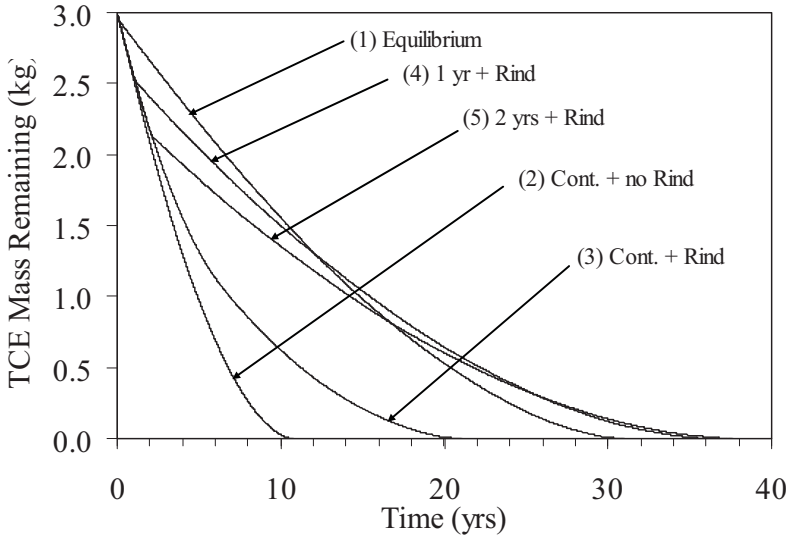

Figure 8 – Influence of rind formation on treatment effectiveness for Suite 1. Chemical oxidation initiated at t = 0 years. Label descriptors refer to simulations identified in Table 2.

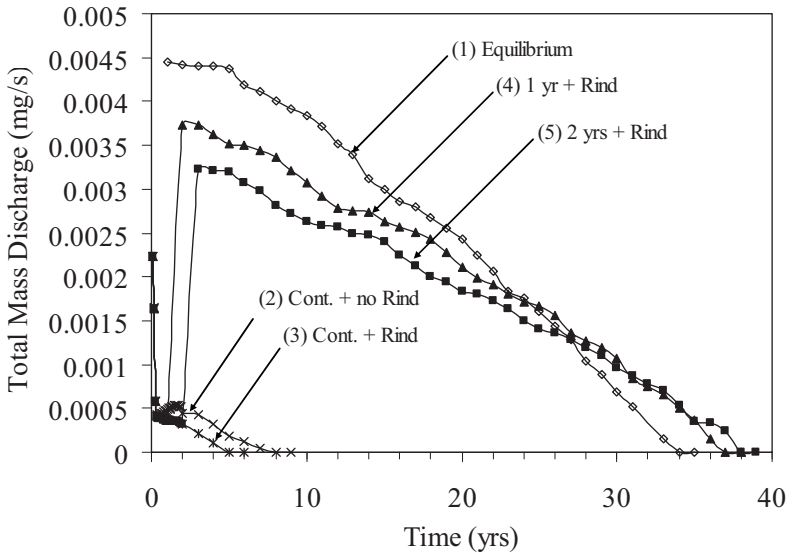

Figure 9 - Comparison of total boundary mass discharge for different chemical oxidation treatment for Suite 1. Label descriptors refer to simulations identified in Table 2.

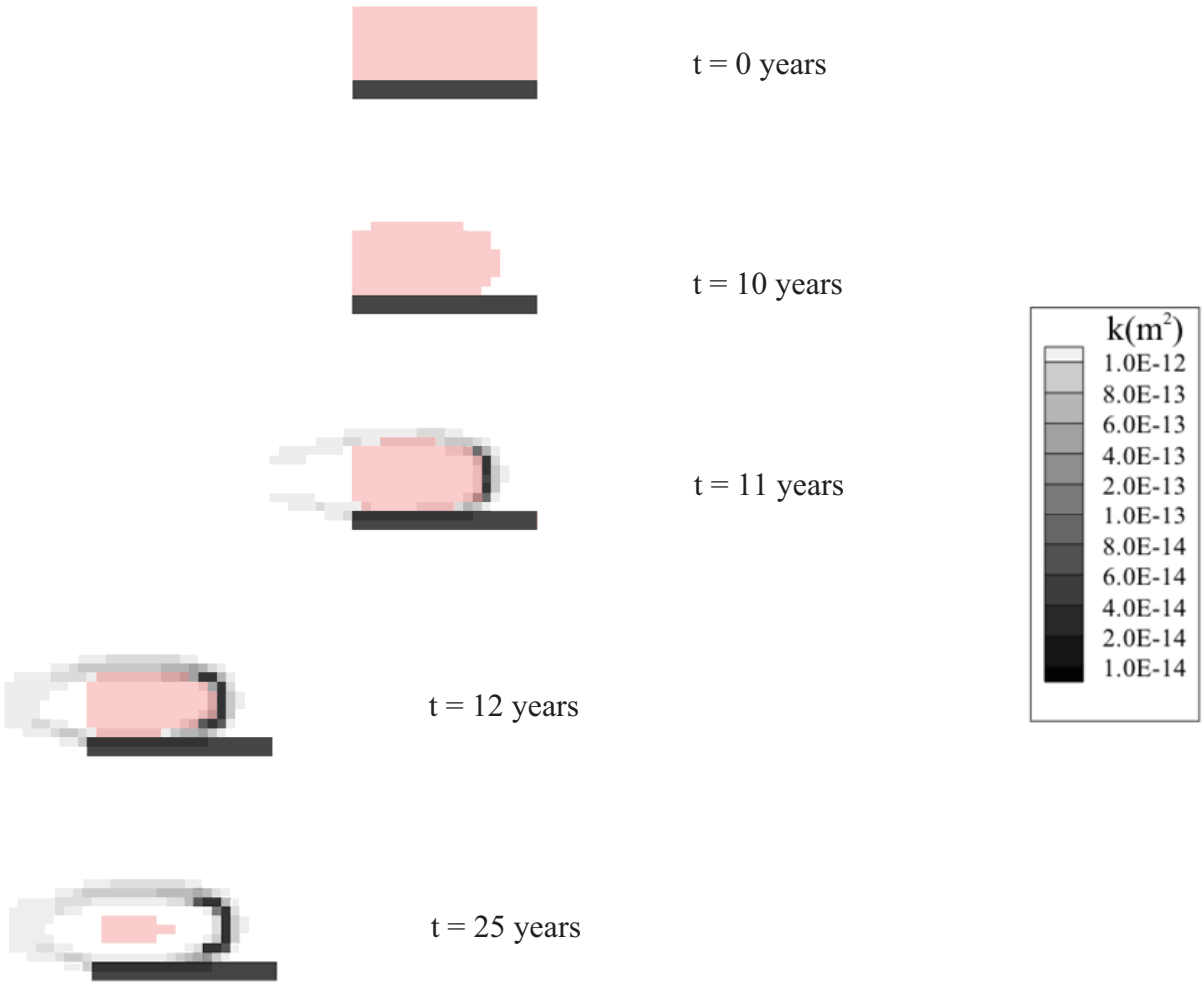

Figure 10 – Time sequence of S_{nw} and k for Simulation 9 (refer to Table 2) for a cross-section through the source zone. Permeabilities are identified in the legend. Red denotes nodes with $S_{nw} > 0$, not the actual saturation.

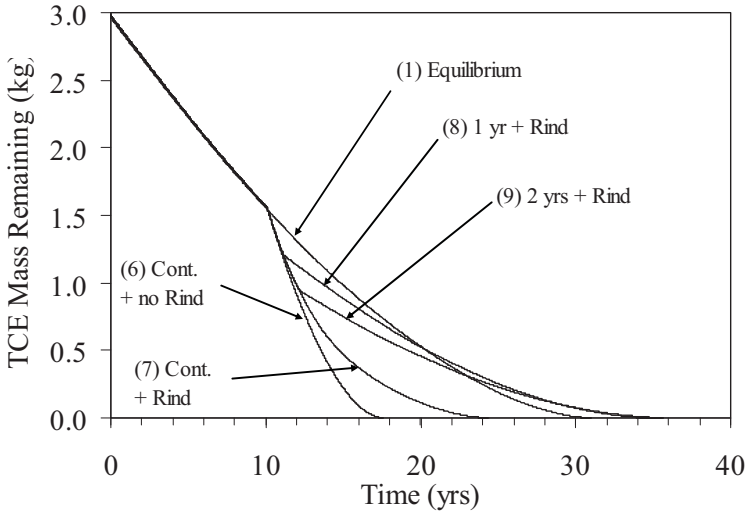

Figure 11 – Influence of rind formation on treatment effectiveness after 10 years of dissolution prior to treatment for Suite 2. Chemical oxidation initiated at t = 10 years. Label descriptors refer to simulations identified in Table 2.

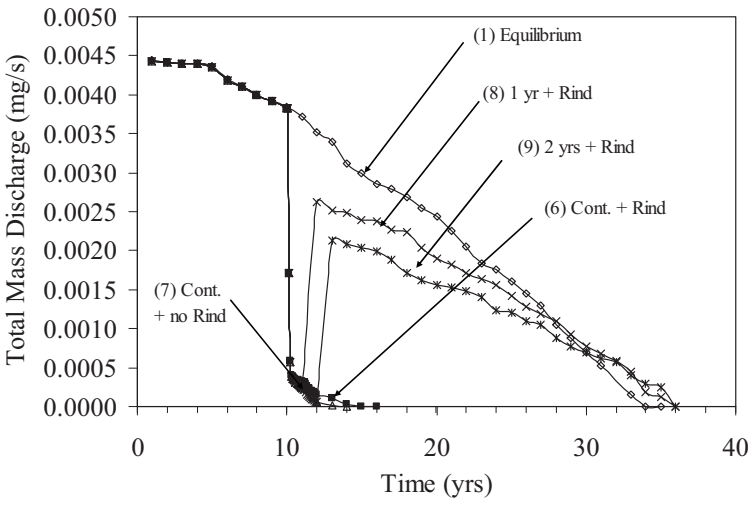

Figure 12 - Comparison of total boundary mass discharge for different chemical oxidation treatment scenarios initiated after 10 years of dissolution for Suite 2. Chemical oxidation initiated at t = 10 years. Label descriptors refer to simulations identified in Table 2.

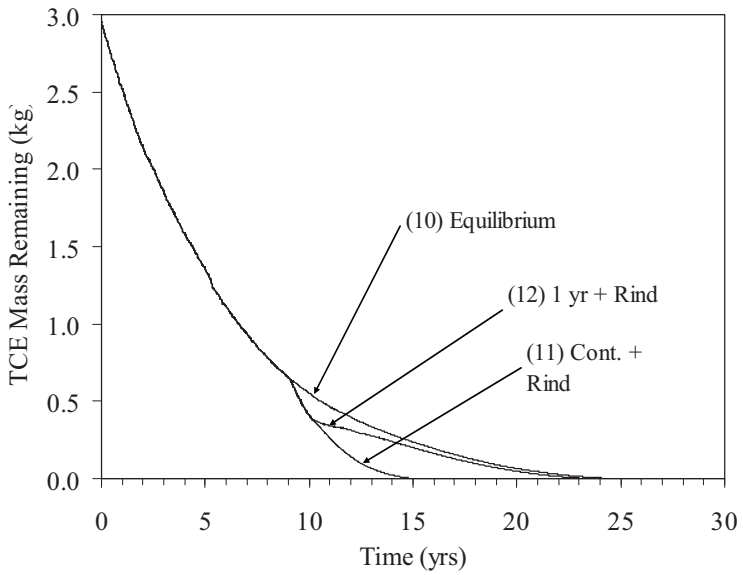

Figure 13 – Influence of rind formation on treatment effectiveness after 9 years of dissolution prior to treatment for Suite 3. Chemical oxidation initiated at t = 9 years. Label descriptors refer to simulations identified in Table 2.

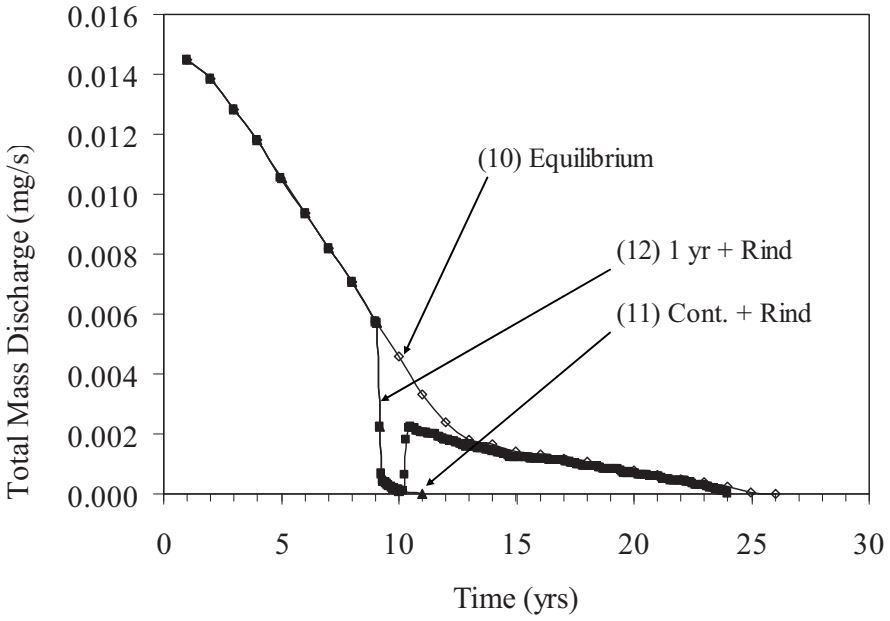

Figure 14 - Comparison of total boundary mass discharge for dissolution and 1 year of chemical oxidation treatment initiated after 9 years of dissolution for Suite 3. Label descriptors refer to simulations identified in Table 2.

APPENDIX D

CONSOLIDATED MEDIA MODELING

Section D.1

Fractured Clay Chemical Oxidation Numerical Model Development and Summary of Simulation Results

Abstract

A two-dimensional, transient flow and transport numerical model was developed to simulate in-situ chemical oxidation (ISCO) of trichloroethylene (TCE) and tetrachloroethylene (PCE) by potassium permanganate in fractured clay. This computer model incorporates DNAPL dissolution, reactive aquifer material, multi-species matrix diffusion, and kinetic formulations for the oxidation reactions. A sensitivity analysis for two types of parameters, hydrogeological and engineering, including matrix porosity, matrix organic carbon, fracture aperture, potassium permanganate dosage, and hydraulic gradient was conducted. Remediation metrics investigated were the relative rebound concentrations arising from back diffusion, and percent mass destroyed. No well-defined correlation was found between the magnitude of rebound concentrations during post-remedy monitoring and the amount of contaminant mass destroyed during the application. Results indicate that all investigated parameters affect ISCO remediation in some form. Results indicate that when advective transport through the fracture is dominant relative to diffusive transport into the clay matrix (large System Peclet Number), permanganate is more likely to be flushed out of the system and treatment is not optimal. If the System Peclet Number is too small, indicating that diffusion into the matrix is dominant relative to advection through the fracture, permanganate does not traverse the entire fracture, leading to post-remediation concentration rebound. Optimal application of ISCO requires balancing advective transport through the fracture with diffusive transport into the clay matrix.

Introduction

Upon release to the subsurface, dense, non-aqueous phase liquids (DNAPLs) such as chlorinated solvents, PCB oils, creosote and coal tar will distribute themselves in the form of both disconnected blobs and ganglia of organic liquid referred to as residual, and in higher saturation distributions referred to as pools. Pooled DNAPL is distinguished from residual DNAPL in that pools represent a continuous fluid distribution throughout the pore space over a spatial scale significantly greater than that associated with residual DNAPL. If the DNAPL reaches a fractured clay aquitard, pooling of the DNAPL will take place until the capillary pressure exceeds the fracture entry pressures, at which point entry into the fractures takes place (Kueper and McWhorter 1991; Pankow and Cherry 1996). As in porous media, both residual and pooled DNAPL can form in fractures (Longino and Kueper, 1999). The longevity of residual and pooled DNAPL in fractures will be governed by a variety of factors including the ground water velocity, the aqueous solubility of the DNAPL components, and the rate of diffusion into the clay matrix (Parker et al. 1994).

Remediation of fractured clay impacted by DNAPLs can be challenging given the significant amount of mass that may have diffused into the clay matrix. Past studies have demonstrated that in-situ chemical oxidation (ISCO) using potassium permanganate ($KMnO_4$) can be successful in destroying chlorinated ethenes such as tetrachloroethene (PCE) and trichloroethene (TCE) in porous media (Vella and Veronda, 1992; Gates et al., 1995; Siegrist et al., 1995; Schnarr et al., 1998; Yan and Schwartz, 1999; Zhang and Schwartz, 2000a,b; Li et al., 2000; Hood and Thomson, 2000; MacKinnon and Thomson, 2002; Schroth et al., 2001; Conrad et al., 2002; Marvin et al., 2002; Urynowicz and Siegrist, 2005) and in fractured media (Struse et al.,2002; Tunnicliffe and Thomson, 2004). These studies have examined various aspects of the $KMnO_4$ ISCO process

including MnO_2 precipitate formation, reaction kinetics, interphase mass transfer, diffusive transport of the oxidant, and the influence of natural oxidant demand (NOD).

Post-remediation monitoring has indicated that some field sites experience a rebound in concentration of the target contaminant following the application of $KMnO_4$ (e.g., Goldstein et al., 2004; Marvin et al., 2004; Allen et al., 2004; Crother et al., 2004). A pilot-scale study of ISCO in fractured shale by Goldstein et al. (2004), for example, found that dissolved contaminant concentrations rebounded from nearly non-detectable levels to pre-injection levels within six months of ceasing $KMnO_4$ injections. It was suggested that if significant amounts of contaminant mass in the rock matrix are not treated, post-remediation concentration rebound will occur in the fractures as a result of back diffusion from the matrix. Marvin et al. (2004) suggested that rebound concentrations could be influenced by an increased rate of diffusion stemming from pore space alterations caused by consumption of organic carbon by permanganate.

The objective of this model is to investigate the role of both hydrogeological properties and engineering parameters on concentration rebound following the application of ISCO in fractured clay. Understanding the causes of concentration rebound is important in designing field applications of ISCO, in selecting an appropriate length of time for post remedy monitoring, and in setting stakeholder expectations. This study focuses on chlorinated ethenes and makes use of numerical simulation. The use of numerical simulation allows time scales on the order of years to decades to be studied in a timely and cost effective manner. Previously published numerical models for ISCO of chlorinated ethenes by permanganate were developed by Zhang and Schwartz (2000a,b), and Hood and Thomson (2000). These models focused on porous media and accounted

for chemical reactions, solute transport, NAPL dissolution, and aquifer oxidant demand. The model developed by Zhang and Schwartz (2000b) also tracked changes in porosity and permeability due to mineral precipitation, and the results were compared to published data from laboratory and field experiments. The modeling presented here differs from previously published work in that it is focused on fractured clay and an understanding of the interaction between advective/dispersive transport in fractures and diffusive transport in the clay matrix.

Model Development

Model Domain

The presented numerical simulations are based on a two-dimensional (2D) fracture-matrix system in which the results can be scaled up using symmetry to represent a larger, three-dimensional (3D) parallel fractured system subject to unidirectional groundwater flow. In order to minimize computational run times, lines of symmetry were located along the center of the fractures and the matrix blocks so that the modeled domain consisted of a half fracture and a half matrix block. Figure 1 illustrates how the modeled domain is scaled up to represent a 3D domain 15 m long in the direction of ground water flow, 20 m wide orthogonal to the direction of ground water flow, and 5 m high. The modeled domain is a 2D vertical slice of the 3D domain. It should be noted that although the presented domain incorporates horizontal fractures, the results are directly applicable to a set of vertical fractures having the same hydraulic characteristics (i.e., aperture, spacing and applied hydraulic gradient) as the modeled horizontal fractures since diffusion is independent of orientation. The source zone emplaced within the fracture is 5 m long, 20 m wide, and is initially assigned a specified non-wetting phase (DNAPL) saturation. Constant head boundaries were applied to the upgradient and downgradient ends of the domain, producing unidirectional ground

water flow in the fracture subject to advection and longitudinal dispersion. Longitudinal and vertical transverse (2D) diffusion are permitted in the matrix.

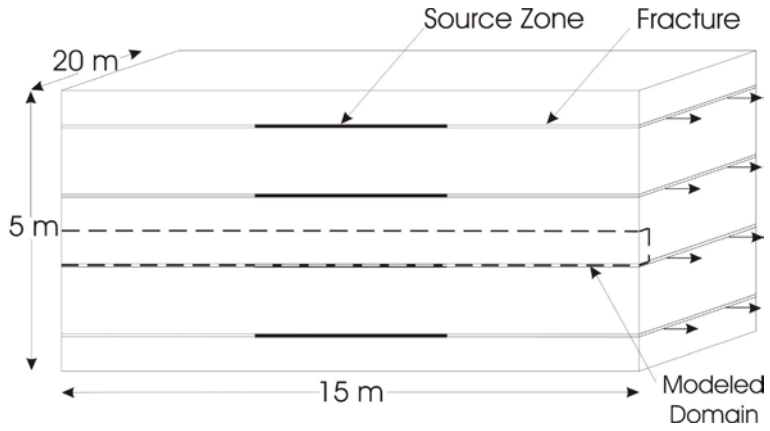

Figure 1 – Model domain and scaled up system

Model Formulation

The chemical oxidation process was modeled using RT3D (Reactive Multispecies Transport in Three-Dimensional Groundwater Systems), a finite difference based reactive transport software program (Clement, 1997; Clement et al., 1998). Reaction packages were developed for ISCO of TCE and PCE by permanganate, multi-species diffusion, mass transfer, and steady state flow governed by the constant head boundary conditions and the presence of DNAPL in the source zone. The code was also altered to allow for a decreasing retardation factor for the contaminant as the organic aquifer material becomes consumed by permanganate during the ISCO remediation process.

In RT3D, the governing equation of contaminant transport of the mobile species is (Clement, 1997; and Clement et al., 1998):

$$\frac{\partial(\theta C_m^n)}{\partial t} = \frac{\partial}{\partial x_i}\left(\theta D_{ij}^n \frac{\partial C_m^n}{\partial x_j}\right) - \frac{\partial}{\partial x_i}\left(\theta v_i C_m^n\right) + q_s C_s^n + \sum R_m \,, \;\; i,j = x,y,z \tag{1}$$

while the immobile species governing equation is:

$$\frac{\partial(\theta C_{im}^n)}{\partial t} = \sum R_{im} \tag{2}$$

where D_{ij} is the hydrodynamic dispersion tensor [L^2T^{-1}], v_i is the average linear groundwater velocity [LT^{-1}], q_s is a volumetric flux representing sources and/or sinks [T^{-1}], R is the rate of all reactions [$ML^{-3}T^{-1}$], θ is the porosity, and t is time [T]. The superscript n denotes the species number, while the subscripts m and im designate mobile and immobile species, respectively. The subscript s denotes a source or a sink. Sorption of the contaminant is represented through a retardation factor (R_s) defined as:

$$R_s = 1 + \frac{\rho_b}{\theta} K_{oc} f_{oc} \tag{3}$$

where ρ_b is the soil dry bulk density, K_{oc} is the organic carbon partition coefficient, and f_{oc} is the fraction organic carbon.

The nodal hydraulic conductivity of the fracture (K) is calculated as:

$$K = \frac{e^2 k_{rw} \rho_w g}{12 \mu_w} \tag{4}$$

where e is the fracture aperture [L], k_{rw} is the relative permeability of the wetting phase [-], ρ_w is the density of the wetting phase [ML^{-3}], g is the gravitational constant [MT^{-2}], and μ_w is the viscosity of the wetting phase [$ML^{-1}T^{-1}$]. The harmonic mean of the nodal hydraulic conductivities was calculated and multiplied by the hydraulic gradient across the fracture to obtain the wetting phase flux in the fracture. The average linear ground water velocity (v) for each individual node was

calculated by dividing the flux by the local wetting phase saturation. The relative permeability (k_{rw}) term in (4) was calculated using the Brooks – Corey constitutive model (Brooks and Corey, 1966) with a pore size distribution index of 2.5 and a residual wetting phase saturation of 0.1. Application of the Brooks – Corey constitutive model to represent capillary behavior in fractures was selected on the basis of Reitsma and Kueper (1994).

DNAPL to water mass transfer is treated here as an equilibrium process. Although non-equilibrium mass transfer has been observed in fractured systems (e.g., Glass and Nicholl 1995; Dickson and Thomson 2003), the relatively small aperture fractures considered in this study result in complete DNAPL dissolution in relatively short periods of time, regardless of what mass transfer model is adopted.

The oxidation of TCE by permanganate is represented as (Yan and Schwartz, 1999):

$$C_2Cl_3H + 2MnO_4^- \rightarrow 3Cl^- + 2CO_2 + H^+ + 2MnO_2(s) \quad (5)$$

The oxidation of PCE by permanganate is represented as (Yan and Schwartz, 1999):

$$C_2Cl_4 + 2MnO_4^- \rightarrow 4Cl^- + 2CO_2 + 2MnO_2(s) \quad (6)$$

Laboratory batch experiments reported in the literature have found that the oxidation of both TCE and PCE can be described with 2nd-order kinetic reaction rate constants. The rate constants for TCE were found to range from 0.65 (± 0.1) $M^{-1}s^{-1}$ to 0.8 (± 0.12) $M^{-1}s^{-1}$ (Yan and Schwartz, 1999; Hood et al., 2002), while for PCE they ranged from 0.028 (± 0.001) $M^{-1}s^{-1}$ to 0.045 (± 0.03) $M^{-1}s^{-1}$ (Yan and Schwatrz, 1999; Huang et al., 2001; Hood et al., 2002; Dai and Reitsma, 2004). The model developed here adopts rate constants of 0.65 $M^{-1}s^{-1}$ and 0.045 $M^{-1}s^{-1}$ for TCE and PCE,

respectively, which are consistent with the above studies at relatively neutral pH values. Changes in system pH and the subsequent influence on kinetic rate constant are not modeled in this study.

With respect to the formation MnO_2, a trial simulation that incorporated precipitate formation resulted in significant permeability reduction of the fracture. Because the simulated domain adopts unidirectional flow, there is no opportunity for flow bypassing. Inclusion of precipitate formation resulted in plugging of the fracture and a significant reduction in groundwater flow. The simulations presented here do not incorporate MnO_2 precipitate formation in the fractures or the matrix.

During ISCO, permanganate is consumed by the organic aquifer material (OAM) located in the matrix. It is anticipated that the natural oxidant demand (NOD) of the OAM will have a significant effect on the efficacy of ISCO remediation. The reaction between OAM and permanganate has been suggested by Mumford (2002) to be:

$$3CH_2O + 4MnO_4^- \rightarrow 3CO_2 + 4MnO_2(s) + H_2O + 4OH^- \quad (7)$$

In the model developed by Zhang and Schwartz, (2000a), a kinetic rate constant of 450 $M^{-1}s^{-1}$ for the OAM was assumed as it was thought that the kinetic reaction rate for OAM (kNOD) would be much greater than the reaction rate constants for the chlorinated compounds. This large kinetic rate constant is based on a conceptual model suggested by Barcelona and Holm (1991) and effectively assumes instantaneous reaction with OAM, producing a permanganate transport front which is dependent on OAM. In comparison, Mumford et al. (2005) suggest that the consumption of MnO_4 by OAM may have two very different reaction rates; the first being controlled by a fast, or instantaneous, reaction and the second by a slower reaction. Mumford (2002) performed column

experiments and fitted the resulting data to a numerical model, which indicated that reaction rate constants of $3x10^{-2}$ $M^{-1}s^{-1}$ to $3x10^{-5}$ $M^{-1}s^{-1}$ (using equation 7) substantiated the kinetic conceptual model for NOD. A model developed by Hood and Thomson (2002) to investigate the impact of diffusion and NOD on permanganate in porous media used reaction rate constants varying from $3x10^{-3}$ $M^{-1}s^{-1}$ to $3x10^{-5}$ $M^{-1}s^{-1}$. In this study the OAM is assumed to be composed solely of organic carbon (f_{oc}) and a second order reaction rate constant (kNOD) of $3x10^{-5}$ $M^{-1}s^{-1}$ is adopted.

Based on the above, the kinetic reaction equations incorporated into the model for TCE are (similar for PCE) [Zhang and Schwartz, 2000a]:

$$\frac{\partial[TCE]}{\partial t} = \frac{-k_{TCE}[TCE][MnO_4^-]}{R_{TCE}} \tag{8}$$

where R_{TCE} is the retardation factor defined in (3). For permanganate:

$$\frac{\partial[MnO_4^-]}{\partial t} = -2k_{TCE}([TCE]+[TCE_{sorbed}])[MnO_4^-] - 4k_{NOD}[OAM][MnO_4^-] \tag{9}$$

where the coefficients 2 and 4 are derived from stoichiometry. For OAM (Mumford, 2002):

$$\frac{\partial[OAM]}{\partial t} = -3k_{NOD}[OAM][MnO_4^-] \tag{10}$$

For sorbed TCE:

$$\frac{\partial[TCE_{sorbed}]}{\partial t} = -k_{TCE}[TCE_{sorbed}][MnO_4^-] \tag{11}$$

Simulation of advection and dispersion in the fracture, and diffusion into the clay matrix were verified through comparison to analytical solutions by Bear (1972), Tang et al. (1981), and Sudicky and Frind (1982). The reaction package for TCE was tested by comparing model results to 1D

porous media column experiments conducted by Schroth et al. (2001). The verification work can be found in Mundle (2006).

The developed model was discretized using a nodal spacing in the longitudinal direction of 0.1 m, resulting in a total of 150 nodes in the direction of ground water flow. The discretization in the matrix varied from a node spacing of 0.0025 m next to the fracture, transitioning to 0.0135 m at the matrix centerline. Verification simulations comparing the developed model to an analytical solution for solute transport in a system of parallel fractures subject to matrix diffusion (Sudicky and Frind, 1982) indicated that this nodal spacing is adequate in representing the diffusion process. Depending on the fracture spacing, the model incorporated approximately 65 rows of nodes in the clay matrix and a total of approximately 9,000 nodes in the entire model domain.

Outline of Simulations

Table 1 presents the base case simulation (Run A) input parameters. The base case consists of a 75 μm fracture containing a 5 m long DNAPL source zone with a specified non-wetting phase saturation of 0.34. The constant head boundaries result in a hydraulic gradient of 0.05 across the ends of the fracture. The DNAPL is permitted to dissolve and form a plume for a period of two years, at which point in time $KMnO_4$ is applied for five years at a concentration of 5 g/L. The $KMnO_4$ is applied immediately upgradient of the source zone (a distance of 5 m from the upgradient domain boundary). The clay matrix is assigned an effective porosity of 0.3, an f_{oc} of 0.003, and a kNOD of 3×10^{-5} $M^{-1}s^{-1}$. The base case adopts a fracture spacing of 1 m.

Table 1 – Base Case Values

Parameter	Unit	Value
DNAPL	[-]	TCE
Aperture (e)	[μm]	75
DNAPL Saturation (S_{nw})[a]	[-]	0.34
Hydraulic Gradient (∇h)	[-]	0.05
Initial Time	[years]	2
Remediation Time	[years]	5
$KMnO_4$ Dosage	[g/L]	5
Matrix Porosity (θ_m)[b]	[-]	0.3
Fraction of Organic Carbon (f_{oc})	[-]	0.003
OAM Reaction Rate Constant (kNOD)	$[M^{-1}s^{-1}]$	$3x10^{-5}$
Injection Location (upstream from source)	[m]	0.1
Tortuosity[b]	[-]	0.3
Bulk Density[b]	$[kg/m^3]$	1400
Fracture Spacing (S)	[m]	1.0
Organic Carbon Partition Coefficient (K_{oc})	[L/kg]	126
TCE Free Solution Diffusion Coefficient[c]	$[m^2/s]$	$1.01x10^{-9}$
PCE Free Solution Diffusion Coefficient[c]	$[m^2/s]$	$9.4x10^{-10}$
MnO_4 Free Solution Diffusion Coefficient[d]	$[m^2/s]$	$1.63x10^{-9}$
TCE Reaction Rate Constant[e] (kTCE)	$[M^{-1}s^{-1}]$	0.65

a Longino and Kueper, 1999
b Johnson et al., 1989
c Pankow and Cherry, 1996 (25 C)
d Lide, 2004
e Yan and Scwartz, 1999

In addition to the base case, two sets of simulations were carried out to investigate the influence of hydrogeological parameters and engineering parameters on concentration rebound. Table 2 outlines the simulations investigating hydrogeological parameters. The simulations involve a sensitivity to contaminant type (PCE), fracture aperture, initial non-wetting phase saturation, matrix porosity, matrix f_{oc}, kNOD, and fracture spacing. Table 2 also lists the base case (Run A) along with a

simulation in which ISCO is not applied (Run B). Table 3 presents the simulations investigating engineering parameters. The simulations involve a sensitivity to hydraulic gradient, length of time until ISCO is applied (initial time), the length of time that ISCO is applied (remediation time), the $KMnO_4$ dosage, and the location of the injection. Table 3 also lists the base case (Run A) and no ISCO simulation (Run B) for comparison purposes.

Table 2 – Outline of simulations investigating hydrogeological parameters

Run	Changed Parameter Value
A	Base case (See Table 1)
B	No ISCO
C	PCE (K_{oc} = 364 L/kg; kPCE = 0.045 $M^{-1}s^{-1}$)
D	e = 37.5 µm
E	e = 150 µm
F	S_{nw} = 0.15
G	S_{nw} = 0.60
H	θ_m = 0.15
I	θ_m = 0.45
J	f_{oc} = 0.0015
K	f_{oc} = 0.006
L	kNOD = $3x10^{-3}$ $M^{-1}s^{-1}$
M	S = 0.5 m

Table 3 – Outline of simulations investigating engineering parameters

Run	Changed Parameter Value
A	Base Case (See Table 1)
B	No ISCO
N	$\nabla h = 0.025$
O	$\nabla h = 0.01$
P	Initial Time = 1 week
Q	Initial Time = 20 years
R	Remediation Time = 1 year
S	Remediation Time = 10 years
T	Remediation Time = 6 month on/off pulses for 5 years
U	$KMnO_4$ Dosage = 2.5 g/L
V	$KMnO_4$ Dosage = 7.5 g/L
W	Injection Location = 3.6 m

Results and Discussion

Base Case and No ISCO Simulations

A comparison between the base case (Run A) and no ISCO (Run B) simulations demonstrated that (i) ISCO will destroy TCE mass located in both the fractures and the matrix (Figure 2), (ii) dissolved concentrations of TCE will decrease throughout the fracture while permanganate injection takes place, and (iii) concentration rebound occurs once ISCO is terminated (Figure 3). The discussion that follows makes use of Figures 2 and 3, as well as cross-section plots that depict the distribution of TCE and MnO_4^- in the clay matrix at various times (Figures 4 through 7).

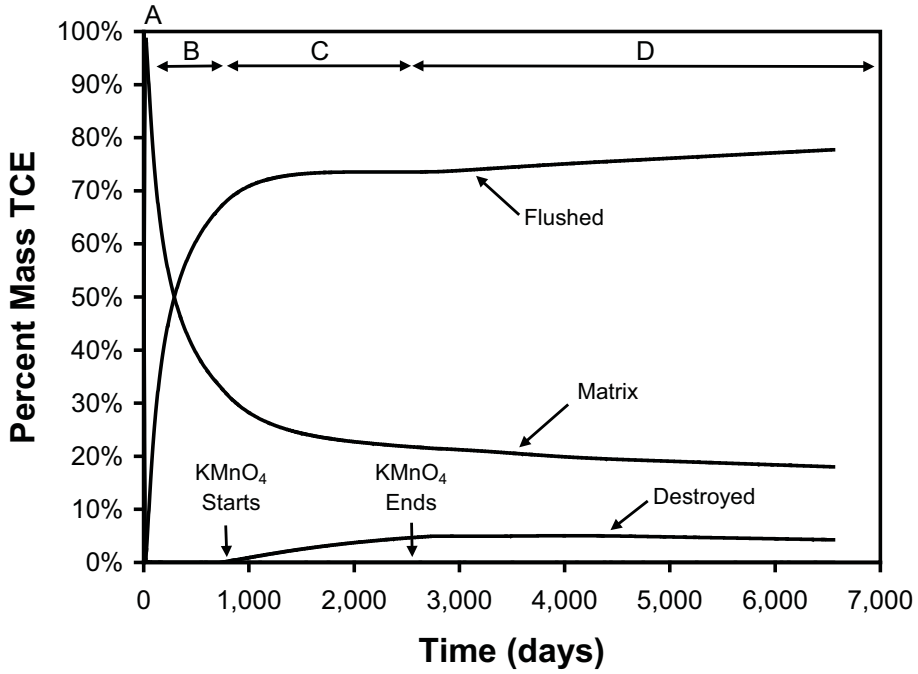

Figure 2 – Base case location of mass. After 21 days the percentage of mass in the fracture is less than 0.5%. Stage A represents period of DNAPL presence; Stage B represents pre-remediation plume development period; Stage C represents application of ISCO; Stage D represents post-remediation period.

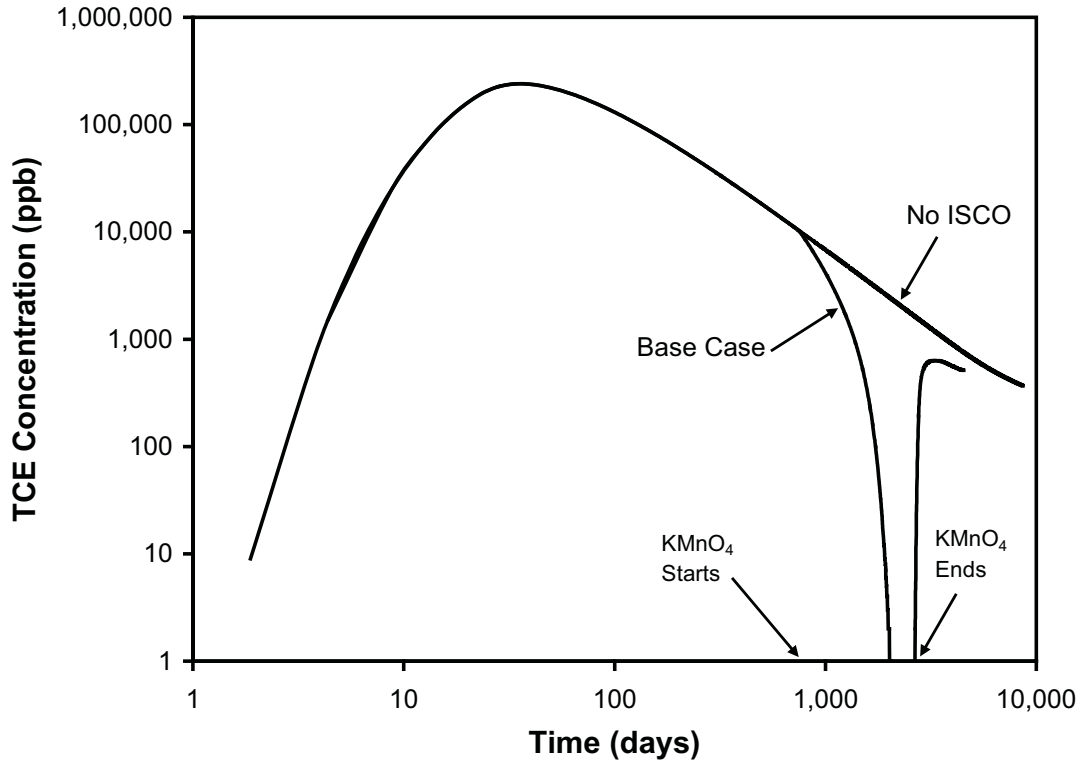

Figure 3 – Concentration of TCE versus time at outlet of system for both the base case and no ISCO simulations

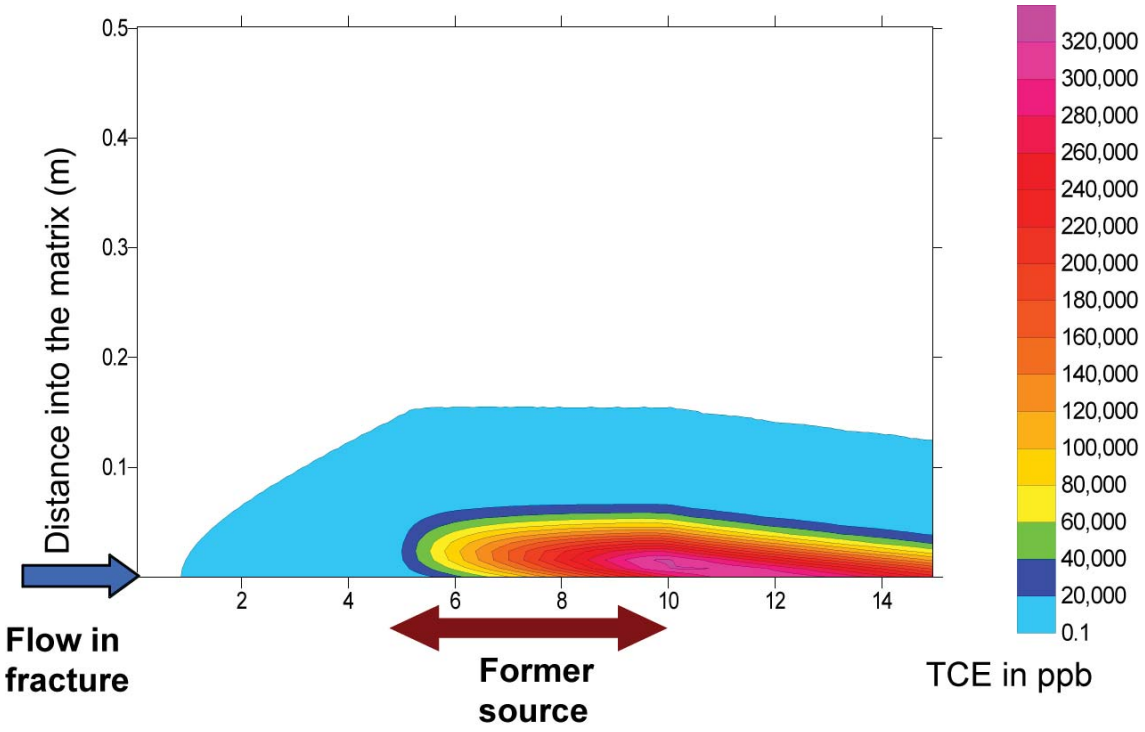

Figure 4 – Base case distribution of TCE in clay matrix at 44 days following start of simulation (DNAPL dissolution period, Stage A). $KMnO_4$ has not yet been applied.

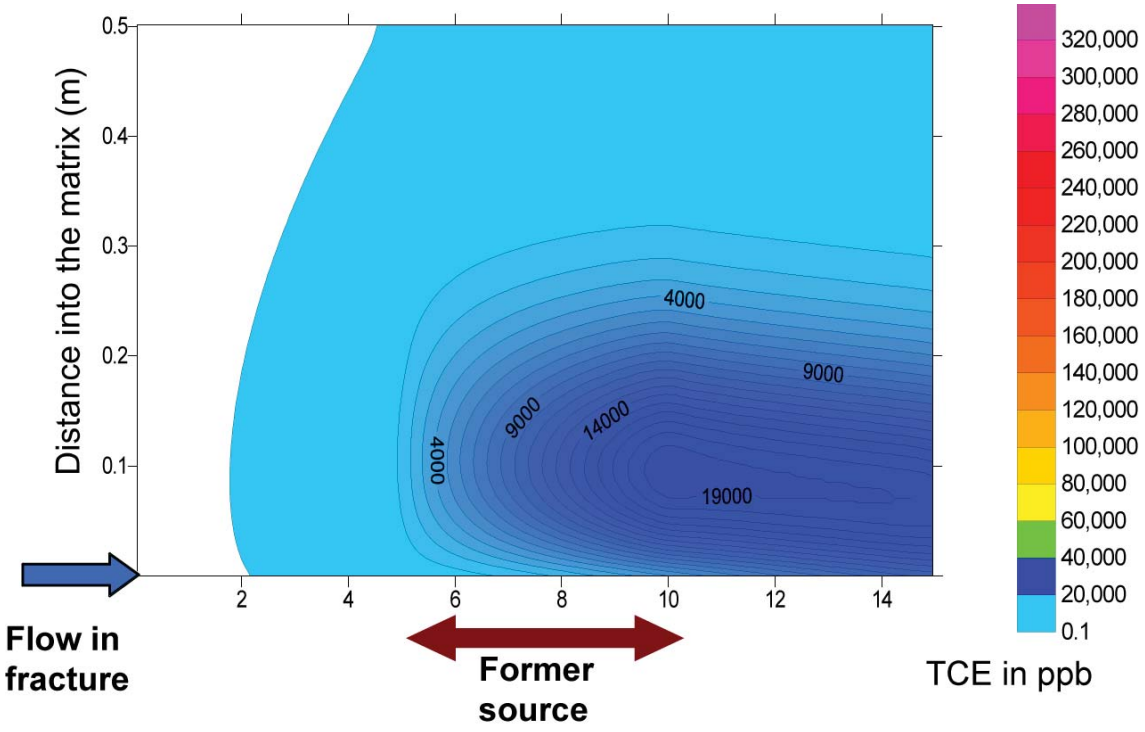

Figure 5 – Base case distribution of TCE in clay matrix at 700 days following start of simulation (plume development, Stage B). $KMnO_4$ has not yet been applied.

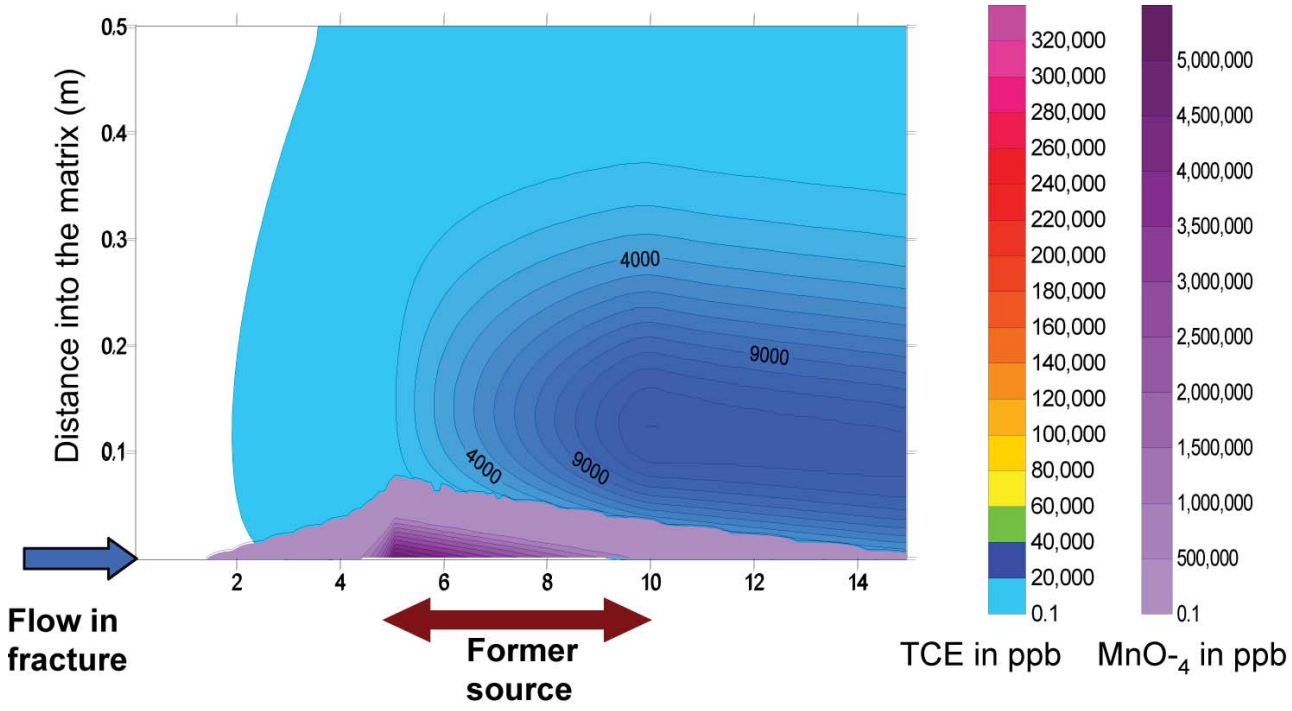

Figure 6 – Base case distribution of TCE and MnO_4^- in clay matrix at 1050 days following start of simulation (permanganate injection, Stage C).

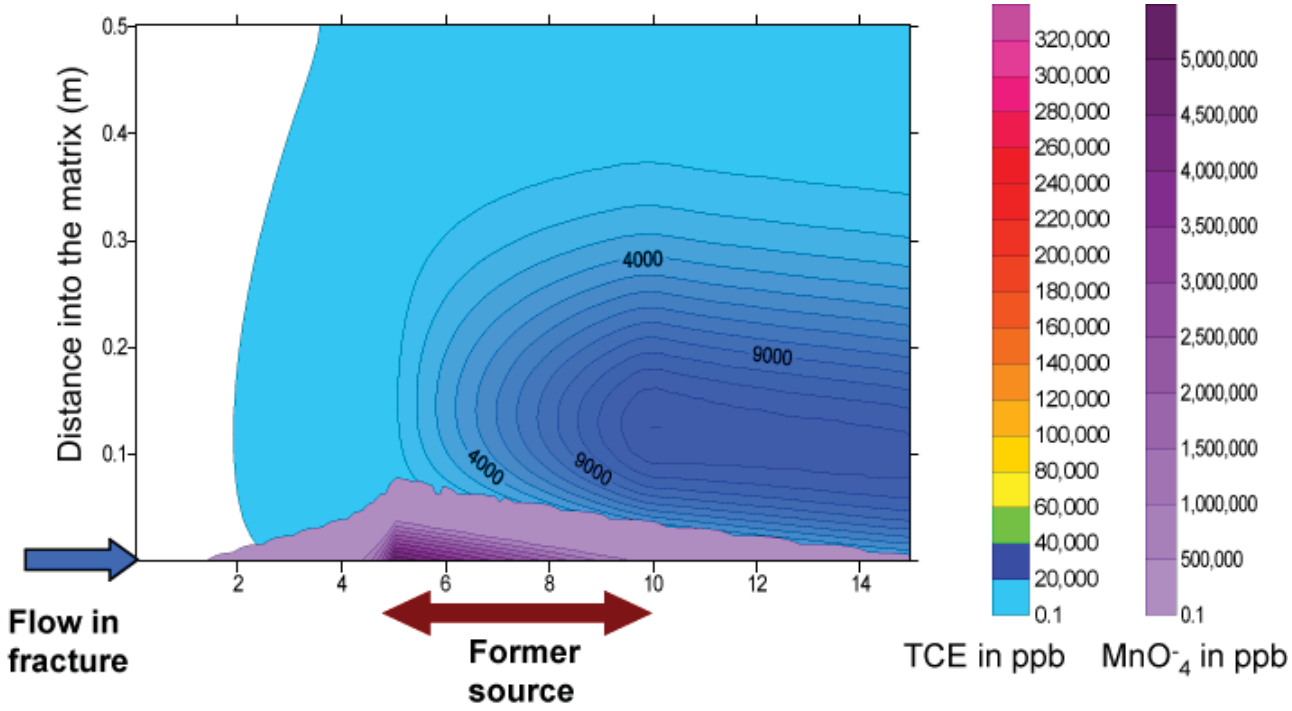

Figure 7 – Base case distribution of TCE in clay matrix at 3106 days following start of simulation (post permanganate injection, Stage D).

Figure 2 illustrates the location of TCE mass within the domain with respect to time for the base case (note that the percentage mass in the fracture is less than 0.5% and cannot be discerned on Figure 2). Four distinct stages of the mass distribution exist and are labeled as A through D. Stage A corresponds to the period of DNAPL dissolution and initial plume development subject to forward diffusion into the clay matrix. This stage is relatively short, which reflects the short time period required for contaminant mass to fully dissolve from the NAPL phase into the aqueous phase. Figure 4 presents a cross section view of TCE concentration throughout both the fracture and matrix at a time of 44 days following the start of the simulation; at this time dissolution of the NAPL phase is nearly complete. Both the mass distribution results (Figure 2) and Figure 4 indicate that during Stage A, a significant amount of TCE mass diffuses directly into the matrix adjacent to the source zone. At the end of the dissolution stage over 98% of the TCE mass is located in the matrix.

Once the DNAPL mass has completely dissolved, the post DNAPL dissolution plume development stage (B) begins. Figure 5 shows a cross section view of TCE concentration at a time of 700 days. During Stage B TCE within the matrix diffuses both deeper into the matrix and back into the fracture (diffusion in opposite directions from a concentration high within the matrix). As TCE diffuses back into the fracture it will advect and disperse downstream in the fracture and either re-enter the matrix at locations further downstream of the source zone, or be flushed out of the domain. Back diffusion plays an important role during the plume development stage as evidenced by the fact that the percent mass in the matrix falls from 98% to 34% during stage B, and the percent flushed increases from 1% to 67% over the same time period (Figure 2).

Stage C is the period during which permanganate injection takes place. Immediately following the onset of injection, TCE mass begins to be destroyed. Figure 6 shows the cross section view of both TCE and permanganate concentrations at a time of 1050 days. As the penetration of the fracture by permanganate continues, the percent mass of TCE flushed from the domain begins to level off whereas the mass back diffusing from the matrix does not. It can be seen in Figure 6 that this results from permanganate having fully penetrated the length of the fracture, allowing newly back diffused mass to be destroyed before it reaches the end of the domain.

Once permanganate injection ceases, the post treatment stage (D) begins. At this point the percent mass destroyed quickly levels off (Figure 2) and the amount of TCE flushed out of the domain begins to increase again. Figure 7 shows that permanganate has been fully consumed by 3106 days and that the concentration gradient of dissolved TCE in the matrix is resulting in TCE back diffusion into the fracture. The increase in the percent mass flushed from the domain occurring during this stage results in the rebound in dissolved concentration seen in Figure 3.

The amount of rebound occurring post treatment is quantified here in relative terms to allow comparison amongst the various simulations. The relative rebound is defined as the maximum value of dissolved concentration of the contaminant at the outlet of the domain following permanganate application (i.e., maximum concentration during Stage D) divided by the dissolved concentration of the contaminant immediately prior to permanganate injection (i.e., concentration at the beginning of Stage C). It is acknowledged here that rebound can also be quantified in other ways. The methodology adopted here recognizes the fact that baseline concentrations are typically

obtained immediate prior to remedy application (corresponding to the concentration at the beginning of Stage C), and that concentration is typically tracked on a quarterly or semi-annual basis for compliance purposes for several years following remedy application (hence the use of the maximum concentration during Stage D). For the base case simulation the relative rebound is calculated to be 0.059.

The amount of mass destroyed as a result of permanganate injection is also quantified here in relative terms to allow comparison amongst the various simulations. The percent mass destroyed is defined as the amount of contaminant mass destroyed divided by the total amount of contaminant mass present at the start of oxidant injection. For the base case simulation, the percent mass TCE detroyed by chemical oxidation is 15.3%.

Hydrogeological Parameters

Relative Rebound

The relative rebound concentrations for the hydrogeological parameter simulations are presented in Figure 8. Run D (37.5 μm fracture aperture) is not presented because TCE concentrations at the exit of the domain were not affected by permanganate injection. The lack of a concentration reduction in Run D is attributable to two things. Firstly, due to the decreased hydraulic conductivity of the fracture, significantly less mass of permanganate is required to maintain an injection concentration of 5 g/L. Secondly, when the aperture is decreased, diffusion will become a more influential transport process in comparison to advection. Both result in a decrease in the ability for permanganate to fully penetrate the fracture length, which is supported by the fact that no permanganate breakthrough curve occurs at the outlet of the fracture in this simulation.

Investigation of Run E indicates that an increase in aperture results in a decrease in the relative TCE concentration rebound. This is attributable to the fact that significantly more permanganate is injected into the system to maintain a constant permanganate concentration of 5 g/L at the injection node. In addition, the fractures are supplied with a higher flux of clean water at the inlet which causes dilution of TCE back-diffusing from the clay matrix post treatment.

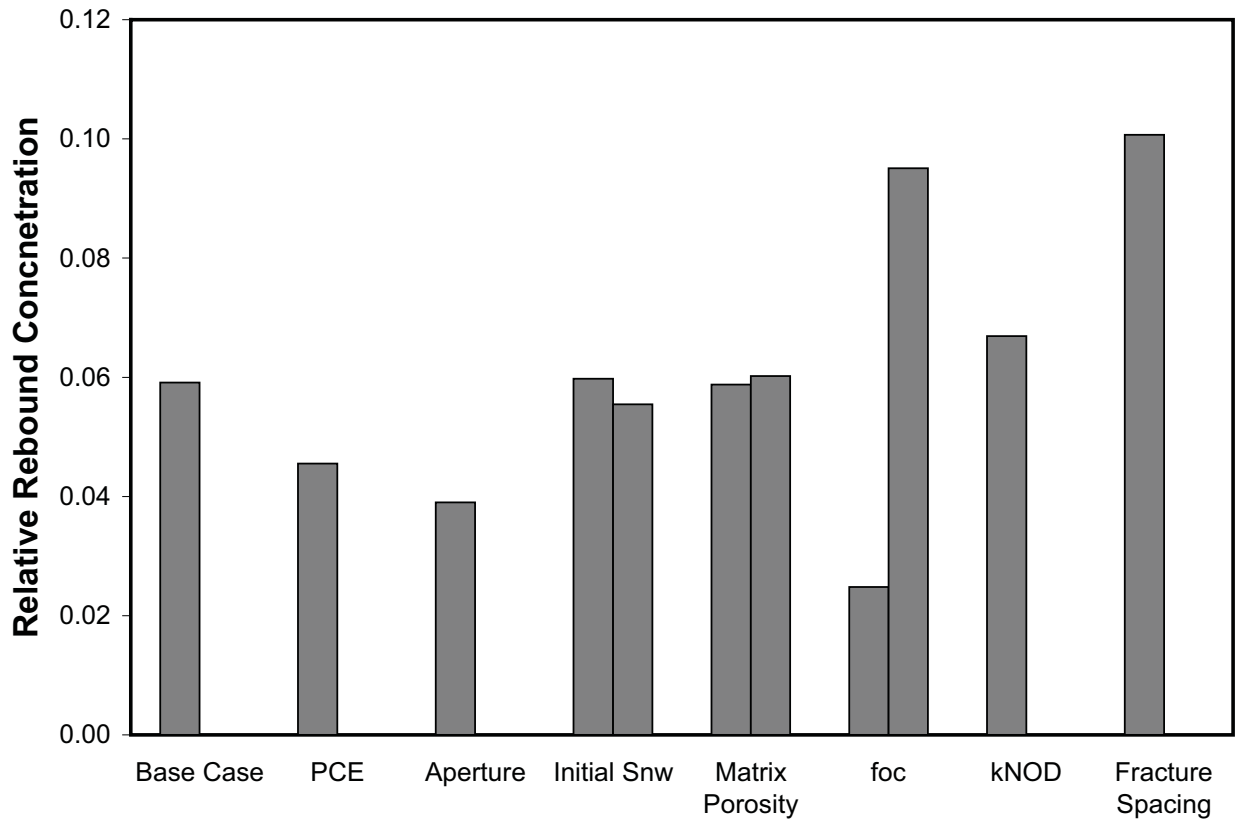

Figure 8 – Relative rebound concentrations for hydrogeological parameters (Table 2). Where two simulations involve changes to the same parameter, the results are presented next to each other. The first result corresponds to a decrease in the input parameter while the second corresponds to an increase relative to the base case. Except for bar 2, all results apply to TCE.

The relative rebound concentration for PCE (Run C) is less than that of the base case (TCE). At the end of the simulation (t = 12 years), twice as much PCE mass remained sequestered in the matrix in comparison to that of the TCE base case. The decrease in relative rebound for PCE is most likely a combination of the increased value of K_{oc} and a decreased value of kPCE. The increase in K_{oc} results in a greater ability for the contaminant to adsorb to the OAM present within the matrix, increasing retardation and therefore decreasing the rate of PCE back diffusion post treatment. The decrease in kPCE in comparison to kTCE will result in less contaminant destruction during the remediation process.

Decreasing the fracture spacing (Run M) resulted in a greater concentration rebound as a result of the shorter diffusion length scales (reduced distance between the fracture and the matrix line of symmetry). An increase in the matrix f_{oc} (Run K) also increased the relative rebound, likely attributable primarily to greater consumption of permanganate by OAM. An increase in relative rebound also occurred in response to an increase in the kinetic reaction rate constant for OAM (Run L). Increasing kNOD increases the sharpness of the permanganate front advancing into the matrix and therefore decreases the ability of permanganate to penetrate the matrix. This results in a steep TCE concentration gradient driving diffusion back into the fracture post remediation, relatively unimpeded by adsorption.

Varying the initial non-wetting phase saturations (Runs F and G) resulted in little difference to relative rebound. This stems from the fact that a significant amount of time has passed before injection begins, therefore resulting in little difference in the amount of contaminant mass remaining in permanganate accessible areas of the matrix. Also showing little sensitivity with

regards to rebound concentration was the matrix porosity (Runs H and I). This may be the result of the model formulation, however, as the matrix tortuosity (and therefore the effective diffusion coefficient) were not varied in response to changes in porosity.

Percent Mass Destroyed

The percent mass destruction for the hydrogeological parameter simulations is presented in Figure 9. The percent PCE mass destroyed (7.95%) is less than that for TCE (15.3%) because of the fact that more PCE mass was initially placed into the fracture. The higher density of PCE results in more mass compared to TCE for a specified initial DNAPL saturation.

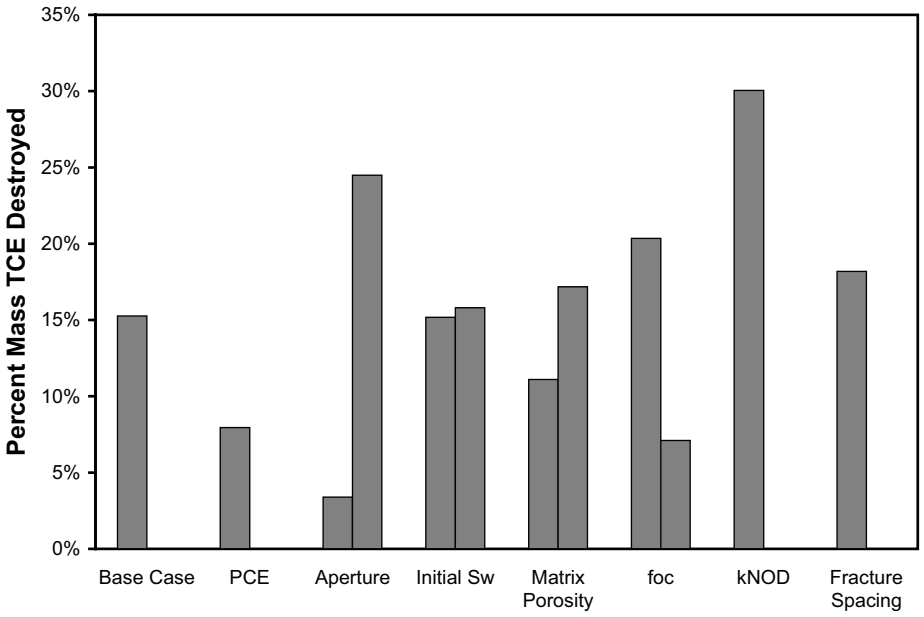

Figure 9 – Percent contaminant mass destroyed for hydrogeological parameters (Table 2). Where two simulations involve changes to the same parameter, the results are presented next to each other. The first result corresponds to a decrease in the input parameter while the second corresponds to an increase relative to the base case. Except for bar 2, all results apply to TCE.

A positive correlation exists between percent mass destruction and fracture aperture, initial DNAPL saturation, matrix porosity, and the reaction rate of the OAM (higher values of these parameters resulted in a higher percent mass destruction). The percent mass destruction was most sensitive to changes in fracture aperture stemming from the fact that the flowrate of water through the fracture is proportional to the aperture cubed. Given a constant concentration boundary condition at the oxidant injection point, it follows that the mass loading of permanganate into the system is proportional to the aperture cubed.

The percent mass TCE destroyed decreased as f_{oc} increased. Doubling the f_{oc} from 0.003 to 0.006 resulted in the percent mass destroyed to drop from 15.3% to 7.1% and is attributable to an increase in permanganate consumption by the OAM. Decreasing the fracture spacing from 1 m (base case) to 0.5 m (Run M) resulted in the percent mass TCE destroyed increasing from 15.3% to 18.2%. The distance TCE must diffuse to reach the line of symmetry in the clay matrix decreases with a decrease in fracture spacing. The TCE forward diffusion process is therefore halted earlier and the back diffusion length scale is shortened, allowing permanganate to more readily come into contact with TCE.

Engineering Parameters

Relative Rebound

The relative rebound concentrations for the engineering parameter simulations are presented in Figure 10. Of the various parameters varied in Runs N through W (Table 3), the initial time allowed for plume formation (length of Stages A and B) exhibited the greatest influence on rebound concentrations (Runs P and Q). The more time allowed for TCE to diffuse into the matrix,

the less accessible TCE will be to permanganate. This indicates that if ISCO is applied when a significant amount of contaminant mass is still present in or near the fracture, the more effective the technology will be in reducing rebound concentrations. The one week emplacement time simulation (Run P) was included as a bounding case, recognizing however that ISCO would typically not be applied this soon following a DNAPL release to fractured clay.

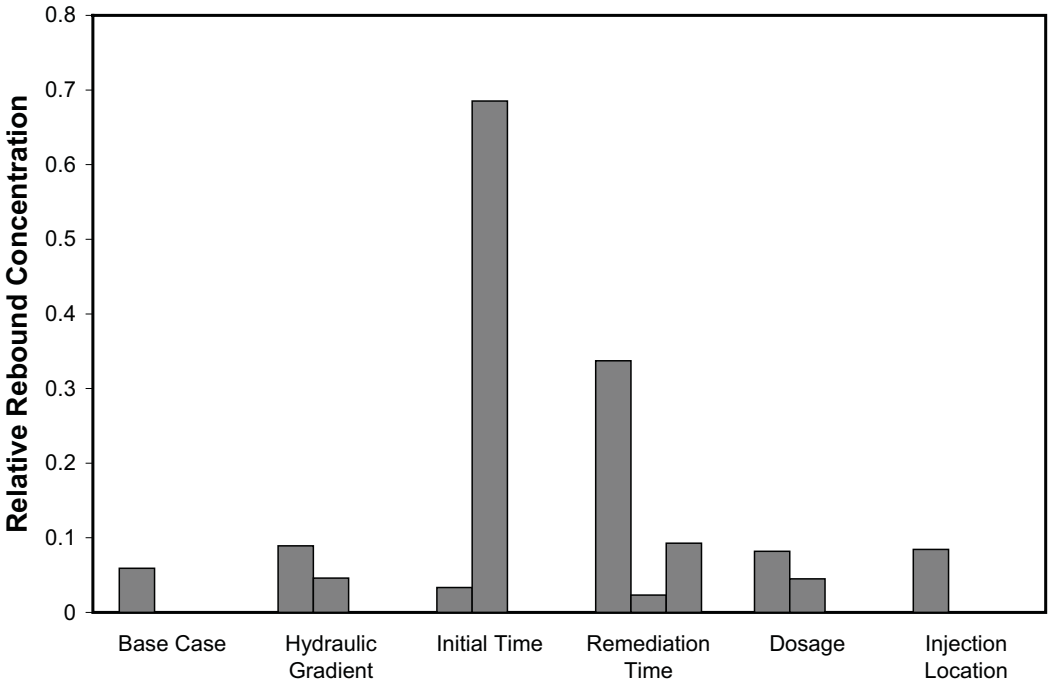

Figure 10 – Relative rebound concentrations for engineering parameters (Table 3). Where two simulations involve changes to the same parameter, the results are presented next to each other. The first result corresponds to a decrease in the input parameter while the second corresponds to an increase relative to the base case. For the remediation time sensitivity, three changes to the base case were evaluated (Runs R, S and T).

Changes in the length of time that permanganate is injected also exhibited a strong influence of rebound concentrations (Runs R, S and T). Given that the rate of TCE destruction in the clay matrix is limited by the rate that permanganate can diffuse, it is clear that longer applications of

ISCO will result in lower rebound concentrations. Applying the oxidant in 6 month pulses (Run T) results in less than half the amount of permanganate injected compared to the base case. This leads to less TCE mass destroyed and higher rebound concentrations stemming from back diffusion. With respect to the influence of hydraulic gradient, it was found that a reduction in the hydraulic gradient resulted in no permanganate breakthrough at the outlet of the fracture. The lack of permanganate breakthrough at the exit of the system indicates that the oxidant did not fully penetrate the fracture length, and therefore was not able to treat all back-diffusing TCE. The practical implication of this is that a lack of oxidant breakthrough at the end of the system may be an indication that significant rebound concentrations may ultimately occur.

Percent Mass Destroyed

The percent mass destruction of TCE for the engineering parameter simulations is presented in Figure 11. An inverse correlation exists between the percent of TCE mass destroyed and initial time and permanganate injection location. As the length of pre-injection time increases, the amount of time allowed for the contaminant to be flushed out of the domain also increases. What TCE mass does remain is sequestered deep within the matrix, unavailable to react with the permanganate. With respect to moving the injection location from 0.1 m (base case) to 3.6 m (Run W) upstream of the source zone, the percent TCE mass destroyed during remediation is halved, dropping from 15.3% to 7.58%. This indicates that in order to maximize TCE destruction during ISCO, the remediation system should be designed to incorporate a permanganate injection location as close as possible to the source zone. Similar to the variable aperture results, the percent mass of TCE destroyed was found to decrease when the hydraulic gradient was both increased and decreased.

As is discussed further on in this paper, maximum mass destruction requires an optimal balance between advective flux in the fracture and diffusive flux in the matrix.

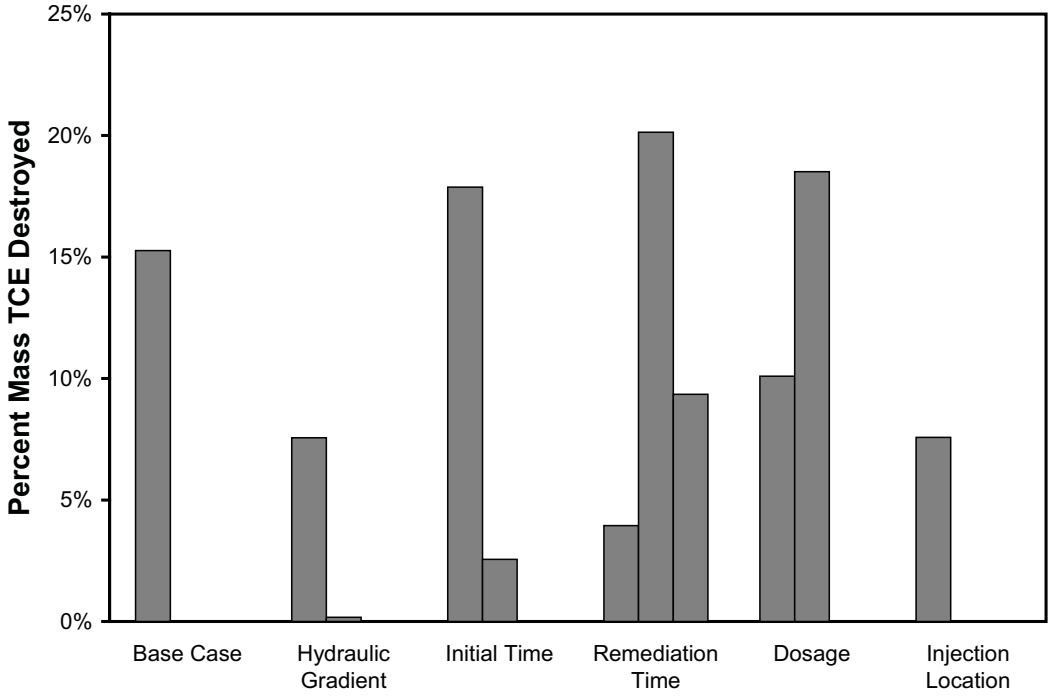

Figure 11 – Percent contaminant mass destroyed for engineering application parameters (Table 3). Where two simulations involve changes to the same parameter, the results are presented next to each other. The first result corresponds to a decrease in the input parameter while the second corresponds to an increase relative to the base case. For the remediation time sensitivity, three changes to the base case were evaluated (Runs R, S and T).

Relationship Between Rebound Concentration and Mass Destroyed

Figure 12 presents a plot of percent mass destroyed versus rebound concentration for all simulations carried out in this study (absent the No ISCO simulation). Figure 12 indicates that when rebound concentrations are high, the percent of contaminant mass destroyed for the simulation is low. More interesting, however, is that the comparison also indicates that no

relationship exists between the two metrics when rebound concentrations are low. These results suggest that conclusions regarding the amount of mass destroyed at a site cannot be based on the magnitude of rebound concentrations.

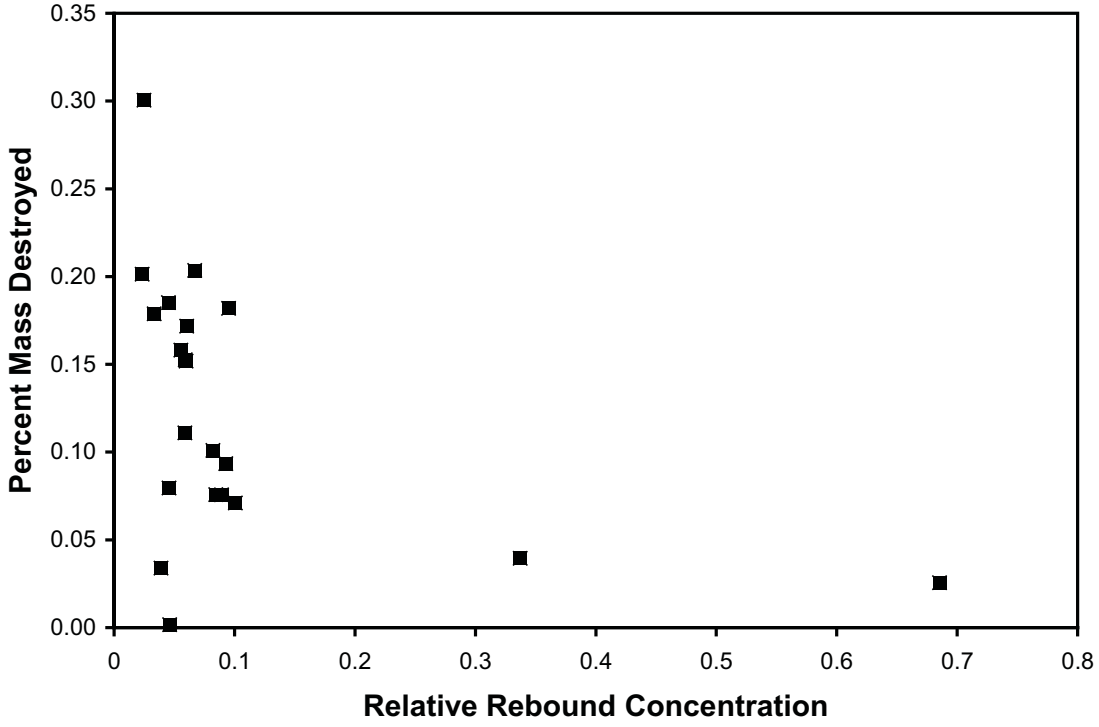

Figure 12 – Relationship between relative rebound concentrations and percent mass destroyed

System Peclet Number

As discussed previously, no clear correlation was found to exist between the percent mass destroyed and either fracture aperture or hydraulic gradient. The mass of permanganate injected varies with the aperture and the hydraulic gradient because a constant injection concentration is maintained at the injection location. Larger fracture apertures and larger hydraulic gradients therefore result in a higher rate of oxidant mass loading to the system. A higher rate of oxidant

mass loading may not be cost effective, however, if significant amounts of oxidant are found to flush through the system too quickly. A 'System Peclet Number' is defined here to quantify the rate of advection in the fracture relative to the rate of diffusion in the matrix:

$$Pe = \frac{vL}{D_o} \tag{12}$$

where D_o is the free solution diffusion coefficient [L^2T^{-1}], L is a characteristic length (in this case the fracture aperture [L]), and v is the ground water velocity in the fracture [LT^{-1}]. When the ground water velocity is low, diffusion is the dominant process, resulting in a small System Peclet Number and a greater amount of the permanganate diffusion into the matrix. This limits the ability of permanganate to fully penetrate the fracture and results in incomplete treatment of the source zone.When the ground water velocity is high, advection and dispersion processes are dominant. A large System Peclet Number results and significant amounts of both the contaminant and oxidant may be flushed out of the domain at early time rather than diffusing into the matrix.

Figures 13 and 14 present the relative rebound concentrations and normalized percent TCE mass destroyed, respectively, versus the System Peclet Number for the simulations that influence ground water velocity. Figure 13 shows that as the velocity and therefore the System Peclet Number decreases, the relative rebound of TCE at the outlet increases. Note also that Run D (reduced aperture, therefore low System Peclet Number) resulted in no influence on outlet TCE concentrations. The difference in relative rebound between Runs O and E are small, suggesting that increasing the System Peclet Number past a certain point may not significantly aid in decreasing rebound concentrations. Inspection of Figure 14 reveals that the simulations with a higher System Peclet Number were relatively ineffective in destroying TCE mass.

The results found here suggest that the System Peclet Number can be used to assist in the design of an ISCO application once it has been determined whether minimizing rebound concentrations or maximizing TCE destruction is the goal. If minimizing rebound concentration is of most importance, achieving a threshold System Peclet Number may be beneficial. In comparison, if maximum TCE destruction is desired, a low System Peclet Number may be most effective in achieving the goal.

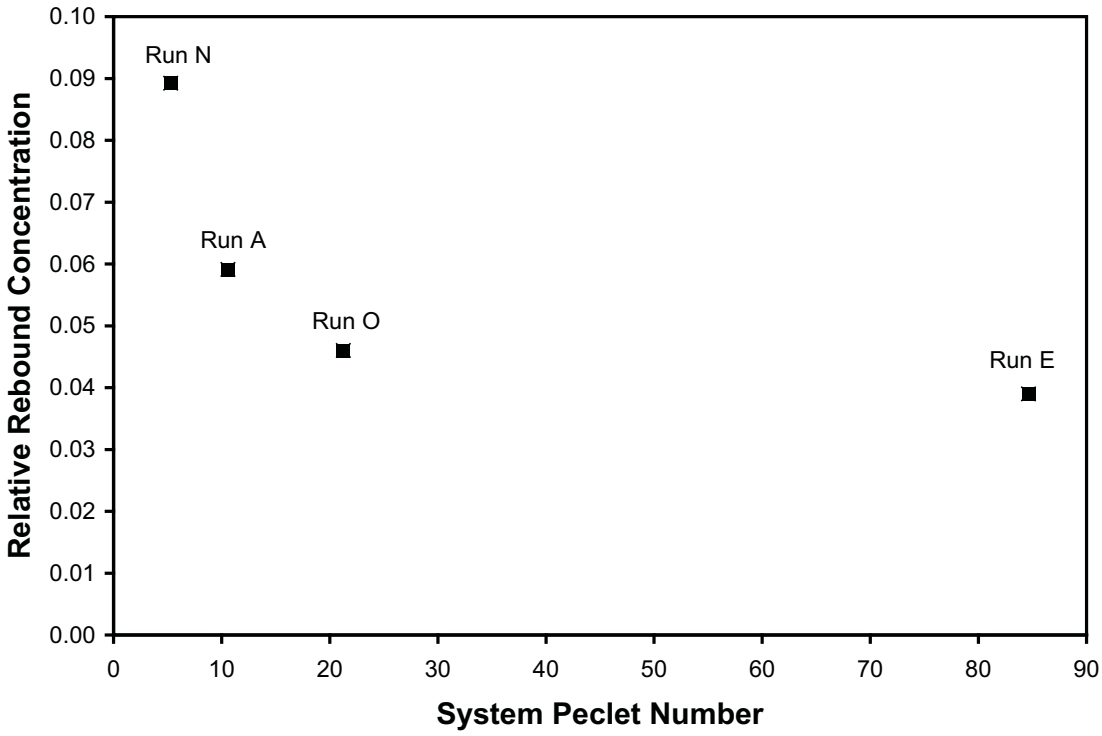

Figure 13 – Relative rebound concentration versus System Peclet Number for simulations that influence ground water velocity in the fracture.

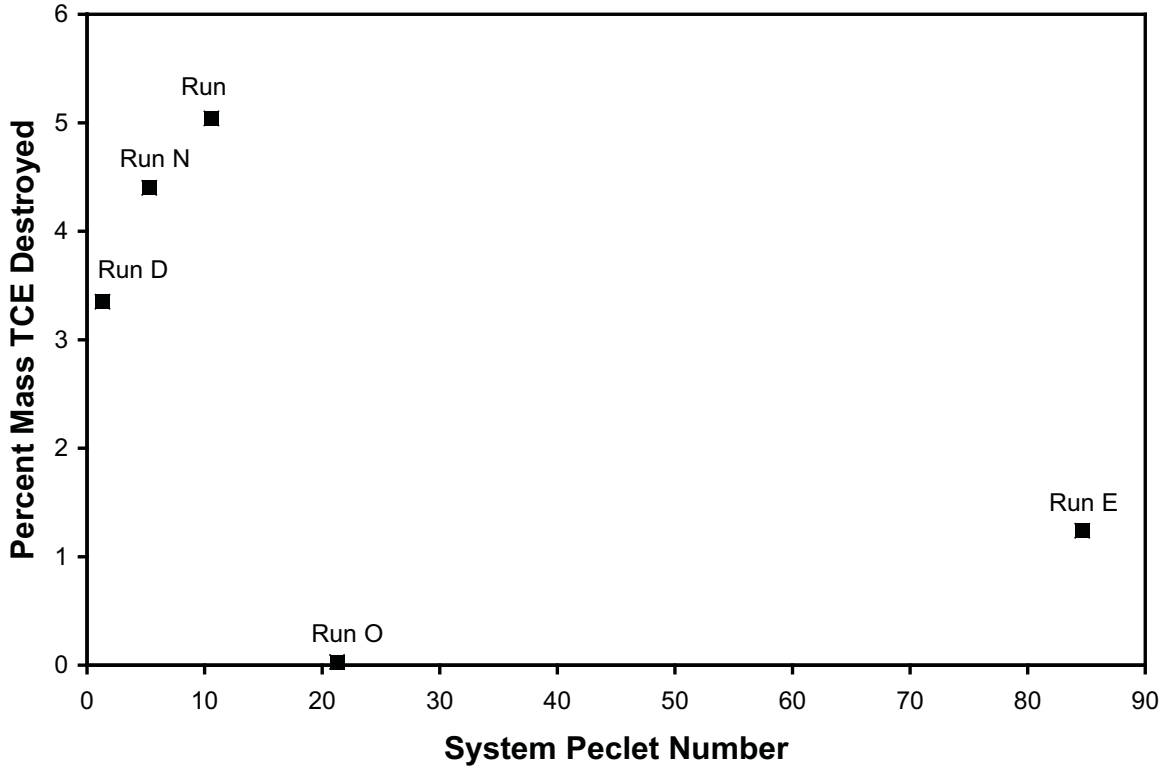

Figure 14 – Percent mass TCE destroyed versus System Peclet Number for simulations that influence ground water velocity in the fracture.

Conclusions

Modeling results indicate that all parameters investigated in this study exerted some influence on the percent mass of TCE destroyed and rebound concentrations following permanganate injection. With regards to the hydrogeological parameters, the most influential parameters governing rebound concentrations resulting from back diffusion were the clay matrix f_{oc} and the fracture spacing. Higher f_{oc} values and lower fracture spacing both resulted in higher rebound concentrations at the exit of the system. With respect to the amount of contaminant mass destroyed, lower fracture aperture values resulted in increased amounts of mass destruction, but only to a certain limit after which effective delivery of the permanganate was precluded. Lower matrix f_{oc} values and higher matrix porosity also resulted in greater amounts of contaminant mass destruction. The results of

this study suggest that time and effort to characterize the clay matrix and its diffusive characteristics may be warranted prior to field application of ISCO.

Analysis of the engineering parameters found that it is important to characterize the source zone with respect to source and plume location. Injecting oxidant immediately upgradient of the source zone will minimize permanganate consumption by uncontaminated OAM. Remediation of sites where the DNAPL phase has long been depleted as a result of dissolution into the aqueous phase may be challenging because the contaminant mass may have become sequestered deep within the matrix and therefore inaccessible to permanganate. Remediation strategies using short permanganate injection time lengths of 1 year or less, and pulsed remediation schemes, were not as effective as the base case injection scheme.

Two parameters that are very important to consider in designing a remediation system are the fracture aperture and the hydraulic gradient, both of which affect the velocity within the fracture. It is important to achieve a balance between the advective transport of permanganate and TCE through fractures and diffusion of permanganate and TCE in the clay matrix. This balance can be quantified using the System Peclet Number. In the scenario considered here, a threshold System Peclet Number was required to minimize relative rebound concentration and a low System Peclet Number was required to achieve large amounts of TCE mass destruction. This study indicates that the amount of contaminant mass destroyed may be relatively independent of the rebound concentration observed during post remediation monitoring. As a result, it is suggested that the design of a system may vary significantly depending on whether degree of mass destruction, or contaminant concentration reduction, is the adopted remediation metric.

References

Allen, T.J., J. Dablow, B. Marvin, M.L. Barackman, J. Baker, and B. Blanford. 2004. TCE oxidation by potassium permanganate injection to enhance groundwater remediation. In *Chemical-Based Remediation Technologies (2C-06)*. Battelle Press.

Barcelona, M.J. and T.R. Holm. 1991. Oxidation-reduction capacities of aquifer solids. *Environmental Science and Technology*, no. 25: 1565-1572.

Bear, J. 1972.*Dynamics of °uids in porous media*. New York: American Elsevier Publishing Company.

Brooks, R.H. and Corey, A.T., 1966. Properties of porous media affecting fluid flow. J. Irrigation and Drainage, Division American Society of Civil Engineering, 92, IR2: 61-88.

Clement, T.P., Y. Sun, B.S. Hooker, and J.N. Petersen. 1998. Modeling multispecies reactive transport in ground water. *Groundwater Monitoring and Remediation*, no. 18: 79-92.

Clement, T.P. 1997. RT3D - A modular computer code for simulating reactive multi-species transport in 3-dimensional groundwater systems. Battelle Pacific Northwest National Laboratory Research Report, PNNL-SA-28967.

Conrad, S.H., R.J. Glass, and W.J. Peplinski. 2002. Bench-scale visualization of DNAPL remediation processes in analog heterogeneous aquifers: surfactant floods and in situ oxidation using permanganate. *Journal of Contaminant Hydrology*, no. 58: 13-49.

Crother, R.A., J. Shipley, and R.A. Vogl. 2004. Changes in water quality due to potassium permanganate injection. In *Chemical-Based Remediation Technologies (2C-38)*. Battelle Press.

Dai, Q. and S. Reitsma. 2004. Kinetic study of permanganate oxidation of tetrachloroethylene at a high pH under acidic conditions. *Remediation*, no. 14: 67-79.

Fetter, C.W. *Contaminant Hydrology*. 1993. New Jersey: Prentice Hall,

Gates, D.D., R.L. Siegrist, and S.R. Cline. 1995. Chemical oxidation of volatile and semivolatile organic compounds in soil. 88th Annual Meeting and Exhibition, Air and Waste Management Association.

Goldstein, K.J., A.R. Vitolins, D. Navon, B.L. Parker, S. Chapman, and G.A. Anderson. 2004. Characterization and pilot-scale studies for chemical oxidation remediation of fractured shale. *Remediation*, no. 14: 19-37.

Hood, E.D. and N.R. Thomson. 2000. Numerical simulation of in situ chemical oxidation.

In *Chemical Oxidation and Reactive Barriers; remediation of chlorinated and recalcitrant compounds, International Conference on Remediation of Chlorinated and Recalcitrant Compounds*. Battelle Press.

Hood, E.D. and N.R. Thomson. 2002. Impact of diffusion and natural oxidant demand on permanganate into low-permeability porous media. In *Chemical Oxidation and Reactive Barriers; remediation of chlorinated and recalcitrant compounds, International Conference on Remediation of Chlorinated and Recalcitrant Compounds*. Battelle Press.

Hood, E.D., N.R. Thomson, D. Grosse, and G.J. Farquhar. 2002. Experimental determination of the kinetic rate law for the oxidation of perchloroethylene by potassium permanganate. *Chemosphere*, no. 40: 1383-1388.

Huang, K.C., G.E. Hoag, P. Chheda, B.A. Woody, and G.M. Dobbs. 2001. Oxidation of chlorinated ethenes by potassium permanganate: a kinetic study. Journal of Hazardous Materials, no. B87:155-169.

Johnson, R.L., J.A. Cherry, and J.F. Pankow. 1989. Diffusive contaminant transport in natural clay: A field example and implications for clay-lined waste disposal sites. *Environmental Science and Technology*, no. 23: 340-349.

Kueper, B.H., and D.B. McWhorter. 1991. The behavior of dense, nonaqueous phase liquids in fracture clay and rock. *Ground Water*, no. 29, vol. 5:716-728.

Li, X.D. and F.W. Schwartz. 2000. Efficiency problems related to permanganate oxidation schemes. in: Wickamanayake, g.b., gavaskar, a.r., chen, a.s.c. (eds). In *Chemical Oxidation and Reactive Barriers: Remediation of Chlorinated and Recalcitrant Compounds, International Conference on Remediation of Chlorinated and Recalcitrant Compounds*, 41-48. Battelle Press.

Lide, D.R. (Editor) 2004. *CRC Handbook of Chemistry and Physics*, 85th edition. CRC Press.

Longino, B.L. and B.H. Kueper. 1999. Nonwetting phase retention and mobilization in rock fractures. *Water Resources Research*, no. 35: 2085-2093.

MacKinnon, L.K. and N.R. Thomson. 2002. Laboratory in situ chemical oxidation of a perchloroethylene pool using permanganate. *Journal of Contaminant Hydrology*, no. 56: 49-74.

Marvin, B.K., J. Chambers, A. Leavitt, and C.G. Schreier. 2002. Chemical and engineering challenges to in situ permanganate remediation. In *International Conference on Remediation of Chlorinated and Recalcitrant Compounds*. Battelle Press.

Marvin, B.K., J. Chambers, A. Leavitt, and C.G. Schreier. 2004. Chemical and engineering challenges to in situ permanganate remediation. In *Chemical-Based Remediation Technologies (2C-04)*. Battelle Press.

Mumford, K.G. 2002. Investigation of natural oxidant demand reactions in a sandy aquifer

material. Master's diss., Department of Civil Engineering, University of Waterloo.

Mumford, K.G., N.R. Thomson, and R.M. Allen-King. 2005. Bench scale investigation of permanganate natural oxidant demand kinetics. *Environment Science and Technology*, no. 29: 2835-2840.

Mundle, K., 2006. Concentration Rebound Following In Situ Chemical Oxidation in Fractured Clay. M.Sc. thesis, Department of Civil Engineering, Queen's University, Kingston, Ontario, Canada.

Pankow, J. F. and John A. Cherry. 1996. *Chlorinated Solvents and Other DNAPLs in Groundwater*. Portland: Waterloo Press.

Parker, B.L., R.W. Gillham, and J.A. Cherry. 1994. Diffusive disappearance of immiscible-phase organic liquids in fractured geologic media. *Ground Water*, no. 32: 805-820.

Reitsma, S. and Kueper, B.H., 1994. Laboratory measurement of capillary pressure saturation curves in a natural rock fracture. *Water Resources Research*, 30(4), pp. 865-878.

Schnarr, M., C. Farquhar, E. Hood, T. Gonullu, and B. Stickney. 1998. Laboratory and controlled field experiments using potassium permanganate to remediate trichloroethylene and perchloroethylene dnapls in porous media. *Journal of Contaminant Hydrology*, no. 29: 205-224.

Schroth, M.H., M. Oostrom, T.W. Wiestma, and J.D. Istok. 2001. In-situ oxidation of trichloroethene by permanganate: Effects on porous medium hydraulic properties. *Journal of Contaminant Hydrology*, no. 20: 79-98.

Siegrist, R.L., O.R. West, M.I. Morris, D.A. Pickering, D.W. Greene, C.A. Muhr, D.D. Davenport, and J.S. Gierke. 1995. In situ mixed region vapor stripping in low-permeability media. 2. full-scale field experiments. *Environmental Science and Technology*, no. 29: 2198-2207.

Struse, A.M., R.L. Siegrist, H.E. Dawson, and M.A. Urynowicz. 2002. Diffusive transport of permanganate during in situ oxidation. *Journal of Environmental Engineering*, no. 128: 327-334.

Sudicky, E.A. and E.O. Frind. 1982. Contaminant transport in fractured porous media: Analytical solutions for a system of parallel fractures. *Water Resources Research*, no. 8: 1634-1642.

Tang, D.H., E.O. Frind, and E.A. Sudicky. 1981. Contaminant transport in fractured porous media: Analytical solution for a single fracture. *Water Resources Research*, no. 17: 555-564.

Tunnicliffe, B.S. and N.R. Thomson. 2004. Mass removal of chlorinated ethenes from rough-walled fractures using permanganate. *Journal of Contaminant Hydrology*, no. 75: 91-114.

Urynowicz, M.A and R.L. Siegrist. 2005. Interphase mass transfer during chemical oxidation of TCE DNAPL in an aqueous system. *Journal of Contaminant Hydrology*, no. 80: 93-106.

Vella, P.A. and B. Veronda. 1992. Oxidation of trichloroethylene: Comparison of potassium permanganate and fenton's reagent, chemical oxidation technologies for the nineties. Technomin, Lancaster, PA, USA,

Yan, Y.E. and F.W. Schwartz. 1999. Oxidative degradation and kinetics of chlorinated ethylenes by potassium permanganate. *Journal of Contaminant Hydrology*, no. 27: 343-365.

Zhang, H. and F.W. Schwartz. 2000a. Simulating the in situ oxidative treatment of chlorinated ethylenes by potassium permanganate. *Water Resources Research*, no. 36: 3031-3042.

Zhang, H., and F.W. Schwartz, 2000b. Simulation of oxidative treatment of a chlorinated compounds by permanganate, Second International Conference on Remediation of Chlorinated and Recalcitrant Compounds, Monterey, May 22-25, pp 1-16.

APPENDIX D.2

DNAPL SOURCE ZONE REMEDIATION IN FRACTURED ROCK: MODEL DEVELOPMENT AND TESTING

DNAPL IN FRACTURED ROCK: MODEL DEVELOPMENT

The model developed for this work (DNAPL3DRX-FRAC) involves the coupling of the three-dimensional two-phase flow model (DNAPL3D) (Gerhard et al., 1998, 2001; Gerhard and Kueper, 2003a,b,c; Gerhard et al., 2007) and RT3D, a three-dimensional multi-species contaminant transport model with non-linear kinetic reactions (Clement, 1997; Clement et al., 1998). This coupling was executed with DNAPL3D-RX (West et al., 2008) using a split-operator approach following Grant and Gerhard (2004). Within a time step, DNAPL migration is initially simulated using DNAPL3D. The contaminant solute is then added to the aqueous phase at nodes with DNAPL present via equilibrium or non-equilibrium mass transfer routines (Grant and Gerhard, 2004; Grant and Gerhard, 2007b). RT3D is then employed within the same time step to simulate advection, dispersion and reactions of the solute. Finally, the phase saturations are updated at the end of the time step in accordance with the amount of mass transferred from the DNAPL to the aqueous phase. Although DNAPL3D-RX is three-dimensional, all fractured rock simulations presented in this work are two-dimensional. The model's relevant characteristics and governing equations are presented here, along with verification against available analytical solutions and tests of model performance. Also provided are charts illustrating the logic of model construction as applied to the three technologies.

1 GOVERNING EQUATIONS

DNAPL3D

The fluid fluxes can be mathematically described by extending Darcy's law to multiphase flow:

$$q_W = -\frac{k_{ij}k_{r,W}}{\mu_W}\left(\frac{\partial P_W}{\partial X_j} + \rho_W g \frac{\partial Z}{\partial X_j}\right) \qquad \text{i, j = x, y, z} \qquad (1)$$

$$q_{NW} = -\frac{k_{ij}k_{r,NW}}{\mu_{NW}}\left(\frac{\partial P_{NW}}{\partial X_j} + \rho_{NW} g \frac{\partial Z}{\partial X_j}\right) \qquad \text{i, j = x, y, z} \qquad (2)$$

where q_W and q_{NW} are the wetting phase and non-wetting phase fluxes respectively [L/T], k_{ij} are the medium permeability [L^2], $k_{r,W}$ and $k_{r,NW}$ are the relative permeabilities to the wetting and non-wetting phases respectively [-], μ_W and μ_{NW} are the wetting and non-wetting phase viscosities respectively [M/LT], P_W and P_{NW} are the wetting and non-wetting phase pressures, respectively [M/LT^2], ρ_W and ρ_{NW} are the wetting and non-wetting fluid densities respectively [M/L^3]; g is the gravitational constant [L/T^2].

Equations 1 and 2 are then substituted into the continuity equations for mass balance of the wetting and non-wetting fluid phases giving the following simultaneous equations:

$$\frac{\partial}{\partial X_i}\left[\frac{k_{ij}k_{r,W}}{\mu_W}\left(\frac{\partial P_W}{\partial X_j} + \rho_W g \frac{\partial Z}{\partial X_j}\right)\right] = \theta \frac{\partial S_W}{\partial t} \qquad \text{i, j = x, y, z} \qquad (3)$$

$$\frac{\partial}{\partial X_i}\left[\frac{k_{ij}k_{r,NW}}{\mu_{NW}}\left(\frac{\partial P_{NW}}{\partial X_j}+\rho_{NW}g\frac{\partial Z}{\partial X_j}\right)\right]=\theta\frac{\partial S_{NW}}{\partial t} \qquad \text{i, j = x, y, z} \qquad (4)$$

where S_W and S_{NW} are the wetting and non-wetting saturations respectively [-], θ is the porosity of the porous medium [-].

Although equations 3 and 4 contain four unknowns: P_W, P_N, S_W and S_N, the two pressures unknowns are related to the capillary pressure, where:

$$P_C = P_{NW} - P_W \qquad (5)$$

while the saturations are related by:

$$S_W + S_{NW} = 1 \qquad (6)$$

By substituting equations 5 and 6 to replace P_{NW} and S_{NW} in equations 3 and 4, the final two partial differential equations (Kueper and Frind, 1991) in terms of two unknowns P_W and S_W are:

$$\frac{\partial}{\partial X_i}\left[\frac{k_{ij}k_{r,W}}{\mu_W}\left(\frac{\partial P_W}{\partial X_j}+\rho_W g\frac{\partial Z}{\partial X_j}\right)\right]=\theta\frac{\partial S_W}{\partial t} \qquad \text{i, j = x, y, z} \qquad (7)$$

$$\frac{\partial}{\partial X_i}\left[\frac{k_{ij}k_{r,NW}}{\mu_{NW}}\left(\frac{\partial\left(P_C+P_W\right)}{\partial X_j}+\rho_{NW}g\frac{\partial Z}{\partial X_j}\right)\right]=-\theta\frac{\partial S_W}{\partial t} \qquad \text{i, j = x, y, z} \qquad (8)$$

Equations 7 and 8 are solved simultaneously to predict the movement of wetting and

non-wetting phases with respect to both space and time. Their solution further requires definition of constitutive relationships for capillary pressure $P_C\ (S_W)$ and relative permeability $kr(S_W)$, which introduces nonlinearity via *Sw*. The equations are solved in a node-centered finite difference domain via discretized equations that are second order accurate in space and first order accurate in time and are solved fully implicitly via Newton Raphson iteration as discussed in Gerhard and Kueper, 2003.

RT3D

In RT3D, the governing equations of contaminant transport of the mobile and immobile species are (Clement, 1997; and Clement et al., 1998):

$$\frac{\partial(\theta C_m^n)}{\partial t} = \frac{\partial}{\partial x_i}\left(\theta D_{ij}^n \frac{\partial C_m^n}{\partial x_j}\right) - \frac{\partial}{\partial x_i}\left(\theta v_i C_m^n\right) + q_s C_s^n + \sum R_m \quad \text{i, j = x, y, z} \qquad (9)$$

$$\frac{\partial(\theta C_{im}^n)}{\partial t} = \sum R_{im} \qquad (10)$$

where D_{ij} is the hydrodynamic dispersion tensor [L^2/T], v_i is the average linear groundwater velocity [L/T], q_s is a volumetric flux representing sources and/or sinks [T^{-1}], R is the rate of all reactions [M/L^3T], and *t* is time [T].

The superscript *n* denotes the species number, while the subscripts *m* and *im* denote the mobile and immobile species respectively; the subscript *s* denotes a source or a sink. Sorption of the contaminant (assuming a linear sorption isotherm) is represented through a retardation factor (R_s) defined as:

$$R_s = 1 + \frac{\rho_b}{\theta} K_{oc} f_{oc} \qquad (11)$$

where ρ_b is the soil dry bulk density [M/L^3], K_{oc} is the organic carbon partition coefficient [L^3/M], and f_{oc} is the fraction organic carbon [-].

The advection and dispersion of individual solute species was solved using the standard explicit finite-difference method (Clement, 1997; Clement et al., 1998); while there are several solver options available to the user in RT3D, testing with the template sites revealed that the former technique was a good balance between memory usage and computational run-time. All solute reactions were solved using the automatic switching Gear-stiff/non-stiff solver option in RT3D.

Fractured Rock

DNAPL3D, RT3D, and DNAPL3D-RX were developed and previously only employed for simulating scenarios involving unconsolidated porous media. Modifications to handle fractured porous media were developed for this thesis and are presented below.

The fracture hydraulic conductivity used in the model was calculated according to (Kueper and McWhorter, 1991; Witherspoon et al., 1980):

$$K = -\frac{e^2 k_{rw} \rho_w g}{12 \mu_\omega} \qquad (12)$$

where e is the hydraulic aperture of the fracture [L] and, k_{rw} is the relative permeability [-]. The relative permeability (k_{rw}) term was calculated using the Brooks – Corey constitutive model (Brooks and Corey, 1966). The Brooks – Corey constitutive model

was demonstrated to be a valid for representing capillary pressure functions in fractures by Reitsma and Kueper (1994). The harmonic mean of the nodal hydraulic conductivities was calculated and multiplied by the hydraulic gradient across the fracture to obtain the wetting phase flux in the fracture. The average linear ground water velocity (v) for each individual node was calculated by dividing the flux by the local wetting phase saturation.

DNAPL to water mass transfer is treated as an equilibrium process in the simulations presented in this work. Although researchers have reported both equilibrium (e.g., Miller et al. 1998; Frind et al. 1999) and non-equilibrium (e.g., Glass and Nicholl, 1995; Dickson and Thomson, 2003) mass transfer in experimental fractured systems, the focus in the majority of this work is on behaviour of remediation systems after substantial aging periods for the DNAPL source zone (e.g., 20 years). Additionally, sensitivity tests revealed that in most cases all DNAPL dissolves in the first few years of aging irregardless of the mass transfer routine chosen. In an attempt to acquire a more in-depth understanding of the effects of mass transfer models on fractured rocks, a rate-limited model adopted from Dickson and Thomson (2003) was incorporated into the model. This rate-limited model was then employed in a single comparison simulation for the surfactant flushing study.

The entry pressure of each fracture was calculated according to (Kueper and McWhorter, 1991):

$$Pe = \frac{(2 \times IFT)}{e} \qquad (13)$$

where, P_e is the fracture entry pressure [M/LT^2], IFT is the interfacial tension between DNAPL and water [M/L], and e is the hydraulic aperture of the fracture [L] (assumed to be representative of the hydraulic aperture giving rise to the first connected non-wetting phase pathway through the computational cell of interest along main drainage). In this equation, DNAPL is assumed to be perfectly nonwetting, hence the contact angle in this equation (as compared to equation 2.11) is assumed to be 0°. In all the simulations presented in this work, the entry pressure of the matrix is assumed to be sufficient to prevent the penetration of DNAPL; this assumption provides the technologies considered the best opportunity for success by restricting the DNAPL mass to the connected fracture network which is accessible by injected treatment fluids.

2.0 GRIDDING ROUTINE

Purpose of Gridding Routine

As demonstrated by Slough et al., (1999), if fracture elements in a domain are not sufficiently discretized, an over-prediction of the volume of DNAPL that continues to migrate vertically at the intersection of a vertical and horizontal fracture can occur. In addition, correctly capturing the diffusion of aqueous compounds into and out of the matrix requires sufficiently fine grid resolution (Slough et al., 1999). By finely discretizing the fracture and adjacent matrix nodes in a rock domain (e.g., at the scale of one centimetre or less), this problem can be accurately resolved. However, such fine

resolution implies that traditional (i.e., equal grid spacing) methods of discretization will lead to a large computational expense.

A gridding routine was therefore developed specifically for this work to refine the nodal spacing of a two-dimensional finite difference domain such that appropriate node size reduction occurs only in those nodes that represent fractures and in the adjacent matrix nodes. This permits DNAPL migration and aqueous species diffusion to be captured accurately while minimizing the overall number of nodes. The routine takes a coarsely-discretized finite difference domain and refines it so that the width of fracture nodes are equal exactly to the user-specified aperture and grid spacing in the matrix progressively increases with perpendicular distance outwards from the fracture; beyond a specified distance from all fractures, the coarse grid is retained. It applies to 2D finite difference domains consisting of any number of vertical and horizontal fractures of varying length and intersections. It assumes no variability of aperture along the length of a particular fracture, but permits a distribution of apertures across the domain. The degree of grid refinement and the distribution of spacing between the new (refined) nodes are left flexible, controlled by user-defined variables.

Method

The procedure used to refine nodal spacing is presented here, using an example of a single (original, coarse) node with width *DX* containing a vertical fracture with an aperture of 'e', as presented in a cross-sectional view of Figure 1(a), The user specifies how many refined nodes (*N*) will be contained in a fracture-containing coarse node after

regridding. The coarse node is then divided into '*N*' regridded nodes; Figure 1(b) illustrates the example of *N*=9. Since the distributions to the left and the right side of the fracture are symmetrical, and identical calculations are employed for the right of the fracture, the following discussion refers only to the left half of the fracture node.

A new node (*i*=0) is defined in the centre of the coarse node, such that:

$$\Delta x_0 = e \qquad (14)$$

The number of matrix nodes to be generated in one half of the coarse node, NNSC, is:

$$NNSC = \frac{(N-1)}{2} \qquad (15)$$

FRACD equals the distance from the fracture wall to the edge of the coarse node, representing half of the total distance to be refined into matrix nodes:

$$FRACD = \frac{(DX-e)}{2} \qquad (16)$$

Finally, the width of each sub-node is determined through:

$$\Delta x_i = FRACD \left[\frac{\left(e^i\right)^{CF1}}{\left(\sum_{i=1}^{NNSC} e^i\right)^{CF2}} \right] \qquad i = 1, \text{NNSC} \qquad (17)$$

where, *CF1* and *CF2* are user defined spacing control factors. As shown in Table 1, by choosing different combinations of the control factors, the regridded matrix nodes can be subdivided equally, or with linearly or exponentially increasing nodal widths with distance from the fracture. These are illustrated for a one-dimensional case in Figure 1(b), (c) and (d).

Table 1. Regridding Options for Near-Fracture Matrix Nodes and Associated Spacing Control Factors for Equation 17

	Exponentially Increasing Spacing	Linearly Increasing Spacing	Equal Spacing
CF1	1	1	0
CF2	1	0	1

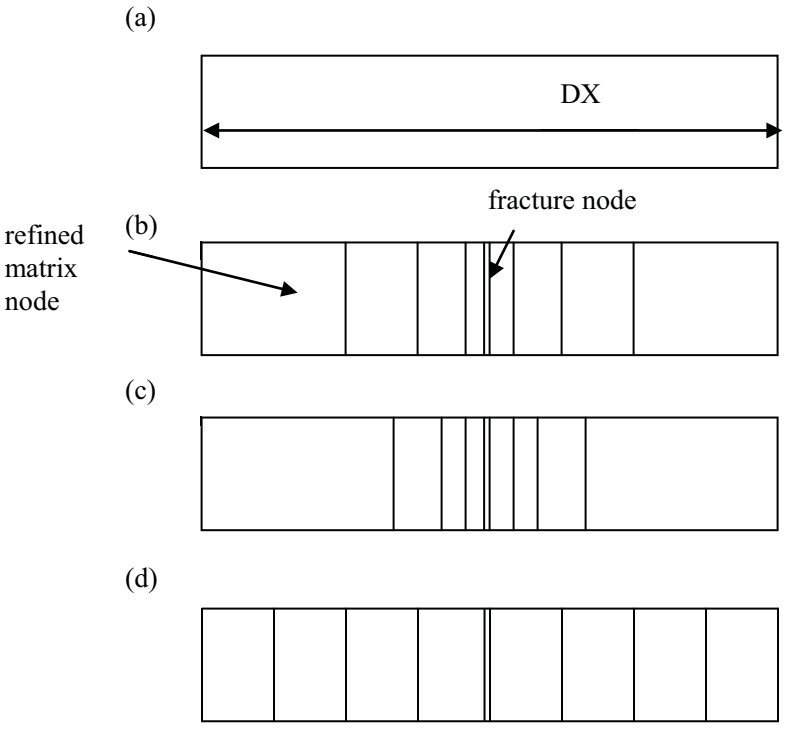

Figure 1: Example of grid refinement on a single coarse node occupied by a vertical fracture employing N=9 and (a) no refinement, (b) linear increasing refinement, (c) exponentially increasing refinement, and (d) equally spaced refinement.

Equations 14 – 17 are applied iteratively across the entire original domain in both

horizontal and vertical directions to achieve refinement in and around all fractures and fracture intersections. Figure 2 presents the cross sectional view of a two-dimensional single fracture intersection, while Figures 3 (a) – (c) provide examples of GR being applied to a two-dimensional singe fracture intersection. In these examples, the original coarse grid contains 81 nodes while the refined domain after GR contains 144 nodes.

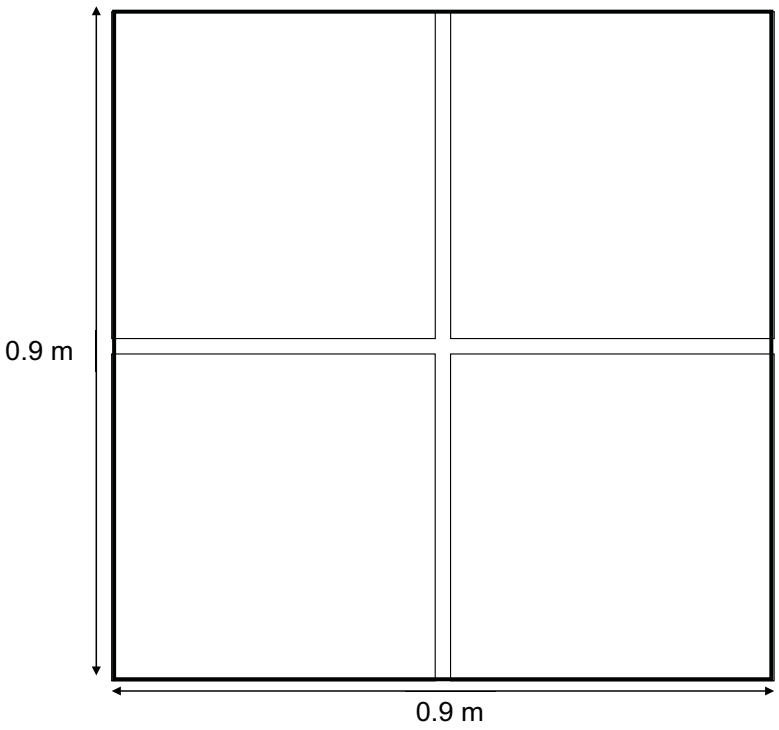

Figure 2: A fracture intersection 0.9m by 0.9m

(a)

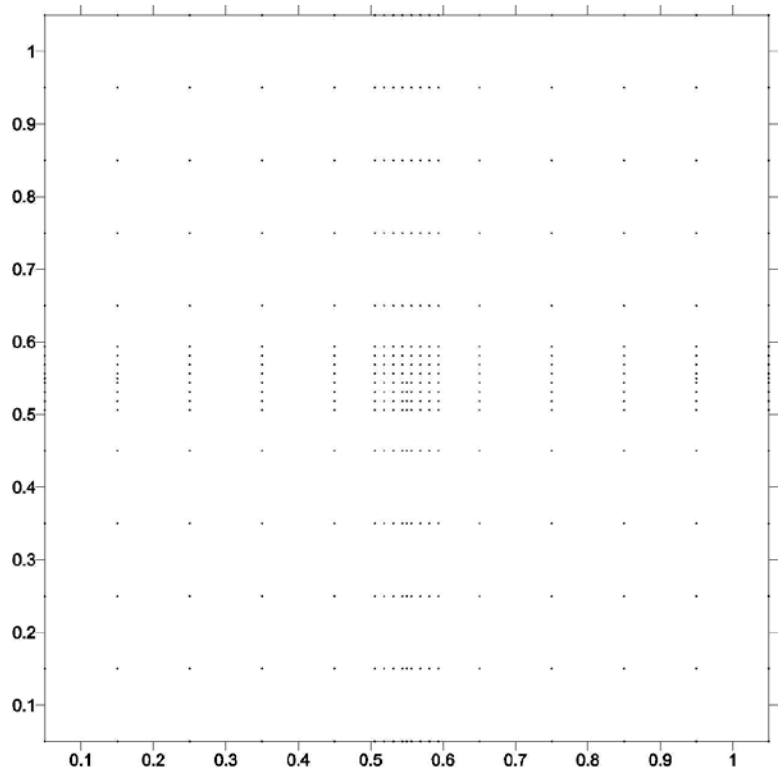

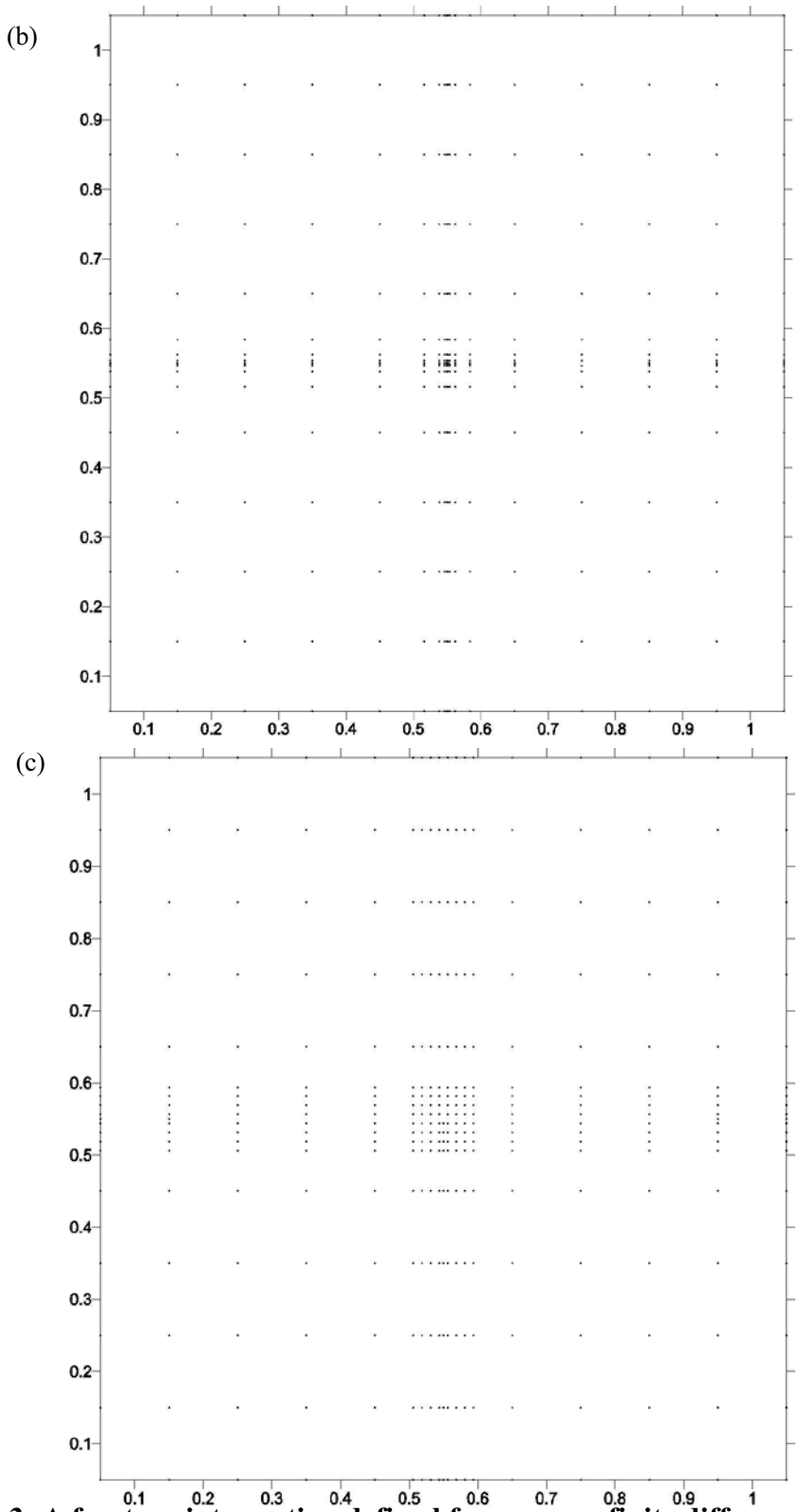

Figure 3: A fracture intersection defined for a coarse finite difference domain with DX=DY=0.1; the domain after grid refinement using (a) equal spacing; (b) exponential spacing and (c) increasing spacing; with N = 9. The dots identify node centers.

3.0 VERIFICATION AND MODEL TESTING

Advection-Dispersive Transport

After DNAPL3DRX-FRAC was developed, various steps were carried out to build confidence in the new model. These steps included comparing advective-dispersive transport in the matrix against the Ogata and Banks (1961) one-dimensional analytical solution. The aim of this verification process is to ensure the advection –dispersion package of the model is running properly.

In this simulation, the physical setting of a one-dimensional horizontal column was used. The nodes in this column were coarsely discretized with a 0.05m discretization. Steady-state flow of groundwater is assumed with the lefthand boundary node assigned a constant concentration of 1000mg/L of TCE solute. A constant hydraulic gradient of 0.004 flowing from left to right was employed. The matrix medium in the column was assigned a porosity of 0.077 (i.e., similar to a sandstone domain) (Lipson et al., 2005) and a longitudinal dispersivity of 0.01 in the x-direction. Figure 4 presents both the analytical and numerical solution over the entire column.

Two Phase Flow

The second check carried out for the model was done by comparing the model with McWhorter and Sunada (1990). This check was done to ensure the two-phase flow equations are solved correctly. The analytical solution consisted of a one-dimensional horizontal column initially saturated with wetting phase throughout. The material in the column was assigned a permeability of $5 \times 10^{-11} m^2$, a porosity of 0.35, a residual wetting phase saturation of 0.05, a pore size distribution index of 2.0, and a displacement pressure

of 2000Pa. Figure 5 presents both the analytical and numerical solution along the column for four separate time of 0.6, 2.9, 5.8 and 9.3 days respectively.

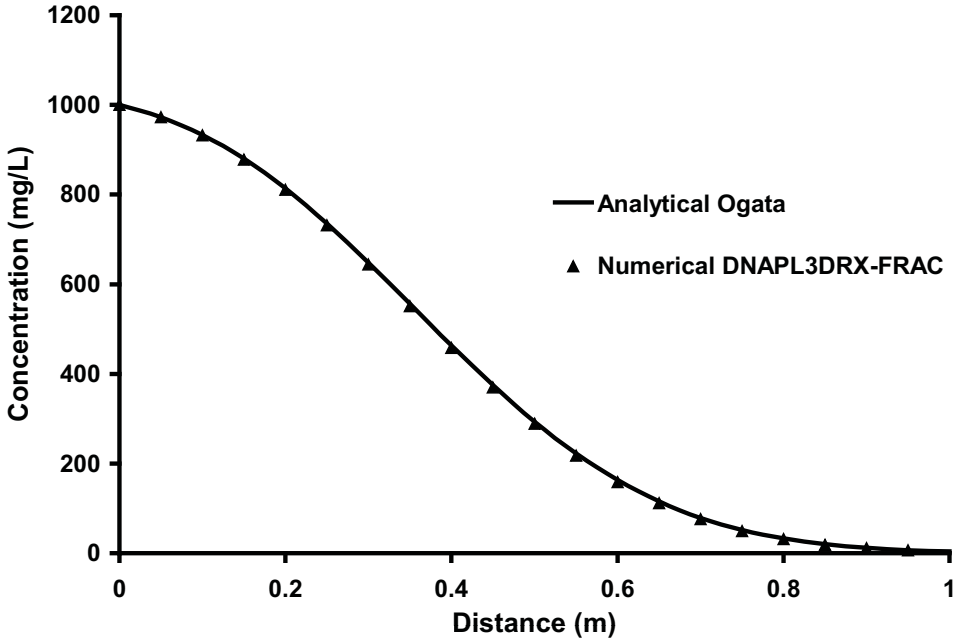

Figure 4: Verification of DNAPL3DRX-FRAC against Ogata and Banks (1961)

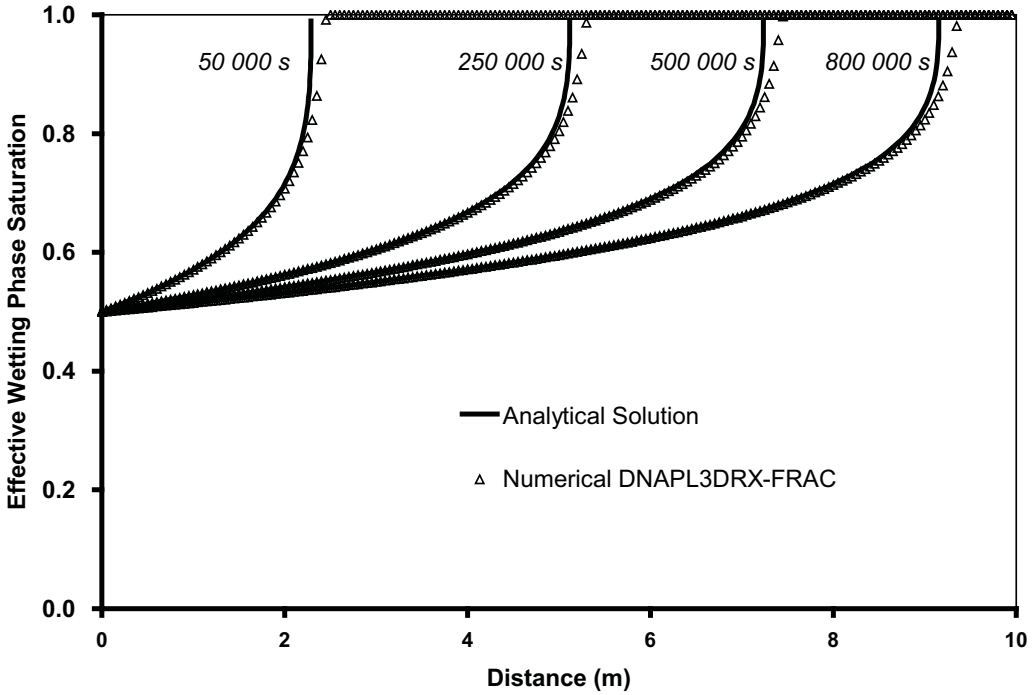

Figure 5: Verification of DNAPL3DRX-FRAC against McWhorter and Sunada (1990)

Matrix Diffusion

In order to gain a proper insight of the required degree of discretization to adequately capture diffusion gradients in the matrix, DNAPL3DRX-FRAC was verified with the analytical solution developed by Sudicky and Frind (1982). This analytical solution solves for transient contaminant transport in a set of discrete, parallel fractures situated in a diffusion-dominated porous matrix. For verification, a two-dimensional domain 10.0 m x 1.05 m with a single vertical fracture running through the entire domain was used.

The domain exhibited a coarse gridding of 0.05 m and the nodes containing the fracture were discretized using the 'exponentially increasing spacing' gridding method as described in the previous section with increasingly refinement (N = 3, 5, 15). The matrix medium in the domain was assigned a porosity of 0.3 and a permeability of $1x10^{-17}m^2$. A constant concentration of 1400mg/L of solute was injected from the top of the fracture and allowed to flow through the entire fracture. A diffusion coefficient of $1x10^{-9}$ m^2/s was assumed for the solute in this simulation. Since the analytical model of Sudicky and Frind (1982) (CRAFLUSH) only provides the solution for half the domain, in order to compare the results from both models, Figure 6 presents the numerical and analytical solution starting from the centre of the fracture to 0.4m of the right side of the matrix. From this figure, it is observed that as, as expected, increased matrix discretization results in more accurate simulation of the analytical solution. However, as discretization increases, more memory is required and the speed of the simulation decreases. For example, as the near-fracture discretization of 0.05 m increased from 3 to 5 to 15 nodes, the total root-mean-squared error between the numerical and analytical

solutions decreased from 22.9 mg/L to 12.5 mg/L to 7.76 mg/L but the speed of the simulation decreased approximately 5 folds with each increase. It was determined that, for field scale simulations in this work, a reasonable compromise between speed and accuracy was reached at N=5 for the GR routine throughout the domain.

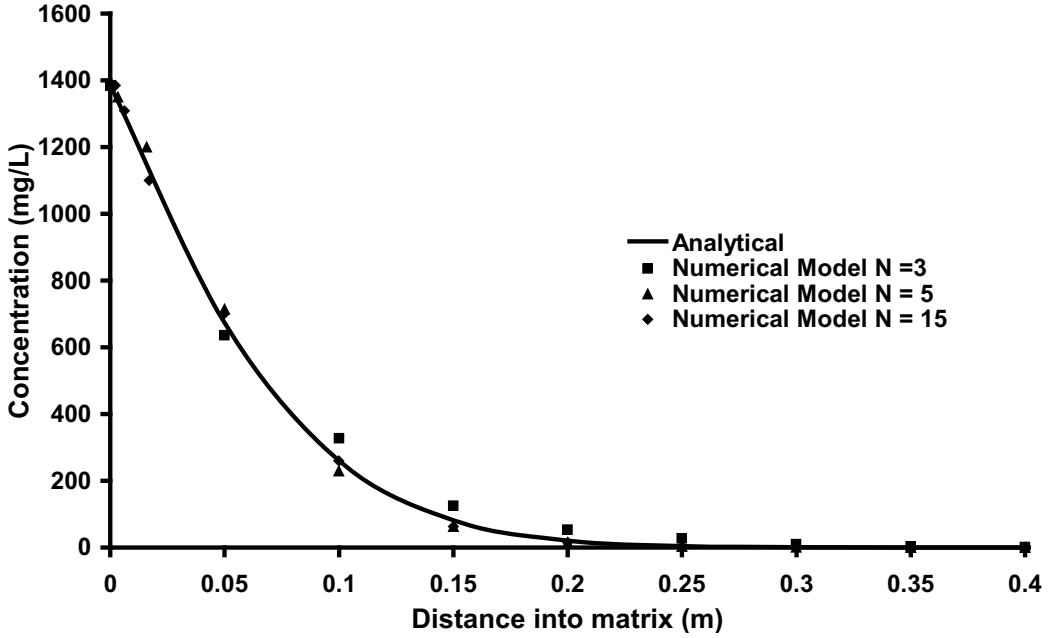

Figure 6: Verification of DNAPL3DRX-FRAC for a solute diffusion in single half-fracture and adjacent matrix against Sudicky and Frind (1982).

Sorption

RT3D typically calculates the change in concentration of a mobile species due to various sorption isotherms, but does not track the mass of sorbed contaminant. For this project, tracking the amount of chlorinated solvent sorbed to soil particles was important as permanganate will destroy the sorbed mass as well as the aqueous phase mass. Code was written to explicitly treat sorbed contaminant as an immobile species and the local (nodal) amount was calculated following the approach of Mundle et al. (2007) in which the concentration of sorbed TCE (*Cs*) was back calculated based upon the solved concentration of dissolved TCE (*Cw*):

$$C_s = C_w Kd \frac{\rho}{\theta} \qquad (18)$$

where $Kd = K_{oc} \times f_{oc}$ (Karickhff et al., 1979), K_{oc} is the organic carbon partition coefficient (L^3M^{-1}), and *foc* is the local (i.e., nodal) fraction of organic carbon (-), ρ is the dry bulk density (ML^{-3}), and θ is the porosity (-). To verify that this approach was being correctly implemented, the concentration of chlorinated solvent was graphed against the concentration of soluble chlorinated solvent in one node. As shown in Figure 7, the employed linear isotherm is confirmed.

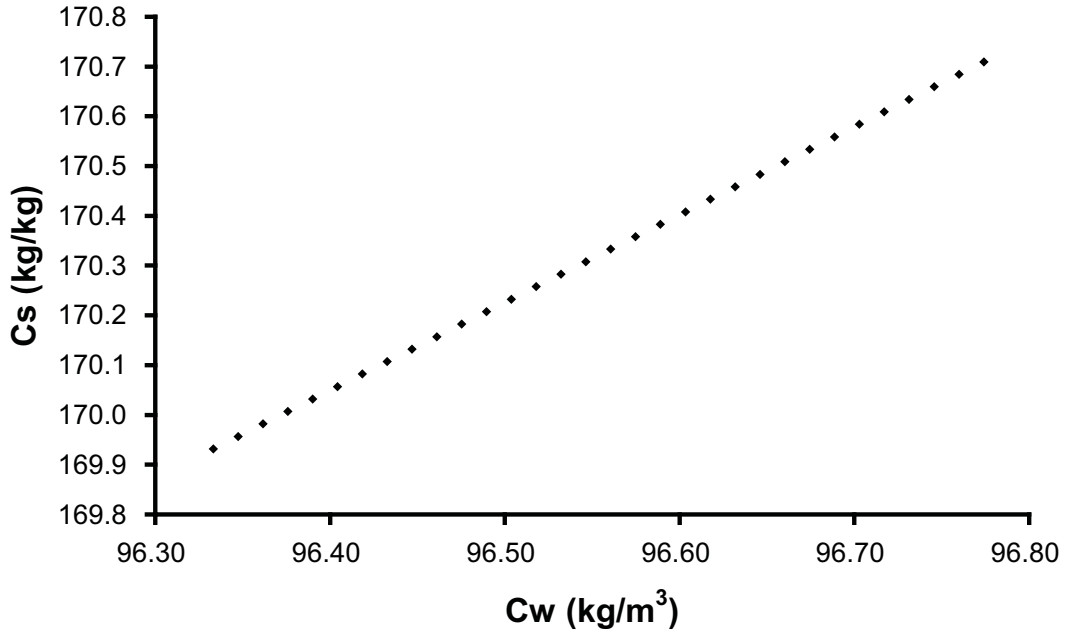

Figure 7: Verification of linear sorption within the model for a single node.

Abriola et al. (2005) found that sorption of Tween-80 to sand conformed to a Langmuir isotherm. The Langmuir sorption isotherm is described as (Fetter, 1993):

$$\frac{C_w}{C_s} = \frac{1}{\alpha\beta} + \frac{C_w}{\beta} \qquad (19)$$

where α is an adsorption constant related to the binding energy (L^3M^{-1}) and β is the maximum amount of solute that can be adsorbed by the solids (MM^{-1}).

To verify that this approach was being correctly implemented, data from Abriola et al. (2005) was employed and the concentration of solvent was graphed against the concentration of sorbed solvent in one node. By employing a maximum sorption capacity of 0.17 mg/g and an adsorption constant of 0.12 L/mg, the Langmuir sorption isotherm is demonstrated in Figure 8.

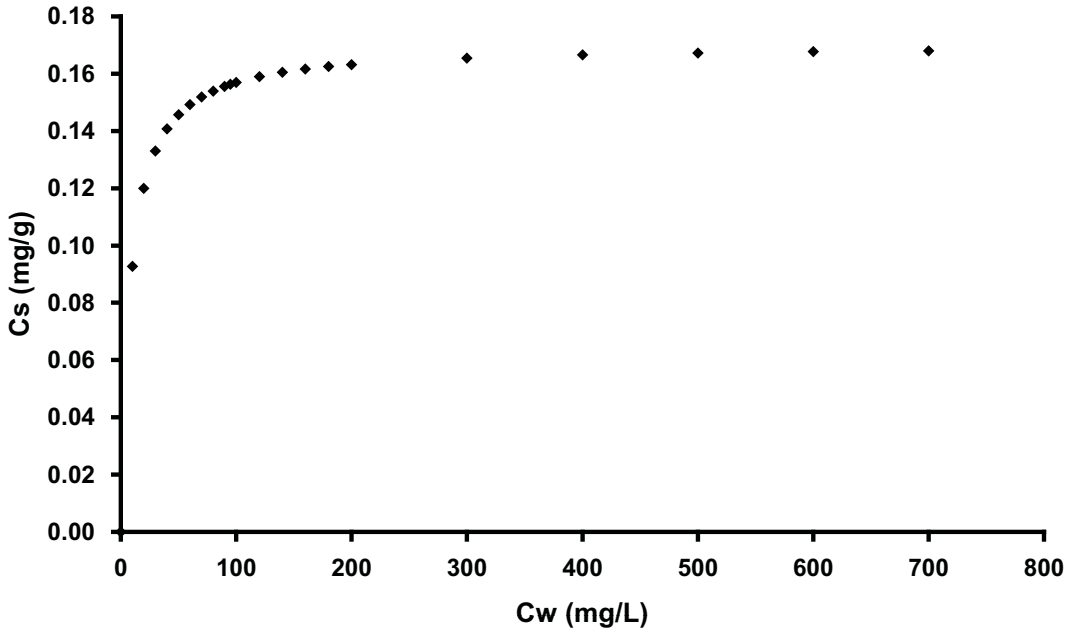

Figure 8: Verification of Langmuir sorption within the model for a single node.

Testing on Multi-Fracture Scenarios

The first study examined multi-phase flow (only) in fractures using a 13m by 13m domain with two orthogonal fractures cross-cutting the centre of the domain (Figure 9). The domain was first discretized using a coarse nodal spacing of 0.1m while the nodes that contain the two fractures were refined using N=7, and by employing 'exponentially increasing spacing'; this resulted in a total of 18495 nodes in the domain. The DNAPL distribution at t=100,000 s is plotted in Figure 10. An identical simulation, in which the fracture nodes were not refined, was conducted (N=1; total of 16900 nodes in domain).

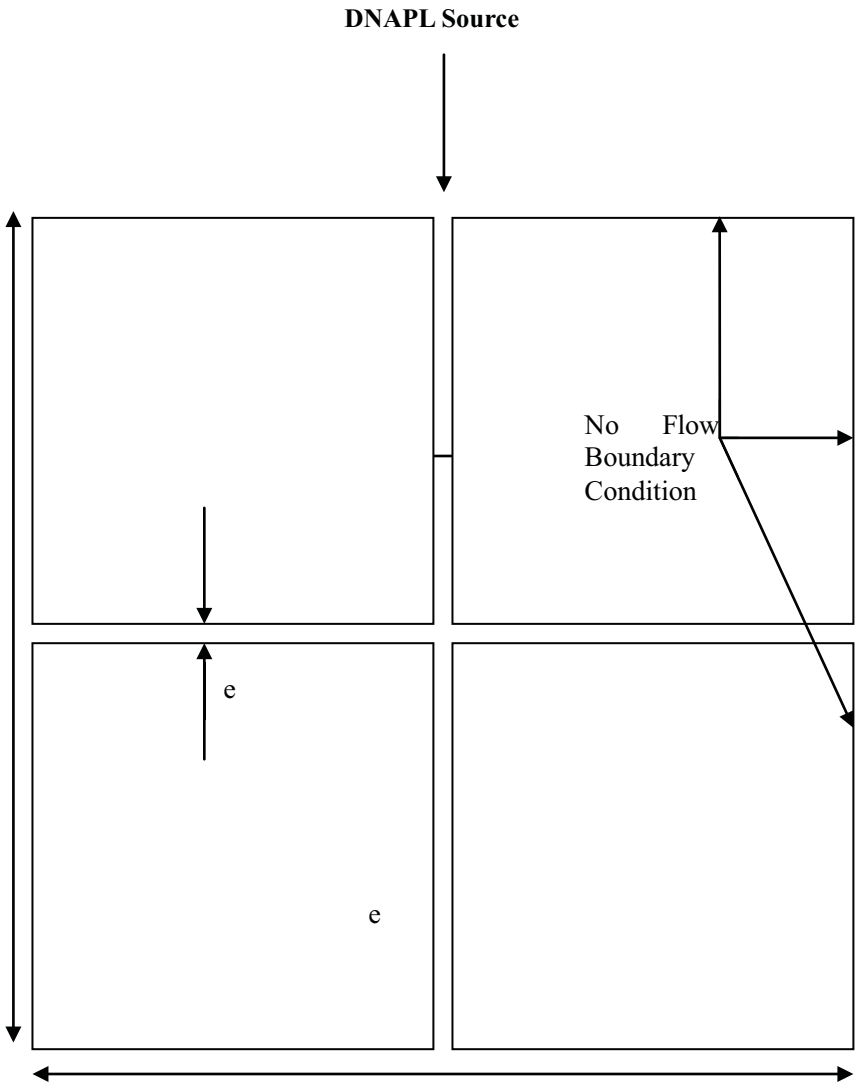

Figure 9 A pair of identical 1m long fractures, one oriented vertically and the other oriented horizontally.

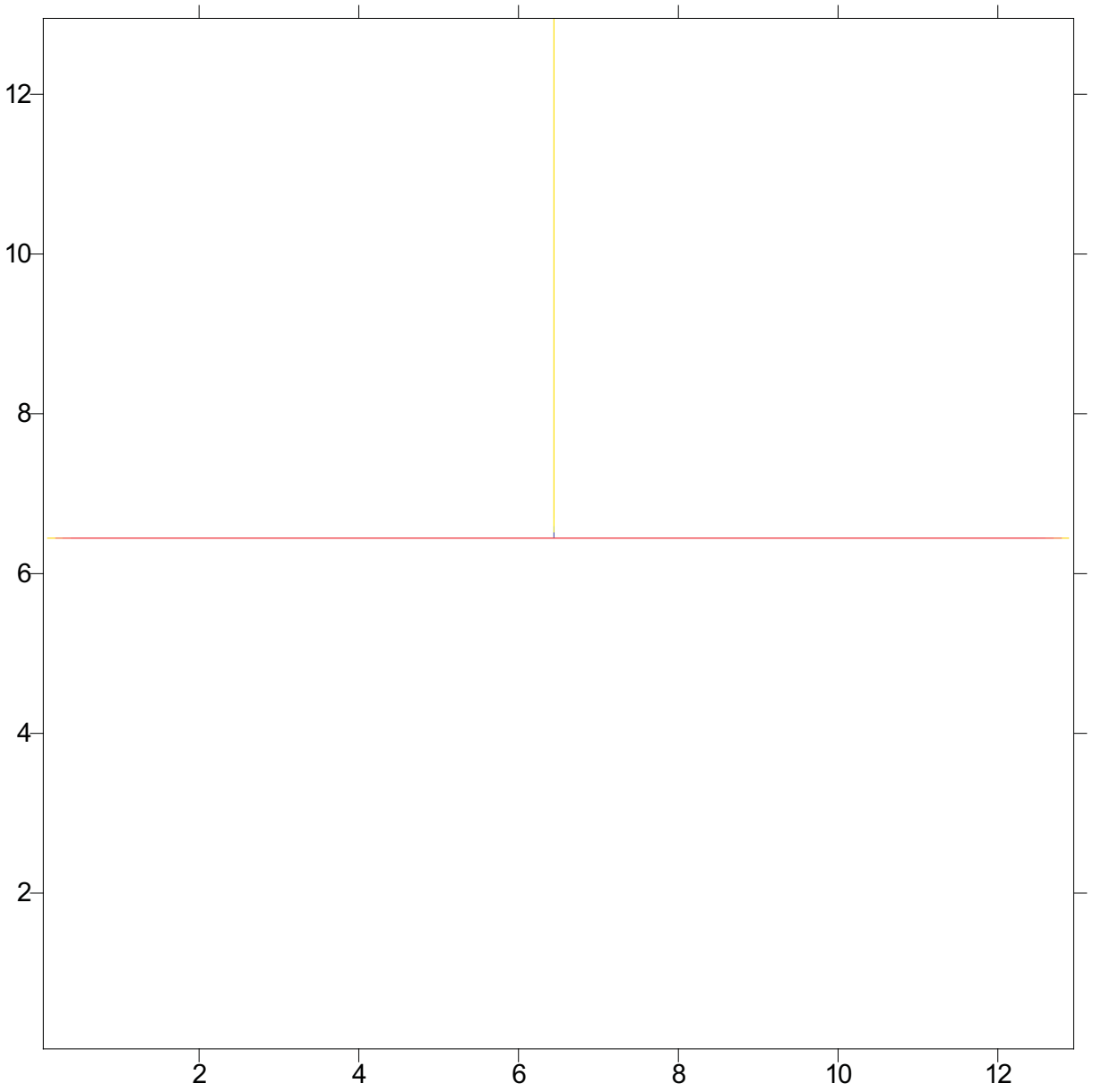

Figure 10: A 13m by 13m domain with the nodes that contain the two fractures variably discretized into seven exponentially spaced sub-nodes. The rest of the matrix is discretized using a 0.1m nodal spacing.

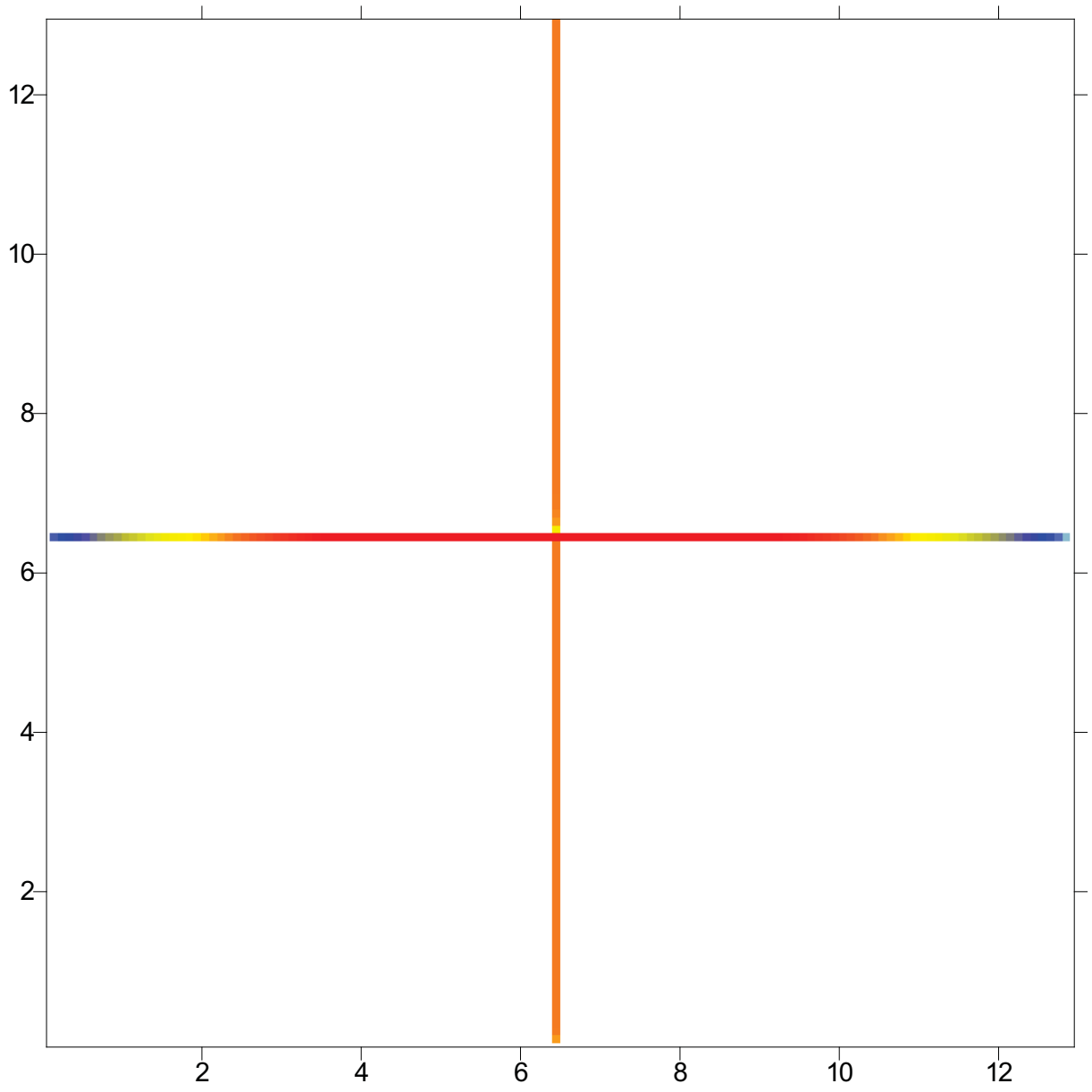

Figure 11: A 13m by 13m domain discretized uniformly using a 0.1m nodal spacing.

The DNAPL distributions at t=100,000 s for the two simulations are presented in Figures

10 and 11 respectively. The results indicate that the uniformly discretized domain results in a higher degree of vertical migration predicted and a lower degree of lateral migration predicted; in fact, it predicts penetration of the vertical fracture beyond the fracture intersection that the more accurate (refined) simulation suggests should not occur. This underscores the importance of sufficient nodal refinement in the vicinity of fracture intersections for properly simulating DNAPL migration. This finding agrees generally with the observations of Slough et al. (1999); where if fracture elements in a domain are not sufficiently discretized, an over-prediction of the volume of DNAPL that continues to migrate vertically at the intersection of a vertical and horizontal fracture can occur. As demonstrated by Slough et al., (1999), by finely discretizing the fracture and adjacent matrix nodes in a rock domain (e.g., at the scale of one centimetre or less), this problem can be accurately resolved.

The second study was a more comprehensive test, employing a larger scale domain with multiple vertical and horizontal fractures, multiphase flow, mass transfer and advective-dispersive-diffusive transport. Two simulations were conducted in which only the fraction of organic carbon (f_{oc}) was varied (0.005 vs 0.0005).

For both simulations, a domain of 20m by 5m with 3 horizontal and 4 vertical fractures was adopted for this study. The porosity of the matrix and fractures were assigned 0.077 and unity respectively. The coarse, uniformly discretized domains employed DX = 0.25 m and DY=0.25 m, for an original domain of 1600 nodes. Grid refinement was conducted using N = 5, and exponential increasing node spacing was employed resulting in a final domain with 3072 nodes.

At t = 0, TCE DNAPL was released into the domain across the entire top boundary by specifying a non-wetting phase saturation of 0.3 and wetting phase pressure of zero. Constant head specified at the side boundaries during DNAPL migration established a zero hydraulic gradient across the domain. The water table was set to be coincident with the top boundary. The bottom boundary was set so as to permit the free exit of both water and DNAPL, while the side boundaries permitted only the flow of water. DNAPL was permitted to flow into the domain for 0.5 years, at which time saturations had achieved steady state values. The DNAPL source was then terminated, and DNAPL redistribution was simulated for 6 months, at which time DNAPL movement had ceased. DNAPL dissolution was not simulated during the DNAPL migration period.

At t = 1 year, the side boundary conditions were changed to provide a hydraulic gradient of 0.005 from left to right across the domain that was maintained throughout the remainder of the simulation. DNAPL dissolution, aqueous phase transport, diffusion, and sorption of TCE was enabled for 1 year (t=1 yr – 2 yr). During this period, a constant concentration of 550 mg/L TCE was specified at the left boundary, representing upgradient contamination entering the domain. The solubility of TCE was specified to be 1100 mg/L with a TCE free solution diffusion coefficient of 1.01 $x10^{-9}$ m^2/s (Pankow and Cherry, 1996).

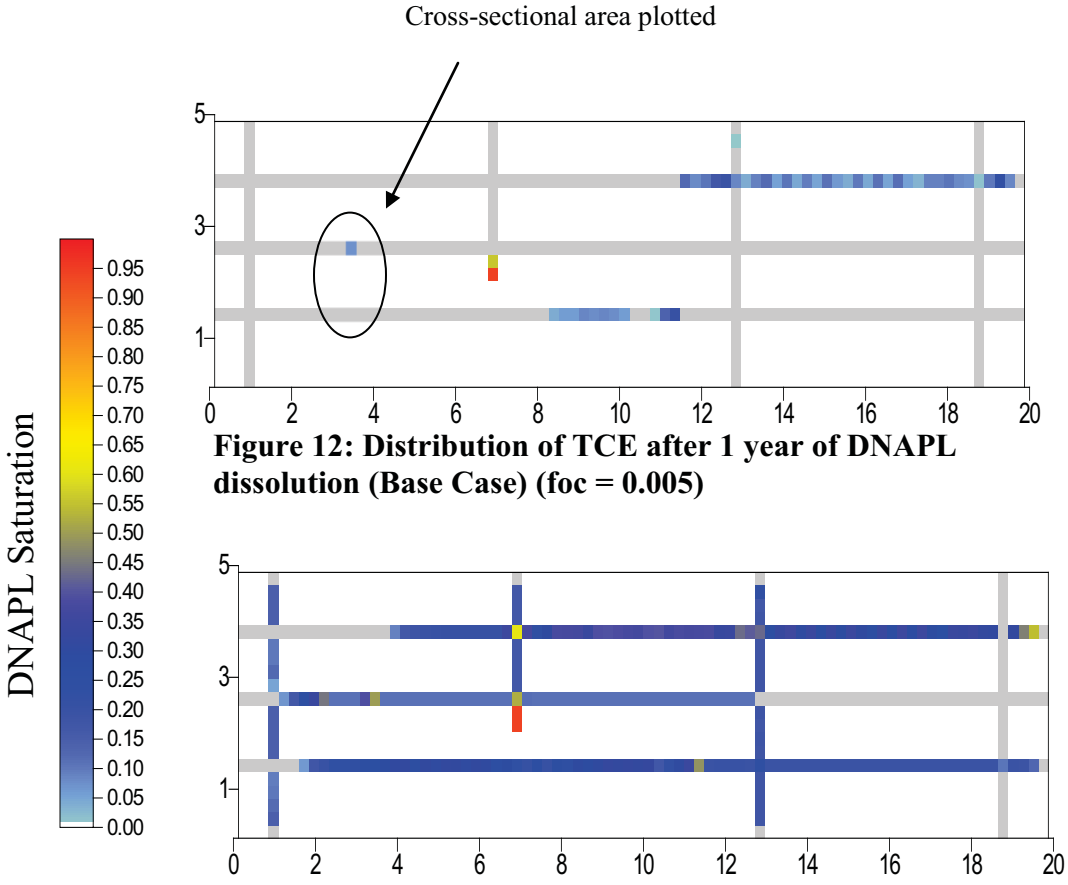

Figure 12: Distribution of TCE after 1 year of DNAPL dissolution (Base Case) (foc = 0.005)

Figure 13: Distribution of TCE after 1 year of DNAPL dissolution (foc = 0.0005).

Note: Fractures are exaggerated in the above figures for visual purpose.

As demonstrated by Figures 12 and 13, the amount of DNAPL that remained in the domain increases, after one year of dissolution, with a lower f_{oc}. In addition, as demonstrated via Figures 14 and 15, with a lower f_{oc}, the amount of solute sorbed decreases dramatically, while the amount of solute that remained in the domain as aqueous phase increases. This inverse relationship between the persistence of DNAPL and f_{oc} is consistent with expectations (e.g., Pankow and Cherry, 1996).

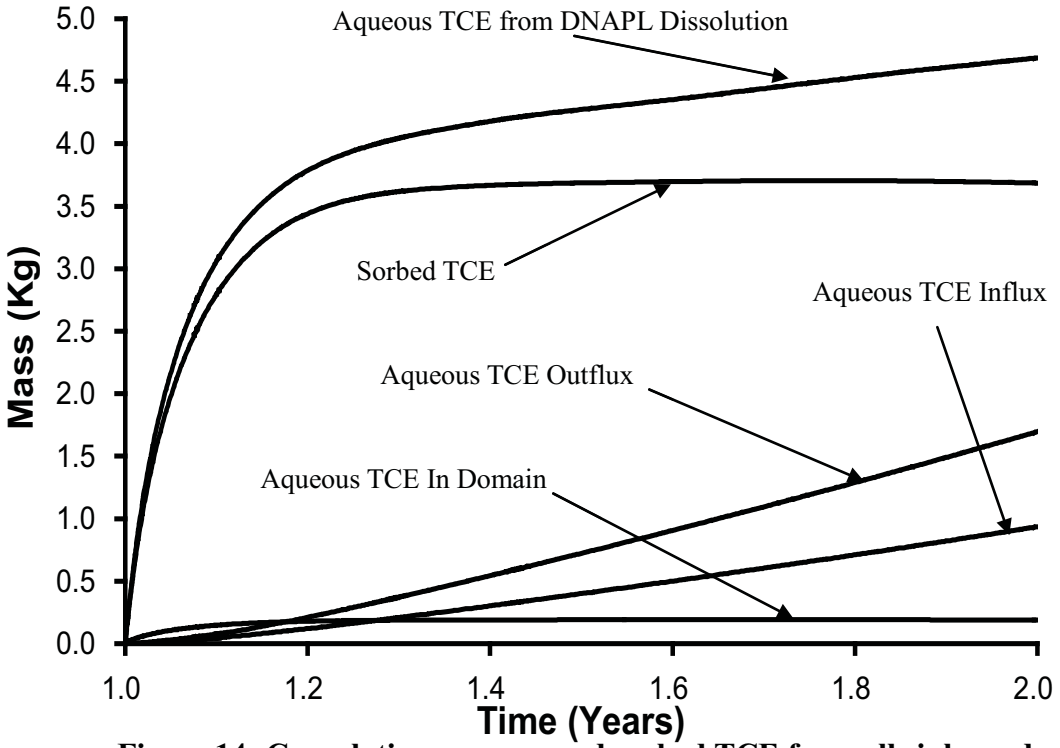

Figure 14: Cumulative aqueous and sorbed TCE from all sinks and sources after 1 year of dissolution (foc = 0.005).

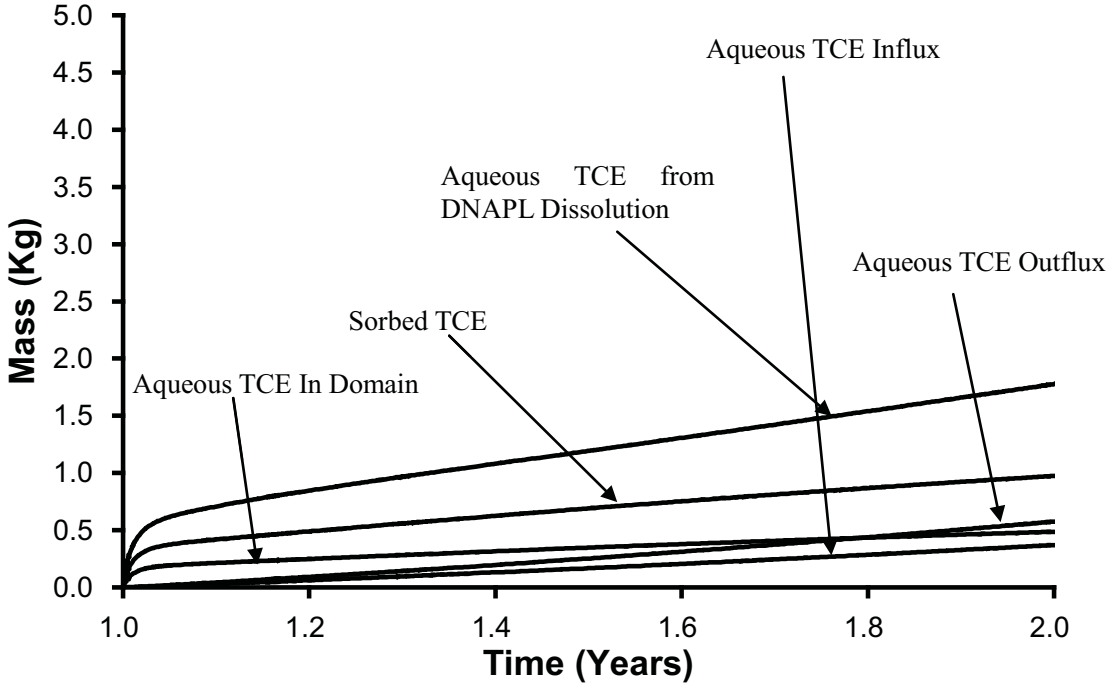

Figure 15: Cumulative aqueous and sorbed TCE from all sinks and sources for lower foc simulation after 1 year of dissolution (foc = 0.0005).

Figure 14 and 15 presents the cumulative mass of all TCE species inside the field scale sandstone domain for the period 1 yr ≤ t ≤ 2yrs (i.e., for the first year of dissolution) for the f_{oc} = 0.005 and the f_{oc} = 0.0005 cases, respectively. Figure 14 illustrates that the majority of aqueous TCE arising from DNAPL dissolution diffuses into the matrix and then sorbs at early time. The amount of sorbed TCE peaks after approximately 0.5 yrs of dissolution, after which the majority of dissolving TCE flows out of the domain through the fractures, as evidenced by the difference between the aqueous TCE influx and outflux plots (and the steady mass of aqueous TCE in the domain).

Figure 15 illustrates that a 10-fold reduction in the f_{oc} results in approximately a two-thirds reduction in the amount of aqueous TCE arising from dissolution after 1 year. It further demonstrates that sorption accounts for a smaller, although still significant, percentage of the aqueous TCE arising from dissolution and the cumulative mass sorbed has not yet peaked after 1 year. In addition, the figure shows that despite the reduced total mass of TCE dissolved, a higher cumulative TCE mass is present in the aqueous phase in the low f_{oc} case. Finally, it is noted that the cumulative TCE influx (from the left hand side boundary condition) is reduced in the low f_{oc} case as a result of reduced aqueous phase velocity through the source zone: the high DNAPL saturations that persist result in reduced wetting phase relative permeability in the fractures. These results provide confidence that diffusion and sorption are being properly simulated by the model.

Figure 16 provides a sequence of aqueous TCE concentration profiles across a horizontal fracture and the adjacent matrix on either side (the specific cross-section chosen is

indicated in Figure 12) after the simulation was continued for a further of 19 years. Figure 16 presents the data during the site aging period (i.e., $t \leq 21$ yrs). As demonstrated in this figure, the concentration is equal to solubility within the fracture at t=4 yrs since DNAPL is still present (see Figure 12). Once DNAPL in the fracture dissolves away (approx. t=3 yrs) the concentration in the fracture drops significantly, and from t=6 yrs until t=21 yrs it steadily increases due to the upgradient aqueous TCE source. Note that, despite its proximity to the upgradient boundary, the fracture never reaches the 550 mg/L influent concentration due to diffusion and sorption in the 3 m interval.

Overall, these series of figures provide confidence that the key processes of multiphase flow, mass transfer, advective-dispersive transport, matrix diffusion (forward and backwards) are all simulated in agreement with expectations. The reactions specific to the various treatment technologies examined are tested in the respective studies to follow.

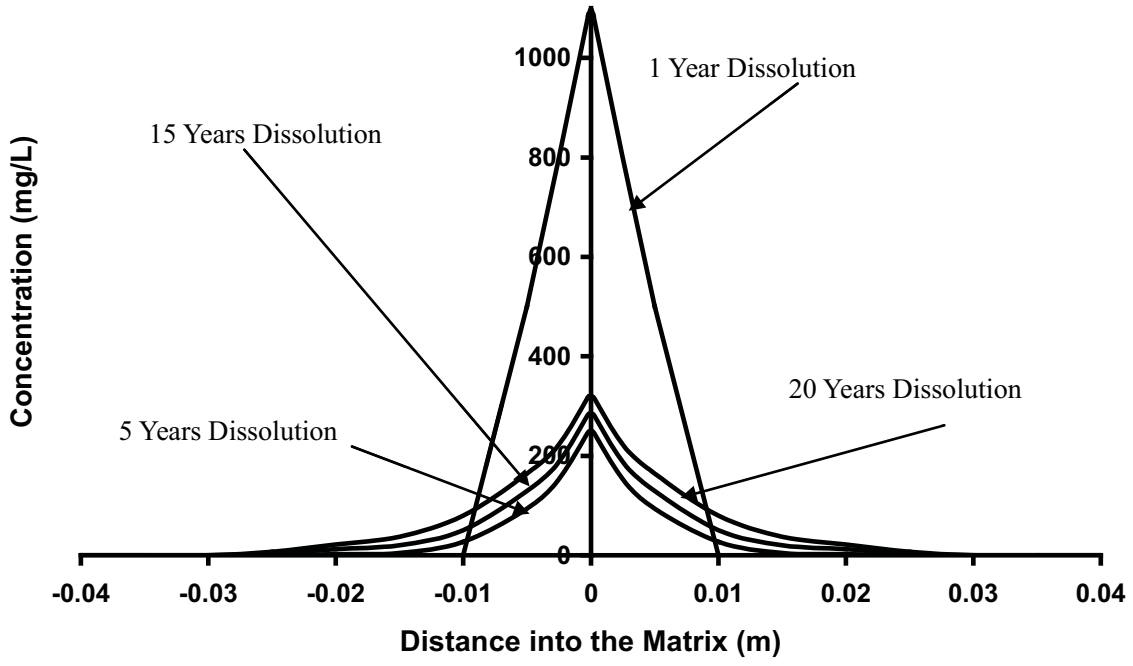

Figure 16: Various concentration profiles into the matrix over time.

A layout of the model for chemical-oxidation and enhanced bioremediation is displayed in Figure 17. Figure 18 demonstrates the model layout for surfactant flushing.

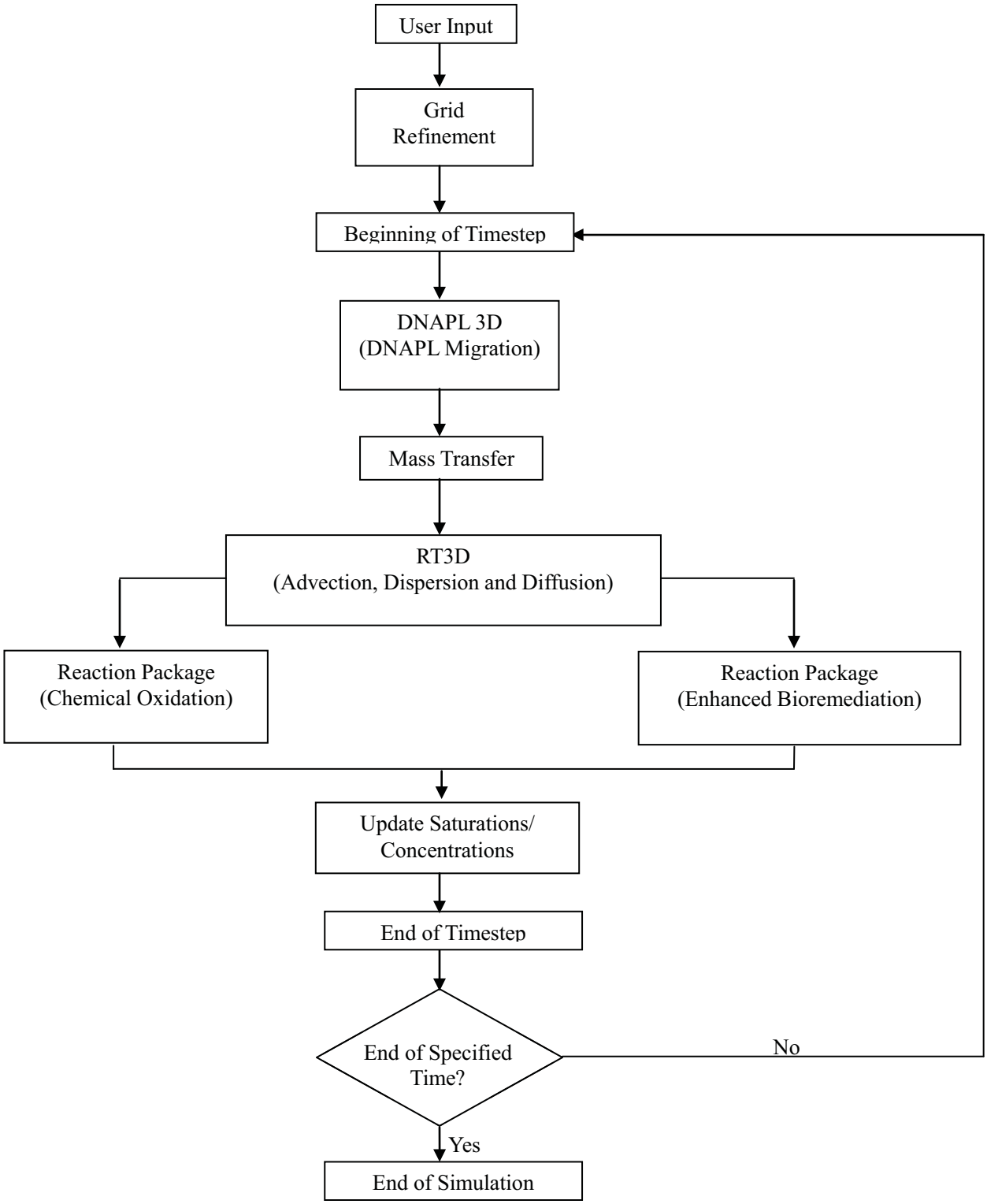

Figure 17: Model structure for chemical oxidation and enhanced bioremediation.

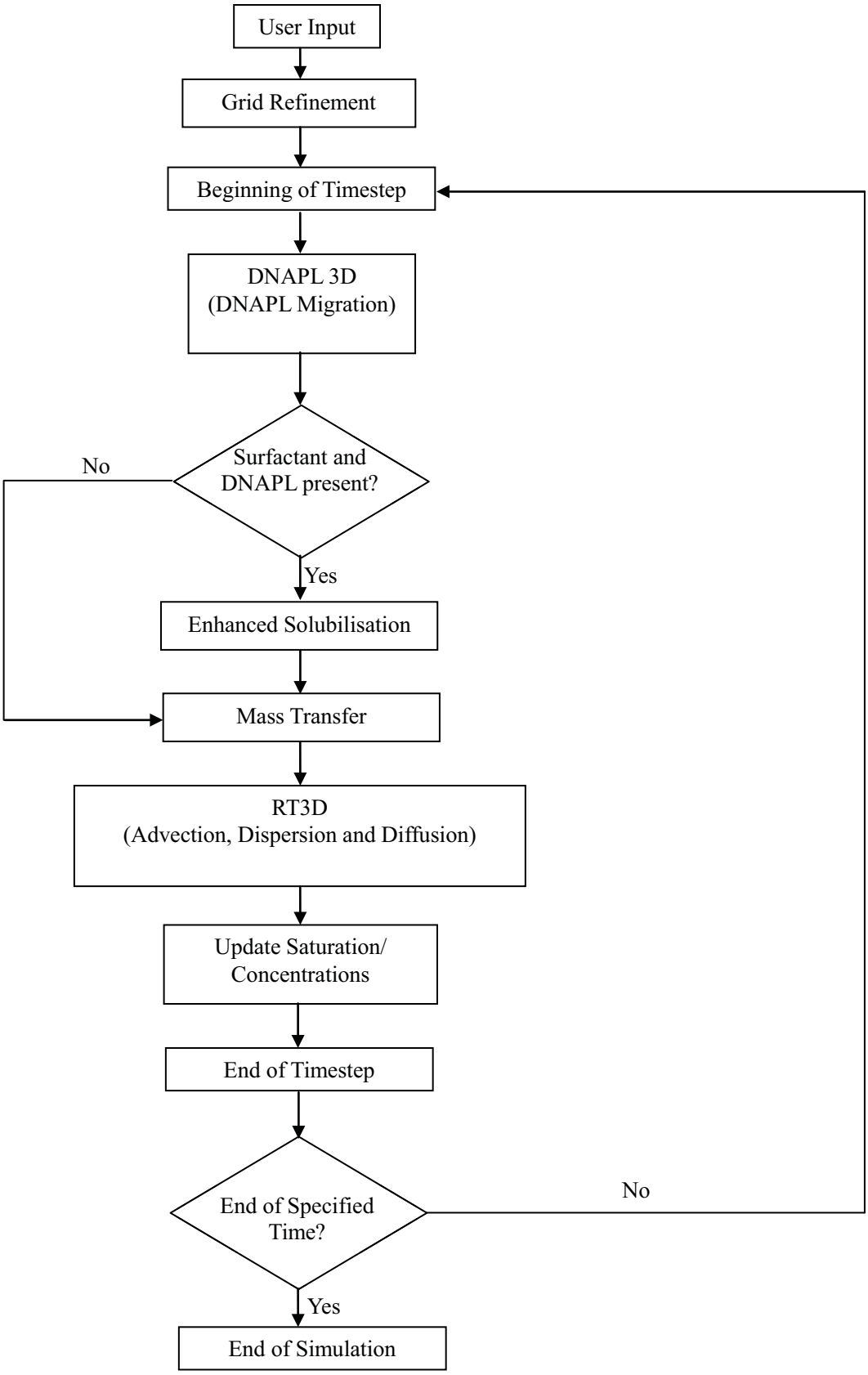

Figure 18: Model structure for surfactant flushing.

APPENDIX B.3

NUMERICAL SIMULATION OF DNAPL SOURCE ZONE REMEDIATION WITH *IN SITU* CHEMICAL OXIDATION (ISCO): FRACTURED ROCK

ABSTRACT

Fractured rock formations represent a valuable source of groundwater aquifers and can be highly susceptible to contamination by dense, non-aqueous phase liquids (DNAPLs). Numerical simulations were conducted to investigate the benefits and challenges of *in situ* chemical oxidation (with permanganate) for chlorinated solvent DNAPL in fractured rock aquifers at the field scale. An established finite difference multiphase flow-transport-reaction simulator was employed after modification with a gridding routine (GR); the GR was designed to permit sufficient grid refinement within and near fractures to adequately capture DNAPL migration and aqueous species diffusion while maximizing computationally efficiency. Simulations were conducted in two-dimensional cross-section with fracture apertures constant within fractures but varying across the source zone. In each of the 9 simulations conducted, a DNAPL release stage was followed by a 20-year site ageing stage prior to simulating a chemical oxidation treatment stage followed by a 5-year post-treatment stage. The suite of simulations examined (i) permanganate injection concentration, (ii) pulsed-injection strategy, (iii) bedrock type (sandstone, shale, and granite), and (iv) DNAPL type (TCE and tetrachloroethylene, PCE). Results confirm that matrix diffusion and sorption to matrix organic carbon dominates the fate of chlorinated solvent in the source zone during site ageing, although the depth of matrix contamination is reduced in those scenarios characterized by increased peclet number (e.g., granite). In all of the cases considered, the efficiency of oxidant utilization was observed to be poor, with greater than 90% of the injected permanganate consumed by the natural oxidant demand. In sandstone (7 simulations), the contaminant mass destroyed was never greater than 11% of the total mass present in

the system despite injecting more than 3 times the theoretical oxidant demand for the chlorinated solvent. Oxidant destruction exceeded supply in all sandstone cases, causing virtually no treatment to occur when injection was not active. In all cases, the narrow spatial and temporal extent of the ISCO treatment relative to the extent of diffusive matrix contamination limited any effective influence on the long term mass discharge from the source zone.

1.0 INTRODUCTION

Dense nonaqueous phase liquid (DNAPL) contamination of fractured geologic media is a long-standing and challenging environmental issue. In fractured bedrock aquifers where DNAPL is excluded from the matrix, fluid movement will be limited to the interconnected fracture porosity (Ross and Lu, 1999; Wealthall, 2002). Such exclusion is possible since matrix permeabilities in rock are typically low while matrix entry pressures are correspondingly high (Kueper and McWhorter, 1991). Thus, DNAPL flow in a fracture network is often restricted to the open fractures, which therefore serve as the primary pathways for DNAPL movement in the subsurface (Pankow and Cherry, 1996). For many bedrock aquifers, the fractures represent only 0.001-0.1% of the bulk volume of the rock mass (Mackay and Cherry, 1989), allowing even a small amount of DNAPL to migrate a significant distance (Reitsma and Kueper, 1994).

In fractured porous media, dissolution can occur within the fracture plane as well as into the porous matrix surrounding the fracture (matrix diffusion). The fate of DNAPL residing in a fractured rock mass may be governed by matrix diffusion for the case of high DNAPL solubility and high matrix porosity (Parker and Gillham, 1994). The amount of DNAPL mass available to dissolve and diffuse into the matrix is dictated primarily by the amount of residual formed during the initial migration event (Longino and Kueper, 1999). The driving force for diffusion into the matrix is provided by the concentration gradient between the aqueous phase present at the fracture surface and the essentially immobile pore water in the matrix. As dissolution and diffusion proceeds, the amount of DNAPL in the fracture is diminished and, eventually, a substantial fraction

of the contaminant mass may be transferred to the matrix. The diffusing aqueous phase contaminant in the matrix can both further penetrate the matrix and can sorb to the matrix solid (Parker et al., 1994).

The restoration of fractured porous media contaminated by DNAPL is often more difficult than for unconsolidated porous media. This is due to the difficulty in identifying the source zone, and also the fact that many traditional remedial technologies (e.g., pump and treat) are relatively ineffective in highly heterogeneous environments such as fractured rock (Powers et al. 1992; National Research Council 1994). The reason is that little or no water flushes through dead-end fracture segments or through the porous but relatively impervious matrix, both of which are likely to retain the bulk of the contaminated mass (Mackay and Cherry, 1989). Clean water flushed through the fractures can reverse the concentration gradients thereby permitting mass to be removed from the matrix. However, the relatively slow rate of release of contaminants from the clay/rock matrix by backwards diffusion, coupled with the potentially appreciable contaminant mass contained in dissolved and sorbed form in the matrix, can cause a long-term bleed of contaminants into the aquifer during remediation (USEPA, 2003b). Furthermore, if pumping is ceased before all of the contaminant is removed, the contaminant concentrations in the groundwater will typically rebound (USEPA, 2003b).

Previous studies of groundwater and DNAPL flow in fracture rock have illustrated that the degree of interconnection between the overburden, uppermost weathered bedrock layer, and bedrock units, as well as the lateral continuity, hydraulic properties and the

heterogeneity of the fracture system are all issues that impact the hydraulic behaviour of the system (Lerner et al., 2002; Wealthall et al., 2001; Kueper and McWhorter, 1991).

Chemical oxidation, commonly referred to as in-situ chemical oxidation (ISCO) involves the injection of an oxidizing agent to chemically degrade chlorinated solvents into non-toxic by-products in the subsurface. An extensive review of the different chemical oxidization agents and their associated chemistry with respect to tetrachloroethene (PCE), trichloroethene (TCE), dichloroethene (DCE), and organic aquifer materials (OAM) was presented by Seol et al. (2003). Many laboratory and field studies have investigated ISCO of DNAPL in aquifers characterized by relatively uniform conditions and with limited heterogeneity (e.g., Vella and Veronda 1992; Yan and Schwartz 1999; Schnarr et al. 1998; Yan and Schwartz, 1999; Zhang and Schwartz 2000; Hood and Thomson 2000; MacKinnon et al., 2002; Schroth et al. 2001; Conrad et al. 2002). However, only a limited number of studies are available for more complex sites and, in particular, those with fractured bedrock (Siegrist, 2001).

Williams and Spiers (2002) carried out two phases of laboratory studies to evaluate the effectiveness of ISCO for remediation of impacted groundwater in a fractured bedrock aquifer using sodium permanganate. These studies demonstrated that fractured rock environments, despite their inherent complexity and heterogeneity, can be quite suitable for successful sodium permanganate applications. In particular, that work argued that fractured rock provides an environment often low in natural organic matter resulting in naturally low demand for oxidant material.

MacKinnon et al. (2002) conducted a series of laboratory treatability studies under simulated site conditions, using materials from two fractured bedrock sites, to examine the influence of performance factors on the oxidative reduction of TCE and PCE by potassium permanganate ($KMnO_4$) in fractured rock. They found minimal penetration of the oxidant into the rock matrix, likely due to the low porosity of the shale and siltstone employed. The study concluded that the oxidant demand resulting from diffusive loss of $KMnO_4$ into the bedrock matrix is unlikely to have a significant impact on oxidant delivery in the field during an extended treatment using permanganate. Specifically, it was concluded that permanganate exhibited the ability to degrade high concentrations of TCE and PCE within very short time frames (days to weeks). However, the study acknowledged that the positive results may have been biased due to pulverization of the bedrock samples prior to testing, a process which significantly increased the surface area available for reaction relative to that expected during field application.

While microcosm studies with crushed bedrock material are valuable, they may overestimate the benefits of chemical oxidation by oversimplifying the system. For example, it is widely accepted that the majority of groundwater and DNAPL flow that occurs through a fracture is highly influenced by the aperture distribution (Tsang and Tsang, 1987; Anderson and Thomson, 1999). Thus, the influence of the fracture network distribution at real sites is expected to dominate the spatial and temporal distribution of DNAPL and of oxidant, as well as on their contact time. In addition, changes in the (effective) aperture distribution due to the formation of reaction by-products during ISCO could potentially influence aqueous transport pathways and

DNAPL mass transfer rates. Laboratory research has demonstrated that the precipitation of manganese dioxide (MnO_2(s)) decreases the hydraulic conductivity between 50 and 90% (Schroth et al., 2001) in sand-packed columns, and resulted in pore plugging and the formation of a distinct manganese oxide layer in the vicinity of the NAPL that reduced the post-treatment mass transfer (Mackinnon et al., 2002; Conrad et al., 2002; Urynowicz and Siegrist, 2005).

Tunnicliffe and Thomson (2004) demonstrated the incapability of a $KMnO_4$ flush to increase the bulk mass removal rate for two single vertical fractures in a laboratory environment. Permanganate solution was flushed through each of the well characterized fractures to remove emplaced DNAPL. The rapid reduction of flow observed in this study for the initial stage of the oxidant flush suggests that flow obstructions developed within the fractures altering the aperture distribution. Tunnicliffe and Thomson (2004) suggested that the resulting development of MnO_2(s) in and around existing diffusion controlled regions plugs the pore structure of the fractures. This had the effect of limiting permanganate diffusion into both existing and newly formed stagnant zones and, simultaneously, the diffusion of the organic compound towards remaining flow pathways.

Various numerical models have been developed to look into both single (e.g., Tsang and Tsang, 1987; Reitsma, 1992) and multiphase flow in fractures (e.g., Parker and Park 2004; Mundle et al., 2007; Pruess and Tsang, 1990; Eikemo et al., 2009). A conceptual model developed by Kueper and McWhorter (1991) found that in both clay and rock, DNAPL will preferentially enter the larger apertures due to their lower displacement pressures. A

numerical model developed by Harrison et al. (1992) found that fractures as small as 10 μm in a clayey aquitard can greatly increase the transport of dissolved contaminants into underlying aquifers.

Numerical models for the ISCO of chlorinated solvents with permanganate have been previously developed for unconsolidated porous media (Hood and Thomson, 2000; Zhang and Schwartz, 2000; West et al, 2008). West et al. (2008) conducted a series of numerical simulations to evaluate the efficacy of in situ chemical oxidation with permanganate for TCE and PCE in heterogeneous unconsolidated porous media at the field scale. It was found that source zone remediation can be effective during, or shortly following, the period of active treatment. However, over the long-term, depending on the dissolution kinetics and the characteristics of the aquifer, the benefit of partial treatment can be greatly reduced due to dissolution tailing. This work suggested that a large fraction of injected permanganate may be competitively consumed by the natural oxidant demand (NOD) at field sites. In addition, the performance of permanganate was also found to be highly variable due to MnO_2 (i.e., rind) formation, DNAPL architecture, and geologic characteristics. That work emphasized the difference between the simplicity of batch studies and the complexity of field scenarios and how, for the latter, heterogeneity and fluid access issues may dominate overall performance.

Only one study has been published modelling the effectiveness of ISCO in fractured porous media. Mundle et al. (2007) developed a pseudo-two-dimensional, transient flow and transport numerical model to simulate ISCO of TCE and PCE by potassium

permanganate in clay containing a single fracture. This work suggested that the NOD of the organic material may significantly reduce the efficiency of ISCO remediation in fractured rock. To the author's knowledge, no systematic studies exist of ISCO in fractured bedrock at the field scale.

The objective of this work is to examine the benefits and challenges of DNAPL source zone remediation by ISCO in fractured aquifers at the field scale. This paper employs numerical simulation to investigate the sensitivity of DNAPL source zone treatment with $KMnO_4$ to a variety of site and engineering design parameters. In so doing, the research aims to cast light on the fractured rock scenarios under which ISCO may be expected to provide cost-effective benefit.

2.0 MODEL DEVELOPMENT

Model Description

The model developed for fractured rock simulations (DNAPL3DRX-FRAC) involves the coupling of the three-dimensional two-phase flow model (DNAPL3D) (Gerhard et al., 1998, 2001; Gerhard and Kueper, 2003 a,b,c; Gerhard et al., 2007) and RT3D, a three-dimensional multi-species contaminant transport model with non-linear kinetic reactions (Clement,1997; Clement et al.,1998). This coupling was first developed for simulations involving unconsolidated porous media as DNAPL3D-RX (West et al., 2008) using a split-operator approach following Grant and Gerhard (2004). Within a time step, DNAPL migration is initially simulated using DNAPL3D. The equations solved are identical to those of the porous media model (Gerhard and Kueper, 2003c):

$$\frac{\partial}{\partial x_i}\left[\frac{k_{ij}k_{r_W}}{\mu_W}\left(\frac{\partial P_W}{\partial x_j}+\rho_W g\frac{\partial z}{\partial x_j}\right)\right]+S_W(\alpha+\theta\beta)\frac{\partial P_W}{\partial t}-\theta\frac{\partial S_W}{\partial t}=0\,,\qquad i,j=x,y,z \qquad (1)$$

$$\frac{\partial}{\partial x_i}\left[\frac{k_{ij}k_{r_{NW}}}{\mu_{NW}}\left(\frac{\partial(P_W+P_c)}{\partial x_j}+\rho_{NW} g\frac{\partial z}{\partial x_j}\right)\right]+(1-S_W)(\alpha)\frac{\partial P_W}{\partial t}+\theta\frac{\partial S_W}{\partial t}=0\,,\ i,j=x,y,z \qquad (2)$$

where P is pressure {M L^{-1} T^{-2}}, P_C is capillary pressure {M L^{-1} T^{-2}}, k_{ij} is the intrinsic permeability tensor {L^2}, k_r is relative permeability {-}, μ is dynamic viscosity {M L^{-1} T^{-1}}, ρ is fluid density {M L^{-3}}, θ is porosity {-}, S is phase saturation {-}, g is gravitational acceleration {L T^{-2}}, α is porous medium compressibility {M^{-1} L T^2}, β is wetting phase compressibility {M^{-1} L T^2}, t is time {T}, and x, y, z denote spatial coordinates. The subscripts W and NW specify the wetting and non-wetting phase, respectively. DNAPL3DRX-FRAC employs a finite difference formulation in which the primary variables, P_W and S_W, are solved fully implicitly using Newton Raphson iteration.

The contaminant solute is then added to the aqueous phase at nodes with DNAPL present via equilibrium or non-equilibrium mass transfer routines (Grant and Gerhard, 2004). RT3D is then employed within the same time step to simulate advection, dispersion, diffusion, and reactions for the solute (Clement, 1997; and Clement et al., 1998):

$$\frac{\partial(\theta C_m^n)}{\partial t}=\frac{\partial}{\partial x_i}\left(\theta D_{ij}^n\frac{\partial C_m^n}{\partial x_j}\right)-\frac{\partial}{\partial x_i}\left(\theta v_i C_m^n\right)+q_s C_s^n+\sum R_m\,,\quad i,j=x,y,z \qquad (3)$$

$$\frac{\partial(\theta C_{im}^n)}{\partial t}=\sum R_{im} \qquad (4)$$

where D_{ij} is the hydrodynamic dispersion tensor {L^2 T^{-1}}, v_i is average linear

groundwater velocity {L T^{-1}} obtained from the multiphase flow model, q_s is volumetric flux representing sources and/or sinks {T^{-1}}, R is the rate of a single reaction {M L^{-3} T^{-1}}, and t is time {T}. The superscript n denotes the species number, the subscripts m and im designate mobile and immobile species, respectively, and the subscript s denotes a source or a sink. Finally, the phase saturations are updated at the end of the time step in accordance with the amount of mass transferred from the DNAPL to the aqueous phase.

For this work, the model was further modified for simulating DNAPL migration, mass transfer, and advective-dispersive-diffusive-reactive transport in fractured porous media environments. The model is capable of simulating the sustained release of DNAPL across one or multiple fractures as well as the redistribution of DNAPL to residual and stable pools after the termination of the source. Further details are provided in Appendix B2: Fractured Rock Model Development.

The detailed submodels of $P_C(S_W)$ and $k_r(S_W)$ of Gerhard and Kueper (2003a,b) employed, which incorporate key hysteresis and other characteristics of DNAPL invasion and trapping, have been validated against physical experiments in homogeneous and heterogeneous unconsolidated porous media (Gerhard and Kueper, 2003a,b; Grant et al., 2007). The underlying form of the constitutive relationships has been demonstrated, however, to also well represent multiphase flow in natural, rough walled fractures (Reitsma and Kueper, 1994). In this work, it is therefore assumed that the constitutive model of Gerhard and Kueper (2003a,b) is a reasonable basis for simulating DNAPL migration and redistribution in fractured porous media. It is noted that the DNAPL

migration simulations in this work are only employed to provide reasonable initial conditions for ISCO treatment scenarios and thus the conclusions on remediation performance are not expected to be sensitive to the constitutive model employed.

Accuracy in simulating matrix diffusion by multiple aqueous phase constituents was achieved by developing and implementing a grid refinement (GR) technique described in Section 3.2

Chemical Oxidation Reactions

For the purpose of this study, the subsequent discussion is limited to chemical oxidation of PCE and TCE DNAPL by $KMnO_4$. The stoichiometry of chemical oxidation of PCE and TCE, respectively, by $KMnO_4$ can be described as (Seol et al., 2003; Yan and Schwartz, 1999):

$$C_2Cl_4 + 2MnO_4^- \rightarrow 4Cl^- + 2CO_2 + 2MnO_2(s) \quad (5)$$

$$C_2Cl_3H + 2MnO_4^- \rightarrow 3Cl^- + 2CO_2 + 2MnO_2(s) + H^+ \quad (6)$$

The relevant reaction kinetics are (West et al., 2008):

$$\frac{\partial[TCE]}{\partial t} = \frac{-K_{rxns}[TCE][MnO_4^-]}{R_{TCE}} \quad (7)$$

$$\frac{\partial[TCE_s]}{\partial t} = -K_{rxns}[TCE][MnO_4^-] \quad (8)$$

$$\frac{\partial[MnO_4^-]}{\partial t} = -2K_{rxns}[TCE][MnO_4^-] \quad (9)$$

$$\frac{\partial[MnO_2]}{\partial t} = 2K_{rxns}[TCE][MnO_4^-] \qquad (10)$$

where the square brackets [ ] denote molar concentration, *Krxns* is the second-order reaction constant between aqueous TCE and MnO_4^- $\{M^{-1}\ L^3\ T^{-1}\}$ and $[TCE_s]$ is the concentration of sorbed TCE.

During ISCO, permanganate reacts with organic aquifer material (OAM). For the purposes of this study, it was presumed that OAM was homogeneous throughout the rock matrix and not present in the fractures. The reaction between OAM and permanganate was represented (Mumford et al., 2005):

$$3CH_2O + 4MnO_4^- \rightarrow 3CO_2 + 4MnO_2(s) + H_2O + 4OH^- \qquad (11)$$

The reaction rate was modelled (Mundle et al., 2007):

$$\frac{\partial[OAM]}{\partial t} = -M_{MnO_4^-/OAM} K_{OAM}[OAM][MnO_4^-] \qquad (12)$$

where K_{OAM} is the second-order kinetic reaction rate constant. The OAM is assumed to comprise solely of organic carbon (*foc*) with an associated K_{OAM} of $1x10^{-6}$ m^3/kg s (Hood and Thomson, 2002).

The model simulates OAM, sorbed contaminant mass and MnO_2 as immobile species, while the contaminant solute and MnO_4 are simulated as mobile aqueous species. To simulate the reaction of $KMnO_4$ with both sorbed and aqueous chlorinated solvents, it

was necessary to modify RT3D so that sorbed compounds were treated as an explicit species. A linear sorption isotherm (Mundle et al., 2007) was employed, in which the concentration of sorbed TCE (*Cs*) was back calculated based upon the solved concentration of dissolved TCE (*Cw*) :

$$C_s = C_w Kd \frac{\rho}{\theta} \qquad (13)$$

where $Kd = K_{oc} \times f_{oc}$ (Karickhff et al., 1979), K_{oc} is the organic carbon partition coefficient (L^3M^{-1}), and *foc* is the local (i.e., nodal) fraction of organic carbon (-), ρ is the dry bulk density (ML^{-3}), and θ is the porosity (-).

The proper functioning of this sorption isotherm for TCE was subsequently verified at both the scales of a single node and field scale simulation (see Appendix B2). The model also accounts for species-dependent diffusion coefficients (West et al., 2008).

The retardation factor is computed locally from the nodal *foc* concentration (e.g., Fetter, 1993):

$$R_i = 1 + Koc \times foc_i \frac{\rho}{\theta} \qquad (14)$$

where ρ is the dry bulk density (ML^{-3}), θ is the porosity of the matrix (-), and *Koc* is the organic carbon partition coefficient (L^3M^{-1}). While *R* is commonly defined as the ratio of the velocity of groundwater to that of the sorbing contaminant, when incorporated into the governing advection-dispersion equation (Equation 3) it has the effect of reducing not only advective velocity but also hydrodynamic dispersion (in the case of rock matrix, this

is pure diffusion) by this factor (e.g., Fetter, 1993). Sorption is known to reduce the rates of both advection and diffusion (Lyman et al., 1992), but it is acknowledged that a linear reduction in diffusion with respect to R is a widely held and almost universally applied assumption (Pankow and Cherry, 1996). The role of R in sorption with respect to matrix diffusion is acknowledged in Lyman et al (1992) in presentation of an equation for 'rock capacity factor' α, which measures a rock's capacity to store organic contaminants, that is identical to (15) where $\alpha = R/\theta$ (Equation 10.2, pg 265). In this work, as OAM is consumed by permanganate, the decreasing foc is reflected in decreasing R and decreasing α which corresponds to a reduction in the sorptive capacity of the matrix.

While the model simulates the production of $MnO_2(s)$ via (5, 6 and 11), permeability reduction associated with MnO_2 accumulation is not considered in this work. Since all the simulations presented are in two dimensions, it is expected that including pore-clogging would significantly restrict the flow field in a manner that may not be representative of three-dimensional behaviour (e.g., bypassing in the third dimension). For this reason, the presented results should be considered as a 'most promising' envelope of results for the elimination of DNAPL by $KMnO_4$ in fractured rock, since rind formation is known to inhibit achievement of this objective (e.g., Tunnicliffe and Thomson, 2004; West et al., 2008).

Model Verification

Advective-dispersive transport was verified against the Ogata and Banks (1961)

one-dimensional analytical solution (see Section 3.3.1 for details). DNAPL migration in a horizontal fracture was verified against the one-dimensional analytical solution of McWhorter and Sunada (1990) (see Section 3.3.2 for details). Simulations of transient contaminant transport in a set of discrete, parallel fractures situated in a diffusion-dominated rock matrix were verified against the analytical solution of Sudicky and Frind (1982) (see Appendix B2). Additional simulations were conducted to provide confidence in the developed model for scenarios/processes for which analytical solutions do not exist, including (i) one-dimensional simulations of DNAPL dissolution and lateral diffusion from a DNAPL occupied vertical fracture, and (ii) DNAPL migration, dissolution, and aqueous phase diffusion in a domain characterized by a single, orthogonal fracture intersection (see Appendix B2). This body of work established that the governing equations were being solved correctly and provided confidence in the modelling approach and developed GR. Furthermore, these simulations provided insight into the minimum degree of discretization required in order to adequately capture diffusion gradients in the matrix (see Appendix B2).

The chemical oxidation reaction kinetics (Equations 7 – 10) were verified in DNAPL3D-RX-FRAC by successfully reproducing the published simulations of a one-dimensional DNAPL dissolution and $KMnO_4$ treatment scenario in an unconsolidated porous medium (West et al., 2008). West et al. (2008), in turn, demonstrated successful reproduction of column ISCO experiments by Schroth et al. (2001) that employed residual TCE DNAPL treated by potassium permanganate. Results with three different DNAPL dissolution routines, and their simulated impact on

TCE degradation by $KMnO_4$, are shown in Figure 1. The plot demonstrates that DNAPL3DRX-FRAC has accurately implemented both the mass transfer and chemical oxidation reaction kinetics.

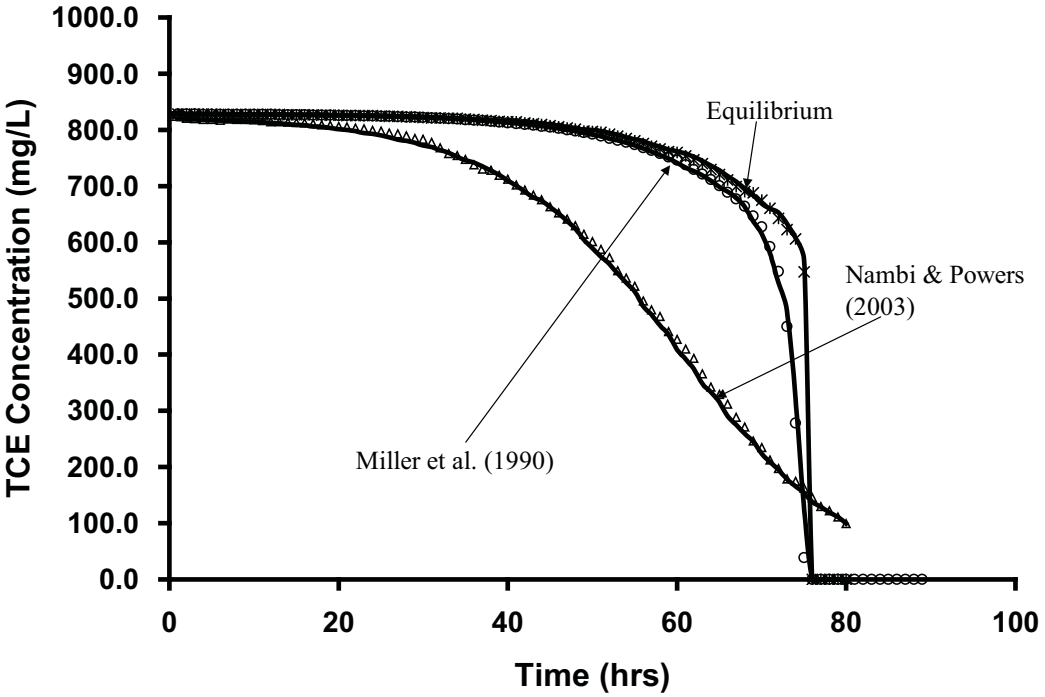

Figure 1: Verification of DNAPL3D-RX FRAC with model results from West et al. (2008) for various mass transfer expressions. Note: Results from West et al. (2008) are indicated with solid lines while results from DNAPL3DRX-FRAC are indicated by symbols.

3.0 NUMERICAL SIMULATIONS

Modelled Scenario

This section describes characteristics common to all of the simulations conducted in this thesis, while the next details the characteristics of the individual runs. All simulations consider a portion of a fractured rock formation within a field scale DNAPL source zone via a two-dimensional, vertical cross-section domain 20 m wide × 5 m high with unit depth. This domain exhibits an underlying, coarse, uniformly discretized grid with

nodes that are $\Delta x = 0.25$m and $\Delta y = 0.25$m (total of 1600 coarse nodes). A network of horizontal and vertical fractures, with an aperture distribution and fracture density appropriate for the rock type considered (refer to Table 2 for the three different rock type properties), was then defined as an overlay. Grid refinement was then conducted using the GR parameters determined as optimal from preliminary analyses (5 refined nodes per coarse node, exponentially increasing spacing with distance from fracture; see Appendix B2 for details). This resulted in an approximate doubling of the number of nodes; for example, for the base case with 7 fractures, the final domain exhibited 3072 nodes with the fracture nodes dimensioned in width equal to the fracture aperture and with matrix nodes as small as $\Delta x = 2.5 \times 10^{-4}$ m and $\Delta y = 7.6 \times 10^{-4}$ m in the matrix immediately adjacent to fracture intersections.

The matrix was assigned a uniform distribution of initial OAM at a representative concentration for each rock type (Table 2). The assigned porosity of fractures was unity and fractures were not assigned any OAM (and thus do not exhibit sorption). Lipson et al. (2005) studied a system of equally spaced fractures from the field and determined that when matrix diffusion effects are dominant, fracture retardation can be assumed equal to unity.

Each simulation evolved according to five distinct stages: (i) DNAPL Release, (ii) DNAPL Redistribution, (iii) Site Ageing, (iv) Treatment Application, and (v) Post-Treatment Ageing. For all stages, the water table was set to be coincident with the top boundary. During the DNAPL Release and DNAPL Redistribution stages, constant

head specified at the side boundaries during DNAPL migration established a zero hydraulic gradient across the domain. The bottom boundary permitted the free exit of both water and DNAPL. At t = 0, the 'DNAPL Release' stage began by specifying a constant nonwetting phase saturation of 30% across the entire top boundary. Note that in this work, DNAPL is considered the nonwetting fluid. DNAPL was permitted to flow into the domain for 6 months, by which time it was established that saturations had achieved steady state values (i.e., DNAPL inflow at the top equalled DNAPL outflow at the bottom). The DNAPL source was then terminated, and DNAPL redistribution was simulated for 6 months, at which time it was established that DNAPL movement had effectively ceased. Thus, at the end of the 'DNAPL Redistribution' stage, at t_{TOTAL} = 1 yr, the fracture network exhibited a complex distribution of DNAPL pools and residual characteristic of the fracture network of the rock type under investigation. DNAPL dissolution was not simulated during the DNAPL emplacement stages in order to better distinguish the fate of TCE during the Site Ageing stage; while a simplification, it is not expected that this assumption significantly impacts the conclusions of this work.

For the 'Site Ageing' stage, the side boundaries were modified such that a groundwater hydraulic gradient of 0.005 from left to right across the domain was established. DNAPL dissolution, aqueous phase transport, diffusion, and sorption of aqueous phase chlorinated solvent were simulated for 20 years during this stage (i.e., 1 yr $\leq t_{TOTAL} \leq$ 21 yrs). During this stage, a constant aqueous phase concentration of 550 mg/L TCE was specified along the entire left boundary, representing the impact of additional upgradient DNAPL upon the domain. This recognized that only a subsection of a typical source

zone was simulated and resulted in (i) increased longevity of the DNAPL by reducing the concentration gradient driving dissolution and (ii) additional mass loading to the matrix within the domain.

In the 'Treatment Application' stage, chemical oxidation was initiated by injecting a constant aqueous phase concentration of 2.5g/L MnO_4 for 2 years (i.e., 21 yrs $\leq t_{TOTAL} \leq$ 23 yrs) at the horizontal fractures along the left boundary (i.e., analogous to a fully screened well). During permanganate application, the hydraulic gradient across the domain was increased to 0.025 to represent active amendment conditions. As well, the upgradient TCE boundary condition was terminated (assuming complete and instantaneous treatment of the upgradient source zone); while this is highly idealized, it provides the best opportunity for success within the domain and thus supports viewing these results as approximating a best case for the technology. In all cases, stoichiometric calculations confirm that the total mass of MnO_4 injected is greater than the theoretical MnO_4 mass required to destroy all the TCE in the domain at the start of the Treatment stage; for example, in the base case 45.5 kg (382 moles) of MnO_4 was injected which, compared to the 7.3kg (55.6 moles) of TCE mass in the domain, represents an excess of 300% (considering that 1 mole of TCE is destroyed by 2 moles of MnO_4, Equation 6).

Following the Treatment stage, an additional five years were simulated (i.e., 23 yrs $\leq t_{TOTAL} \leq$ 28 yrs). During this Post-Treatment stage, the ambient hydraulic gradient of 0.005 was again employed, but no upgradient concentration of any species (i.e.,

permanganate or TCE) was applied.

Several assumptions were employed in this work to facilitate reasonable simulation times:

1. All fractured rock simulations presented are two-dimensional; this assumption likely benefits the technology since the reduced dimensionality is expected to reduce bypassing of the treatment fluid around DNAPL-occupied fractures;
2. The matrix is presumed to have a sufficient displacement pressure so as to exclude DNAPL entry; this assumption likely benefits the technology because the highest fraction of DNAPL is retained in the fractures which are most accessible to the treatment fluid;
3. Advection of groundwater through the matrix is assumed to be negligible; this is reasonable given that the high permeability contrast between the fractures and matrix. For example, for the sandstone Base Case, the matrix permeability is approximately 6 orders of magnitude less than the average fracture permeability. The Peclet number for the matrix ($Pe = vx/D$ where v is horizontal velocity in matrix) if advection were not neglected is 0.166; since $Pe<1$ it is reasonable to assume that the matrix is diffusion dominated and advection is negligible (Trivedi et al., 2008).
4. Equilibrium mass transfer from DNAPL to aqueous phase was assumed; this assumption also favours improved performance of the technology by maximizing aqueous phase solvent concentrations.

Base Case and Sensitivity Simulations

Table 1 presents the suite of 10 simulations conducted in this study. The base case considered a fractured sandstone template site. Table 2 presents the parameters employed to characterize the sandstone as well as the other two rock types (shale and granite). The sandstone domain, employed in all simulations except Run 7 and Run 8, is presented in Figure 2a. The sandstone parameters were chosen to be broadly representative of North American sandstone aquifers (e.g., Lipson et al., 2005). Table A1 (Supplementary Information) provides, for each rock type, the observed ranges for each parameter synthesized from the literature. Table 3 reveals that this sandstone exhibits - relative to the other template rock types - low fracture density, low mean aperture (125μm), high matrix porosity (7.7%), and intermediate foc (0.005).

The sandstone base case employed TCE as the DNAPL released and as the aqueous phase and sorbed chlorinated compound subsequently targeted by ISCO. Fluid properties and reaction parameters are listed in Table 4. The base case also employed a continuous injection of $KMnO_4$ at 2.5 g/L for 2 years during the Treatment stage (Table 1).

Table 1 Field Scale ISCO Fractured Rock Simulations

Run No.	DNAPL Type	Material	KMnO4 Concentration (mg/L)	Pulsing	Pulsing Strategy
1 (Base Case)	TCE	Sandstone	2500	No	Continuous KMnO4 Injection for 2 Years
2	TCE	Sandstone	5000	No	Continuous KMnO4 Injection for 1 Year
3	TCE	Sandstone	1250	No	Continuous KMnO4 Injection for 4 Years
4	TCE	Sandstone	2500	Yes	3 Months On 3 Months Off for 4 Years
5	TCE	Sandstone	2500	Yes	6 Months On 3 Months Off for 4 Years
6	TCE	Sandstone	2500	Yes	12 Months On 12 Months Off for 4 Years
7	TCE	Shale	2500	No	Continuous KMnO4 Injection for 2 Years
8	TCE	Granite	2500	No	Continuous KMnO4 Injection for 2 Years
9	PCE	Sandstone	2500	No	Continuous KMnO4 Injection for 2 Years

Table 2 Properties of Field Scale Fractured Rock Template Sites

Rock Type	Fracture Spacing (m)	Matrix Permeability (m^2)	Matrix Porosity	Foc	Bulk Density (g/cm^3)	Matrix Tortuosity	Fracture Aperture Range (μm)	Mean Aperture (μm)
Sandstone	6.0 (Ver) [*] 1.0 (Hor) [a]	1.05×10^{-15}	7.7% [a]	0.005 [a]	2.49 [a]	0.2 [a]	25 - 230 [a]	125
Shale	4.0 (Ver) [*] 1.0 (Hor) [*]	1.05×10^{-15}	3.0% [b]	0.009 [*]	2.619 [**]	0.1 [*]	50 - 250 [c]	150
Granite	2.0 (Ver) [d] 2.0 (Hor) [d]	1.05×10^{-15}	0.1% [*]	0.0005 [*]	2.697 [**]	0.05 [*]	100 - 500 [e]	300

[a] *Lipson et al., 2005*
[b] *Morris and Johnson, 1967*
[c] *Jardine et al., 1999*
[d] *Sousa 2007*
[e] *Sausse 2002*
**Data supplied by B.H Kueper (personal communication) based upon consulting experience on sites of all three rock types.*
*** Calculated using Bulk Density = Grain Density x (1-porosity), assuming a grain density of 2.7 for Shale and Granite.*
Ver – Vertical Fractures
Hor – Horizontal Fractures

Table 3 Fracture Density of Field Scale Fractured Rock Template Sites

	Sandstone	Shale	Granite
Fracture Length (m)	77.0	82.0	84.0
Density (m^{-1})*	0.77	0.82	0.84

**Fracture Length / Total Domain Area*

Table 4 Fluid Properties and Reaction Parameters

Parameter	Notation	Value
TCE Density [a]	ρ_{NWtce}	1460 kg/m^3
TCE Viscosity [a]	μ_{NWtce}	0.0005 Pa s
TCE Solubility [a]	$Solub_{TCE}$	1100 mg/L
TCE Koc [a]	KOC_{TCE}	126 L/kg
PCE Density [a]	ρ_{NWpce}	1630 kg/m^3
PCE Viscosity [a]	μ_{NWpce}	0.0009 Pa s
PCE Solubility [a]	$Solub_{PCE}$	200 mg/L
PCE Koc [a]	KOC_{PCE}	364 L/kg
TCE Free Solute Diffusion Coefficient [b]	D^O_{TCE}	1.01 x10^{-9} m^2/s
PCE Free Solute Diffusion Coefficient [b]	D^O_{PCE}	9.40 x10^{-10} m^2/s
MnO_4^- Free Solute Diffusion Coefficient [c]	D^O_{MnO4}	1.63 x 10^{-9} m^2/s
Kinetic Reaction Rate for TCE [d]	K_{TCE}	4.11 x 10^{-3} m^3/kg s
Kinetic Reaction Rate for PCE [d]	K_{TCE}	2.85 x 10^{-4} m^3/kg s
Kinetic Reaction Rate for OAM [e]	K_{OAM}	1.0 x 10^{-6} m^3/kg s

a – Pankow and Cherry (1996)
b –Wilke and Chang (1955) at 25°C
c - Lide (2004)
d – Yan and Schwartz (2000)
e –Hood and Thomson (2002)

As illustrated in Table 1, Runs 1 - 6 examine variations in treatment strategy, while Runs 7-8 and 9 explore the influence of site conditions and different DNAPLs respectively. All parameters, boundary conditions, and source conditions were established identically to the base case for all simulations, except for changing the parameter(s) whose influence was being examined in each study. It is noted that for all simulations except Runs 7 and 8, the results during the DNAPL Release, DNAPL Redistribution, and Site Ageing stages are identical with the differences occurring from the start of the Treatment stage.

It is noted that a 'No ISCO' case (Run 10) was simulated for comparison purposes. This simulation was identical to the base case in all respects but one: the 2-year Treatment stage employed identical boundary conditions as the base case except no upgradient concentration of permanganate was applied.

Injected Potassium Permanganate Concentration

In Runs 1-3, the concentration of $KMnO_4$ injected was increased by 100% and reduced by 50% relative to the base case (Table 1). All of these values are within the range of those employed in field studies (Geosyntec, 2007). In order to ensure the total volume of $KMnO_4$ injected was kept constant, the injection period was changed accordingly (Table 1). This sensitivity study comprised three simulations.

Pulsed Injection of Permanganate

The effects of pulsing are examined in Runs 1 and 4-6 by subdividing the base case injection period (2 years) into equal length $KMnO_4$ injection on and off intervals.

Pulsed injection intervals of 3 months, 6 months and 12 months were examined. Pulsed treatment has been demonstrated to be valuable in other remediation options (e.g., Gerhard et al., 2001) and has been considered for permanganate in unconsolidated porous media as a means to reduce rind formation and increase destructive capacity for a given mass of treatment fluid injected (e.g., Thomson et al., 2008). This sensitivity study comprised four simulations.

Rock Type

Runs 1, 7, and 8 compare ISCO performance in three different types of fractured rock at the field scale, each exhibiting a characteristic set or range of hydrogeological parameters (Table 2). Figure 2 presents the distribution of intrinsic permeability for the three domains, illustrating the distribution of fractures. In each case, the mean aperture is at the midpoint of the range specified in the table. It is noted that, characteristic of these rock types in natural environments, the shale template site exhibits (relative to the other two) intermediate fracture density, low mean aperture (150μm), intermediate matrix porosity (3%), and high *foc* (0.009) while the granite exhibits high fracture density, high mean aperture (300μm), low matrix porosity (0.1%), and low *foc* (0.0009).

DNAPL Type

Runs 1 and 9 compare performance for TCE and PCE in the sandstone domain. The full set of PCE fluid parameters employed for Run 9 are presented in Table 4. Note that, while the boundary conditions in each run were identical, the distribution of DNAPL resulting from infiltration and redistribution were not identical due to contrasting fluid

properties. As well, different solubilities and sorptive capacities resulted in different distributions of aqueous phase and sorbed phase concentrations after the Site Ageing stage. This sensitivity study comprised of two simulations.

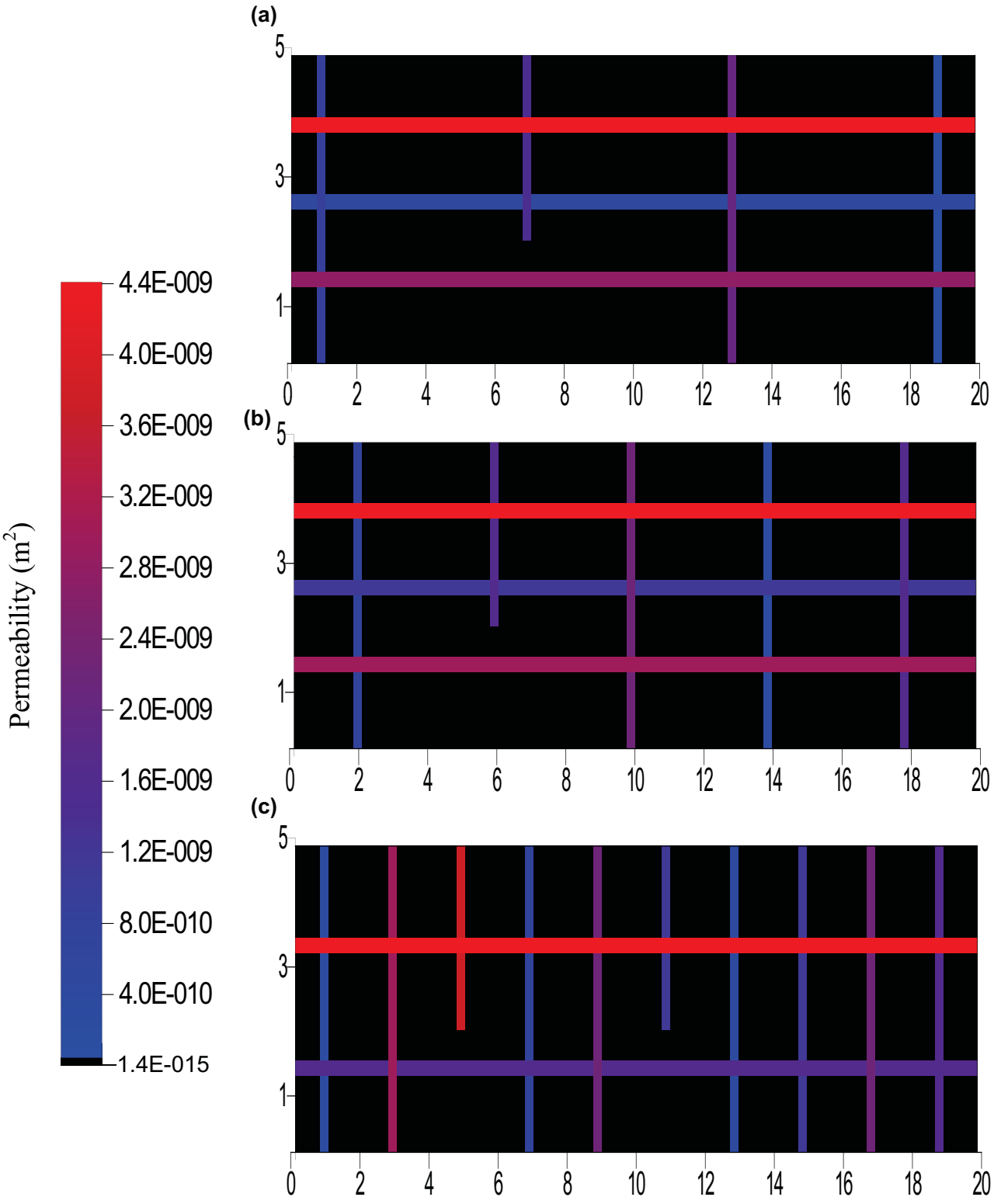

Figure 2: Distribution of permeability for the field scale fractured rock domains: (a) sandstone, (b) shale, and (c) granite. Colour corresponds to fracture permeability according to the scale bar provided; matrix permeability is uniform (black). Note that distance is in metres, domain is vertically exaggerated, and fracture apertures are exaggerated for visual purposes.

4.0 RESULTS AND DISCUSSION

Table 5 summaries a selection of key numerical results for all 10 simulations conducted in this study. These data will be discussed as each set of simulations is presented.

Table 5: Summary of Results for All ISCO Simulations

Run No.	DNAPL St 2 (kg)	DNAPL St 3 (kg)	Aq + Sorb St 3 (kg)	MnO_4 Inject (kg)	DNAPL St 5 (kg)	Aq + Sorb St 5 (kg)	Mass Discharge St 5 (10^{-3} mg/s)	MnO_4 React (kg)	CS React (kg)
1	5.26	0.00	7.3	45.5	0.00	5.10	3.97	44.9	0.78
2	5.26	0.00	7.3	44.8	0.00	5.25	4.21	44.3	0.82
3	5.26	0.00	7.3	45.0	0.00	4.85	3.56	44.4	0.80
4	5.26	0.00	7.3	44.7	0.00	4.86	3.56	44.2	0.81
5	5.26	0.00	7.3	45.1	0.00	4.86	3.56	44.6	0.80
6	5.26	0.00	7.3	45.4	0.00	4.86	3.56	44.9	0.78
7	6.86	0.01	6.8	59.6	0.00	3.05	0.36	41.9	2.33
8	11.53	4.23	0.68	538.8	4.17	0.37	0.02	23.2	0.30
9	6.03	0.11	3.3	46.7	0.08	2.59	0.67	46.1	0.22
10	5.26	0.00	7.3	0.0	0.00	5.18	4.06	0.00	0.00

St 2 = mass present at the end of Stage 2 (DNAPL redistribution)
St 3 = mass present at the end of Stage 3 (Site Ageing)
St 5 = mass present at end of Stage 5 (Post-Treatment)
DNAPL = mass of DNAPL present
Aq + Sorb = combined mass of aqueous and sorbed chlorinated solvent present
MnO_4 Inject = mass of MnO4 injected during the treatment period
Mass Discharge = mass per time of chlorinated solvent leaving the domain at the end of Post-Treatment stage
MnO_4 React = total mass of MnO_4 that reacted (with OAM + chlorinated solvent in all phases)
CS React = total mass of chlorinated solvent (in all phases) destroyed by MnO_4

Base Case Results

Figures 3(a) and 3(b) illustrate the distribution of the TCE DNAPL at the end of the infiltration and redistribution phases, respectively (relevant to all simulations except Runs 7 - 9). Figures 3(a) and 3(b) reveal a heterogeneous distribution of DNAPL pools (i.e., connected phase) and residual (i.e., trapped blobs and ganglia) due to the influence of capillary forces (and, specifically, fracture entry pressures), the order of encounter of fractures, and the permeability contrasts between fractures. At the end of the DNAPL infiltration stage, the average local DNAPL saturation (i.e. average saturation of all nodes containing DNAPL) was 0.75, the mass of DNAPL in the domain equaled 11.68 kg, the DNAPL volume was 0.008 m^3 (compared to a total fracture volume of 0.012 m^3) with 100% of the nodes on drainage (i.e., DNAPL displacing water). At the end of DNAPL redistribution stage, the average DNAPL saturation was 0.3, the DNAPL volume was 0.0036 m^3 (equal to a mass of 5.26 kg) and the pool to residual ratio was 71:29%. Note in Figure 3(b) that, as expected, the lone remaining pool exhibiting a high DNAPL saturation resides in a vertical dead-end fracture, and other pools of various lengths occur in horizontal fractures, separated by areas of residual DNAPL.

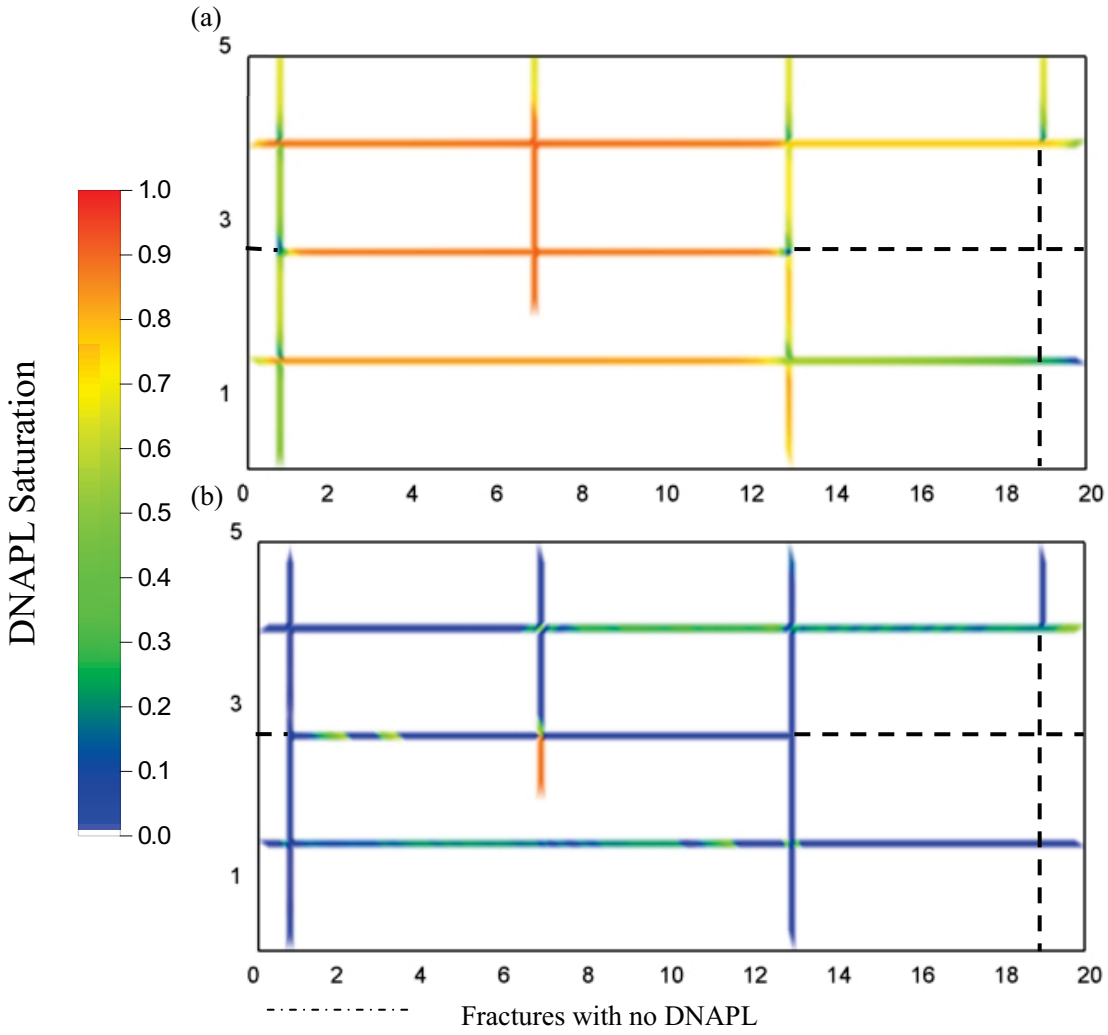

Figure 3: DNAPL distribution for Base Case at (a) t_{TOTAL} = 0.5 years when DNAPL inflow and outflow are equal, and (b) t_{TOTAL} = 1 year when all DNAPL migration has ceased.

Figure 4 illustrates the distribution of aqueous phase TCE at the end of the 20 year Site Ageing stage (t_{TOTAL} = 21 years). Evident are the expected diffusion halos in the sandstone matrix blocks adjacent to fractures containing DNAPL as well as those horizontal fractures without DNAPL but subject to significant aqueous mass flux (Figure 3b). However, it is noted that due to the lack of DNAPL in the rightmost vertical fracture (i.e., x=19.0 m) and continuous injection of aqueous TCE in the horizontal

upgradient, no aqueous phase TCE surrounding the immediate vicinity of this fracture is noted. At this time, no DNAPL remained in the domain. This occurred despite the constant influent concentration equal to 50% of TCE solubility. The reason is the substantial TCE sink provided by matrix diffusion and sorption. At this time, the total mass of TCE in the domain was 7.3 kg, of which 99% resided in the matrix; of the mass in the matrix, 98% was sorbed and only 2% remained in the aqueous phase. The significant porosity and foc of the sandstone matrix combine so that it acts as a substantial sink for TCE, rapidly promoting DNAPL dissolution. The complete disappearance of DNAPL from fractures in sandstones and similar scenarios is not unexpected (Parker et al., 1994).

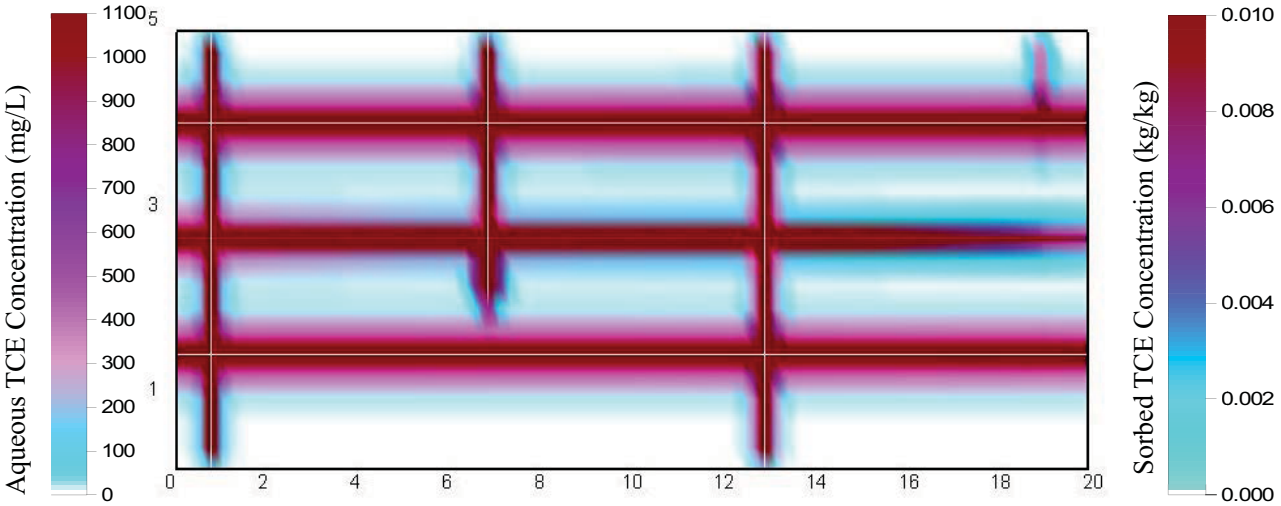

Figure 4: Distribution of aqueous and sorbed TCE after 20 years (t_{TOTAL} = 21 years) of DNAPL dissolution (i.e., Site Ageing stage).

Figure 5 provides the concentration of aqueous and precipitated species throughout the domain after the Treatment stage (i.e., 2 years of MnO_4 injection, t_{TOTAL} = 23 years). It reveals the limited penetration of MnO_4 at this time, due to its reaction with TCE in the

fractures and its diffusion and subsequent destruction by OAM, aqueous TCE, and sorbed TCE in the matrix. As expected, that absence of TCE is most prominent in the fractures near the injection boundary, although it should be noted that TCE concentrations also decrease due to an ongoing mass flux of TCE flux out of the downgradient boundary. Horizontal penetration is noted to be least in the middle fracture, which exhibits the smallest aperture (see Figure 2a). It is further noted that the horizontal extent of $MnO_2(s)$ penetration closely corresponds to the extent of TCE disappearance.

Figure 6 provides the concentration of aqueous TCE throughout the domain after the Post-Treatment stage (i.e., 5 years after the completion of MnO_4 injection, t_{TOTAL} = 28 years). Back diffusion of TCE solute into the fractures is observed while all of the MnO_4 has been consumed.

Figure 7 plots the evolution of the aqueous TCE concentration profile along a cross-section perpendicular to the fracture (in this case for the top horizontal fracture with the cross-section located 3.0 m from the left side boundary). In this figure, back diffusion of TCE into the fracture after the MnO_4 injection is demonstrated. At t_{TOTAL} = 21 years, the maximum aqueous TCE concentration was observed. Over the 2 year injection period, the concentration of aqueous TCE in the fracture decreased from approximately 325mg/L to 20mg/L as a result of the treatment and the eliminated upgradient boundary condition. However, the concentration profile within the fracture is observed to rebound as back diffusion begins during the Post-Treatment stage. Figure 7 further illustrates that the concentration profile in the matrix is little affected by the

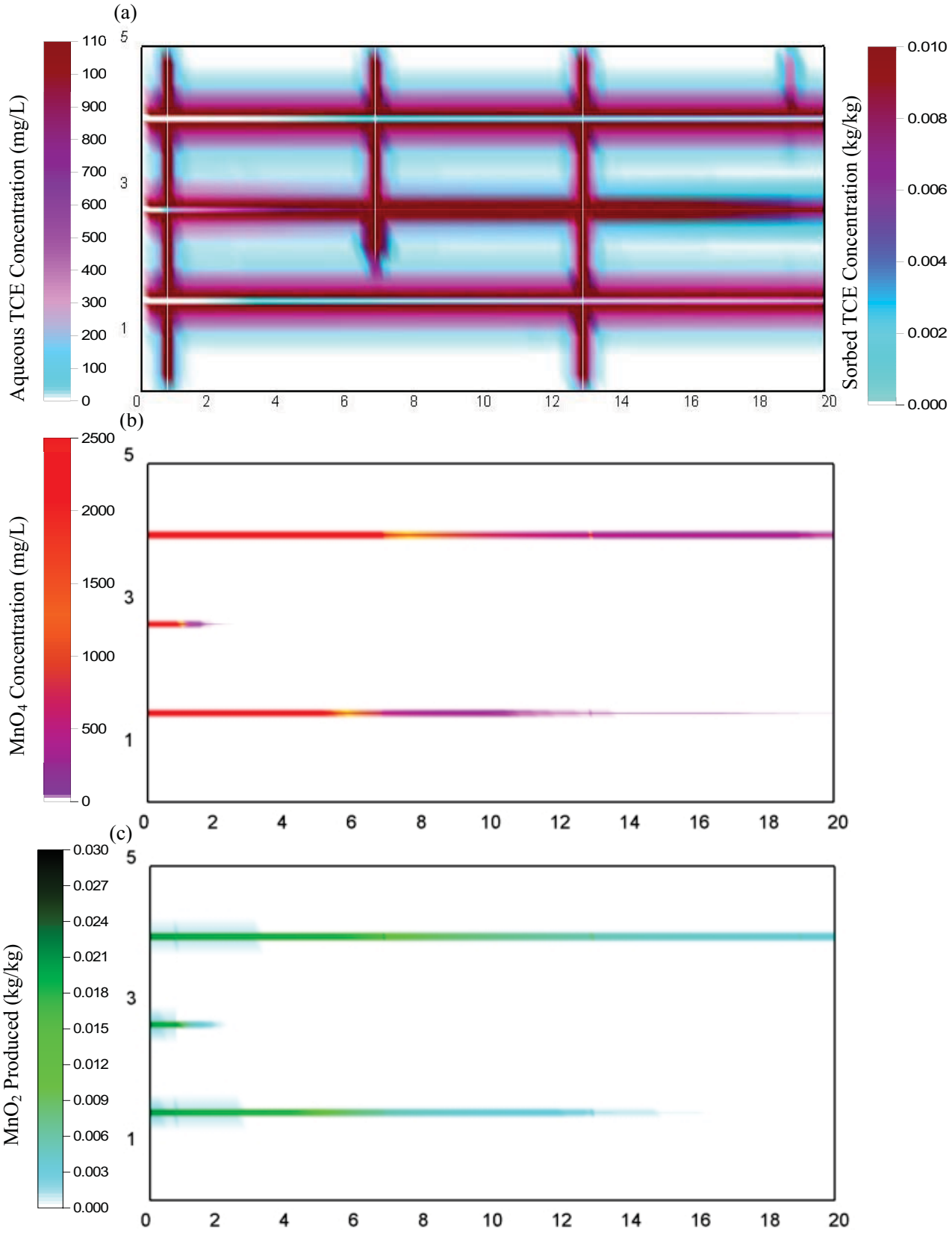

Figure 5: Distribution of aqueous species concentrations at t_{TOTAL} =23 years for Base Case after 2 years of chemical oxidation (i.e., Treatment stage): (a) TCE, (b) MnO_4, (c) MnO_2.

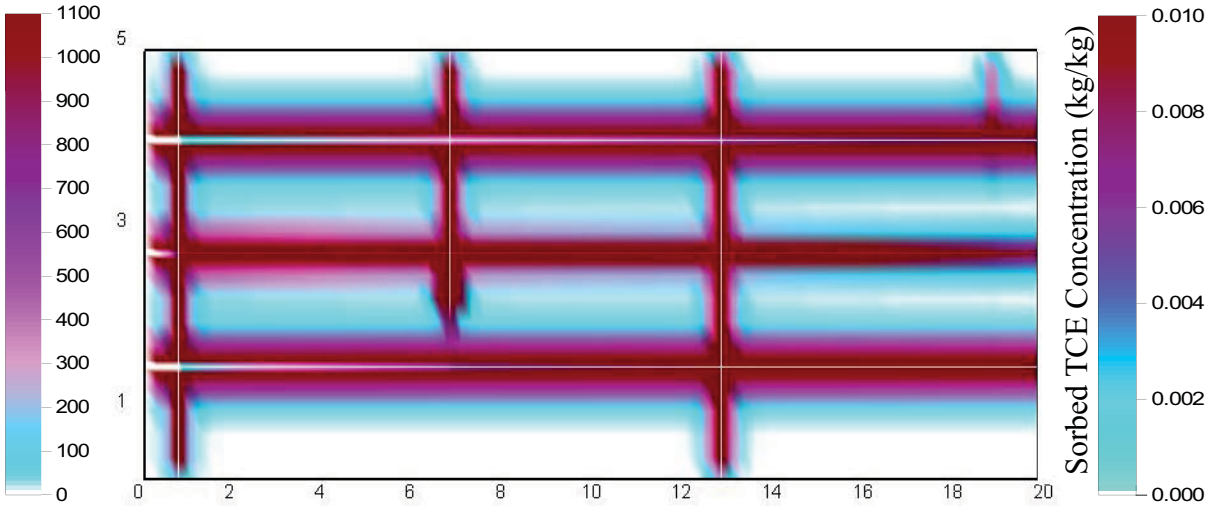

Figure 6: Distribution of aqueous TCE concentrations at t_{TOTAL} =28 years for Base Case, 5 years after chemical oxidation (i.e., Post-Treatment stage).

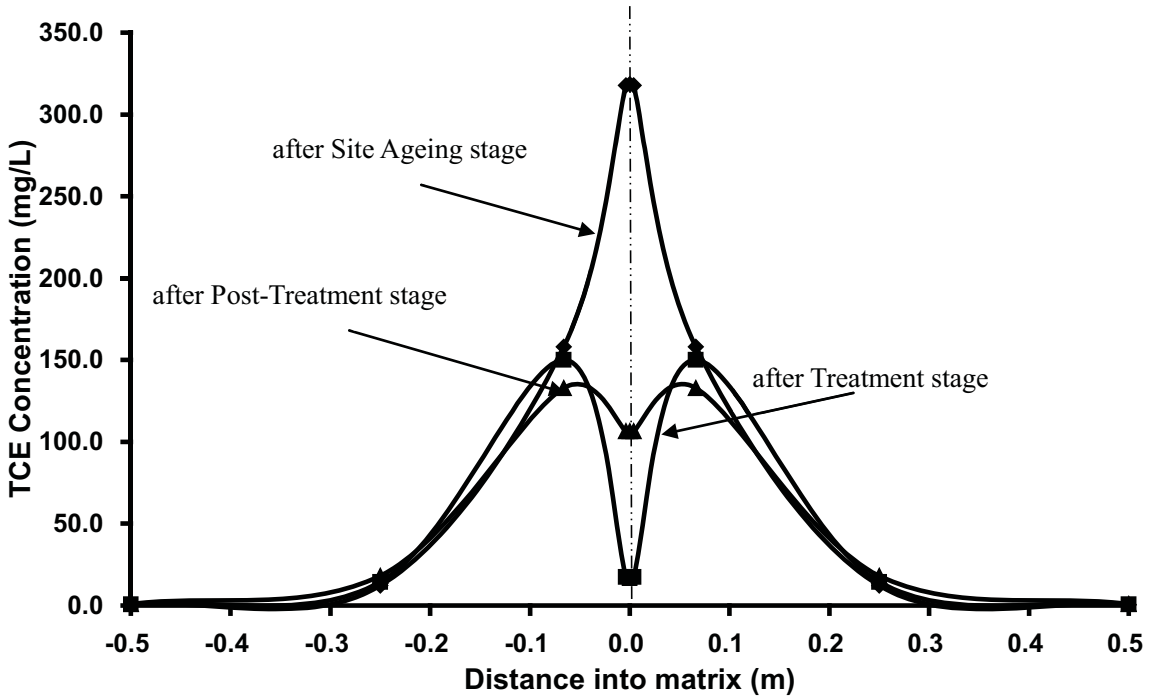

Figure 7: Concentration profile of aqueous TCE across a single fracture for the Base Case. Shown is a 1.0 m cross-section across a horizontal fracture (dotted line denotes location of the facture).

chemical oxidation treatment, indicating that (as observed in Figure 5) the permanganate had minimal interaction with the TCE in the matrix.

Figure 8 presents cumulative mass plots of all sinks and sources of TCE during the base case simulation. Summed totals of the sinks and sources in this plot, where:

Mass Dissolved + Mass Influx =

Mass Destroyed + Mass Outflux + Mass Sorbed + Mass In Domain (16)

reveal that the model has excellent mass balance for TCE (plots not shown to improve clarity of the figure); this was further confirmed by excellent computed mass balance on all modelled species. The figure reveals that the majority of DNAPL dissolution occurred rapidly at the beginning of the simulation due to partitioning to groundwater in the fractures, diffusion into the matrix, and simultaneously a rapid increase in sorbed TCE in the matrix. Until t_{TOTAL} = 3 years, TCE flux out of the domain was greater than flux into the domain due to a proportion of the dissolved TCE exiting via fracture flow. However, beyond this time, with dissolution virtually complete, TCE influx exceeded outflux as the incoming background TCE contributed to a steady rise in mass retained via sorption. It is also noted the cumulative mass of aqueous TCE in the domain (sum of that in the fractures and matrix) is a small fraction of the amount sorbed.

Figure 8 further illustrates that when MnO_4 was injected, at t_{TOTAL} = 21 years, the amount of TCE solute destroyed began to rise. However, the magnitude of this rise was less than the magnitude of the reduction in sorbed TCE. The additional desorption occurred for two reasons: (i) as a result of back-diffusion induced by the flushing of aqueous TCE out of the domain via fracture flow, and (ii) the reduction in sorptive capacity caused by

the destruction of OAM. During the Post-Treatment stage, as illustrated by Figure 8, the amount of aqueous TCE destroyed increases at a rate that is minor (i.e. 0.0024 kg over 5 years of post-treatment dissolution) relative to that achieved during the Treatment stage (i.e., 0.78 kg over 2 years of MnO_4 injection).

Figure 9 presents the cumulative mass in the domain of the species involved in the oxidation reactions; note that the time axis originates at the beginning of the Treatment stage. This figure reveals that the rate of MnO_4 consumption was essentially constant during the injection period. Of the total mass of 382 moles of MnO_4 injected (i.e., 45.5 kg MnO_4), at the end of the Treatment stage 95.7% had been consumed by OAM while 4.3% had been consumed by TCE. Of the 7.3 kg of aqueous TCE solute present in the domain at the end of the 20 year Site Ageing stage, only 0.78 kg (i.e., 10.7% of the initial mass) was destroyed by the injected MnO_4 at the end of the 5-year Post-Treatment stage.

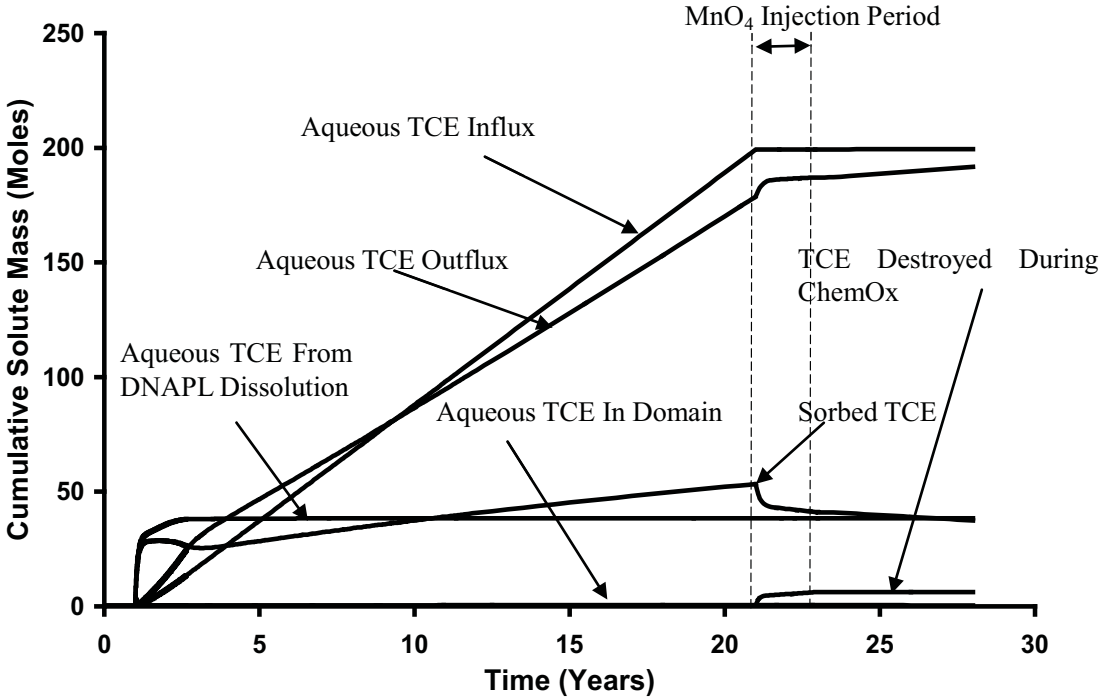

Figure 8: Cumulative aqueous and sorbed TCE from all sinks and sources for Base Case.

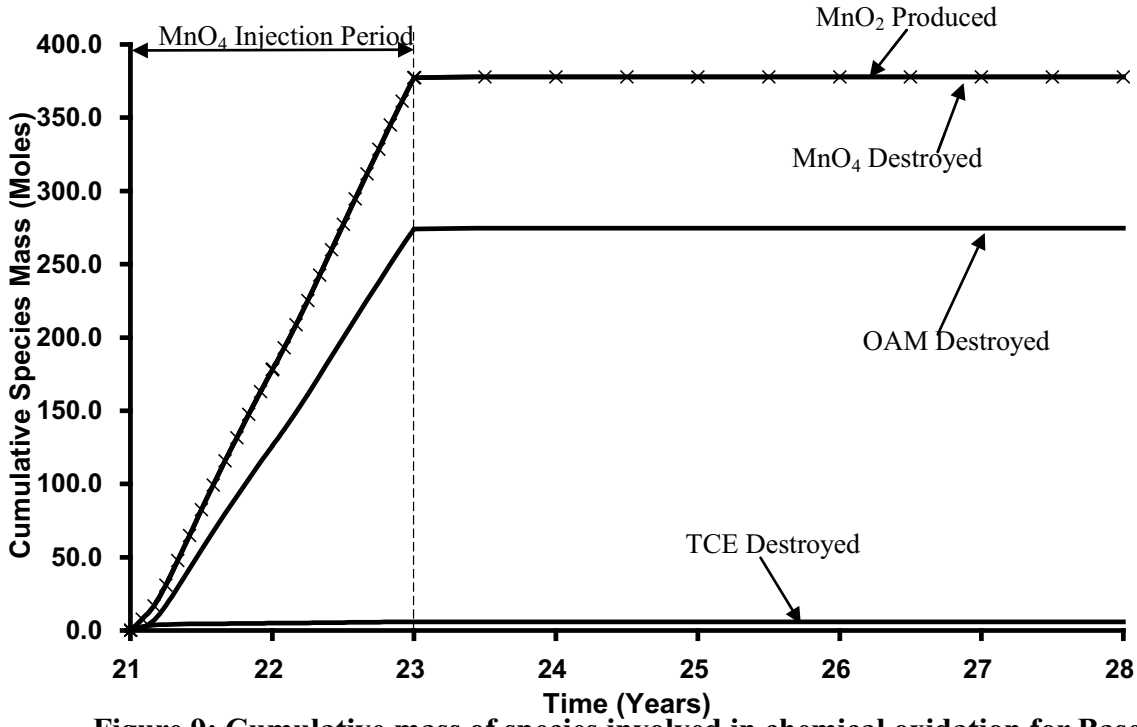

Figure 9: Cumulative mass of species involved in chemical oxidation for Base Case.

Figure 10 presents the TCE mass discharge at the downgradient boundary of the domain for the base case and No ISCO simulations. The figure illustrates that mass discharge initially increased during the Ageing stage as the DNAPL dissolved, peaked when all DNAPL has disappeared, then decreased to a constant level. The very slowly increasing mass discharge at the exit reflects the mass influx at the inlet modified by a significant amount of forward diffusion from the matrix that decreases slowly with time. The mass flux then spiked at the start of the Treatment stage due to the increase in hydraulic gradient (from 0.005 to 0.025) that flushed out the fractures. The mass discharged after treatment is substantially lower than before treatment, but this is largely a function of removing the constant influx of TCE solute. Comparison with the No ISCO simulation in Figure 10 reveals the small but not insignificant effect of treatment to further reduce the mass flux during the Treatment stage. However, it also reveals that the

Post-Treatment mass discharge is essentially identical for the two cases (see also Table 5). This illustrates that, for the base case scenario modelled, ISCO effectively targeted TCE in the hydraulically active fractures during treatment but had a relatively insignificant influence on the TCE in the matrix that was responsible for long term mass flux. Total TCE mass in the domain at the end of the simulations were 5.103 kg and 5.179 kg (1.5% difference) for the base and No ISCO cases, respectively.

Figure 11 presents the average TCE solute concentration in each of the three horizontal fractures at the downgradient boundary. The figure first demonstrates that concentrations in none of the three fractures were in equilibrium with the matrix after 20 years of Site Ageing, as evidenced by exit concentrations less than the 550 mg/L specified at the upgradient boundary. This agrees with Figure 4 in that large concentration gradients span only 0.5 m into the matrix even after 20 years. Figures 4 and 11 also reveal that higher exit concentrations correlate to higher degrees of mass loading to the matrix, which in turn result from higher initial DNAPL saturation present in these fractures. The gradual increase in exit concentrations observed for all three fractures during the Site Ageing period reflects the gradual loading of the matrix such that forward diffusion gradients are reduced.

During the Treatment stage, Figure 11 reveals that the two larger fractures (i.e., 178μm and 230μm) experienced concentrations that decreased significantly; this was primarily due to dilution by injected water rather than chemical oxidation (as evidenced by the similarity to the No ISCO case). Flow rates in these fractures were so large that reverse

diffusion from the matrix could not occur fast enough to significantly elevate concentrations. However, soon after the commencement of the Treatment stage, a small concentration rebound is observed in the No ISCO case while the base case observed no such rebound (Figure 11b); this difference accounts for the mass flux difference observed (Figure 10) and illustrates the relative benefit of MnO_4 penetration and treatment in the larger fractures (Figure 5b). Later in the Post-Treatment stage, steady concentrations attained only 20-25% of the pre-treatment amounts and no difference was observed between the ISCO and No ISCO cases; this reflects the long term bleed from matrix-bound TCE and the inability of the 2-year treatment to significantly affect this stored mass (see also Table 5).

In contrast, Figure 11 reveals that TCE concentrations in the smallest horizontal facture (i.e., 76 μm, the central fracture in Figure 5) increased during the Treatment stage. This occurred because the rate of groundwater flow, although elevated, was still low relative to the rate of reverse diffusion (occurring downgradient from the limited zone of MnO_4 penetration, Figure 5b) so that mass entering the fracture impacted the exit concentrations. The fact that no significant difference is observed in solute concentrations before and after treatment in this fracture reveals further that both the upgradient TCE boundary condition and the small MnO_4 treated zone have no impact on the exit boundary after 5 years. And the lack of significant difference from the No ISCO case reveals the negligible influence of treatment on such low-flow fractures (given a constant head boundary condition, which results in the majority of injected water flowing through the larger aperture fractures).

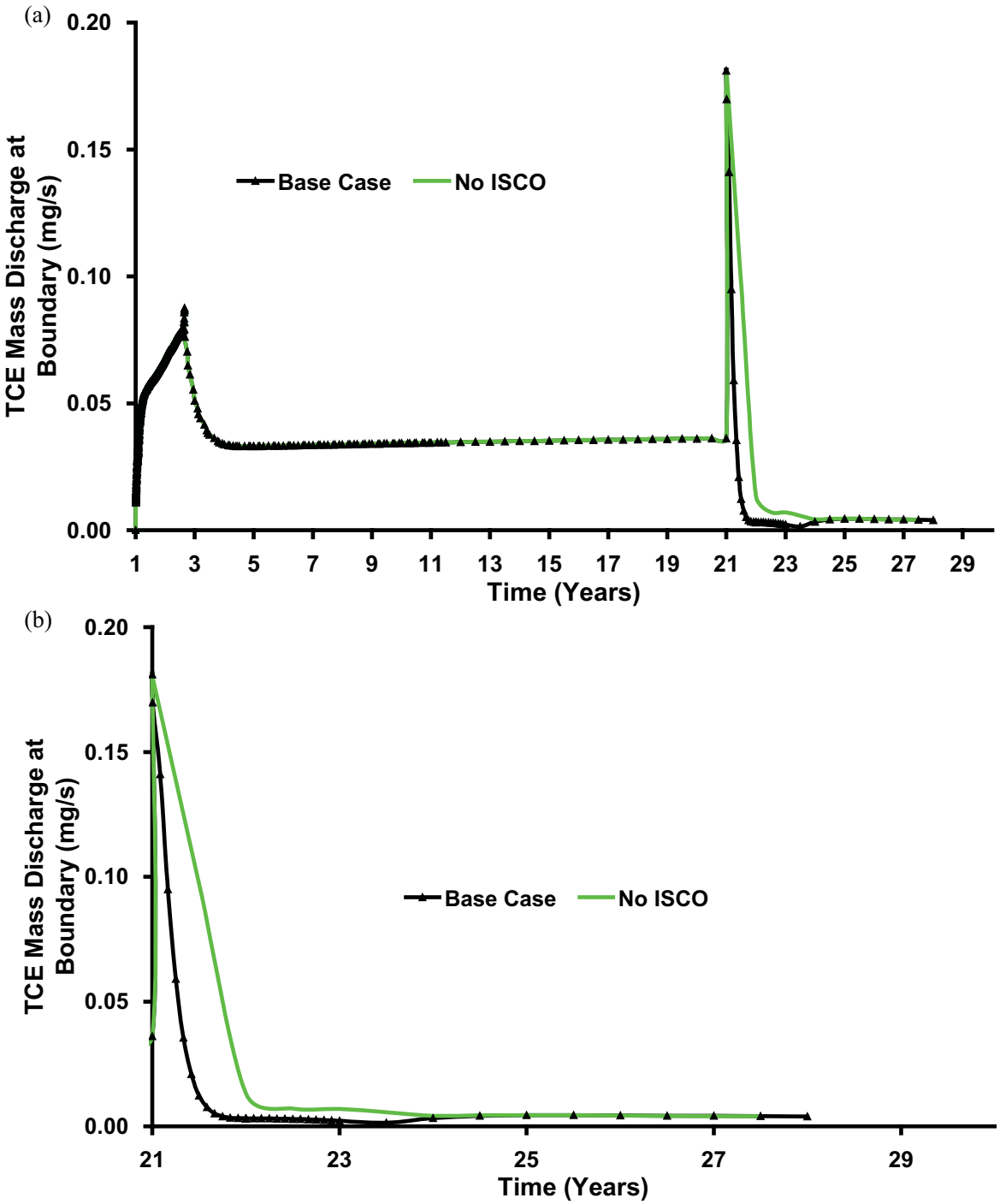

Figure 10: Comparison of total boundary mass discharge for base case with (a) a simulation where no ISCO was carried out and (b) since the start of the Treatment Stage only (timescale expanded for clarity).

(a)

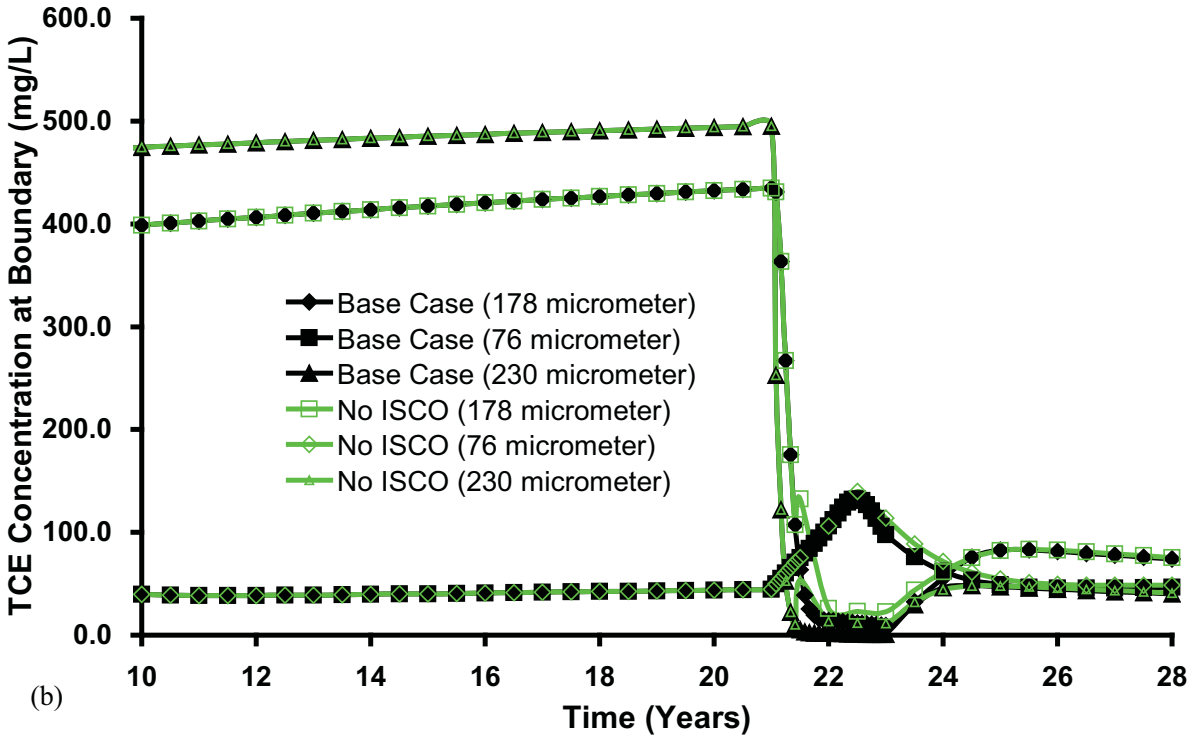

(b)

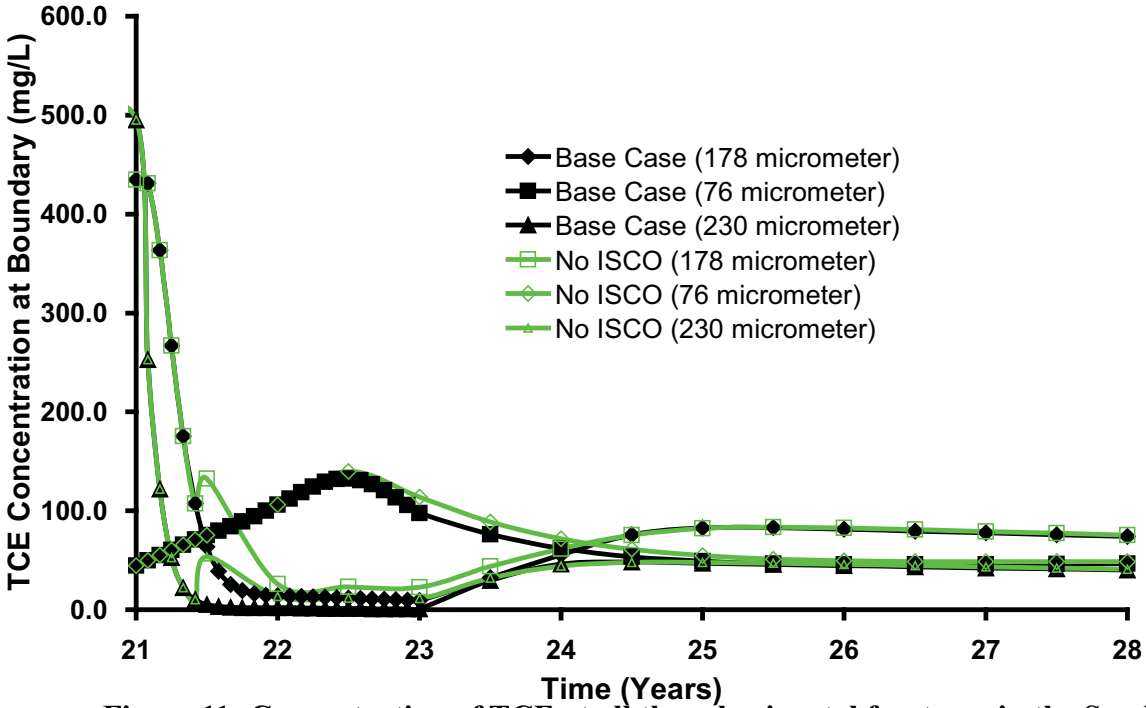

Figure 11: Concentration of TCE at all three horizontal fractures in the Sandstone base case at the downgradient boundary over (a) the latter 18 years, and (b) since the start of the Treatment stage only (timescale expanded for clarity).

Sensitivity to Potassium Permanganate Concentration

Figure 12 plots the cumulative mass of TCE destroyed for Runs 1, 2, and 3, in which the injected concentration of MnO_4 was varied but the total mass injected was kept constant (by varying the length of the Treatment stage). Note that the plot shows data from the start of the Treatment stage only. It reveals that, for the scenario considered, the rate of TCE mass destruction is a function of the injected MnO_4 concentration, but the total TCE mass destroyed is only a function of the total mass of oxidant injected.

Furthermore, once the injection process ceased, additional TCE destruction was negligible in all three cases. This occurs because of the limited pathways available for permanganate transport, and the fact that oxidant demand (from OAM + TCE) significantly exceeds oxidant supply in all three simulations. In addition, the Post-Treatment period is dominated by reverse diffusion of TCE mass and all three simulations have similar, negligible effect on the matrix-stored mass. No significant difference between the 3 cases is observed during the Post-Treatment stage with respect to mass flux (Figure 13) or exit concentrations of MnO_4 (figure not shown). Moreover, the distribution of TCE, MnO_4, and MnO_2 are observed to be essentially identical after the Treatment stage (compare Figure 5 and Figures A1 and A2 in Supplementary Information).

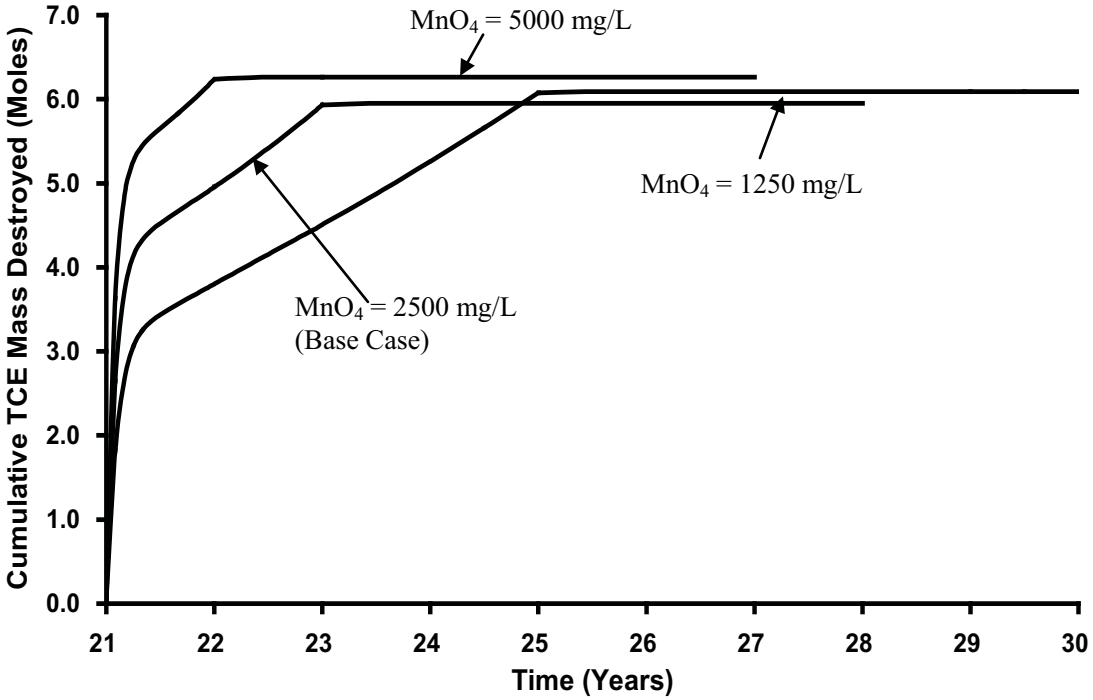

Figure 12: Cumulative mass of TCE destroyed for various MnO4 concentrations.

(a)

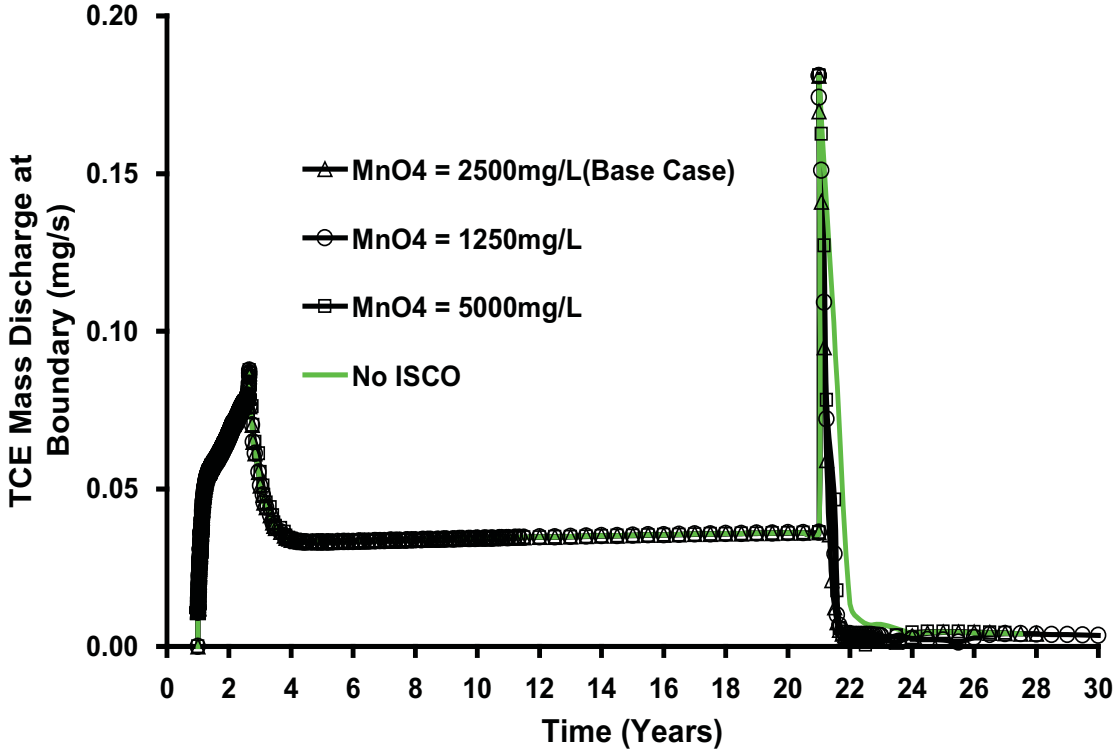

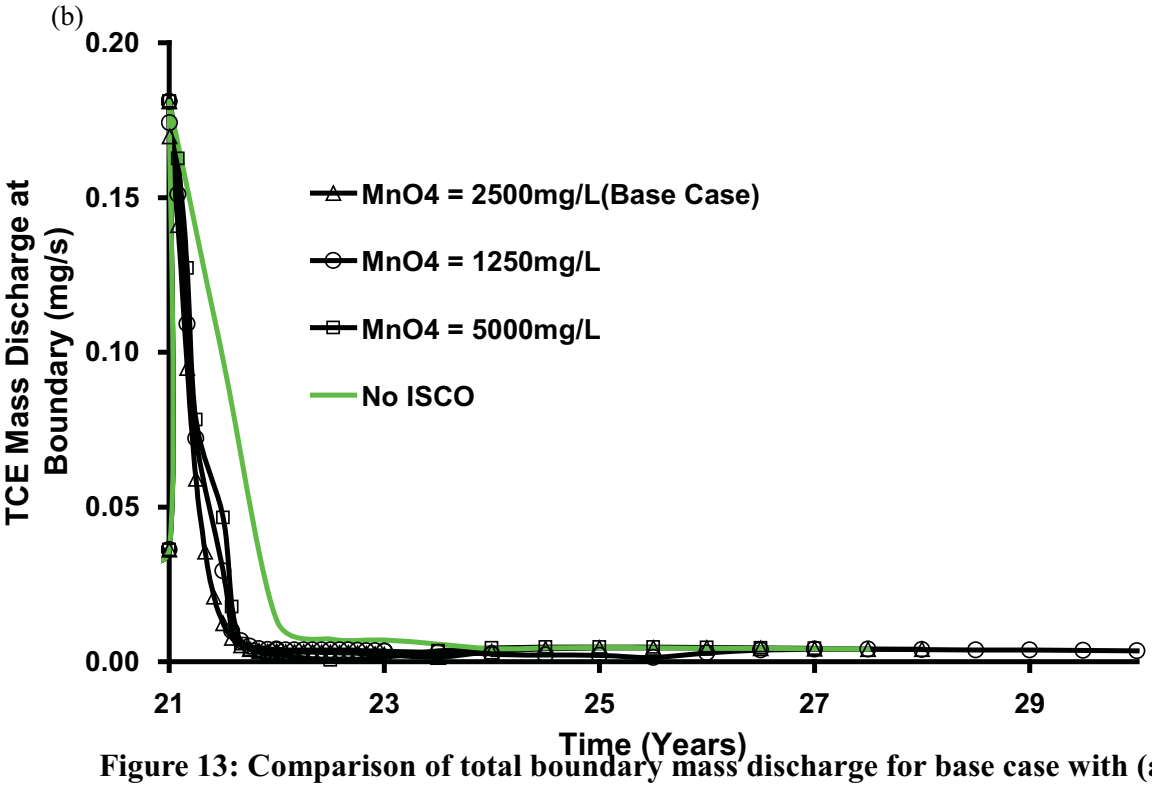

Figure 13: Comparison of total boundary mass discharge for base case with (a) various MnO4 concentration injected and (b) since the start of the Treatment stage only (timescale expanded for clarity).

Sensitivity to Pulsed Injection

Figure 14 plots the cumulative mass of TCE destroyed for Runs 1, 4, 5 and 6, in which the MnO_4 was added via pulsed injection periods of varying length, including no pulsing, ensuring that the total mass injected was constant (by varying the length of the Treatment stage). As demonstrated in Figure 14, the total mass of TCE destroyed at the end of the Treatment stage (and thereafter) is nearly identical in all cases due to the fact that the cumulative injected MnO_4 mass is constant. No significant difference between the 4

cases is observed during the Post-Treatment stage with respect to mass flux (Figure 15) or exit concentrations of MnO_4 (figure not shown). Moreover, the distribution of TCE, MnO_4, and MnO_2 are observed to be essentially identical after the Treatment stage (compare Figure 6 and Figures A3, A4 and A5 in Supplementary Information). Figure 15(b) reveals that for each interlude between a MnO_4 pulse, TCE mass flux begins to rise immediately due to reverse diffusion delivering mass to the hydraulically active fractures and then decreases at the start of the next pulse as MnO_4 reacts with TCE in the fractures. This reconfirms that the injected permanganate was quickly consumed by the high oxidant demand in the matrix of the fractured rock. and that no residual permanganate remained to provide ongoing treatment of TCE mass bleeding into the fractures during the pump-off periods.

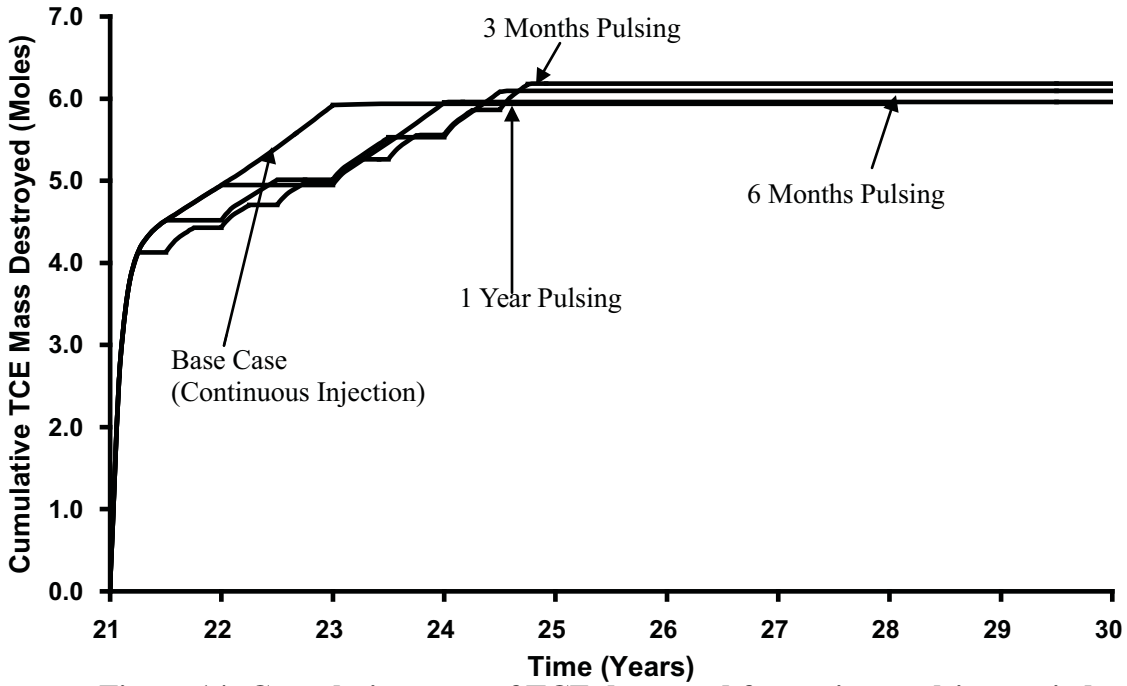

Figure 14: Cumulative mass of TCE destroyed for various pulsing periods.

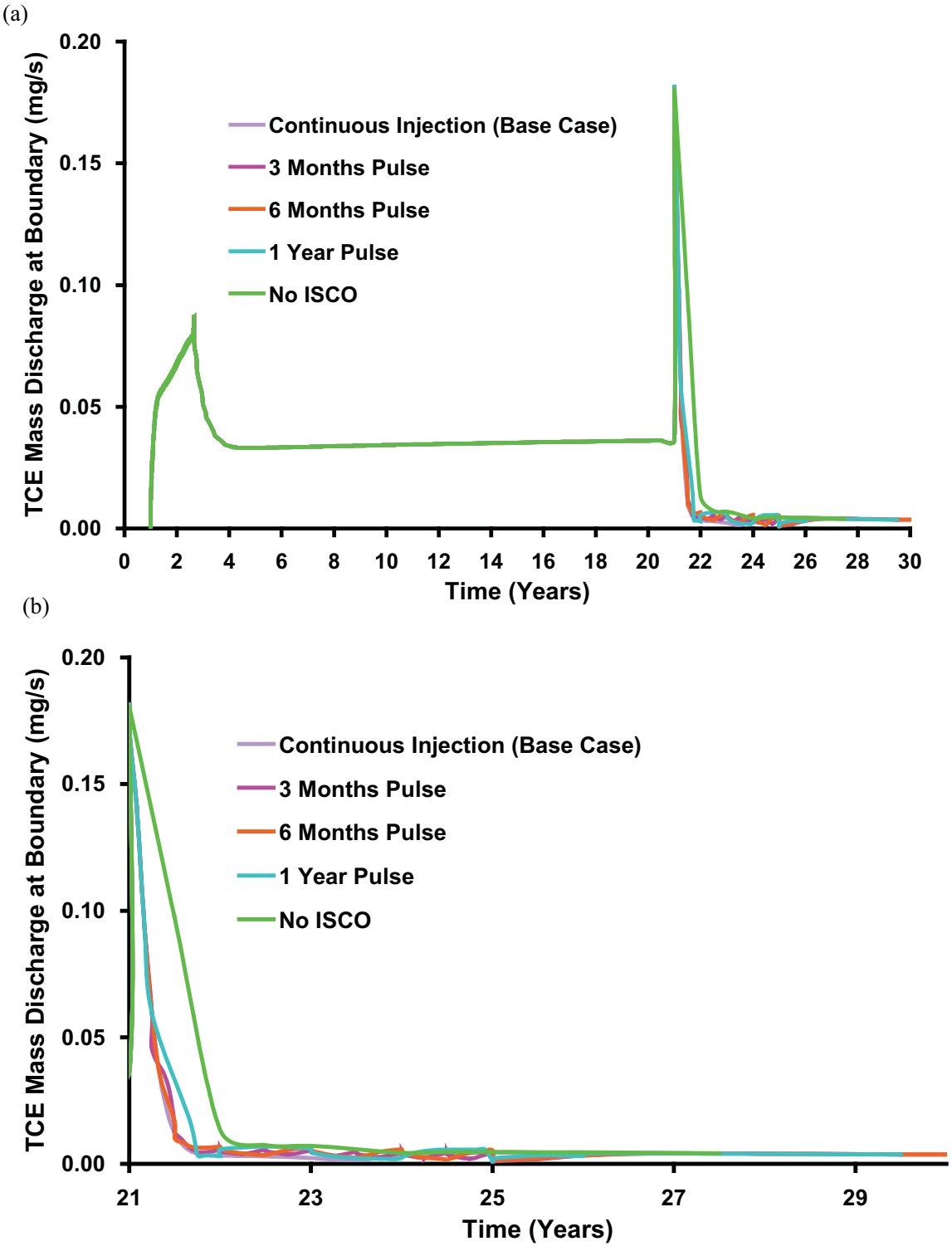

Figure 15: Comparison of total boundary mass discharge for base case with (a) various pulsing method and (b) since the start of the Treatment stage only (timescale expanded for clarity).

Sensitivity to Rock Type

At the end of the DNAPL Infiltration stage, the average DNAPL saturation was 0.75, the volume of DNAPL in the domain was 0.008 m^3, 0.01 m^3 and 0.018 m^3 for sandstone, shale and granite with 100% of the invaded nodes on drainage for all 3 rock types. At the end of the DNAPL redistribution stage, the average DNAPL saturation was 0.3 for all 3 rock types, the volume of DNAPL was 0.0036 m^3 , 0.0047 m^3 and 0.0079 m^3 while the pool to residual ratio was 71:29%, 72:28% and 90:10% for sandstone, shale and granite respectively. The distributions of TCE DNAPL at the end of the redistribution stage for each rock type are illustrated in Figure 3 and Figure A6, Supplementary Information.

At the end of the 20 years Site Ageing stage (t_{TOTAL} = 21 years) the total mass of aqueous and sorbed TCE in the domain was 7.3 kg (55.6 moles), 6.8kg (50.8 moles) and 0.68 kg (5.08 moles) for sandstone, shale and granite respectively. In each case, 97-99% of the total mass resided in the matrix, of which 97-98% was sorbed and only 1-2% remained in the aqueous phase. Although no DNAPL was left in the sandstone and shale domain at this time, 4.23 kg of DNAPL was found present in the granite domain. This observation is consistent with the findings in Parker et al. (1994) where it was suggested that due to the low porosity in granite, DNAPL could remain present in the fractures for decades. Figure 16 illustrates the distribution of aqueous phase TCE in the sandstone, shale and granite simulations at the end of the 20 year Site Ageing stage. In each case, the matrix immediately surrounding the fractures exhibits diffusion halos of TCE. However, the depth and extent of TCE penetration of the matrix is observed to be highly dependent on properties of both the fractures and the matrix for each rock type. The combination of

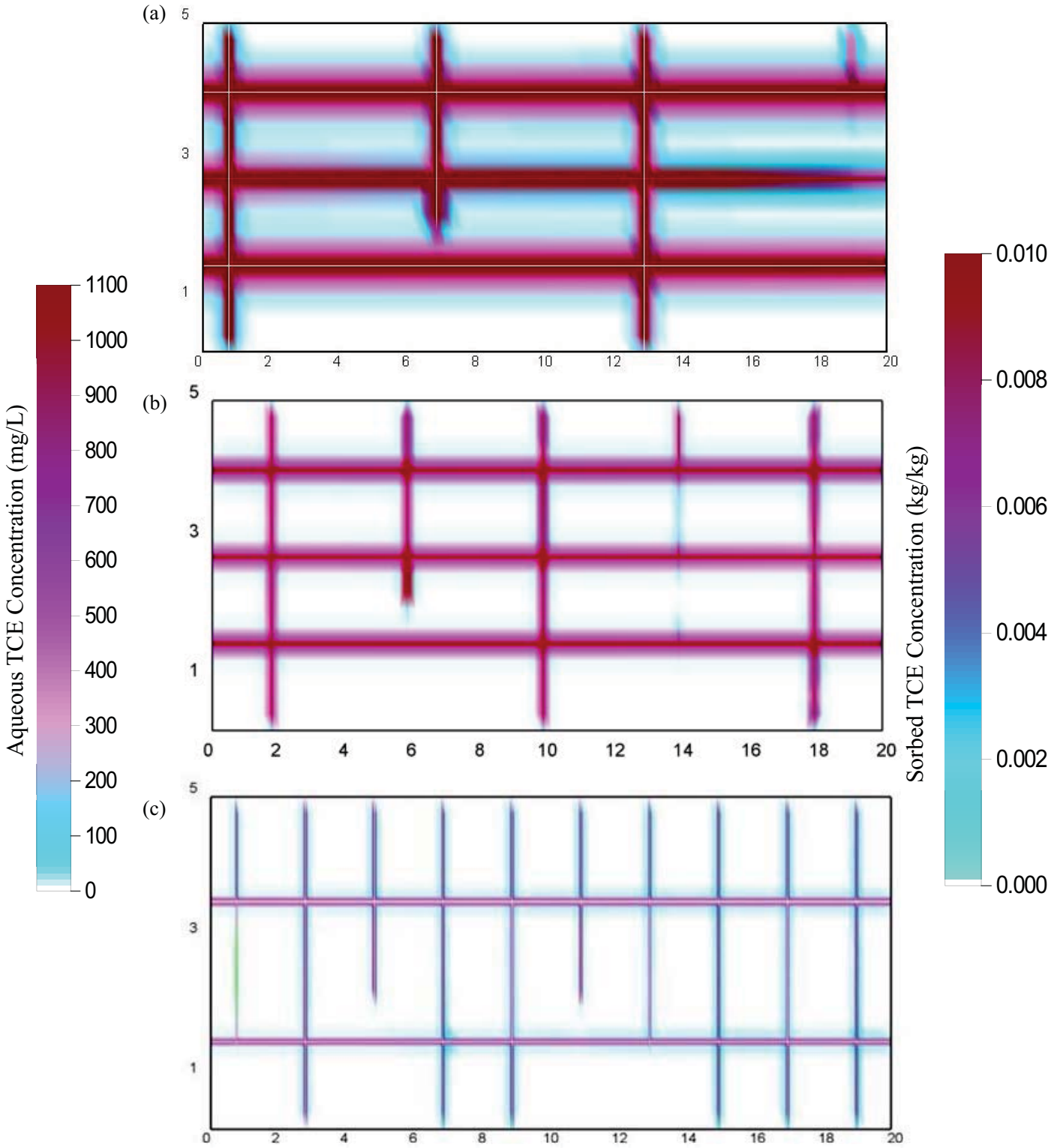

Figure 16: Distribution of aqueous TCE after 20 years (t_{TOTAL} = 21 years) of DNAPL dissolution (i.e., Site Ageing stage) in (a) Sandstone, (b) Shale and (c) Granite.

these impacts residence time of TCE in the source zone and it is the relative rates of TCE transport through fractures versus diffusion to the matrix that affects the final distribution of mass.

The effective diffusion rate is proportional to matrix tortuosity multiplied by the free solute diffusion coefficient (Bear, 1972; Pankow and Cherry, 1996); referring to Table 2 for the three rock types, the product of these two values is 2.02 $x10^{-10}$ m^2/s for the sandstone, 1.01x 10^{-10} m^2/s for the shale, and 5.05 x 10^{-11} m^2/s for the granite. Countering this is the sorptive capacity of the matrix, which is proportional to foc and inversely proportional to porosity (Equation 13). The (pre-treatment) matrix retardation coefficient R (Equation 14) is 21, 100 and 170 for sandstone, shale and granite, respectively. This corresponds to rock capacity factors, α, values of 270, 3300, and 170,000 for sandstone, shale, and granite, respectively. Overall the depth of penetration of TCE into the matrix in a direction perpendicular to the fractures is expected to be proportional to the effective diffusion rate divided by the rock capacity factor; this is calculated for sandstone, shale, and granite as 7.4 x 10^{-13}, 3.0 x 10^{-14}, and 3.0 x 10^{-16}, respectively. Figure 16 confirms that the ability of TCE to penetrate to depth in the matrix follows the order of this calculation, namely sandstone > shale > granite.

With respect to the impact of rock fractures on mass storage and mass flux, the dominant properties are fracture density, mean aperture, and distribution of apertures. In particular, the residence time of TCE in the horizontal fractures is key. The mean aperture of the horizontal fractures only for sandstone, shale, and granite are 161 μm, 192

μm, and 400 μm, respectively. The mean horizontal groundwater velocities across the domain (in the absence of DNAPL) for sandstone, shale, and granite were found to be 1.06 x 10^{-4} m/s, 1.50 x10^{-4} m/s, and 6.54 x 10^{-4} m/s, respectively. These correspond to mean residence times across the 20 m domain for sandstone, shale, and granite of 2.21 days, 1.56 days, and 0.36 days, respectively.

Figure 17 demonstrates that the mass discharge of TCE out of the right boundary of the domain during the Site Ageing stage follows the order granite > shale > sandstone. The vertical axis of Figure 18 demonstrates that the percentage of initial TCE mass retained in the domain at the end of Site Ageing follows the order sandstone > shale > granite (see also Table 5 for the mass retained in domain). These two results, mass lost to advection versus mass retained via sorption, reflect the overall balance of residence time versus matrix diffusion. Peclet number (Pe) for fractured rock is defined as the ratio of advection to diffusion rates, $Pe = ve/(D^o\tau)$, where v is the advective velocity in the fracture, e is the mean aperture, D^o is the free solute diffusion coefficient and τ is the matrix tortuosity (e.g., Fetter, 1993). Here v is taken as the mean horizontal advective velocity across each domain and e is the mean aperture of all horizontal fractures for each rock type. Figure 18 reveals that the percentage of TCE retained (in aqueous and sorbed forms) exhibits a linear dependence on the log(Pe) for the three rock types ($R^2 = 0.9923$) at the end of the Site Ageing stage (i.e., $t_{TOTAL} = 21$ years). This confirms expectations that lower Pe (i.e., lower advective velocity, smaller apertures, higher effective diffusion) corresponds to increased matrix diffusion (e.g., sandstone) while higher Pe corresponds to increased mass loss via advection (e.g., granite). Note that this relationship is specific

to the 3 domains tested; it is expected that more scatter would be observed if more simulations were conducted with a wider range of properties of each rock type.

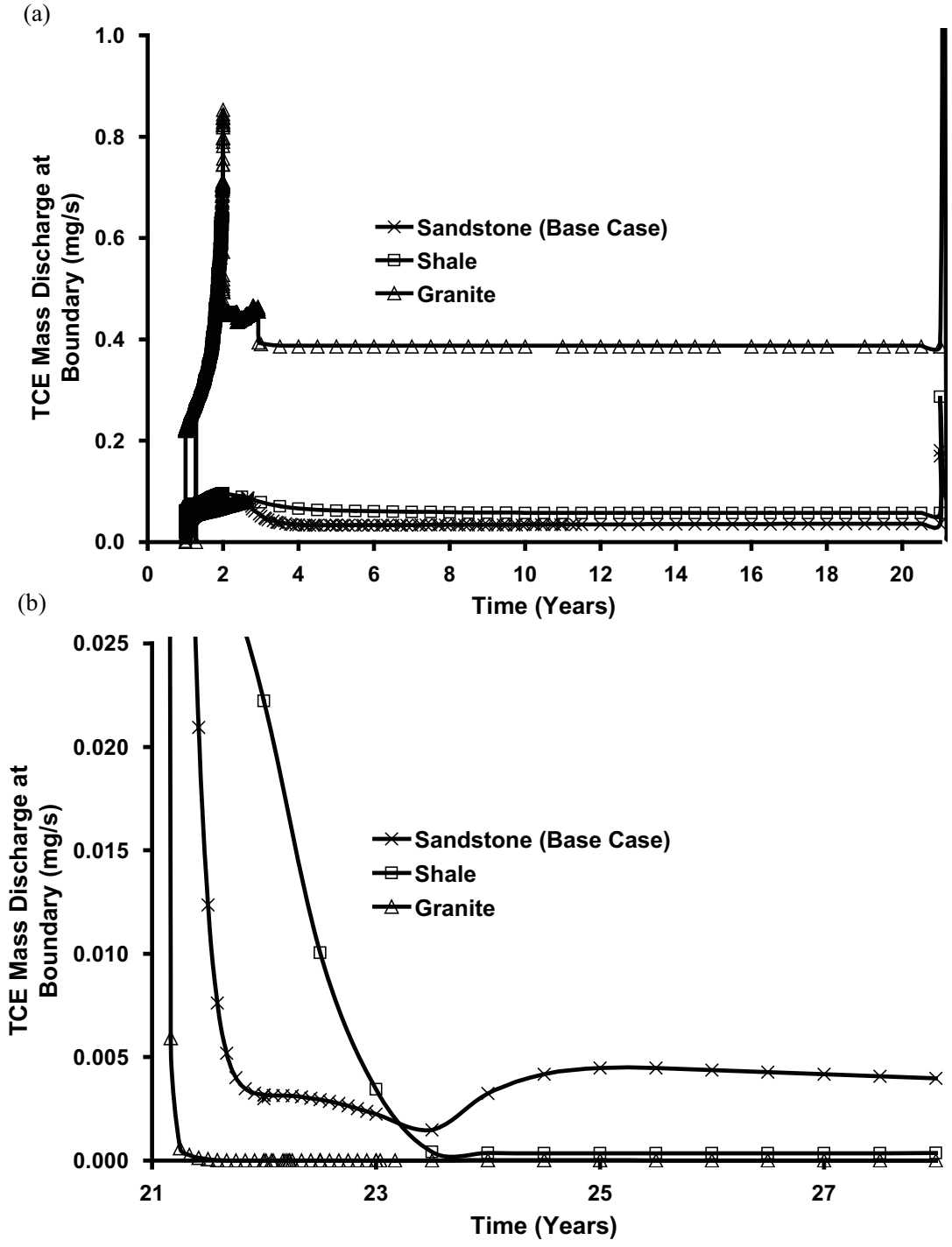

Figure 17: Comparison of total boundary mass discharge for different rock types; (a) from the beginning of the simulation to end of Site Ageing stage and (b) Treatment stage only (timescale expanded for clarity).

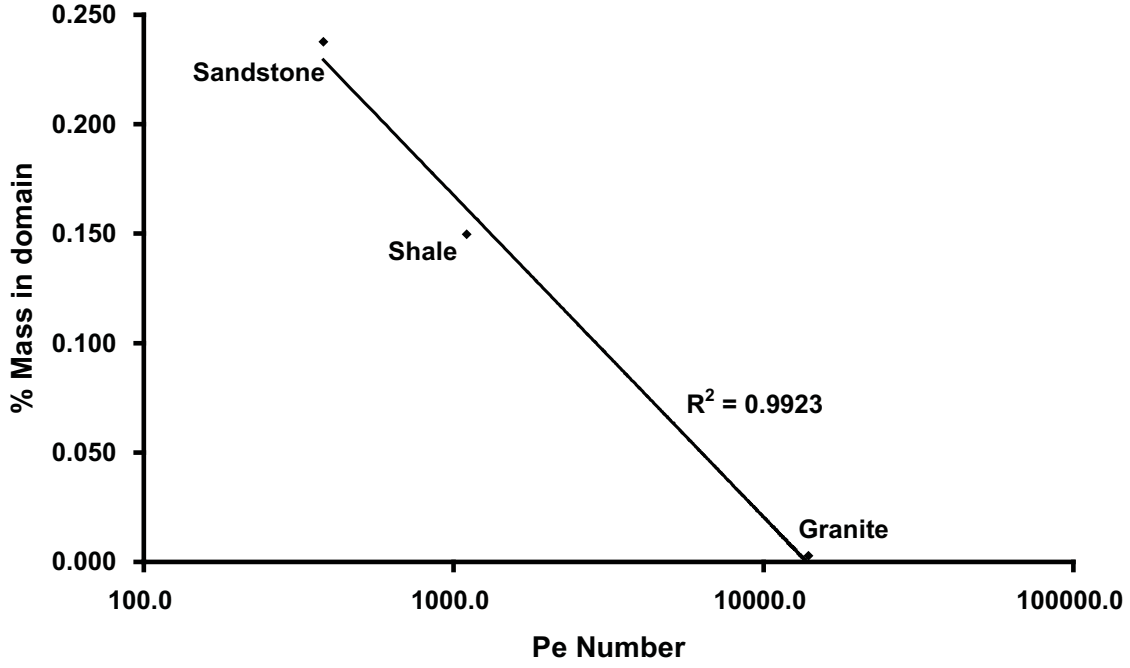

Figure 18: Mass of aqueous and sorbed TCE in various rock domains at end of Site Ageing stage (i.e., t_{TOTAL} = 21 years) vs. Peclet number (log scale) for each individual domain.

During the Treatment stage, 45.5 kg (382 moles), 59.6 kg (501 moles) and 538.8 kg (4531 moles) of MnO_4 were injected into the domain for sandstone, shale and granite respectively. The amount of MnO_4 injected is equivalent to 3.4 times, 4.5 times and 40.8 times greater than the theoretical MnO_4 mass required to destroy all the TCE in the domain at the start of the Treatment stage. The differences in MnO_4 mass injected are due the differences in bulk effective horizontal hydraulic conductivity while treatment period, injection concentration and hydraulic gradient were all held constant.

As demonstrated in Figure 19, the total moles of aqueous TCE destroyed is 5.94 moles, 17.7 moles and 2.26 moles for sandstone, shale and granite respectively. This mass destroyed is equivalent to 10.7%, 34.8% and 44.5%, respectively, of the initial mass

present in the respective domains prior to the Treatment stage. It is not surprising that the percentage of TCE mass destroyed increases as the depth of penetration of TCE into the matrix decreases, since the TCE is more available for reaction in the fractures than the matrix. In terms of efficiency, measured as the moles of TCE destroyed per moles of MnO_4 injected, the values for the sandstone, shale, and granite are 0.016, 0.035, and 0.0005, respectively. In all 3 rock types, the majority (specifically 69% – 91%) of the total mass destroyed was accomplished in the first 4 months of the two-year Treatment period. The change in slope (i.e., rate of mass destruction) indicates that the injected MnO_4 destroys the contaminant mass easily accessed, in the fracture and stored in the matrix immediately adjacent to the fractures, at early time but is less able to access the TCE mass deeper in the matrix in all rock types. It is noted that MnO_4 has a diffusion coefficient of the same order of magnitude as TCE and, since it is not subject to sorption (i.e., R=1), its diffusive flux into the matrix is approximately one (sandstone) to two (shale and granite) orders of magnitude greater than TCE.

Recall that diffusive flux is highest for the sandstone, decreased one order of magnitude for shale, and decreased two orders of magnitude for granite. This, in part, explains the poor loading of TCE into the matrix for granite (discussed above, Figures 16 and Figure A9, Supplementary Information) and the limited extent of TCE destruction (Figure 19). This also helps account for the observed differences between sandstone and shale in the Figure 19 despite the similar initial mass of TCE present in the domain (7.3 kg for sandstone and 6.8kg for shale) at the beginning of the Treatment period. It is noted that, in the case of shale, the end of TCE destruction after 1 year in Figure 19 suggests that this

is the length of time required for the MnO_4 to reach the limit of the TCE diffusion halo in the matrix, at least within the small portion of the domain that MnO_4 actually penetrated (this is confirmed by Figure A10 in Supplementary Information). Figure A11 (a) and (b) in Supplementary Information further demonstrates that after 1 year of MnO_4 injection, aqueous TCE concentration both within the matrix and fracture of the shale domain remained relatively constant over time. On the other hand, Figure A11 (c) (Supplementary Information) revealed MnO_2 continued to increase over time until the end of the Treatment stage (i.e., t_{TOTAL} = 23 years); this indicates that a majority of injected MnO_4 after the first year of Treatment was consumed by the organic carbon within the matrix. However, the same figures for sandstone (Figures 5 and 19) indicate that additional TCE would have been destroyed if the treatment period had been extended since the rate of mass destruction was still increasing and matrix contamination persisted.

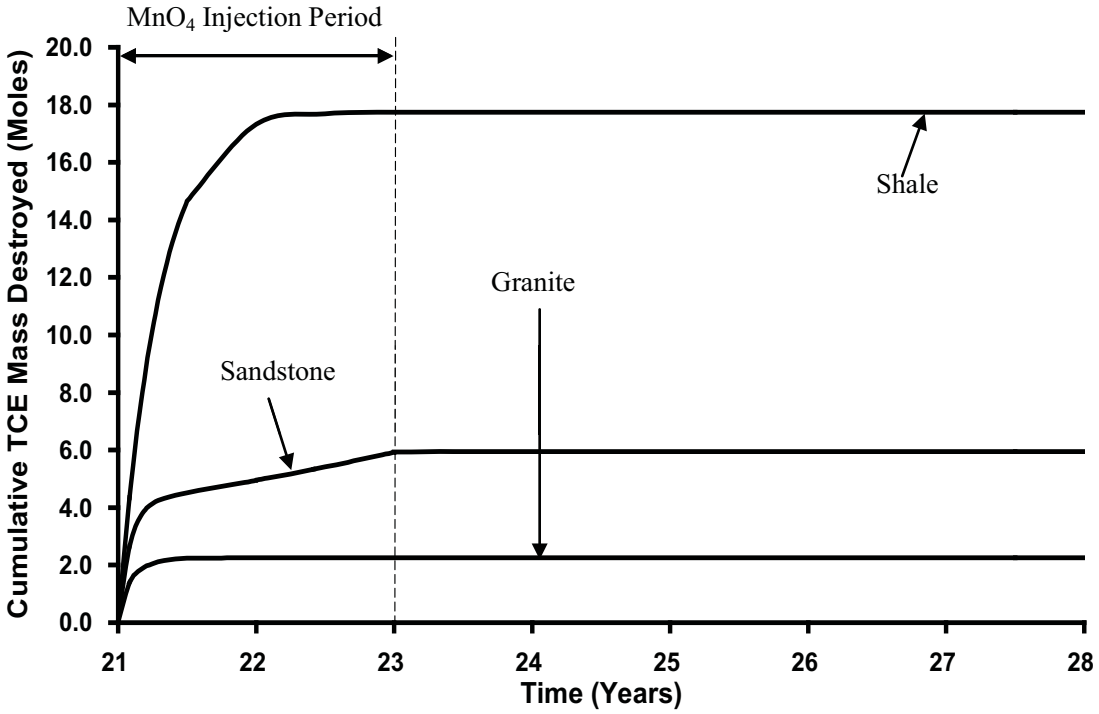

Figure 19: Cumulative mass of TCE destroyed for various rock types.

Sensitivity to DNAPL Type

In this study, results were compared between PCE and TCE; in contrast to the previous simulations, the distribution of DNAPL at the start of the Site Ageing stage was not identical. At the end of the DNAPL Infiltration stage, the average DNAPL saturation was 0.75 while the volume of DNAPL in the domain was 0.008 m^3 (compared to a total fracture volume of 0.012 m^3) with 100% of the nodes in drainage in both simulations. At the end of the DNAPL redistribution stage, the average DNAPL saturation was 0.3 for both TCE and PCE , the volume of DNAPL present was 0.0036 m^3 (5.26 kg) and 0.0037 m^3 (6.03 kg), and the pool to residual ratio was 71:29% and 51:49% for TCE and PCE, respectively (Figures 3 and A14 respectively). The higher density of PCE, leading to higher mobility and more DNAPL migration out of the bottom of the domain, is most likely the cause of the reduced pool-to-residual ratio in that case.

At the end of the Site Ageing stage (t_{TOTAL} = 21 years) the total mass of TCE and PCE in the domain was 7.3 kg (55.6 moles) and 3.3kg (20.2 moles) respectively (Table 5). As demonstrated by Figure 20, the PCE DNAPL was almost completely dissolved after 16 years of Site Ageing (t_{TOTAL} = 17 years), as compared to only 2.5 years for TCE (base case, Figure 8). One reason for this is the lower solubility of PCE (Table 4). Another reason is that the PCE DNAPL in the fractures caused reduced relative permeability to water; in conjunction with a fixed gradient, this caused reduced water flux through the source zone. Figure 21 confirms that identical boundary conditions resulted in considerably different time series of water discharge (m^3/s) at the exit boundary. Both simulations experience increasing water discharge as DNAPL dissolves until the

maximum is achieved when no DNAPL remains, but the rate of increase varies due to the difference in DNAPL dissolution rates. The reduced aqueous phase relative permeability in the fractures in the presence of PCE DNAPL resulted in reduced water velocities and, in turn, even further reduced aqueous PCE mass flux. Grant and Gerhard (2007b) comment upon this dynamic link between DNAPL saturation and water velocity and its impact on the evolution of source zones in unconsolidated porous media. Of the 3.3 kg (20.2 moles) PCE mass in the domain at the end of Site Ageing, more than 99.9% resided in the sandstone matrix, of which 98.7% was sorbed and only 1.3% remained in the aqueous phase.

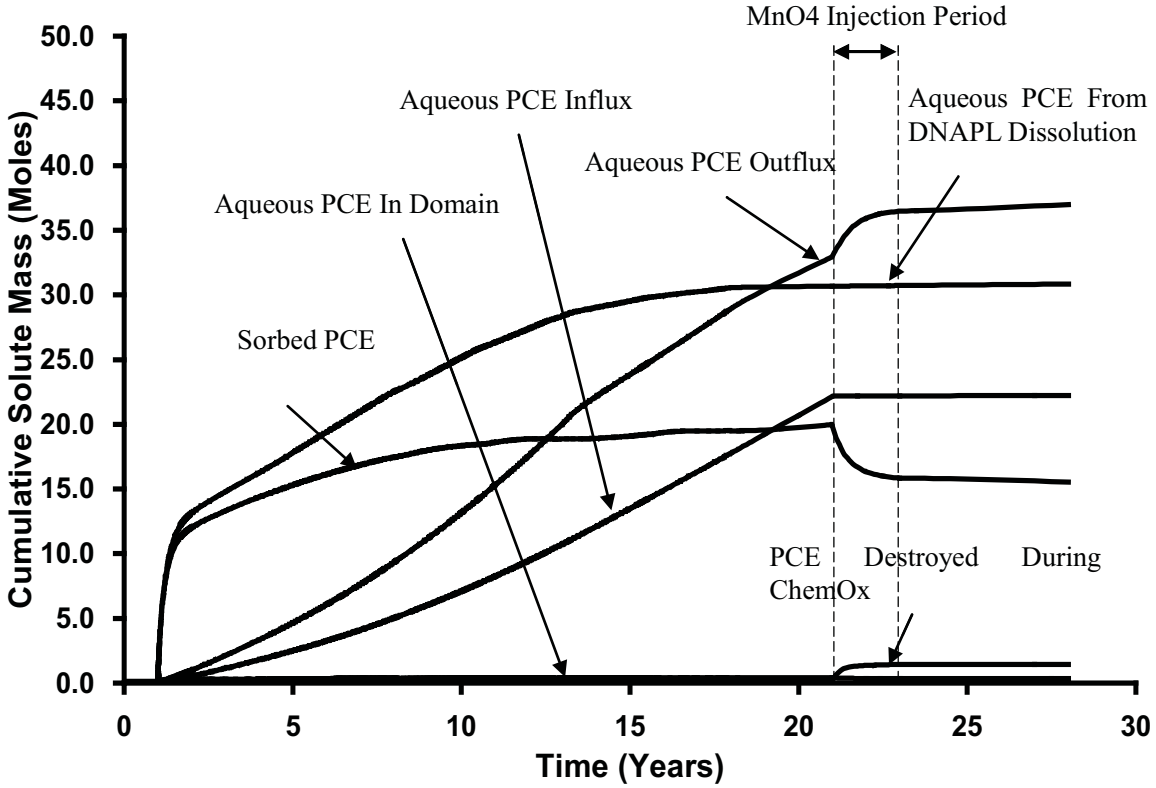

Figure 20: Cumulative aqueous and sorbed PCE from all sinks and sources for PCE Simulation.

The distribution of aqueous and sorbed PCE at the end of Site Ageing is shown in Figure A15, Supplementary Information, as compared to that for TCE at the same time (Figure 4). There are a number of reasons why the depth of matrix penetration for PCE is considerably less than TCE. First, the constant concentration of aqueous solvent provided at the upgradient boundary throughout the Site Ageing stage (50% solubility) was much lower for PCE (100mg/L) than TCE (550mg/L). In addition, the R and alpha value for PCE is 60 and 780, while for TCE is 21 and 270, this is because the Koc for PCE is approximately 3 times greater than TCE (Table 4). The effective diffusion rate for PCE is 1.88 x 10^{-10} m^2/s while for TCE it is 2.02 x 10^{-10} m^2/s. Therefore, the diffusion rate divided by the rock capacity factor for PCE is 2.4 x 10^{-13}, while for TCE it is 7.4 x 10^{-13}. For these reasons, although the initial volume of DNAPL was similar in both simulations, the mass present in the PCE domain at the end of the Site Ageing stage (3.3 kg) is much lower than the TCE domain (7.3 kg).

As demonstrated in Figure 22, although the total permanganate injected into the domain is similar in both simulations, the total mass destroyed by the injected permanganate is much lower for PCE (1.32 moles) than TCE (5.94 moles). As a fraction of the mass present, this represents 6.5% and 10.7% of the total mass destroyed for PCE and TCE, respectively. The changing rate of chlorinated solvent destruction (i.e., the decreasing slopes in Figure 22) is likely due to differences in the distribution of the contaminants in the matrix and the one order of magnitude lower reaction rate between MnO_4 and PCE versus MnO_4 and TCE (Table 4).

While it appears for the TCE case that it would have benefited from continued oxidant injection, the PCE case is clearly approaching an asymptotic limit within the two-year treatment period.

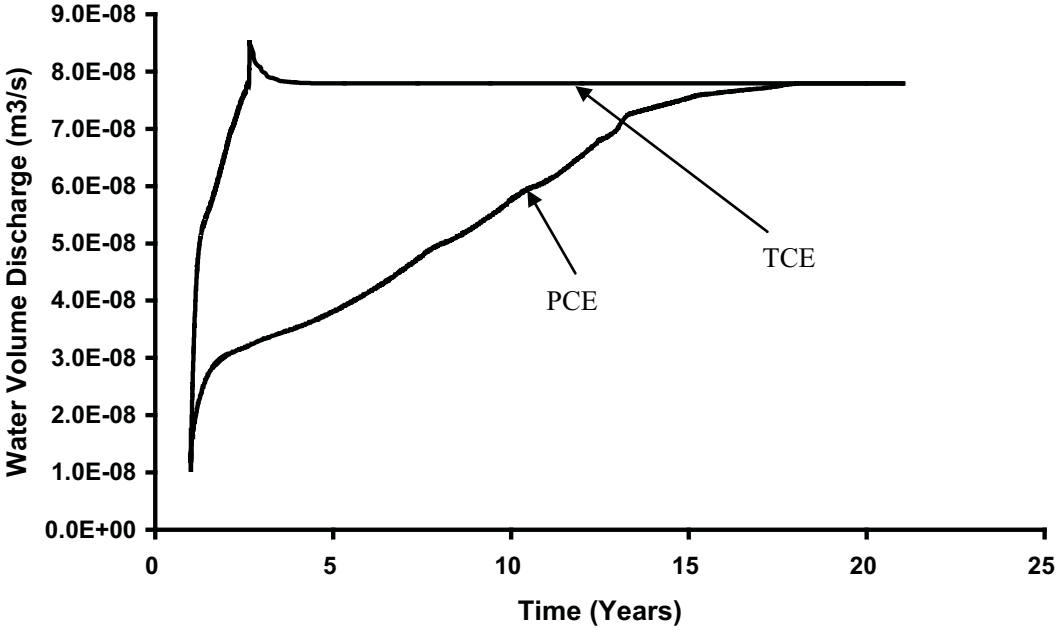

Figure 21: Downgradient water volume discharge for (i) TCE and (ii) PCE Simulations.

Figure 23 indicates the mass outflux at the boundary rebounds after the Treatment stage as a result of reverse diffusion. This rebound was observed to be much higher in the TCE than the PCE simulation (Table 5). This reflects that the same factors that promote increased forward diffusion in the TCE case (lower R, higher concentration gradients due to higher solubility) also result in increased reverse diffusion.

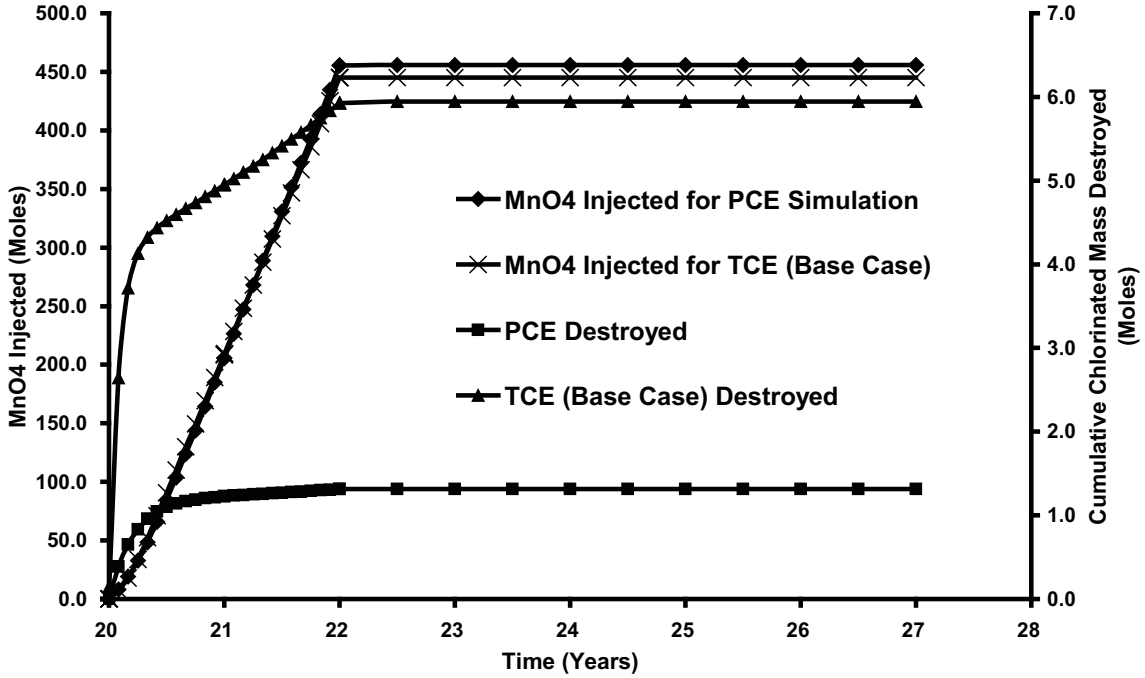

Figure 22: Cumulative mass of (i) contaminants mass destroyed (right axis) and (ii) MnO_4 injected.

(a)

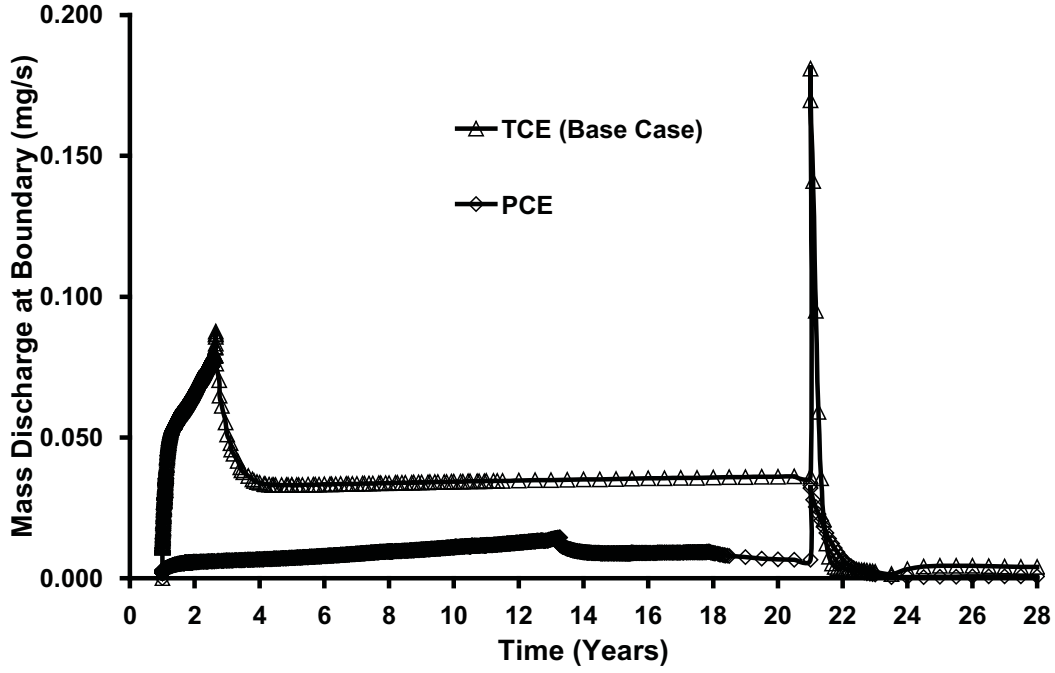

(b)

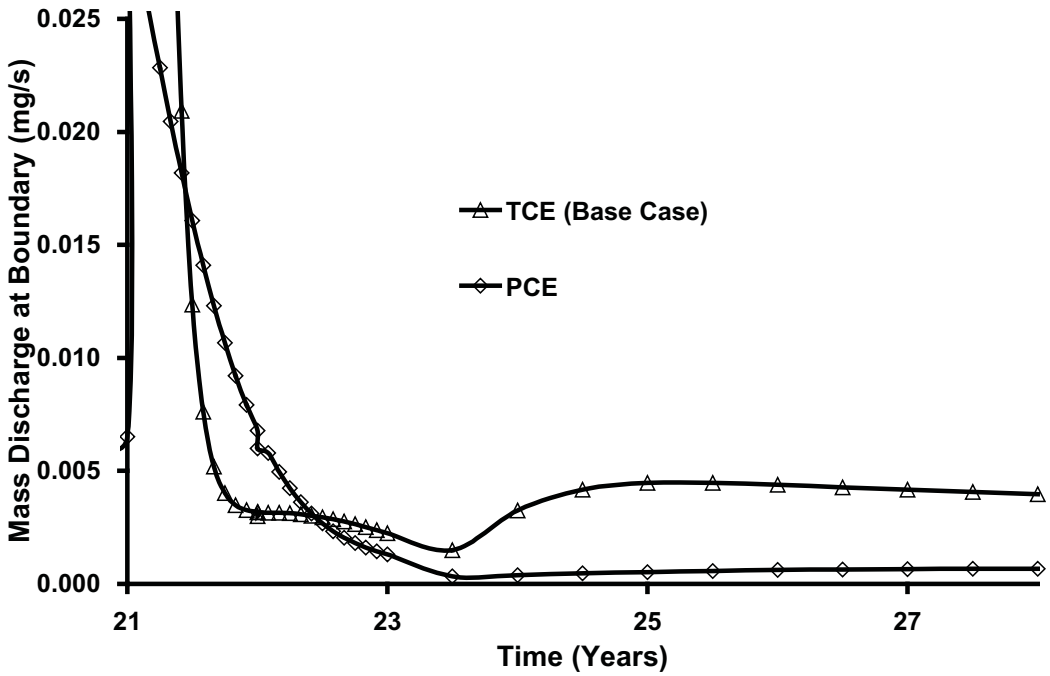

Figure 23: Comparison of total boundary mass discharge for (a) various DNAPL (b) Treatment stage only (timescale expanded for clarity).

5.0 CONCLUSIONS

In all of the cases considered here, after 20 years of Site Ageing, the majority (>97%) of the mass in the domain was sorbed to the matrix. The efficiency of oxidant provision was observed to be poor across the suite of scenarios, with greater than 90% of the injected MnO_4^- consumed by natural oxidant demand.

For scenarios in which diffusive flux is significant (e.g., sandstone/TCE simulations) substantial mass becomes stored in the matrix via forward diffusion. High diffusive flux is promoted by high matrix porosity, high diffusion coefficient, high aqueous solvent concentrations (i.e., high solubility), and low sorptive capacity (i.e., low Koc and/or low foc). The extent to which source zone mass is retained in the matrix was observed to be

inversely proportional to the logarithm of the mean peclet number of the horizontal fractures. Vertical fractures, contaminated by the downward vertical movement of DNAPL and its subsequent dissolution and diffusion, appear to be relatively unaffected by horizontally driven chemical oxidation.

In the high diffusive flux scenarios, permanganate injection appears to be relatively inefficient. Across all the sandstone simulations, the contaminant mass destroyed was never greater than 11% of the total mass present in the domain after injecting never less than 3 times the theoretical demand from TCE. Mass destruction, while highest at early time for the most accessible TCE, did continue at a significant rate throughout the injection period. The same factors that resulted in significant forward diffusion of TCE prior to treatment were observed to result in significant destruction (i.e., forward penetration of MnO_4 and TCE reverse diffusion during treatment, resulting in ongoing treatment of the matrix). Oxidant demand and rate of destruction exceeded supply in all sandstone cases, causing virtually no treatment to occur when injection was not active.

Additionally, in these high diffusive flux scenarios, and for the same reasons, reverse diffusion was significant after treatment ceased. It is not possible in this work to quantify the reduction in mass discharge or concentration rebound associated directly with treatment in the domain due to the upgradient mass flux of contaminant coincidentally terminated at the end of the Site Ageing stage. Chemical oxidation clearly suppressed mass discharge and exit concentrations during active treatment in sandstone. However, following treatment the mass discharge and downgradient

concentrations quickly rebounded to reveal no significant difference relative to a No ISCO case.

Higher mass destruction ratios were observed in the shale and granite scenarios, with TCE mass reduced during treatment 35% and 45%, respectively. However, these scenarios did not exhibit more efficient use of the injected oxidant. Rather, high large scale peclet numbers associated with these rock types were found to correspond to significantly reduced TCE forward diffusion, thereby concentrating the TCE near the fractures and increasing access of the oxidant.

The total mass of PCE destroyed via the injected permanganate was found to be 6.5% of the total mass present in the domain at the start of the Treatment stage. This difference in mass destroyed from the base case (i.e., 10.7%), is mainly due to differences in the distribution of the contaminants in the matrix and the one order of magnitude lower reaction rate between MnO_4 and PCE versus MnO_4 and TCE. The rebound of mass discharge at the boundary after the Treatment stage was observed to be higher in the TCE than in the PCE simulation. The same factors that limit forward diffusion for PCE relative to TCE (increased sorption, reduced concentration gradients) also result in reduced reverse diffusion, resulting in much lower PCE concentration rebound and long term mass discharge at the boundary.

For the sandstone base case investigated, all of the metrics examined proved insensitive to the injection strategy (varied concentration or pulsed injection). Because oxidant

demand and destruction rate always exceeded supply, the only relevant parameter was the total mass of MnO_4 injected. Extrapolating forward, it is estimated that approximately 678 total kg of MnO_4 (15 times the current mass injected) would have been required to destroy the 7.3 kg of TCE present in the domain. In the PCE, shale, and granite cases, no such 'complete treatment' calculation is possible since all observed sharp declines in the rate of destruction after the first 4 months of treatment, indicating that the diffusive flux limitations in these cases were a significant barrier to further clean-up. In all cases, the short duration of the treatment relative to the long duration of site ageing was an impediment to effectively changing the mass discharge in the long term.

It is acknowledged that numerous assumptions and simplifications were employed in this work. In the majority of circumstances, the assumptions were chosen to present a 'best case' scenario that favours effective treatment (e.g., no rind formation, constant injection concentration with elevated gradient, two-dimensional flow with little opportunity for bypassing, etc.). This approach underscores the challenges associated with effectively treating aged source zones in fractured rock with ISCO. The limited number of simulations conducted using specific site templates on a small field scale implies that these results cannot be directly extended to a wide variety of complex real sites. Nevertheless, it is expected that the diffusive flux limitations and OAM demand inefficiencies impeding effective treatment observed here are likely widely applicable to chlorinated solvent-impacted fractured rock scenarios.

6.0 SUPPLEMENTARY INFORMATION

Table A1: Summary of Different Rock Properties for Sandstone, Shale and Granite

Parameters	Sandstone	Shale	Granite
Porosity (%)	2.2 – 49.0 [a]	1.0 – 47.0 [h]	0.5 – 7.2 [o]
Matrix Permeability (m^2)	$2 \times 10^{-13} – 9 \times 10^{-15}$ [b]	$1 \times 10^{-17} – 1 \times 10^{-21}$ [i]	$9 \times 10^{-16} – 2 \times 10^{-21}$ [p]
Foc (-)	0.0002 – 0.01 [c]	0.005 – 0.006 [j]	-
Bulk Density (g/cm^3)	2.06 – 2.64 [d]	1.34 – 2.33 [k]	2.63 – 2.69 [q]
Fracture Apertures (μm)	10 – 100000 [e]	30 – 102 [l]	448 – 748 [r]
Fracture Spacing (m)	0.01 – 10.0 [f]	2.0 – 200.0 [m]	0.98 – 2.80 [s]
Matrix Tortuosity (-)	0.2 – 1.6 [g]	0.37 – 0.45 [n]	1.29 – 1.43 [t]

[a] *Lipson et al., 2005; Morris and Johnson, 1967; Baraka-Lokmane, 2002; Hitchmough et al., 2007; Lima and Niwas 2000; Mohnke and Yaramanci, 2008; Dutton and Loucks, 2010; Gooddy et al., 2002; Bloomfield et al., 2001; Pape et al., 2006.*
[b] *Dana and Skoczylas, 2002; Wulff et al., 2000.*
[c] *Lipson et al., 2005; Gooddy, unplublished data.*
[d] *Lipson et al., 2005; Dana and Skoczylas, 2002.*
[e] *Hitchmough et al., 2007; Lipson et al., 2005; Allen et al., 1998.*
[f] *Hitchmough et al., 2007; Lipson et al., 2005; Allen et al., 1998.*
[g] *Hitchmough et al., 2007; Lipson et al., 2005.*
[h] *Gutierrez et al. 2000; Morris and Johnson, 1967; Busch et al., 2008; Cumbie and McKay, 1999; Gwo et al., 2007; Jardine et al., 1999; Silva et al., 2008.*
[i] *Gutierrez et al. 2000; Garavito et al. 2006.*
[j] *Busch et al., 2008; Jardine et al., 1989.*
[k] *Busch et al., 2008; Cumbie and McKay, 1999; Gwo et al., 2007.*
[l] *Jardine et al., 2002; Jardine et al., 1999; Cumbie and McKay, 1999.*
[m] *Jardine et al., 1999; Jardine et al., 2002.*
[n] *Busch et al., 2008; Gwo et al., 2007; Jardine et al., 2002.*
[o] *Chaki et al., 2008; Hu and Mori, 2008; Vasconcelos et al., 2008; Schild et al., 2001.*
[p] *Chaki et al., 2008; Sausse et al., 2006; Vilks et al., 2003.*
[q] *Sausse et al., 2006; Chaki et al., 2008.*
[r] *Sausse 2002.*
[s] *Sousa 2007.*
[t] *Vilks et al., 2003.*

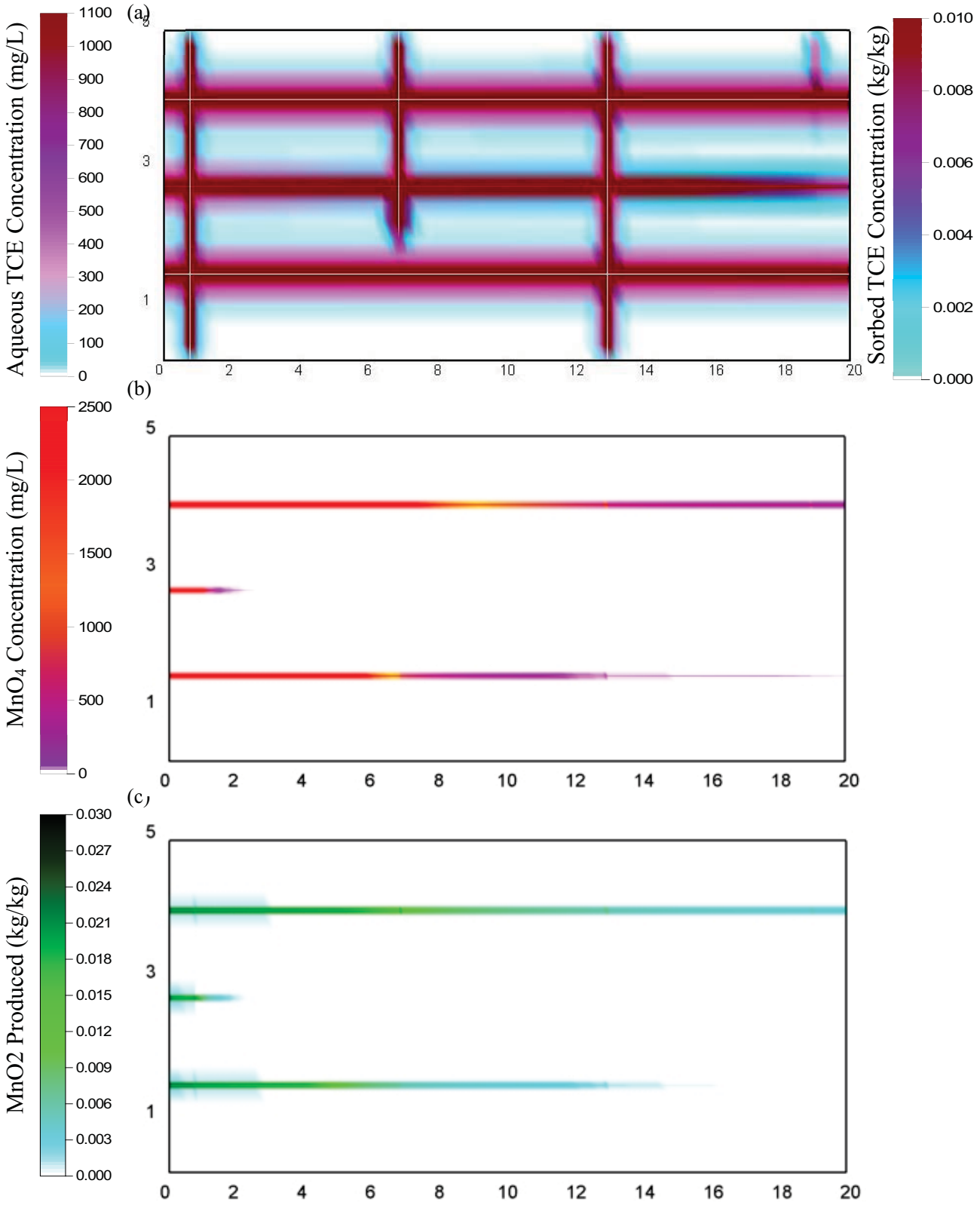

Figure A1: Distribution of aqueous species concentrations at t_{TOTAL} =23 years for 5000 mg/L of MnO4 Simulation, after 2 years of chemical oxidation (i.e., Treatment stage): (a) TCE, (b) MnO_4, (c) MnO_2

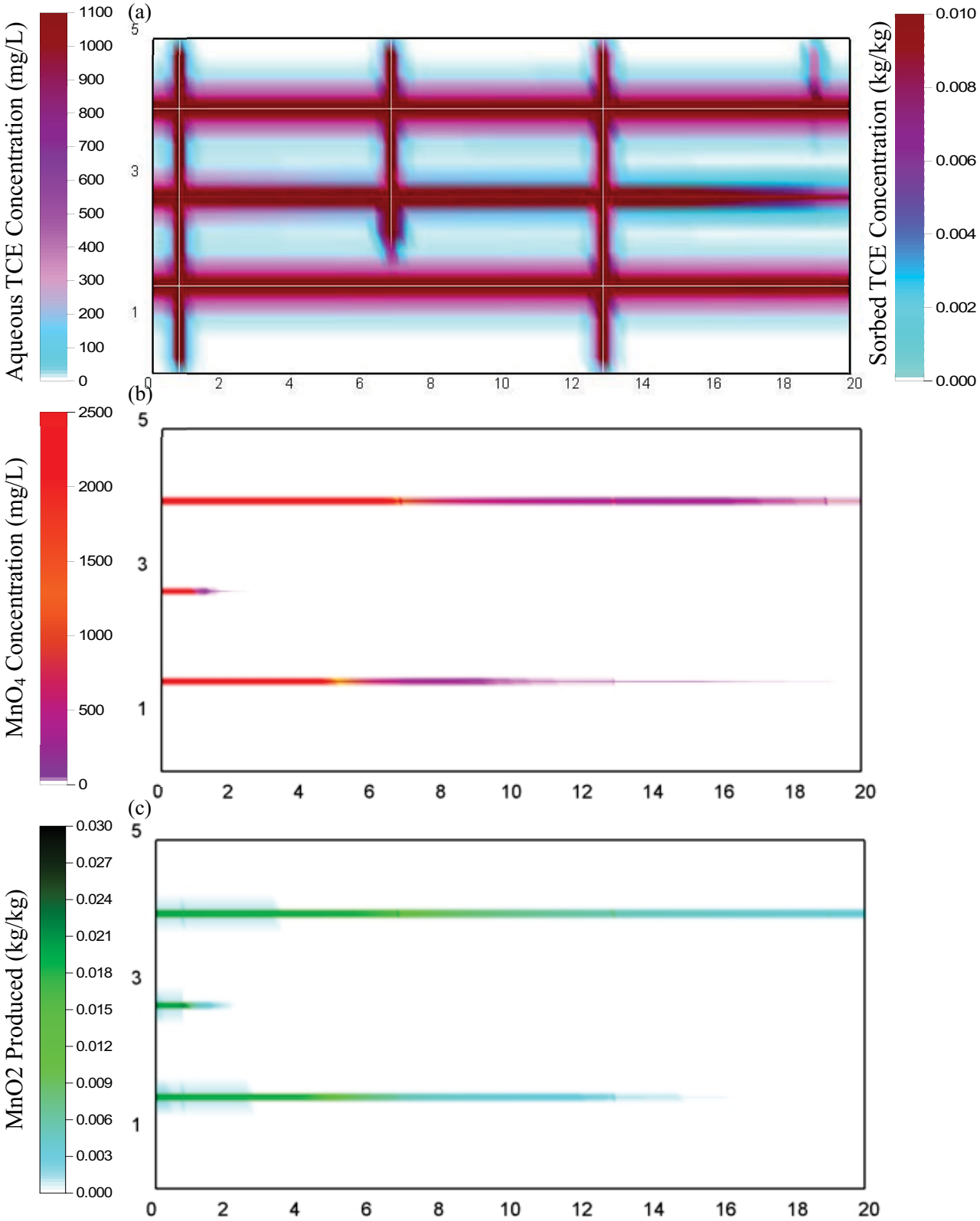

Figure A2: Distribution of aqueous species concentrations at t_{TOTAL} =23 years for 1250 mg/L of MnO4 Simulation, after 2 years of chemical oxidation (i.e., Treatment stage): (a) TCE, (b) MnO_4, (c) MnO_2

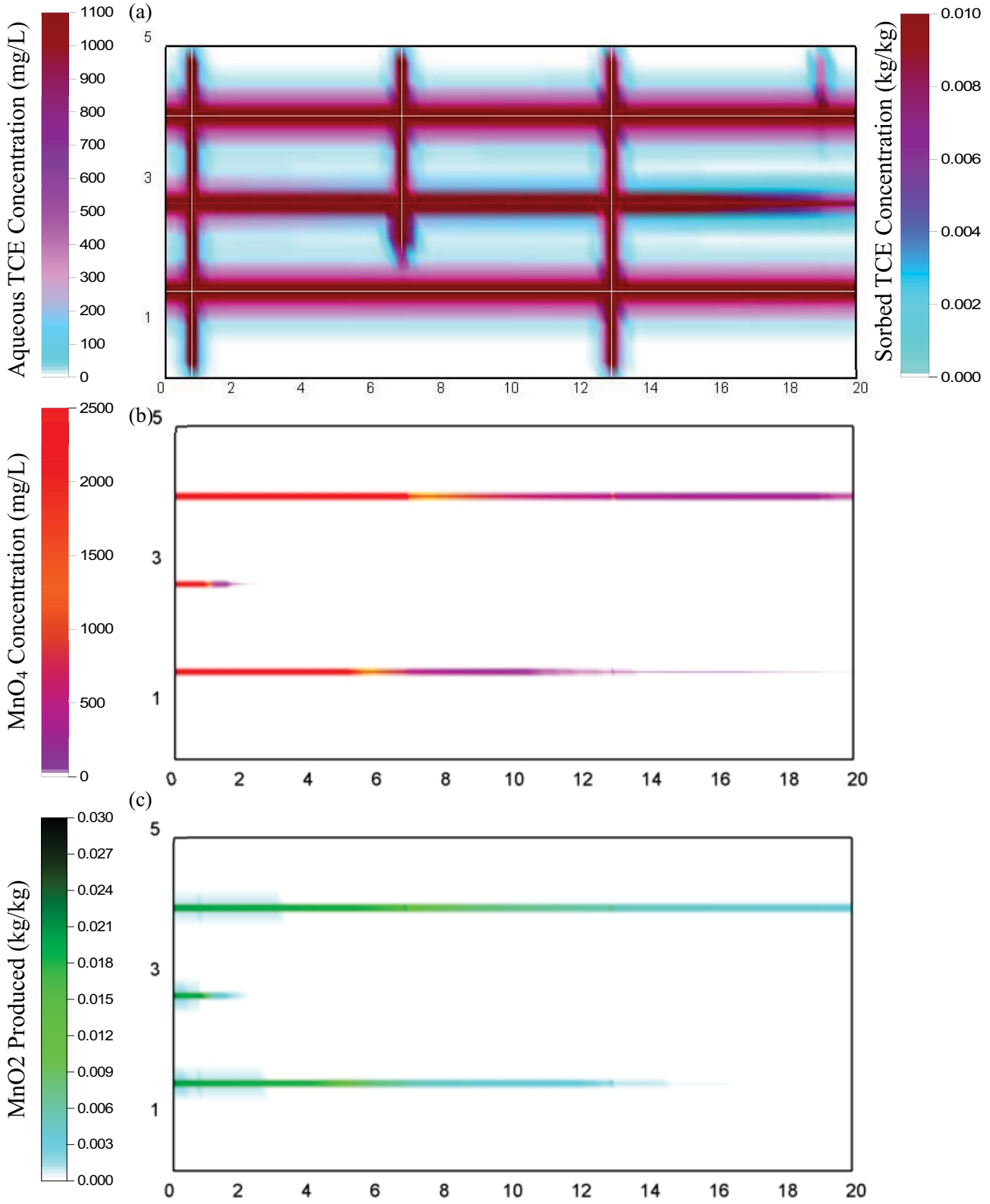

Figure A3: Distribution of aqueous species concentrations at t_{TOTAL} =23 years for 3 Months Pulsing Simulation, after 2 years of chemical oxidation, aging period: (a) TCE, (b) MnO_4, (c) MnO_2

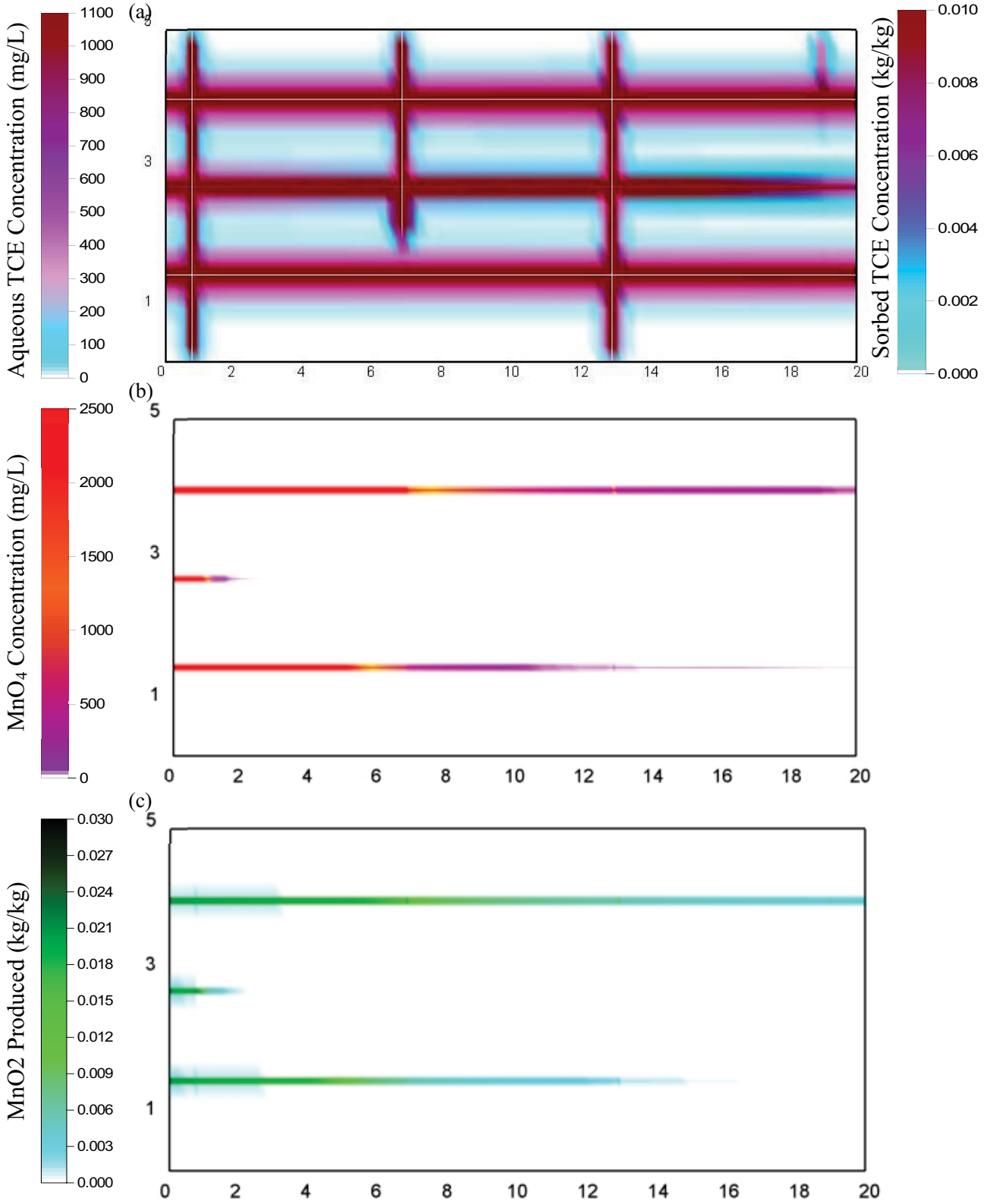

Figure A4: Distribution of aqueous species concentrations at t_{TOTAL} =23 years for 6 Months Pulsing Simulation, after 2 years of chemical oxidation, aging period: (a) TCE, (b) MnO_4, (c) MnO_2

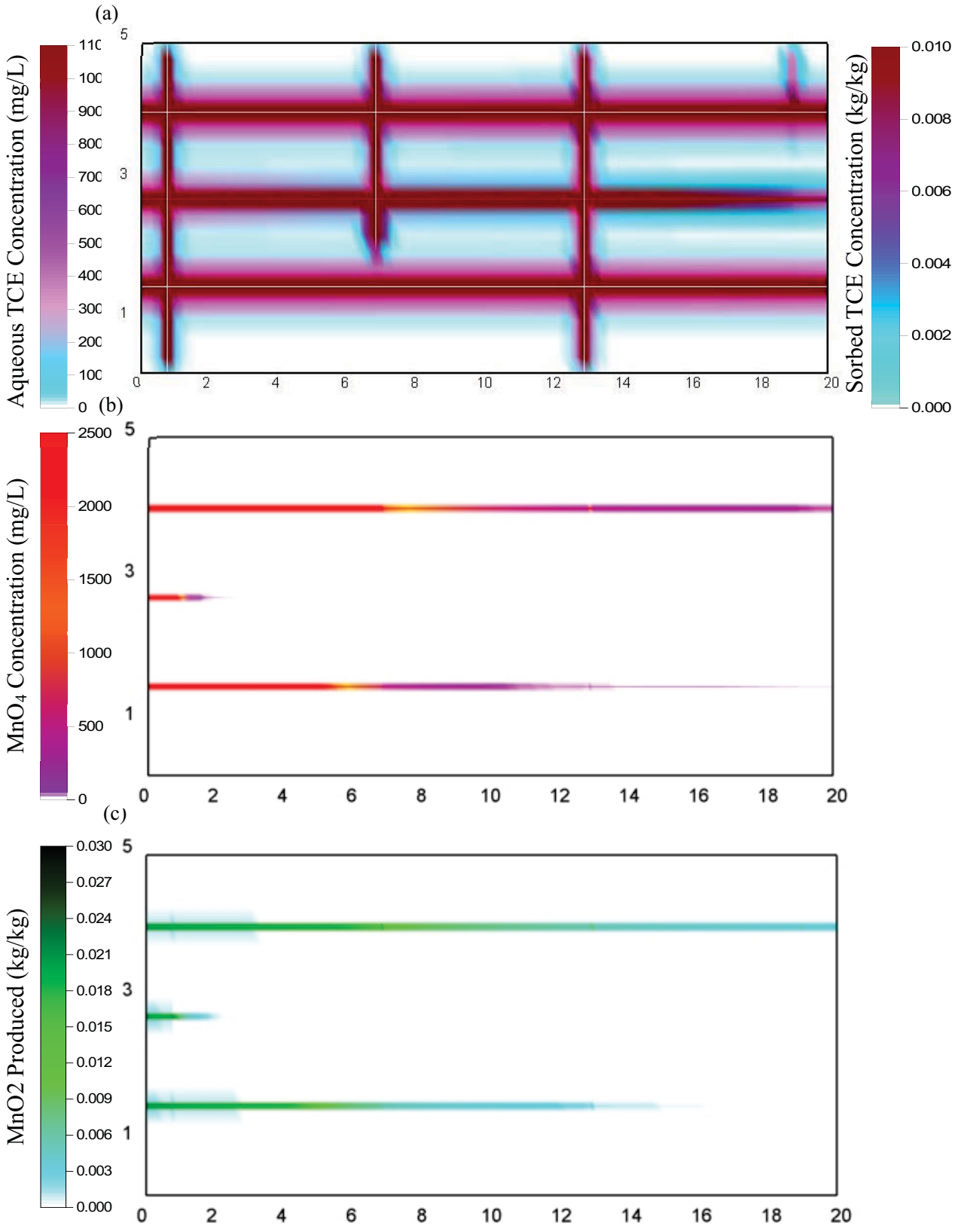

Figure A5: Distribution of aqueous species concentrations at t_{TOTAL} =23 years for 1 Year Pulsing Simulation, after 2 years of chemical oxidation, aging period: (a) TCE, (b) MnO_4, (c) MnO_2

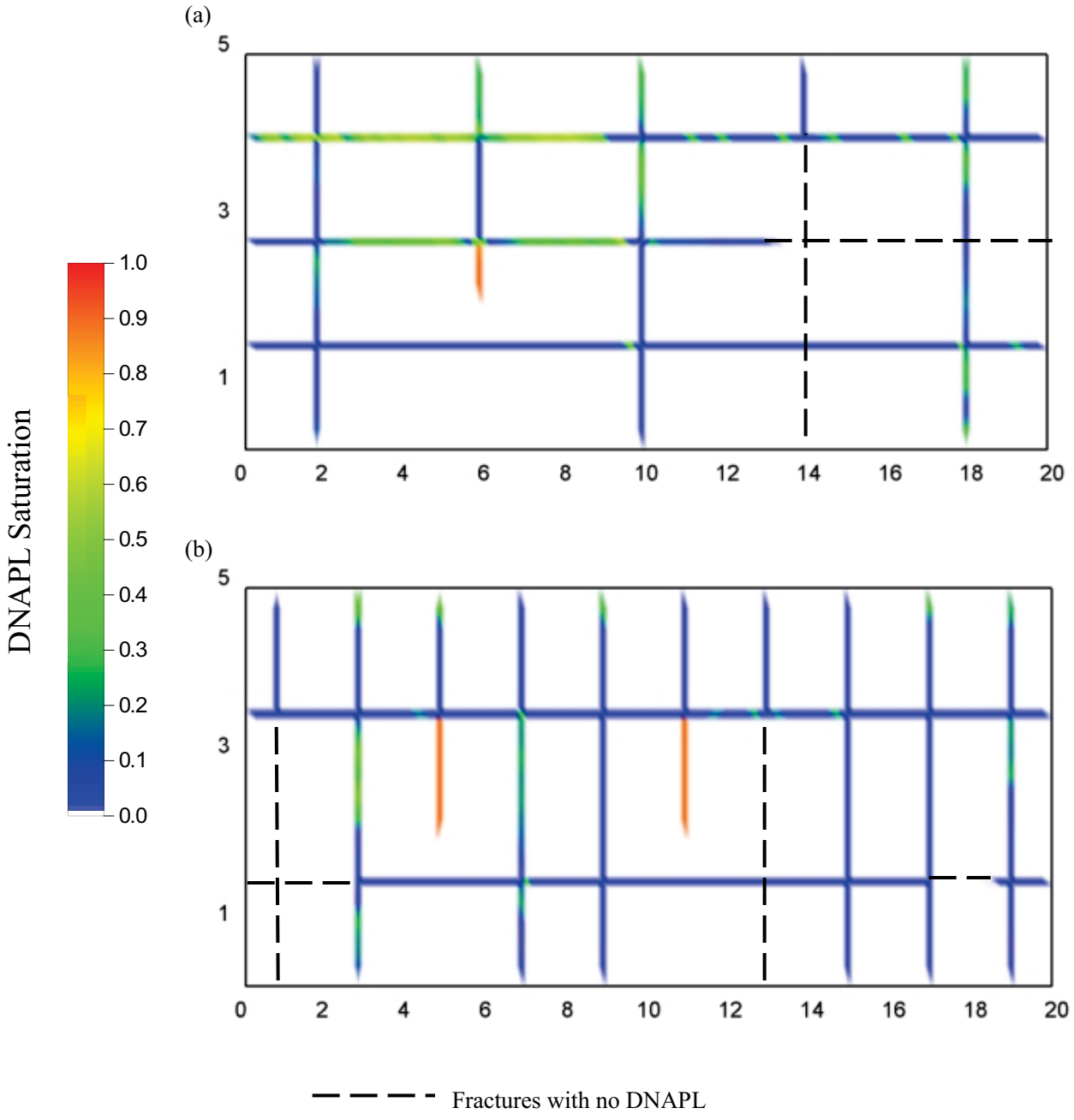

Figure A6: DNAPL distribution for (a) Shale and (b) Granite at t_{TOTAL} = 1 year when all DNAPL migration has ceased.

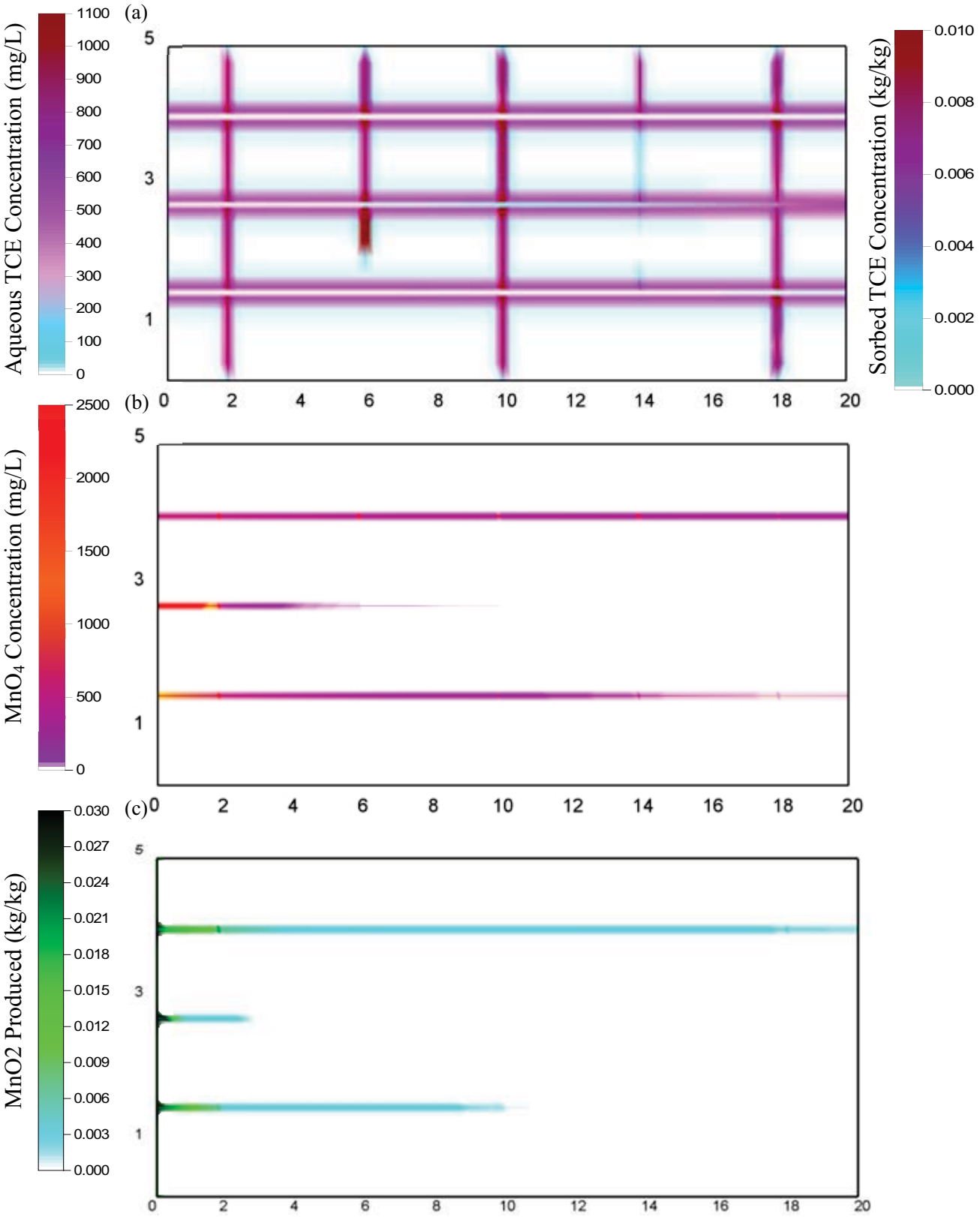

Figure A7: Distribution of aqueous species concentrations at t_{TOTAL} =23 years for Shale, after 2 years of chemical oxidation, aging period: (a) TCE, (b) MnO_4, (c) MnO_2

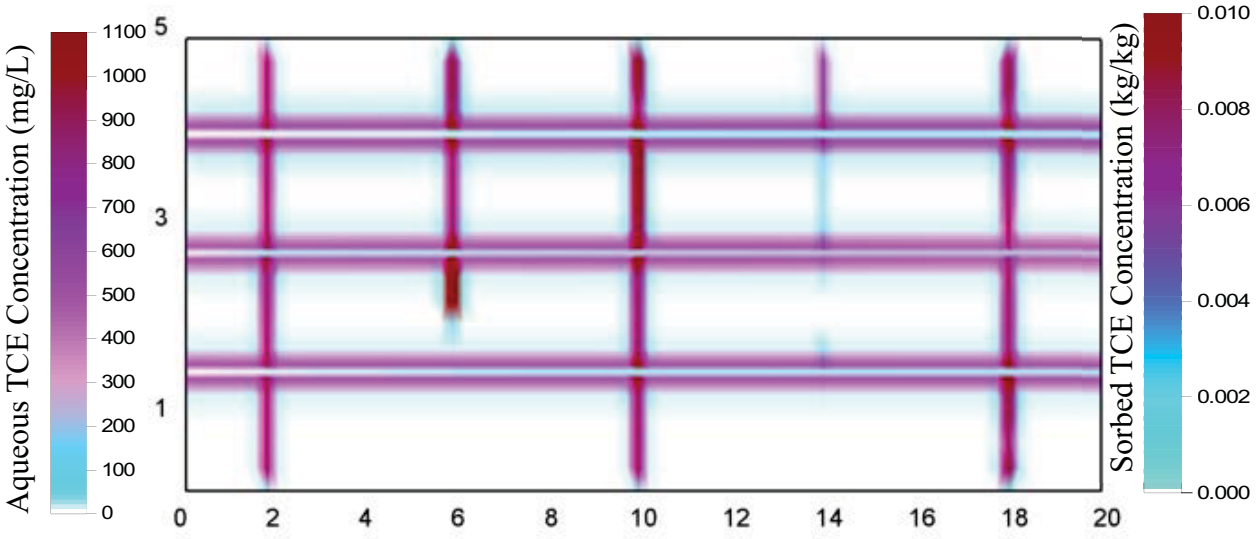

Figure A8: Distribution of aqueous TCE concentrations at t_{TOTAL} =28 years for Shale, 5 years after chemical oxidation

(a)

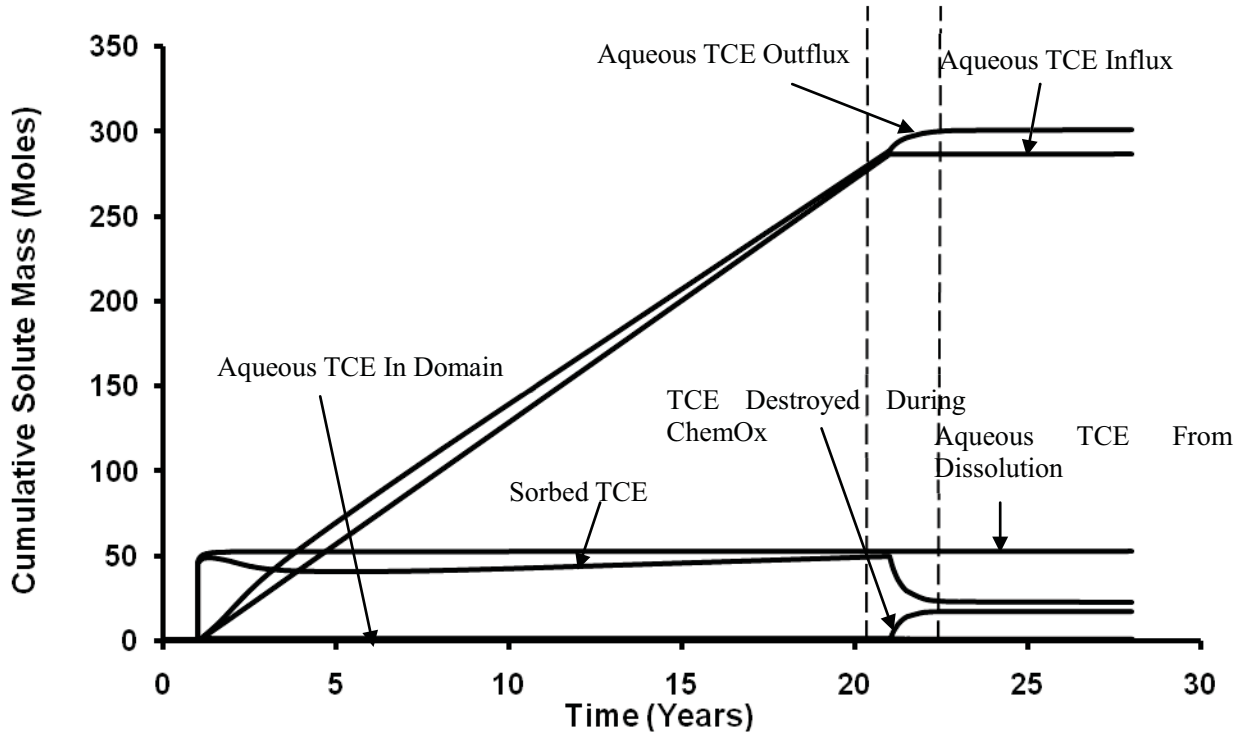

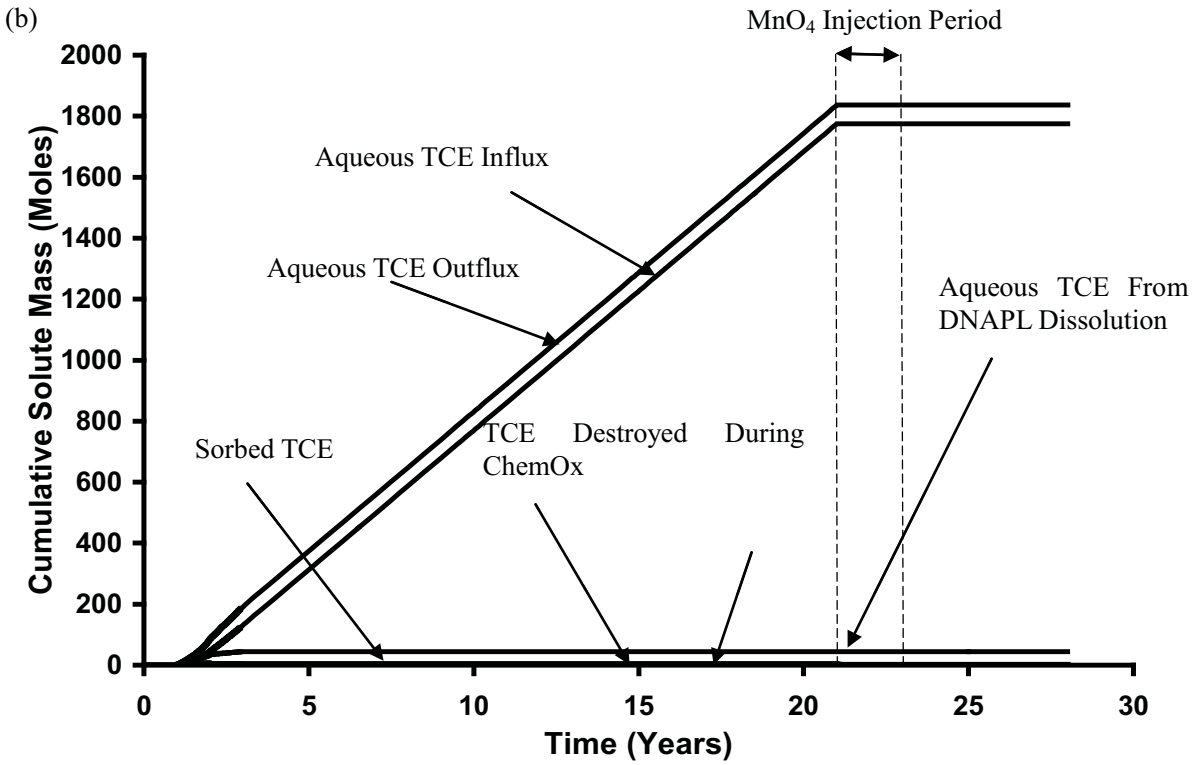

Figure A9: Cumulative aqueous and sorbed TCE from all sinks and sources for (a) Shale Simulation and (b) Granite Simulation.

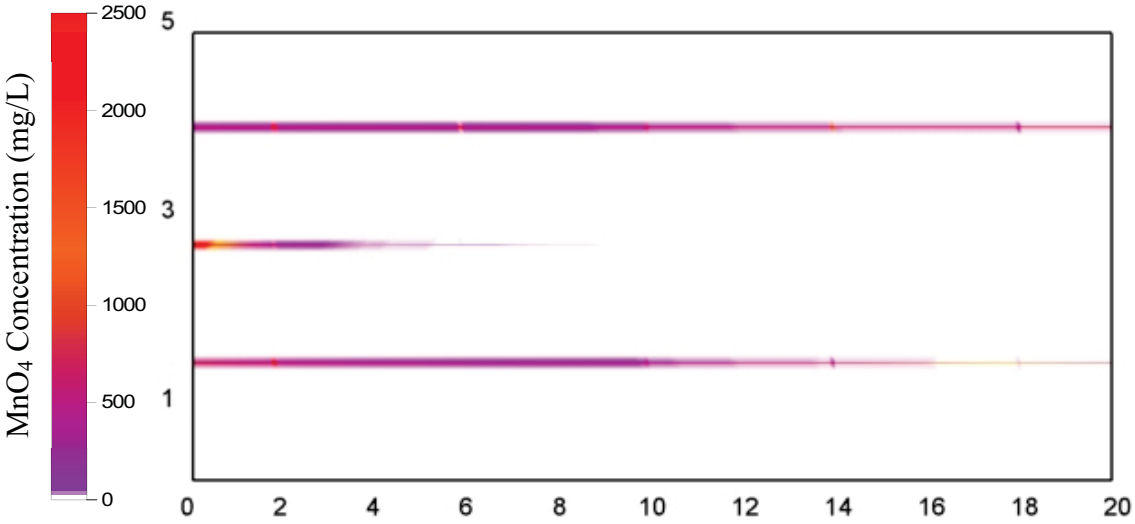

Figure A10: Distribution of MnO4 concentrations at t_{TOTAL} =22 years for Shale, 1 years after chemical oxidation

(a)

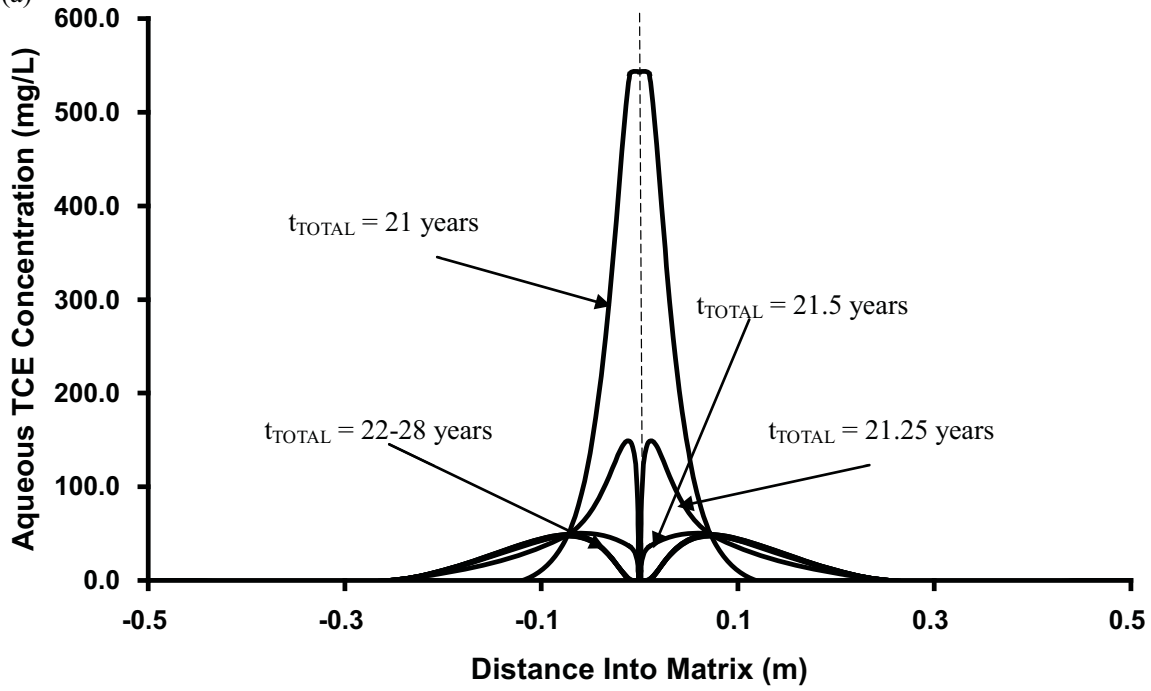
600.0
500.0
400.0
300.0
200.0
100.0
0.0
Aqueous TCE Concentration (mg/L)
-0.5
-0.3
-0.1
0.1
0.3
0.5
Distance Into Matrix (m)
t_{TOTAL} = 21 years
t_{TOTAL} = 21.5 years
t_{TOTAL} = 22-28 years
t_{TOTAL} = 21.25 years

(b)

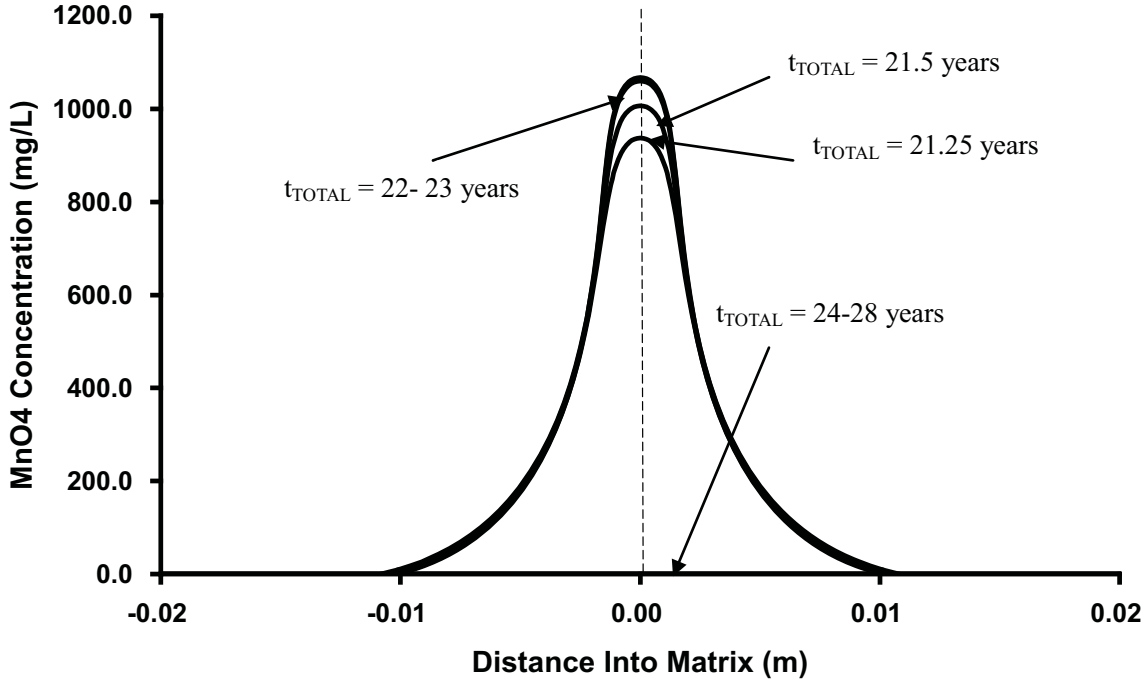
1200.0
1000.0
800.0
600.0
400.0
200.0
0.0
MnO4 Concentration (mg/L)
-0.02
-0.01
0.00
0.01
0.02
Distance Into Matrix (m)
t_{TOTAL} = 21.5 years
t_{TOTAL} = 21.25 years
t_{TOTAL} = 22- 23 years
t_{TOTAL} = 24-28 years

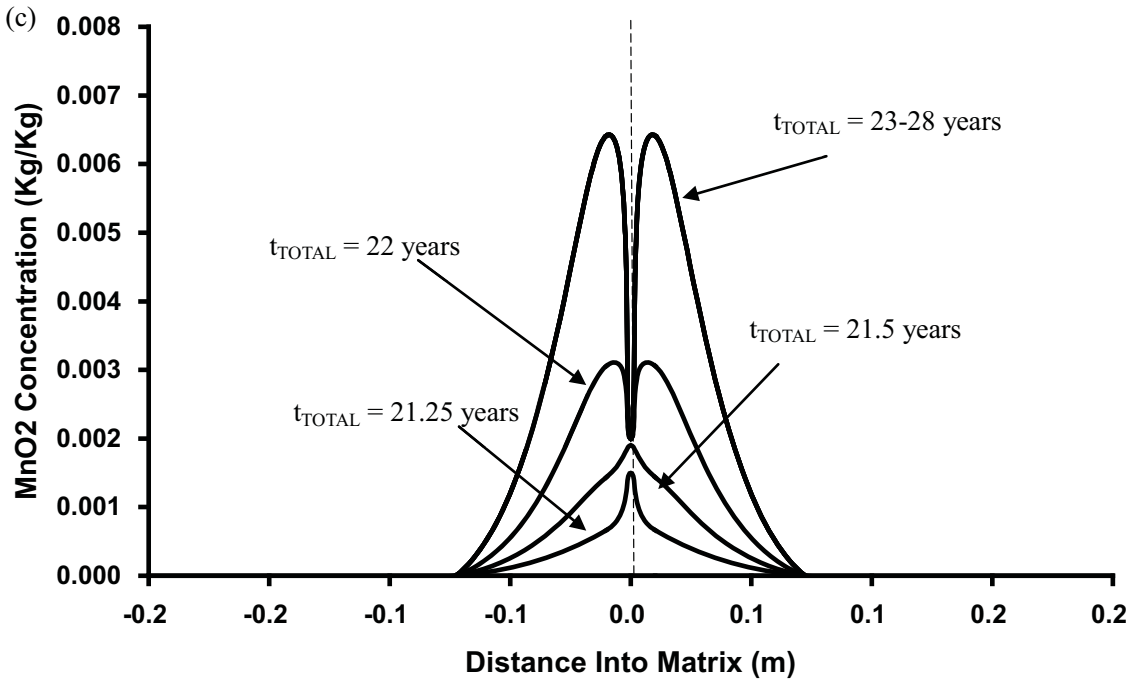

Figure A11: Concentration profile of (a) aqueous TCE; (b) MnO_4 and (c) MnO_2across a single fracture for the Base Case. Shown is a 1.0 m cross-section across a horizontal fracture (dotted line denotes location of the facture).

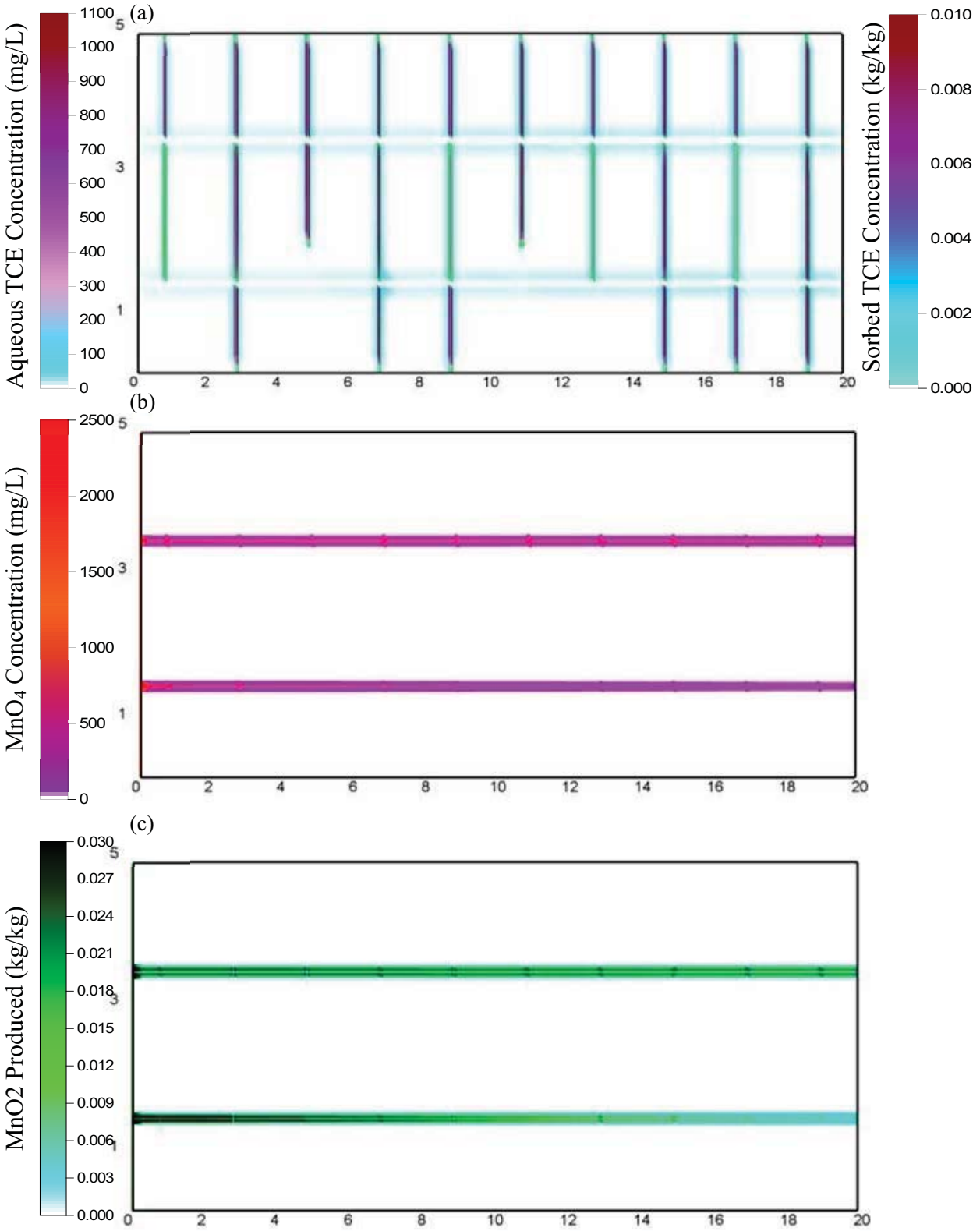

Figure A12: Distribution of aqueous species concentrations at t_{TOTAL} =23 years for Granite, after 2 years of chemical oxidation, aging period: (a) TCE, (b) MnO_4, (c) MnO_2

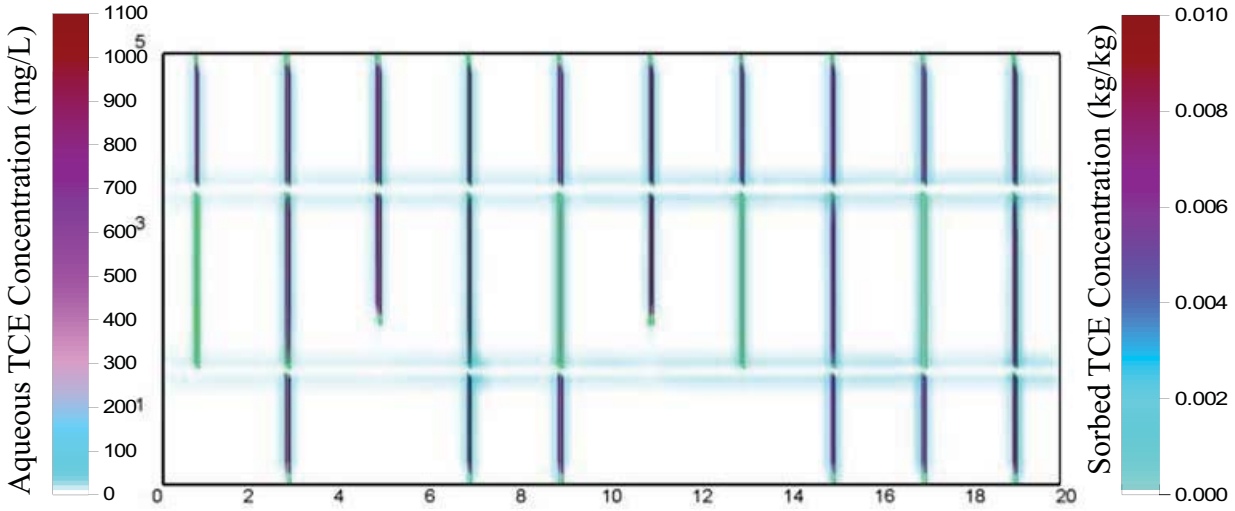

Figure A13: Distribution of aqueous TCE concentrations at t_{TOTAL} =28 years for Granite, 5 years after chemical oxidation

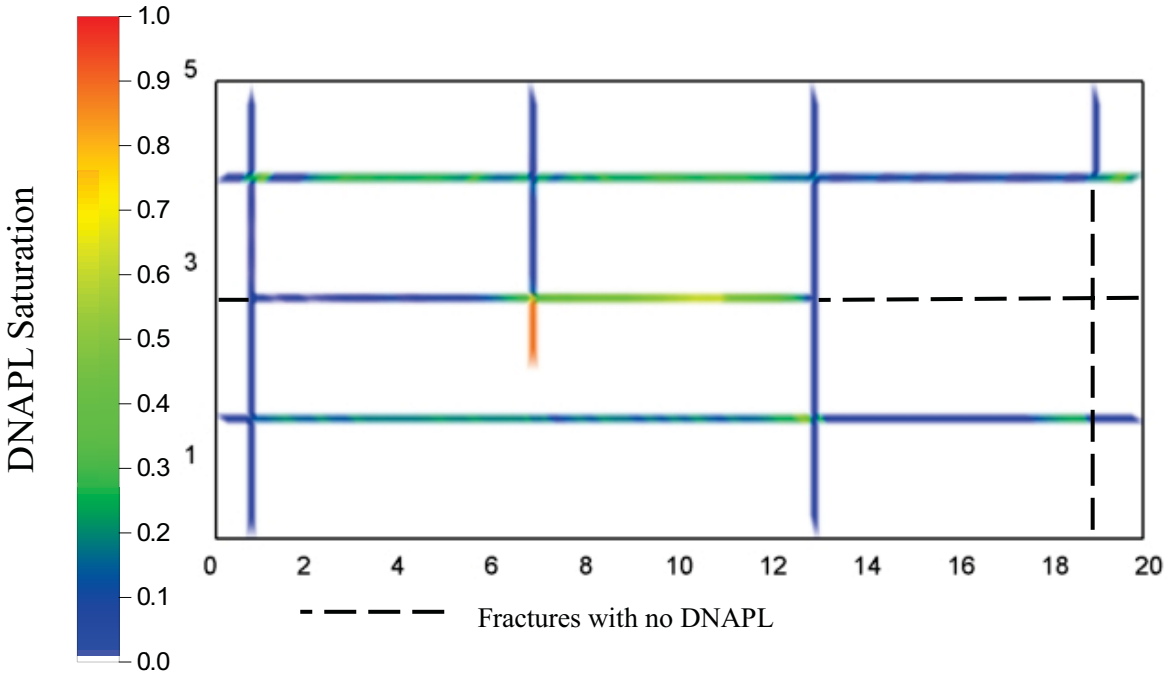

Figure A14: DNAPL distribution for PCE Simulation at t_{TOTAL} = 1 year when all DNAPL migration has ceased.

Figure 3.8: Verification of Langmuir sorption

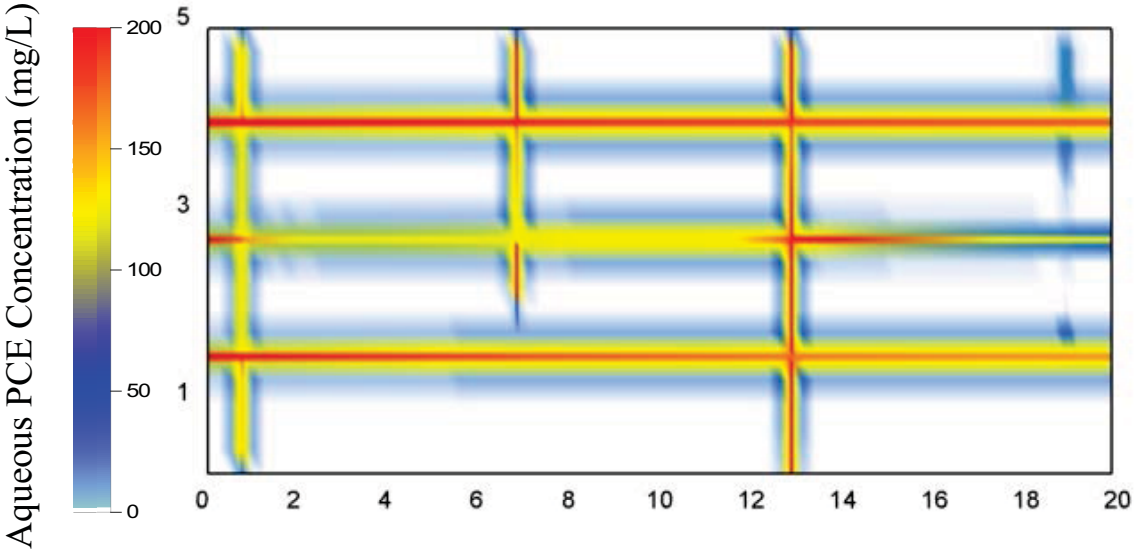

Figure A15: Distribution of aqueous PCE after 20 years of site aging (i.e., t_{TOTAL} = 21 years) for PCE simulation.

APPENDIX D.4

NUMERICAL SIMULATION OF DNAPL SOURCE ZONE REMEDIATION WITH ENHANCED IN SITU BIOREMEDIATION (EISB): FRACTURED ROCK

ABSTRACT

Numerical simulations were conducted to investigate the benefits and challenges of enhanced *in situ* bioremediation (EISB) (with lactate) for trichloroethylene (TCE) and tetrachloroethylene (PCE) DNAPL in fractured rock aquifers at the field scale. An established finite difference multiphase flow-transport-reaction simulator was employed with a gridding routine. Simulations were conducted in two-dimensional cross-section with fracture apertures constant within fractures but varying across the source zone. In each of the 13 simulations conducted, a DNAPL release stage was followed by a 20-year site ageing stage prior to simulating an EISB treatment stage followed by a 5-year post-treatment stage. The suite of simulations examined (i) lactate injection concentration, (ii) pulsed-injection strategy, (iii) bedrock type (sandstone, shale, and granite), and (iv) DNAPL type (TCE and PCE).

The effectiveness of EISB was observed to vary widely across the suite of scenarios. A critical factor was the assumed spatial distribution of the microbial consortium; the TCE mass fraction reduced to ethene decreasing from 74% (microbes assumed to be in the fractures and matrix) to 0.006% (microbes assumed in the fractures only). EISB effectiveness during and after the treatment process was found to be sensitive to total mass of lactate injected but not the rate of lactate injection, pulsed injection, or lactate concentration. In addition, the results are highly sensitive to the first-order decay rates assigned to the microbes in the matrix, indicating that EISB effectiveness is expected to decrease dramatically with factors such as increased inhibition and competition for hydrogen. Furthermore, it was revealed that DNAPL type and rock type significantly

affect EISB performance in the case of matrix bioremediation, with increased performance associated with increased diffusive flux of lactate to the matrix-bound contaminant mass (i.e., source zones characterized by lower peclet numbers). Overall, the results indicate that relatively ideal conditions (i.e., low inhibition, high microbial concentrations throughout the matrix, and low peclet number) are required for EISB to be effective. In contrast with in situ chemical oxidation, the simulations suggest that ongoing EISB treatment of the matrix after lactate injection ceases is possible under these ideal conditions. However, if bioremediation activity is restricted to the fractures, ongoing treatment of back-diffusing contaminant mass is relatively insignificant and no difference in post-treatment downgradient mass discharge is observed from the identical scenario with no EISB applied.

1. INTRODUCTION

Enhanced In Situ Bioremediation (EISB) is increasingly being used as a remediation approach for contaminated aquifers. EISB has been demonstrated to effectively remediate/contain the spread of contaminants (including many chlorinated solvents) while converting a significant fraction of their mass to harmless byproducts (National Research Council, 1994). Laboratory and field research conducted over the last decade has shown that micro-organisms that are naturally present in subsurface environments possess the capability to degrade chlorinated ethenes (e.g., tetrachloroethylene (PCE), trichloroethene (TCE), dichloroethylene (DCE) and vinyl chloride (VC)) to non-toxic end-products such as ethene, carbon dioxide, and chloride (Suthersan and Payne, 2005).

Under anaerobic conditions, chlorinated aliphatic hydrocarbons (CAHs) such as PCE may be metabolized by indigenous microorganisms. The reductive dechlorination process results in the sequential transformation of PCE into TCE, DCE, VC, ethene, and finally carbon dioxide and chloride. With each step, a chlorine atom is removed from the compound resulting in a less oxidized molecule. For this natural process to occur, hydrogen (the electron donor) takes the place of chlorine in the CAH (the electron acceptor) during reduction. When the process is documented to proceed without interference this is referred to as natural attenuation. Based on site-specific conditions, including the specific microorganisms present and the availability of hydrogen and nutrients (e.g., phosphorus) required by the microorganisms, the rates and degree of completeness of biodegradation varies between sites (Kozar et al., 2002). Typically, the process can be accelerated via addition of a carbon substrate and/or nutrients (biostimulation) and even further by injecting a microbial consortium of known degraders (bioaugmentation) (Major et al., 2002).

While hydrogen can be injected directly (e.g., Adamson et al., 2003), more typical is to provide a carbon substrate (e.g., lactate, ethanol, pentanol, glucose) that is converted to hydrogen via fermentative microorganisms (Ellis et al., 2000; Major et al., 2002; Fennell et al., 1997; Carr and Hughes, 1998; Wu et al., 1998; Yang and McCarty, 1998; Yang and McCarty, 2000a)). Engineering design of these technologies is rapidly evolving, although to date there is considerable uncertainty in determining the quantities of carbon substrate required and the impacts of dosing requirements on field performance (Hood et al., 2007). Lactate is one of the most common carbon substrates used in the industry

and research studies (Sung et al., 2003; Christ and Abriola, 2007; Hood et al., 2007; Sorenson, 2002). Due to its high solubility, maintaining sufficient concentrations of hydrogen to support EISB typically requires continuous dosing with lactate throughout the treatment period (Major et al., 2002). Emulsified Vegetable Oil (EVOs) on the other hand has been recognized as a promising remediation technique that does not require continue dosing (Long and Borden, 2006). Dechlorination may be slowed or inefficient in the presence of competing electron accepting processes that consume the available hydrogen, including sulphate reduction, iron reduction, and methanogenesis (Chapelle, 1996).

While the majority of laboratory and field work has focused on EISB for relatively dilute CAH plumes, it has been demonstrated that the approach has potential for treating dense non-aqueous phase liquid (DNAPL) source zones (e.g., Seagren et al., 1994; Yang and McCarty, 2000; Yang and McCarty, 2002). Not only are the fermentors and dehalogenataors able to metabolize CAHs at concentrations previously assumed toxic, the suppression of methanogensis in these environments favours efficient dechlorination (Yang and McCarty, 2000). Furthermore, EISB within the source zone has additional benefits of reducing DNAPL longevity by increasing the driving force for mass transfer to the aqueous phase (Seagren et al., 1994; Yang and McCarty, 2000; Yang and McCarty, 2002; Christ et al., 2005; Amos et al., 2007).

The majority of laboratory work, field trials, and field applications of EISB have been conducted in unconsolidated porous media aquifers (e.g., sands and gravels). However,

the nature and extent of these processes in fractured rock are not well-understood. There is some field evidence that biodegradation of chlorinated solvents can occur in the vadose zone of fractured rock settings (e.g., Conrad et al., 1997b), but major questions remain as to how to characterize the extent of naturally occurring biological activity and how to stimulate and monitor it for the remediation of contaminated aquifers. Newell et al. (2006) reported downgradient source concentration decay rates to range from as low as 0.34/year for TCA to 0.11/year for TCE.

Kalish et al. (1964) observed permeability reductions due to bacterial clogging via injection experiments with sandstone cores. It was found that in high permeability, bacterial clogging is limited to 5 to 6 inches, while in low permeability cores clogging zones were noted to be less than 2 inches. It was also found that depending on the bacteria size, the depth of penetration into the cores can similarly varies. Charbonneau et al. (2006) found that biofilm formed within dolostone cores reduces the effective porosity via radial diffusion experiments with a conservative tracer. In other works, Yu and Pinder (1994) and de Beer et al. (1997) observed significant reductions in effective diffusivity for various solutes due to biofilm formation.

Previously, deep fractured rock vadose zones in arid regions have been thought of as biologically inactive, due to dry conditions and minimal organic matter (Palumbo et al., 1994). Although the numbers of indigenous bacteria are ubiquitous and have been found in such environments, albeit in low numbers, experiments have indicated that their activity may be stimulated with the addition of water, nutrients and organic carbon

(Palumbo et al., 1994; Colwell et al., 1992). Additionally, studies of microbial activity in deep fractured granite rock have shown a diverse microbial population to be attached to the fracture walls (Pedersen 1990), and evidence has been presented for natural biodegradation (intrinsic bioremediation) of chlorinated ethenes in a fractured dolomite aquifer (Yager et al. 1997). In general, there is a significant knowledge gap regarding the effectiveness of EISB in fractured rock at the field scale.

Numerous numerical models have been developed for simulating chlorinated ethene transport and degradation. Dechlorination kinetics have been approximated by first-order (Carr et al., 2000; Sleep and Sykes, 1993), Michaelis-Menten (Haston and McCarty, 1999) and Monod-type expressions (Chu et al., 2004; Cupples et al., 2004a,b; Christ and Abriola, 2007). The latter two forms often include limitations on the rate of dechlorination due to the availability of hydrogen (e.g., Fennell and Gossett, 1998; Amos et al., 2007) and competition between CAHs (Cupples et al., 2004a,b; Yu and Semprini, 2004). Depending on the quantities of alternate electron acceptors present, competition for hydrogen can be neglected (Cupples et al., 2004a; Amos et al., 2007) or included (Fennel and Gossett, 1998; Lee et al., 2004; Christ and Abriola, 2007). A few models consider excessive acid formation limiting the rate of dechlorination (Zhuang and Pavlostathis, 1995; Cope and Hughes, 2001; Lee et al., 2002; Adamson et al., 2004). In general, models that employ first-order decay expressions incorporate all of the sources of limitation implicitly in the rate constant. A few models explicitly include DNAPL dissolution (Carr et al., 2000; Chu et al., 2003; Widdowson, 2004; Amos et al., 2007; Christ and Abriola, 2007). To the author's knowledge, no models have been developed

or employed to investigate EISB in fractured rock.

The objective of this work is to examine the benefits and challenges of DNAPL source zone remediation by EISB in fractured rock aquifers. This paper employs numerical simulation to investigate the sensitivity of DNAPL source zone treatment with lactate to a variety of site history and engineering design parameters. In so doing, the research casts light on the fractured rock scenarios under which EISB may be expected to provide cost-effective benefit.

2. Model Development

A more detail description on the model development of DNAPL3DRX-FRAC is provided in Appendix B2. The processes described here are aimed to provide the reader with an understanding of the approach being adopted to develop the bioremediation package of the model.

Bioremediation Equations

For the purpose of this study the subsequent discussion is limited to anaerobic bioremediation of chlorinated solvent DNAPLs employing lactate as the organic substrate.

H_2, the direct electron donor, is obtained via the in situ fermentation of injected lactate and employed by reductive dehalogenating microorganisms to dechlorinate contaminants such as PCE, TCE, DCE, and VC (Cornuet et al., 2000). The fermentation of lactate

and of its byproduct acetate may be represented as follows (Macbeth et al., 2004):

$$\underset{\text{Lactate}}{C_3H_5O_3} + 2H_2O \rightarrow \underset{\text{Acetate}}{C_2H_3O_2} + CO_2 + H_2O + 2H_2 \quad (1)$$

$$\underset{\text{Acetate}}{C_2H_3O_2} + 4H_2O \rightarrow 2CO_2 + 2H_2O + 4H_2 \quad (2)$$

Equations 1 and 2 indicate that each mole of lactate is theoretically capable of producing 6 moles of hydrogen. In reality, a number of factors will reduce the amount of H_2 available to dechlorinating bacteria, such as incomplete fermentation and the presence of competing terminal electron accepting processes (e.g., Yang and McCarty, 1998). Fermentation processes are not explicitly simulated in this work; instead a hydrogen yield coefficient, Y_{H2}, is employed to describe the fraction of the theoretical maximum H_2 available to dechlorinating microorganisms:

$$\text{Lactate} \rightarrow Y_{H2}\ 6[H_2] \quad (3)$$

The microbial mediated sequential reductive dechlorination of PCE and its daughter products are modelled as follows (Clement, 1997):

$$\underset{\text{PCE}}{C_2Cl_4} + H_2 \rightarrow \underset{\text{TCE}}{C_2HCl_3} + HCl \quad (4)$$

$$\underset{\text{TCE}}{C_2HCl_3} + H_2 \rightarrow \underset{\text{DCE}}{C_2H_2Cl_2} + HCl \quad (5)$$

$$\underset{\text{DCE}}{C_2H_2Cl_2} + H_2 \rightarrow \underset{\text{VC}}{C_2H_3Cl} + HCl \quad (6)$$

$$\underset{\text{VC}}{C_2H_3Cl} + H_2 \rightarrow \underset{\text{Ethene}}{C_2H_4} + HCl \quad (7)$$

In 9 – 12, H_2 is not explicitly modelled as an independent chemical species. Rather, 8 is inserted into 9 – 12, such that [H_2] is replaced by $(1/6)Y_{H2}$ [lactate]. In this way, fermentation is assumed to occur in respond to local (i.e., nodal) demand for H_2 and dechlorination can only proceed in nodes where lactate and chlorinated ethenes are co-located. Moreover, tracking of lactate mass in space and time ensures that the extent of dechlorination at a given node cannot exceed the potential supply of H_2 in a given timestep. In this way, the physical distribution of lactate in the fractures and matrix, relative to the distribution of chlorinated ethenes, is a dominant factor in determining bioremediation success in these simulations.

Hydrogen yield coefficients in the range 0.20 – 1.0 are reasonable depending on the efficiency of the fermentors, fate of acetate, and availability of competing electron accepting processes (Robinson et al., 2009). It is reasonable not to permit H_2 to build-up and transport in the subsurface since H_2 is typically scavenged by an electron accepting process as soon as it becomes available (Fennell et al., 1997; Yang and McCarty, 1998) and therefore H_2 concentrations in these systems tend to remain very low. Moreover, it is reasonable to simulate that H_2 is generated in response to the presence of H_2 sinks (i.e., electron accepting processes) (Robinson et al., 2009). However, the adopted methodology does imply that all electron accepting processes (dechlorination + others) occur only in tandem when in fact they occur independently.

By using a split-operator approach for transport processes (Clement, 1997; Clement et al., 1998), the relevant kinetic equations treated as first-order processes are as follows

(Clement 1997):

$$\frac{d[PCE]}{dt} = -\frac{K_P[PCE]}{R_P} \quad (8)$$

$$\frac{d[TCE]}{dt} = \frac{Y_{T/P}K_P[PCE] - K_{T1}[TCE]}{R_T} \quad (9)$$

$$\frac{d[DCE]}{dt} = \frac{Y_{D/T}K_T[TCE] - K_{D1}[DCE]}{R_D} \quad (10)$$

$$\frac{d[VC]}{dt} = \frac{Y_{V/D}K_{D1}[DCE] - K_{V1}[VC]}{R_V} \quad (11)$$

$$\frac{d[ETH]}{dt} = \frac{Y_{E/V}K_{V1}[VC] - K_{E1}[ETH]}{R_E} \quad (12)$$

$$\frac{dy[Cl]}{dt} = \frac{Y1_{C/P}K_{P1}[PCE] + Y1_{C/T}K_{T1}[TCE] + Y1_{C/D}K_{D1}[DCE] + Y1_{C/V}K_{V1}[VC]}{R_C} \quad (13)$$

where the square brackets [ ] denote molar concentration, *KP, KT1, KD1, KV1,* and KE1 are first-order anaerobic degradation rates $\{M^{-1}\ L^3\ T^{-1}\}$ for PCE, TCE, DCE, VC, and ETH, respectively; RP, RT, RD, RV, RE, and RC are retardation factors for the chlorinated ethenes, respective; YT/P, YD/T, YV/D, and YE/V are chlorinated compound yield coefficients for the respective chlorinated ethenes (their values, computed from 9 – 12, are: 0.79, 0.74, 0.64 and 0.45, respectively); Y1C/P, Y1C/T, Y1C/D, and Y1C/V are yield values for chloride (their values, computed from 8 – 11, are: 0.21,0.27, 0.37, and 0.57, respectively).

The retardation factor is computed locally from the nodal *foc* concentration (e.g., Fetter, 1993):

$$R_i = 1 + Koc \times foc_i \frac{\rho}{\theta} \quad (14)$$

where ρ is the dry bulk density (ML^{-3}), θ is the porosity of the matrix (-), and *Koc* is the organic carbon partition coefficient (L^3M^{-1}) (see Section 4.3.2 for details). Reductive dechlorination is assumed to occur only in the aqueous phase of the chlorinated products (Domenico 1987).

First-order kinetics for dechlorination represents the assumption that there are no rate-limiting factors (e.g., nutrients are in excess, microbial populations not inhibited by, for example, non-neutral pH or high concentrations of chlorinated ethenes). In this study, the microbial populations are not simulated explicitly, but rather are implicitly assumed to be mature populations of constant concentration that are relatively immobile. The model permits the microbial consortium (i.e., fermentors and dechlorinators) to be present on the fracture surface only or in both the fracture and the matrix (as defined by the user). This flexibility is permitted since the depth of penetration of the microorganisms into the matrix; which was found to be dependent on the size of the microbial involved (Cumbie and MacKay, 1999; Becker et al., 2003; Driese and MacKay, 2004), and the extent of dechlorination occurring in rock matrices remains an open research question.

Equations 8 – 13 are implemented in the model by employing the inbuilt RT3D sequential dechlorination reaction module. The reaction module was, however, modified to allow for transport and in situ fermentation of lactate to (implicitly) generate H_2. The model explicitly simulates all chlorinated ethenes (PCE, TCE, DCE, VC) as well as their end-products (Cl, ETH) and lactate as mobile aqueous species. RT3D was

modified to account for species-dependent diffusion coefficients (West et al., 2008) and to permit the retardation factor of each species to be computed locally from the fraction of organic carbon (f_{oc}) at each node. The adsorption of lactate, however, is assumed to be negligible (Wu et al., 2007).

Using equations 4 – 13, the simplification 3, and robust first-order rate constants for dechlorination results in predictions of bioremediation proceeding to the maximum extent possible at a node for a given timestep limited only by the local availability of lactate at that time. While this is a gross oversimplification of reality, it is appropriate for the simulations in this work that focus on the field scale feasibility of bioremediation in fractured rock from an engineering perspective. This approach ensures that fermentation is not the limiting factor for success in these simulations. Moreover, employing the first-order kinetic approach and rate constants representing healthy dechlorinating populations, there are no geochemical or microbiological limits on the rate of dechlorination. These generous assumptions create a 'best case' scenario for bioremediation in which the success of the EISB application depends most significantly on the physical flow and transport processes in fractured rock (i.e., the spatial and temporal distribution of lactate and chlorinated ethenes in both fractures and matrix).

Model Verification

A more detail description on the model verification process of DNAPL3DRX-FRAC is provided in Appendix B2. For the purpose of this study the subsequent discussion is limited to the verification of the bioremediation package of the model.

The bioremediation reaction kinetics equations 8 – 13 were verified by reproducing and comparing the results of a single horizontal fracture simulation using DNAPL3DRX-FRAC and the original inbuilt RT3D sequential dechlorination reaction module in RT3D. Fluid properties and reaction parameters are listed in Table 1. Note that in order to effectively compare the results with the original inbuilt RT3D sequential reaction module, the effects of lactate fermentation was neglected in this verification test.

The verification simulation considers a representative sandstone formation at the scale of a localized DNAPL source zone via a two-dimensional domain 20 m wide × 2.25 m high with unit depth. The coarse, uniformly discretized domain employed DX = 0.25m and DY = 0.25m. A single horizontal fracture was defined with an aperture of 128μm. Grid refinement was then conducted using N = 5 together with the 'exponentially increasing' spacing option.

A 5.0m pool of TCE, 1.0m from the left hand boundary, characterized by an effective wetting phase saturation of 0.3 was placed within the fracture at the start of the simulation (Figure 1). The watertable was set to be coincident with the top boundary while the bottom boundary permitted the free exit of both water and DNAPL. Side boundaries were modified such that a hydraulic gradient of 0.005 from left to right across the domain was established throughout the entire simulation. DNAPL was then allowed to redistribute for 1 year with no DNAPL dissolution or reactions permitted. Following the cessation of NAPL movement, DNAPL dissolution, aqueous phase transport and EISB were simulated for 1 year. The microbial consortium was assumed to be present

in the matrix and fractures equally and the first-order rate constants were applied in the presence of chlorinated compounds since fermentation was ignored. As demonstrated by Figure 2 the results generated by DNAPL3DRX-FRAC were an exact match to the results produced by the original inbuilt RT3D sequential dechlorination reaction module.

In order to provide confidence in the in-situ organic substrate fermentation process added to the model, an expanded version of this verification exercise was conducted. All conditions were identical, except that following the end of the first year, the hydraulic gradient was increased to 0.025 for 2 years during which lactate was injected at a constant concentration of 2.0 g/L from the left-hand boundary. At the end of 2 years of lactate injection (i.e., t_{TOTAL} = 3 years), lactate injection was terminated and the hydraulic gradient was reduced back to 0.005. Following the EISB stage, an additional five years were simulated. In this case, dechlorination is only permitted to occur in the presence of sufficient lactate (i.e., H_2) in both the fracture and the matrix.

As demonstrated by Figure 3, and in contrast to Figure 2, the various TCE daughter products only begin to form when lactate was injected into the domain at t_{TOTAL} = 2 years. Mass balance of chloride, lactate and chlorinated compounds was found to be excellent for both the global domain and for single nodes (figure not shown). These simulations provide confidence in the model to calculate both the bioremediation reaction stoichiomtery (equations 3 – 7), reaction kinetics (equations 8 – 13), and the dependence of dechlorination on lactate fermentation as intended.

Table 1 Fluid Properties and Reaction Parameters for Verification Simulation

Parameter	Notation	Value
TCE Density [a]	ρ_{NWtce}	1460 kg/m^3
TCE Viscosity [a]	μ_{NWtce}	0.0005 Pa s
TCE Solubility [a]	$Solub_{TCE}$	1100 mg/L
TCE Free Solute Diffusion Coefficient [b]	D^O_{TCE}	1.01 x10^{-9} m^2/s
PCE Free Solute Diffusion Coefficient [b]	D^O_{PCE}	9.40 x10^{-10} m^2/s
DCE Free Solute Diffusion Coefficient [b]	D^O_{DCE}	9.03 x10^{-10} m^2/s
VC Free Solute Diffusion Coefficient [b]	D^O_{VC}	1.06 x10^{-10} m^2/s
Ethene Free Solute Diffusion Coefficient [b]	D^O_{Eth}	1.34 x10^{-9} m^2/s
Chloride Free Solute Diffusion Coefficient [b]	D^O_{Cl}	2.03 x10^{-9} m^2/s
First-Order PCE Degradation Rate [c]	K_{PCE}	0.0413 / Day
First-Order TCE Degradation Rate [c]	K_{TCE}	0.0481 / Day
First-Order DCE Degradation Rate [c]	K_{DCE}	0.0326 / Day
First-Order VC Degradation Rate [c]	K_{VC}	0.0300 / Day
Hydrogen Yield Coefficient	Y_{H2}	0.50

a – Pankow and Cherry (1996)
b –Wilke and Chang (1955) at 25^{o}C
c –Suarez and Rifai (1999)

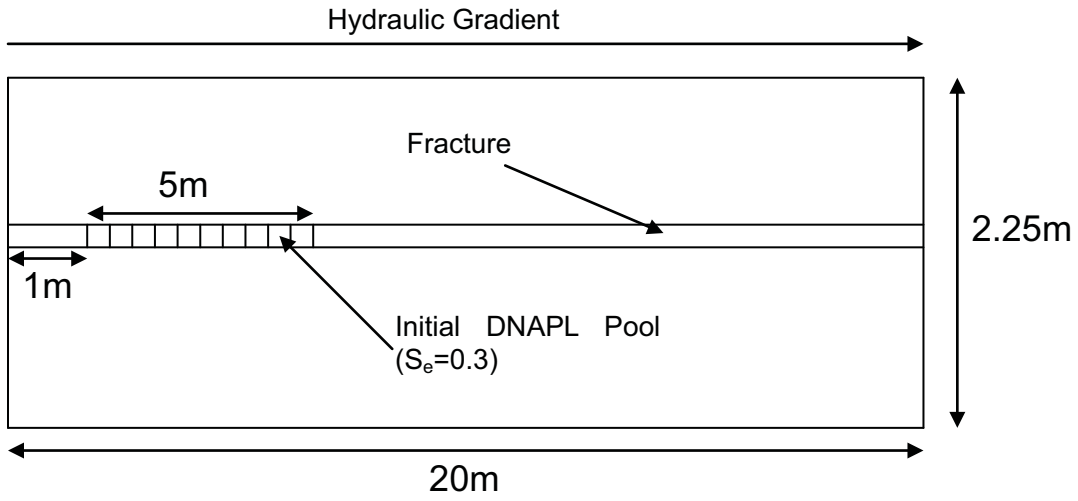

Figure 1: Sketch of domain layout for verification simulation.

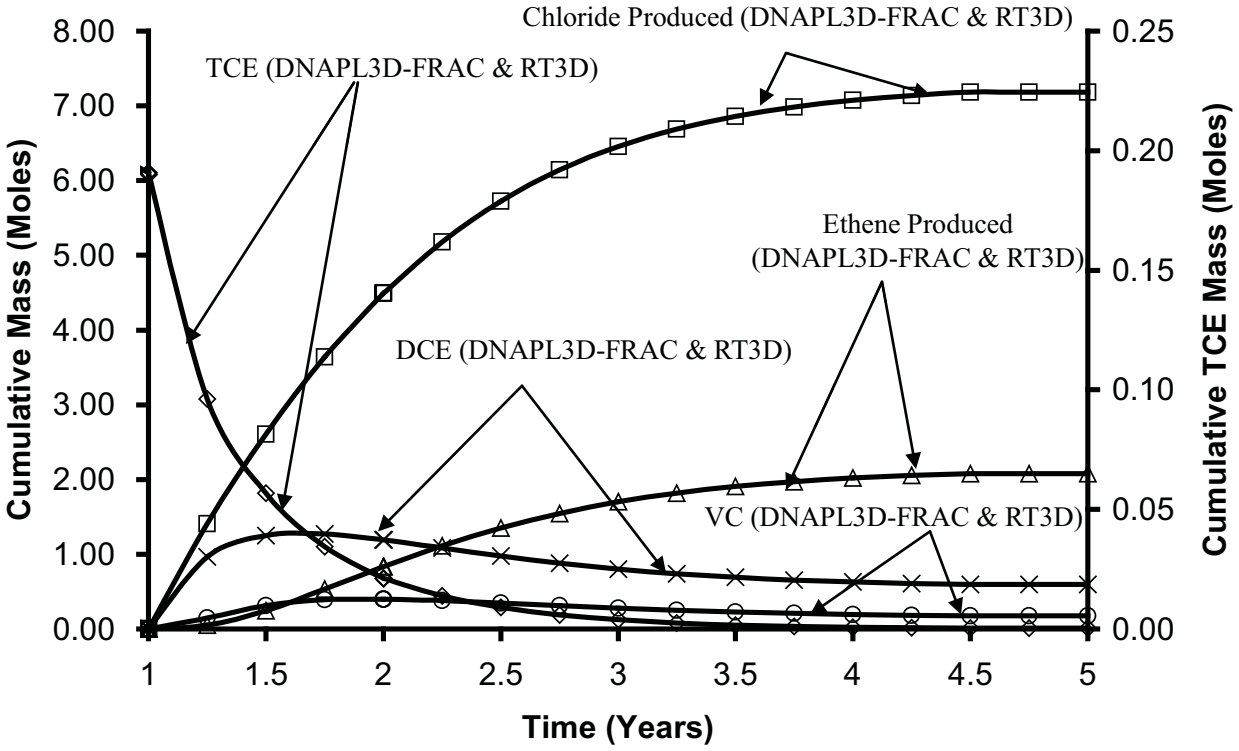

Figure 2: Cumulative aqueous mass of TCE and various chlorinated by-products in the domain over time.

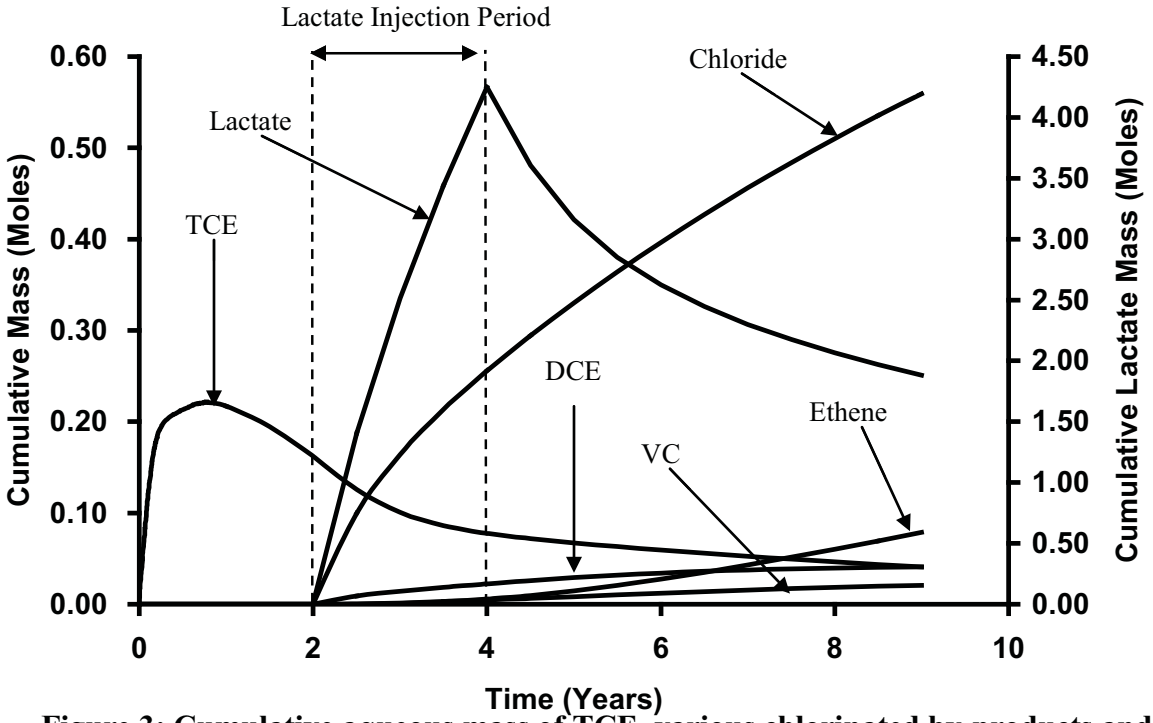

Figure 3: Cumulative aqueous mass of TCE, various chlorinated by-products and lactate in the domain over time.

3. NUMERICAL SIMULATIONS

Modelled Scenario

This section describes characteristics common to all of the simulations conducted for the bioremediation study (See Section 4.4.1 for the layout of the domain, boundary conditions and the five distinct stages applicable to each simulation), while the next details the characteristics of the individual runs. Note that stages one to three (i.e., i) DNAPL Release, (ii) DNAPL Redistribution, (iii) Site Ageing) are similar for both ISCO and EISB simulations.

During the 'Treatment Application' stage, EISB was initiated by injecting a constant aqueous phase concentration of 2.0g/L lactate (Geosyntec, 2007) for 2 years (i.e., 21 yrs $\leq t_{TOTAL} \leq$ 23 yrs) along a fully screened well at the left boundary (with penetration of the

formation assumed only at the horizontal fractures intersecting the well). During lactate application, the hydraulic gradient across the domain was increased to 0.025 to represent active amendment conditions. As well, the upgradient chlorinated solvent injection was terminated (assuming complete and instantaneous treatment of upgradient source zone); while this is unrealistic, it provides the best opportunity for success within the domain and thus supports viewing these results as approximating a best case for the technology. In all cases, stoichiometric calculations confirm that the total mass of lactate injected is greater than the theoretical lactate mass (accounting for the hydrogen yield coefficient assumed, 0.50) to theoretically dechlorinate all TCE and its daughter-products in the domain at the start of the Treatment stage. For example, for the Base Case, 48.5 kg or 545 moles of lactate was injected, compared to the 7.3kg or 55.6 moles of TCE mass in the domain, representing an excess of 980% (given that 1 mole of TCE is reduced to ethene by 1 mole of lactate (via 3 moles of hydrogen, when $Y_{H2} = 0.50$ in Equation 3).

Following the Treatment stage, an additional five years were simulated (i.e., 23 yrs $\leq t_{TOTAL} \leq$ 28 yrs). During this Post-Treatment stage, the ambient hydraulic gradient of 0.005 was again employed, but no upgradient concentration of any species (i.e., lactate or chlorinated solvent) was applied.

Several assumptions were employed in this work to facilitate reasonable simulation times:

1. All fractured rock simulations presented are two-dimensional; this assumption likely benefits the technology since the reduced dimensionality is expected to

reduce bypassing of the treatment fluid around DNAPL-occupied fractures;

2. The matrix is presumed to have a sufficient displacement pressure so as to exclude DNAPL entry; this assumption likely benefits the technology because the highest fraction of DNAPL is retained in the fractures which are most accessible to the treatment fluid;
3. Advection of groundwater through the matrix is assumed to be negligible; this is reasonable given that the high permeability contrast between the fractures and matrix. For example, for the sandstone Base Case, the matrix permeability is approximately 6 orders of magnitude less than the average fracture permeability. The Peclet number for the matrix (Pe = vx/D where v is horizontal velocity in matrix) if advection were not neglected is 0.166; since Pe<1 it is reasonable to assume that the matrix is diffusion dominated and advection is negligible (Trivedi et al., 2008).
4. Equilibrium mass transfer from DNAPL to aqueous phase was assumed; this assumption also favours improved performance of the technology by maximizing aqueous phase solvent concentrations.
5. Lactate is assumed not to sorb (Wu et al., 2007) and reductive dechlorination is assumed to occur only in the aqueous phase of the chlorinated products (Domenico, 1987).

Base Case and Sensitivity Simulations

Table 2 presents the suite of 13 simulations conducted in this study. The Base Case considered a fractured sandstone template site. Table 3 presents the parameters

employed to characterize the sandstone as well as the other two rock types (shale and granite). The sandstone domain, employed in all simulations except Run 10 and Run 11, is presented in Figure 4a. The sandstone parameters were chosen to be broadly representative of North American sandstone aquifers (e.g., Lipson et al., 2005). Table A1 (Appendix A) provides, for each rock type, the observed ranges for each parameter synthesized from the literature. Table 4.3 reveals that this sandstone exhibits - relative to the other template rock types - low fracture density, low mean aperture (125μm), high matrix porosity (7.7%), and intermediate foc (0.005).

The Base Case employed TCE as the DNAPL released and as the aqueous phase and sorbed chlorinated compound subsequently targeted by EISB. Fluid properties and reaction parameters are listed in Table 4. The Base Case also employed a continuous injection of lactate at 2.0 g/L for 2 years during the Treatment stage (Table 2).

Table 2. Field Scale EISB Fractured Rock Simulations

Run No.	DNAPL Type	Material	Lactate Concentration (mg/L)	Rate	Pulsing Strategy	Bioremediation Location
1 (Base Case)	TCE	Sandstone	2000	Mean	Continuous Lactate Injection for 2 Years	Fracture + Matrix
2	TCE	Sandstone	2000	Mean	Continuous Lactate Injection for 2 Years	Fracture
3	TCE	Sandstone	2000	High	Continuous Lactate Injection for 2 Years	Fracture + Matrix
4	TCE	Sandstone	2000	Low	Continuous Lactate Injection for 2 Years	Fracture + Matrix
5	TCE	Sandstone	2000	Mean	3 Months on 3 Months Off for 4 Years	Fracture + Matrix
6	TCE	Sandstone	2000	Mean	6 Months on 6 Months Off for 4 Years	Fracture + Matrix
7	TCE	Sandstone	2000	Mean	1 Year on 1 Year Off for 4 Years	Fracture + Matrix
8	TCE	Sandstone	1000	Mean	Continuous Lactate Injection for 4 Years	Fracture + Matrix
9	TCE	Sandstone	4000	Mean	Continuous Lactate Injection for 1 Year	Fracture + Matrix
10	TCE	Shale	2000	Mean	Continuous Lactate Injection for 2 Years	Fracture + Matrix
11	TCE	Granite	2000	Mean	Continuous Lactate Injection for 2 Years	Fracture + Matrix
12	PCE	Sandstone	2000	Mean	Continuous Lactate Injection for 2 Years	Fracture + Matrix
13	TCE	Sandstone	0	Mean	No Treatment	Fracture + Matrix

Table 3. Properties of Field Scale Fractured Rock Template Sites

Rock Type	Fracture Spacing (m)	Matrix Permeability (m^2)	Matrix Porosity	Foc	Bulk Density (g/cm^3)	Matrix Tortuosity	Fracture Aperture Range (μm)	Mean Aperture (μm)
Sandstone	6.0 (Ver) [*] 1.0 (Hor) [a]	1.05×10^{-15}	7.7% [a]	0.005 [a]	2.49 [a]	0.2 [a]	25 - 230 [a]	125
Shale	4.0 (Ver) [*] 1.0 (Hor) [*]	1.05×10^{-15}	3.0% [b]	0.009 [*]	2.619 [**]	0.1 [*]	50 - 250 [c]	150
Granite	2.0 (Ver) [d] 2.0 (Hor) [d]	1.05×10^{-15}	0.1% [*]	0.0005 [*]	2.697 [**]	0.05 [*]	100 - 500 [e]	300

[a] *Lipson et al., 2005*
[b] *Morris and Johnson, 1967*
[c] *Jardine et al., 1999*
[d] *Sousa 2007*
[e] *Sausse 2002*
**Data supplied by B.H Kueper (personal communication) based upon consulting experience on sites of all three rock types.*
*** Calculated using Bulk Density = Grain Density x (1-porosity), assuming a grain density of 2.7 for Shale and Granite.*
Ver – Vertical Fractures
Hor – Horizontal Fractures

Table 4 Fluid Properties and Reaction Parameters

Parameter	Notation	Value
TCE Density [a]	ρ_{NWtce}	1460 kg/m^3
TCE Viscosity [a]	μ_{NWtce}	0.0005 Pa s
TCE Solubility [a]	$Solub_{TCE}$	1100 mg/L
PCE Density [a]	ρ_{NWpce}	1630 kg/m^3
PCE Viscosity [a]	μ_{NWpce}	0.0009 Pa s
PCE Solubility [a]	$Solub_{PCE}$	200 mg/L
TCE Free Solute Diffusion Coefficient [b]	D^O_{TCE}	1.01 x10^{-9} m^2/s
PCE Free Solute Diffusion Coefficient [b]	D^O_{PCE}	9.40 x10^{-10} m^2/s
DCE Free Solute Diffusion Coefficient [b]	D^O_{DCE}	9.03 x10^{-10} m^2/s
VC Free Solute Diffusion Coefficient [b]	D^O_{VC}	1.06 x10^{-10} m^2/s
Ethene Free Solute Diffusion Coefficient [b]	D^O_{Eth}	1.34 x10^{-9} m^2/s
Chloride Free Solute Diffusion Coefficient [b]	D^O_{Cl}	2.03 x10^{-9} m^2/s
Lactate Free Solute Diffusion Coefficient [c]	D^O_{Lac}	2.57 x 10^{-9} m^2/s
First-Order PCE Degradation Rate [d]	K_{PCE}	0.0413 / Day
First-Order TCE Degradation Rate [d]	K_{TCE}	0.0481 / Day
First-Order DCE Degradation Rate [d]	K_{DCE}	0.0326 / Day
First-Order VC Degradation Rate [d]	K_{VC}	0.0300 / Day
Hydrogen Yield Coefficient	Y_{H2}	0.50

a – Pankow and Cherry (1996)
b –Wilke and Chang (1955) at 25°C
c – Lide (2004)
d – Suarez and Rifai (1999)

As illustrated in Table 2, Runs 5 - 9 examine variations in treatment strategy, while Runs 2 - 4 and 10 - 12 explore the influence of site conditions. All parameters, boundary conditions, and source conditions were established identically to the Base Case for all simulations, except for changing the parameter(s) whose influence was being examined in each study. It is noted that for all simulations except Runs 10, 11 and 12, the results during the DNAPL Release, DNAPL Redistribution, and Site Ageing stages are identical with the differences occurring from the start of the Treatment stage.

It is noted that a 'No EISB' case was simulated for comparison purposes. This simulation was identical to the Base Case in all respects but one: no lactate was injected during the Treatment stage. As a result, no fermentation or reductive dechlorination processes were simulated in this simulation.

Microorganisms in Fractures/Matrix

Although bacteria has been known to reside within both fractures and matrix (Crow, 1968; National Research Council, 1984), in order to examine the influence of the spatial distribution of microorganisms in fractured rock aquifers, the Base Case (Run 1) assumed significant biological activity in both the fractures and in the matrix (homogeneously distributed) while Run 2 assumed the microbiological consortium being present only in the fractures. This sensitivity study comprised two simulations, representing the endpoints of a spectrum of possible configurations.

Dechlorination Rate Parameters

The overall influence of the rate at which the chlorinated ethenes are being dechlorinated was examined. It is known that the dechlorination rate parameters can vary significantly depending on many factors including the scale and format of the study (e.g., microcosm, column, or field) (Suarez and Rifai, 1999), the type of microbial community present (Yu and Semprini, 2004), microbial concentration (Fennell et al., 1997), and a wide variety of inhibiting factors such as pH (Lowe et al.,1993), H_2S concentrations (Kalyuzhnyi et al., 1997), PCE/TCE toxicity (Bailey 1986), etc. In this study, a first-order approach is employed that lumps all of these effects together, allowing an investigation of the impact of modified dechlorination rates without reference to the specific cause of the modification. The first-order rate parameters used in this study were obtained from Suarez and Rifai (1999). The first-order rate parameters for all chlorinated ethenes in Run 3 are increased by one order of magnitude while the rate parameters used in Run 4 are decreased by one order of magnitude relative to the Base Case. These values are representative of rates recorded from previous laboratory experiments and previous sites respectively. This sensitivity study comprised three simulations.

Pulsed Injection of Organic Substrate

The effects of pulsing were examined by subdividing the Base Case injection period (2 years) into periodic, equal length lactate injection on and off intervals. Pulsed injection intervals of 3 months (Run 5), 6 months (Run 6) and 12 months (Run 7) were examined. Pulsed treatment has been demonstrated to be valuable in other DNAPL remediation options, such as waterflooding (Gerhard et al., 2001) and is often considered for other

treatment options involving injected fluids to reduce operation and maintenance costs while maintaining performance (e.g., reducing biofouling of wells during enhanced bioremediation). In all cases, the application period was adjusted so that the total mass of lactate injected was identical. This sensitivity study comprised four simulations.

Organic Substrate Concentration

To examine the influence of lactate concentration, the concentration at the injection well was halved (1 g/L, Run 8) and doubled (4 g/L, Run 9) relatively to the Base Case. In order to ensure that the total mass of lactate injected was kept constant, the injection period was changed accordingly (4 years and 1 year, respectively). This sensitivity study comprised three simulations.

It is noted that these simulations also represent a sensitivity study to Y_{H2} (i.e., hydrogen yield for dechlorination per mole of lactate). Run 8 represents a Y_{H2} of 0.25 (i.e., decreased efficiency, for example due to high sulphate concentrations in the groundwater) and Run 9 represents a Y_{H2} of 1.0 (i.e., perfect efficiency, complete fermentation of lactate and acetate to H_2 and no competition or losses) for a 2g/L lactate injection concentration. The study can be viewed from either perspective, since the model is formulated (equation 3) such that the extent of dechlorination is dependent upon the product of the molar concentration of lactate and the yield coefficient.

Rock Type

Runs 1, 10, and 11 compare EISB performance in three different types of fractured rock

at the field scale, each exhibiting a characteristic set or range of hydrogeological parameters (Table 3). Figure 4 presents the distribution of intrinsic permeability for the three domains, illustrating the distribution of fractures. In each case, the mean aperture is at the midpoint of the range specified in the table. It is noted that, characteristic of these rock types in natural environments, the shale template site exhibits (relatively) intermediate fracture density, low mean aperture (150μm), intermediate matrix porosity (3%), and high *foc* (0.009) while the granite exhibits high fracture density, high mean aperture (300μm), low matrix porosity (0.1%), and low *foc* (0.0009).

DNAPL Type

Runs 1 and 12 compare performance for both TCE and PCE in the sandstone domain. The full set of PCE fluid parameters employed for Run 12 is presented in Table 4. Note that while the boundary conditions in each run were identical, the distribution of DNAPL resulting from infiltration and redistribution were different due to the contrasting fluid properties. As well, different solubilities and sorptive capacities resulted in different distributions of aqueous phase and sorbed phase concentrations after the Site Ageing stage. This sensitivity study comprised two simulations.

4. RESULTS AND DISCUSSION

Table 5 summaries a selection of key numerical results for all 13 simulations conducted in this study. These data will be discussed as each set of simulations is presented.

Table 5: Summary of Results for All ISCO Simulations

Run No.	DNAPL St 2 (kg)	DNAPL St 3 (kg)	Aq + Sorb St 3 (kg)	Lactate Inject (kg)	DNAPL St 5 (kg)	Aq + Sorb St 5 (kg)	Mass Discharge St 5 (10^{-3} mg/s)	Lact React (kg)	CS React (kg)
1	5.26	0.00	7.3	48.5	0.00	0.018	0.017	3.180	7.77
2	5.26	0.00	7.3	48.5	0.00	5.140	3.885	0.017	0.07
3	5.26	0.00	7.3	48.5	0.00	0.000	0.000	2.200	8.97
4	5.26	0.00	7.3	48.5	0.00	2.940	2.340	0.724	2.45
5	5.26	0.00	7.3	48.5	0.00	0.003	0.003	3.530	7.83
6	5.26	0.00	7.3	48.5	0.00	0.003	0.003	3.450	7.83
7	5.26	0.00	7.3	48.5	0.00	0.003	0.003	3.181	7.83
8	5.26	0.00	7.3	48.5	0.00	0.003	0.003	3.521	7.83
9	5.26	0.00	7.3	48.5	0.00	0.041	0.040	2.895	7.70
10	6.86	0.01	6.8	35.1	0.00	0.971	0.293	2.902	0.61
11	11.53	4.23	0.68	436.3	4.10	0.378	0.017	0.001	0.01
12	6.03	0.11	3.3	48.5	0.04	0.474	0.116	1.181	2.61
13	5.26	0.00	7.3	0.0	0.00	5.180	3.956	0.000	0.00

St 2 = mass present at the end of Stage 2 (DNAPL redistribution)
St 3 = mass present at the end of Stage 3 (Site Ageing)
St 5 = mass present at end of Stage 5 (Post-Treatment)
DNAPL = mass of DNAPL present
Aq + Sorb = combined mass of aqueous and sorbed chlorinated solvent present
Lactate Inject = mass of lactate injected during the treatment period
Mass Discharge = mass per time of chlorinated solvent leaving the domain at the end of Post-Treatment stage
Lact React = total mass of lactate that reacted with chlorinated solvent in all phases
CS React = total mass of chlorinated solvent (in all phases) dechlorinated

Base Case Results

Figures 5a and 5b illustrate the distribution of the TCE DNAPL at the end of the infiltration and redistribution phases, respectively (relevant to all simulations except Runs 10, 11, and 12). Figures 5a and 5b reveal a heterogeneous distribution of DNAPL pools (i.e., connected phase) and residual (i.e., trapped blobs and ganglia) due to the influence of capillary forces (and, specifically, fracture entry pressures), the order of encounter of fractures, and the permeability contrasts between fractures. At the end of the DNAPL infiltration stage, the average DNAPL saturation was 0.75, the mass of

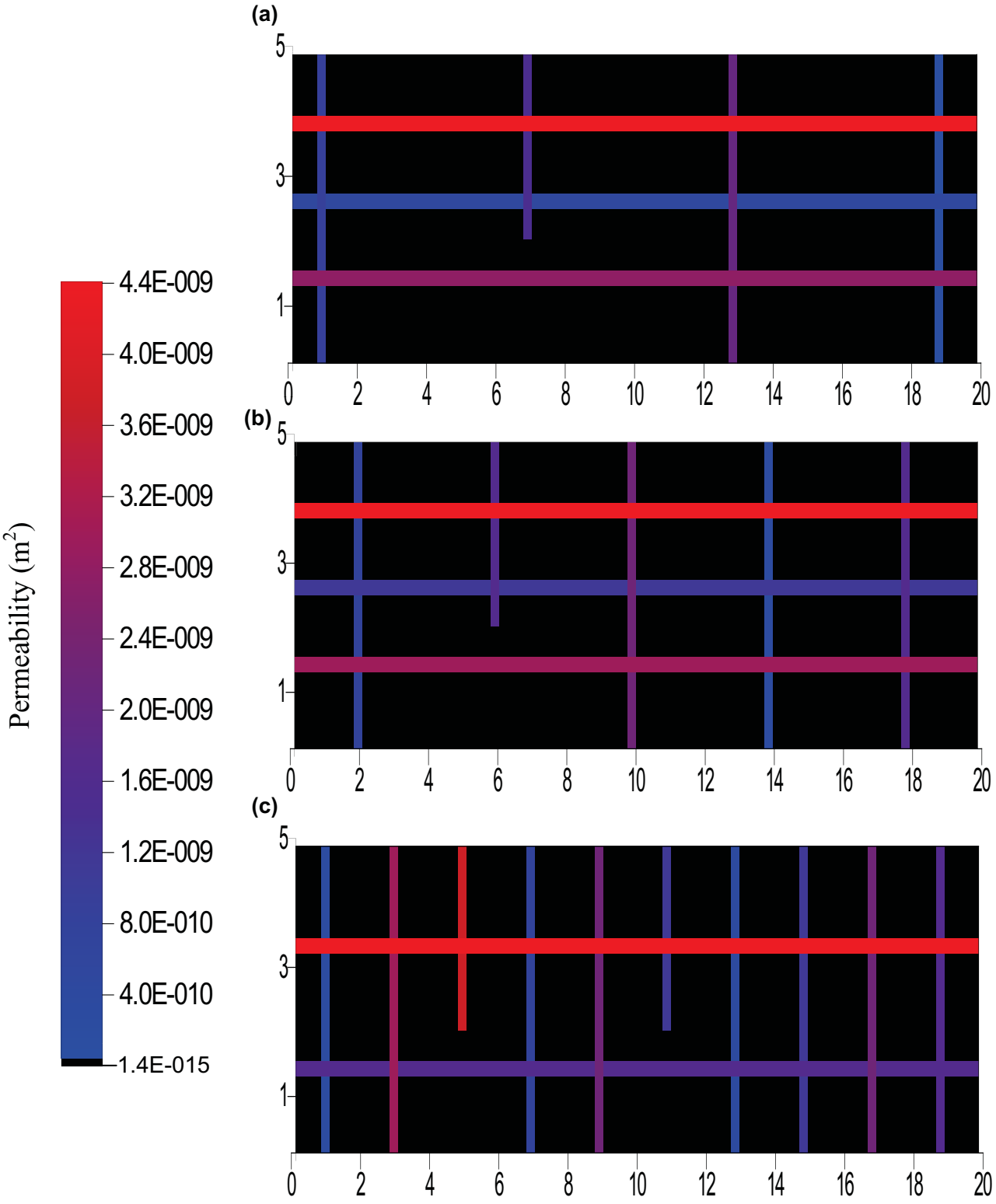

Figure 4: Distribution of permeability for the field scale fractured rock domains: (a) sandstone, (b) shale, and (c) granite. Colour corresponds to fracture permeability according to the scale bar provided; matrix permeability is uniform (black). Note that fracture apertures are exaggerated for visual purposes.

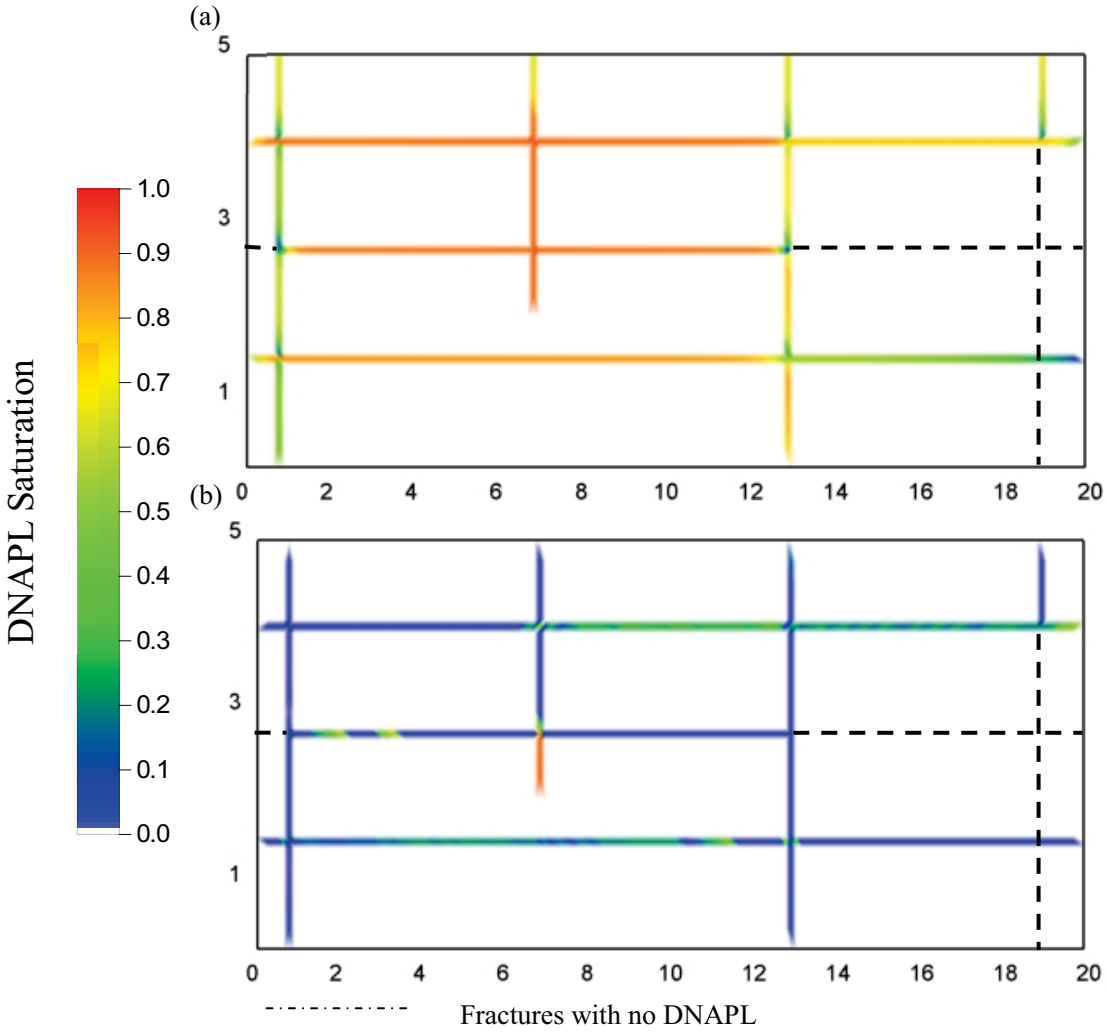

Figure 5: DNAPL distribution for Base Case at (a) t_{TOTAL} = 0.5 years when DNAPL inflow and outflow are equal, and (b) t_{TOTAL} = 1 year when all DNAPL migration has ceased.

DNAPL in the domain equaled 11.68 kg, the DNAPL volume was 0.008 m^3 (compared to a total fracture volume of 0.012 m^3) with 100% of the nodes on drainage (i.e., DNAPL displacing water). At the end of DNAPL redistribution stage, the average DNAPL saturation was 0.3, the DNAPL volume was 0.0036 m^3 (equal to a mass of 5.26 kg) and the pool to residual ratio was 71:29%. Note in Figure 5b that, as expected, the lone remaining pool exhibiting a high DNAPL saturation resides in a vertical dead-end

fracture, and other pools of various lengths occur in horizontal fractures, separated by areas of residual DNAPL.

Figure 6 illustrates the distribution of aqueous phase TCE at the end of the 20 year Site Ageing stage (t_{TOTAL} = 21 years). Evident are the expected diffusion halos in the sandstone matrix blocks adjacent to fractures containing DNAPL as well as those horizontal fractures without DNAPL but subject to significant aqueous mass flux (Figure 5b). At this time, no DNAPL remained in the domain. This occurred despite the constant influent concentration equal to 50% of TCE solubility. The reason is the substantial TCE sink provided by matrix diffusion and sorption. At this time, the total mass of TCE in the domain was 7.3 kg, of which 99% resided in the matrix; of the mass in the matrix, 98% was sorbed and only 2% remained in the aqueous phase. It appears that the matrix acts as a substantial sink for TCE, rapidly promoting DNAPL dissolution and solvent diffusion.

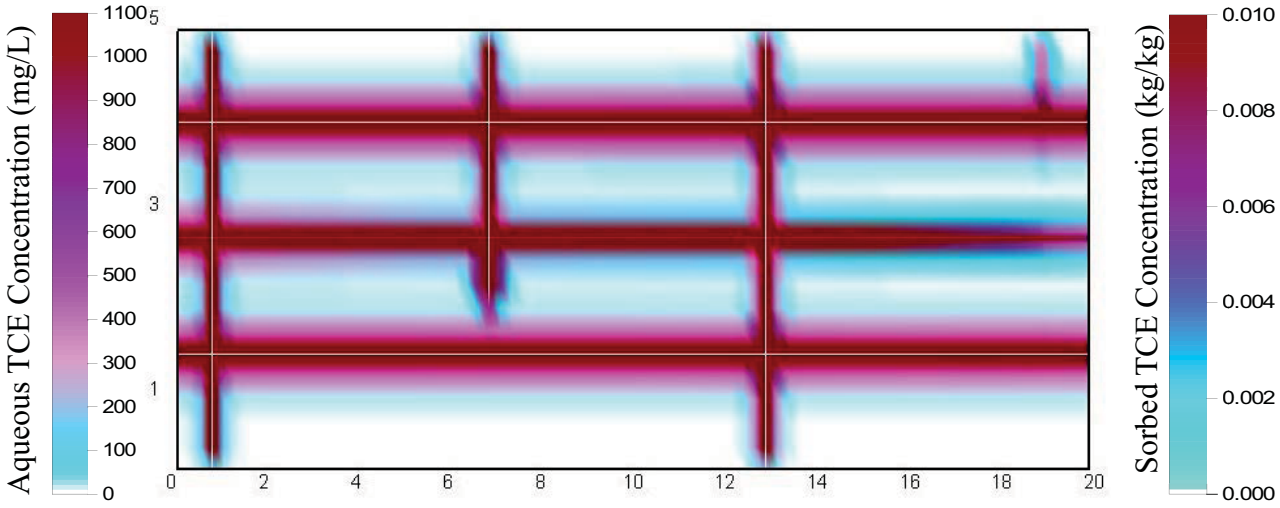

Figure 6: Distribution of aqueous and sorbed TCE after 20 years (t_{TOTAL} = 21 years) of DNAPL dissolution (i.e., Site Ageing stage).

Figure 7 provides the concentration of aqueous TCE and its various daughter-products throughout the domain after the Treatment stage (i.e., 2 years of lactate injection, t_{TOTAL} = 23 years). It reveals that the majority of the initial aqueous TCE mass present in the domain has been converted to daughter-products. It is noted that, by this time, the injected lactate has successfully penetrated the full extent of all the three horizontal factures present in the domain as well as a significant distance into the matrix. Figure 7e further demonstrates that chloride, a commonly used measure of the extent of reductive dechlorination, was present to some degree in most of the domain.

Figure 8 presents the concentration of aqueous TCE and its daughter-products throughout the domain at the end of the Post-Treatment stage (i.e. 5 years after lactate injection, t_{TOTAL} = 28 years). During this stage, further dechlorination of all chlorinated ethenes was observed; the lactate remaining (Figure 7f) clearly provided a continuing source of electron donor. This is confirmed by further decreases in the spatial distribution of TCE, DCE and VC (Figures 8a, b, and c, respectively) and the simultaneous increase in ethene and chloride concentration (Figures 8d and e). Figure 8f reveals that lactate has widely penetrated the domain and is nearing depletion within and near both horizontal and vertical fractures. Moreover, there is a strong correlation between the areas of lactate depletion and high concentrations of the non-toxic products ethene and chloride. Thus, while reverse diffusion and fracture flushing no doubt is occurring in the Post-Treatment phase, the figures suggest that significant dechlorination continues to occur within fractures and within the adjacent matrix.

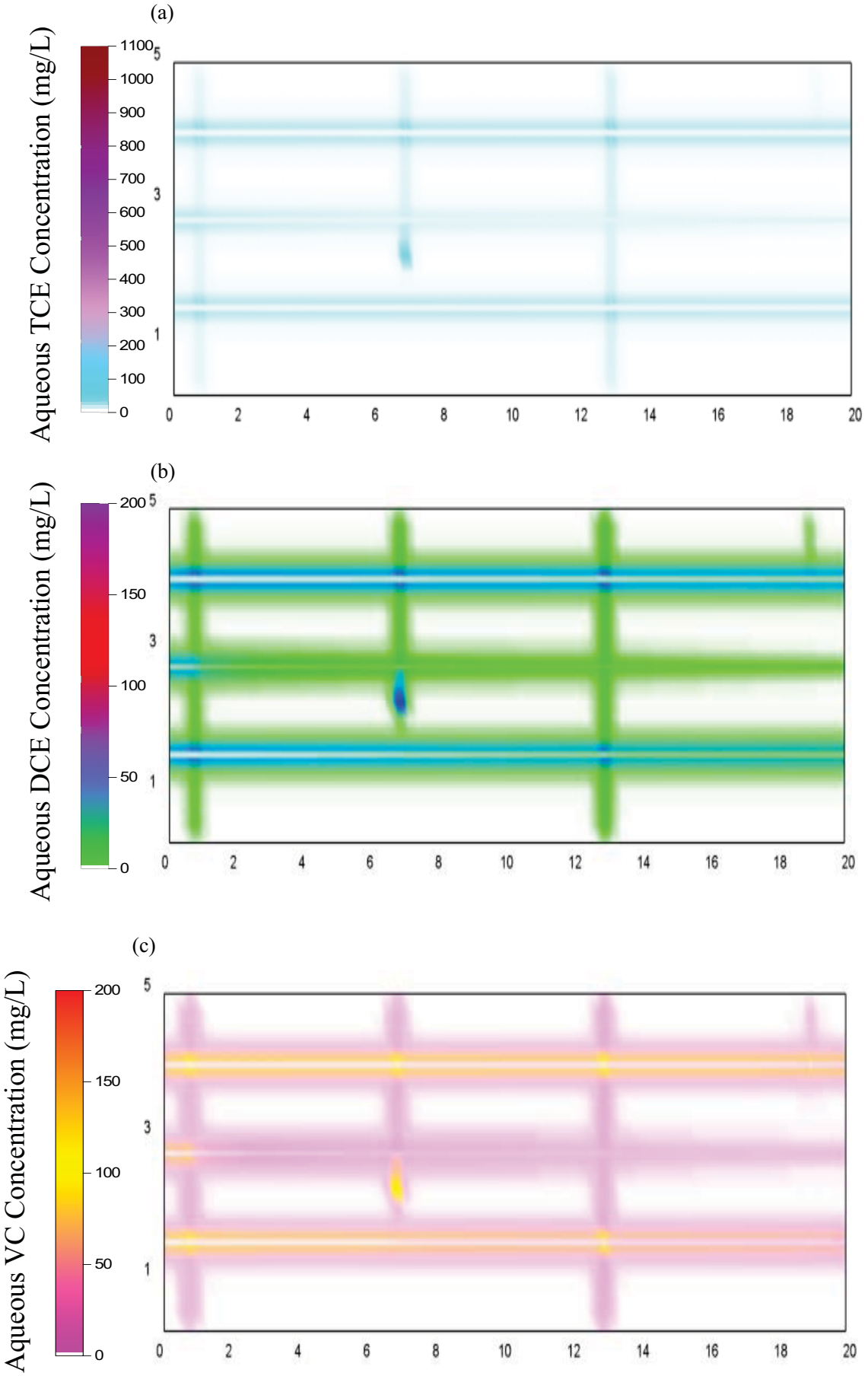
(a)
Aqueous TCE Concentration (mg/L)
1100
1000
900
800
700
600
500
400
300
200
100
0
5
3
1
0
2
4
6
8
10
12
14
16
18
20
(b)
Aqueous DCE Concentration (mg/L)
200
150
100
50
0
5
3
1
0
2
4
6
8
10
12
14
16
18
20
(c)
Aqueous VC Concentration (mg/L)
200
150
100
50
0
5
3
1
0
2
4
6
8
10
12
14
16
18
20

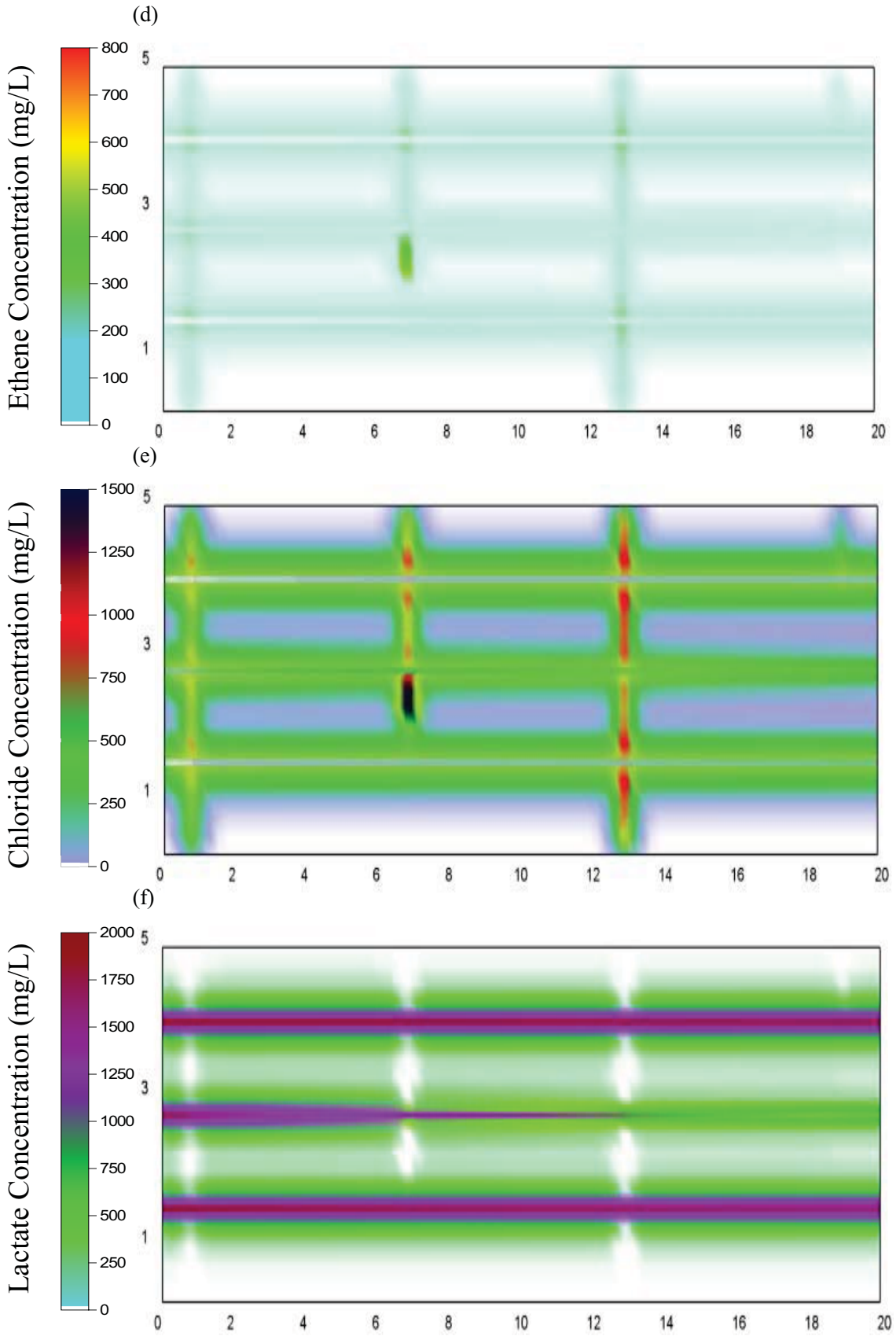

Figure 7: Distribution of aqueous species concentrations at t_{TOTAL} =23 years for Base Case after 2 years of lactate injection (i.e., Treatment stage): (a) TCE; (b) 1,1, DCE; (c) VC; (d) Ethene; (e) Chloride; (f) Lactate.

Figure 9 presents cumulative mass plots of all sinks and sources of TCE during the Base Case simulation. Summed totals of these plots, in which:

Mass Dissolved from DNAPL + Mass Inflow - Mass Destroyed - Mass Discharged = Mass Sorbed + Mass Aqueous in Domain (15)

revealed that the model has excellent mass balance (plots not shown to improve clarity of the figure) and this was confirmed by excellent computed mass balance on all species. The figure reveals that the majority of DNAPL dissolution occurred rapidly at the beginning of the simulation due to DNAPL dissolution and diffusion, corresponding to a rapid increase in sorbed TCE in the matrix. Until t_{TOTAL} = 3 years, TCE flux out of the domain was greater than flux into the domain due to a proportion of the dissolved TCE exiting via fracture flow. However, beyond this time, with dissolution virtually completed, TCE flux into the domain exceeded the flux out as the incoming background TCE contributed to a steady rise in mass retained via sorption. It also reveals that the cumulative mass of aqueous TCE in the domain (sum of that in the fractures and matrix) was a small fraction of the amount sorbed.

Figure 9 further illustrates that when lactate was injected, at t_{TOTAL} = 21 years, the amount of 'TCE Reduced During EISB' began to rise. Over the 2-year treatment period the total amount of 'TCE Reduced During EISB' was approximately 13% less than the magnitude of the reduction in sorbed TCE. The additional desorption occurred mainly as a result of back-diffusion induced by the low concentrations of TCE in the flowing

horizontal fractures.

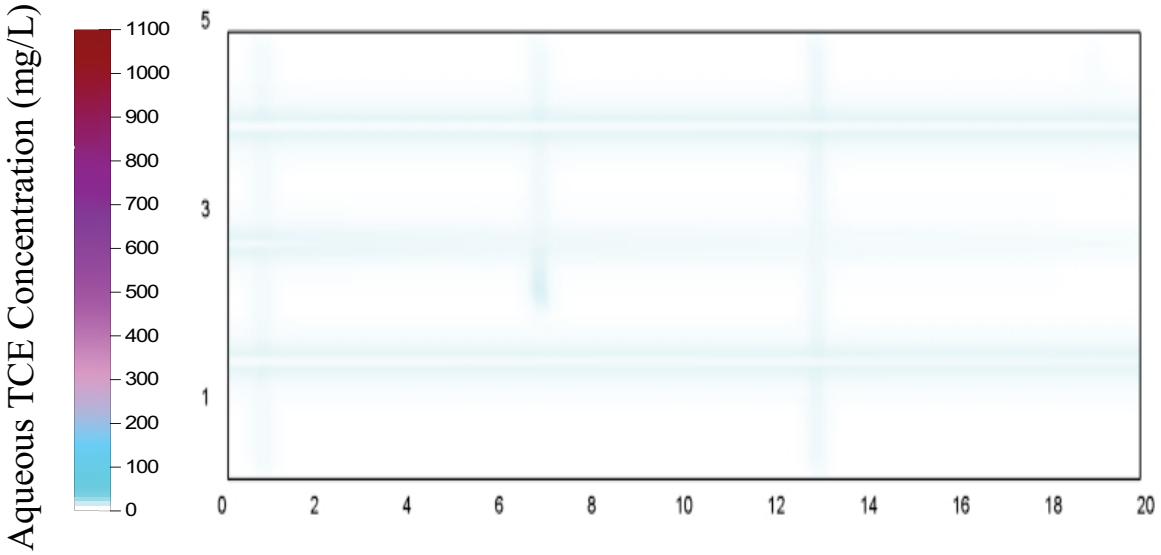

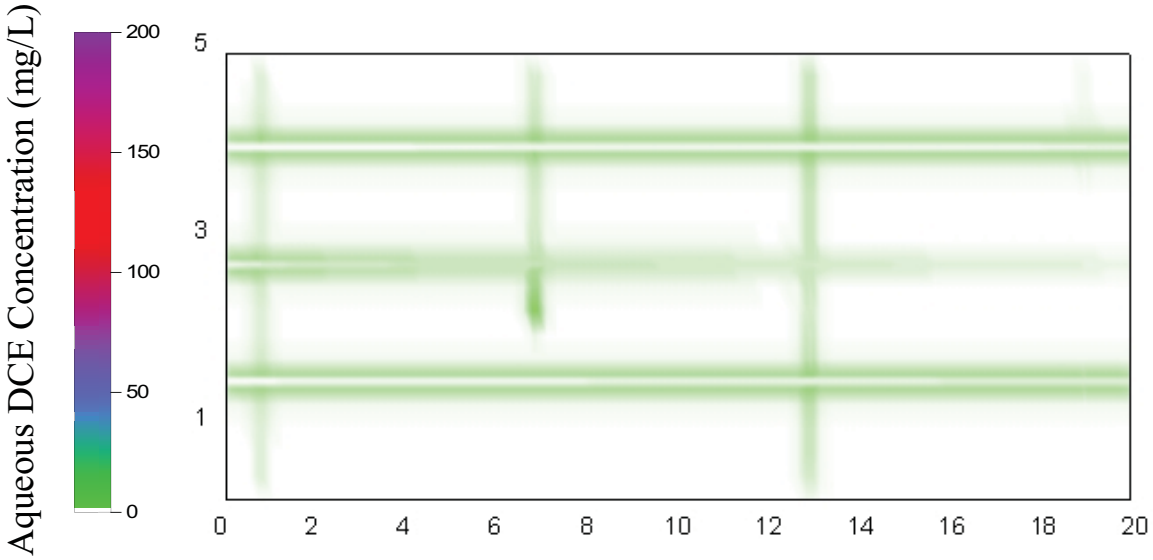

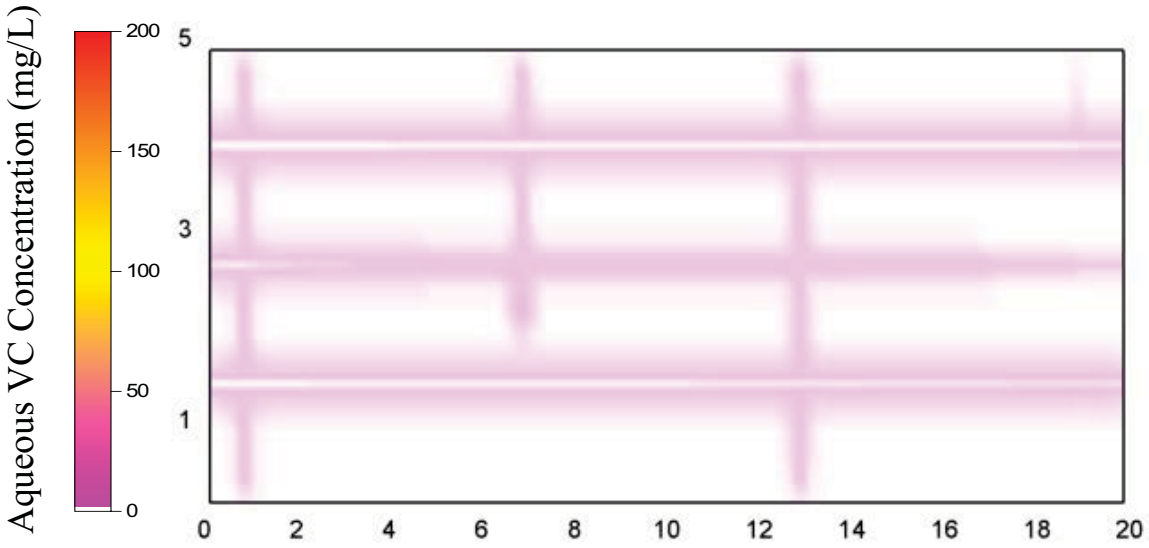

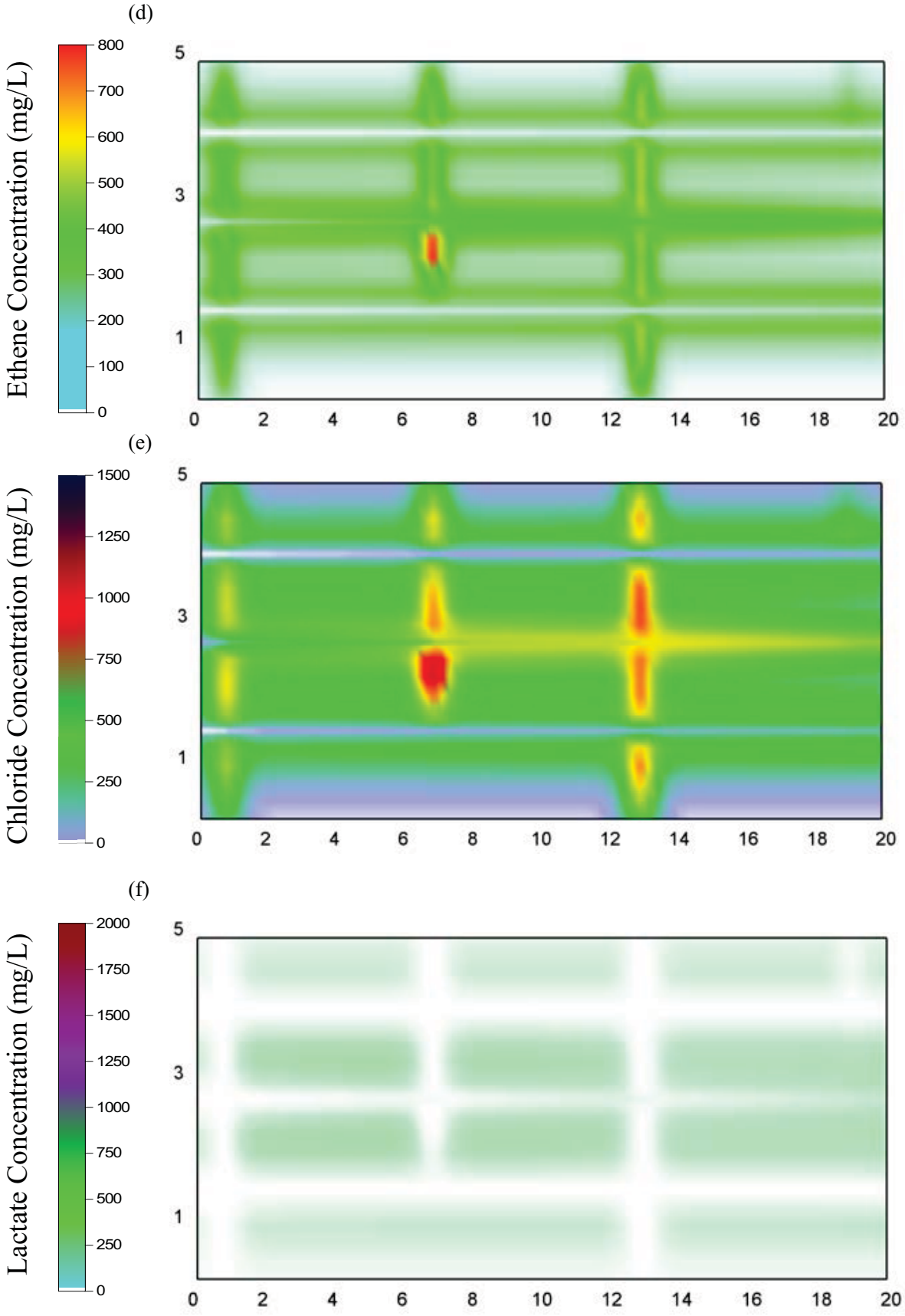

Figure 8: Distribution of aqueous species concentrations at t_{TOTAL} =28 years for Base Case (i.e., 5 years Post-Treatment stage): (a) TCE; (b) 1,1, DCE; (c) VC; (d) Ethene; (e) Chloride; (f) Lactate.

Figure 9 further reveals that the rate of TCE destruction rapidly declines with time: from rapid destruction due to early-time remediation of the fractures to successively lower rates associated with the comingling of organic substrate with chlorinated solvents at successive depths into the matrix. Interestingly, Figure 9 reveals that the rate of TCE destruction appears to be unaffected by termination of the treatment application at the injection well; this underscores that sufficient lactate was present in the matrix during the Post-Treatment stage to continue dechlorination.

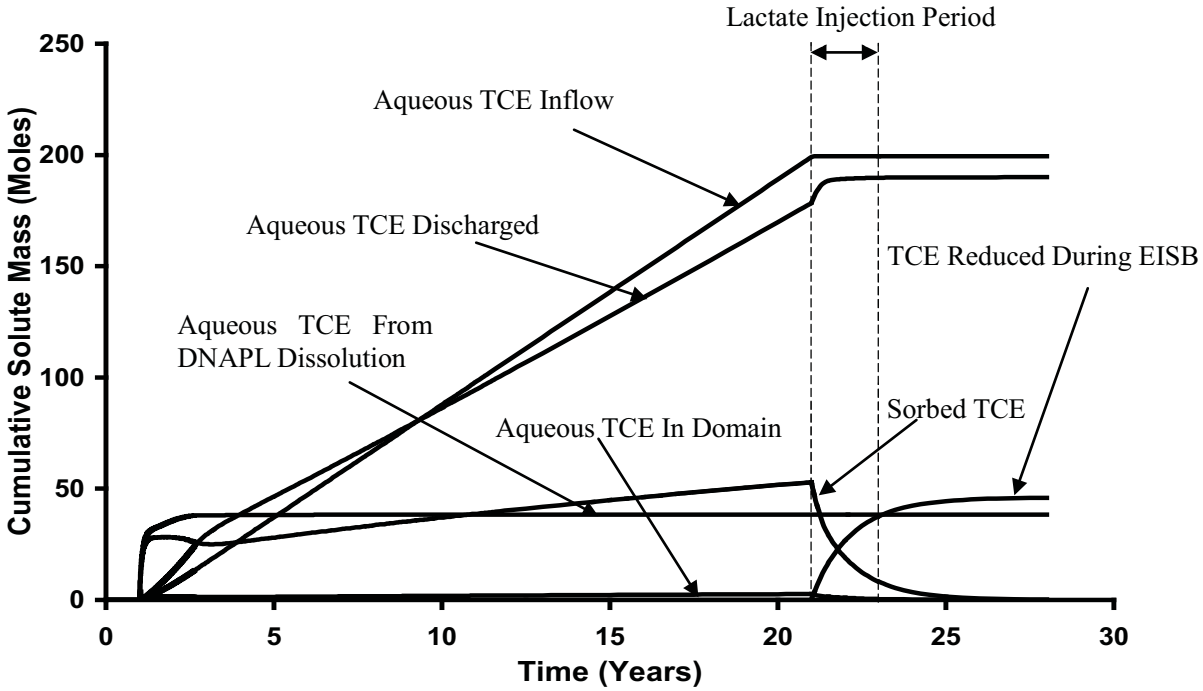

Figure 9: Cumulative aqueous and sorbed TCE from all sinks and sources for base case.

Figure 10 presents the cumulative mass in the domain of the species involved in EISB; note that the time axis originates at the beginning of the Treatment stage. This figure reveals that the rate of chloride being produced during lactate injection period was constant, indicating a steady rate of chlorinated products being reduced. It confirms that this rate was relatively unaffected by the termination of the lactate injection. Analysis

of Figure 10 reveals that of the 7.3 kg of TCE (aqueous plus sorbed) present in the domain at the end of the 20 years Site Ageing stage (t_{TOTAL} = 21 years), approximately 67.6% was successfully converted to daughter products (DCE + VC + ETH) by the end of the treatment period, and 6.03 kg (i.e., 82.6%) was converted by the end of Post-treatment period (t_{TOTAL} = 28 years). Of the TCE mass dechlorinated, 89.0% was converted to ethene.

Figure 10 reveals that reductive dechlorination continues at ever diminishing rates throughout the Post-Treatment period. At t_{TOTAL} = 25.5 years, the chloride and ethene curves reveal that the amount of chloride production was less than the amount being flushed out of the domain. This occurred despite 5.2 moles of lactate and a total of 7.5 moles of chlorinated ethenes still present in the domain at this time. As demonstrated by Figure 8a through c and Figure 8f, the remaining 5.2 moles of lactate in the domain were embedded deep within the matrix while the remaining chlorinated ethenes were present nearer to the fractures. This suggests that while an excess of lactate was injected, matrix diffusion (both forward and reverse) caused a deficiency in electron donor in the matrix near the fractures at late time. It is noted that the lactate, with no sorption or retardation, exhibits a diffusive rate approximately 20 times greater than the chlorinated compounds in sandstone. Thus, it is likely that relatively rapid reverse diffusion of the lactate will result in eventual comingling with the chlorinated ethenes and therefore more complete clean-up in time is theoretically possible.

Figure 11 reveals that of the 545 moles of lactate injected, 91.3% was flushed out of the

domain via advection in the fractures, while only 6.5% was consumed by the TCE, DCE and VC in the domain; the difference (2.2%) remains unreacted, embedded within in the matrix 5-years post-treatment.

Figure 12 presents the total mass discharged at the right-hand boundary of the domain for the Base Case and 'No EISB' simulations. The figure illustrates that the TCE mass discharge decreased dramatically in the 'No EISB' case because (i) the upgradient TCE source was removed, and (ii) the gradient was increased from 0.005 to 0.025. Nevertheless, during the Treatment stage (i.e., t_{TOTAL} = 21 to 23 years), the Base Case exhibited a lower mass discharged than the 'No EISB' at all times by 59% to 71%. Moreover, during the Post-Treatment stage, the 'No EISB' simulation exhibited a low but relatively constant mass discharge associated with reverse diffusion. Meanwhile, the mass discharged in the Base Case during this period was not detectable (i.e., <0.0001 mg/s).

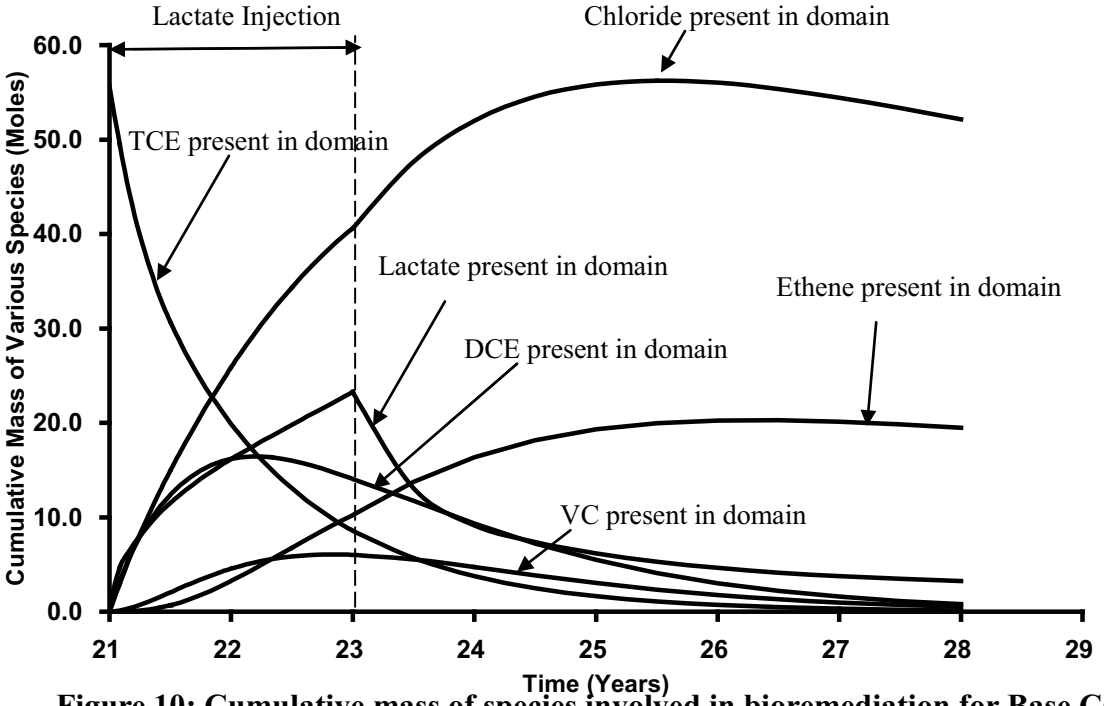

Figure 10: Cumulative mass of species involved in bioremediation for Base Case.

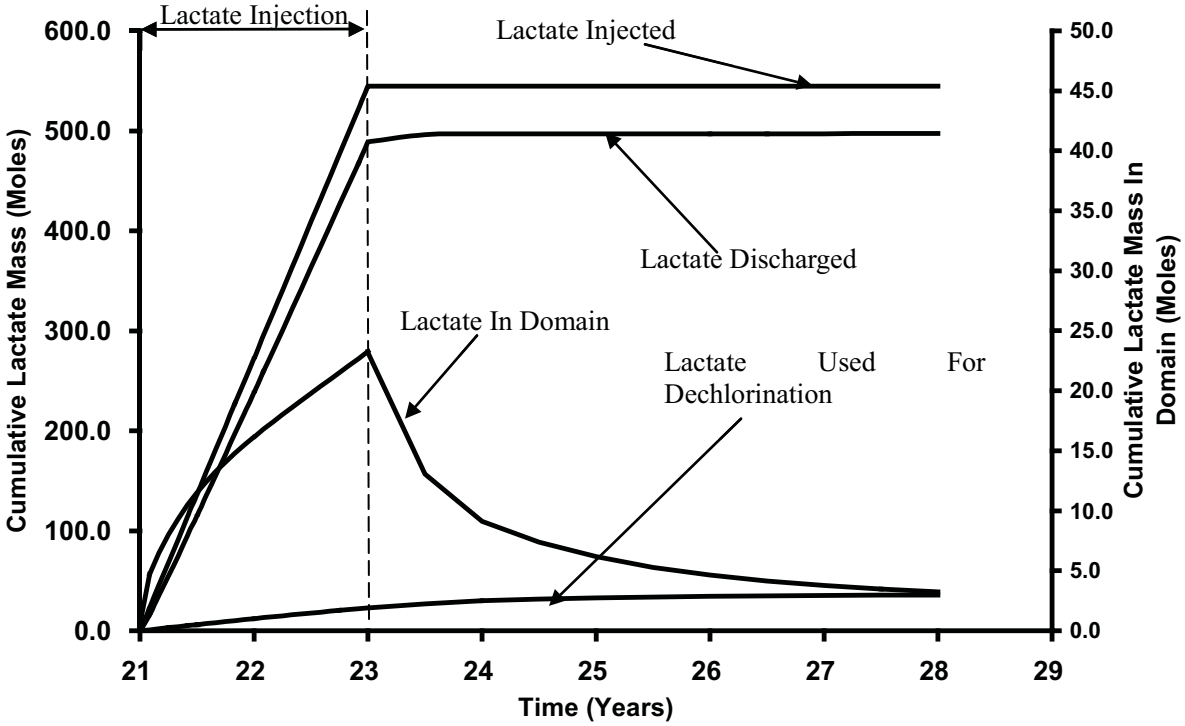

Figure 11: Cumulative mass of lactate involved in bioremediation for Base Case. Note: The plot 'lactate in domain' uses the right axis.

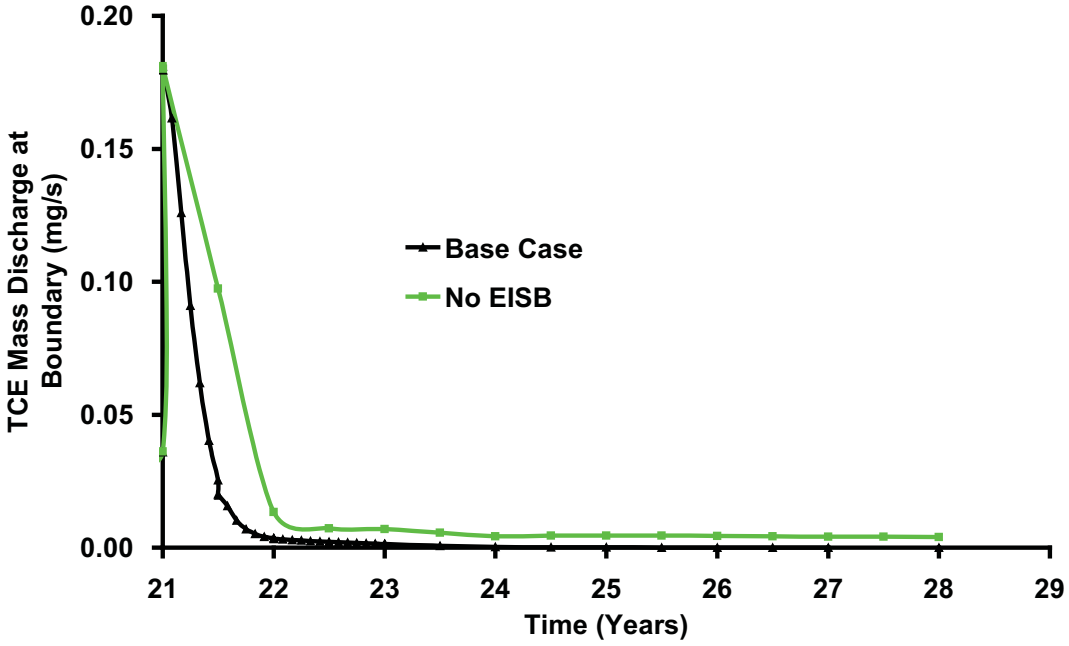

Figure 12: Comparison of total boundary mass discharge (TCE) for base case with a simulation where no lactate was injected.

Figure 13 plots the TCE solute concentration for each of the three horizontal fractures at the downgradient boundary. This figure demonstrates, during the Treatment Stage, that the rapid concentration decrease observed in the larger aperture fractures (e.g., 178μm and 230μm) in the Base Case is indistinguishable from that of the 'No EISB' case. However, for the smallest facture aperture (i.e., 76 μm), considerably lower concentrations are observed in the Base Case since the significant concentrations of TCE emerging from back-diffusion and flushing (in particular, associated with the TCE-loaded dead-end fracture, see Figure 7a) observed in the 'No EISB' case are treated by reductive dechlorination. The difference in downgradient concentrations in the Post-Treatment period is dramatic, with ongoing treatment of back-diffusing TCE (via primarily destruction in the matrix) in the EISB Base Case.

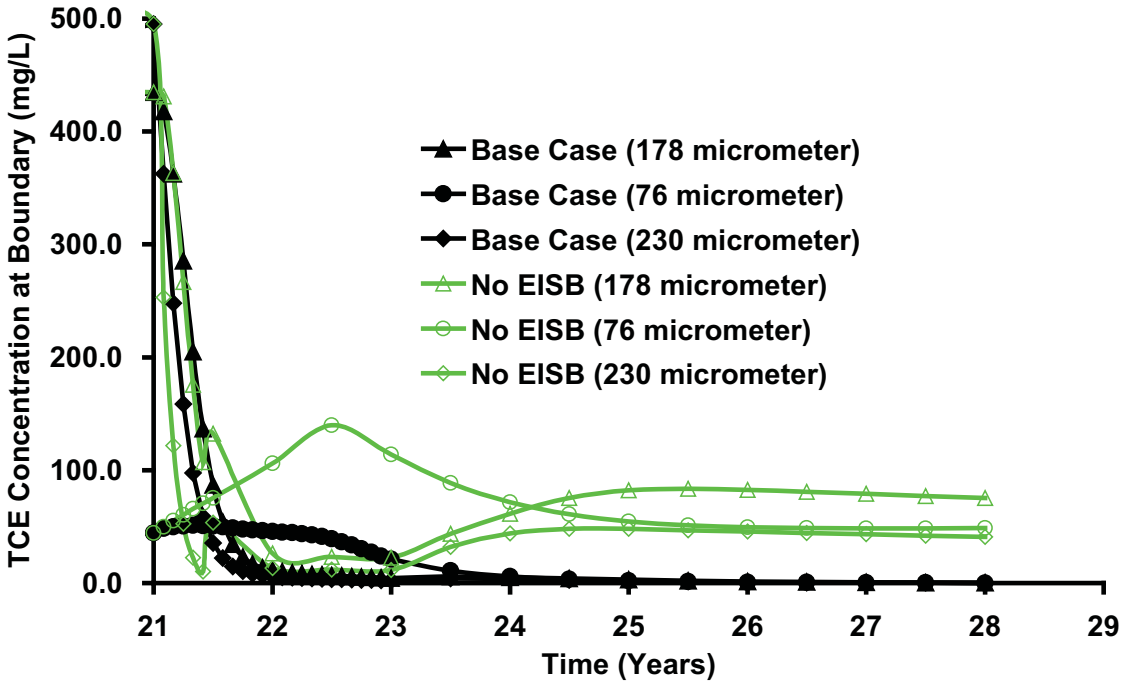

Figure 13: Concentration of TCE in various horizontal fractures at downgradient boundary.

Sensitivity Simulations

In order to compare the impact various parameters have on the effectiveness of bioremediation in fractured rock at the field scale, two metrics were chosen: (i) the total mass of chloride generated, and (ii) total mass of VC dechlorinated to ETH (since accumulation of toxic VC is a significant concern for bioremediation applications).

Sensitivity to Microorganisms in Fractures/Matrix

Figure 14 demonstrates that, despite a similar amount of lactate delivered, the mass of total TCE dechlorinated for microorganisms active in the fractures only (Run 2) is 98.8% less than the Base Case (compare to Figure 10; notice the altered vertical axis for all species except TCE and lactate). As expected, the majority of the dechlorination for Run 2 occurred in the first 6 months of treatment due to direct interaction of TCE and lactate within the fractures. However, such a small fraction of the total TCE is present in the fractures (1%) that even very effective treatment in this region has negligible impact on total mass treated. A small amount of sustained dechlorination is observed in the Post-Treatment period due to back-diffusion of sorbed TCE and coincident back-diffusion of lactate into the fractures. Nevertheless, the total extent of dechlorination, as revealed through chloride production (Figure 15) demonstrates the significantly reduced effectiveness of EISB when microorganisms are not active in the rock matrix. These results are consistent with the concentration distributions of the various species (see Figure B1, Supplementary Information for Run 2, Figure 8 for Base Case), where only 1% of the initial total TCE mass present in the domain was demonstrated to be reduced (Table 5).

Figure 16 demonstrates that, in fact, the TCE mass discharge at the downgradient boundary was very similar for Run 1 and Run 2 during the initial lactate injection period. In both cases, a more rapid decrease than the 'No EISB' case in the first 6 months was observed associated with mass destruction in the fractures. However, in the Post-Treatment period the TCE mass discharged (as revealed in Table 5) in the 'fracture bioremediation only' simulation is only slightly lower than the 'No EISB' case, revealing the inability to effectively treat back-diffusing TCE mass. This is because during the Post-Treatment period, the rate of bioremediation is limited by the back-diffusion rate of lactate from the matrix. A similar conclusion is obtained by examining the downgradient concentration at each horizontal fracture (Figure 17).

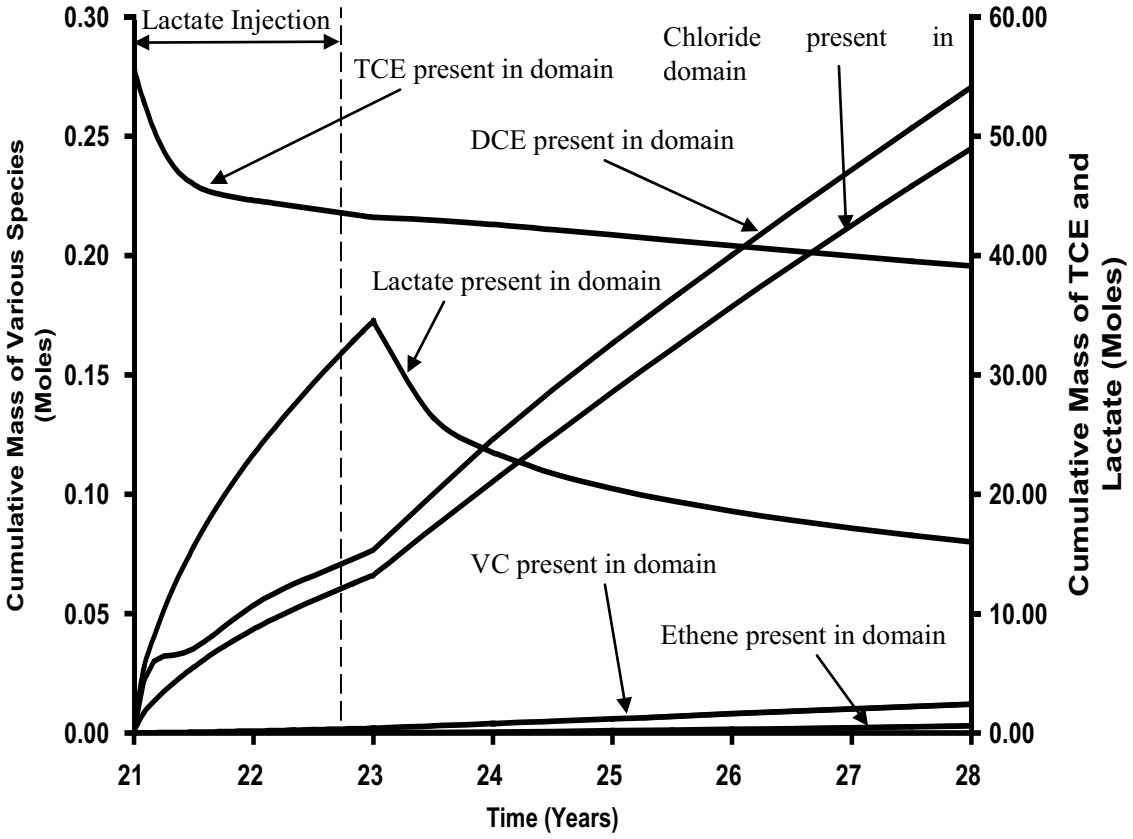

Figure 14: Cumulative mass of species involved in bioremediation for the case when indigenous bacteria is only present in fractures.

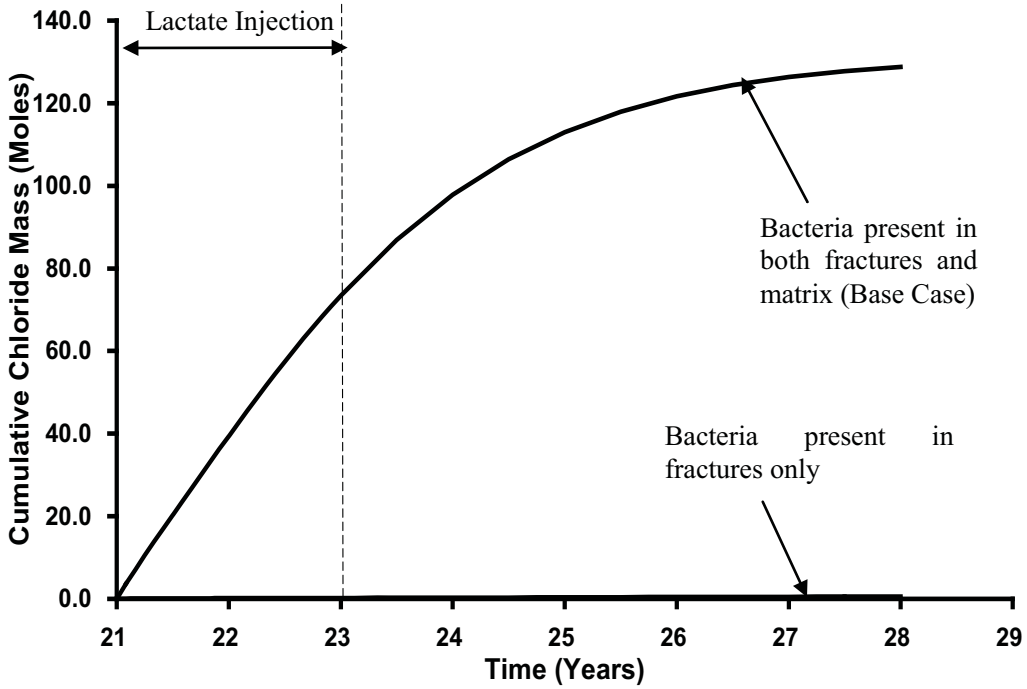

Figure 15: Cumulative mass of chloride produced for microorganisms active in the matrix and fractures (base case) versus in fractures only (Run 2).

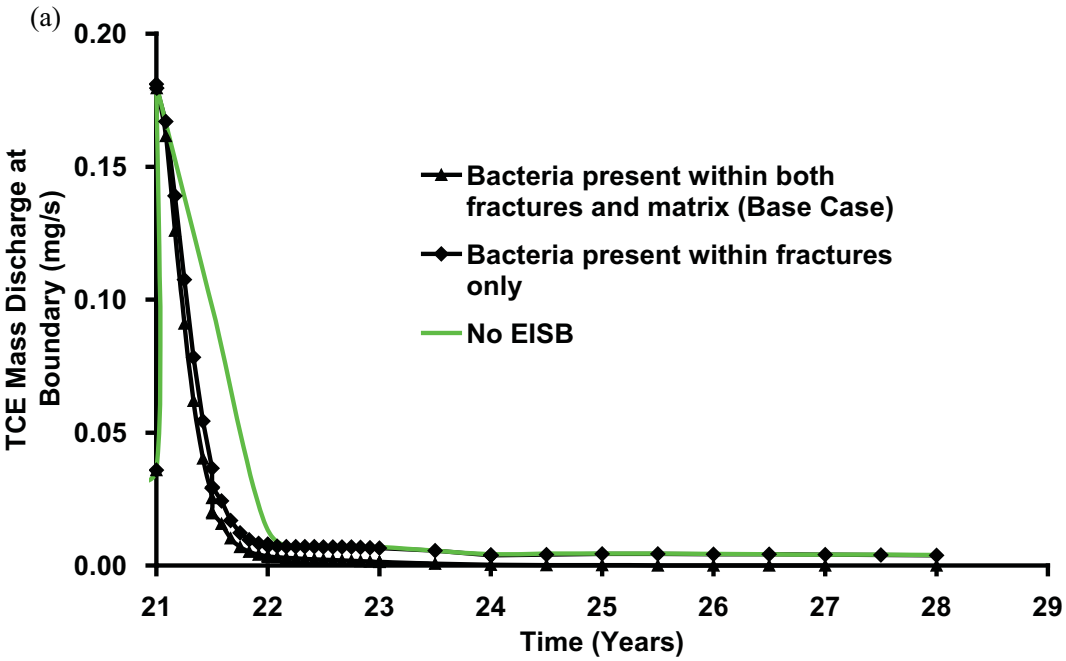

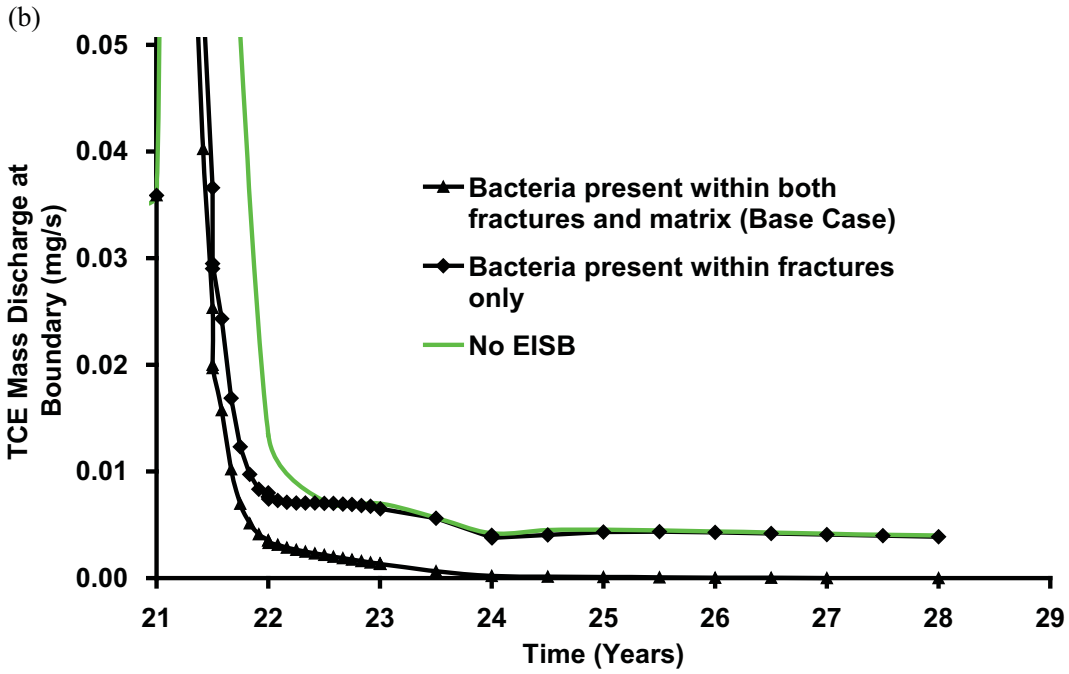

Figure 16: Comparison of total boundary mass discharge (TCE) for base case with (a) bioremediation within fractures only and (b) since the start of the Treatment Stage only (timescale expanded for clarity).

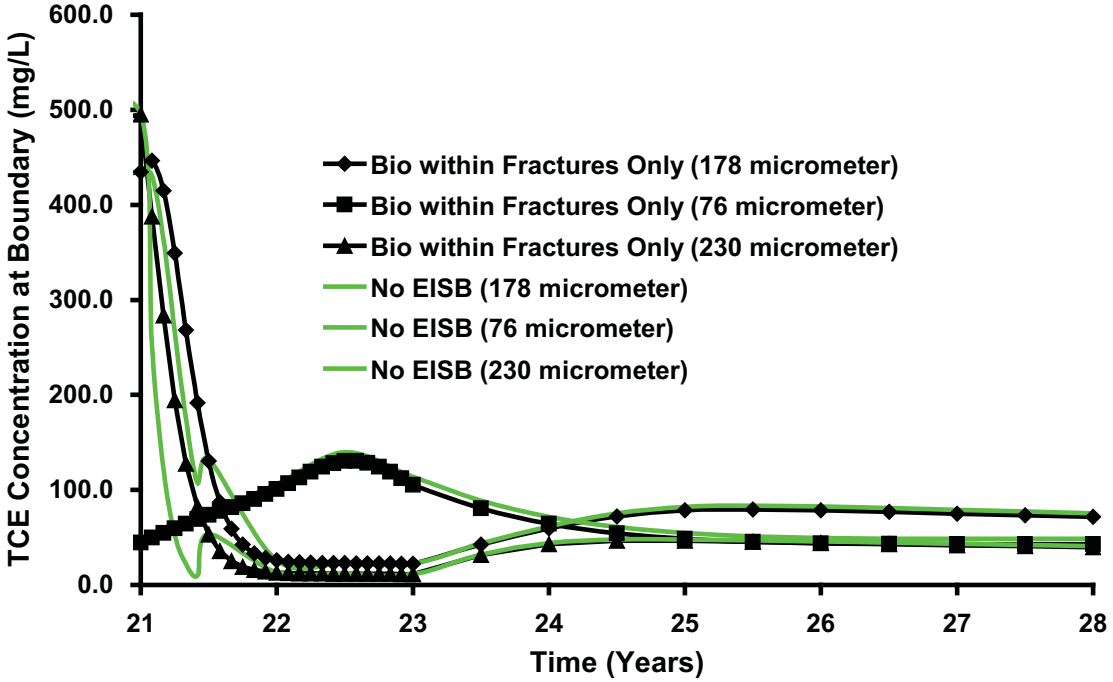

Figure 17: Concentration of TCE in various horizontal fractures at downgradient boundary for bioremediation within fractures only.

Sensitivity to Dechlorination Rate Parameters

As demonstrated in Figure 18, the total extent of dechlorination (as measured by the mass of chloride being produced) is highly sensitive to the first-order decay rate parameters. For example, when the decay rate parameters were increased by one order of magnitude (Run 3), all anaerobic dechlorination ceased approximately one year after lactate injection began. Figure 19a, plotting the cumulative mass of the key species in the domain for this simulation, illustrates that all the chlorinated products in the domain have been reduced to non-detect after one year. In contrast, when the decay rates were lowered by one order of magnitude, chloride production and ethene slowed dramatically (Figure 18 and Figure 19b). The total mass of chloride produced during the Treatment and Post-Treatment period was 150, 129 and 25 moles and the total mass of TCE reduced was 52.3, 45.9 and 18.7 moles for the high, median (Base Case) and low decay rates, respectively. This indicates that the overall bioremediation efficiency was more sensitive to decreases in decay rates than increases for this scenario; this is likely due to the fact that the Base Case already exhibited such a high degree of remediation. Concentration distribution images for the key species support these findings (Figure B2, Supplementary Information).

Figure 19b further reveals that the cumulative mass of the daughter-products of TCE is on the increase by the end of the simulation; indicating that dechlorination is still taking place within the domain at late times.

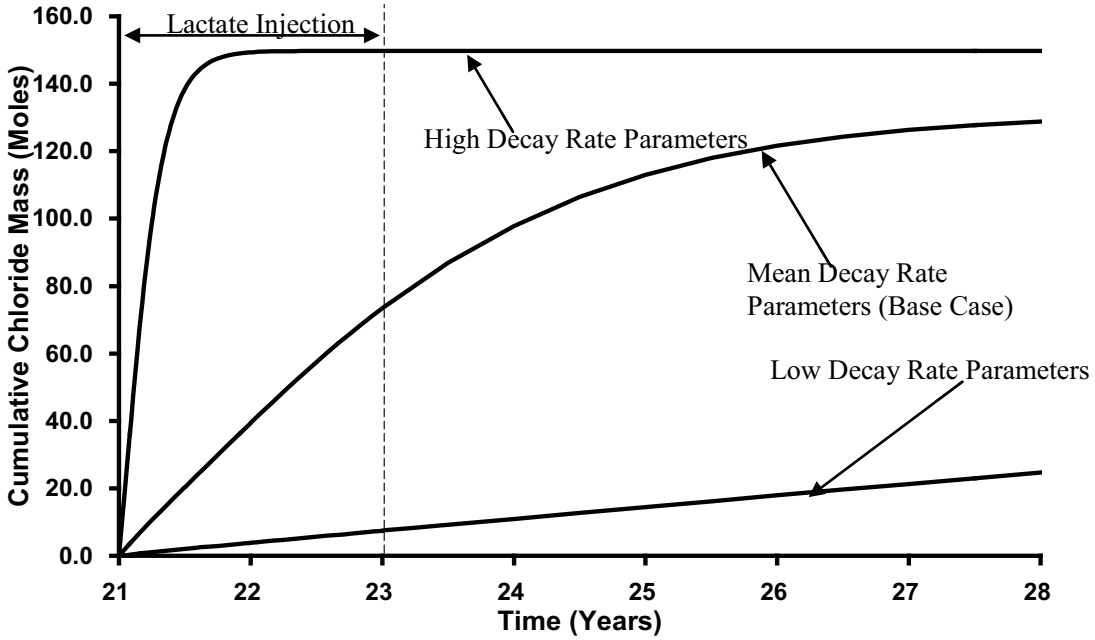

Figure 18: Cumulative mass of chloride being produced over time for different decay rate parameters.

Figure 20 reveals the TCE mass discharged for the high reaction rates simulation was reduced to non-detect by 6 months of treatment. In contrast, the mass discharged in the low reaction rates simulation is very similar to the 'No EISB' simulation after the first year of treatment. It is noted that there is sufficient amount and distribution of lactate through the subsurface (see Figure B2, Supplementary Information) but that the contact time – even in the diffusion limited matrix – is too low relative to the reduced dechlorination rates for effective treatment.

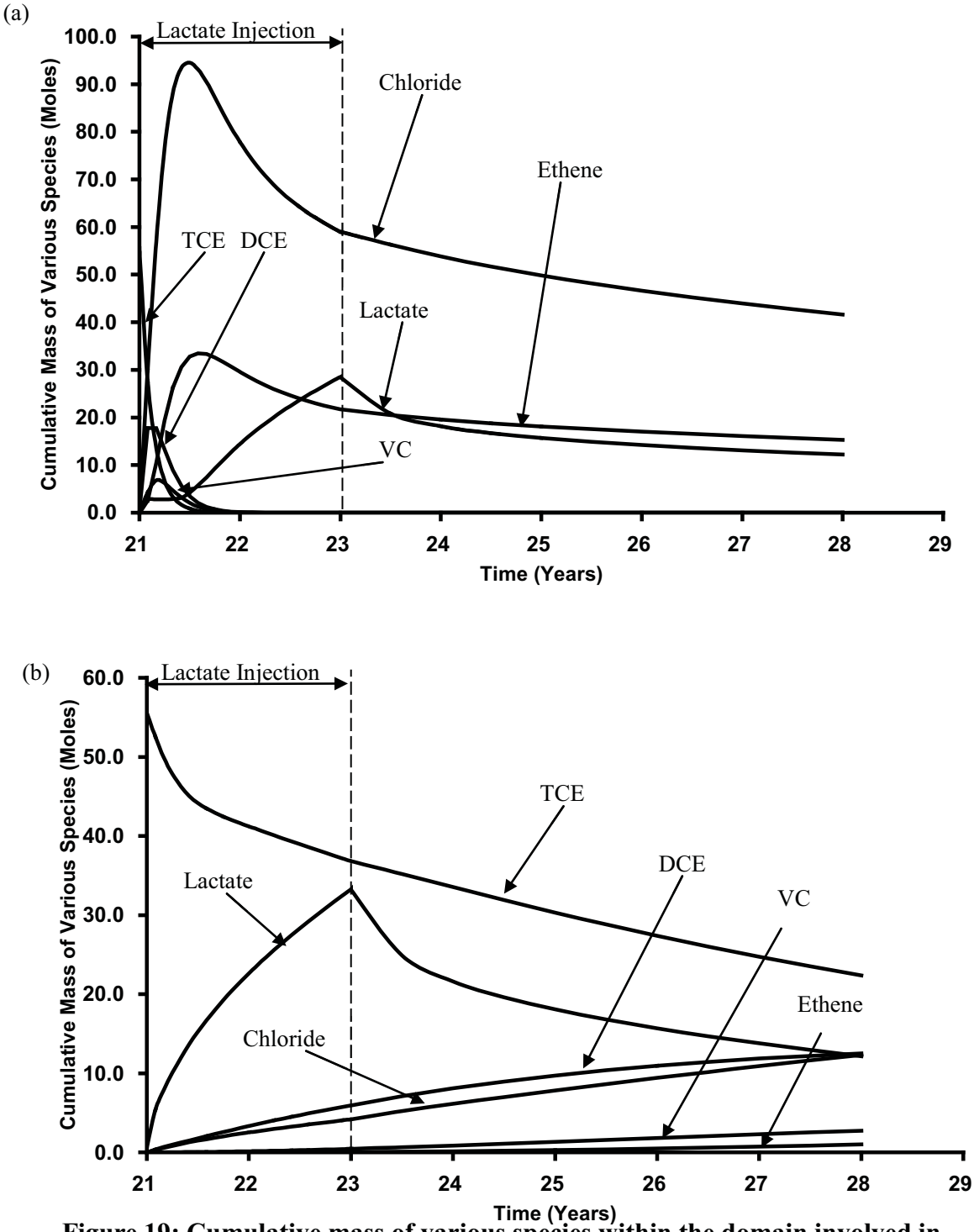

Figure 19: Cumulative mass of various species within the domain involved in (a) high decay rate and (b) low decay rate parameters over time.

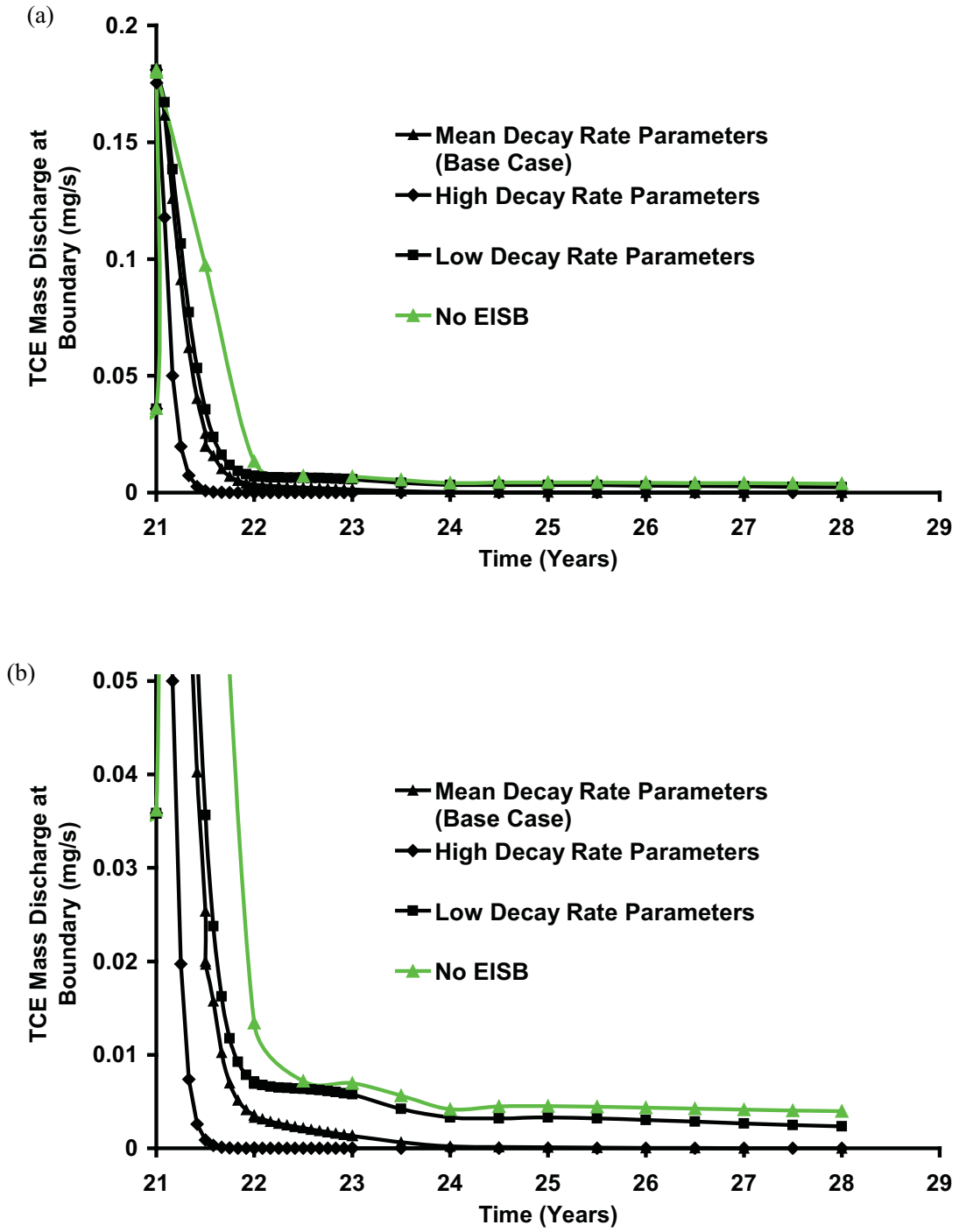

Figure 20: Comparison of total boundary mass discharge (TCE) for base case with (a) various decay rates (b) since the start of the Treatment Stage only (timescale expanded for clarity).

Sensitivity to Pulsed Injection of Organic Substrate

As demonstrated in Figure 21 and 22 the total masses of chloride and ethene produced at the end of the Post-Treatment period for these simulations and their spatial distribution (Figure 8 and Figures B5, B6 and B7 in Supplementary Information) were indistinguishable. Furthermore, Figure 23 illustrates no significant difference in TCE mass discharge was observed for the three cases. The distribution of lactate in this scenario (and thus the extent of dechlorination) is insensitive to pulsing since it remains in excess. It is recognized that, in reality, pulsing may have advantages not observed in this work such as allowing the dissipation of acids so as to recover near-neutral pH, reducing bioclogging, etc. However, with respect to effectively distributing the lactate in a biologically active fractured sandstone, these simulations suggest no significant influence.

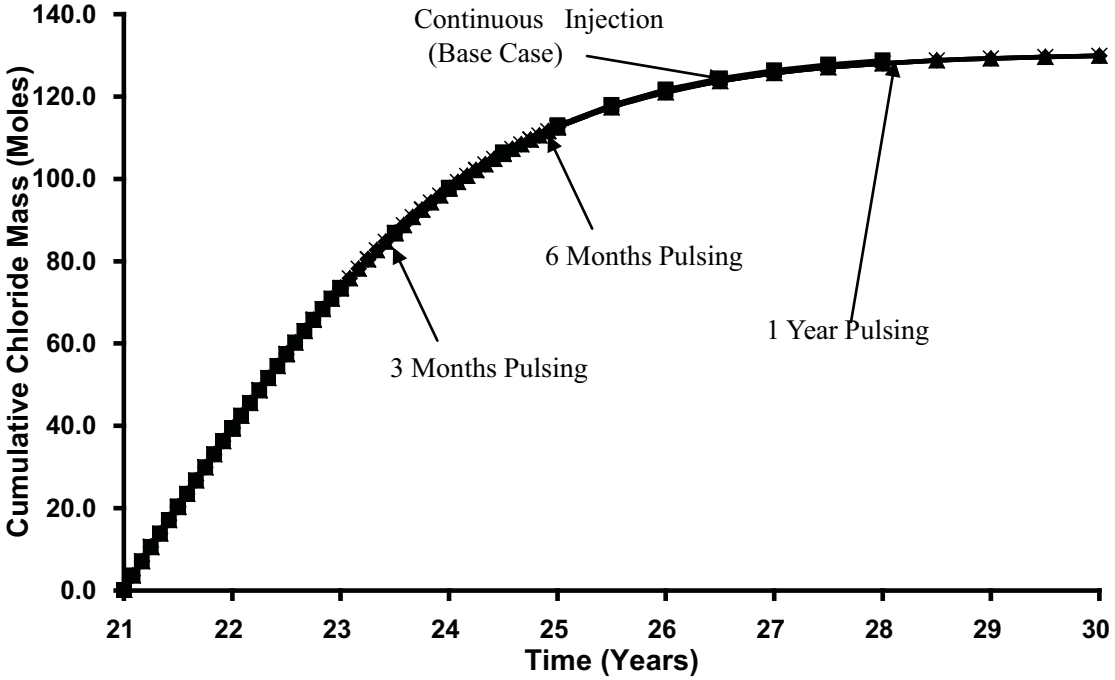

Figure 21: Cumulative mass of ethene being produced over time for different pulsing method.

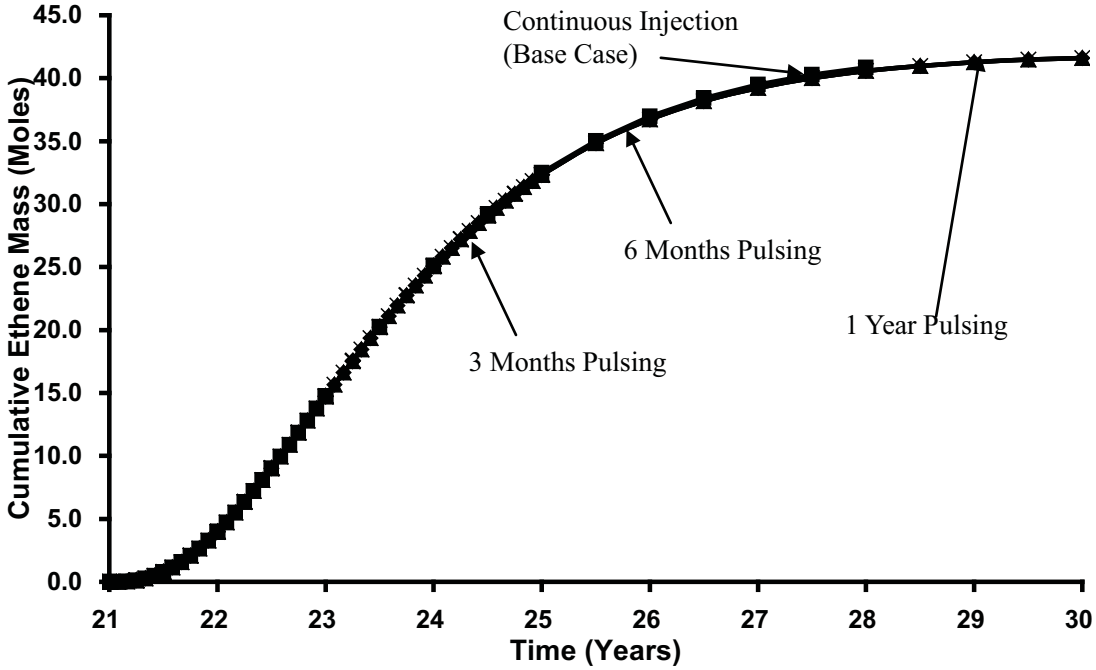

Figure 22: Cumulative mass of ethene being produced over time for different pulsing method.

(a)

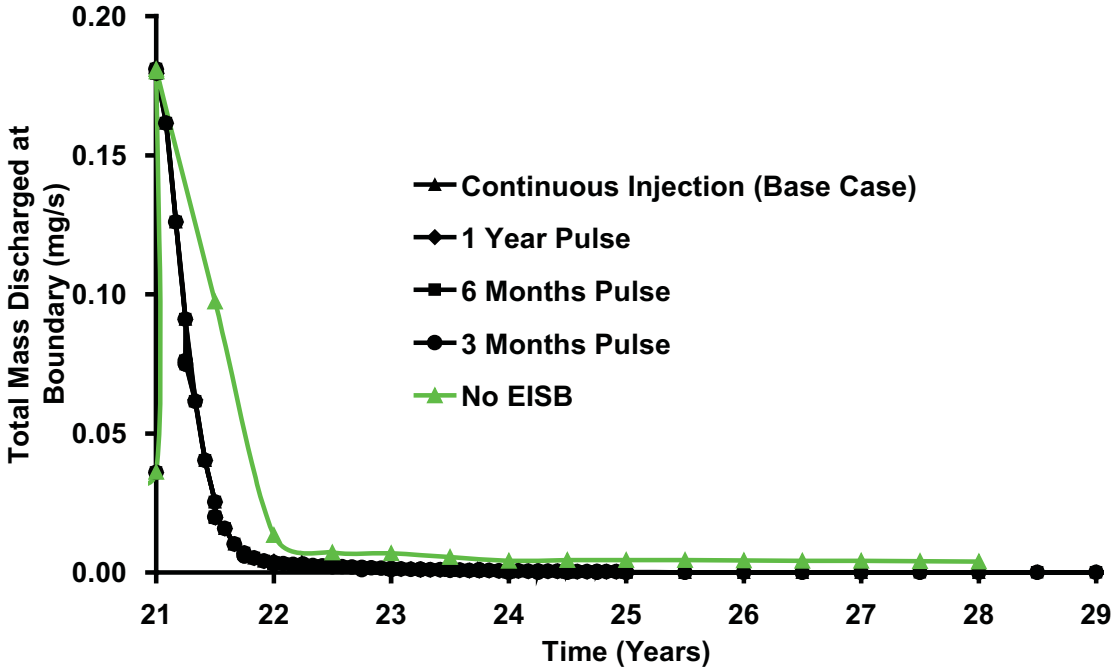

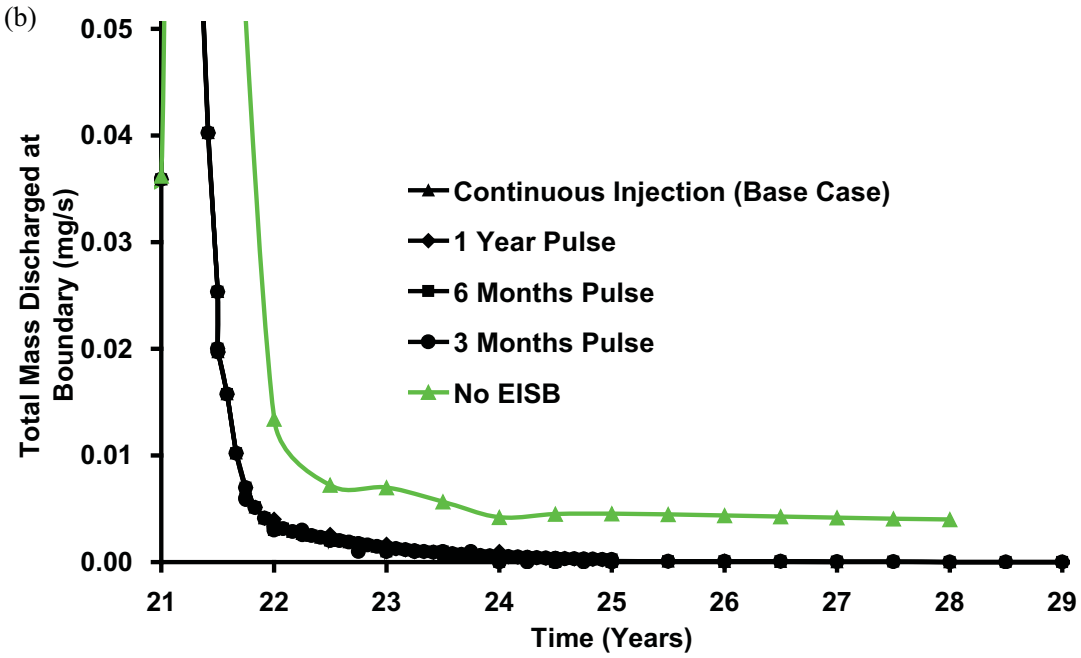

Figure 23: Comparison of total boundary mass discharge (TCE) for base case with (a) various pulsing methods (b) since the start of the Treatment Stage only (timescale expanded for clarity).

Sensitivity to Organic Substrate Concentration

Figure 24, plotting the cumulative mass of chloride produced for 4 g/L, 2 g/L, and 1 g/L (Runs 8, 1, and 9, respectively), reveals that the lactate concentration had virtually no effect on the remediation efficiency (give that the time of injection was adapted to ensure equal total mass injected in each case). Moreover, the amount of each chlorinated ethene transformed with time was essentially identical (Figures B8 and B9, Supplementary Information). Moreover, the distribution of the key species were essentially identical in all three cases at the end of the Post-Treatment stage (Figure 8, and Figures B8 and B9, Supplementary Information).

Figure 25, plotting the cumulative mass discharge of lactate at the downgradient boundary for the three simulations, reveals that, regardless of the concentration injected,

an equivalent total mass exits the domain and, therefore, an equivalent mass penetrates the matrix in all three cases. The fraction of the total moles of lactate that exited the domain relative to that injected is 91.5% in all three cases. Furthermore, no significant difference in the simulations was observed for TCE mass discharge (Figure 26) or TCE distribution (Figures B8 and B9, Supplementary Information). These plots illustrate that the ability of lactate to diffuse throughout the rock matrix was equivalent and substantial in all three cases; clearly the lack of matrix sorption for lactate was critical in this regard and as a result, sensitivity to the concentration gradient from the fractures to the matrix was low (at least at the relatively high concentrations injected here). The results further indicate that the lactate was always in excess, even in the lowest concentration case, and thus the first-order rate constants were likely the factors that limited complete clean-up in these cases.

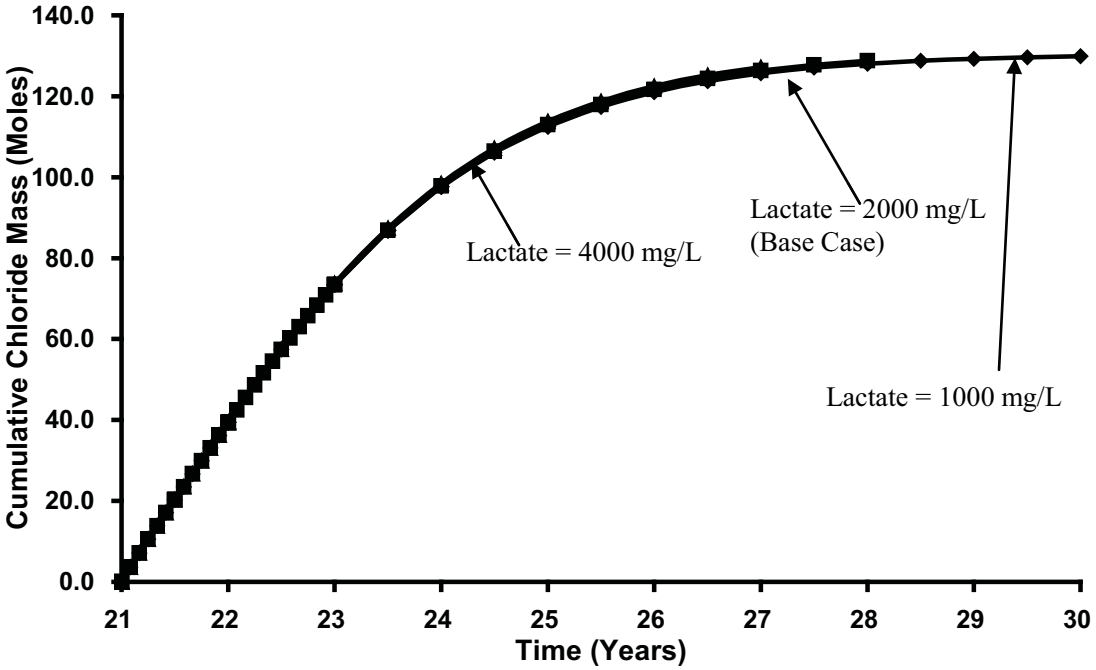

Figure 24: Cumulative mass of chloride being produced over time for different injected concentration.

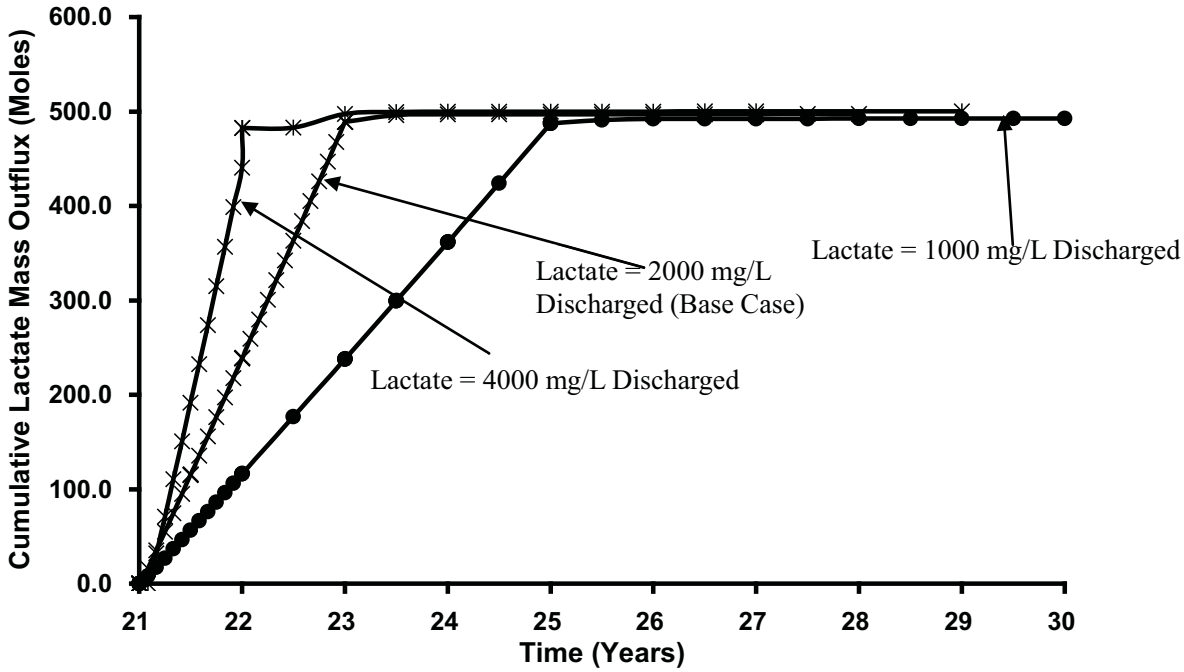

Figure 25: Cumulative mass of lactate discharged over time for different injected concentrations.

(a)

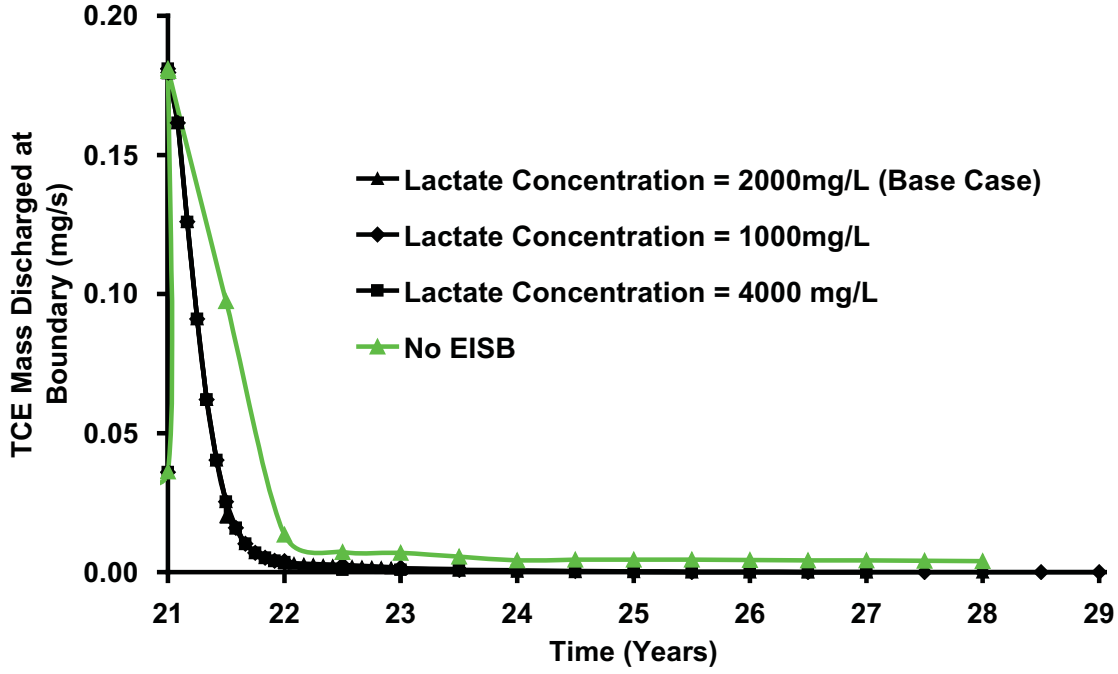

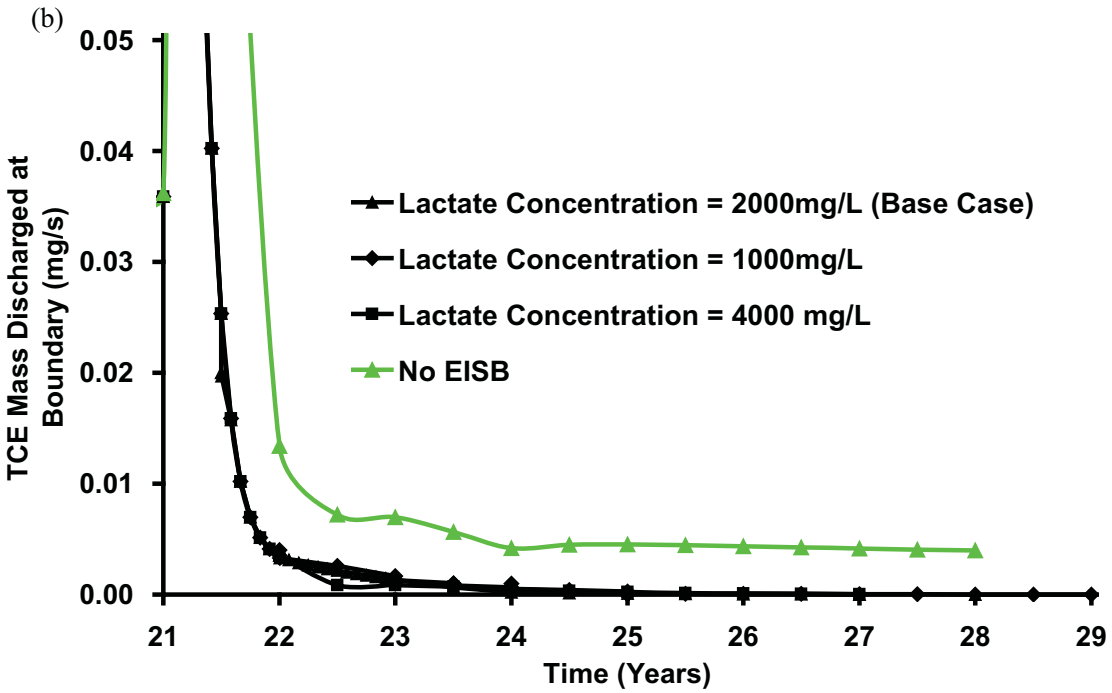

Figure 26: Comparison of total boundary mass discharge (TCE) for base case with (a) various lactate concentration (b) since the start of the Treatment Stage only (timescale expanded for clarity).

Sensitivity to Rock Type

At the end of the DNAPL Infiltration stage, the average DNAPL saturation was 0.75, the volume of DNAPL in the domain was 0.008 m^3, 0.01 m^3 and 0.018 m^3 for sandstone, shale and granite with 100% of the invaded nodes on drainage for all 3 rock types. At the end of the DNAPL redistribution stage, the average DNAPL saturation was 0.3 for all 3 rock types, the volume of DNAPL was 0.0036 m^3 , 0.0047 m^3 and 0.0079 m^3 while the pool to residual ratio was 71:29%, 72:28% and 90:10% for sandstone, shale and granite respectively. The distributions of TCE DNAPL at the end of the redistribution stage for each rock type are illustrated in Figure 4.3 and Figure A6, Appendix A.

At the end of the 20 years Site Ageing stage (t_{TOTAL} = 21 years) the total mass of aqueous

and sorbed TCE in the domain was 7.3 kg (55.6 moles), 6.8kg (50.8 moles) and 0.68 kg (5.08 moles) for sandstone, shale and granite respectively. In each case, 97-99% of the total mass resided in the matrix, of which 97-98% was sorbed and only 1-2% remained in the aqueous phase. Although no DNAPL was left in the sandstone and shale domain at this time, 4.23 kg of DNAPL was found present in the granite domain. This observation is consistent with the findings in Parker e al. (1994) where it was suggested that due to the low porosity in granite, DNAPL could remain present in the fractures for decades. Figure 27 illustrates the distribution of aqueous phase TCE in sandstone, shale and granite at the end of the 20 year Site Ageing stage. In each case, the matrix immediately surrounding the fractures exhibits diffusion halos of TCE. However, given that the matrix is homogeneous, the depth and extent of TCE penetration of the matrix is observed to be highly dependent on properties of both the fractures and the matrix for each rock type. The combination of these impacts residence time of TCE in the source zone and it is the relative rates of TCE transport through fractures versus diffusion to the matrix that affects the final distribution of mass.

Figure 28 demonstrates that the mass flux of TCE out of the right boundary of the domain during the Site Ageing stage follows the order granite > shale > sandstone. The vertical axis of Figure 29 demonstrates that the percentage of initial TCE mass retained in the domain at the end of Site Ageing follows the order sandstone > shale > granite. These two results, mass lost to advection versus mass retained via sorption, reflect the overall balance of residence time versus matrix diffusion (See section 4.5.2.3 for calculations and further details). Peclet number (Pe) for fractured rock is defined as the ratio of

advection to diffusion rates, Pe = ve/($D^o\tau$), where v is the advective velocity in

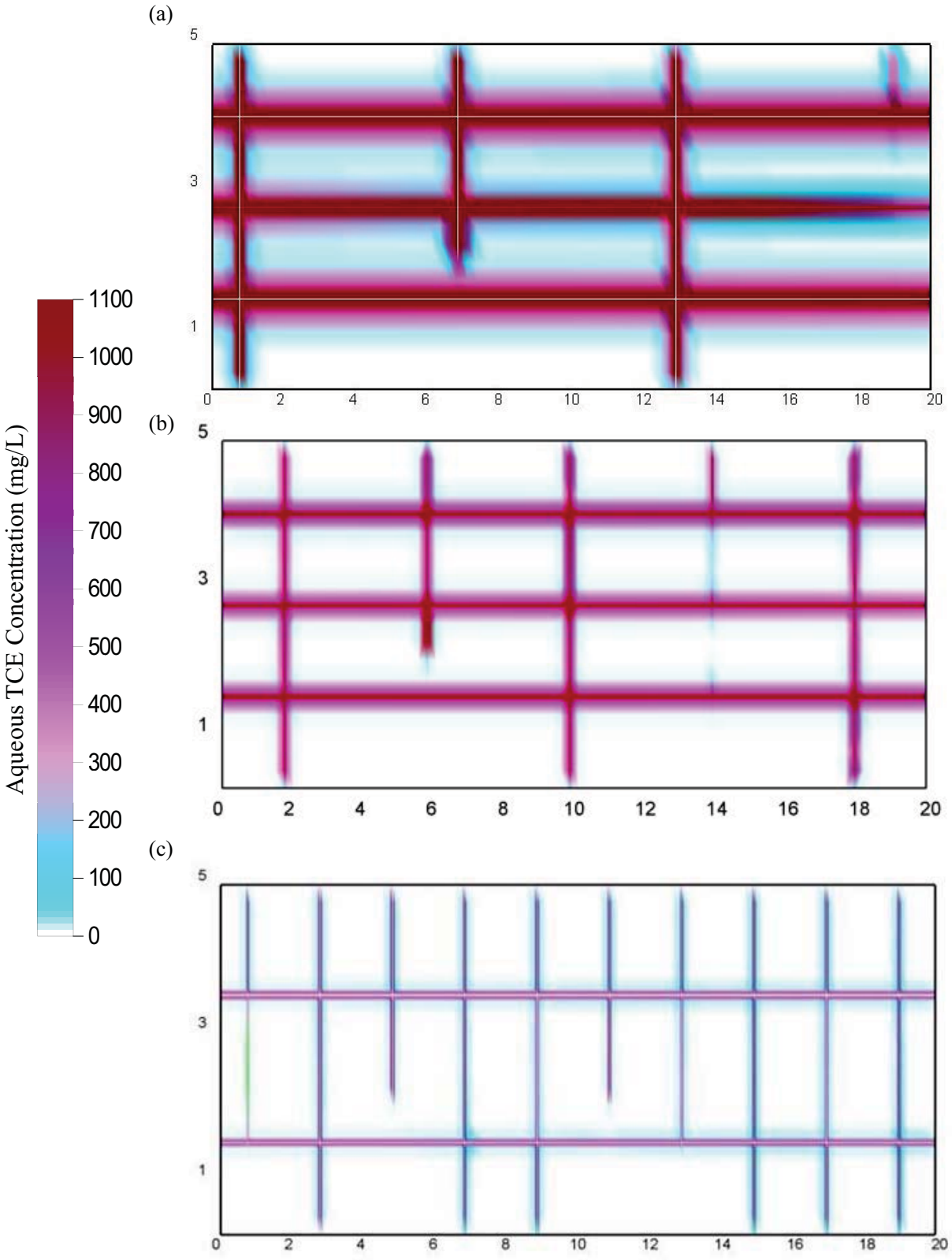

Figure 27: Distribution of aqueous TCE after 20 years (t_{TOTAL} = 21 years) of DNAPL dissolution (i.e., Site Ageing stage) in (a) Sandstone, (b) Shale and (c) Granite.

the fracture, e is the mean aperture, D^o is the free solute diffusion coefficient and τ is the matrix tortuosity (e.g., Fetter, 1993). Here v is taken as the mean horizontal advective velocity across each domain and e is the mean aperture of all horizontal fractures for each rock type. Figure 29 reveals that the percentage of TCE retained (in aqueous and sorbed forms) exhibits a linear dependence on the log(Pe) for the three rock types ($R^2 = 0.9923$) at the end of the Site Ageing stage (i.e., $t_{TOTAL} = 21$ years). This confirms expectations that lower Pe (i.e., lower advective velocity, smaller apertures, higher effective diffusion) corresponds to increased matrix diffusion (e.g., sandstone) while higher Pe corresponds to increased mass loss via advection (e.g., granite).

(a)

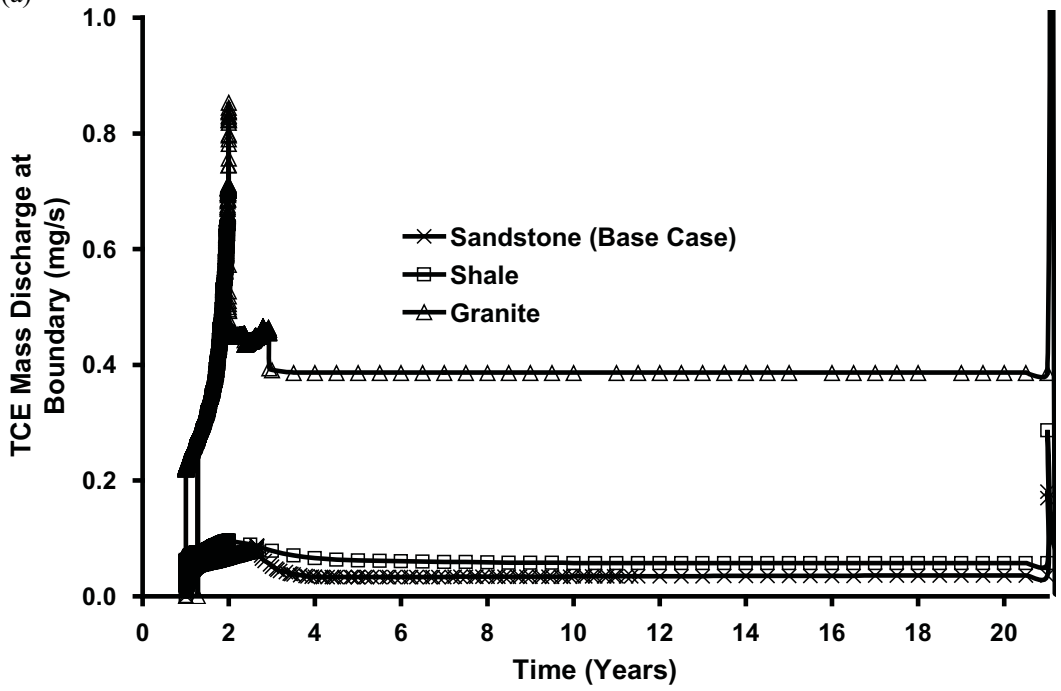

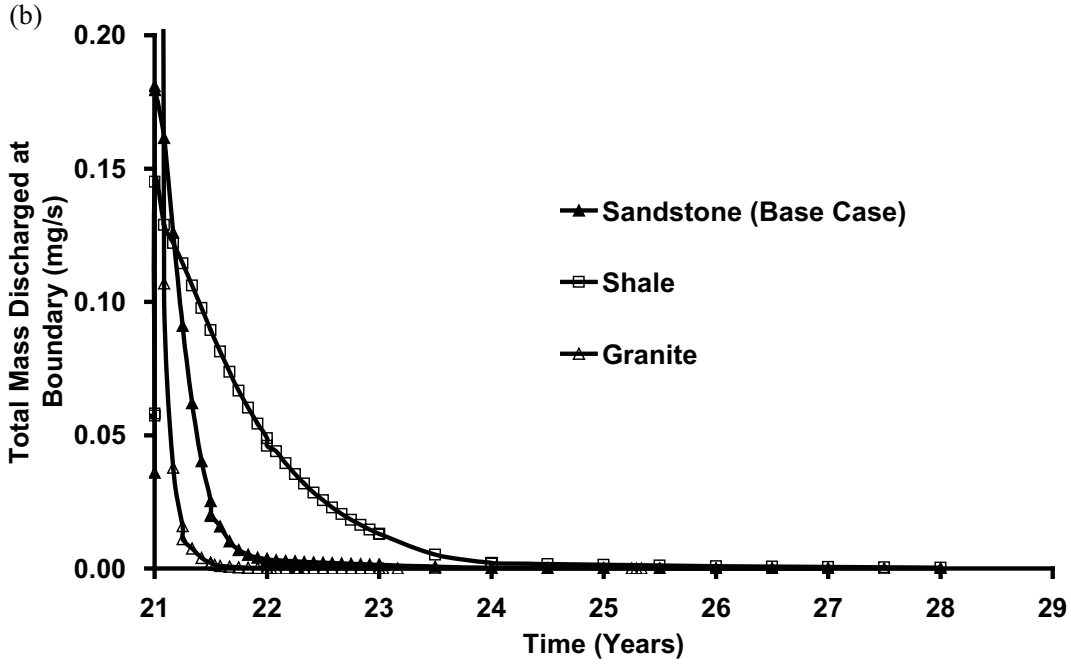

Figure 28: Comparison of total boundary mass discharge for different rock types; (a) from the beginning of the simulation to end of Site Ageing stage and (b) Treatment stage only (timescale expanded for clarity).

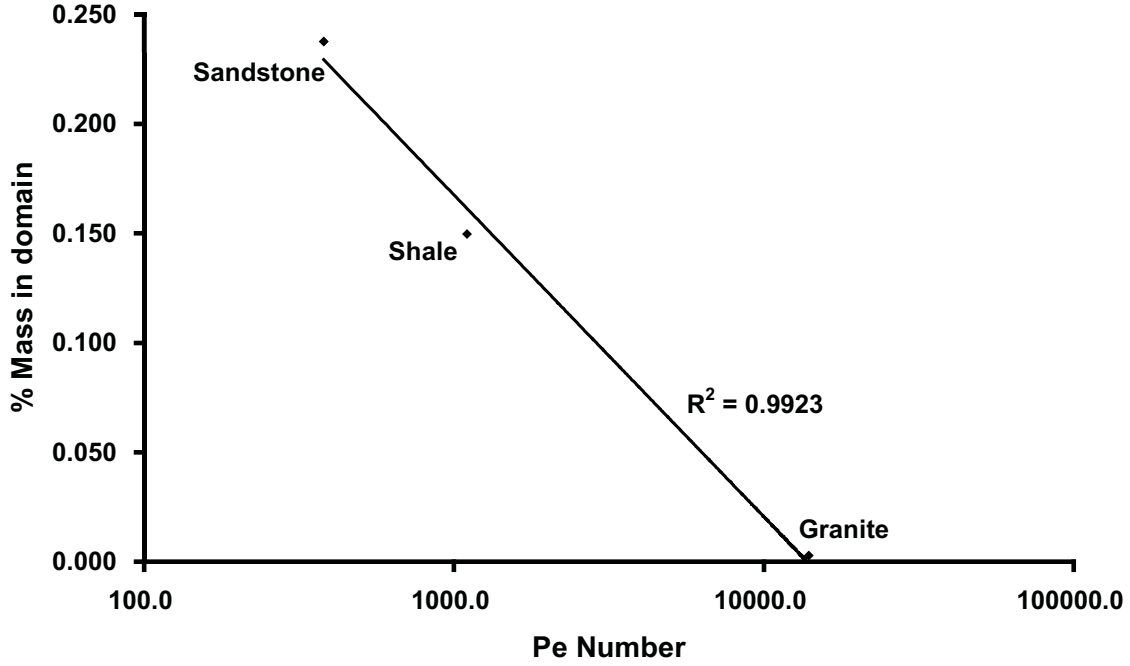

Figure 29: Mass of aqueous and sorbed TCE in various rock domains at end of Site Ageing stage (i.e., t_{TOTAL} = 21 years) vs. Peclet number (log scale) for each individual domain.

During the Treatment stage, 48.5 kg (545 moles), 35.1 kg (394 moles) and 436.3 kg (4900 moles) of lactate were injected into the domain for sandstone, shale and granite respectively (Table 5). The amount of lactate injected is equivalent to 9.8 times, 7.8 times and 964.6 times greater than the theoretical lactate mass required to dechlorinate all the TCE in the domain at the start of the Treatment stage. The differences in lactate mass injected are due the differences in bulk effective horizontal hydraulic conductivity while treatment period, injection concentration and hydraulic gradient were all held constant.

If all TCE present in the domain at the start of the Treatment stage was successfully reduced to ethene, the total mass of chloride produced would have been 166.8 moles, 152.4 moles and 15.24 for sandstone, shale and granite respectively. Figure 30 revealed the total moles of chloride produced were 128.8 moles, 36.8 moles and 0.06 moles for sandstone, shale and granite respectively. Thus, the efficiency of reductive dechlorination in the three rock types were 77.2%, 24.1% and 0.4% for sandstone, shale and granite respectively.

Figure 30 further revealed that the total moles of ethene produced were 40.8 moles, 5.67 moles and 0.0003 moles for sandstone, shale and granite respectively by the end of the simulations. These masses when compared to the TCE mass present in the domain at the start of the Treatment stage, revealed 73.5%, 11.2% and 0.006% of the initial mass has been successfully reduced to ethene.

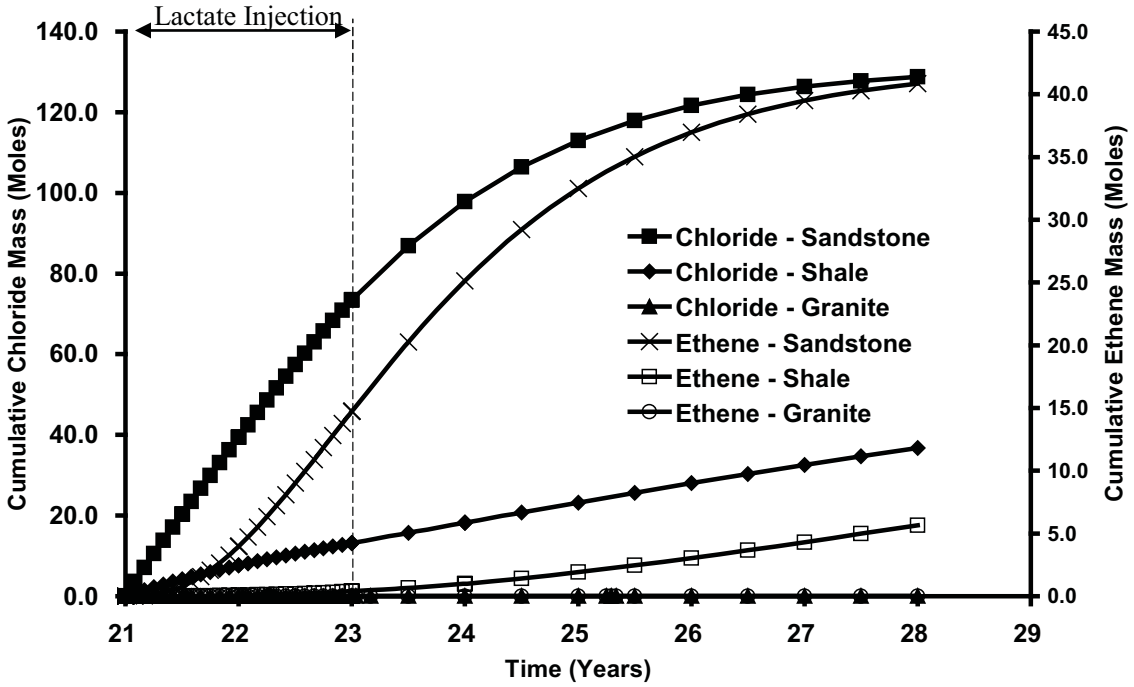

Figure 30: Cumulative mass of chloride and ethene produced over time for different rock types.

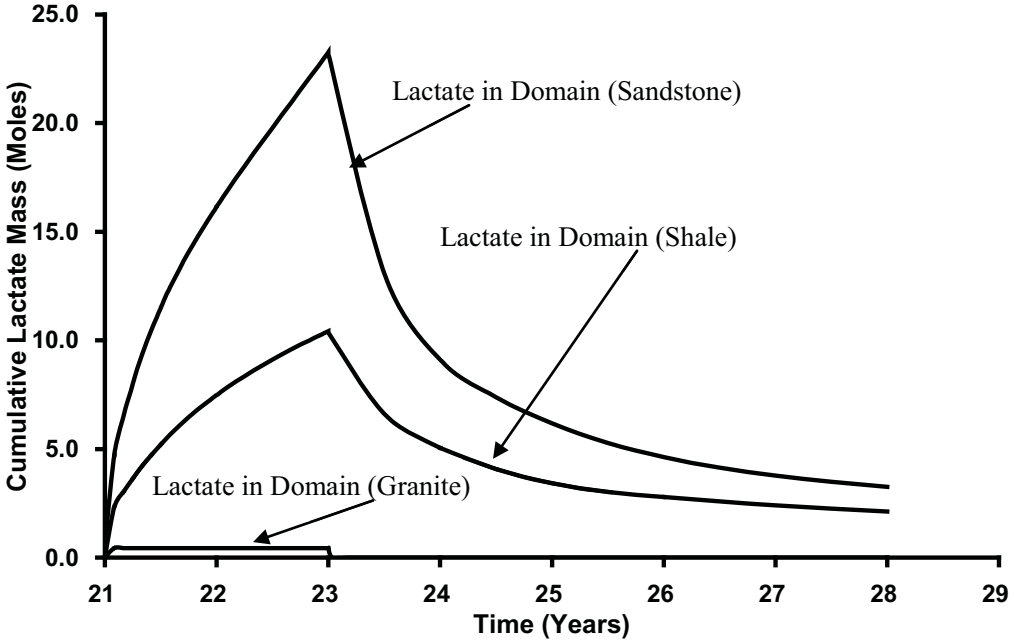

Figure 31: Cumulative mass of lactate present in the domains over time.

Figure 31 demonstrated that once the lactate injection ceased at t_{TOTAL} = 23 years, the cumulative mass of lactate present in the three rock domains began to decrease until the end of the simulation (i.e. t_{TOTAL} = 28 years). Correspondingly, the efficiency of EISB was found to be inversely related with the average Pe for each rock type. With higher Pe (i.e., higher advective velocity - granite), diffusion into the matrix is diminished relative to advection through the factures. Since TCE experienced forward diffusion for 20 years while lactate only has 2 years to penetrate the matrix, Pe has a significant impact on increasing the spatial distribution of lactate in the sandstone versus the granite domain.

Sensitivity to DNAPL Type

In this study, results were compared between PCE and TCE; in contrast to the previous simulations, the distribution of DNAPL at the start of the Site Ageing stage was not identical. At the end of the DNAPL Infiltration stage, the average DNAPL saturation was 0.75 while the volume of DNAPL in the domain was 0.008 m^3 (compared to a total fracture volume of 0.012 m^3) with 100% of the nodes in drainage in both simulations. At the end of the DNAPL redistribution stage, the average DNAPL saturation was 0.3 for both TCE and PCE , the volume of DNAPL present was 0.0036 m^3 (5.26 kg) and 0.0037 m^3 (6.03 kg), and the pool to residual ratio was 71:29% and 51:49% for TCE and PCE, respectively (Figures 5 and A14 of Appendix A respectively). The higher density of PCE, leading to higher mobility and more DNAPL migration out of the bottom of the domain, is most likely the cause of the reduced pool-to-residual ratio in that case.

At the end of the Site Ageing stage (t_{TOTAL} = 21 years) the total mass of TCE and PCE in

the domain was 7.3 kg (55.6 moles) and 3.3kg (20.2 moles) respectively. As demonstrated by Figure 33, the PCE DNAPL was almost completely dissolved after 16 years of Site Ageing (t_{TOTAL} = 17 years), as compared to only 2.5 years for TCE (Base Case, Figure 9). One reason for this is the lower solubility of PCE (Table 4). Another reason is that the PCE DNAPL in the fractures caused reduced relative permeability to water; in conjunction with a fixed gradient, this caused reduced water flux through the source zone. Figure 32 confirms that identical boundary conditions resulted in considerably different time series of water discharge (m^3/s) at the exit boundary. Both simulations experience increasing water discharge as DNAPL dissolves until the maximum is achieved when no DNAPL remains, but the rate of increase varies due to the difference in DNAPL dissolution rates. The reduced aqueous phase relative permeability in the fractures in the presence of PCE DNAPL resulted in reduced water velocities and, in turn, even further reduced aqueous PCE mass flux. Grant and Gerhard (2007b) comment upon this dynamic link between DNAPL saturation and water velocity and its impact on the evolution of source zones in unconsolidated porous media. Of the 3.3 kg (20.2 moles) PCE mass in the domain at the end of Site Ageing, more than 99.9% resided in the sandstone matrix, of which 98.7% was sorbed and only 1.3% remained in the aqueous phase.

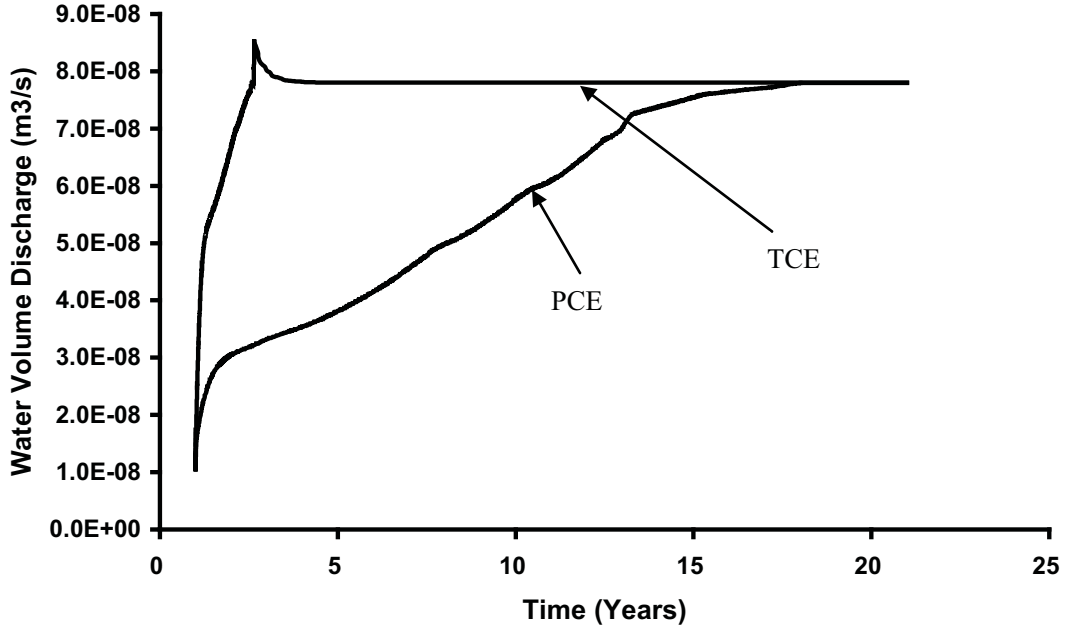

Figure 32: Downgradient water volume discharge for (i) TCE and (ii) PCE Simulations.

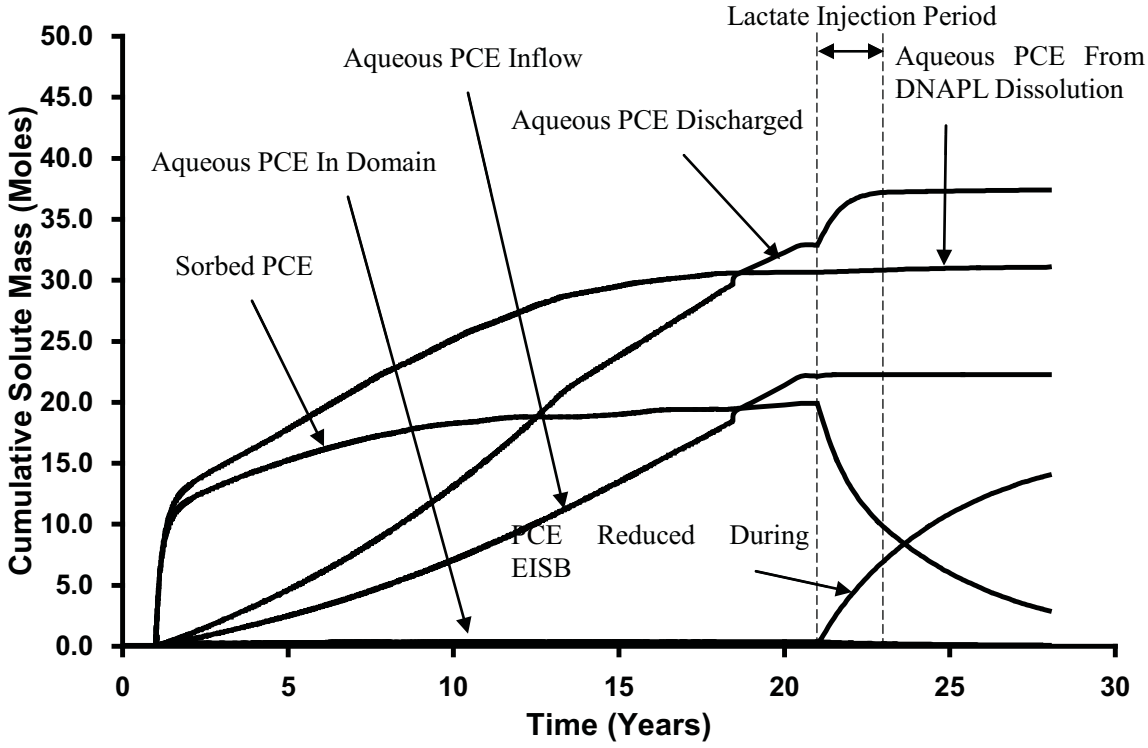

Figure 33: Cumulative aqueous and sorbed PCE from all sinks and sources for PCE Simulation.

The distribution of aqueous and sorbed PCE at the end of Site Ageing is shown in Figure A15, Appendix A, as compared to that for TCE at the same time (Figure 6). There are a number of reasons why the depth of matrix penetration for PCE is considerably less than TCE. First, the constant concentration of aqueous solvent provided at the upgradient boundary throughout the Site Ageing stage (50% solubility) was much lower for PCE (100mg/L) than TCE (550mg/L). In addition, the R and alpha value for PCE is 60 and 780, while for TCE is 21 and 270, this is because the Koc for PCE is approximately 3 times greater than TCE (i.e., KOC_{PCE} = 364 L/kg, KOC_{TCE} = 126 L/kg; Pankow and Cherry, 1996). The effective diffusion rate for PCE is 1.88 x 10^{-10} m^2/s while for TCE it is 2.02 x 10^{-10} m^2/s. Therefore, the diffusion rate divided by the rock capacity factor for PCE is 2.4 x 10^{-13}, while for TCE it is 7.4 x 10^{-13}. For these reasons, although the initial volume of DNAPL was similar in both simulations, the mass present in the PCE domain at the end of the Site Ageing stage (3.3 kg) is much lower than the TCE domain (7.3 kg) (Table 5).

As demonstrated in Figure 34, although the total mass of lactate injected into the domain was similar in both simulations, the total amount of lactate used for chlorinated ethenes reduction was 6.56% for TCE and 2.43% for PCE. This is found despite the fact that 25% more hydrogen (and therefore more lactate) is required to dechlorinate 1 mole of PCE than TCE (Equations 3 – 7). Figure 35 reveals that 73.5% of the initial TCE mass was successfully reduced to ethene as compared to 45% in the PCE simulation. However, Figures 9, and 34 – 36 all reveal that while TCE dechlorination had effectively

run its course (see rates of TCE reduction and chloride production diminishing substantially towards zero) PCE dechlorination rates had not yet started to diminish. The evidence suggests that the bioremediation process was substantially slower for PCE but it is possible that a similar degree of clean-up may have been achieved if a longer post-treatment period was simulated.

There are a number of reasons why PCE bioremediation was substantially slower in these simulations. One reason is due to the lower mass of PCE present at the start of the Treatment stage: with first-order reactions the rate of dechlorination of each chlorinated ethene is proportional to the amount present. A second reason is the higher Koc value for PCE, which implies that, for a given concentration, a higher proportion of PCE than TCE will be sorbed instead of in the aqueous phase (and only the aqueous phase is available to the microorganisms for dechlorination). A third reason is that the PCE dechlorination pathway requires one additional rate-limited step which necessarily slows down the overall conversion rate from parent solvent to ethene.

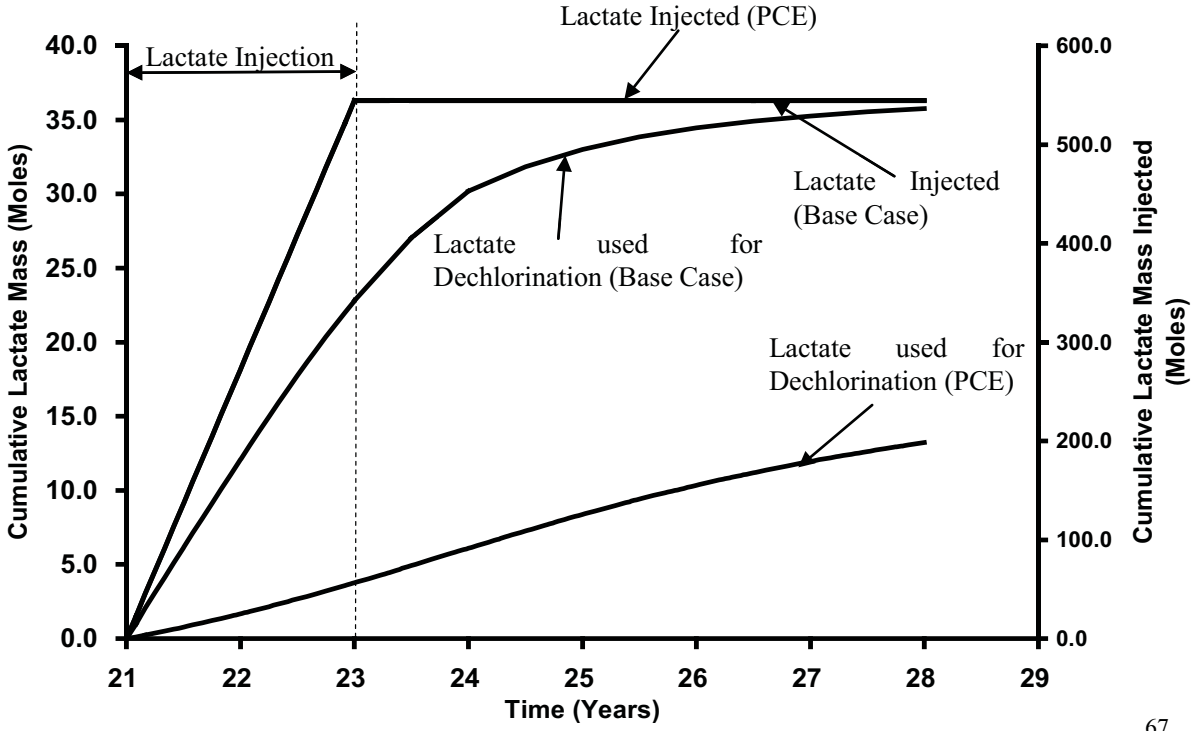

Figure 34: Cumulative mass of lactate over time for different DNAPL simulations.

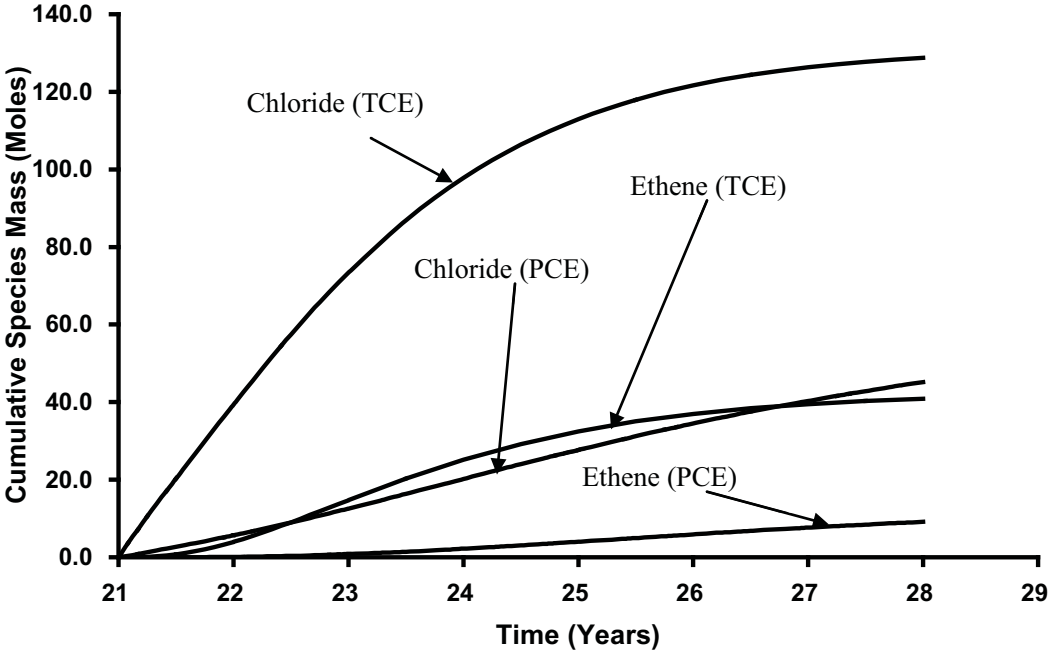

Figure 35: Cumulative mass of chloride and ethene produced over time for different DNAPL simulations.

(a)

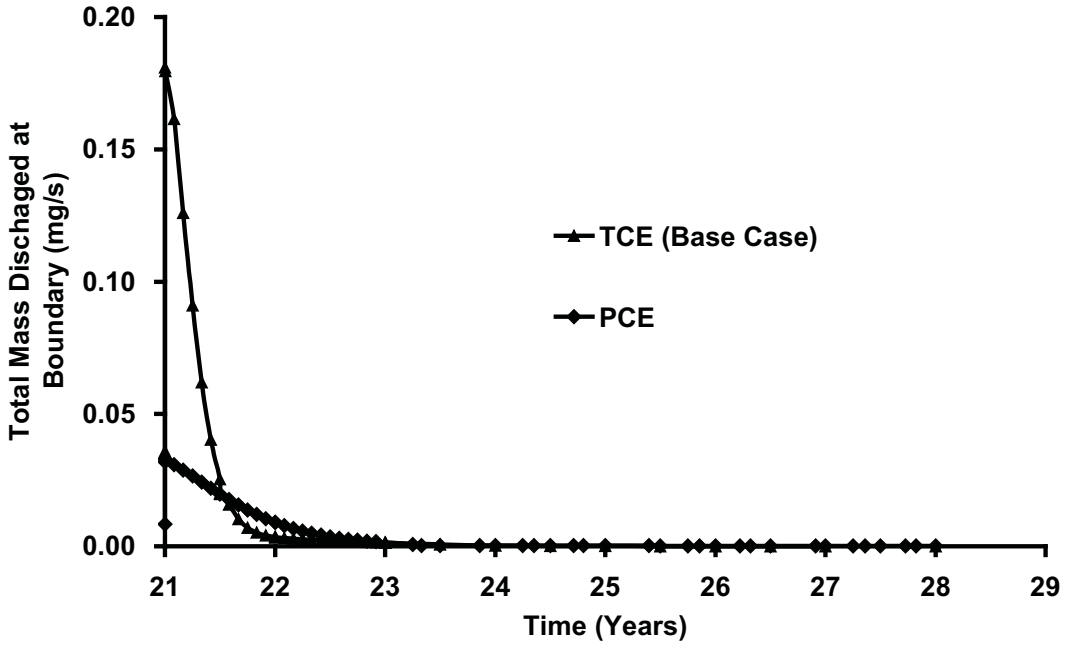

(b)

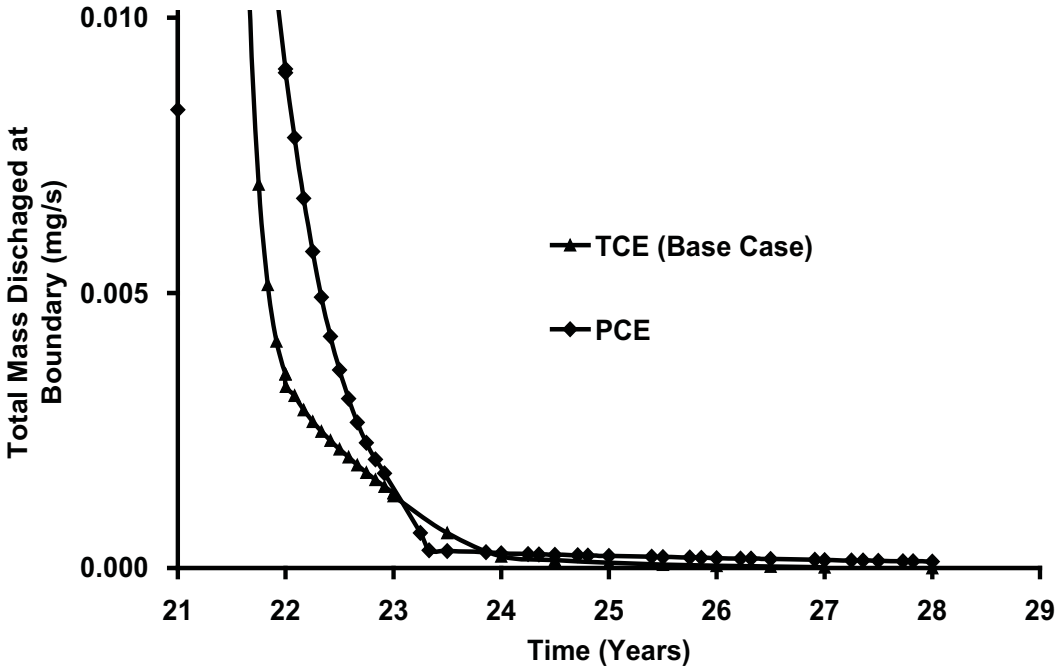

Figure 36: Comparison of total boundary mass discharge for (a) different DNAPL and (b) since the start of the Treatment Stage only (timescale expanded for clarity).

Figure 36 agrees with this analysis since the reduction in PCE mass flux at the downgradient boundary is slower than that for TCE. Figure 36b illustrates that in the case for PCE, downgradient mass discharge did not reduce to non-detect levels by the end of the simulation. Therefore, the untreated PCE mass in the domain acts as a long-term source of contamination to the downgradient boundary. Figure 36 further reveals a rapid change in PCE mass discharged at approximately t_{TOTAL} = 23.3 years, suggesting that dechlorination of PCE is more difficult than TCE.

5. CONCLUSION

In the Base Case, EISB was demonstrated to produce relatively positive results. Of the

total initial mass present, 73.5% was demonstrated to have successfully been reduced to ethene. It was further noted that the size of facture apertures directly affects the downgradient discharge where fractures with smaller apertures were noted to take a longer time before the discharged mass decreases below detection limits as compared to larger fractures. This represents an ideal case, with robust first-order decay rates, active microorganisms throughout the fractures and matrix, presence of TCE rather than PCE, and low peclet numbers that enhance diffusion of lactate to the matrix-bound contaminant.

However, when the bacterial consortium was assumed to be confined to within the sandstone fractures, it was found that the mass of chloride produced was 200 times less than the Base Case. Since the majority of the mass resided in the matrix, lack of bioremediation in the matrix significantly reduced effectiveness of treatment. It is noted that some treatment of back-diffusing TCE occurred in the fractures, but this was significant only for the smallest horizontal fractures, which contribute least to the downgradient mass flux, and thus the overall long-term effect on mass discharge was negligible.

These sensitivity studies suggest that the concentration and the rate at which lactate was injected – given that the total mass injected is identical - have little influence on EISB effectiveness during and after the treatment process. It is acknowledged that this may differ in scenarios where lactate is not in excess or where bioclogging, pH effects, and other complicating factors may plan an important role.

For scenarios in which diffusive flux is significant (e.g., sandstone/TCE simulations) substantial mass becomes stored in the matrix via forward diffusion. High diffusive flux is promoted by high matrix porosity, high diffusion coefficient, high aqueous solvent concentrations (i.e., high solubility), and low sorptive capacity (i.e., low Koc and/or low foc). The results revealed that both the mass of TCE reduced and the time required to reduce this mass can vary significantly in different rock types, with mean fracture Pe observed to be inversely related to the efficiency of EISB. Clearly the rock properties that influence matrix loading of contaminants and diffusive rate of electron donor during the treatment period dominate EISB performance, assuming that effective ESIB is able to occur in the matrix.

EISB was substantially slower for PCE than TCE but it is possible that a similar degree of clean-up may have been achieved if a longer post-treatment period was simulated.

The post-treatment TCE mass discharged was found to be able to achieve negligible levels when (i) bioremediation was assumed to take place throughout the matrix and (ii) first-order biodegradation rates exceeded a threshold. These results indicate that ideal conditions (i.e., inhibition is low, significant dechlorination occurs in the matrix) and favourable scenarios (e.g., low Pe number formations such as sandstone, rapidly degrading compounds such as TCE) may be required for successful application of EISB. This is because success appears to depend on effective penetration of electron donor into the matrix during the treatment period and the ongoing treatment that occurs after

injection ceases.

It is acknowledged that numerous assumptions and simplifications were employed in this work. In the majority of circumstances, the assumptions were chosen to present a 'best case' scenario that favours effective treatment (e.g., constant injection concentration with elevated gradient, two-dimensional flow with little opportunity for bypassing, no Bioclogging, etc.). This approach underscores the challenges associated with effectively treating aged source zones in fractured rock with EISB. The limited number of simulations conducted using specific site templates on a small field scale implies that these results cannot be directly extended to a wide variety of complex real sites. Nevertheless, it is expected that the importance influence of key variables, including decay rate parameters, the spatial distribution of microorganisms, the rock type, and DNAPL type, will likely have similar impacts in field applications of EISB to chlorinated solvent-impacted fractured rock scenarios.

SUPPLEMENTARY INFORMATION

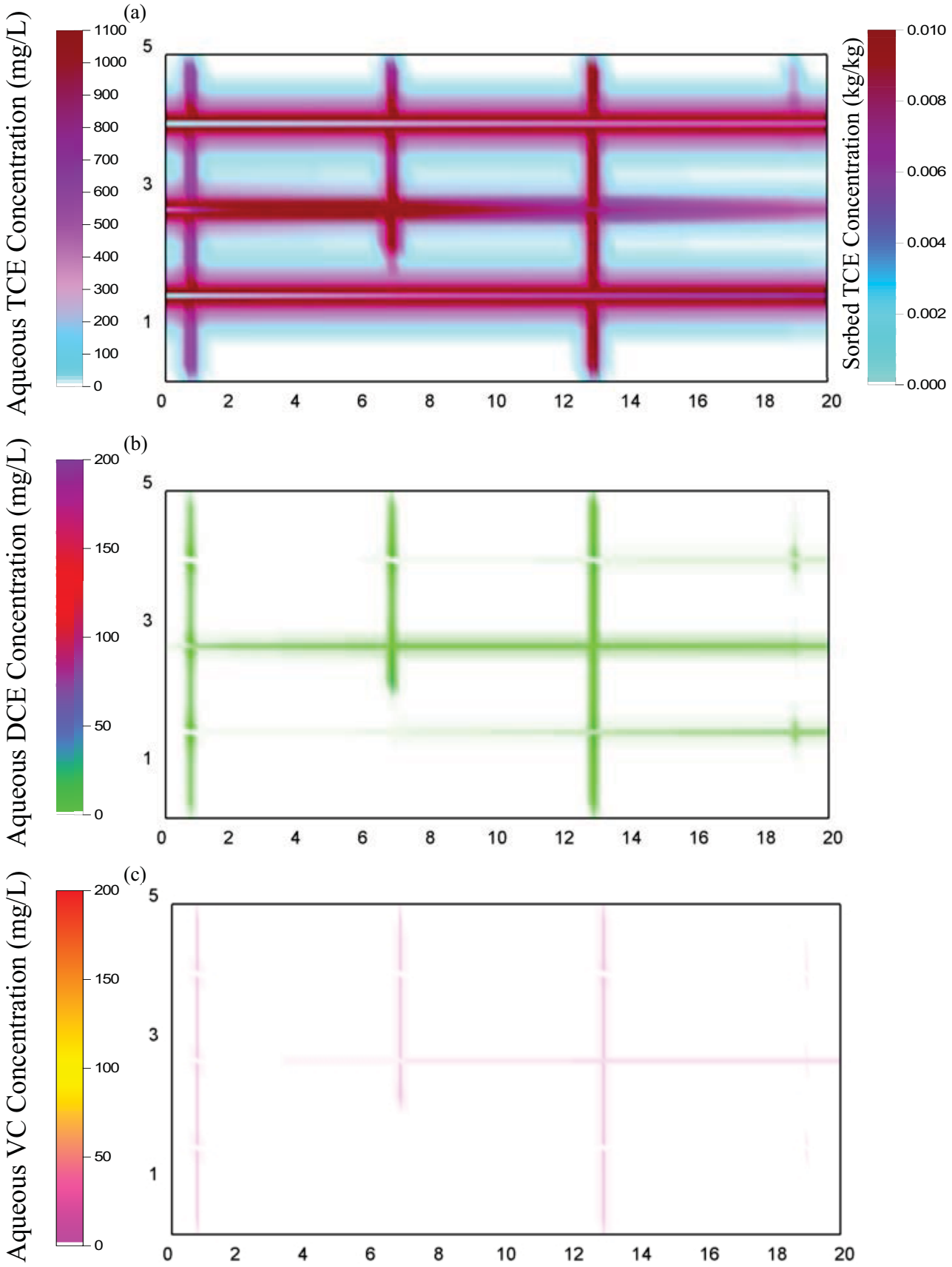

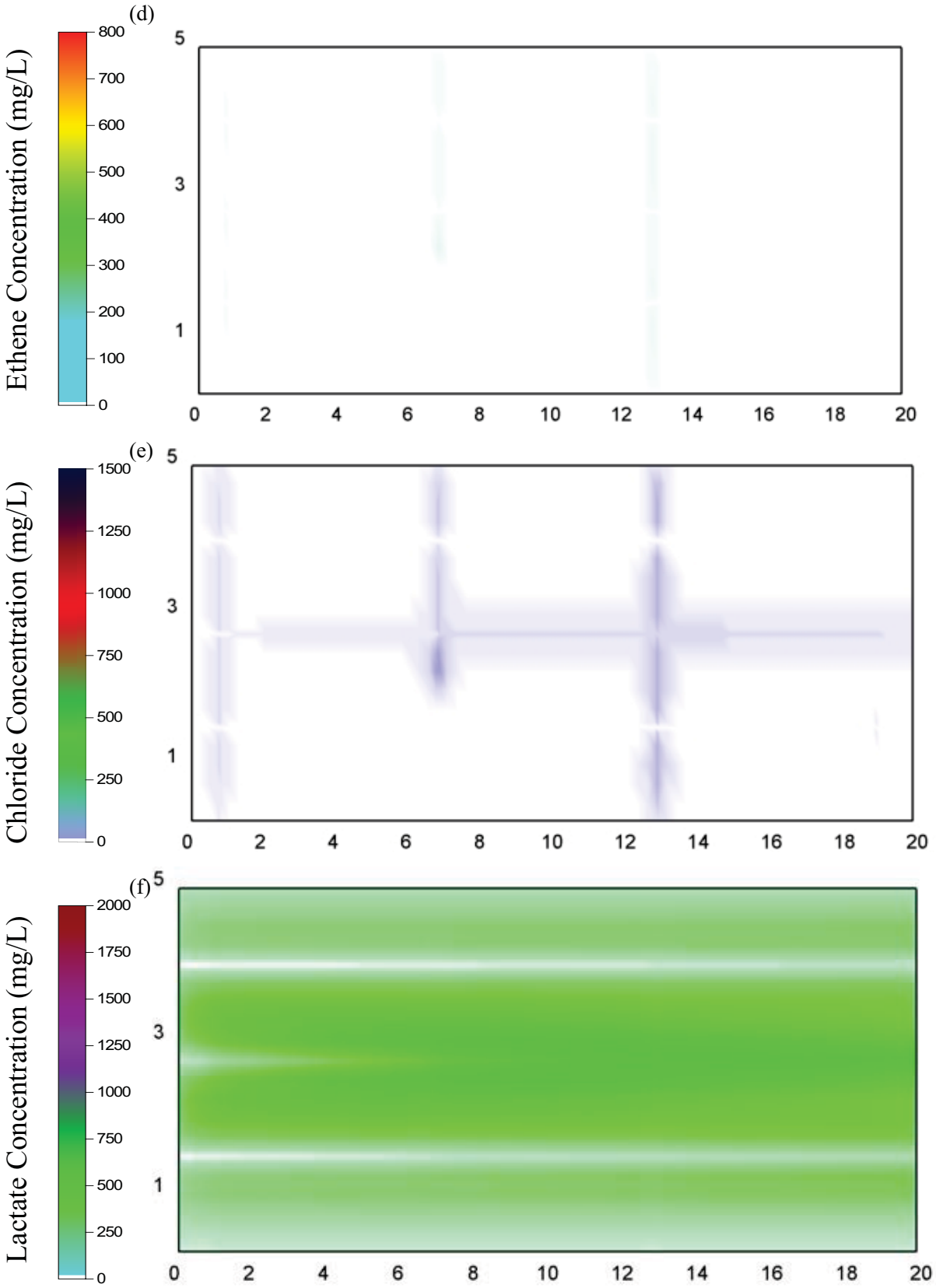

Figure B1: Distribution of (a) Aqueous TCE; (b) Aqueous DCE; (c) Aqueous VC; (d) Ethene; (e) Chloride; (f) Lactate, 5 years after lactate injection for indigenous bacteria present in facture only.

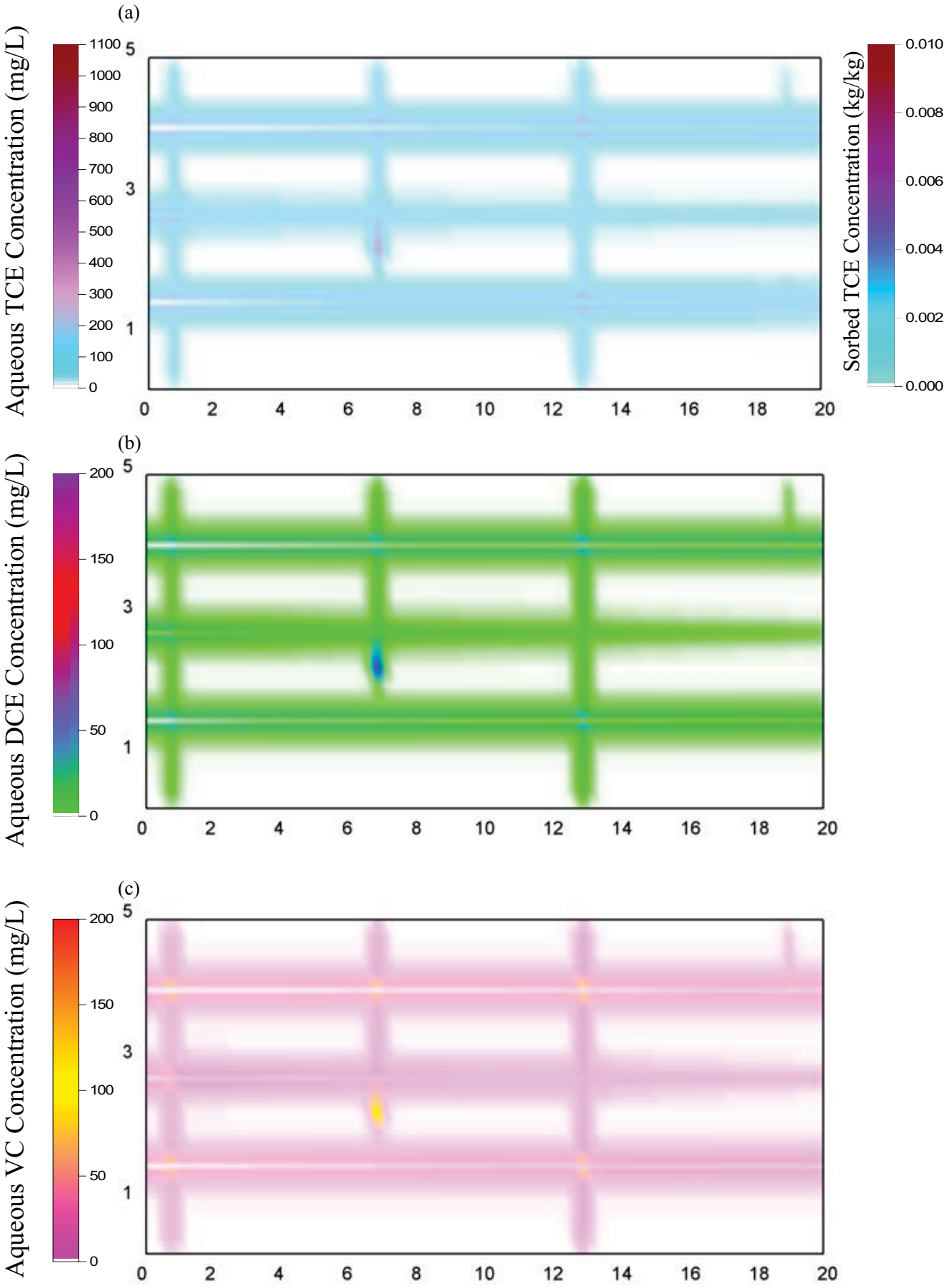
(a)
Aqueous TCE Concentration (mg/L)
1100
1000
900
800
700
600
500
400
300
200
100
0
Sorbed TCE Concentration (kg/kg)
0.010
0.008
0.006
0.004
0.002
0.000
5
3
1
0
2
4
6
8
10
12
14
16
18
20
(b)
Aqueous DCE Concentration (mg/L)
200
150
100
50
0
(c)
Aqueous VC Concentration (mg/L)

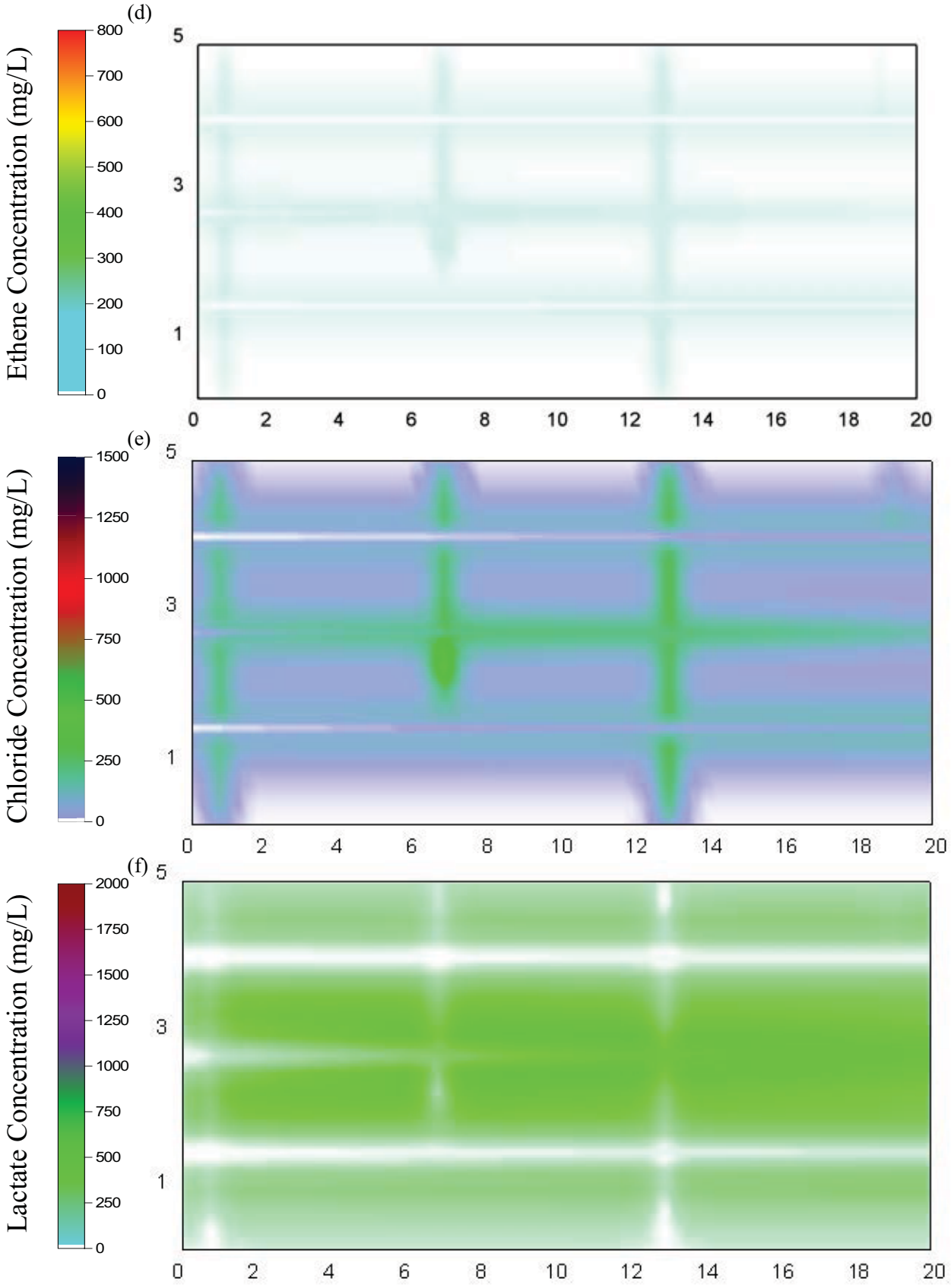

Figure B2: Distribution of (a) Aqueous TCE; (b) Aqueous DCE; (c) Aqueous VC; (d) Ethene; (e) Chloride; (f) Lactate, 5 years after lactate injection for low decay rate.

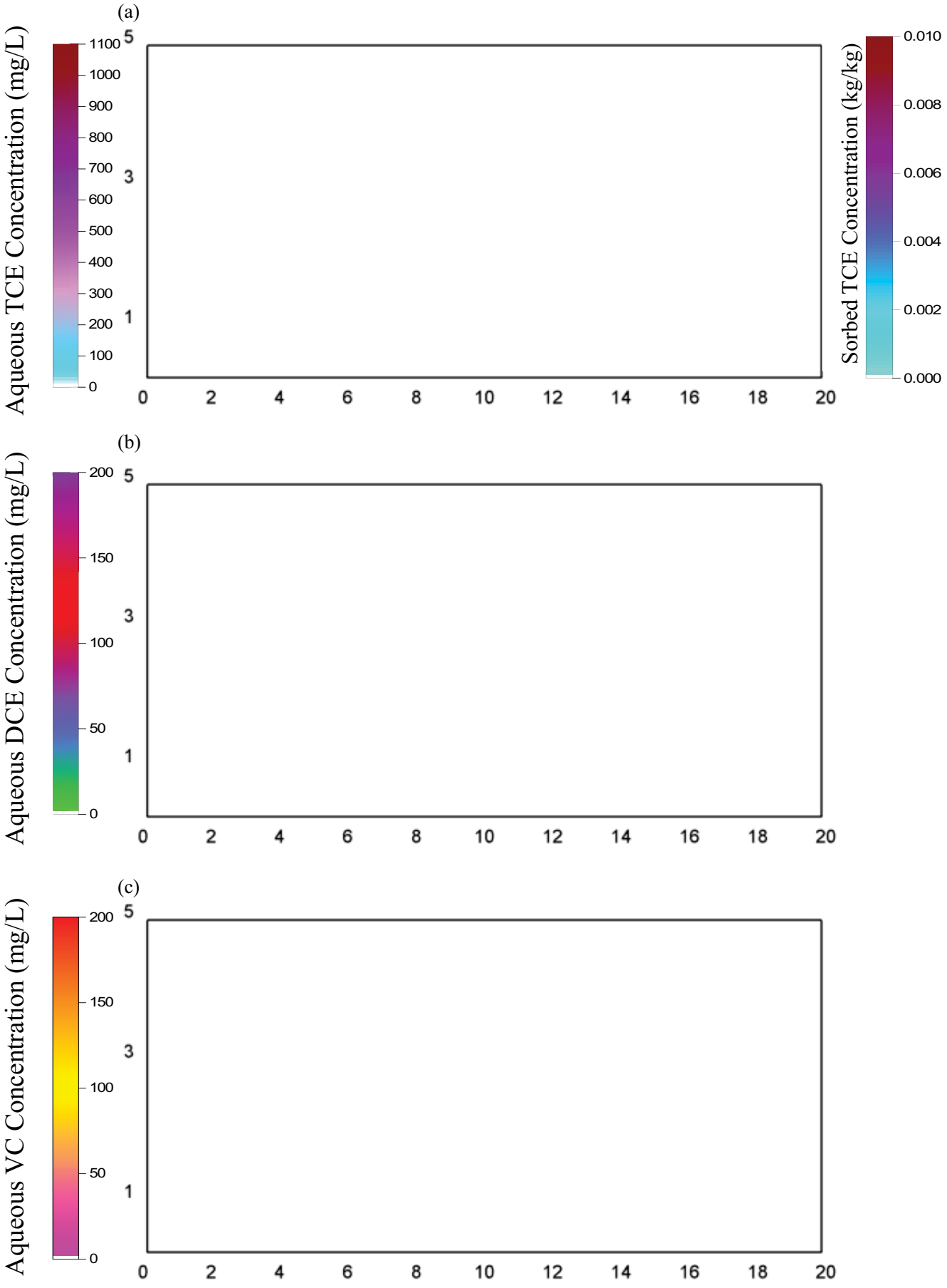
(a)
Aqueous TCE Concentration (mg/L)
1100
1000
900
800
700
600
500
400
300
200
100
0
Sorbed TCE Concentration (kg/kg)
0.010
0.008
0.006
0.004
0.002
0.000
5
3
1
0
2
4
6
8
10
12
14
16
18
20
(b)
Aqueous DCE Concentration (mg/L)
200
150
100
50
0
(c)
Aqueous VC Concentration (mg/L)

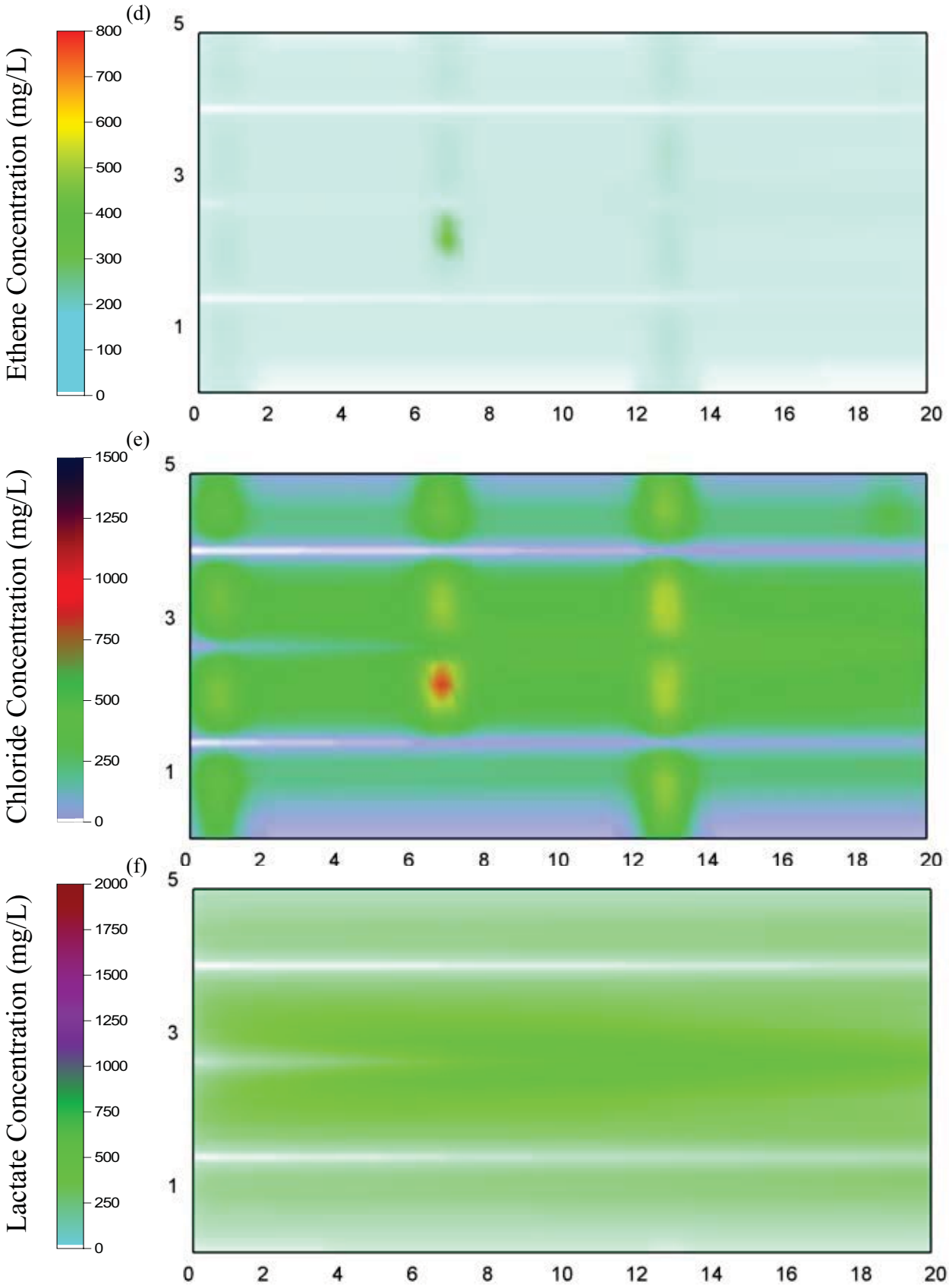

Figure B3: Distribution of (a) Aqueous TCE; (b) Aqueous DCE; (c) Aqueous VC; (d) Ethene; (e) Chloride; (f) Lactate, 5 years after lactate injection for high decay rate.

(a)

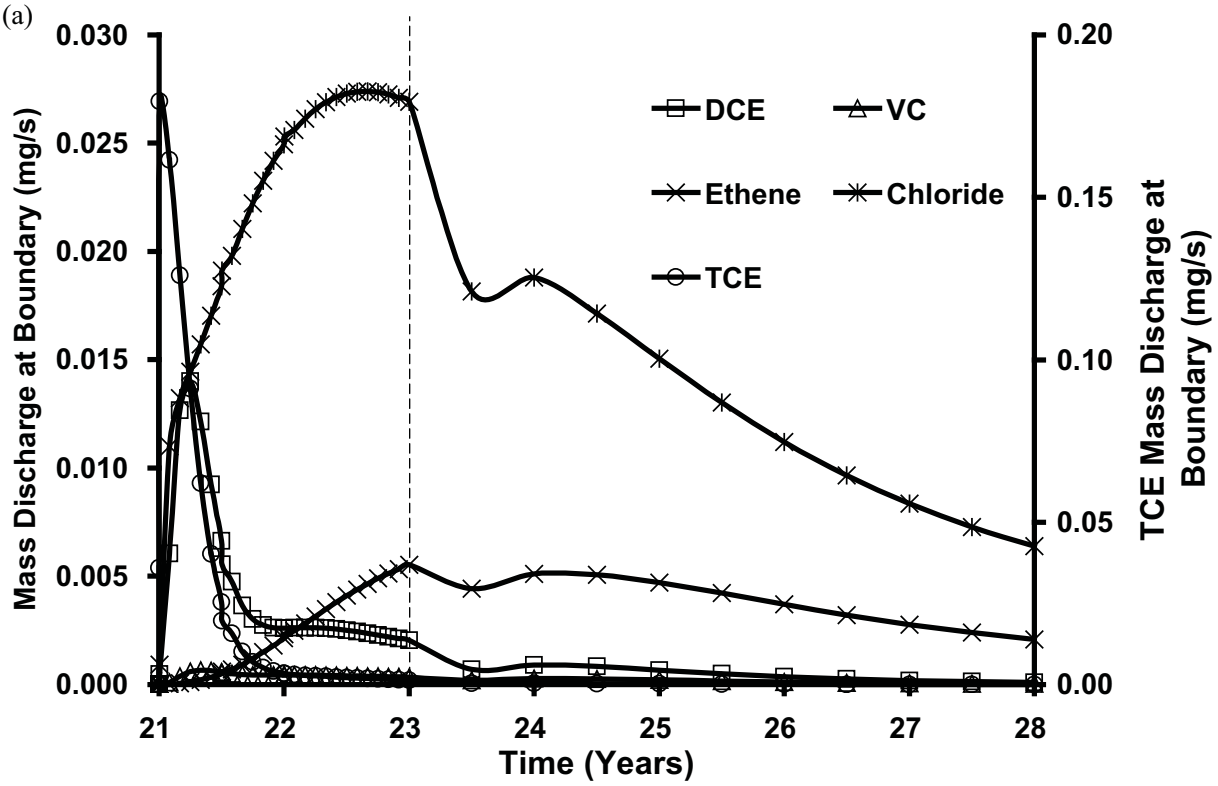
Mass Discharge at Boundary (mg/s)
TCE Mass Discharge at Boundary (mg/s)
Time (Years)
DCE
VC
Ethene
Chloride
TCE
0.030
0.025
0.020
0.015
0.010
0.005
0.000
0.20
0.15
0.10
0.05
0.00
21
22
23
24
25
26
27
28

(b)

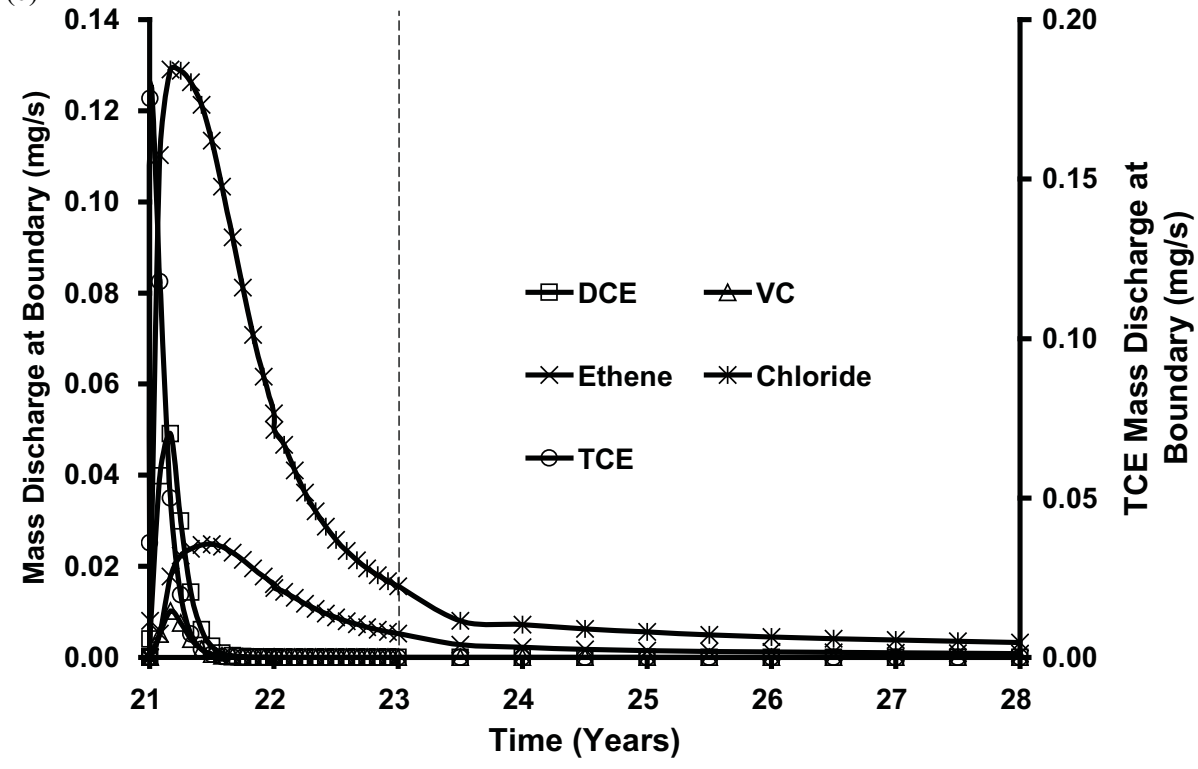
Mass Discharge at Boundary (mg/s)
TCE Mass Discharge at Boundary (mg/s)
Time (Years)
DCE
VC
Ethene
Chloride
TCE
0.14
0.12
0.10
0.08
0.06
0.04
0.02
0.00
0.20
0.15
0.10
0.05
0.00
21
22
23
24
25
26
27
28

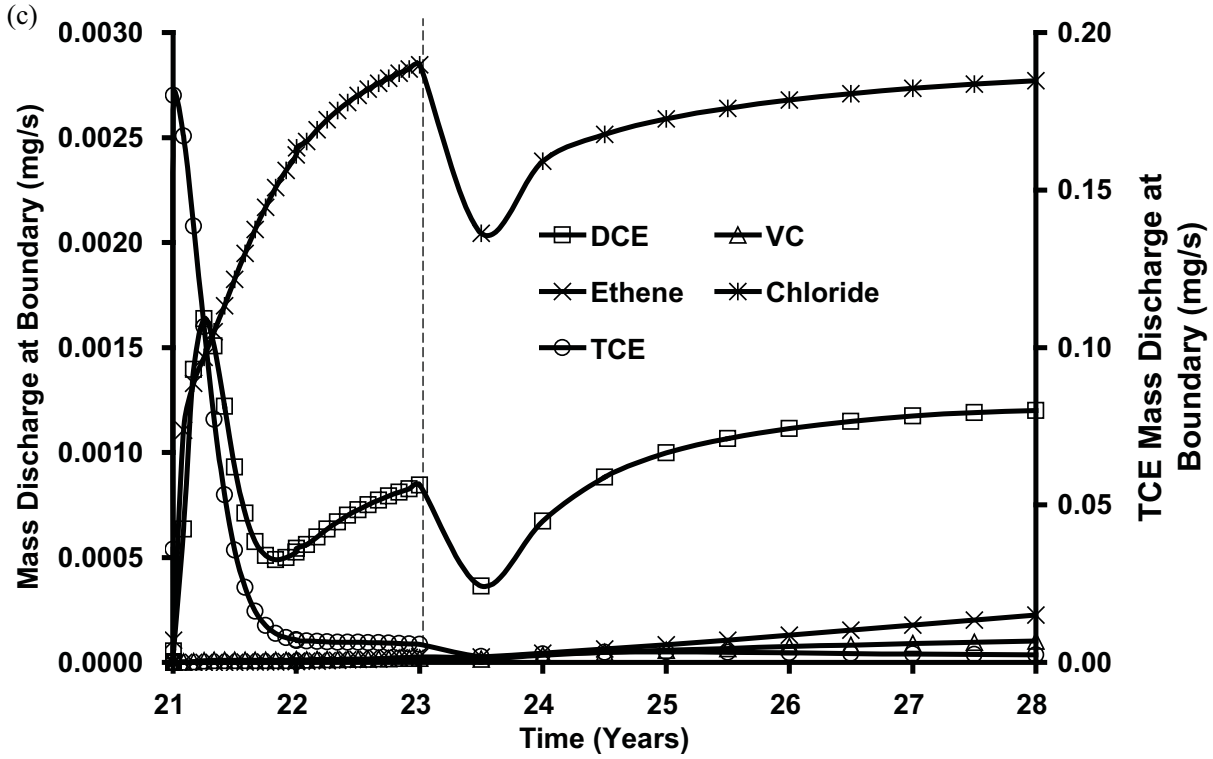

Figure B4: Total boundary mass discharge for various species in (a) Base Case; (b) High Decay Rate Parameter; (c) Low Decay Rate Parameter over time.

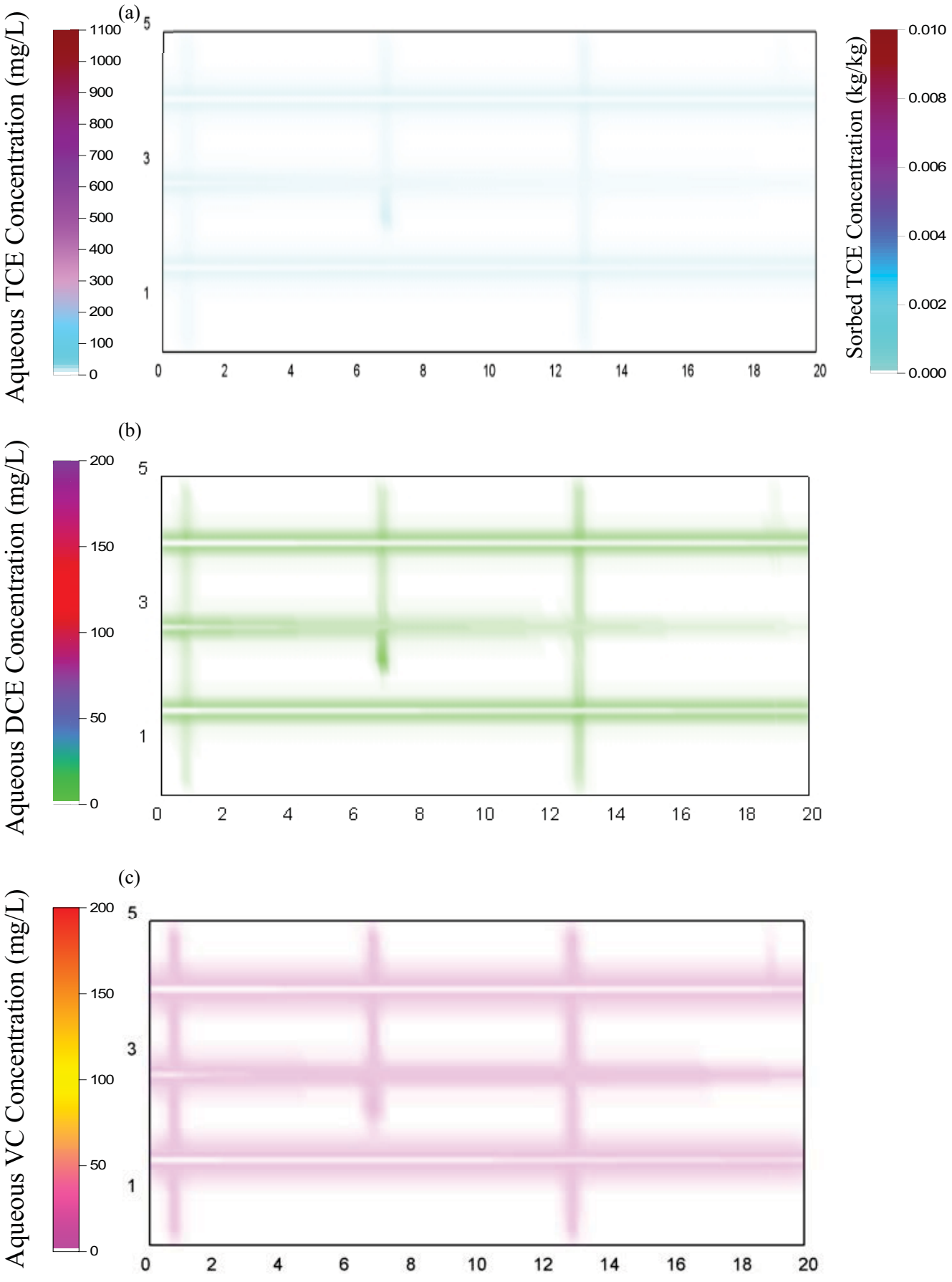
(a)
Aqueous TCE Concentration (mg/L)
1100
1000
900
800
700
600
500
400
300
200
100
0
5
3
1
0
2
4
6
8
10
12
14
16
18
20
Sorbed TCE Concentration (kg/kg)
0.010
0.008
0.006
0.004
0.002
0.000
(b)
Aqueous DCE Concentration (mg/L)
200
150
100
50
0
5
3
1
0
2
4
6
8
10
12
14
16
18
20
(c)
Aqueous VC Concentration (mg/L)
200
150
100
50
0
5
3
1
0
2
4
6
8
10
12
14
16
18
20

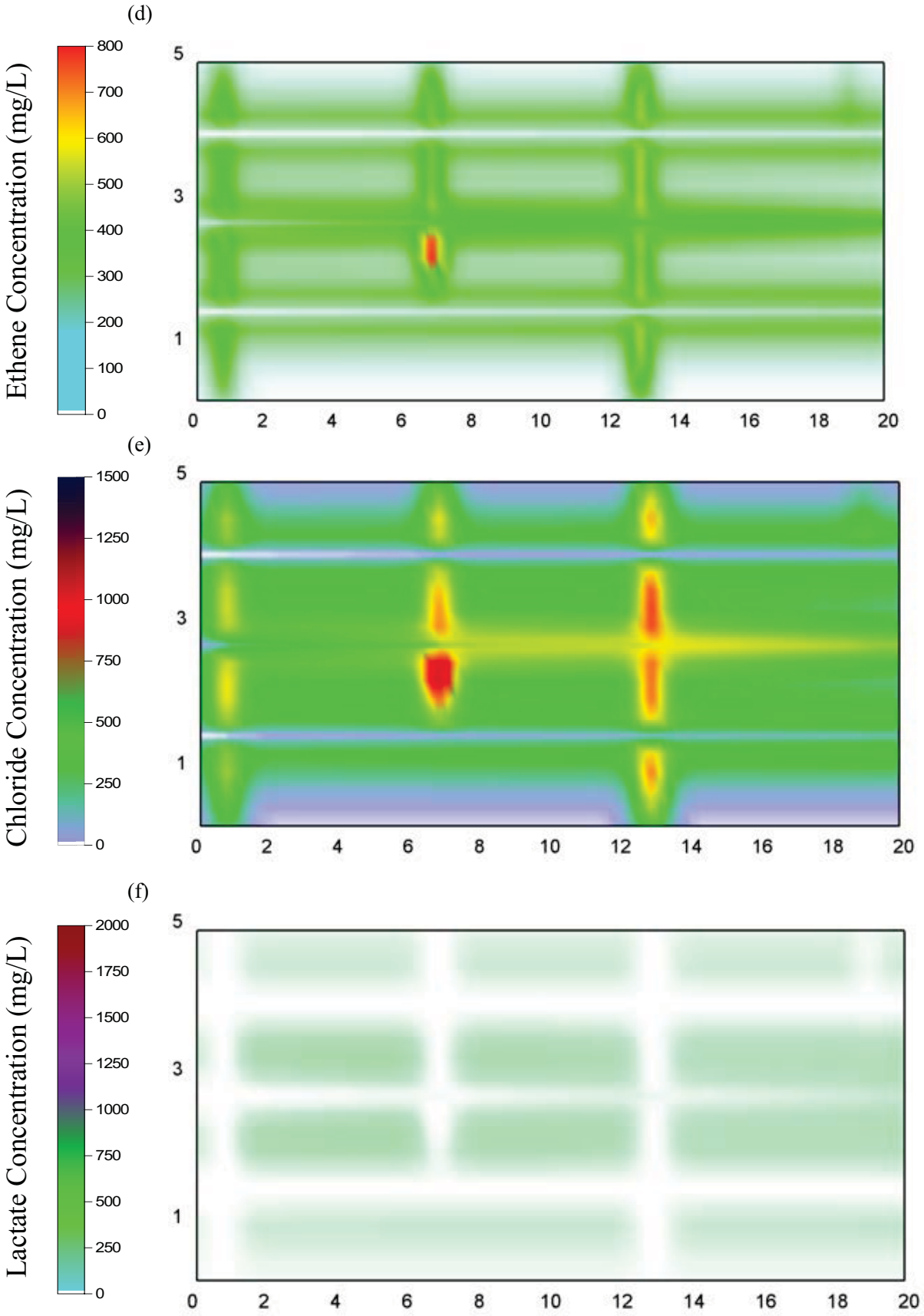

Figure B5: Distribution of (a) Aqueous TCE; (b) Aqueous DCE; (c) Aqueous VC; (d) Ethene; (e) Chloride; (f) Lactate, 5 years after lactate injection for 3 Months pulse injection simulation.

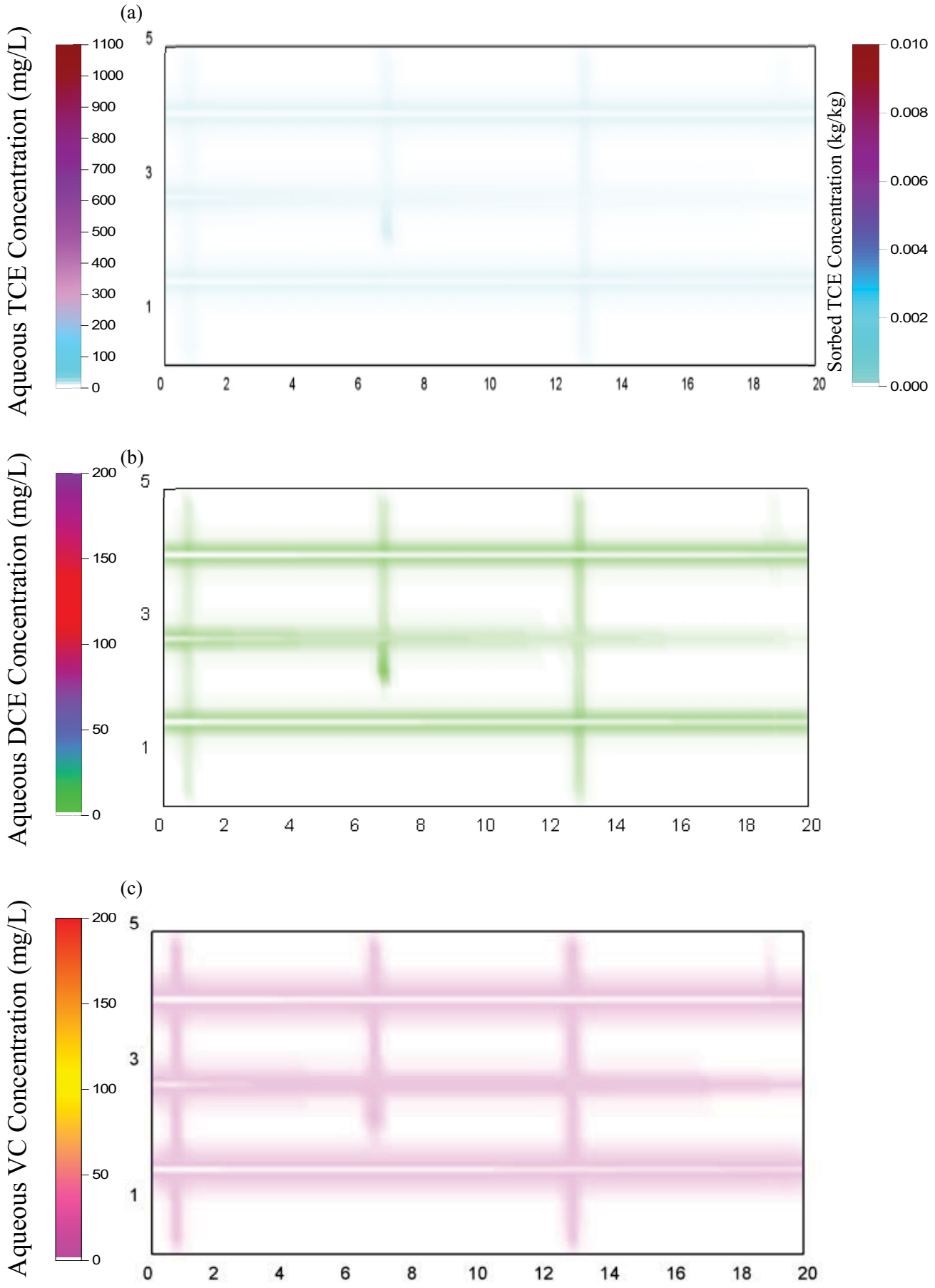
(a)
Aqueous TCE Concentration (mg/L)
1100
1000
900
800
700
600
500
400
300
200
100
0
5
3
1
0
2
4
6
8
10
12
14
16
18
20
Sorbed TCE Concentration (kg/kg)
0.010
0.008
0.006
0.004
0.002
0.000
(b)
Aqueous DCE Concentration (mg/L)
200
150
100
50
0
5
3
1
0
2
4
6
8
10
12
14
16
18
20
(c)
Aqueous VC Concentration (mg/L)
200
150
100
50
0
5
3
1
0
2
4
6
8
10
12
14
16
18
20

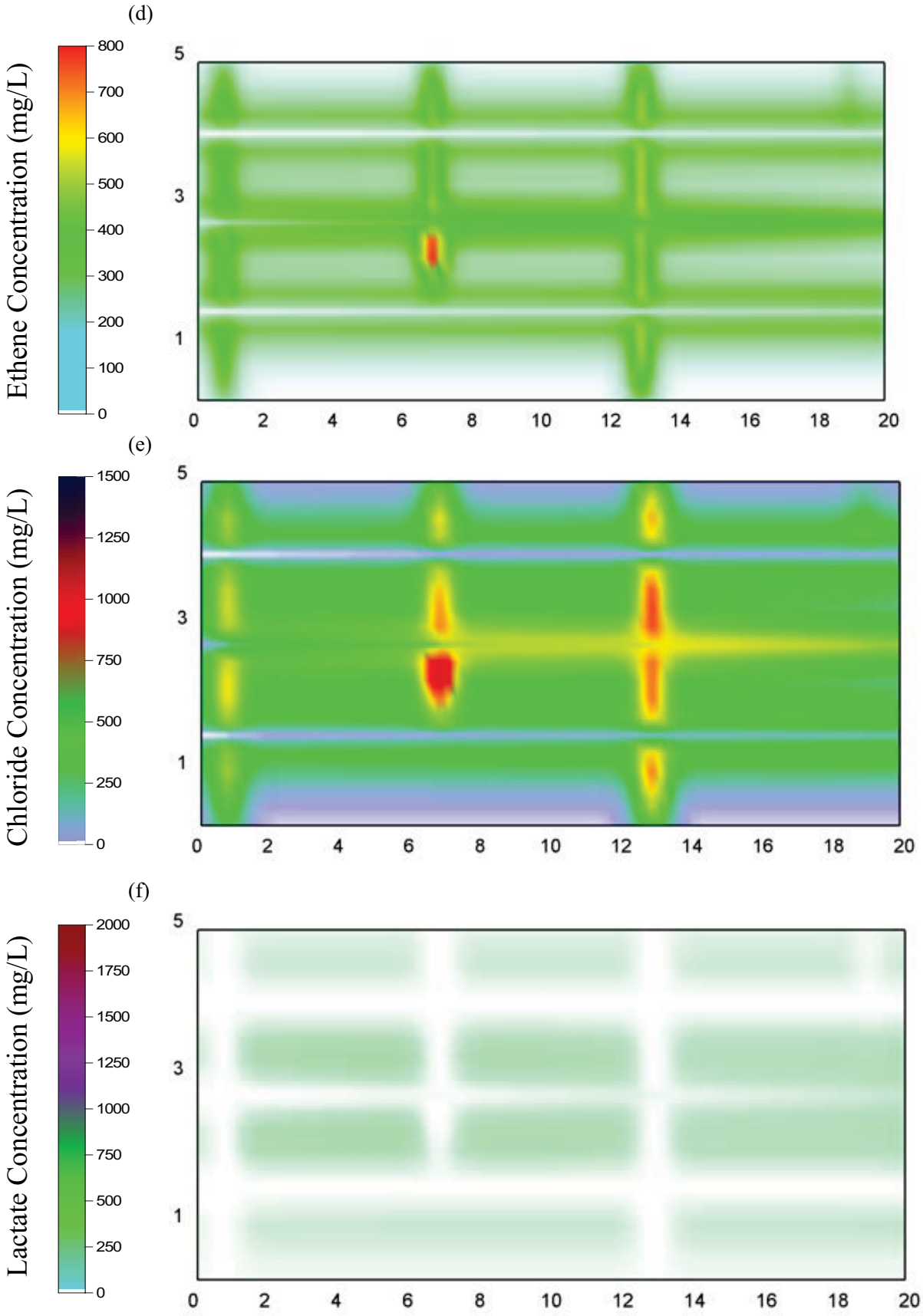

Figure B6: Distribution of (a) Aqueous TCE; (b) Aqueous DCE; (c) Aqueous VC; (d) Ethene; (e) Chloride; (f) Lactate, 5 years after lactate injection for 6 Months pulse injection simulation.

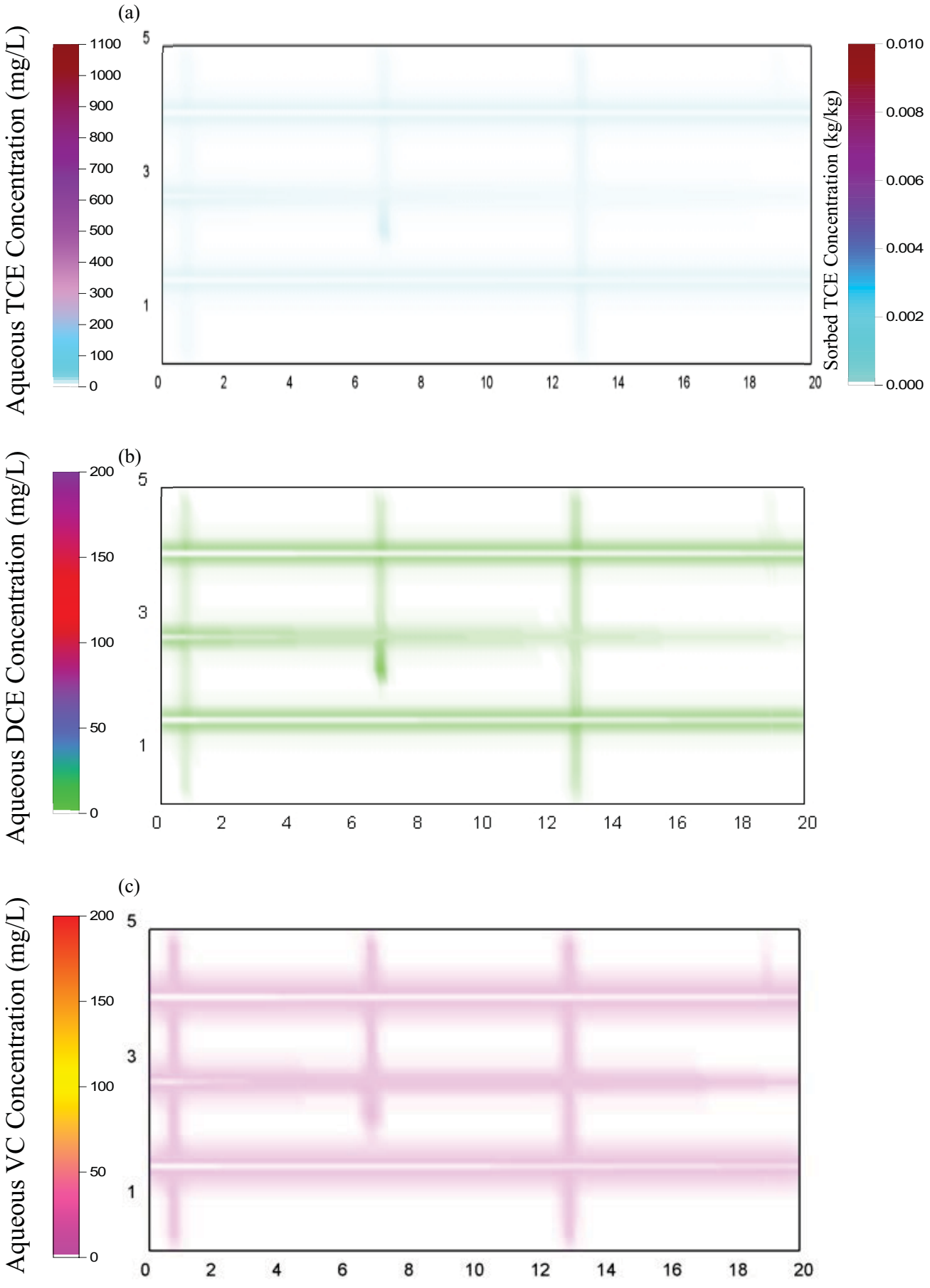
(a)
Aqueous TCE Concentration (mg/L)
1100
1000
900
800
700
600
500
400
300
200
100
0
5
3
1
0
2
4
6
8
10
12
14
16
18
20
Sorbed TCE Concentration (kg/kg)
0.010
0.008
0.006
0.004
0.002
0.000
(b)
Aqueous DCE Concentration (mg/L)
200
150
100
50
0
5
3
1
0
2
4
6
8
10
12
14
16
18
20
(c)
Aqueous VC Concentration (mg/L)
200
150
100
50
0
5
3
1
0
2
4
6
8
10
12
14
16
18
20

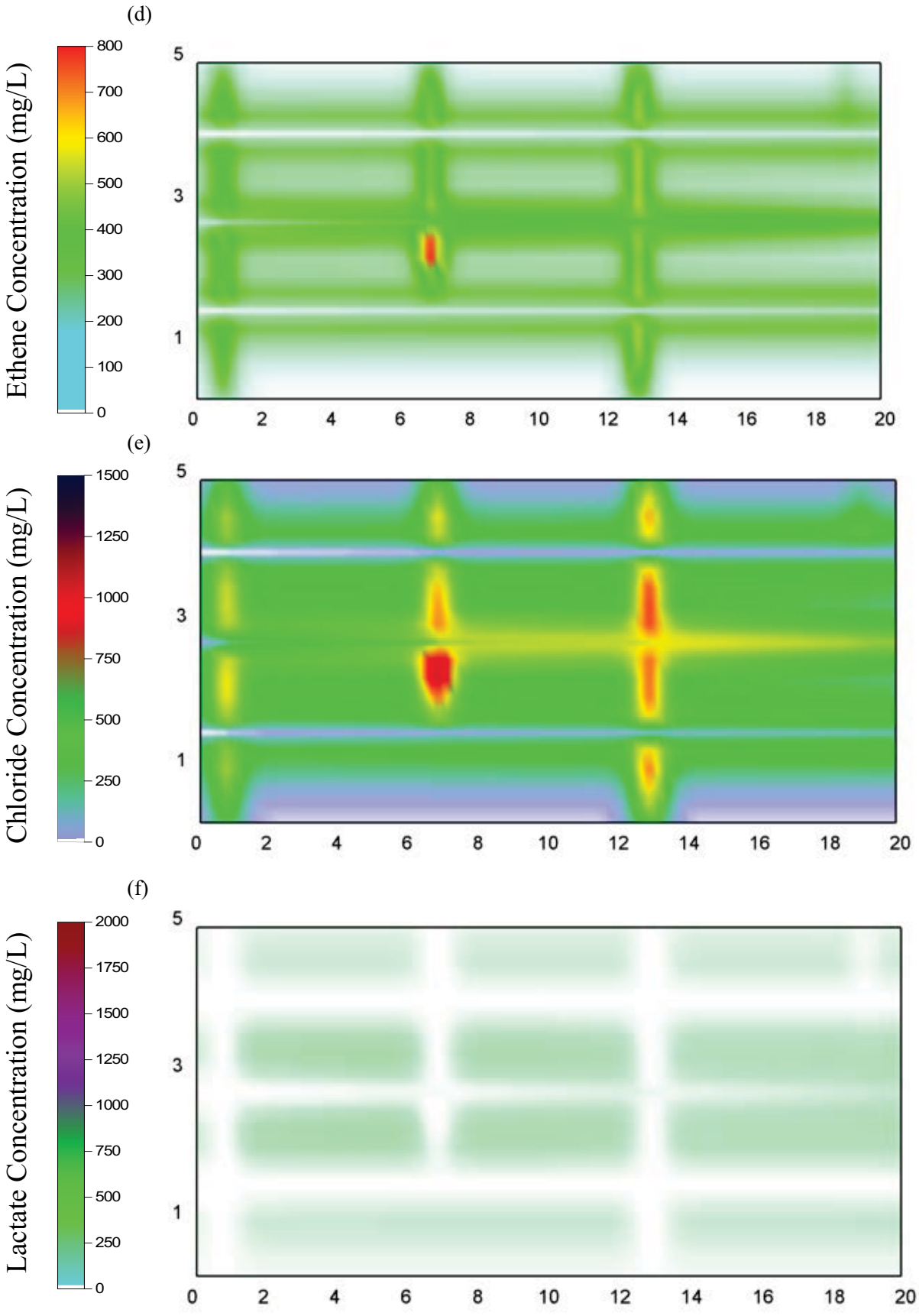

Figure B7: Distribution of (a) Aqueous TCE; (b) Aqueous DCE; (c) Aqueous VC; (d) Ethene; (e) Chloride; (f) Lactate, 5 years after lactate injection for 12 Months pulse injection simulation.

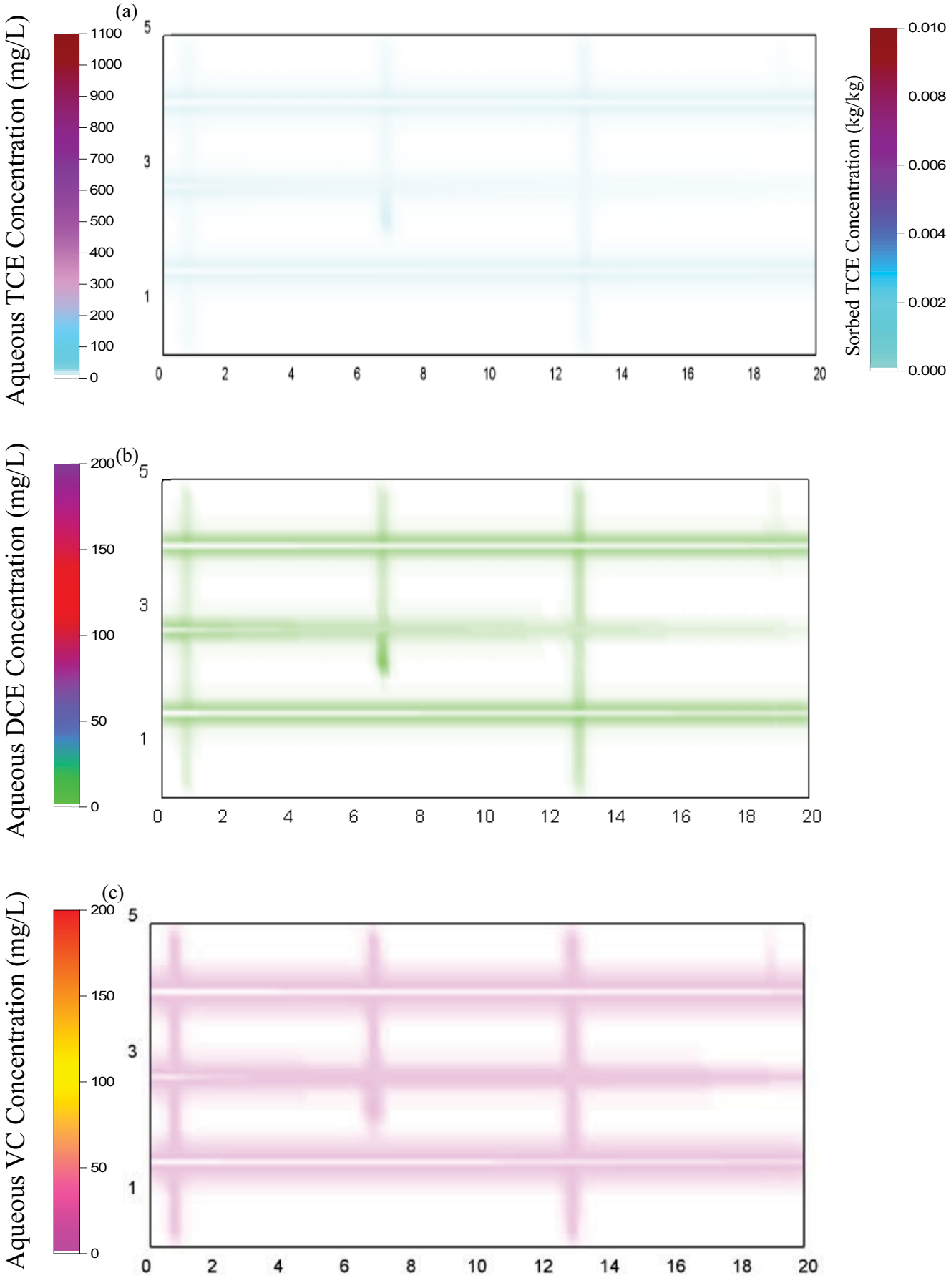
(a)
Aqueous TCE Concentration (mg/L)
1100
1000
900
800
700
600
500
400
300
200
100
0
5
3
1
0
2
4
6
8
10
12
14
16
18
20
Sorbed TCE Concentration (kg/kg)
0.010
0.008
0.006
0.004
0.002
0.000
(b)
Aqueous DCE Concentration (mg/L)
200
150
100
50
0
5
3
1
0
2
4
6
8
10
12
14
16
18
20
(c)
Aqueous VC Concentration (mg/L)
200
150
100
50
0
5
3
1
0
2
4
6
8
10
12
14
16
18
20

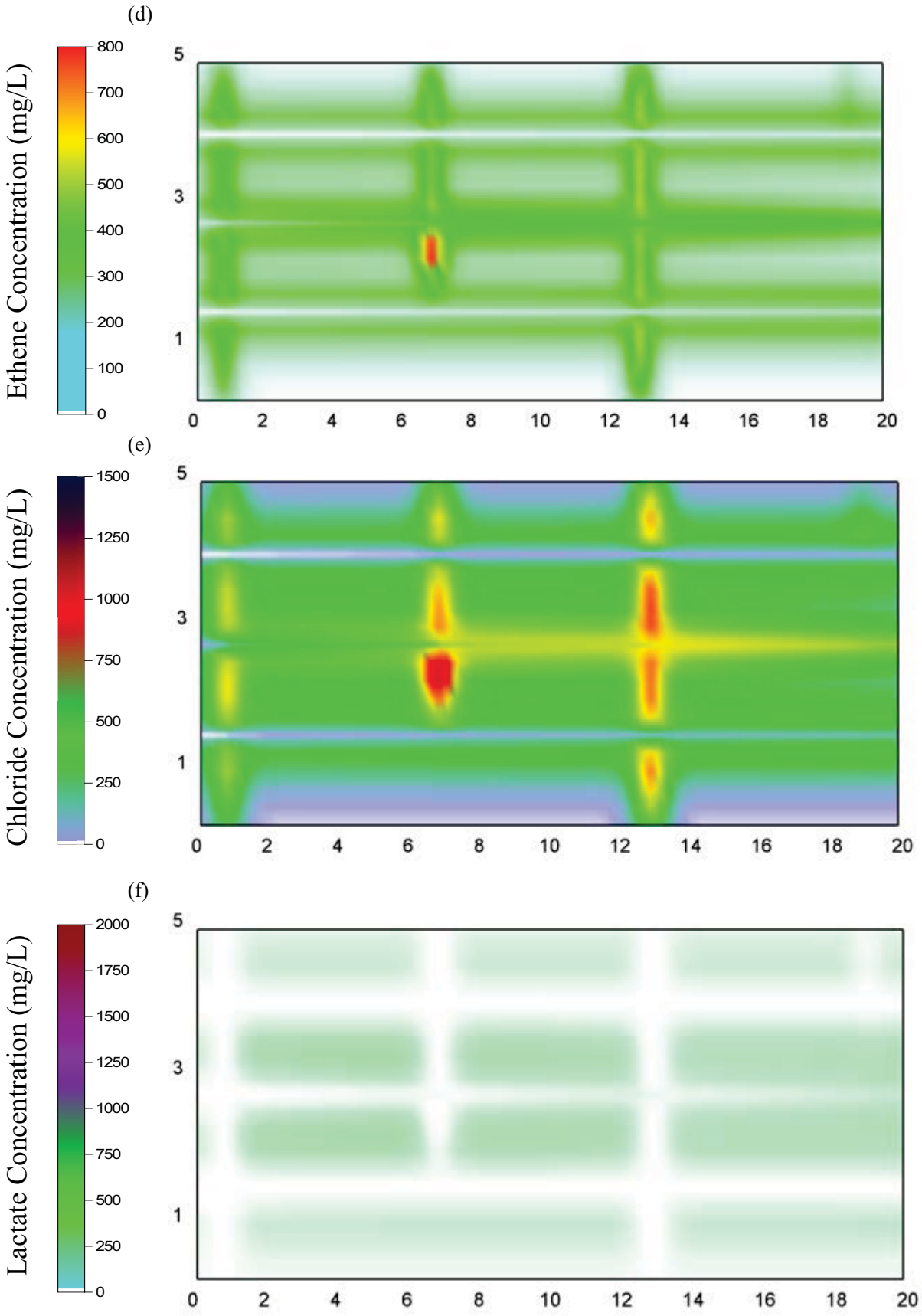

Figure B8: Distribution of (a) Aqueous TCE; (b) Aqueous DCE; (c) Aqueous VC; (d) Ethene; (e) Chloride; (f) Lactate, 5 years after lactate injection for 1000mg/L of lactate injection simulation.

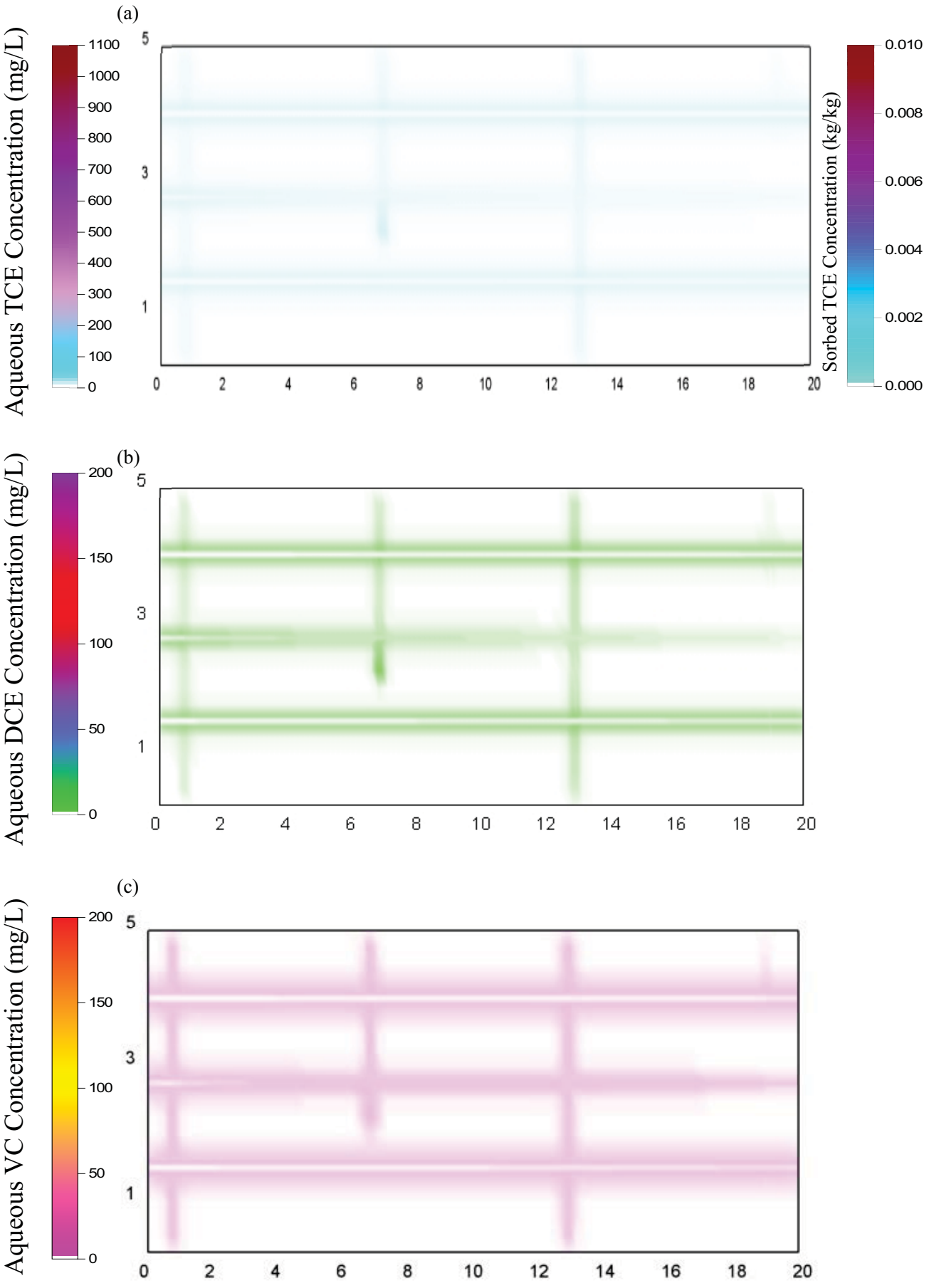
(a)
Aqueous TCE Concentration (mg/L)
1100
1000
900
800
700
600
500
400
300
200
100
0
5
3
1
0
2
4
6
8
10
12
14
16
18
20
Sorbed TCE Concentration (kg/kg)
0.010
0.008
0.006
0.004
0.002
0.000
(b)
Aqueous DCE Concentration (mg/L)
200
150
100
50
0
5
3
1
0
2
4
6
8
10
12
14
16
18
20
(c)
Aqueous VC Concentration (mg/L)
200
150
100
50
0
5
3
1
0
2
4
6
8
10
12
14
16
18
20

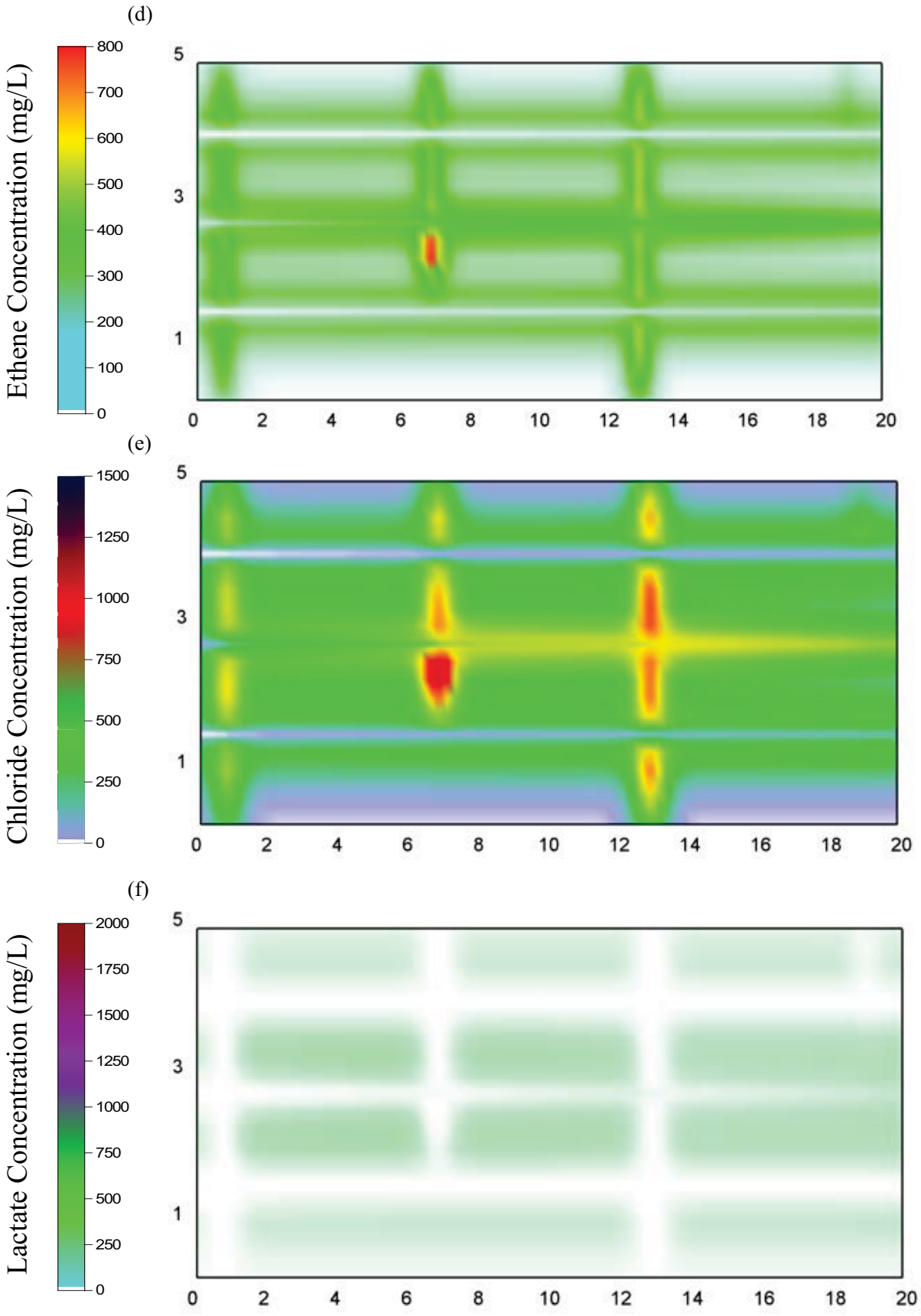

Figure B9: Distribution of (a) Aqueous TCE; (b) Aqueous DCE; (c) Aqueous VC; (d) Ethene; (e) Chloride; (f) Lactate, 5 years after lactate injection for 4000mg/L of lactate injection simulation.

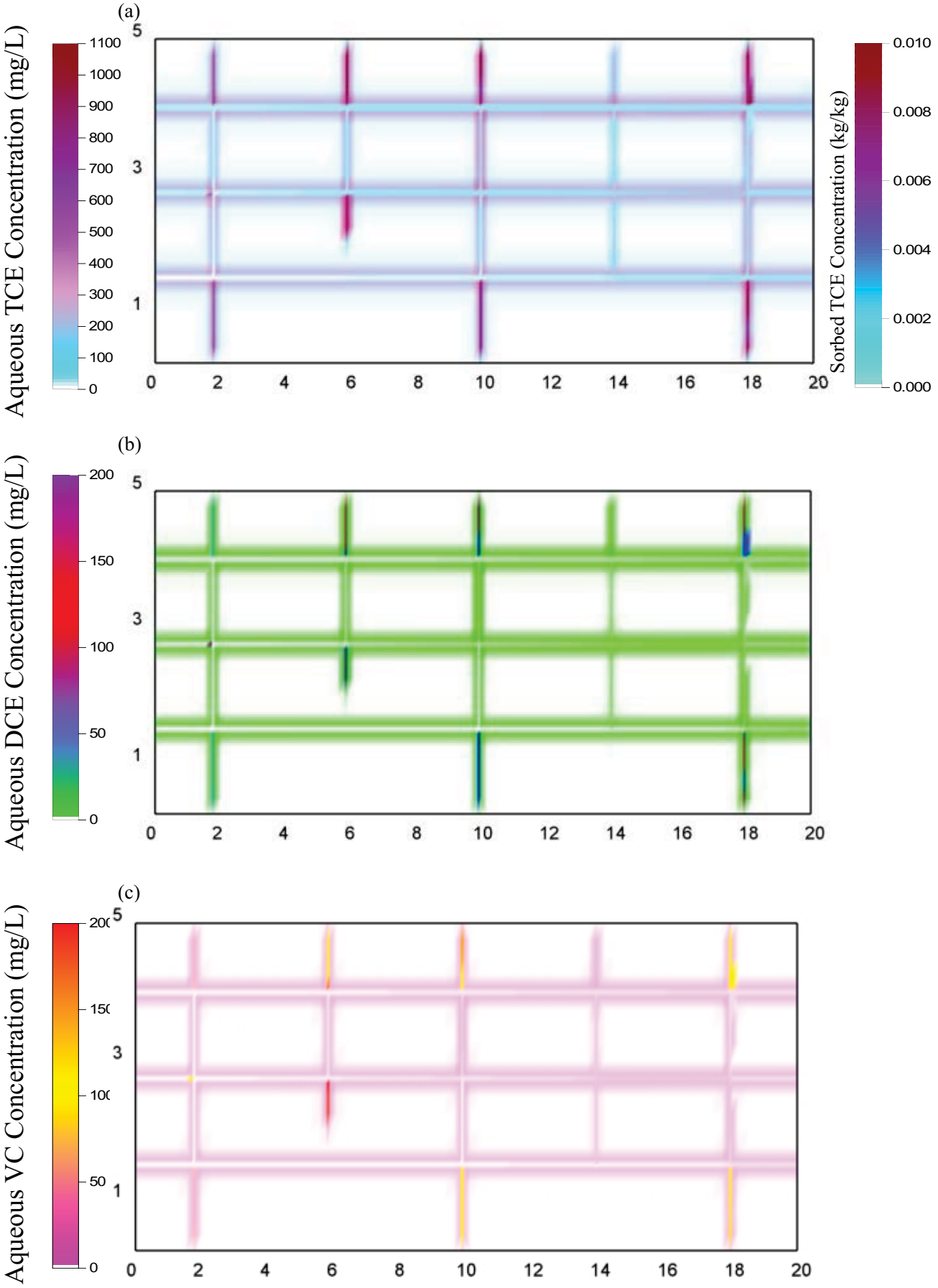
(a)
Aqueous TCE Concentration (mg/L)
1100
1000
900
800
700
600
500
400
300
200
100
0
Sorbed TCE Concentration (kg/kg)
0.010
0.008
0.006
0.004
0.002
0.000
5
3
1
0
2
4
6
8
10
12
14
16
18
20
(b)
Aqueous DCE Concentration (mg/L)
200
150
100
50
0
(c)
Aqueous VC Concentration (mg/L)

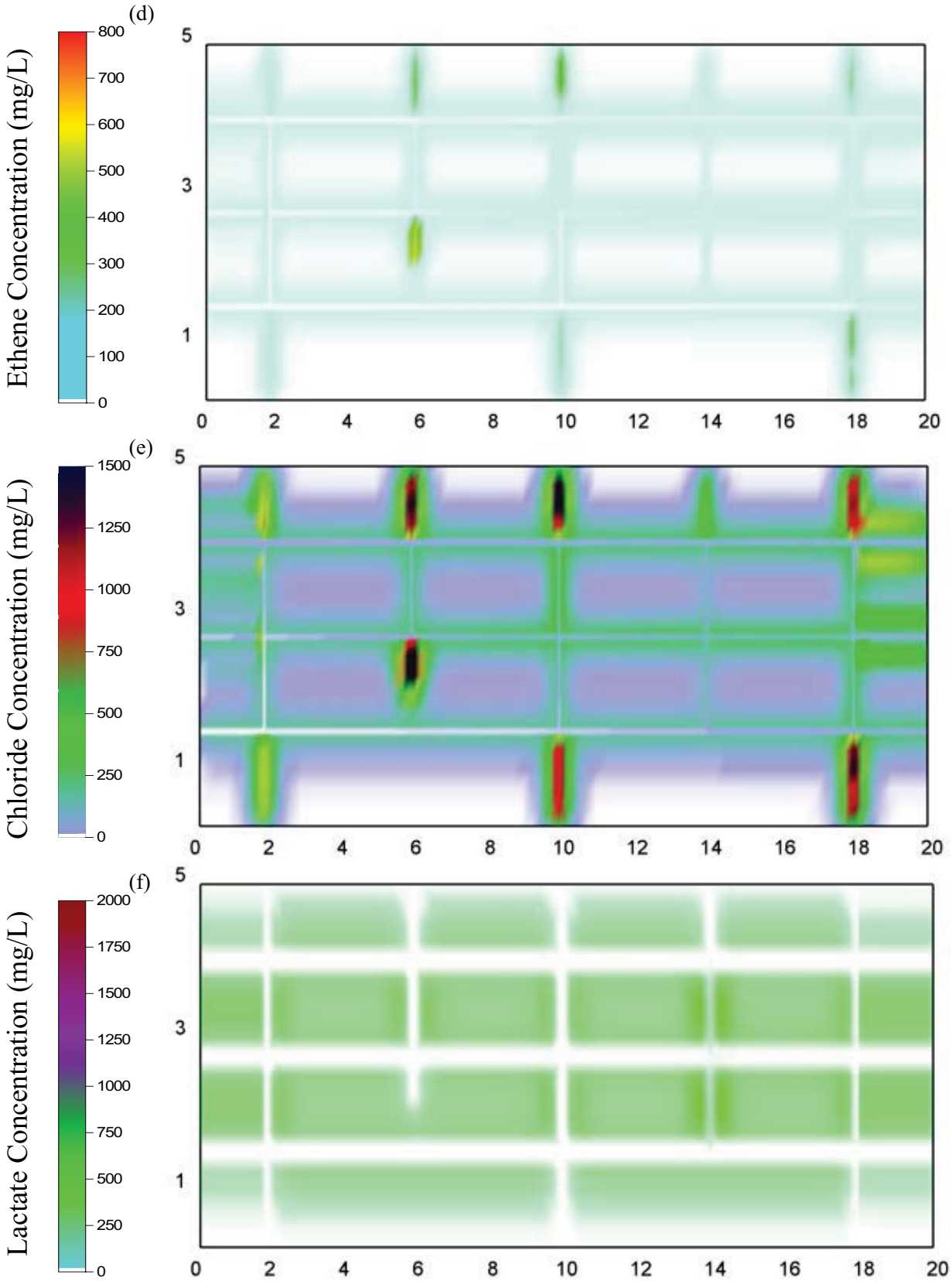

Figure B10: Distribution of (a) Aqueous TCE; (b) Aqueous DCE; (c) Aqueous VC; (d) Ethene; (e) Chloride; (f) Lactate, 5 years after lactate injection for Shale simulation.

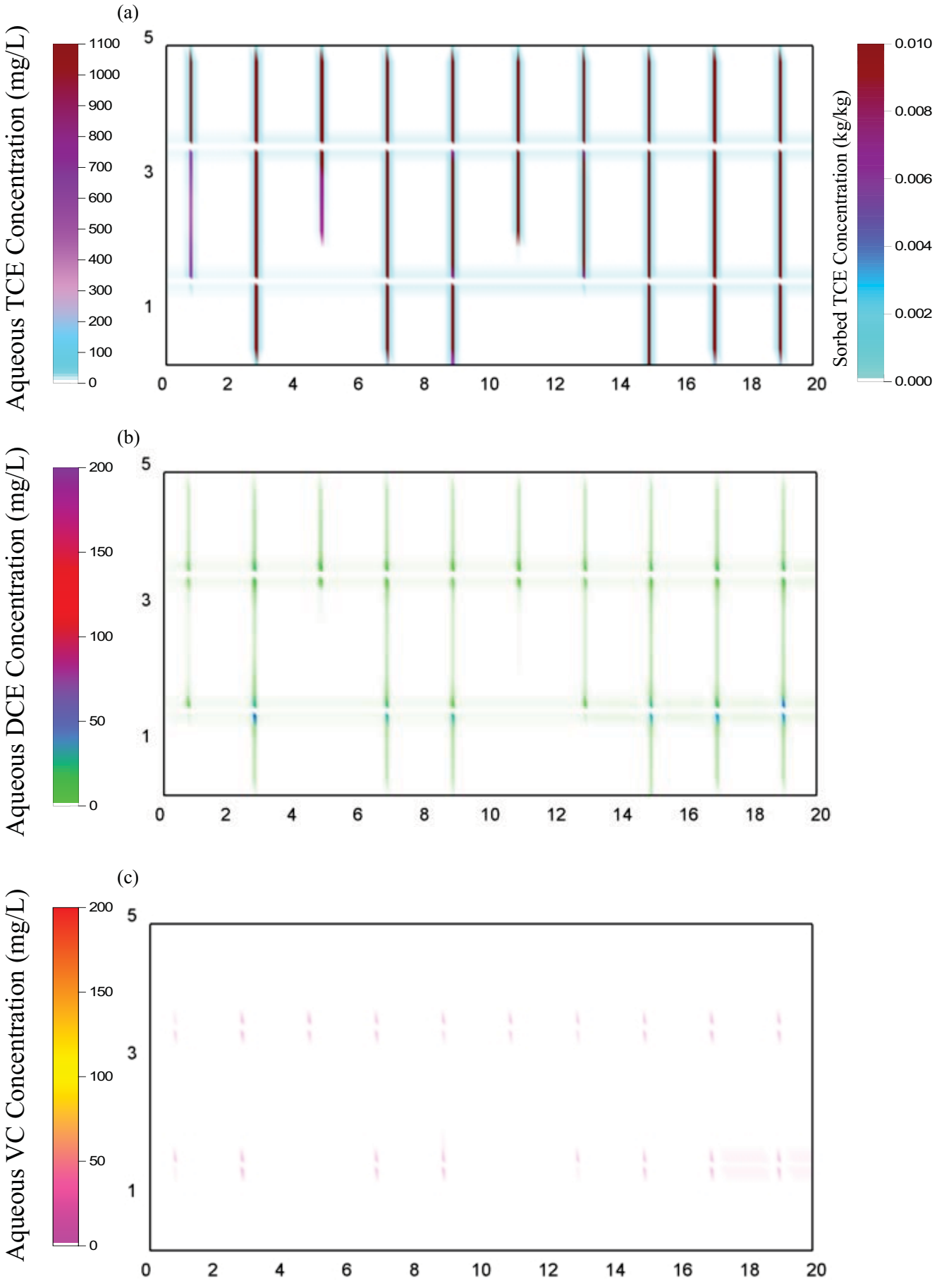
(a)
Aqueous TCE Concentration (mg/L)
1100
1000
900
800
700
600
500
400
300
200
100
0
5
3
1
0
2
4
6
8
10
12
14
16
18
20
Sorbed TCE Concentration (kg/kg)
0.010
0.008
0.006
0.004
0.002
0.000
(b)
Aqueous DCE Concentration (mg/L)
200
150
100
50
0
5
3
1
0
2
4
6
8
10
12
14
16
18
20
(c)
Aqueous VC Concentration (mg/L)
200
150
100
50
0
5
3
1
0
2
4
6
8
10
12
14
16
18
20

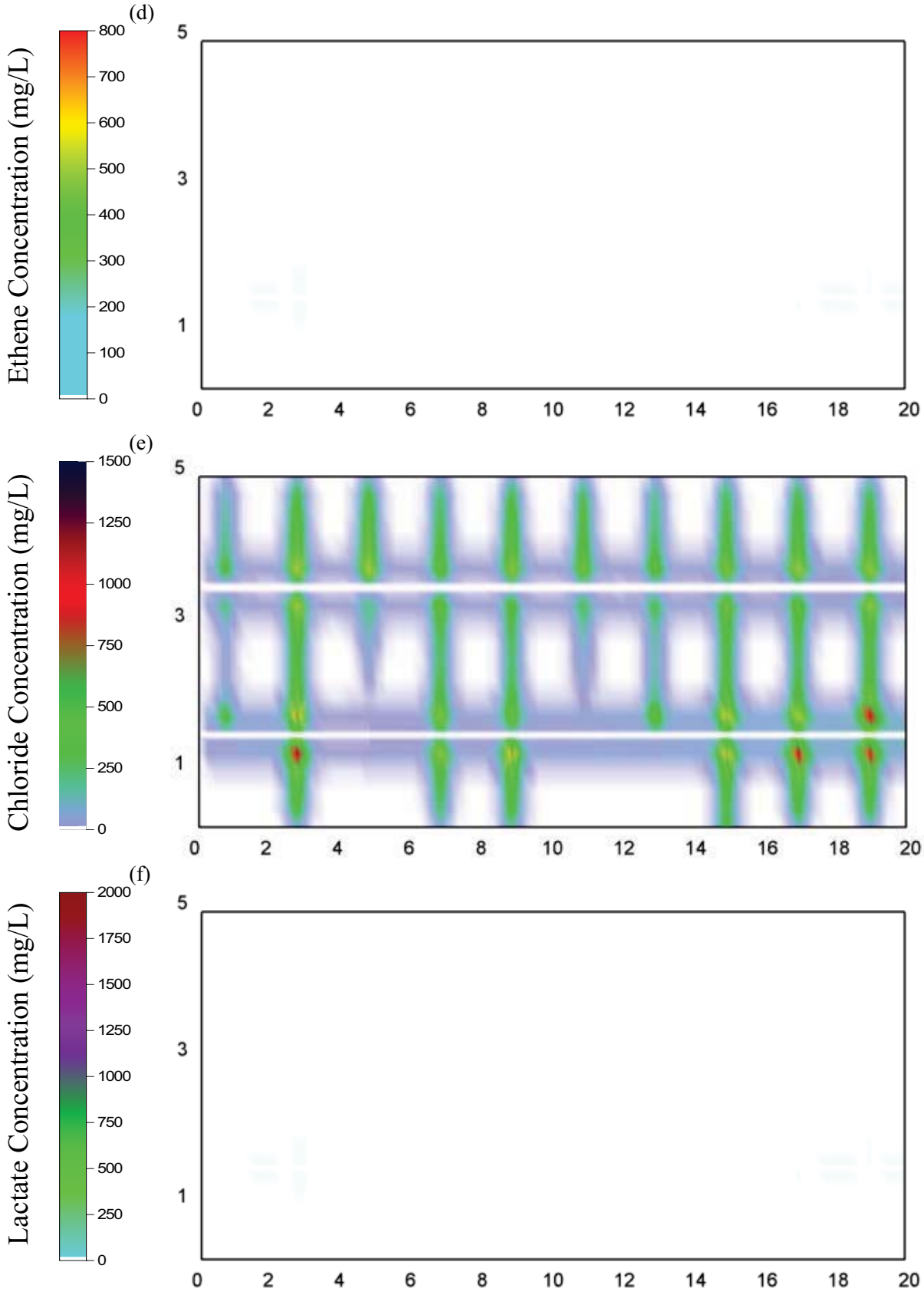

Figure B11: Distribution of (a) Aqueous TCE; (b) Aqueous DCE; (c) Aqueous VC; (d) Ethene; (e) Chloride; (f) Lactate, 5 years after lactate injection for Granite simulation.

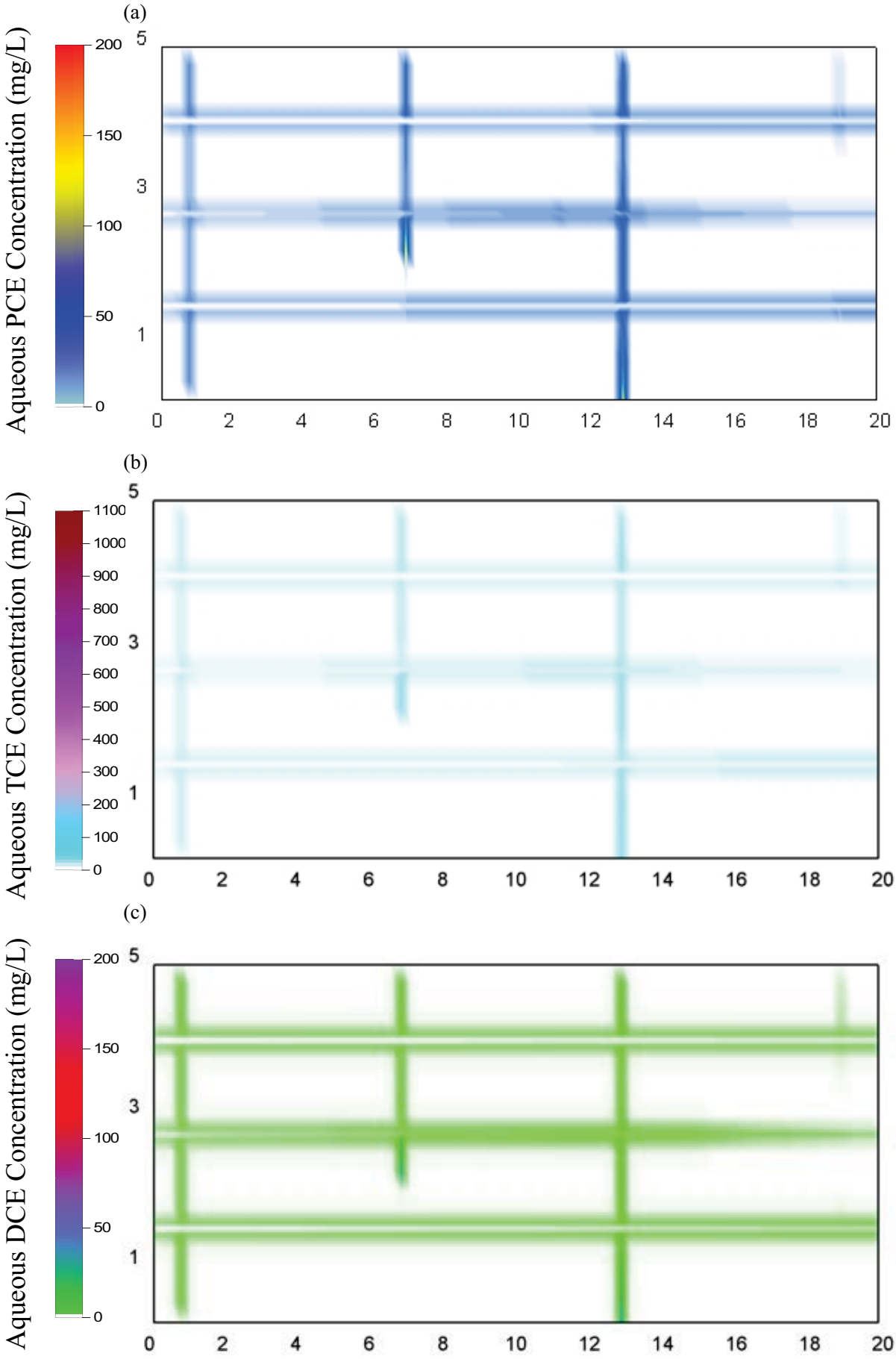
(a)
Aqueous PCE Concentration (mg/L)
200
150
100
50
0
5
3
1
0
2
4
6
8
10
12
14
16
18
20
(b)
Aqueous TCE Concentration (mg/L)
1100
1000
900
800
700
600
500
400
300
200
100
0
5
3
1
0
2
4
6
8
10
12
14
16
18
20
(c)
Aqueous DCE Concentration (mg/L)
200
150
100
50
0
5
3
1
0
2
4
6
8
10
12
14
16
18
20

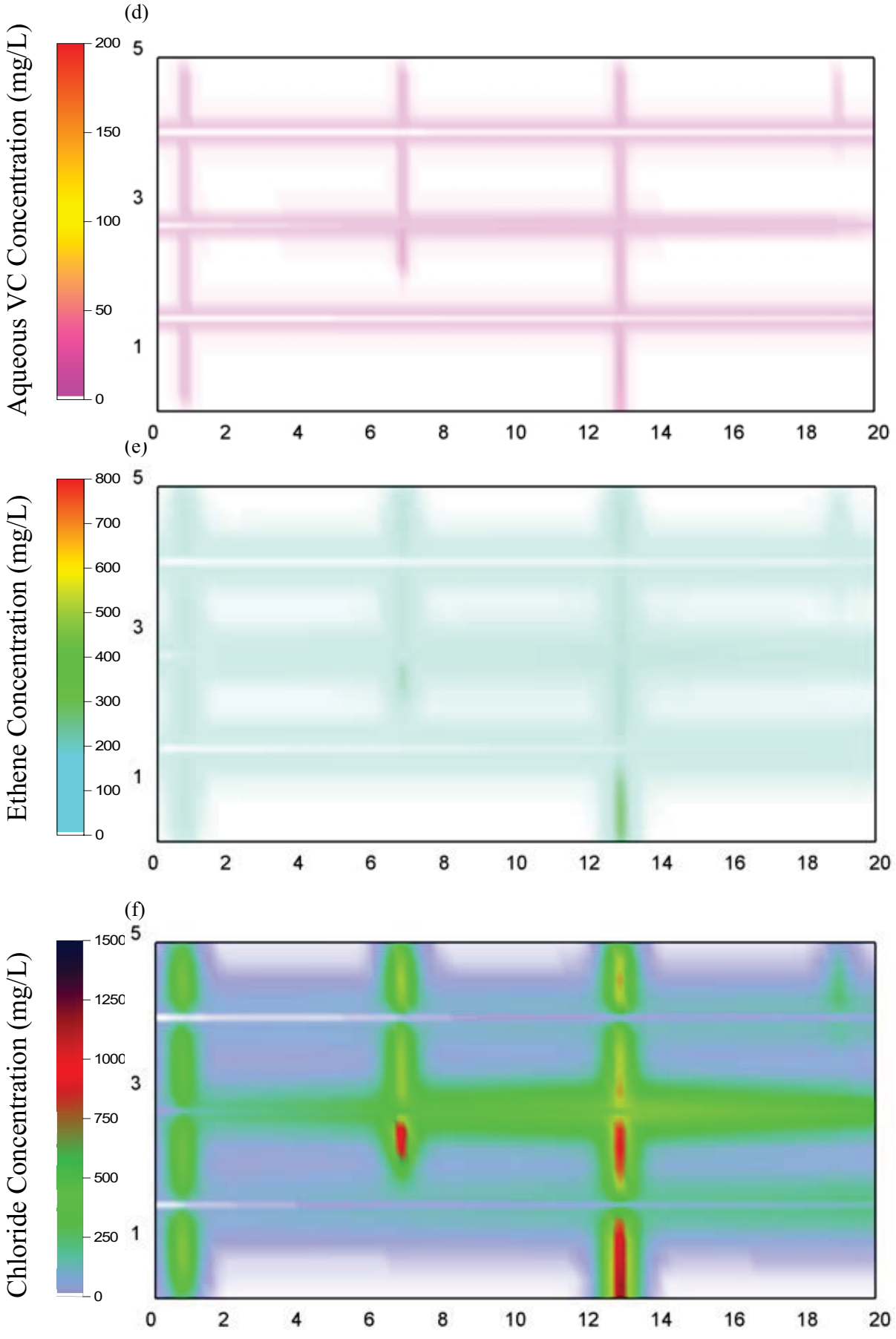
(d)
Aqueous VC Concentration (mg/L)
200
150
100
50
0
5
3
1
0
2
4
6
8
10
12
14
16
18
20
(e)
Ethene Concentration (mg/L)
800
700
600
500
400
300
200
100
0
5
3
1
0
2
4
6
8
10
12
14
16
18
20
(f)
Chloride Concentration (mg/L)
1500
1250
1000
750
500
250
0
5
3
1
0
2
4
6
8
10
12
14
16
18
20

Figure 4.1: Verification of DNAPL3D-RX

(g)

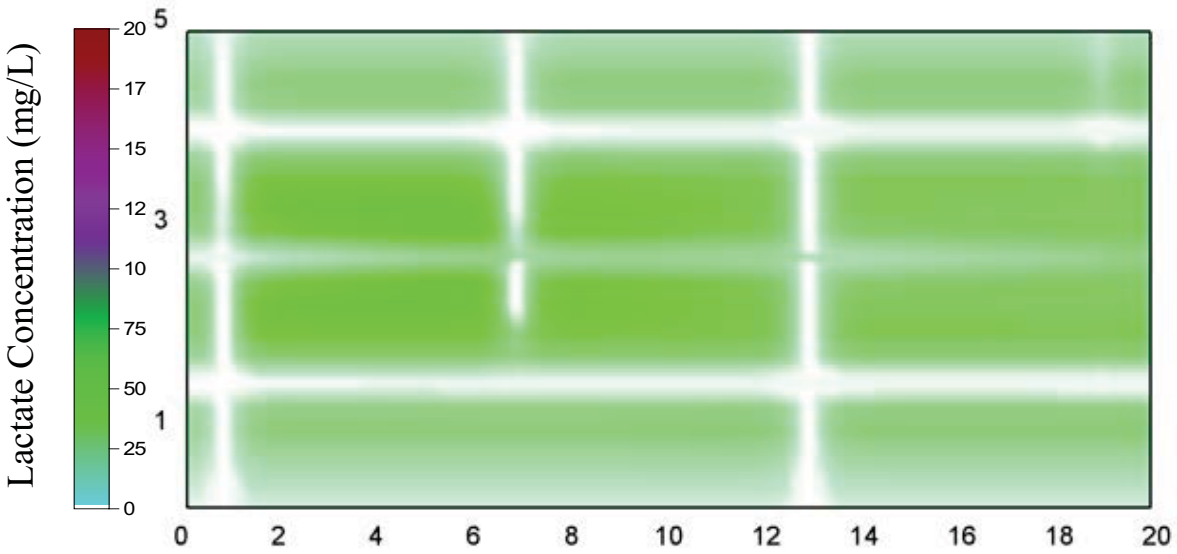

Figure B12: Distribution of (a) Aqueous PCE (b) Aqueous TCE; (c) Aqueous DCE; (d) Aqueous VC; (e) Ethene; (f) Chloride; (g) Lactate, 5 years after lactate injection for PCE simulation.

APPENDIX D.5

NUMERICAL SIMULATION OF DNAPL SOURCE ZONE REMEDIATION WITH SURFACTANT ENHANCED AQUIFER REMEDIATION (SEAR): FRACTURED ROCK

ABSTRACT

Numerical simulations were conducted to investigate the benefits and challenges of *in situ* surfactant flushing for chlorinated solvent dense, nonaqueous phase liquid (DNAPL) in fractured rock aquifers at the field scale. Two-dimensional (cross-section) simulations were conducted with DNAPL3DRX-FRAC, a finite difference multiphase flow-aqueous transport-reaction numerical model developed specifically for fractured rock simulations and augmented with enhanced DNAPL and aqueous solvent solubility for surfactant flooding applications. The base case simulation employed a complex DNAPL distribution in the fracture network generated via a surface release of trichloroethylene (TCE) and site ageing via dissolution and diffusion achieved significant matrix contamination. 11 surfactant flushing simulations with Tween-80 were conducted to explore sensitivity of DNAPL recovery and downgradient mass flux to a number of site specific properties (rock type, DNAPL type, extent of site ageing), engineering parameters (surfactant concentration), and modelling assumptions (mass transfer expression).

Surfactant flushing was found to be effective for DNAPL residing within horizontal fractures; however DNAPL was not removed from dead-end vertical fractures even after 5 years of post-treatment. Furthermore, all simulations predicted limited treatment for both aqueous and sorbed solvent within the matrix. Minimal difference was found in terms of the efficiency of surfactant flushing when the surfactant concentration was increased from 20g/L to 40g/L. Higher treatment efficiencies were observed in the

shale and sandstone while granite, with the largest fraction of initial mass entrapped in vertical fractures, experiences the lowest fraction of mass being recovered among the three rock types. It was further revealed that the aging period of each site, which directly affects the mass of aqueous and sorbed TCE within the matrix surrounding the fractures; affects the amount of TCE molecules being solubilised by surfactant micelles and subsequently the amount of back-diffusion when treatment ceases. When surfactant was applied to different DNAPLs, due to the difference in molar solubilisation ratios (MSRs), it was found that a higher fraction of aqueous PCE mass was entrained into micelles than for TCE. Furthermore, different mass transfer models were found to lead to significant difference to the amount of DNAPL left in the domain by the end of the simulation

1. INTRODUCTION

Surfactants are surface acting agents that concentrate at interfacial regions between two fluid phases (e.g., oil and water). They are amphiphilic agents that exhibit dual behaviour (i.e., affinity for both water and oil). This behaviour is possible due to their molecular structure which is made up of one soluble and one insoluble moiety. Surfactants are classified according to the nature of the hydrophilic portion of the molecule. The head can be positively charged (cationic), negatively charged (anionic), both negatively and positively charged (zwitterionic) or not charged (nonionic) (West and Harwell, 1992). Individual surfactant molecules are single monomers. However, when the aqueous concentration of monomers exceeds a critical value - the critical micelle concentration (CMC) - and the solution is above the limiting Krafft temperature, T_k, the monomers form into spherical clusters called micelles. Micelles exhibit a hydrophilic surface around an lipophilic core.

Due to these properties, micelles are capable of encapsulating non-aqueous phase liquids (NAPLs) and forming microemulsions. As a result, surfactants can decrease the interfacial tension (IFT) between water and NAPL and can increase the effective aqueous solubility of NAPL components. The former allows NAPLs contacted with surfactants to be mobilized towards recovery wells due to a reduction in capillary resistance to flow, while the latter allows NAPL mass to be removed by enhanced dissolution. However, mobilization of DNAPL in particular may cause it to move deeper into former uncontaminated zones (Pankow and Cherry, 1996). For this reason, some researchers recommend using solubilisation rather than mobilization as the primary surfactant

treatment mechanism in DNAPL systems. However, solubilisation of contaminant by the surfactant creates a microemulsion phase that is denser than the surrounding groundwater and can travel downward before being captured by an extraction well (Ramsburg and Pennell, 2002).

Laboratory-scale experiments have demonstrated that DNAPLs can be efficiently recovered in unconsolidated porous media using two-phase (immiscible) displacement technologies (e.g., Lunn and Kueper, 1999; Ramsburg and Pennell, 2002; Miller et al., 2000; Kostarelos et al., 1998). Surfactant-enhanced aquifer remediation has been demonstrated to effectively recover contaminants (including chlorinated solvents) in a variety of subsurface environments, (Taylor et al., 2004; Zhong et al., 2003, Abriola et al., 2005; Suchomel et al., 2007). The use of surfactants for remediation of unconsolidated porous media at field sites contaminated by DNAPL has been investigated by numerous research groups (e.g., Ellis et al., 1986; Gannon et al., 1992; Pennell et al., 1994; Pope and Wade, 1995; Shiau et al., 1995; Fountain et al., 1996; Martel and Gelinas, 1996; Hirasaki et al., 1997).

However, the effectiveness of surfactants in fractured rock is not known. The author has found only one publication investigating the use of surfactants for DNAPL trapped in fractures. Yeo et al. (2003) conducted three bench scale experiments using an artificial two-dimensional fracture network that was made from a 20 cm by 15 cm acrylic plate with a thickness of 2 cm. The removal of DNAPL trapped in vertical dead-end fractures was examined in this study. It was found that a water-flushing method failed to remove DNAPL TCE from fractures, failing to overcome the vertical capillary and gravity forces

that trapped the DNAPL. Subsequently, a fluid denser than TCE (made up of a mixture of 50% water and 50% calcium bromide) was injected into the fracture network, but this too did not displace the TCE DNAPL. However, a mixture of calcium bromide and 0.8% sodium doceyl sulphate surfactant did effectively displace the trapped DNAPL, suggesting that surfactants could act similarly in fractured rock as in unconsolidated porous media.

The objective of this work is to examine the benefits and challenges of DNAPL source zone remediation in fractured bedrock aquifers by surfactants at the field scale. Numerical simulations are employed to evaluate the effectiveness of surfactant remediation via enhanced dissolution as a function of key site parameters (fractured rock type, degree of contamination, DNAPL type) as well as an engineering parameter (surfactant concentration), and a modelling assumption (rate of mass transfer).

2. MODEL DEVELOPMENT AND TESTING

A more detailed description on the development of the model DNAPL3DRX-FRAC is provided in Appendix B2. The processes described here are aimed to provide the reader with an understanding of the approach being adopted to develop the surfactant treatment package of the model.

Surfactant Flushing Kinetics

For the purpose of this study, the subsequent discussion is limited to surfactant flushing of DNAPLs by Tween-80 (polyoxyethylene (20) sorbitan monooleate). Although a number of surfactant types exist, Tween-80 was selected for these studies due to its

frequent use in DNAPL remediation research and field trials (e.g., Abriola et al., 1993; Jafvert et al., 1995; Ramsburg and Pennell, 2002; Ramsburg et al., 2005, Chu and So, 2001; Zhang et al., 2006). Nonionic surfactants such as Tween-80 tend to possess the most desirable characteristics for *in situ* subsurface remediation. For example, nonionic surfactants do not dissociate and do not produce ions in an aqueous solution, they are fairly insensitive to electrolytes, and can be utilized in aqueous solutions with high salinity or significant hardness. Additionally, nonionic surfactants tend to have low biotoxicity and may be biodegradable. Tween-80 is typically applied at concentrations in the range of 2.0 – 6.0% (Abriola et al., 1993; Jafvert et al., 1995; Ramsburg and Pennell, 2002; Ramsburg et al., 2005).

DNAPL solubilisation will be considered the dominant recovery mechanism in this work. DNAPL mobilization is not expected to be as significant a recover mechanism in DNAPL source zones which have undergone considerable redistribution (and loss) of DNAPL outside the treatment zone. This work considers scenarios in which, after termination of the source, DNAPL has been allowed to redistribute freely out of the sides and bottom of the domain prior to remediation commencing in the near-surface fractured rock source zone. Hence much of the DNAPL is at residual and the remaining horizontal DNAPL pools are limited and only present at high saturations in dead-end vertical fractures. Neglecting IFT reduction by Tween-80 in these situations is expected to not have a dominant effect on the conclusions.

Solubilisation

A measure of the effectiveness of a particular surfactant in solubilising a given DNAPL is

known as the molar solubilisation ratio (MSR). MSR is defined as the number of moles of organic compound solubilised per mole of surfactant added to solution (Attwood and Florence, 1983). The MSR may be calculated (Edwards et al., 1991):

$$MSR = \frac{C_{eq}^{CE} - C_{cmc}^{CE}}{\left(C^{Surf} - C_{cmc}^{Surf}\right)} \qquad (1)$$

Where C_{eq}^{CE} (mol/L) is the equilibrium chlorinated ethene solute concentration in the presence of a given surfactant concentration greater than the CMC; C_{cmc}^{CE} (mol/L) is the concentration of chlorinated ethene DNAPL at CMC (normally assumed to be the solubility of the DNAPL); C^{Surf} is the given surfactant concentration and C_{cmc}^{Surf} is the surfactant CMC. C_{cmc}^{Surf} is 13mg/L for Tween-80 (Taylor et al., 2001).

Micellear Partitioning Below DNAPL Solubility

Equation 1 is only valid in the presence of both DNAPL (i.e. $C_{eq}^{CE} > C_{cmc}^{CE}$) and surfactant concentrations greater than the CMC. Since most studies in unconsolidated porous media are particularly focused on the interactions of high surfactant concentrations with excess DNAPL, this equation is typically considered sufficient. However, in fractured rock, the matrix may prevent DNAPL penetration but nevertheless be a significant medium for diffusive transport of both aqueous chlorinated solvents and surfactant monomers/micelles. Thus, it is necessary here to consider surfactant concentrations above the CMC in the presence of chlorinated solvent concentrations that are less than their standard equilibrium solubility (C_{cmc}^{CE}).

Using batch partitioning experiments, Kim et al. (2007) demonstrated a linear correlation between the fraction of chlorinated ethene (TCE and PCE) that remained external to the micelles (extramicellar) as a function of aqueous chlorinated ethene concentration up to their standard aqueous solubilities (Figure 1). The figure further demonstrates that for a given concentration of aqueous PCE and TCE, as the concentration of Tween-80 increased from 0.2 to 1.0 wt%, the extramicellar mass fraction decreased approximately 50% (Figure 1).

Each curve in Figure 1 was averaged to obtain a single ratio of extramicellular chlorinated ethene to total chlorinated ethene concentration as a function of surfactant concentration (Figure 2, for TCE; Figure C1, Supplementary Information, for PCE). An exponential relationship was best-fit to the range of concentrations examined by Kim et al (2007), 0.2% < C^{Surf} < 1.0% (R^2 = 0.989). As shown in Figure 2, this function was extrapolated to obtain a relevant extramicellular ratio for Tween-80 at 4.0%. In the absence of data, a linear function was assumed to apply in the region C^{Surf} < 0.20%. Therefore, the model employs these relationships to determine the equilibrium extramicellular mass fraction of chlorinated ethene at a given surfactant concentration (C_{TCE}^{EX}) in the absence of DNAPL:

TCE:

$$\frac{C_{TCE}^{EX}}{C_0} = 1 - 3.515 C^{Surf},\ 0.0\% \le C^{Surf} \le 0.2\% \qquad (2a)$$

$$\frac{C_{TCE}^{EX}}{C_0} = 0.37 e^{-C^{Surf}},\ C^{Surf} \ge 0.2\% \qquad (2b)$$

PCE:

$$\frac{C_{PCE}^{EX}}{C_0} = 1 - 4.406 C^{Surf}, \quad 0.0\% \le C^{Surf} \le 0.2\% \qquad (3a)$$

$$\frac{C_{PCE}^{EX}}{C_0} = 0.12 e^{-C^{Surf}}, \quad C^{Surf} \ge 0.2\% \qquad (3b)$$

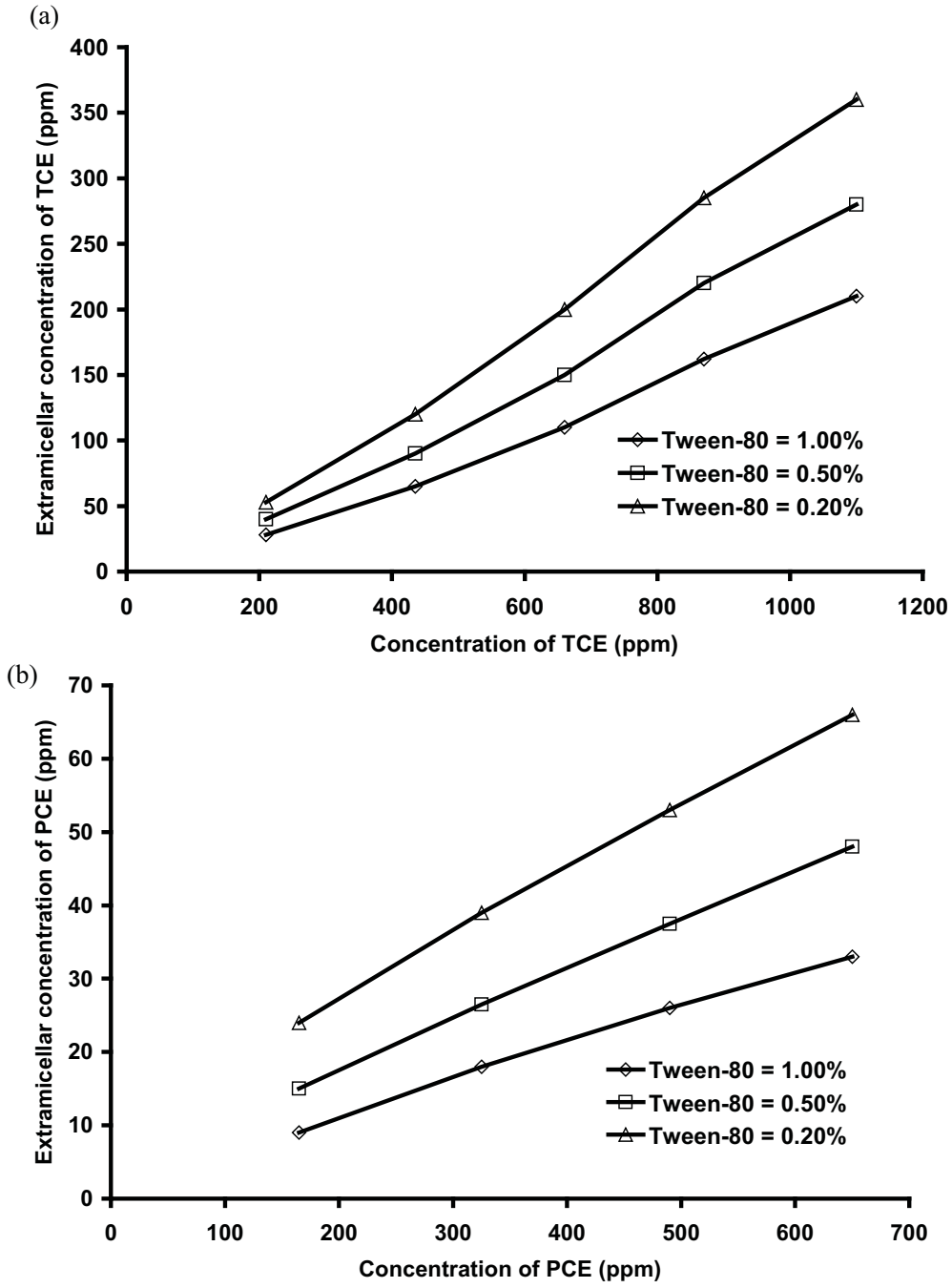

Figure 1: Extramicellar concentration of (a) TCE and (b) PCE in Tween-80 solution (Data extracted from Kim et al., 2007).

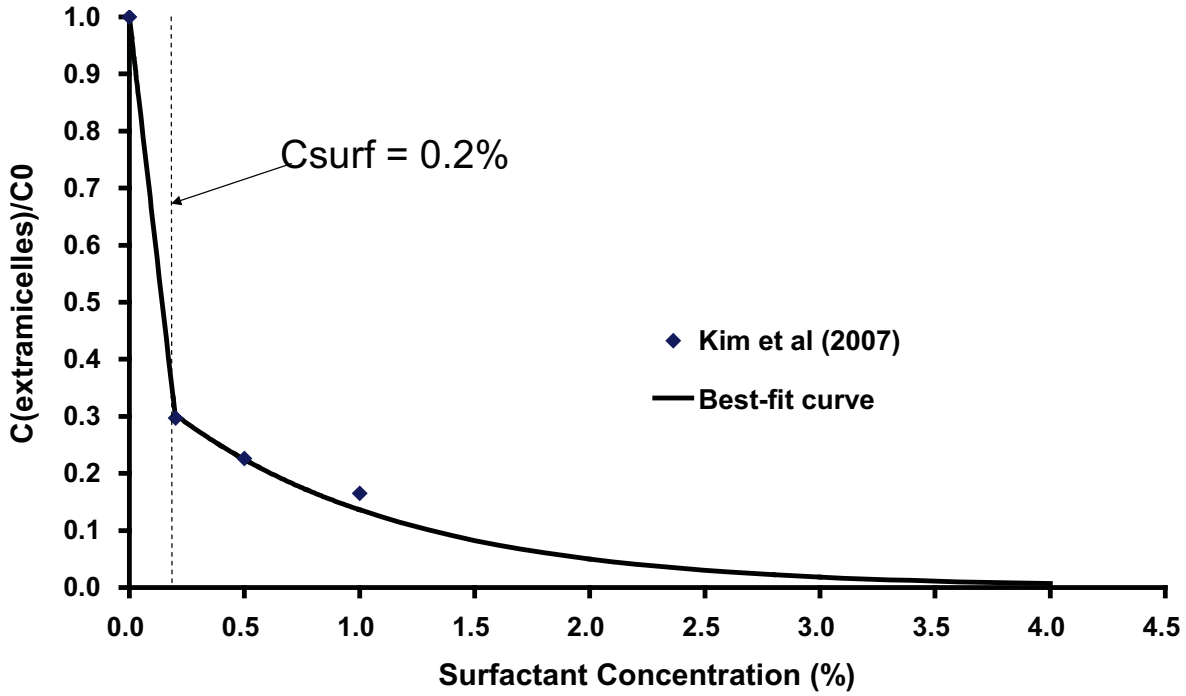

Figure2: Extramicellar best fit curves for TCE based on results extrapolated from Kim et al., 2007.

Surfactant Reaction Module

The model simulates three separate, mobile aqueous species: (1) aqueous chlorinated ethene solute (2) 'surfactant' (monomers and micelles free of chlorinated ethene), and (3) 'micelles' (surfactant micelles containing chlorinated ethene).

Within each timestep, the model determines the distribution of surfactant and treats separately those nodes with DNAPL and those without. For nodes containing DNAPL and if the concentration of surfactant is above the CMC level, C_{eq}^{CE} (the equilibrium concentration of chlorinated ethene for a given surfactant concentration) is determined via Equation 1. Equilibrium mass transfer is assumed in reducing the DNAPL saturation and increasing the concentration of chlorinated ethene in the aqueous phase. If C_{eq}^{CE} exceeds the standard DNAPL aqueous solubility (i.e., 1100mg/L for TCE and

200 mg/L for PCE), all the mass that exceeds the standard solubility is then immediately moved from the aqueous solvent species into the micelle species (i.e., the former decreases in proportion the increase in the latter; no kinetics assumed). As micelles become occupied with solvent, the micelle species increases in concentration and the surfactant species concentration decreases correspondingly (i.e., total surfactant mass is conserved).

For nodes containing chlorinated ethene mass but no DNAPL, (e.g., a matrix node), if the concentration of surfactant is present and above the CMC level, Equations 2 or 3 is employed to determine the amount of mass that partitions into the micelles, and the concentration of all three species are updated accordingly. It is assumed that, once entrained, chlorinated ethene mass will not partition back out of the micelles.

After which, the model calculates the concentration of the micelles for each node by summing up the mass of chlorinated ethene partitioned into the micelles together with the surfactant mass used in this process and dividing it by the molecular weight of the micelle species as determined by the sum of molecular weight of chlorinated ethene and surfactant.

Sorption

Abriola et al. (2005) found that sorption of Tween-80 to sand conformed to a Langmuir isotherm. The retardation factor for a Langmuir sorption isotherm is (Fetter, 1993):

$$R = 1 + \frac{\rho}{\phi}\left(\frac{\alpha\beta}{(1+\alpha C)^2}\right) \qquad (4)$$

where α is an adsorption constant related to the binding energy (L^3M^{-1}), β is the maximum amount of solute that can be adsorbed by the solids (MM^{-1}), ρ is the dry bulk density (ML^{-3}), ϕ is the porosity of the matrix (-) and C is the concentration of the solute (ML^{-3}). Via the batch experiments, Abriola et al. (2005) yielded a maximum sorption capacity of 0.17 ± 0.02 mg/g and an adsorption constant of 0.12 ± 0.04 L/mg.

This finding was consistent with previous studies in which the maximum sorption of Tween-80 by sands having low organic carbon content ranged from 0.16 to 0.19 mg/g (Taylor et al., 2001). In the absence of literature on the sorption capacity of Tween-80 in fractured rocks, a Langmuir isotherm is assumed. In this work, an appropriate fraction of organic carbon is assigned to the matrix for each rock type and thus Equation 4 applies to all matrix nodes. However, the fractures are assumed to be free of organic carbon and thus sorption is negligible in the fractures. Lipson et al. (2005) studied a system of equally spaced fractures from the field and determined that when matrix diffusion effects are dominant, fracture retardation can be assumed equal to 1. Sensitivity to different Tween-80 sorption isotherms is likely small at the high surfactant concentrations (40000 – 60000 mg/l) employed in this work.

For the purpose of this study, the retardation factor for the aqueous chlorinated ethene is calculated as:

$$R_i = 1 + Koc \times foc_i \frac{\rho}{\theta} \qquad (5)$$

where ρ is the dry bulk density (ML^{-3}), θ is the porosity of the matrix (-), and *Koc* is the organic carbon partition coefficient (L^3M^{-1}). No sorption was assumed for the micelles

(Liu et al., 1992). The proper implementation of both retardation isotherms in the model was verified at both the scales of a single node and field scale simulation (see Appendix B2 for details),

Mass Transfer

DNAPL to water mass transfer is treated as an equilibrium process in the simulations presented in this work. It is acknowledged that non-equilibrium mass transfer has been observed in experimental fractured systems (e.g., Glass and Nicholl 1995; Dickson and Thomson 2003). Appendix B2, which examined DNAPL dissolution over substantial aging periods in fractured rock, suggested that the matrix provides such a substantial mass sink that chlorinated solvent DNAPL dissolves relatively rapidly (on the order of years, not decades). Therefore, it may be that DNAPL dissolution in these scenarios is relatively insensitive to mass transfer routine.

However, since surfactant flushing is a mass transfer-dependent technology, the prudent step was taken to incorporate an appropriate rate-limited dissolution model for fractures. Dickson and Thomson (2003) carried out eight long-term dissolution experiments using 1,1,1-trichloroethane (1,1,1-TCA) and trichloroethylene (TCE) in two laboratory-scale dolomitic limestone variable aperture fractures. The experimental data were used in conjunction with statistical techniques to develop a continuous empirical model describing the (initial) pseudosteady and transient stages of dissolution. The model was then used in that work to successfully replicate effluent concentration data from two separate dissolution experiments providing an indication of the expected dissolution behaviour of entrapped DNAPLs.

Sherwood number, proportional to kinetic mass transfer rate, was determined to be (Dickson and Thomson, 2003):

$$Sh = 7.718 R_e^{1.621} \delta^{2.439} Sn^*(t)^{8.826} \qquad Sn^*(t) \geq 1 \qquad (6.6a)$$

$$Sh = 7.718 R_e^{1.621} \delta^{2.439} Sn^*(t)^{4.338} \qquad Sn^*(t) \leq 1 \qquad (6.6b)$$

$$Sn^*(t) = \frac{Sn(t)}{Sn_{8\%}} \qquad (6.6c)$$

where $Sn(t)$ and $Sn_{8\%}$ are the DNAPL saturation and DNAPL saturation when 8% of initial mass is removed, respectively. Re is the Reynold's number and δ is the aperture ratio which takes into account of the range of extreme apertures (δ is taken equal to unity in this study, corresponding to parallel plate fracture geometries). The majority of mass removal was demonstrated to occur during the initial pseudosteady and early transient stages of dissolution (Dickson and Thomson, 2003; Miller et al., 1990). Dickson and Thomson (2003) demonstrated the initial pseudosteady stage to typically last until an average of 8% of the initial mass trapped was removed, or until the initial volumetric DNAPL saturation Sn(t = 0) was reduced by 8% as denoted by $Sn_{8\%}$.

Model Verification

A more detail description on the model verification process of DNAPL3DRX-FRAC is provided in Appendix B2. For the purpose of this study the subsequent discussion is limited to the verification of the surfactant treatment package of the model.

Surfactant Flushing Verification

Since no analytical solution is available for verifying the surfactant model in fractured rock, several steps were taken to build confidence in the developed model. First, a one-dimensional simulation of surfactant flushing of a DNAPL pool in a single horizontal fracture was carried out and compared with calculations via Equation 1. Fluid properties and reaction parameters for this simulation are listed in Table 1. It is noted that, in the absence of a published diffusion coefficient for micelles, this was taken as equal to the diffusion coefficient of Tween-80.

The simulation considers a representative sandstone formation at the scale of a single DNAPL pool via a two-dimensional domain 20 m wide × 2.25 m high with unit depth. The coarse, uniformly discretized domain employed DX = 0.25m and DY = 0.25m. A single, horizontal fracture was defined with an aperture of 128μm. Grid refinement was then conducted using N = 5 together with nodal dimensions increasing exponentially with distance from the fracture.

The initial condition was a stationary 5.0m pool of TCE DNAPL, located in the fracture 1.0 m from the left hand boundary, exhibiting an effective DNAPL saturation of 0.3 (Figure 3). DNAPL migration was not permitted in order to focus on the solubilisation process exclusively in this test. Surfactant solution (4.0% Tween-80) was then injected via the left hand boundary for 1 year. A series of calculations for all three species in the domain were then conducted to check mass balance of all species throughout the entire simulation.

Table 1 Fluid Properties and Reaction Parameters for Verification Simulation

Parameter	Notation	Value
TCE Density [a]	ρ_{NWtce}	1460 kg/m^3
TCE Viscosity [a]	μ_{NWtce}	0.0005 Pa s
TCE Solubility [a]	$Solub_{TCE}$	1100 mg/L
TCE Free Solute Diffusion Coefficient [b]	D^O_{TCE}	1.01 x10^{-9} m^2/s
Tween 80 Free Solute Diffusion Coefficient [c]	$D^O_{Tween\ 80}$	2.00 x10^{-6} m^2/s
Micelles Free Solute Diffusion Coefficient	D^O_{TCEMic}	2.00 x10^{-6} m^2/s

a – Pankow and Cherry (1996)
b –Wilke and Chang (1955) at 25°C
c –Amidon et al. (1982)

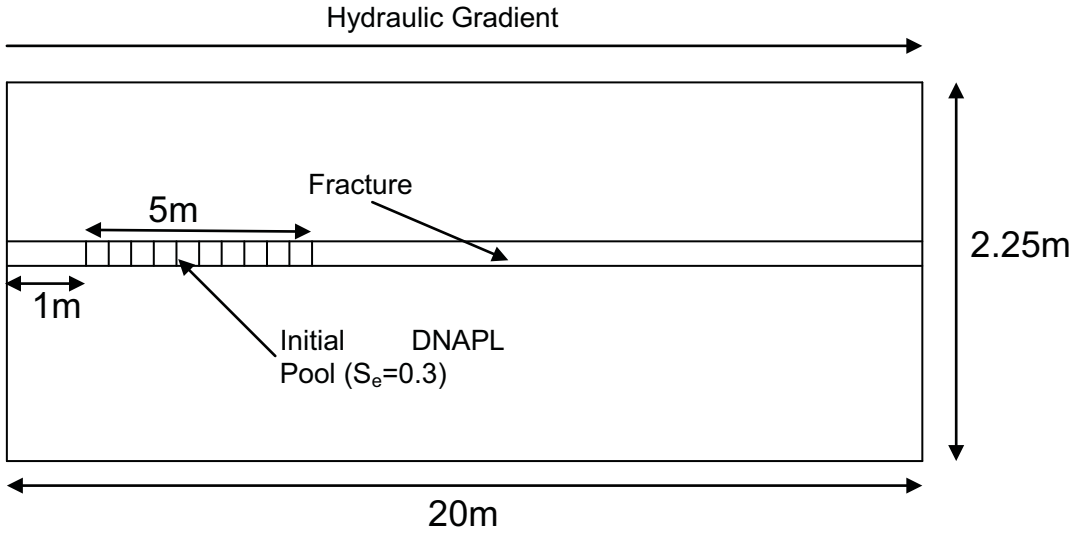

Figure 3: Sketch of domain layout for test simulation.

Figure 4 plots the cumulative concentration of TCE, surfactant and micelles within a node in the horizontal fracture, 1.5m from the left boundary (in the DNAPL pool) over time. Recall that 'surfactant' refers to monomers plus micelles that are TCE-free while 'micelles' refers to the TCE concentration occupying the micelles. It is demonstrated

that as surfactant was injected into the fracture, micelles began to form quickly as the DNAPL was solubilised by the surfactant. By the second month, Figure 4 reveals the TCE solute in the aqueous phase decreases quickly, indicating that DNAPL in this node has been completely solubilised (Figure 5). Figure 4 further demonstrates that prior to the disappearance of DNAPL from this node, the surfactant species concentration in this node was negligible; indicating that virtually all the Tween-80 in this node was used in solubilising the DNAPL in the node. These results are consistent with what one would expect to find with respect to DNAPL solubilisation, providing confidence that the model is working accurately. Additionally, excellent mass balance was observed throughout the entire simulation for all three species (Figure not shown).

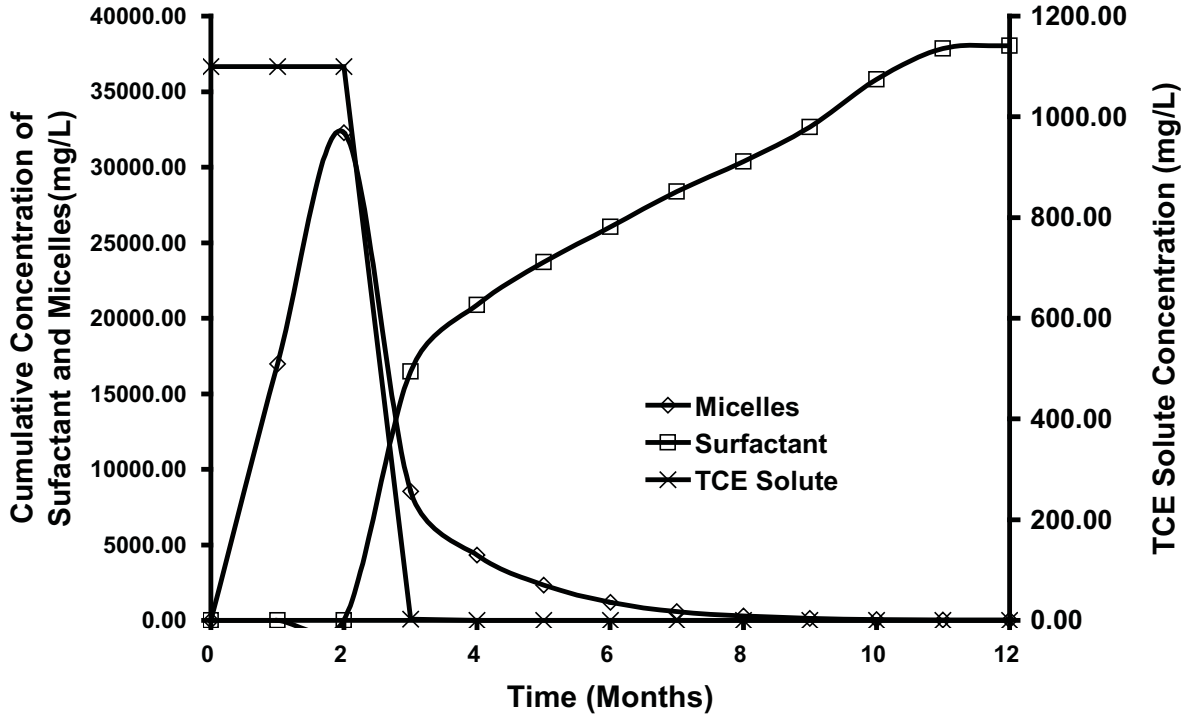

Figure 4: Cumulative aqueous mass of aqueous TCE, micelles, and surfactant species in a node over time for verification run.

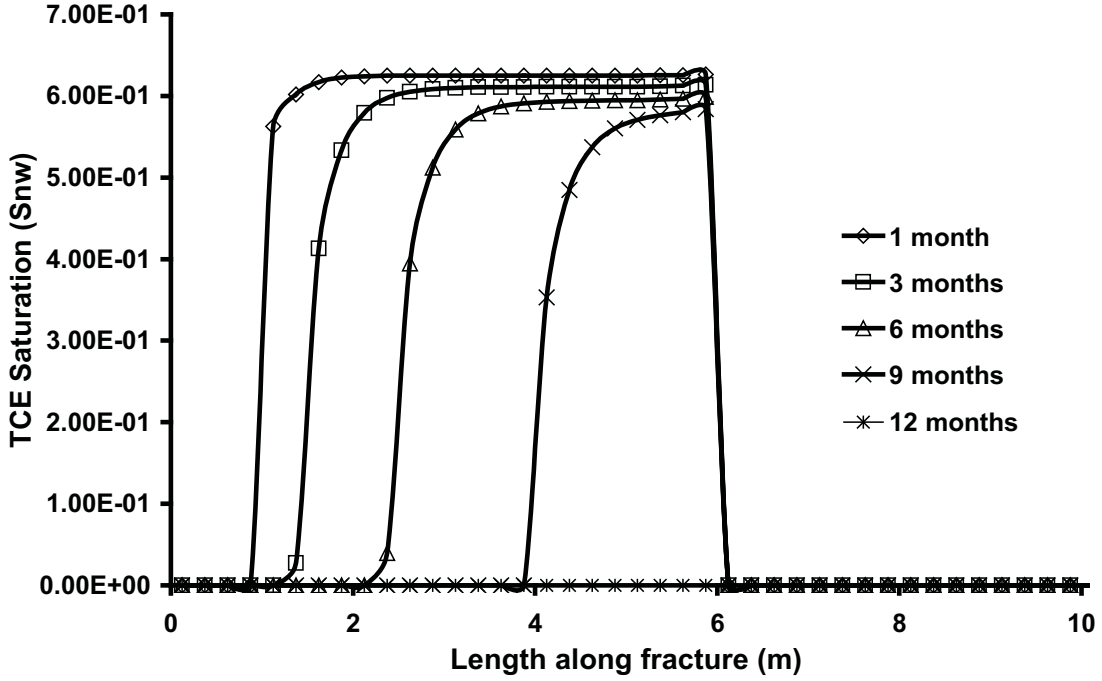

Figure 5: TCE saturation along the length of fracture over time.

The simulation also confirmed that, in addition to DNAPL solubilisation, micellularization of aqueous TCE in the absence of DNAPL is correctly modelled (Equations 2a and 2b) (calculations not shown).

In order to verify the accuracy of the rate-limited mass transfer model, one scenario from Dickson and Thomson (2003) was reproduced. Dickson and Thomson (2003) calibrated their predictions to their laboratory results for DNAPL dissolution in a single rough-walled fracture. As demonstrated by Figure 6, DNAPL3DRX-FRAC predicted similar behaviour to the published results of Dickson and Thomson (2003), providing confidence that the rate-limited mass transfer model is correctly implemented in the code. Altogether, these simulations provide confidence in the model to calculate both the surfactant treatment reaction kinetics equations 1 – 6 and the rate limited mass transfer

process accurately.

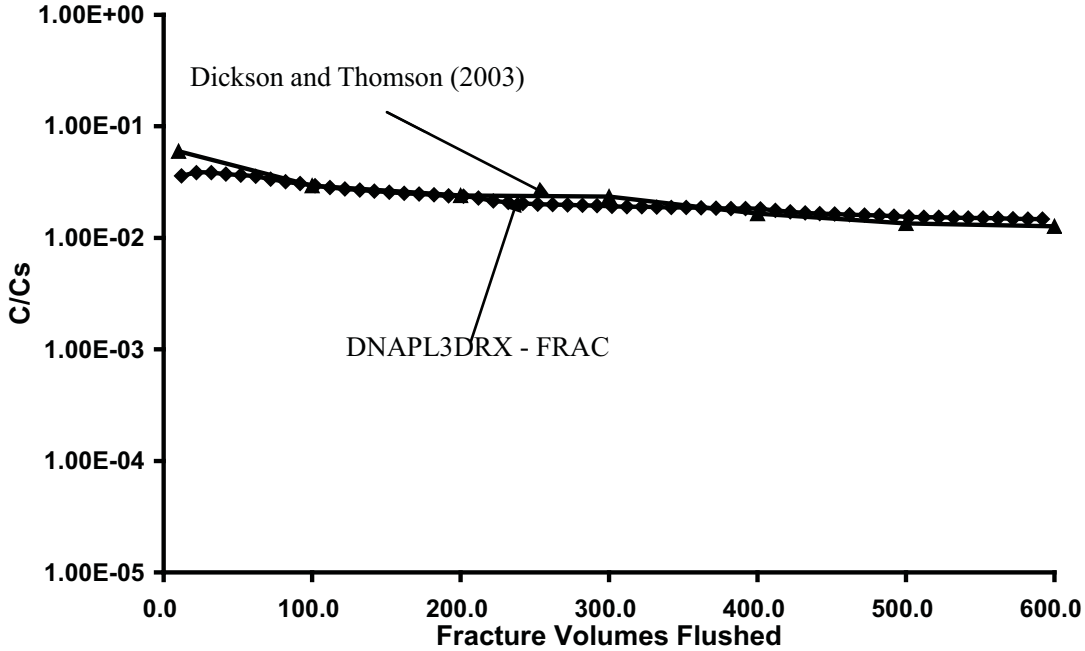

Figure 6: Verification of rate-limited model and compared against results from Dickson and Thomson, 2003.

3. NUMERICAL SIMULATIONS

Modelled Scenario

This section describes characteristics common to all of the simulations conducted for the surfactant treatment study (See Section 4.4.1 for the layout of the domain applicable to each simulation), while the next details the characteristics of the individual runs.

Each simulation in the surfactant treatment study evolved according to six distinct stages: (i) DNAPL Release, (ii) DNAPL Redistribution, (iii) Site Ageing, (iv) DNAPL Mapping, (v) Treatment Application, and (vi) Post-Treatment Ageing. For all stages, the water table was set to be coincident with the top boundary. During the DNAPL Release and

DNAPL Redistribution stages, constant head specified at the side boundaries during DNAPL migration established a zero hydraulic gradient across the domain. Also, the bottom boundary permitted the free exit of both water and DNAPL. At t = 0, the 'DNAPL Release' stage began by specifying a constant DNAPL saturation of 30% across the entire top boundary. Note that in this work, DNAPL is considered the nonwetting fluid. DNAPL was permitted to flow into the domain for 6 months, by which time it was established that saturations had achieved steady state values (i.e., DNAPL inflow at the top equaled DNAPL outflow at the bottom). The DNAPL source was then terminated, and DNAPL redistribution was simulated for 6 months, at which time it was established that DNAPL movement had effectively ceased. Thus, at the end of the 'DNAPL Redistribution' stage, at t_{TOTAL} = 1 yr, the fracture network exhibited a complex distribution of DNAPL pools and residual characteristic of the fracture network of the rock type under investigation.

For the 'Site Ageing' stage, the side boundaries were modified such that a groundwater hydraulic gradient of 0.005 from left to right across the domain was established. DNAPL dissolution, aqueous phase transport, diffusion, and sorption of aqueous phase chlorinated solvent were simulated for 20 years during this stage (i.e., from t_{TOTAL} = 1 yr to t_{TOTAL} = 21 yrs). During this stage, a constant aqueous phase concentration of 550 mg/L TCE was specified along the entire left boundary, representing the impact of additional upgradient DNAPL upon the domain. This recognized that only a subsection of a typical source zone was simulated and resulted in (i) increased longevity of the DNAPL by reducing the concentration gradient driving dissolution and (ii) substantial

mass loading to the matrix within the domain.

At the end of 20 years of 'Site Ageing', for the Base Case (sandstone) it was found that no DNAPL remained. In fact, DNAPL dissolution enhanced by loss of mass via diffusion into the matrix and subsequent sorption depleted the DNAPL in only 3 years. For the Base Case, of the 7.3 kg of aqueous TCE in the domain at the end of the Site Ageing stage, 99% is within the matrix and 98% is sorbed. Clearly, such a scenario would not benefit from surfactant flushing.

In order to pursue the objectives of this work, it was necessary to have a realistic DNAPL distribution as well as a realistic distribution of solvent mass in the matrix. Thus, the DNAPL saturation distribution at t_{TOTAL} = 1 year was overlaid onto the TCE solute concentration distribution from t_{TOTAL} = 21 yrs to generate a new, combined source zone scenario appropriate for surfactant flushing (hereafter referred to as 'DNAPL Mapping'). For the Base Case, this new t_{TOTAL} = 21 yrs scenario exhibited 5.18 kg TCE DNAPL and 7.3 kg TCE solute. This represents a scenario in which a second DNAPL release occurred or long-term, continuous release to the subsurface took place, or one in which the DNAPL mass spilled is so substantial that despite 20 years of dissolution/diffusion/sorption, significant DNAPL remains at the time of treatment.

In the 'Treatment Application' stage, surfactant was initiated by injecting a constant aqueous phase concentration of 40.0 g/L surfactant for 2 years (i.e., 21 yrs $\leq t_{TOTAL} \leq$ 23 yrs) at the horizontal fractures along the left boundary. During surfactant application,

the upgradient TCE injection was terminated (i.e., assuming complete and instantaneous treatment of the upgradient source zone); while this is unrealistic, it provides the best opportunity for success within the domain and thus supports viewing these results as approximating a best case for the technology. In all cases, MSR calculations confirm that the total mass of surfactant injected is greater than the theoretical surfactant mass required to solubilise all the TCE in the domain at the start of the Treatment stage; for example, for the Base Case, 160 kg (122 moles) of surfactant was injected over the Treatment stage and 7.3 kg (55.6 moles) of aqueous TCE mass and 5.18 kg (39.4 moles) of TCE DNAPL was present; this represents an excess of 12.3 times, considering that 1 mole of surfactant is capable of solubilising 9.57 moles of TCE (Taylor et al., 2001) .

Following the Treatment stage, an additional five years were simulated (i.e., 23 yrs $\leq t_{TOTAL} \leq$ 28 yrs) to examine the impact of surfactants and potential rebound of chlorinated solvent concentrations in the post-treatment period. During this stage no upgradient concentration of any species (i.e., surfactant or chlorinated solvent) was applied.

Several assumptions were employed in this work to facilitate reasonable simulation times:

1. All fractured rock simulations presented are two-dimensional; this assumption likely benefits the technology since the reduced dimensionality is expected to reduce bypassing of the treatment fluid around DNAPL-occupied fractures;
2. The matrix is presumed to have a sufficient displacement pressure so as to exclude DNAPL entry; this assumption likely benefits the technology because

the highest fraction of DNAPL is retained in the fractures which are most accessible to the treatment fluid;

3. Advection of groundwater through the matrix is assumed to be negligible; this is reasonable given that the high permeability contrast between the fractures and matrix. For example, for the sandstone Base Case, the matrix permeability is approximately 6 orders of magnitude less than the average fracture permeability. The Peclet number for the matrix (Pe = vx/D where v is horizontal velocity in matrix) if advection were not neglected is 0.166; since Pe<1 it is reasonable to assume that the matrix is diffusion dominated and advection is negligible (Trivedi et al., 2008).

Base Case and Sensitivity Simulations

Table 2 presents the suite of 11 simulations conducted in this study. The Base Case considered a fractured sandstone template site. Table 3 presents the parameters employed to characterize the sandstone as well as the other two rock types (shale and granite). The sandstone domain, employed in all simulations except Run 5 and Run 6, is presented in Figure 7a. The sandstone parameters were chosen to be broadly representative of North American sandstone aquifers (e.g., Lipson et al., 2005). Table A1 (Appendix A) provides, for each rock type, the observed ranges for each parameter synthesized from the literature. Table 4.3 reveals that this sandstone exhibits - relative to the other template rock types - low fracture density, low mean aperture (125μm), high matrix porosity (7.7%), and intermediate foc (0.005).

The sandstone Base Case employed TCE as the DNAPL targeted by the surfactant treatment. Fluid properties and reaction parameters are listed in Table 4. The Base Case employed a continuous injection of surfactant at 40.0 g/L for 2 years during the Treatment stage (Table 2). This concentration is representative of values applied in typical treatment scenarios (e.g., Abriola et al. 1993; Rathfelder et al., 2001)

Table 2. Field Scale Surfactant Flushing in Fractured Rock Simulations

Run No.	DNAPL Type	Material	Surfactant Concentration (mg/L)	Degree of Matrix Loading	Mass Transfer
1 (Base Case)	TCE	Sandstone	40000	20 Years Aging	Equilibrium
2	TCE	Sandstone	20000	20 Years Aging	Equilibrium
3	TCE	Sandstone	60000	20 Years Aging	Equilibrium
4	PCE	Sandstone	40000	20 Years Aging	Equilibrium
5	TCE	Shale	40000	20 Years Aging	Equilibrium
6	TCE	Granite	40000	20 Years Aging	Equilibrium
7	TCE	Sandstone	40000	0 Years Aging	Equilibrium
8	TCE	Sandstone	40000	5 Years Aging	Equilibrium
9	TCE	Sandstone	40000	10 Years Aging	Equilibrium
10	TCE	Sandstone	40000	20 Years Aging	Rate Limited
11	TCE	Sandstone	0.0	20 Years Aging	Equilibrium

Table 3. Properties of Field Scale Fractured Rock Template Sites

Rock Type	Fracture Spacing (m)	Matrix Permeability (m^2)	Matrix Porosity	Foc	Bulk Density (g/cm^3)	Matrix Tortuosity	Fracture Aperture Range (μm)	Mean Aperture (μm)
Sandstone	6.0 (Ver) [*] [a] 1.0 (Hor) [a]	1.05×10^{-15}	7.7% [a]	0.005 [a]	2.49 [a]	0.2 [a]	25 - 230 [a]	125
Shale	4.0 (Ver) [*] 1.0 (Hor) [*]	1.05×10^{-15}	3.0% [b]	0.009 [*]	2.619 [**]	0.1 [*]	50 - 250 [c]	150
Granite	2.0 (Ver) [d] 2.0 (Hor) [d]	1.05×10^{-15}	0.1% [*]	0.0005 [*]	2.697 [**]	0.05 [*]	100 - 500 [e]	300

[a] *Lipson et al., 2005*
[b] *Morris and Johnson, 1967*
[c] *Jardine et al., 1999*
[d] *Sousa 2007*
[e] *Sausse 2002*
**Data supplied by B.H Kueper (personal communication) based upon consulting experience on sites of all three rock types.*
*** Calculated using Bulk Density = Grain Density x (1-porosity), assuming a grain density of 2.7 for Shale and Granite.*
Ver – Vertical Fractures
Hor – Horizontal Fractures

Table 4. Fluid Properties and Reaction Parameters

Parameter	Notation	Value
TCE Density [a]	ρ_{NWtce}	1460 kg/m^3
TCE Viscosity [a]	μ_{NWtce}	0.0005 Pa s
TCE Solubility [a]	$Solub_{TCE}$	1100 mg/L
TCE MSR [b]	MSR_{TCE}	9.57 mol/mol
PCE Density [a]	ρ_{NWpce}	1630 kg/m^3
PCE Viscosity [a]	μ_{NWpce}	0.0009 Pa s
PCE Solubility [a]	$Solub_{PCE}$	200 mg/L
PCE MSR [c]	MSR_{PCE}	5.41 kg/kg

a – Pankow and Cherry (1996)
b – Taylor et al. (2004)
c – Zhong et al. (2003)

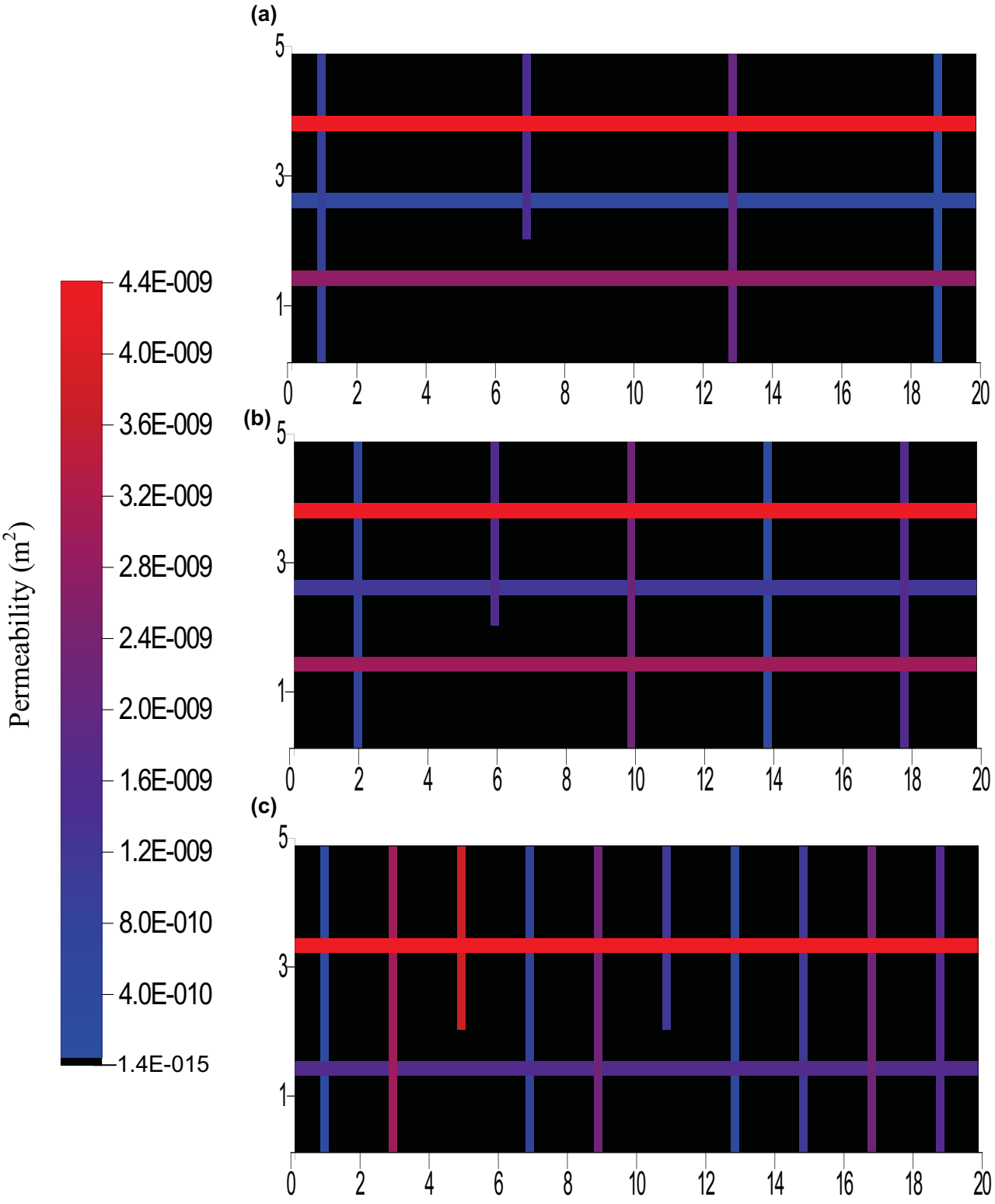

Figure 7 Distribution of permeability for the field scale fractured rock domains: (a) sandstone, (b) shale, and (c) granite. Colour corresponds to fracture permeability according to the scale bar provided; matrix permeability is uniform (black). Note that fracture apertures are exaggerated for visual purposes.

As illustrated in Table 2, Runs 2 - 3 examine variations in treatment strategy, while Runs 4 -10 explore the influence of site conditions. All parameters, boundary conditions, and source conditions were established identically to the Base Case for all simulations, except for changing the parameter(s) whose influence was being examined in each study.

It is noted that a 'No Surfactant' case was simulated for comparison purposes. In all respects but one, this simulation was identical to the Base Case. In this case, the Treatment stage employed identical boundary conditions as the Post-Treatment stage, and thus ambient conditions (in the absence of an updgradient TCE source) were simulated for 7 years following Site Ageing.

Surfactant Concentration

To examine the effects of surfactant concentration, the injected (i.e., boundary) concentration was increased by 50% and reduced by 50% relative to the Base Case in Runs 2 and 3, respectively. These range of concentrations investigated here are within the typical range of Twen-80 concentrations applied at field sites (Abriola et al., 1993; Jafvert et al., 1995; Ramsburg and Pennell, 2002; Ramsburg et al., 2005). In order to ensure the total volume of surfactant injected by the end of the Treatment stage was kept constant, the injection period was changed accordingly to 1.3 years and 4 years when concentration was increased by 50% and reduced by 50% respectively. This sensitivity study comprises of three simulations.

DNAPL

Run 4 utilized PCE DNAPL in the Base Case domain. PCE fluid and reaction parameters are provided in Table 4. For both the TCE and PCE simulations, all boundary conditions and stage parameters were identical. This sensitivity study comprises of two simulations.

Rock Type

Runs 1, 5, and 6 compare surfactant treatment performance in three different types of fractured rock at the field scale, each exhibiting a characteristic set or range of hydrogeological parameters (Table 3). Figure 7 presents the distribution of intrinsic permeability for the three domains, illustrating the distribution of fractures. In each case, the mean aperture is at the midpoint of the range specified in the table. It is noted that, characteristic of these rock types in natural environments, the shale template site exhibits (relatively) intermediate fracture density, low mean aperture (150μm), intermediate matrix porosity (3%), and high *foc* (0.009) while the granite exhibits high fracture density, high mean aperture (300μm), low matrix porosity (0.1%), and low *foc* (0.0009).

Aging Time

To examine the effects of the extent of contaminant penetration into the matrix on surfactant flushing success, Runs 7-9 varied the length of the Site Ageing stage: 0 years, 5 years, and 10 years (the Base Case was 20 years). In each case, before the Treatment stage, the T_{total}=1 year DNAPL distribution in the fractures was overlaid on the simulated distribution of aqueous and sorbed phases present in the matrix. It is acknowledged that by doing so, the total amount of DNAPL mass present was identical but the aqueous and sorbed mass in the domain differed in each simulation. The (aqueous + sorbed) TCE

present at the start of the Treatment stage for Runs 7, 8, 9 and 1 (Base Case) were 0.0 kg, 4.13 kg, 5.33 kg, and 7.3 kg, respectively, while the mass of TCE DNAPL for all of those runs were 5.18 kg. The effectiveness of surfactant flushing will be examined in these cases by considering the percentage of mass removed due to surfactant flushing.

Mass Transfer Model

Since the effectiveness of surfactant flushing is expected to be dependent on the rate of DNAPL mass transfer within the fractures, it is deemed important to examine the effect a rate-limited mass transfer model has on surfactant flushing of fractured rock source zones. The rate-limited model adopted from Dickson and Thomson (2003) was employed to compare with the equilibrium mass transfer relationship (Base Case).

4. RESULTS AND DISCUSSIONS

Table 5 summaries a selection of key numerical results for all 11 simulations conducted in this study. These data will be discussed as each set of simulations is presented.

Table 5: Summary of Results for All Surfactant Flushing Simulations

Run No.	DNAPL St 2 (kg)	DNAPL St 3 (kg)	Aq + Sorb St 3 (kg)	Surf Inject (kg)	DNAPL St 5 (kg)	Aq + Sorb St 5 (kg)	Mass Discharge St 5 (10^{-3} mg/s)	Surf React (kg)	CS React (kg)
1	5.26	5.26	7.30	160.0	0.020	4.32	2.69	4.33	4.16
2	5.26	5.26	7.30	160.0	0.016	4.11	2.42	4.15	3.98
3	5.26	5.26	7.30	160.0	0.021	4.40	2.81	4.39	4.21
4	6.03	6.03	3.30	165.0	0.452	0.92	0.0001	6.50	4.45
5	6.86	6.86	6.80	263.0	0.175	3.34	0.0001	5.03	4.83
6	11.53	11.53	0.68	1730.0	4.075	0.34	0.010	7.47	7.17
7	5.26	5.26	0.00	160.0	0.012	0.40	0.000	3.17	3.04
8	5.26	5.26	4.13	160.0	0.014	1.04	0.019	3.64	3.49
9	5.26	5.26	5.33	160.0	0.019	2.11	0.715	4.08	3.92
10	5.26	5.26	7.30	162.0	0.527	4.11	2.70	3.43	3.25
11	5.26	5.26	7.30	0.0	0.020	7.23	5.62	0.00	0.00

St 2 = mass present at the end of Stage 2 (DNAPL redistribution)
St 3 = mass present at the end of Stage 3 (Site Ageing)
St 5 = mass present at end of Stage 5 (Post-Treatment)
DNAPL = mass of DNAPL present
Aq + Sorb = combined mass of aqueous and sorbed chlorinated solvent present
Surf Inject = mass of surfactant injected during the treatment period
Mass Discharge = mass per time of chlorinated solvent leaving the domain at the end of Post-Treatment stage
Surf React = total mass of surfactant that reacted (with chlorinated solvent in all phases)
CS React = total mass of chlorinated solvent (in all phases) solubilised by surfactant

Base Case Results

Figures 8(a) and 8(b) illustrate the distribution of the TCE DNAPL at the end of the infiltration and redistribution phases, respectively (relevant to all simulations except Runs 5 and 6). Figures 8(a) and 8(b) reveal a heterogeneous distribution of DNAPL pools (i.e., connected phase) and residual (i.e., trapped) due to the influence of capillary forces (and, specifically, fracture entry pressures), the order of encounter of fractures, and the permeability contrasts between fractures. At the end of the DNAPL infiltration stage, the average DNAPL saturation was 0.75, the mass of DNAPL in the domain equaled 11.68 kg, the DNAPL volume was 0.008 m^3 (compared to a total fracture volume of

0.012 m^3) with 100% of the nodes in drainage. At the end of DNAPL redistribution stage, the average DNAPL saturation was 0.3, the volume of DNAPL was 0.0036 m^3 (equal to a mass of 5.18 kg) and the pool to residual ratio was 71:29%. Note in Figure 8(b) that, as expected, the lone remaining pool exhibiting a high DNAPL saturation resides in a vertical dead-end fracture and other pools of various lengths occur in horizontal fractures, separated by areas of residual DNAPL.

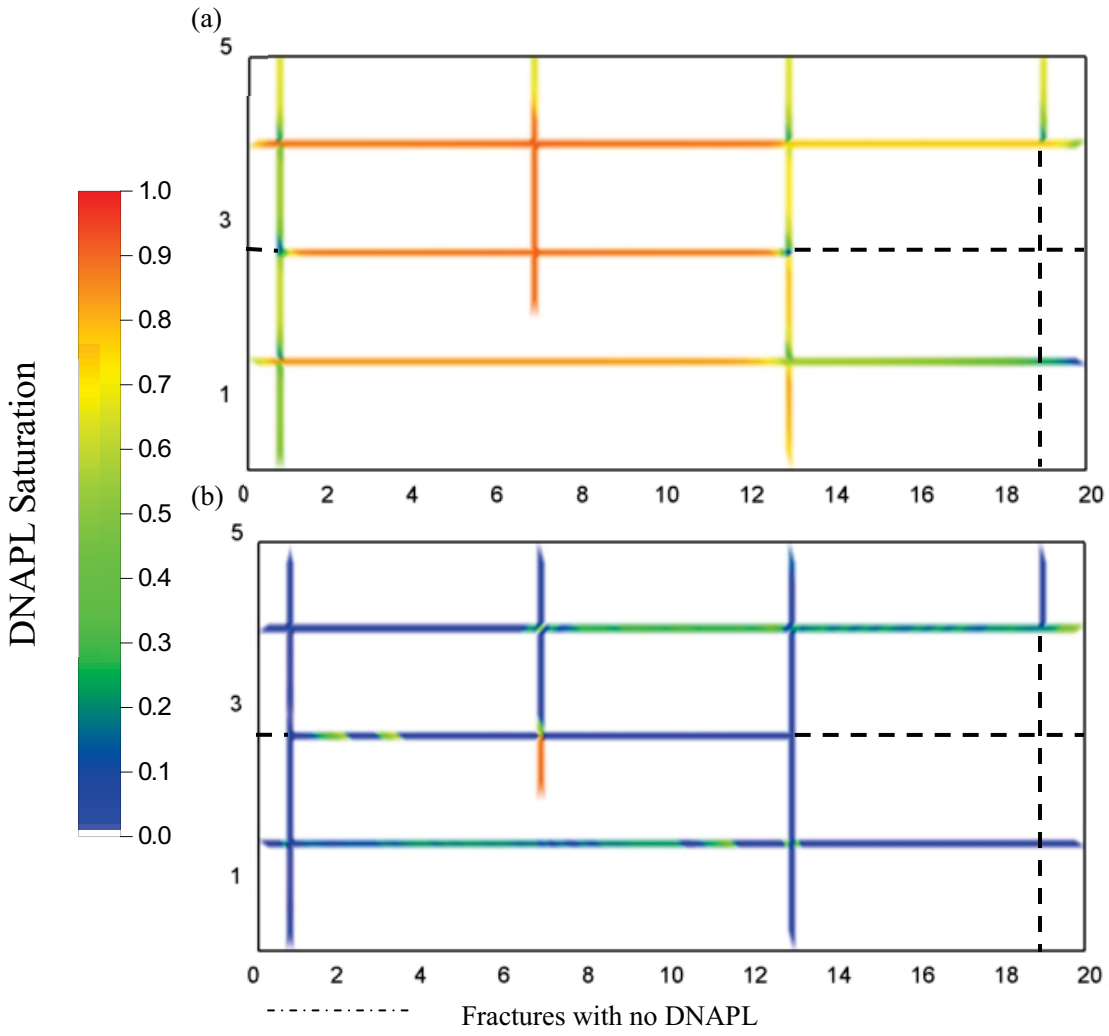

Figure 8: DNAPL distribution for Base Case at (a) t_{TOTAL} = 0.5 years when DNAPL inflow and outflow are equal, and (b) t_{TOTAL} = 1 year when all DNAPL migration has ceased.

Figure 9 illustrates the distribution of aqueous phase TCE at the end of the 20 year Site

Ageing stage (t_{TOTAL} = 21 years). Evident are the expected diffusion halos in the sandstone matrix blocks adjacent to fractures containing DNAPL as well as those horizontal fractures without DNAPL but subject to significant aqueous mass flux (Figure 8b). At this time, no DNAPL remained in the domain. This occurred despite the constant influent concentration equal to 50% of TCE solubility. The reason is the substantial TCE sink provided by matrix diffusion and sorption. At this time, the total mass of TCE in the domain was 7.3 kg, of which 99% resided in the matrix; of the mass in the matrix, 98% was sorbed and only 2% remained in the aqueous phase. It appears that the matrix acts as a substantial sink for TCE, rapidly promoting DNAPL dissolution.

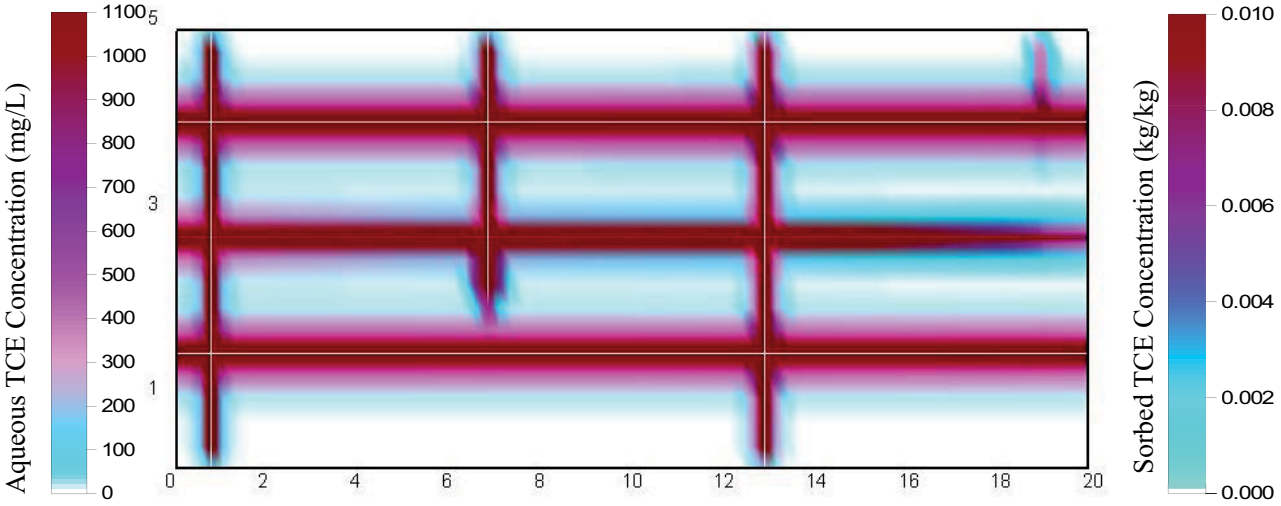

Figure 9: Distribution of aqueous and sorbed TCE after 20 years (t_{TOTAL} = 21 years) of DNAPL dissolution.

Figure 10 provides the concentration plots of aqueous TCE, surfactant, micelles and DNAPL saturation throughout the domain after the Treatment stage (i.e., 2 years of surfactant injection, t_{TOTAL} = 23 years). It is noted by this time, the injected surfactant has traversed the full extent of all three horizontal fractures present in the domain. Figure 10c further demonstrates that micelles in the top and bottom horizontal factures

(largest apertures) have been flushed out, while the middle horizontal fracture still contains micelles as the solubilisation process continues. In addition, Figure 10c demonstrates substantial TCE-occupied micelle mass present in the matrix close to most of the fractures within the domain.

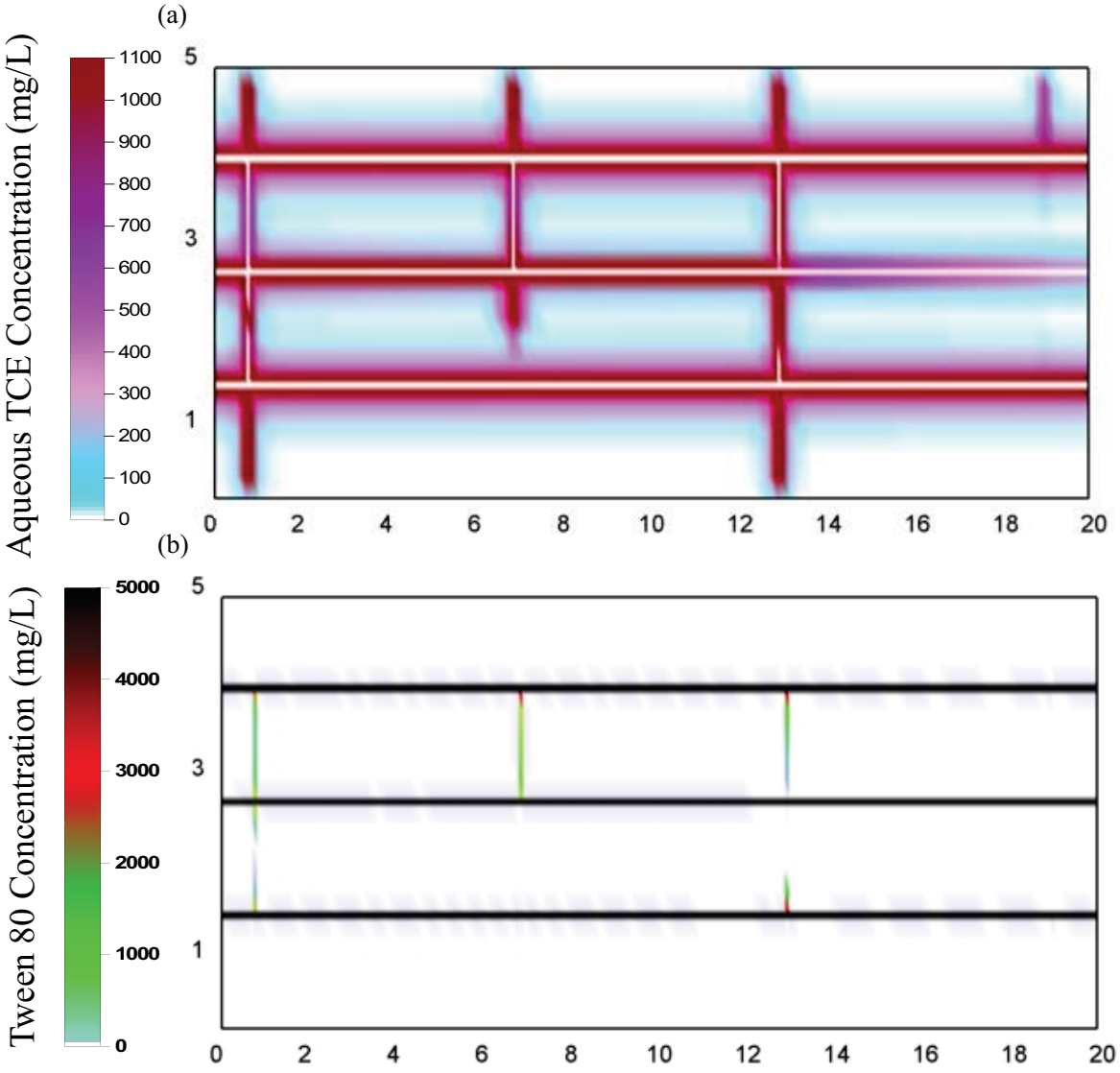

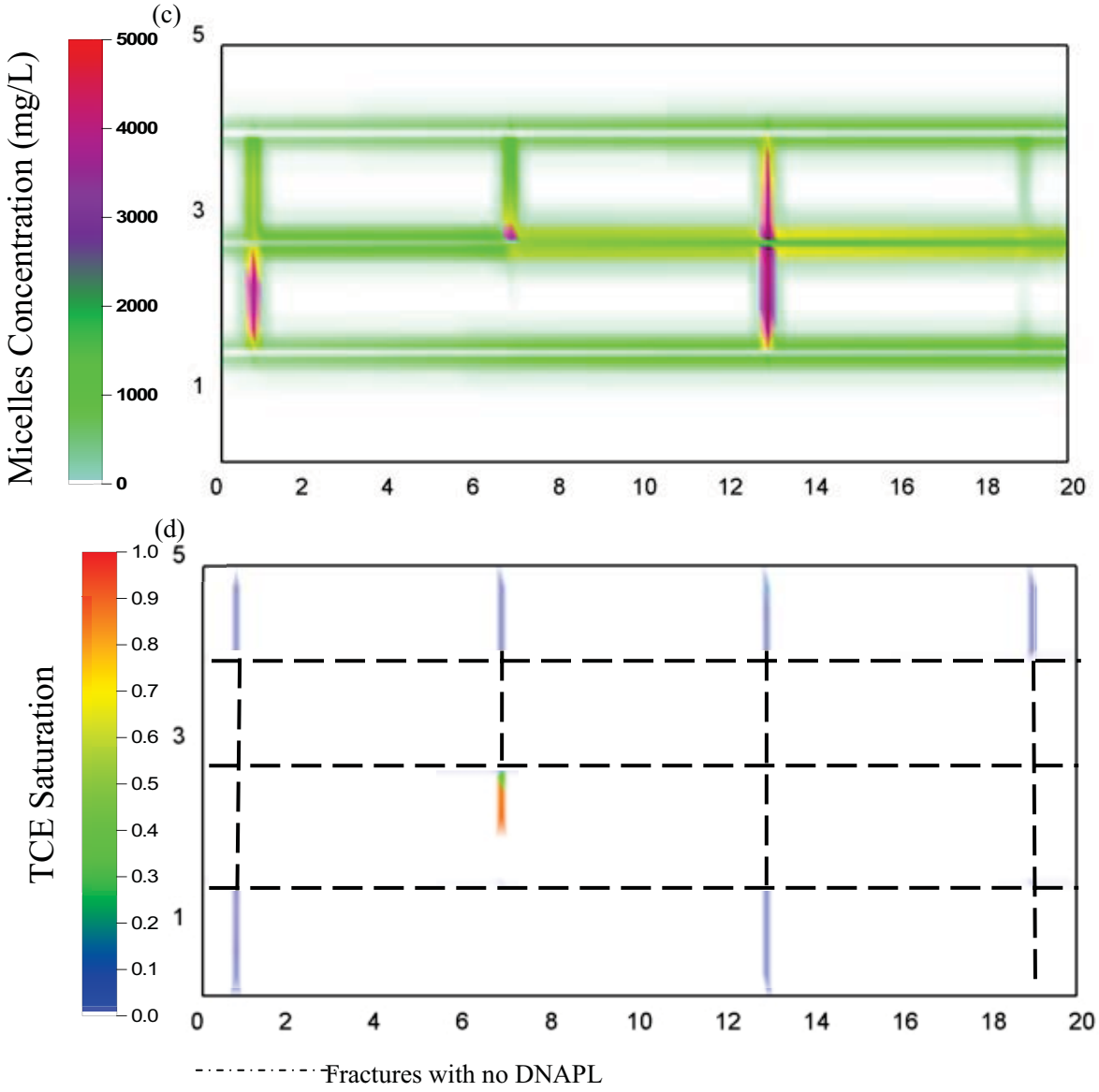

Figure 10: Distribution of (a) Aqueous TCE; (b) Surfactant; (c) Micelles; (d) TCE Saturation, 2 years after surfactant injection.

Figure 11 presents the concentration of aqueous TCE and various species throughout the domain at the end of the post-treatment stage (i.e. 5 years post-surfactant injection, t_{TOTAL} = 28 years). Figure 11d reveals that some DNAPL remains in one of the vertical dead-end fractures; as expected, this is not readily accessed by the surfactant flush. Moreover, the figure illustrates that minimal surfactant remains while forward

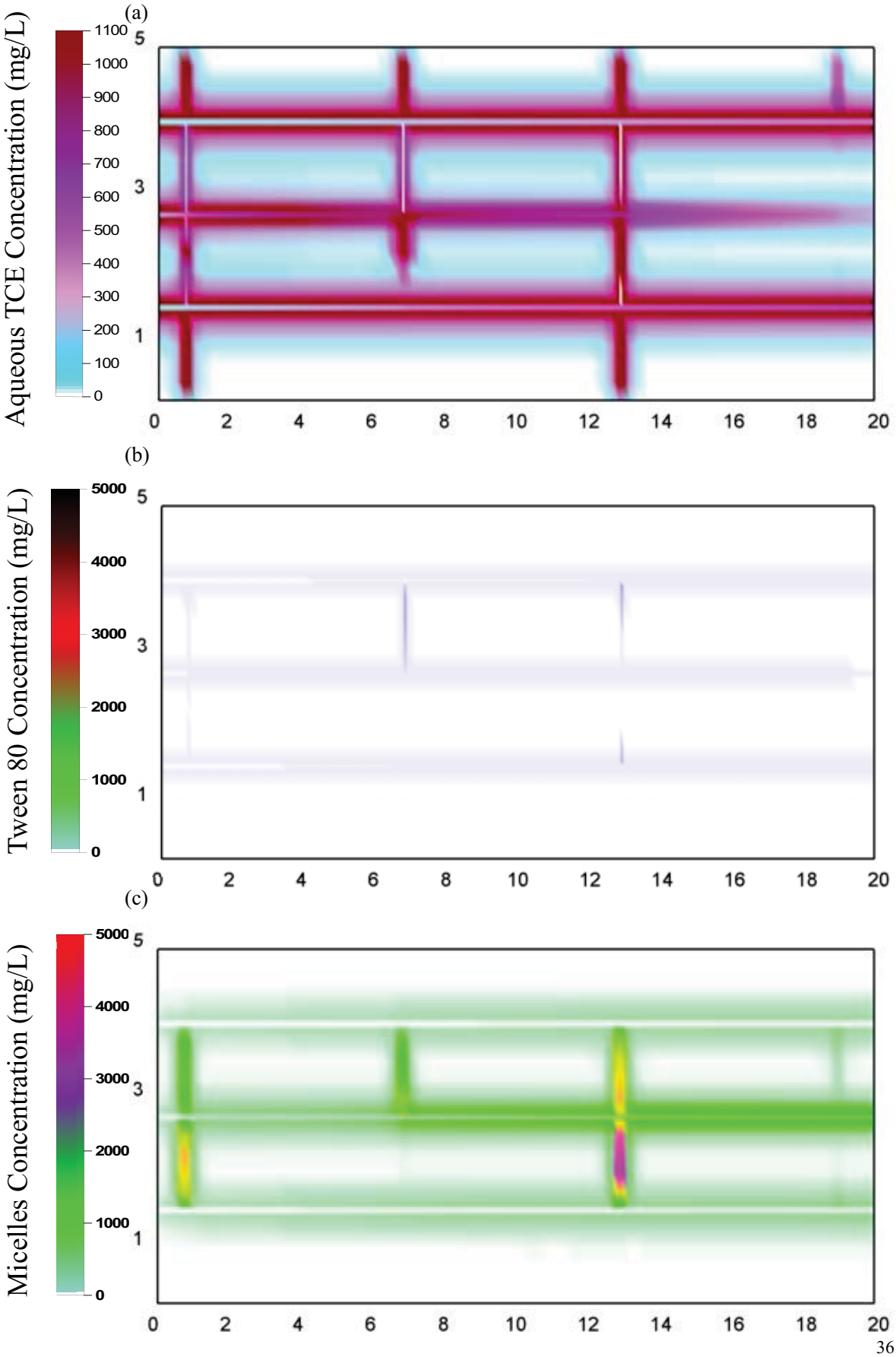
(a)
Aqueous TCE Concentration (mg/L)
1100
1000
900
800
700
600
500
400
300
200
100
0
5
3
1
0
2
4
6
8
10
12
14
16
18
20
(b)
Tween 80 Concentration (mg/L)
5000
4000
3000
2000
1000
0
5
3
1
0
2
4
6
8
10
12
14
16
18
20
(c)
Micelles Concentration (mg/L)
5000
4000
3000
2000
1000
0
5
3
1
0
2
4
6
8
10
12
14
16
18
20

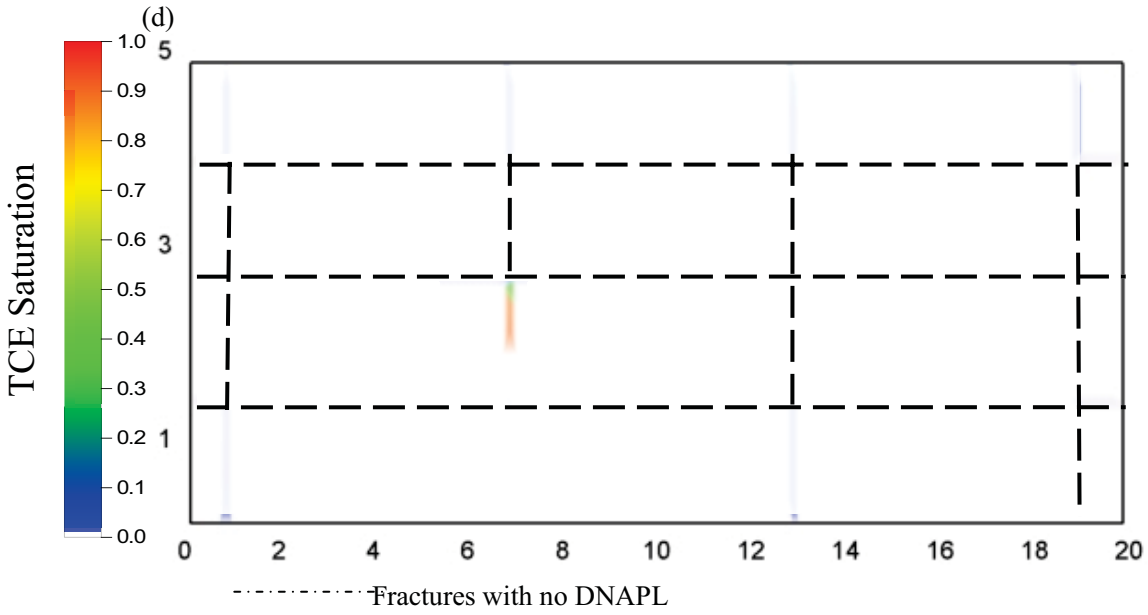

Figure 11: Distribution of (a) Aqueous TCE; (b) Aqueous surfactant; (c) Micelles; (d) TCE saturation, 5 years after surfactant injection.

and backward diffusion are smearing the distribution of TCE and TCE-occupied micelles in the matrix adjacent to the two 'clean' horizontal fractures.

Figure 12 presents cumulative mass plots of all sinks and sources of TCE during the Base Case simulation. Summed totals of these plots, in which:

Mass Dissolute In + Mass Influx = Mass Destroyed + Mass Outflux + Mass Sorbed + Mass In Domain (7)

revealed that the model has excellent mass balance (plots not shown to improve clarity of the figure) and this was confirmed by excellent computed mass balance on all species. The figure reveals that majority of DNAPL dissolution occurred rapidly at the beginning

of the simulation due to DNAPL dissolution and diffusion into the matrix, corresponding to a rapid increase in sorbed TCE in the matrix. Until t_{TOTAL} = 3 years, TCE flux out of the domain was greater than the flux into the domain due to a proportion of the dissolved TCE exiting via fracture flow. However, beyond this time, with dissolution virtually completed, TCE influx exceeded outflux as the incoming background TCE contributed to a steady rise in mass retained via sorption. It was also noted the cumulative mass of aqueous TCE in the domain (sum of that in the fractures and matrix) was a small fraction of the amount sorbed.

At t_{TOTAL}=21 years, as mentioned above, DNAPL distribution at t_{TOTAL} = 1 year, (equivalent to a mass of 5.18 kg) was mapped onto the domain. Figure 12 reveals that as surfactant was injected into the domain, DNAPL solubilisation increases dramatically before reaching a constant level at t_{TOTAL} = 22.3 years. It reveals at this time approximately 96.5% (i.e., 5.0 kg) of initial DNAPL mass present in the fractures has been solubilised by surfactant.

Following the Treatment stage, Figure 12 revealed that although the mass of TCE removed by surfactant continued to increase, this increase throughout the 5 years of Post-Treatment stage only accounts of 0.35% of the total mass removed.

Figure 13 reveals that of the 160 kg of surfactant injected, approximately 94.4% of the total mass was flushed out of the domain, while only 2.71% (Table 5) was used for the solubilisation of TCE while the rest of the surfactant was sorbed onto the matrix of the

fractured rock.

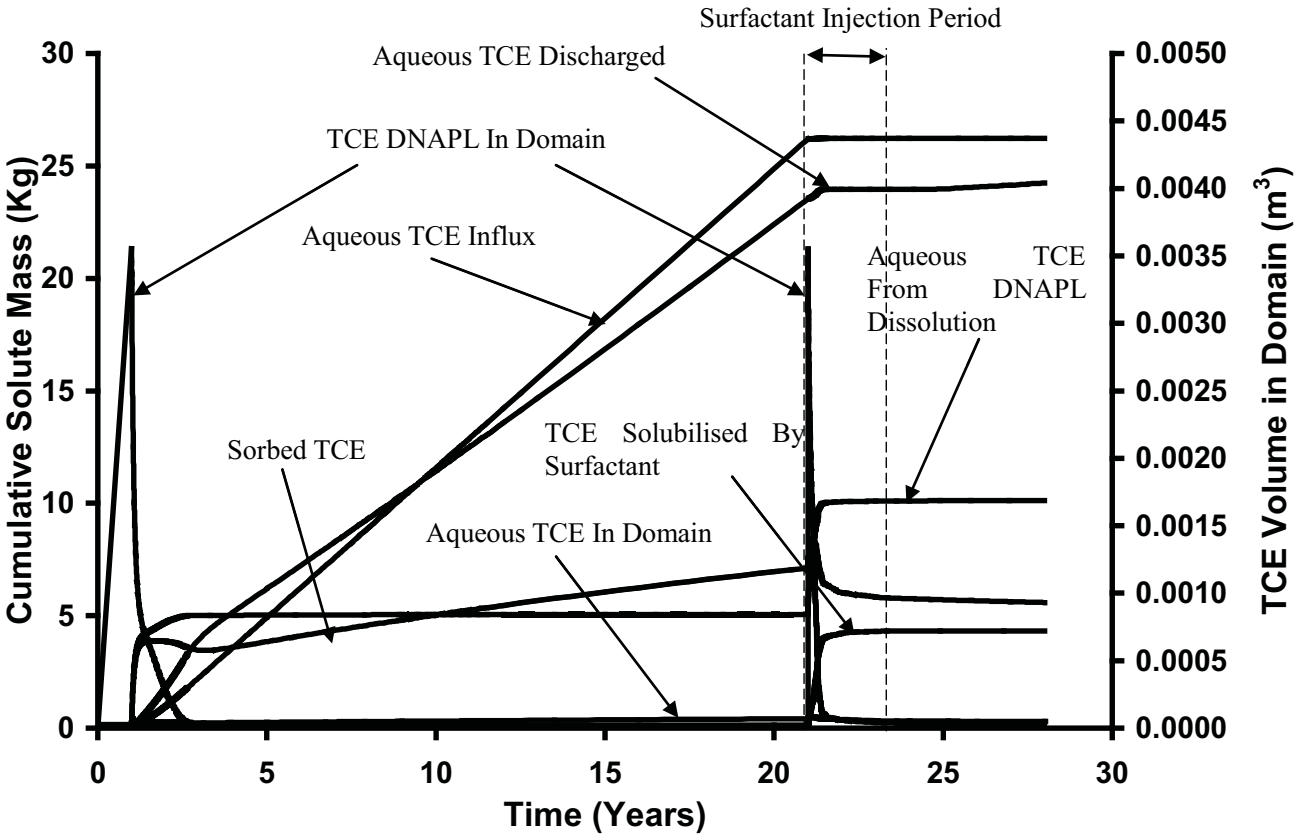

Figure 12: Cumulative aqueous and sorbed TCE from all sinks and sources for Base Case Simulation.

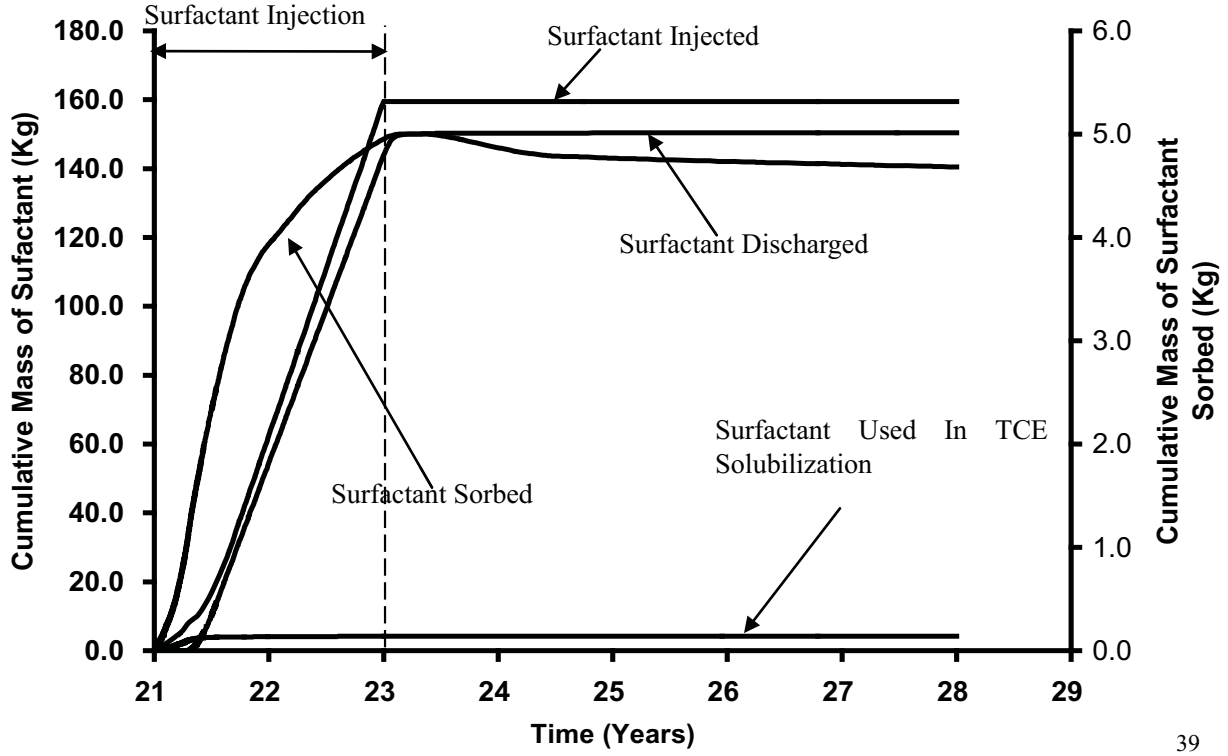

Figure 13: Cumulative aqueous and sorbed surfactant from all sinks and sources for Base Case Simulation.

Figure 14 reveals that, as expected, at the start of the Treatment stage the DNAPL dissolution rate increases dramatically and the amount of TCE encapsulated by micelles rises correspondingly. These rapid increases only last for approximately 6 months while the remaining 78 months of the treatment period show very little additional solublization. This is because most of the DNAPL that could be accessed by the surfactant has been solubilised in the first 6 months of the treatment. It is noted that the amount of sorbed mass decreases equally quickly during the first 6 months of treatment, indicating that desorption was occurring (Figure 12). And as the cumulative mass of micelles stops increasing; the rate of decrease of sorbed mass declines. Throughout the Post-treatment stage, the amount of TCE solubilised is insignificant.

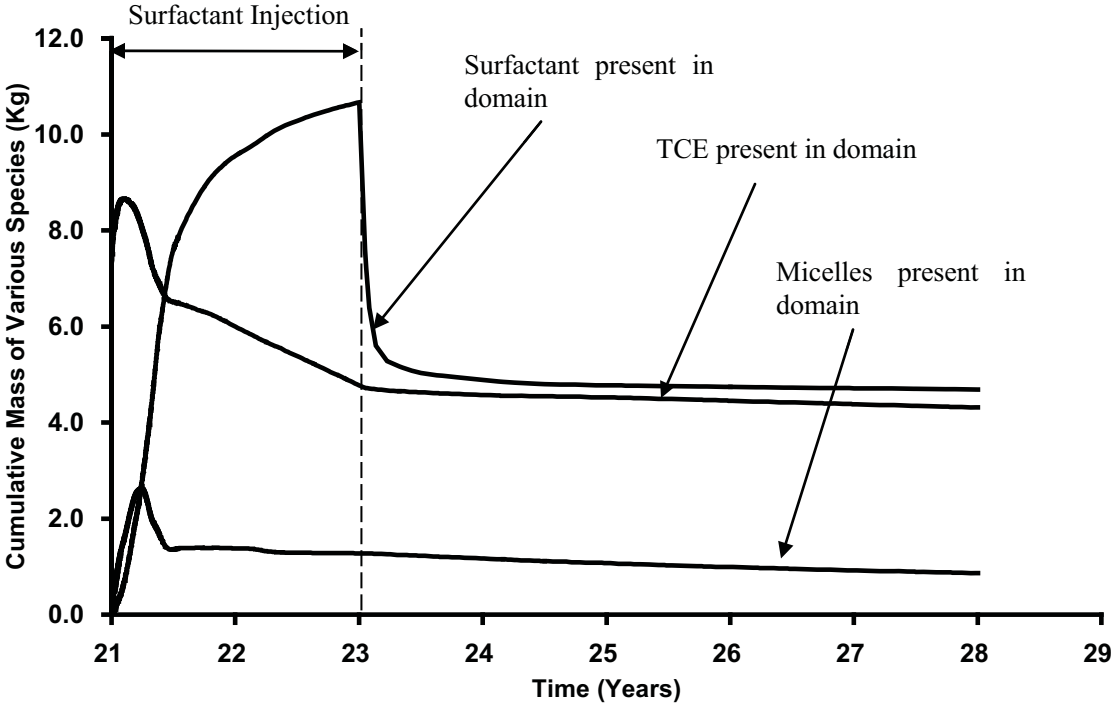

Figure 14: Cumulative mass of TCE, surfactant and micelles for Base Case Simulation.

Figure 15 compares the total TCE solute mass discharged at the right-hand boundary of the domain for the Base Case and the 'No Surfactant' simulation. During the Treatment stage (i.e., t_{TOTAL} = 21 to 23 years), the difference in mass discharged between the 2 simulations were observed to vary significantly. In the 'No Surfactant' simulation, the boundary mass discharge is observed to increase exponentially until t_{TOTAL} = 23.5 years, before decreasing at a relatively steady state to a relatively constant level at t_{TOTAL} = 25.75 years. On the other hand, when surfactant was injected in the Base Case simulation, Figure 15 demonstrates the boundary TCE mass discharge to increase rapidly during the initial Treatment stage before decreasing to negligible level by t_{TOTAL} = 21.4 years. Figure 15 further reveals the mass discharged in the Base Case at t_{TOTAL} = 24.5 years to increase from negligible level to a constant level of 0.002mg/s (Table 5), until the end of the simulation. This trend in the Base Case simulation can be broken down to 3 stages:

1. Due to the mapping of DNAPL into the Base Case, the mass outflux experiences a sudden drop at the beginning of the Treatment stage before steadily increasing due to the DNAPL solubilisation by the injected surfactant.
2. As the majority of the DNAPL within the domain was solubilised by the injected surfactant (i.e., t_{TOTAL} = 21.5 years), the mass discharged decreases to a negligible value. This observation is supported by the corresponding increase in concentration of the micelle species within the domain (Figure 14).

3. In the final stage, after the injection of surfactant has ceased for 1.5 years (i.e. t_{TOTAL} = 24.5 years), the TCE mass outflux is observed to rebound again due to back-diffusion of previously sorbed TCE from the matrix.

It is further observed that the post-treatment mass outflux in the 'No Surfactant' case is approximately 2.8 times more (i.e. 0.0056 mg/s vs. 0.0027 mg/s) than the Base Case (refer to Table 5). This is because of the long-term, back-diffusion of stored TCE mass in the matrix (aqueous + sorbed) and slow dissolution of TCE DNAPL in the fractures (low groundwater velocity pathways). The total TCE mass in the domain at the end of the Post-Treatment stage (aqueous + sorbed + DNAPL) in the source zone is 4.34 kg for the Base Case and 7.25 kg for the No Surfactant case.

Figure 16, which is the same data as 15 but expands the time axis to focus on the first year during treatment, reveals three areas of 'abrupt slope changes' (circled areas) on the TCE mass discharge curve. It is believed these 'abrupt slope changes' are associated with the mass flux through each horizontal fracture in the domain. As demonstrated in Figure 18, depending on the size of the aperture, the downgradient discharge varies for each fracture. The discharge in Figure 16 was dominated at first by the largest aperture fracture (circle 1), followed by the middle aperture fracture (circle 2), and then after both were flushed out, the mass from the smallest aperture fracture finally arrived at the boundary (circle 3).

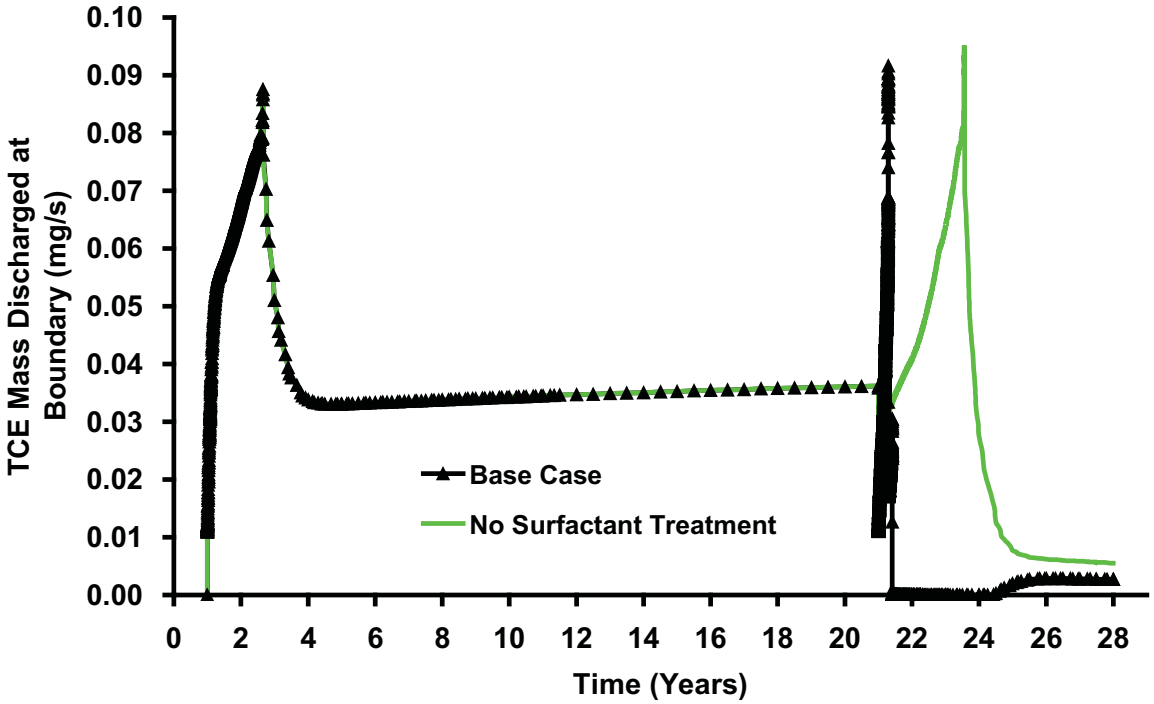

Figure 15: Comparison of total boundary mass discharge (TCE) for (a) base case with a simulation where no surfactant was injected (b) since the start of the Treatment Stage for 1 year only (timescale expanded for clarity).

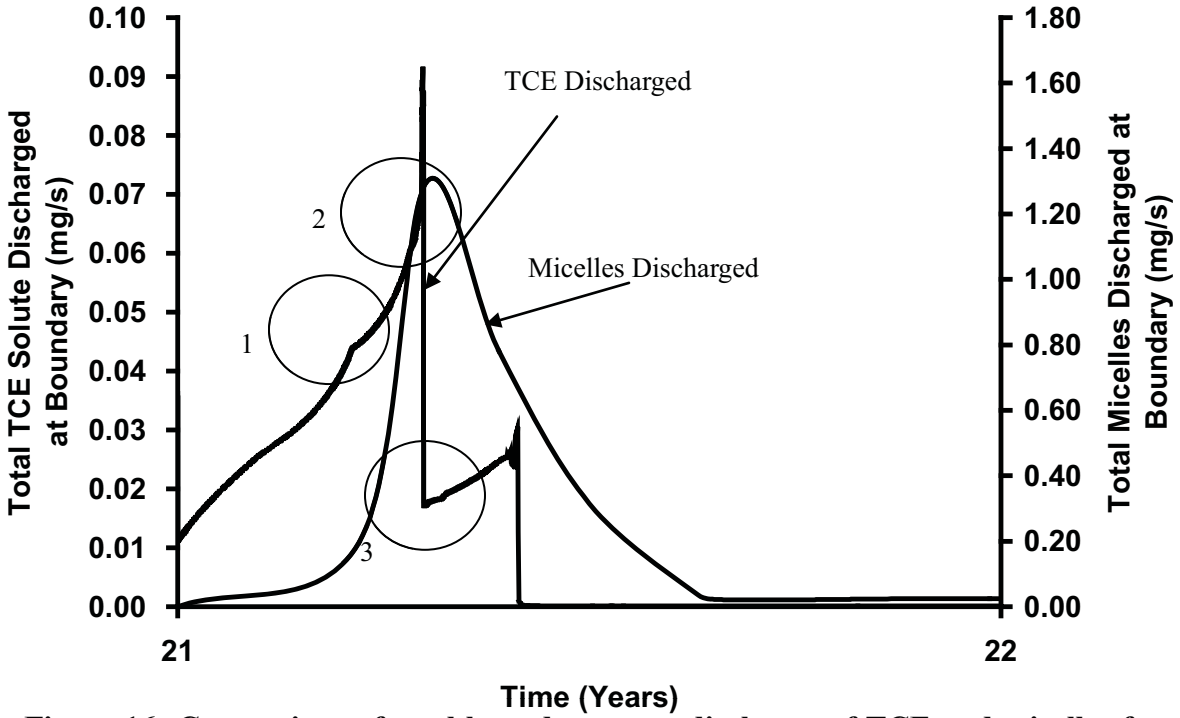

Figure 16: Comparison of total boundary mass discharge of TCE and micelles for base case simulation since the start of the Treatment Stage for 1 year only (timescale expanded for clarity).

Figure 16 further demonstrates that the concentration of micelles discharged at the boundary increased rapidly during the first quarter of the Treatment stage before decreasing to a low, constant concentration at t_{TOTAL} = 21.65 years. Although boundary TCE mass discharge was observed to decrease to negligible level by this time, It is recognised that in every simulation conducted in this study, micelles containing TCE will be discharged downgradient even though the mass discharge for TCE has reached a negligible level.

Figure 17 plots the cumulative downgradient mass discharge of aqueous and entrained TCE in micelles for the base case. During the first 6 months of the Treatment stage, the discharge of TCE mass contained in micelles is observed to increase significantly. It is further noted that the mass of TCE in micelles being discharged is 5.5 times more than the mass of aqueous TCE being flushed out, indicating that surfactant is efficient in solubilising and removing TCE from the domain.

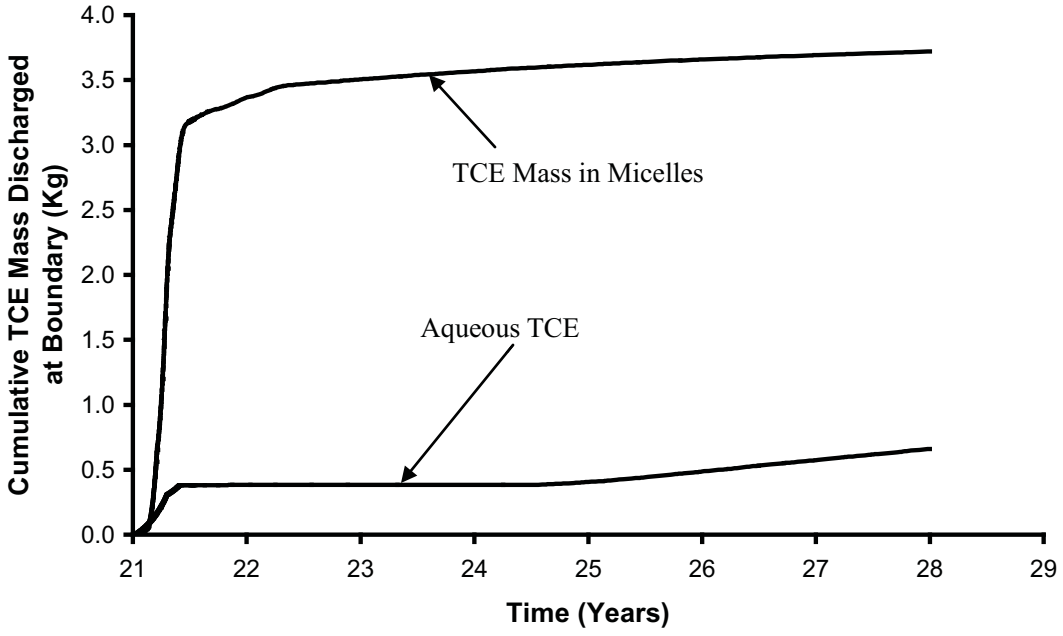

Figure 17: Cumulative TCE mass discharged at downgradient boundary.

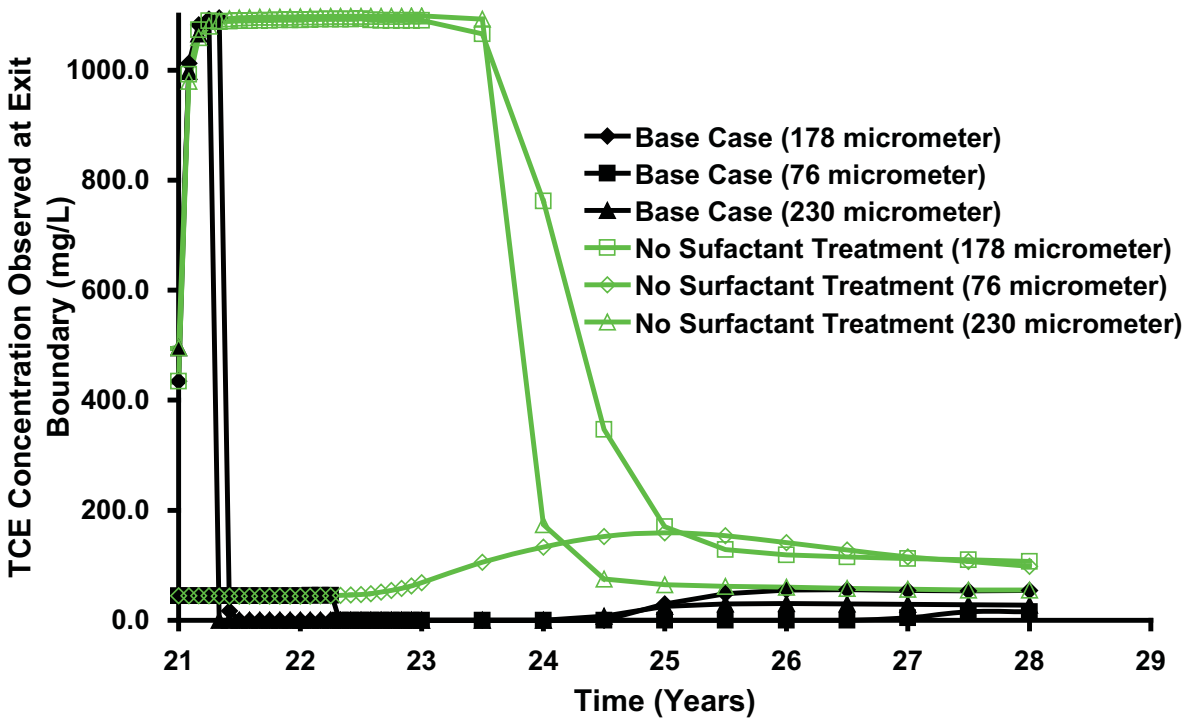

Figure 18: Concentration of TCE in various horizontal fractures at downgradient boundary.

Figure 18 reveals the average discharge of TCE solute concentration within the horizontal fractures at the downgradient boundary can vary significantly over time. This figure demonstrates that in bigger fractures (e.g., 178μm ~ 230μm), the solute concentration decreased significantly during the initial few months of surfactant injection. On the other hand, it was noted that if the fracture aperture was small (i.e., 76 μm), although the initial concentration outflux in this fracture was much lower than the other two larger factures, it took a much longer time before the downgradient outflux was reduced to undetectable limits; probably due to the difficulty in gaining access to both the DNAPL and contaminant solute in these area by the injected surfactant.

Of the 5.18 kg of TCE DNAPL and 7.3 kg aqueous and sorbed TCE present in the domain at the end of the 20 year Site Ageing stage (t_{TOTAL} = 21 years), 0.02 kg and 4.32

kg, respectively (Table 5), remained at the end of the Treatment stage in the Base Case. For the 'No Surfactant' case, 0.02 kg of DNAPL and 7.23 kg of aqueous plus sorbed TCE remained at the end of the Treatment stage. However, the Base Case achieved this DNAPL amount in 7.5 months (Figure 12) versus 31.2 months in the 'No Surfactant' case (Figure C2, Supplementary Information). The difference noted in the matrix-bound TCE is the cause of the observed difference in long-term mass discharge during the Post-Treatment stage.

Sensitivity Simulations

Sensitivity to Surfactant Concentration

Figure 19 presents the volume of DNAPL in the domain over time. Recall that, in order to conserve total surfactant mass injected, the 60 g/L, 40 g/L, and 20 g/L surfactant solutions were injected for 1.3, 2.0 and 4.0 years, respectively. It is revealed that at any time, the higher the concentration of surfactant injected, the lower the volume of DNAPL is present in the domain. Figure 19 further reveals after 6 months of surfactant treatment, more than 90% of the initial DNAPL mass in the domain has been solubilised before reaching a constant level. Mass solubilisation, while highest at early time for the most accessible TCE, accounts for the quick decrease in DNAPL volume during the first 6 months of surfactant treatment. The constant low volume at late time is mainly contributed by the entrapped DNAPL in the dead-end fracture (Figure 11).

Figure 20 plots the cumulative mass of total TCE present in the domain (i.e., sorbed + aqueous + DNAPL) solubilised by surfactant for Runs 1, 2 and 3. It reveals that an

increase from 20 g/L to 40 g/L causes a total improvement of 1.45% of the total TCE recovered (from 3.98 kg to 4.16 kg (Table 5), recalling that the total DNAPL mass in the domain was 5.26 kg). Moreover, the 40 g/L completes solublization in 4.8 months versus 7.8 months for the 20 g/L simulation (Figure 18). However, a further increase from 40 g/L to 60 g/L causes small further improvement in rate or in total amount; the latter because all readily-accessed DNAPL is solubilised. Overall, the sensitivity of the results is minor within the range of concentrations examined. It is expected that more significant deterioration of results would occur if injected concentrations were further reduced.

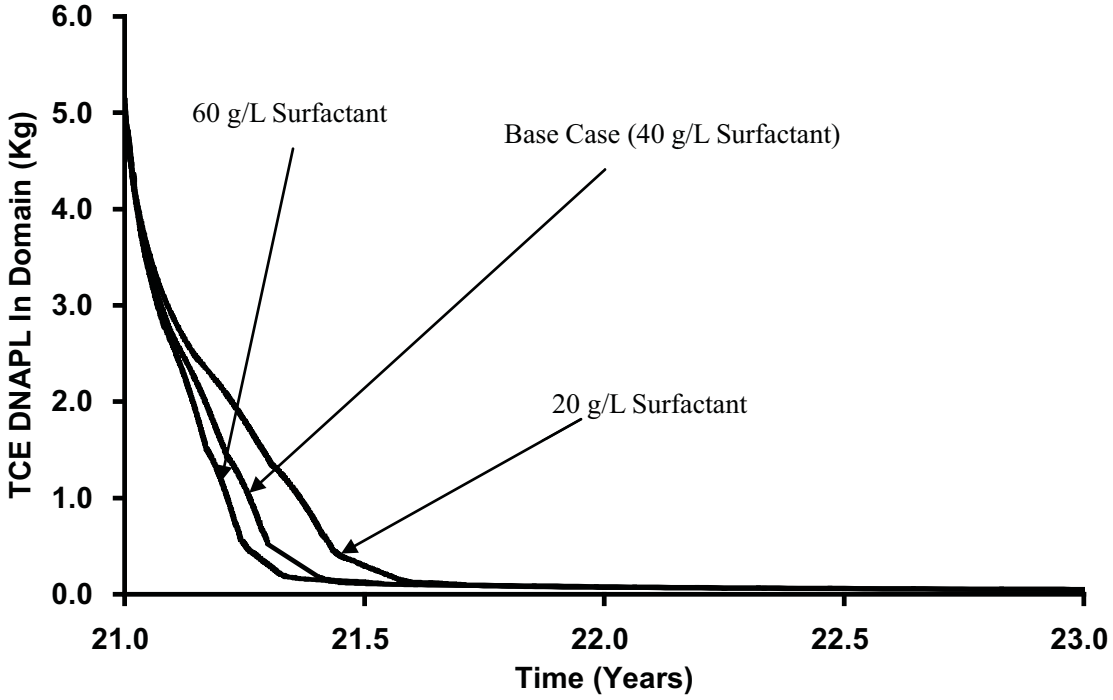

Figure 19: Total TCE DNAPL present in domain over time for (a) Base Case, (b) 20000mg/L and (c) 60000 mg/L of surfactant injected.

Figure 21 plots the cumulative surfactant mass (i.e., TCE-free) discharged at the downgradient boundary for the three simulations. It reveals that higher concentrations of surfactant resulted in a smaller portion of the injected mass leaving the domain without TCE. As demonstrated by Figure 22, a higher proportion of surfactant was used to solubilise the chlorinated ethene present in the domain when a higher concentration of surfactant was injected.

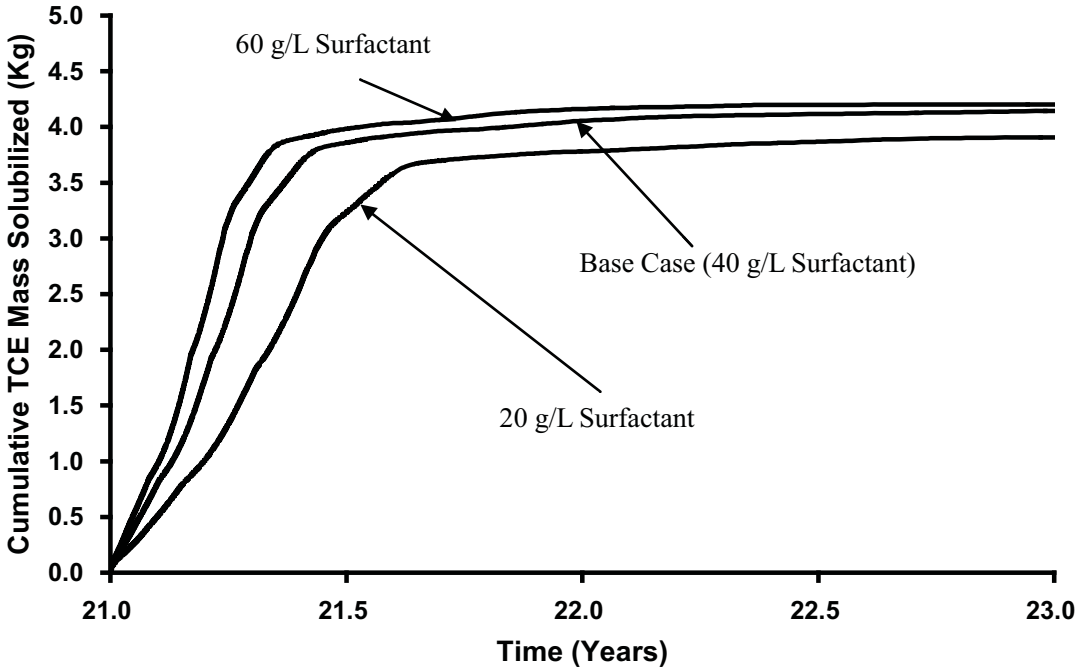

Figure 20: Cumulative mass of TCE solubilised by micelles over time for different injected concentration.

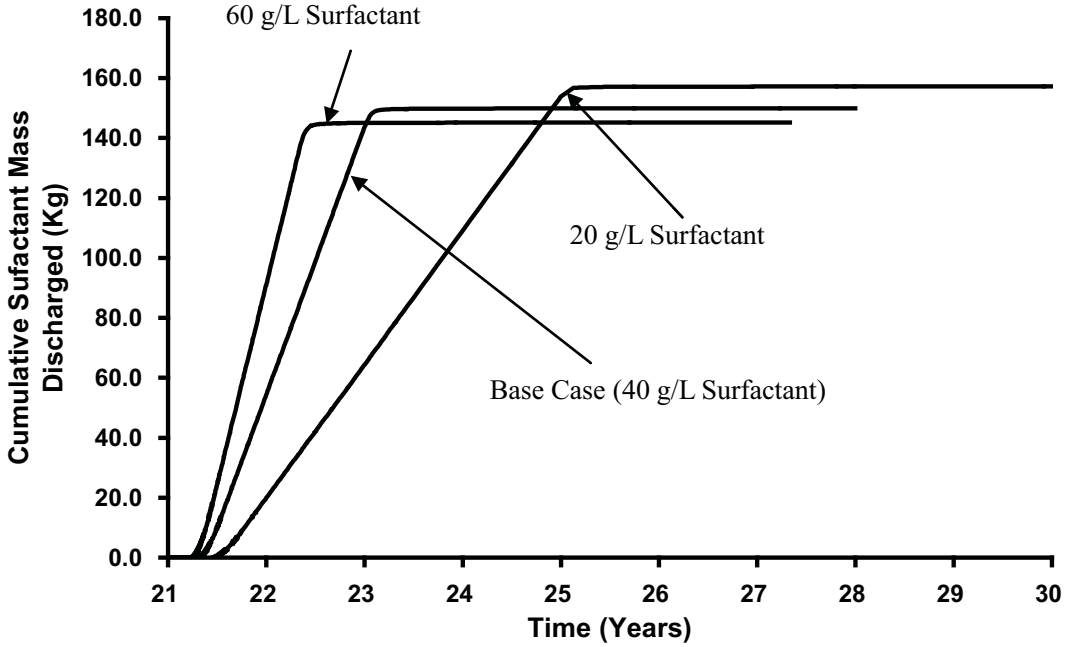

Figure 21: Cumulative mass of surfactant discharged over time for different injected concentration.

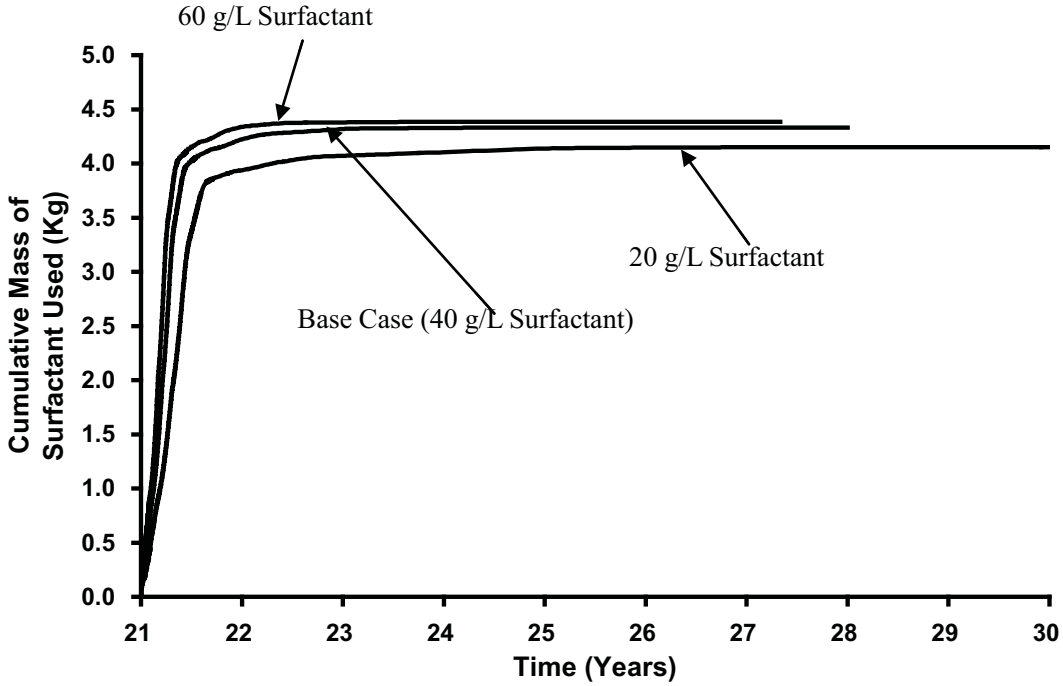

Figure 22: Cumulative mass of surfactant used for solubilising DNAPL over time for different injected concentration.

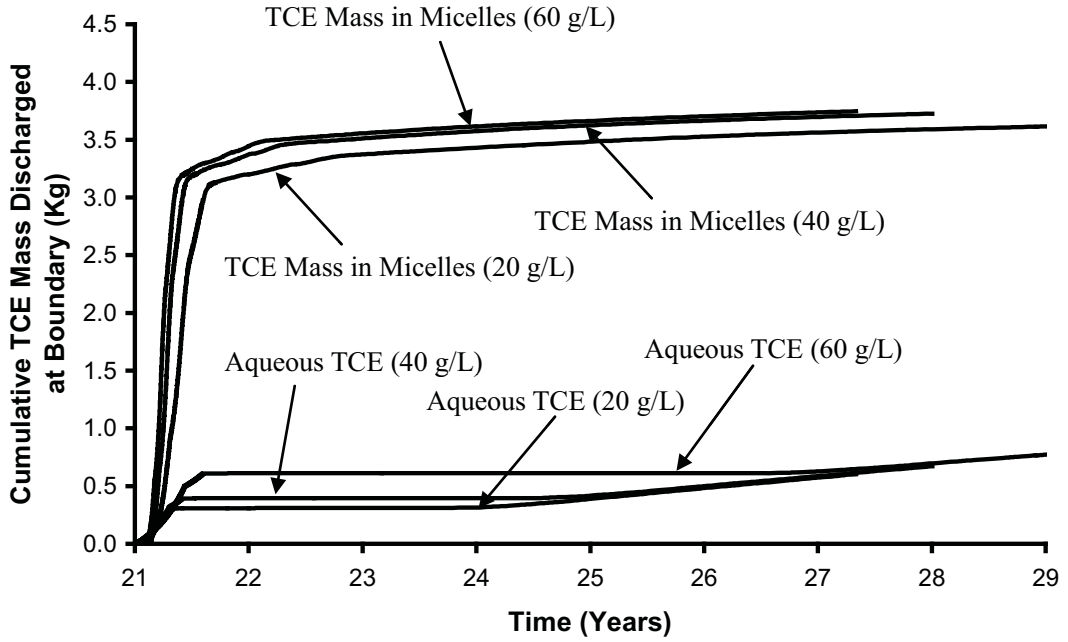

Figure 23: Cumulative TCE mass discharged at downgradient boundary for various concentrations.

Figure 23 plots the cumulative downgradient mass discharge of aqueous and entrained TCE in micelles for all 3 different concentration simulations. During the first 6 months of Treatment stage, the discharge of TCE mass contained in micelles is observed to increase significantly. It is further noted in all 3 simulations, the mass of TCE entrained in micelles being discharged is at least 5.5 times more than the mass of aqueous TCE being flushed out.

No significant difference between the 3 cases is observed during the Post-Treatment stage with respect to mass discharge (Figure C3, Supplementary Information) or exit concentrations of surfactant (figure not shown). Moreover, the distribution of TCE, surfactant, and micelles are observed to be essentially identical after the Treatment stage (compare Figure 11 and Figures C4 and C5 in Supplementary Information).

Sensitivity to DNAPL Type

In this study, results were compared between PCE and TCE. At the end of the DNAPL Infiltration stage, the average DNAPL saturation was 0.5 while the volume of DNAPL in the domain was 0.008 m^3 (compared to a total fracture volume of 0.012 m^3) with 100% of the nodes in drainage in both simulations. At the end of DNAPL redistribution stage, the average DNAPL saturation was 0.3 for both TCE and PCE while the volume of DNAPLs present was 0.0036 m^3 (5.18 kg) and 0.0037 m^3 (6.03 kg) while the pool to residual ratio was 71:29% and 51:49% for TCE and PCE, respectively.

At the end of the Site Ageing stage (t_{TOTAL} = 21 years) the total mass of aqueous and sorbed TCE and PCE in the domain was 7.3 kg (55.6 moles) and 3.3kg (20.2 moles) respectively. Of the PCE mass in the domain, more than 99.9% resided in the matrix, of which 98.7% was sorbed and only 1.3% remained in the aqueous phase.

Although the initial volume of DNAPL injected into the domain was similar in both simulations, it is important to note that the concentration of continuous influx throughout the Site Ageing stage was considerably lower for PCE (100mg/L) than TCE (550mg/L). As a result, the mass present in the PCE-contaminated domain at the end of the Site Ageing stage was much lower than the Base Case. Prior to the Treatment stage, the TCE and PCE DNAPL masses mapped into the domain were 5.18 kg and 6.03 kg, respectively.

As demonstrated in Figure 24, the total mass of surfactant injected into the domain was similar for both the Base Case and the PCE simulation. Despite this, Figure 24 reveals

that the total mass of TCE (i.e., sorbed + aqueous + DNAPL) solubilised by surfactant was slightly lower than that for PCE (4.16 kg versus 4.45 kg). Closer inspection of Figure 24 revealed that initially the rate of TCE solubilisation exceeded PCE solubilisation. This could be explained by (1) higher MSR for TCE (9.57 mol/mol) than PCE (5.41 mol/mol), and (2) larger initial total TCE mass (12.48 kg) than total PCE mass (9.33 kg) (Refer to Table 5). However, after approximately 6 months of treatment, the total mass of PCE being solubilised surpassed the total mass of TCE; this coincides with the time when TCE DNAPL solubilisation was effectively complete (Figure 12; note that PCE DNAPL solubilisation was effectively complete 8 months after the start of the Treatment stage). After the easily accessed DNAPL was removed, increased amount of solubilised TCE was dominated by the partitioning of aqueous solute into micelles. Recall that, at chlorinated ethene concentrations less than solubility (i.e., in absence of DNAPL), the extramicellular fraction of PCE solute is about one-third that of TCE solute (Figure 1, Kim et al., 2007). In other words, under similar conditions, a higher fraction of aqueous PCE mass was entrained into micelles than for TCE, thus leading to the higher PCE recovery at late time observed in Figure 24. This finding is backed by evidence (Figure C6, Supplementary Information) demonstrating that the remediated volume of matrix surrounding the horizontal fractures is larger for the PCE case than the Base Case (Figure 24).

Figure 25 reveals that by the end of the Treatment stage, the chlorinated ethene mass discharge at the downgradient boundary was reduced to nondetectable in both simulations. However, while the mass discharge in for TCE rebounded slightly at t_{TOTAL} = 24.5 years,

no such rebound was observed in the PCE simulation.

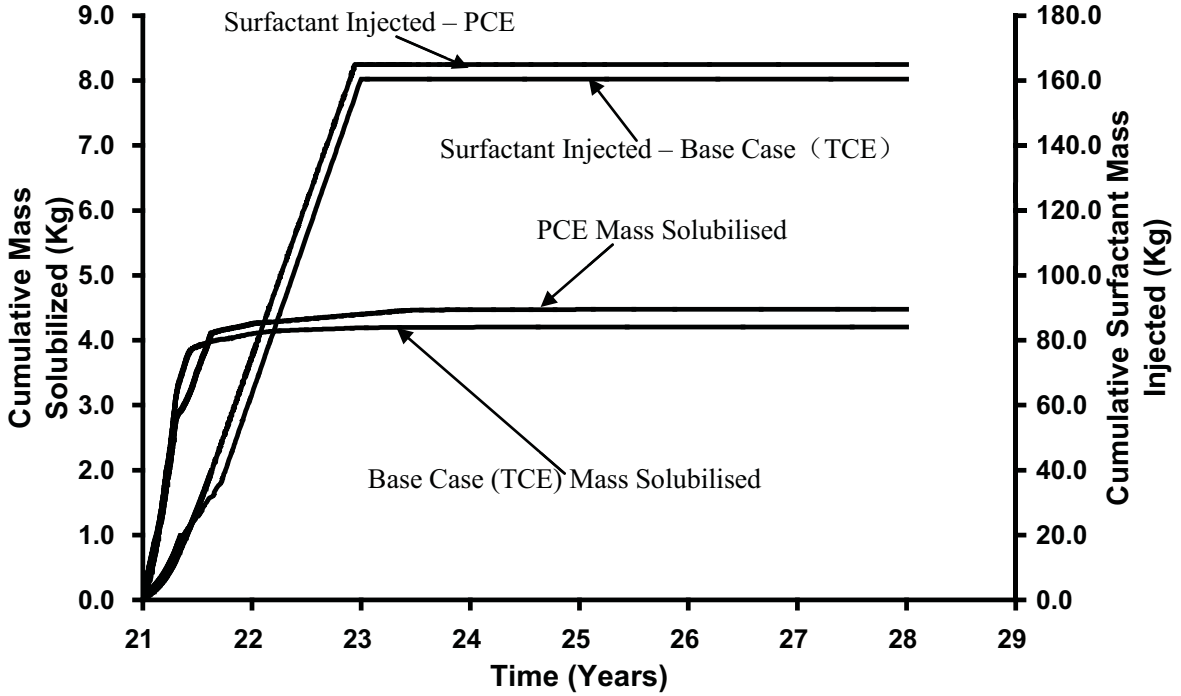

Figure 24: Comparison of cumulative mass solubilised by micelles and surfactant injected for period between 21 to 28 years.

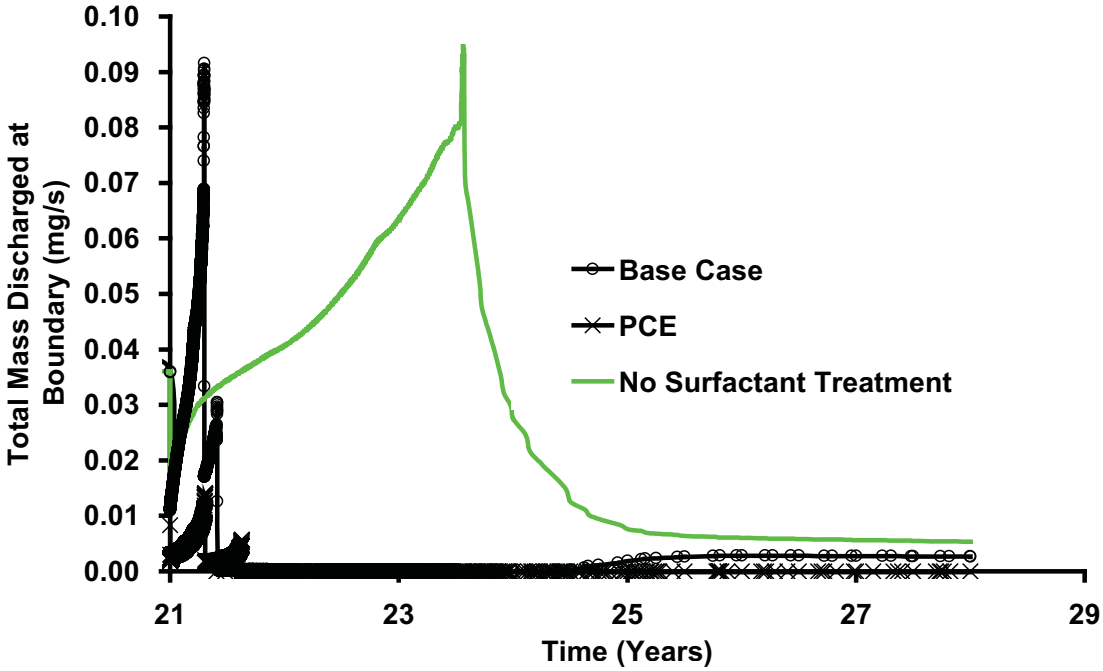

Figure 25: Comparison of total boundary mass discharge for different DNAPL with a simulation where no surfactant treatment (sandstone) was carried out for period between 21 to 28 years.

Figure 26 plots the cumulative discharged mass of aqueous and DNAPL mass entrained in micelles for both PCE and TCE. It is observed in both cases, the discharge for solubilised chlorinated solvent is significantly higher than that exiting the domain in the aqueous phase external to the micelles. Additionally, the discharge of entrained PCE mass is observed to be approximately 8% higher than the entrained TCE mass discharged.

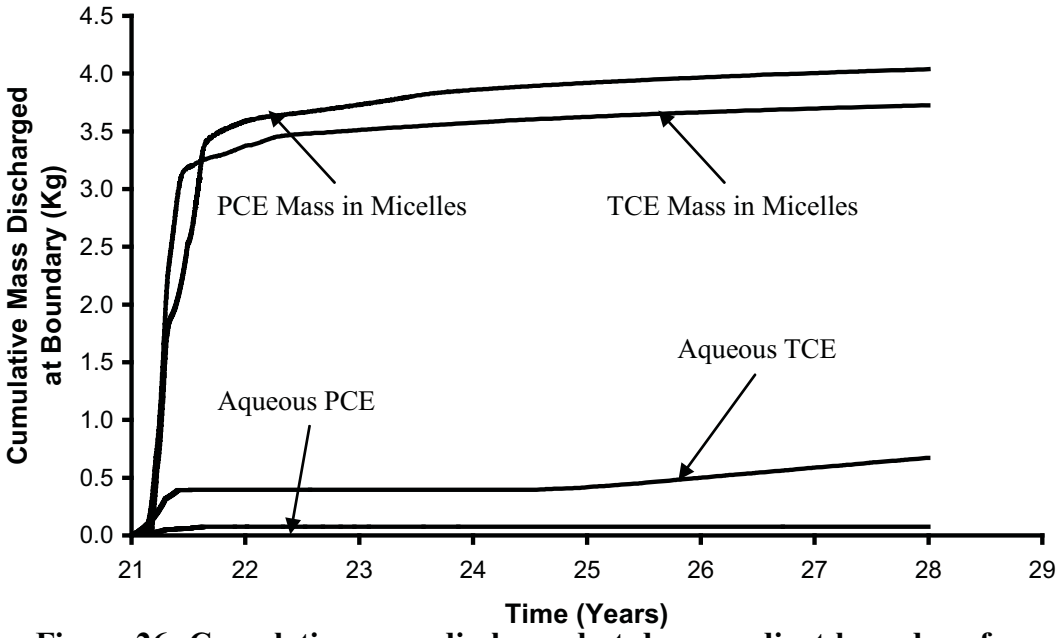

Figure 26: Cumulative mass discharged at downgradient boundary for various DNAPL simulations.

This further corroborates the observation described above that the extramicellar fraction of PCE entrained into micelles is higher than the extramicellar fraction of TCE in the absence of DNAPL, with significant impacts on long term mass discharge.

Sensitivity to Rock Type

At the end of the DNAPL Infiltration stage, the average DNAPL saturation was 0.75, the volume of DNAPL in the domain was 0.008 m^3, 0.010 m^3 and 0.0181 m^3 for sandstone,

shale and granite with 100% of the invaded nodes on drainage for all 3 rock types. At the end of DNAPL redistribution stage, the average DNAPL saturation was 0.3 for all 3 rock types, the volume of DNAPL was 0.0036 m^3 , 0.0047 m^3 and 0.0079 m^3 while the pool to residual ratio was 71:29%, 72:28% and 90:10% for sandstone, shale and granite, respectively. The distribution of TCE DNAPL at the end of the Redistribution stage for all three is illustrated in Figure A6, Appendix A.

At the end of the 20 years Site Ageing stage (t_{TOTAL} = 21 years) the total mass of aqueous and sorbed TCE in the domain was 7.3 kg, 6.8 kg and 0.68 kg for sandstone, shale and granite respectively (Table 5). In each case, 97-99% of the total mass resided in the matrix, of which 97-98% was sorbed and only 1-2% remained in the aqueous phase. Although no DNAPL was left in the sandstone and shale domain at this time, 4.23 kg of DNAPL was present in the granite domain. This observation is consistent with the findings in Parker e al. (1994) where it was demonstrated that due to the low porosity in granite, DNAPL could remain present in the fractures for decades. Figure 27 illustrates the distribution of aqueous phase TCE in sandstone, shale and granite at the end of the 20-year Site Ageing stage. In each case, the matrix immediately surrounding the fractures exhibits diffusion halos of TCE. However, the depth and extent of TCE penetration of the matrix is observed to be highly dependent on properties of both the fractures and the matrix for each rock type. The combination of these impacts residence time of TCE in the source zone and it is the relative rates of TCE transport through fractures versus diffusion to the matrix that affects the final distribution of mass diffusion (See section 4.5.2.3 for calculations and further details).

The vertical axis of Figure 28 demonstrates that the percentage of initial TCE mass retained in the domain at the end of Site Ageing follows the order sandstone > shale > granite. Peclet number (Pe) for fractured rock is defined as the ratio of advection to diffusion rates, $Pe = ve/(D^o\tau)$, where v is the advective velocity in the fracture, e is the mean aperture, D^o is the free solute diffusion coefficient and τ is the matrix tortuosity (e.g., Fetter, 1993). Here v is taken as the mean horizontal advective velocity across each domain and e is the mean aperture of all horizontal fractures for each rock type. Figure 28 reveals that the percentage of TCE retained (in aqueous and sorbed forms) exhibits a linear dependence on the log(Pe) for the three rock types ($R^2 = 0.9923$) at the end of the Site Ageing stage (i.e., t_{TOTAL} = 21 years). This confirms expectations that lower Pe (i.e., lower advective velocity, smaller apertures, higher effective diffusion) corresponds to increased matrix diffusion (e.g., sandstone) while higher Pe corresponds to increased mass loss via advection (e.g., granite).

At t_{TOTAL}=21 years, as mentioned above, DNAPL distribution at t_{TOTAL} = 1 year was mapped onto the domain. As a result, the total TCE DNAPL mass (and total aqueous + sorbed TCE mass) present in sandstone, shale and granite were 5.18 kg (7.30 kg), 6.88 kg (6.67 kg) and 11.53 kg (0.68 kg), respectively, at the beginning of the Treatment stage.

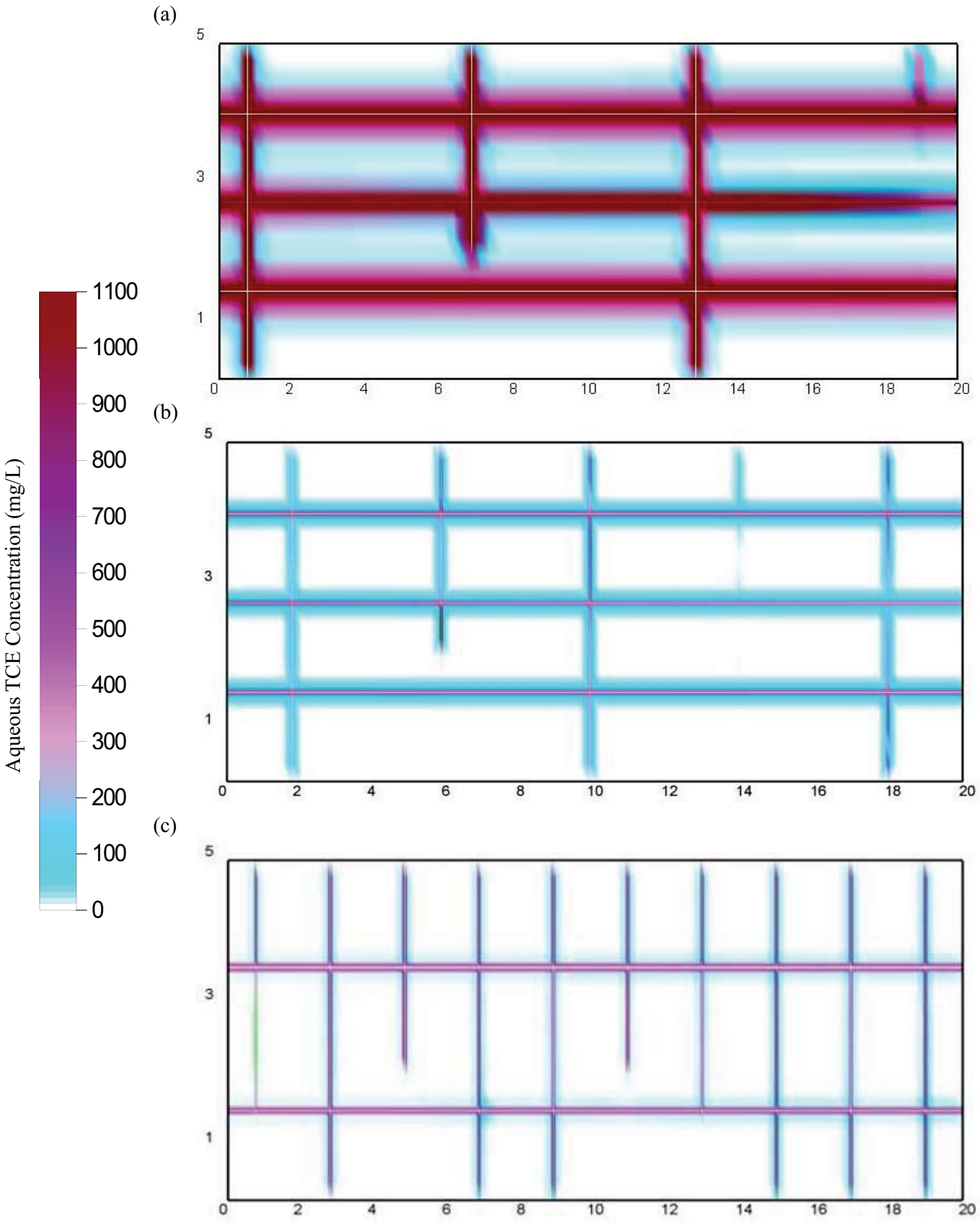

Figure 27: Distribution of aqueous TCE after 20 years (t_{TOTAL} = 21 years) of DNAPL dissolution in (a) Sandstone, (b) Shale and (c) Granite.

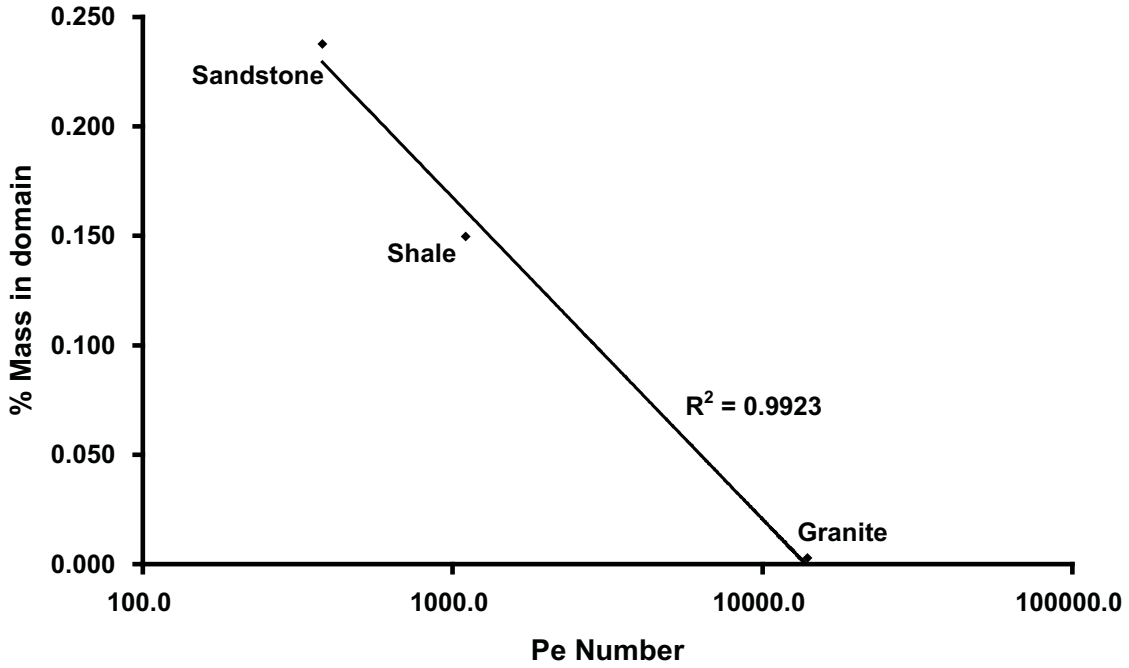

Figure 28: Mass of aqueous and sorbed TCE in various rock domains at end of Site Ageing stage (i.e., t_{TOTAL} = 21 years) vs. Peclet number (log scale) for each individual domain.

Figure 29, presenting the mass of TCE (i.e., sorbed + aqueous + DNAPL) solubilised, reveals that granite (which exhibits the largest mean fracture aperture of the three rock types) exhibits the highest solubilised TCE mass while sandstone (i.e., Base Case) exhibits the lowest. These observations are mainly due to the presence of more DNAPL within the fractures at the start of the Treatment stage. Although granite exhibits the highest solubilised mass among the three rock types investigated, the fraction of mass recovered is only equivalent to 62.1% of the initial DNAPL mass present in the domain at the start of the Treatment stage. Interestingly, this is lower than the 70.2% and 80.2% of chlorinated ethene mass recovered in shale and sandstone respectively. Figure 11 and Figures C7 and C8 of Supplementary Information revealed that vertical fractures, contaminated by the downward vertical movement of DNAPL appear to be relatively

unaffected by horizontally driven surfactant. This is confirmed by the lack of micelles being formed in the vicinity of the vertical fractures, especially near the top and bottom areas of the vertical fractures in the respective domains. Given the largest vertical fracture volume in granite (hence the largest fraction of initial mass entrapped in vertical fractures), it could be understood why granite experienced the lowest fraction of mass being recovered among the three rock types.

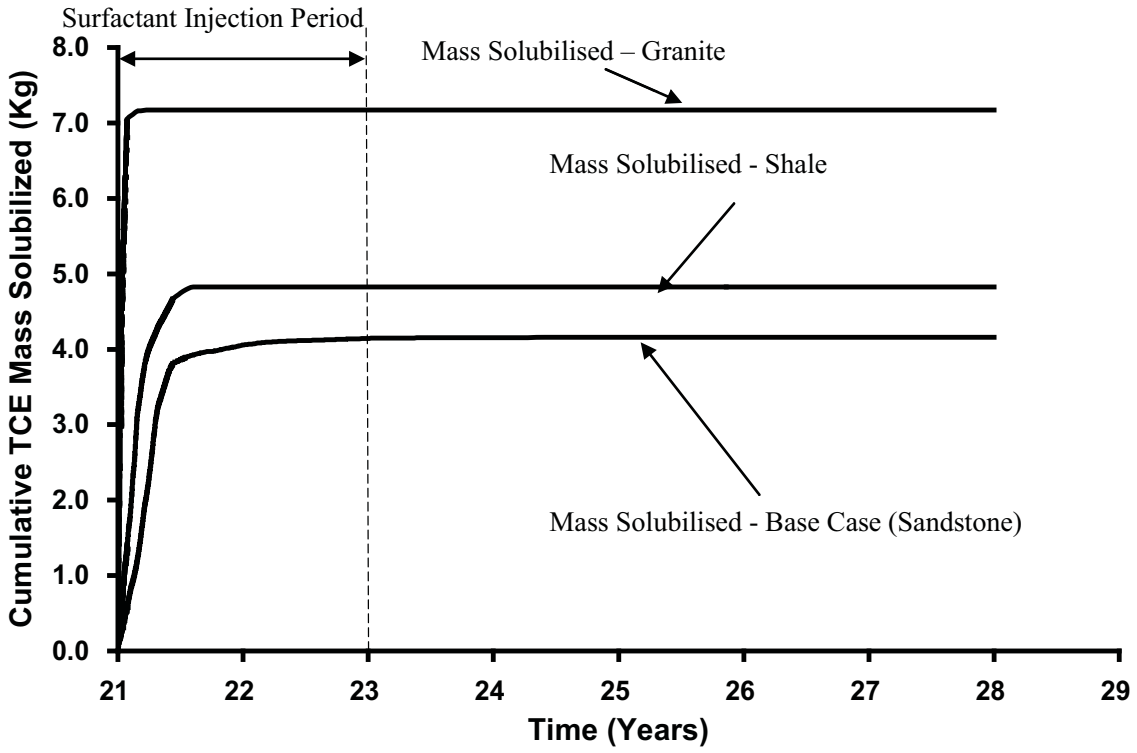

Figure 29: Cumulative TCE mass solubilised by surfactant over time for various rock types.

Figure 30 reveals a total of 160kg, 263kg and 1730kg of surfactant being injected over 2 years for sandstone, shale and granite respectively (Table 5). The amount of surfactant injected is equivalent to 12.3 times, 18.5 times and 136.0 times greater than the theoretical mass required to solubilise and entrain all the TCE in the domain at the start of the Treatment stage. The differences in surfactant mass injected are due the differences

in bulk effective horizontal hydraulic conductivity while treatment period, injection concentration and hydraulic gradient were all held constant. This figure further reveals that of the surfactant injected, only 4.33kg, 5.03kg and 7.47kg (Table 5) were used in the solubilisation and capturing of TCE into micelles in the sandstone, shale and granite, respectively.

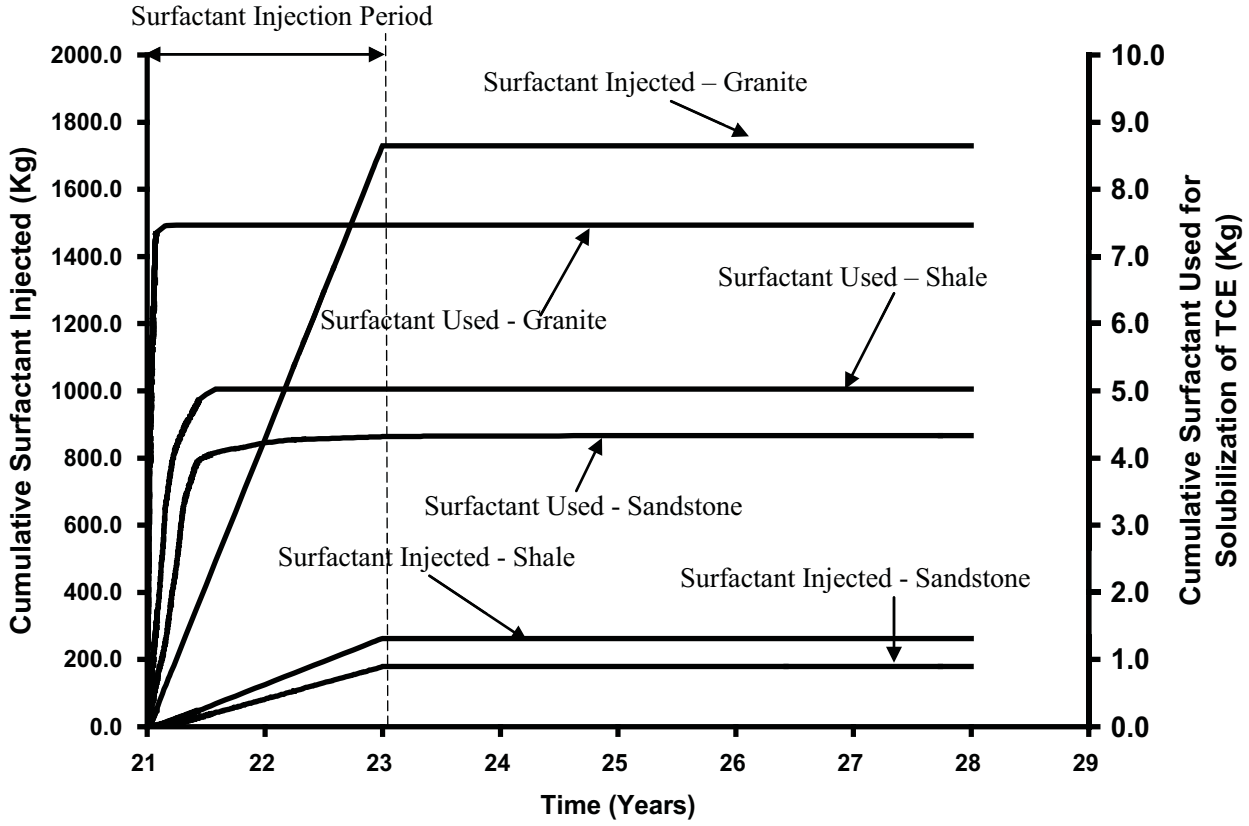

Figure 30: Cumulative surfactant injected and used for TCE solubilization for various rock types simulations.

Figure 31 presents the total boundary mass discharge for the three rock types. As revealed in this figure, the mass discharges for all three simulations were quickly reduced to negligible level in less than half a year after treatment began. Figure 31b further reveals that the mass discharge for granite diminishes at the fastest rate among the three rock types. This confirms expectations that granite with a higher peclet number (i.e., a

more advective dominated domain) allows the injected surfactant to travel through the fractures at a quicker rate, thus in turn solubilises and partitions TCE molecules within the fractures into the surfactant micelles at a faster rate than sandstone and shale (i.e., less advective dominated domains). During the Post-Treatment stage, the 'No surfactant treatment' simulation exhibited a low but relatively constant mass discharge associated with reverse diffusion. Meanwhile, only sandstone (which possesses the highest diffusive flux scenario among the three rock types) exhibited a re-bound in mass discharged while shale and granite both reveal negligible mass discharge level throughout this period.

Figure 32 plots the cumulative discharged mass of aqueous and entrained TCE mass in micelles for sandstone, shale and granite respectively. Although the aqueous mass discharged is similar in all three rock types during the Treatment stage, the sandstone simulation revealed an increase in mass discharge during late times; reaffirming the observation of reverse diffusion in this particular domain. Figure 32 further reveals the mass of entrained TCE being discharged as granite > shale > sandstone. This observation is consistent with the previous findings where granite exhibits the highest solubilised TCE mass while sandstone (i.e., Base Case) exhibits the lowest. Together with the high peclet number (therefore a more advective domain) in granite, it can be understood why granite exhibits the largest amount of entrained TCE mass being discharged out of the domain.

Refer Figure C7 and C8, Supplementary Information for the concentration profiles of all

three aqueous species at t_{TOTAL}=28 years.

（a）

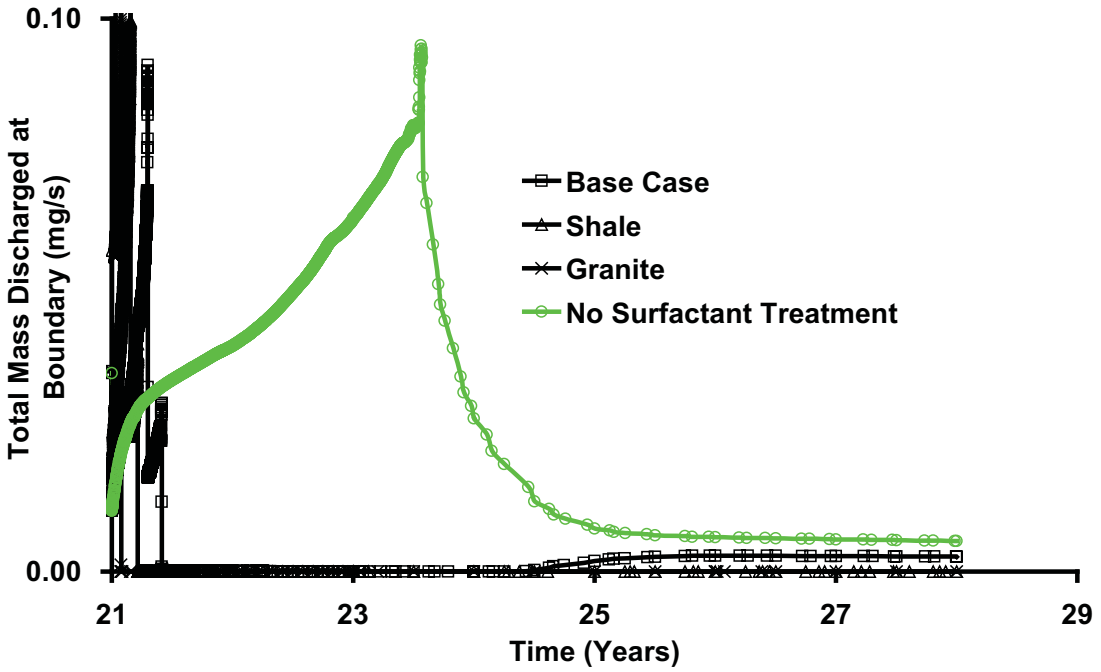

（b）

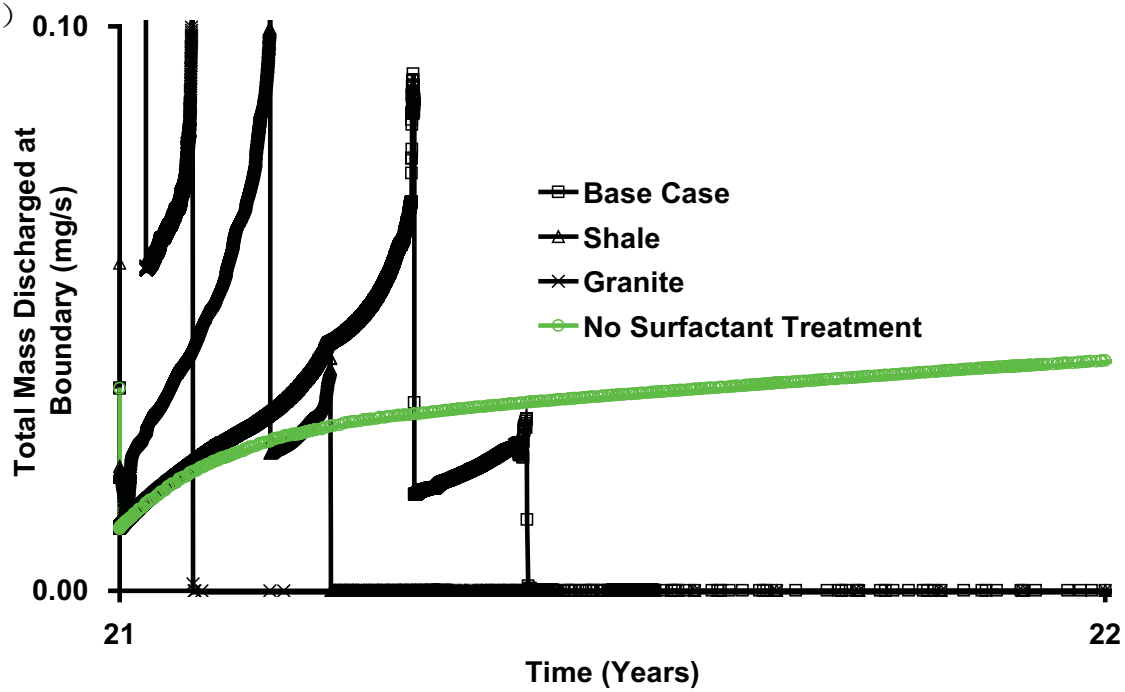

Figure 31: Comparison of total boundary mass discharge for (a) different rock type with a simulation where No surfactant treatment (sandstone) was carried out for period between 21 to 28 years (b) since the start of the Treatment Stage for 1 year only (timescale expanded for clarity).

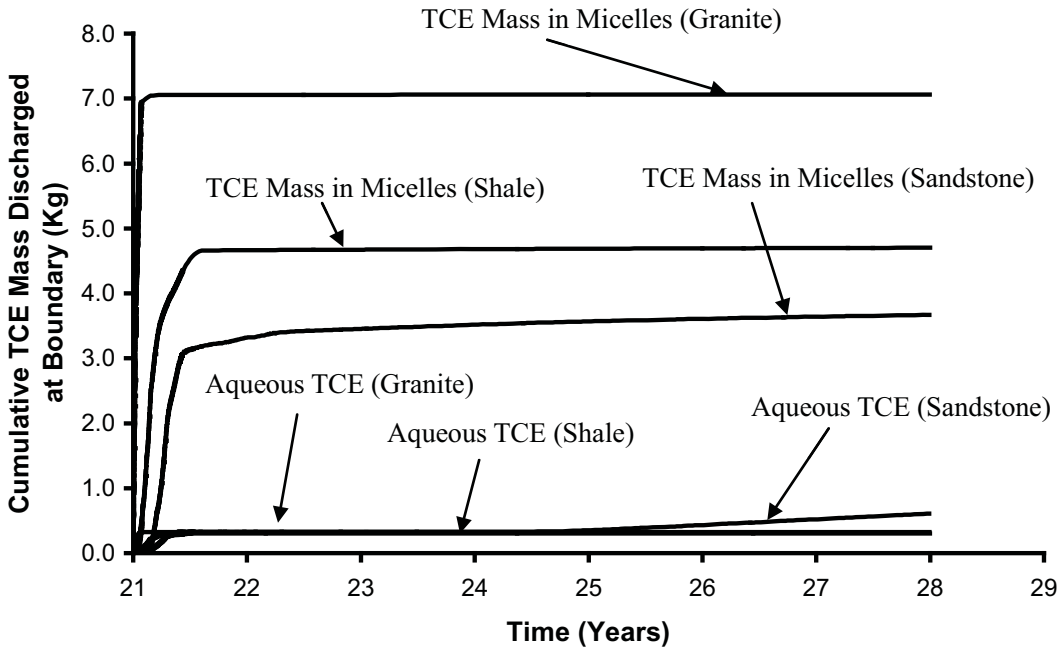

Figure 32: Cumulative mass discharged at downgradient boundary for (a) sandstone; (b) shale and (c) granite.

Sensitivity to Aging Time

In this sensitivity study, the effects of the duration of 'aging' process on surfactant flushing were investigated. In each case, the DNAPL volume and distribution is the same but the aqueous and sorbed TCE mass contaminates the matrix to different extents at the start of treatment. Prior to the Treatment stage, the total aqueous and sorbed TCE present in the domain was 0.00 kg, 4.13 kg, 5.33 kg and 7.30 kg for 0 years, 5 years, 10 years and 20 years aging (Base Case), respectively, while the DNAPL mass in each case was 5.18 kg.

Figure 33 reveals that the total TCE mass (DNAPL solubilised and solute entrained) removed by surfactant is directly related to the extent of TCE loading of the matrix (i.e., aging period). Therefore, some recovery of the matrix-bound TCE is observed.

However, the fraction of initial TCE + aqueous and sorbed mass recovered was 59%, 38%, 37% and 33% for ageing periods of 0 years, 5 years, 10 years and 20 years, respectively. These results underscore that while surfactant flushing of fractures is effective, recovering diffused and sorbed mass in the matrix is relatively inefficient with this inefficiency increasing as the timescale of the site ageing increases relative to the timescale of the treatment.

Figure 34 plots the cumulative TCE (aqueous + sorbed) mass discharged for these 4 simulations. For the purpose of clarity, only the mass discharged for the Treatment and Post-Treatment stages were plotted. This figure reveals that in all cases the downgradient mass discharge was reduced to zero in a short time during the treatment period. It is further noted that only the cases with significant matrix contamination – namely, Site Ageing for 5 years, 10 years and 20 years - exhibited rebound of mass flux

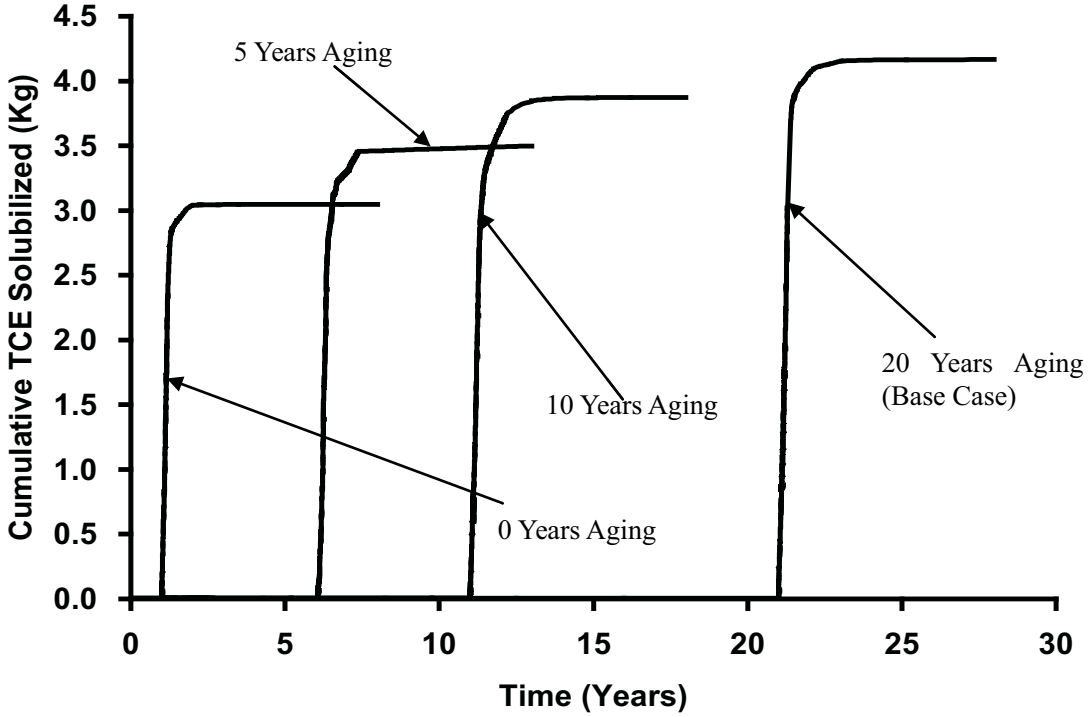

Figure 33: Cumulative mass of TCE solubilised over time for different aging period.

within a 2-year period after terminating treatment. Although only 59% of the initial TCE mass was recovered in the '0 years' Ageing simulation, it is believed the high concentration of surfactant that remained in the vicinity of the factures (Figure C9, Supplementary Information) has prevented a rebound of mass flux after Treatment has ceased. It is revealed that the mass discharge for '5 years', '10 years' and '20 years' aging were 1.91 x 10^{-5} mg/s, 7.15 x 10^{-4} mg/s and 2.69 x 10^{-3} mg/s respectively (Table 5), indicating that the magnitude of rebound is more significant as the length of site ageing increases. As expected, when the extent of rock matrix that was contaminated with aqueous and sorbed TCE increases beyond a threshold amount, a constant volume of surfactant cannot access it all in the limited Treatment period.

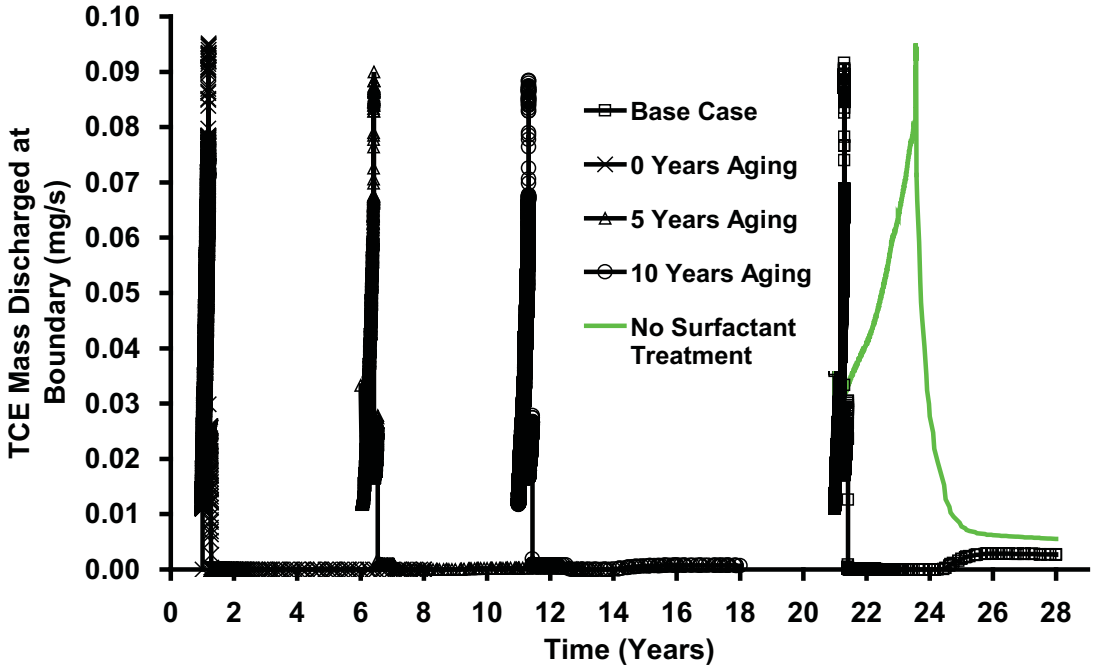

Figure 34: Comparison of total boundary mass discharge for different aging period with a simulation where no surfactant treatment was carried out for period from 2 years of Treatment and 5 years of Post-Treatment.

Figure 35 plots the cumulative downgradient mass discharge of aqueous and entrained TCE in micelles for '0 years', '5 years', '10 years' and '20 years' aging simulation. As per all other simulations, this figure reveals higher entrained TCE mass being discharged than aqueous TCE. It is further revealed that as the years of aging increases, the amount of mass of TCE entrained in micelles being discharged increases accordingly. This agrees with the previous observation that the extent of the total TCE mass (DNAPL solubilised and solute entrained) removed by surfactant is directly related to the extent of TCE loading of the matrix (i.e., aging period).

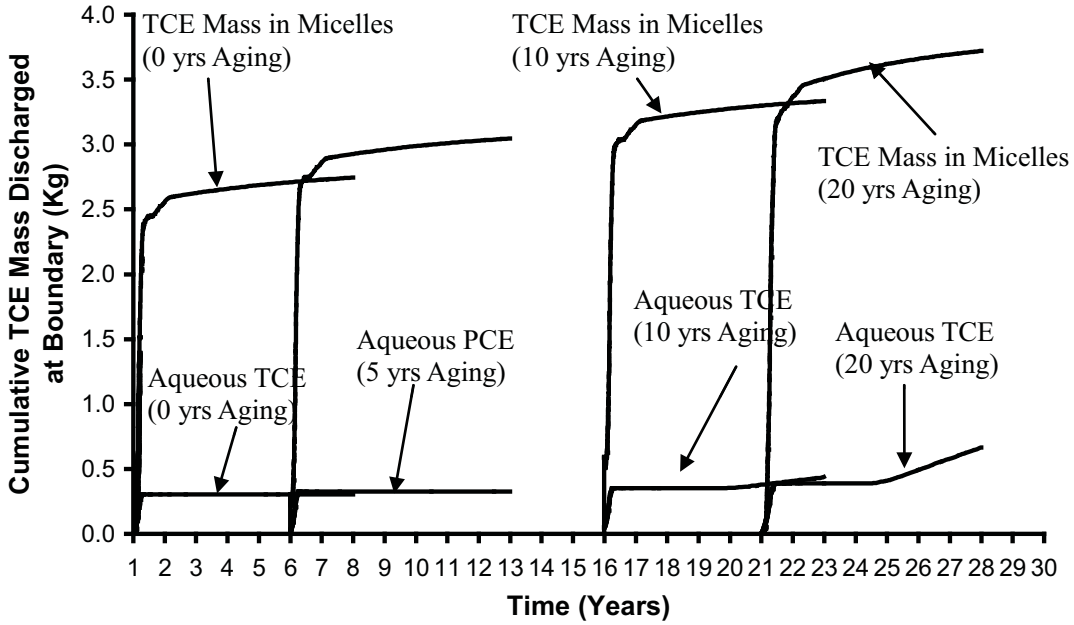

Figure 35: Cumulative mass discharged at downgradient boundary for (a) 0 years aging; (b) 5 years aging (c) 10 years aging and (d) 20 year aging.

Sensitivity to Mass Transfer Model

This sensitivity study compared the influence of the rate-limited mass transfer model of Dickson and Thomson (2003) to that from the equilibrium dissolution model. Figure 36 reveals that although the total mass of surfactant injected into the domain is similar in

each simulation, the total cumulative mass of TCE (i.e., sorbed + aqueous + DNAPL) solubilised in the Base Case was approximately 21% higher than the rate-limited case. Figure 37 reveals the result of a predicted stall in DNAPL mass transfer in the rate-limited case before all the DNAPL was depleted. In this case, a rapid slowdown in mass transfer rate is observed at t_{TOTAL} = 21.5 years. It is believed this slowdown is due to an end of the initial pseudosteady and early transient stages of dissolution, where majority of mass transfer is to take place (Dickson and Thomson, 2003). This is backed-up by Figure 38 where DNAPL saturations in the domain are generally observed to be at 0.1 or less (except for the immediate vicinity of the dead-end vertical fracture), indicating more than 8% of the initial mass has been removed from virtually all locations – a criteria which marked the end of the initial pseudosteady and early transient stages of dissolution.

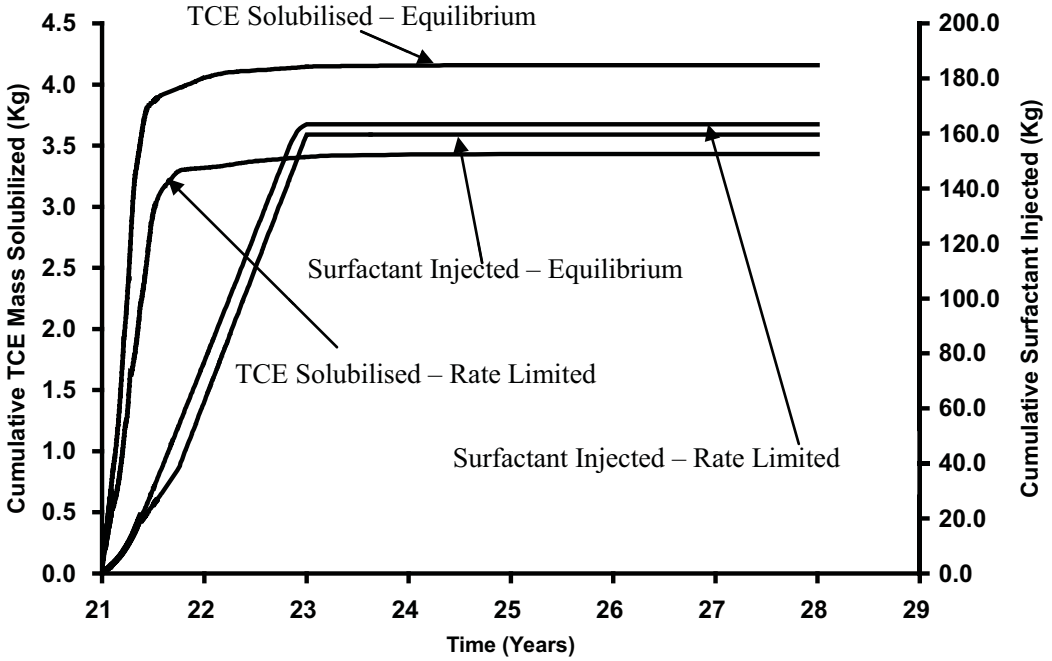

Figure 36: Cumulative TCE captured and Tween-80 injected over time for rate-limited mass transfer simulation.

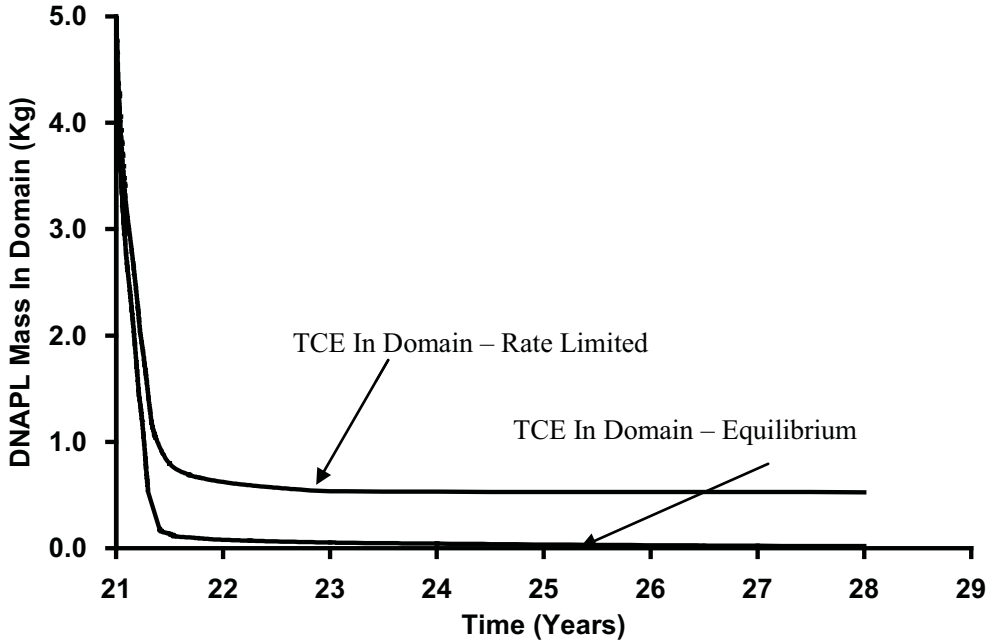

Figure 37: Cumulative TCE mass in domain for (a) rate-limited mass transfer simulation (b) Base Case, over time.

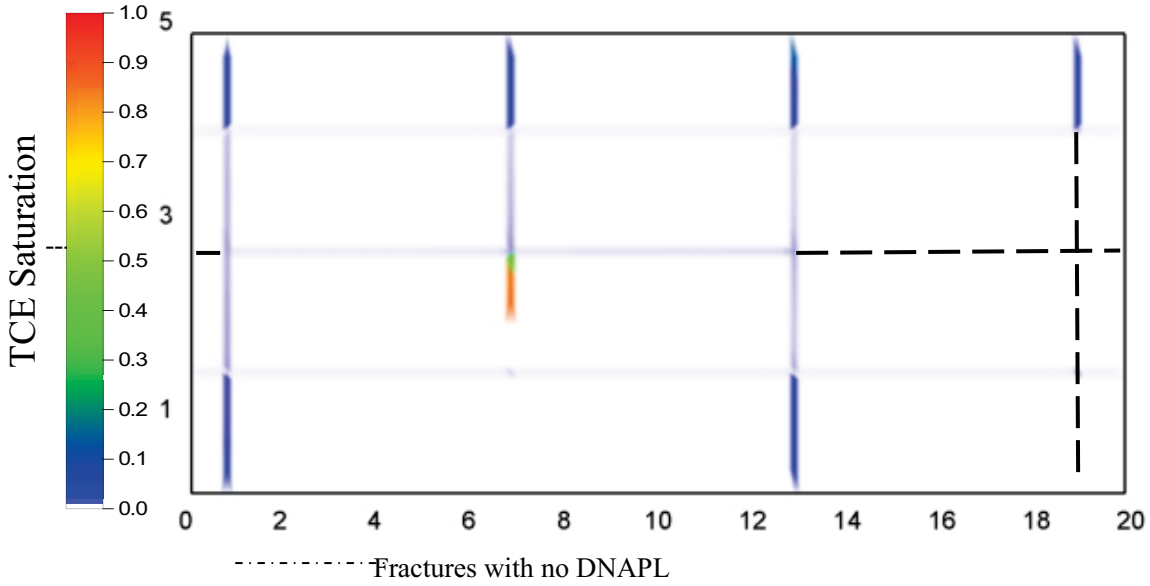

Figure 38: Distribution of TCE saturation, at the end of Treatment stage (i.e., t_{TOTAL} = 23 years).

Figure 39, presenting the total TCE mass discharge from both runs, reveals that during the Treatment stage, the mass discharge in both simulations are reduced to negligible

level in less than one year. However, it is further noted that during the first year of treatment, the mass discharge curve is significantly different in the two simulations. In the rate-limited mass transfer simulation, the decrease in mass discharge is more gradual than the equilibrium mass transfer model simulation with no sharp downturn in the downgradient discharge rate. This is most possibly due to longer presence of DNAPL within the fractures in the rate limited simulation, thus leading to overlapping of the three distinct stages of mass flux through each horizontal fracture in the domain. Figure 39 further reveals that in both simulations a rebound of similar magnitude of boundary mass discharge is observed at late times.

Figure 40 plots the cumulative downgradient mass discharge of aqueous and entrained TCE in micelles for both the equilibrium (i.e. Base Case) and rate-limited mass transfer model. This figure revealed that although the equilibrium model has a higher mass discharge for entrained TCE - a finding consistent with a previous observation where more TCE mass was solubilised in the Base Case; the rate-limited simulation has a higher aqueous TCE mass discharge. Indicating surfactant flushing is less efficient in a rate-limited scenario.

Refer to Figure C12, Supplementary Information for the concentration profiles of all three species at t_{TOTAL}=28 years.

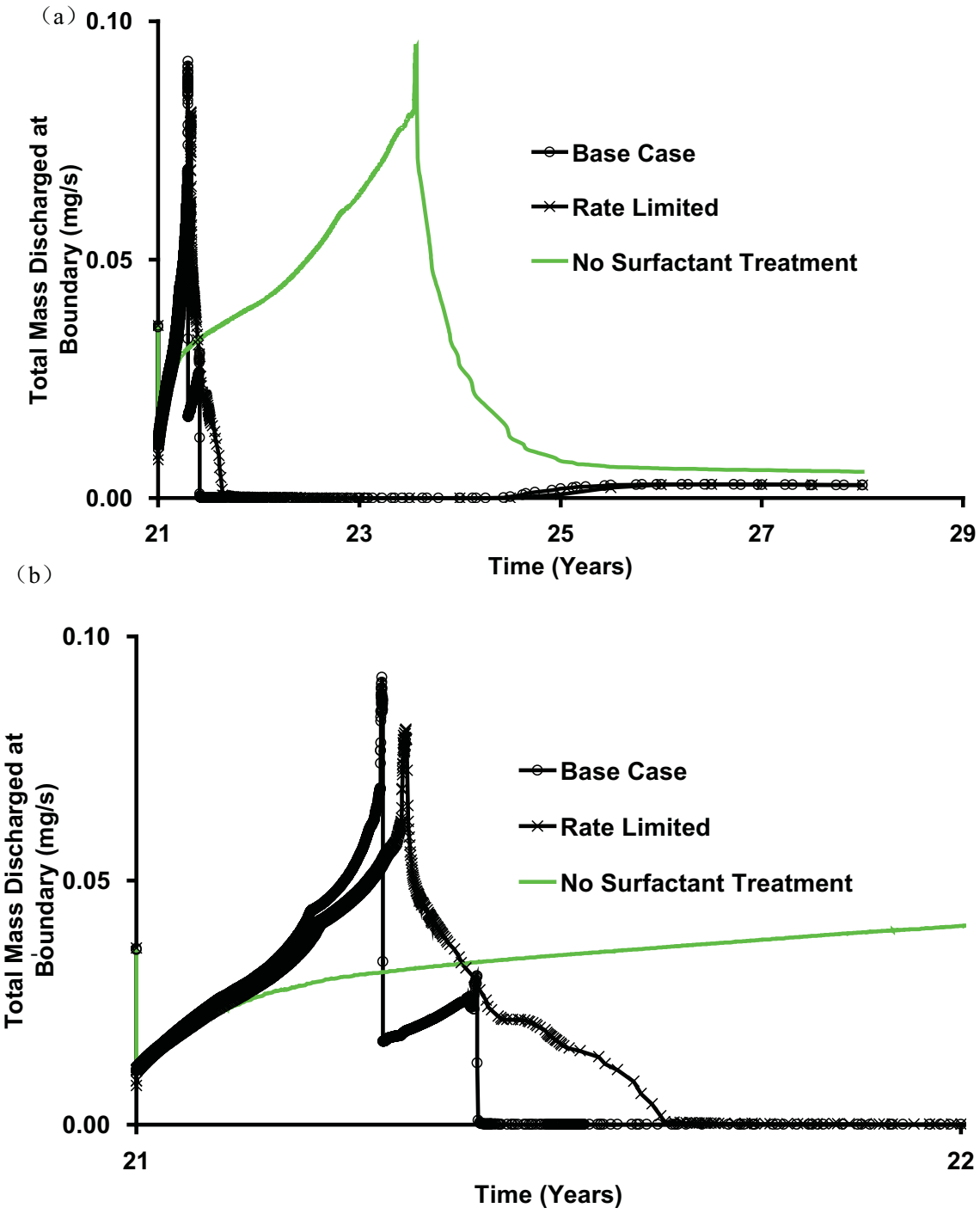

Figure 39: Comparison of total boundary mass discharge for (a) different mass transfer model with a simulation where No surfactant treatment (equilibrium mass transfer) was carried out for period between 21 to 28 years (b) since the start of the Treatment Stage for 1 year only (timescale expanded for clarity).

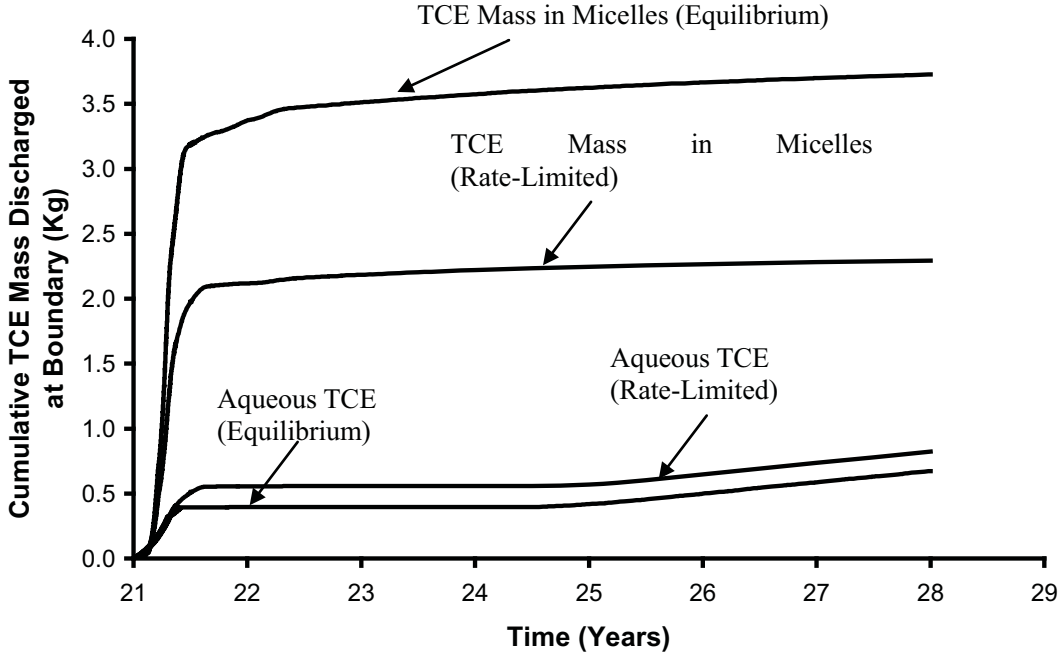

Figure 40: Cumulative mass discharged at downgradient boundary for (a) equilibrium and (b) rate limited mass transfer model.

5. CONCLUSION

Surfactant treatment with Tween-80 was proven to be a relatively effective technique in solubilising and removing DNAPL from the horizontal fractures within the domain. However, by comparing the aqueous and sorbed mass at the start and end of the Treatment stage, it is revealed that surfactant treatment is relatively ineffective in removing the mass that resides within the matrix.

Higher treatment efficiencies were observed in the shale and sandstone, with TCE mass reduced during treatment 70.2% and 80.2% of the initial DNAPL mass, respectively. Results revealed that vertical fractures, contaminated by the downward vertical movement of DNAPL appear to be relatively unaffected by horizontally driven surfactant. Granite, with the largest fraction of initial mass entrapped in vertical fractures,

experiences the lowest fraction of mass being recovered among the three rock types. Furthermore, granite, with the lowest diffusive storage, is able to achieve negligible mass discharge at a faster rate than sandstone and shale. This confirms expectations that granite (higher peclet number, i.e., more advection-dominated domain) allows the injected surfactant to travel through the fractures at a quicker rate, solubilizingses and encapsulating TCE molecules within the fractures at a faster rate than sandstone and shale. DNAPLs were observed in dead-end vertical fractures within all three rock types by the end of all simulations. This indicates that although surfactant treatment may be efficient in solubilising DNAPL in fractures, the injected surfactant experiences difficulty in accessing DNAPL entrapped in dead-end fractures.

As the surfactant concentration was increased from 20g/L to 40g/L, a small improvement in the total mass solubilised was noted. However, a further increase from 40 g/L to 60 g/L causes negligible further improvement in rate or in total amount recovered; the latter because all readily accessed DNAPL is solubilised. The overall percent recovery of chlorinated solvent mass from the source zone decreased with increasing ageing time because, although similar volumes of DNAPL were solubilised, decreasing fractions of the matrix-bound mass was removed.

When surfactant was applied to different DNAPLs it was found that, due to the difference in MSRs, a higher fraction of aqueous PCE mass was entrained into micelles relative to TCE. Unlike for TCE, no rebound in the chlorinated ethene mass discharge was observed in for PCE. This further corroborates the observation that PCE is better

solubilised than TCE, with potential impacts on long term mass discharge.

Different mass transfer models were found to lead to a significant difference in the amount of DNAPL left in the domain by the end of the simulation. By employing a rate-limited mass transfer model, it was found that the amount of DNAPL present in the domain never decreases to a negligible amount (as compared to most DNAPL being solubilised by 4.8 months in the Base Case). The rate-limited model was also found to contribute to significant differences in the boundary mass discharge curve during the first year of surfactant treatment. No sharp downturn in the downgradient discharge rate was observed when the rate-limited mass transfer model was employed, indicating longer presence of DNAPL within the fractures in the rate-limited simulation, thus leading to overlapping of the three distinct stages of mass flux through each horizontal fracture in the domain.

It is acknowledged that numerous assumptions and simplifications were employed in this work. In the majority of circumstances, the assumptions were chosen to present a 'best case' scenario that favours effective treatment (e.g., no sorption of micelles, TCE molecules do not partition back out from the micelles, two-dimensional flow with little opportunity for bypassing, equilibrium mass transfer). This approach underscores the challenges associated with effectively treating aged source zones in fractured rock with surfactant. The limited number of simulations conducted using specific site templates on a small field scale implies that these results cannot be directly extended to a wide variety of complex real sites. For these reasons, these results are not intended to be

predictive; rather they speak to the overall effectiveness of the technique in fractures versus matrix and focus on the relative performance between scenarios.

SUPPLEMENTARY INFORMATION

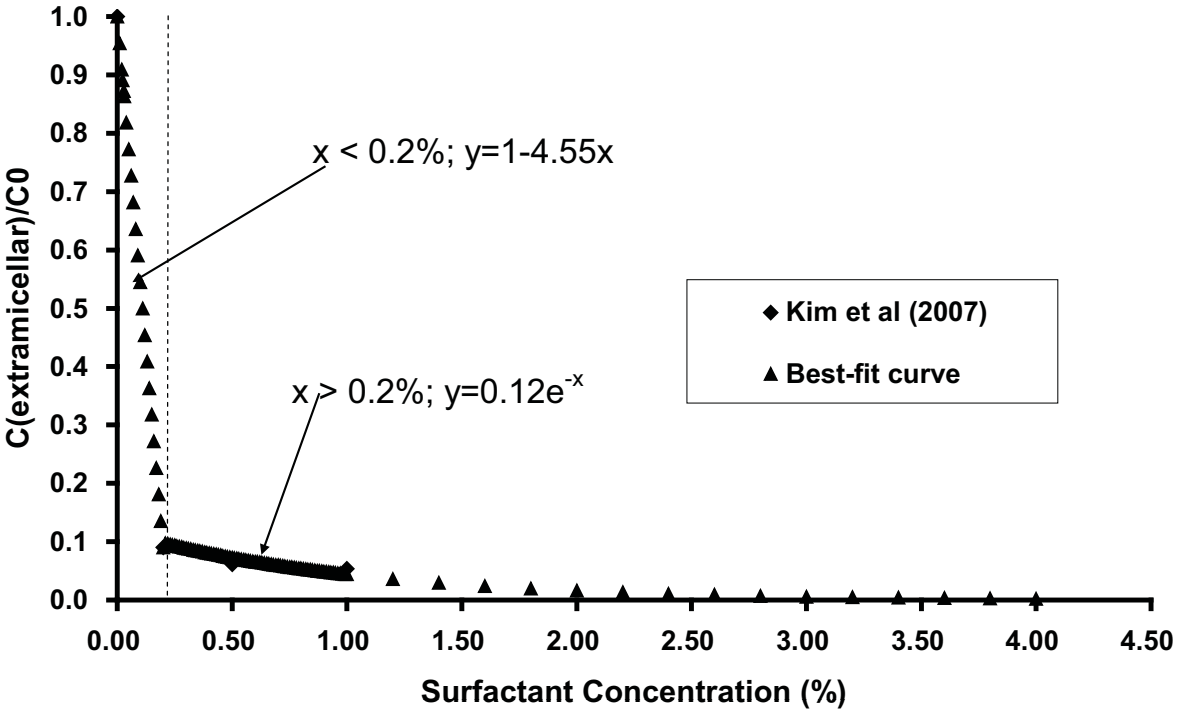

Figure C1: Extramicellar best fit curves for PCE based on results interpolated from Kim et al., 2007.

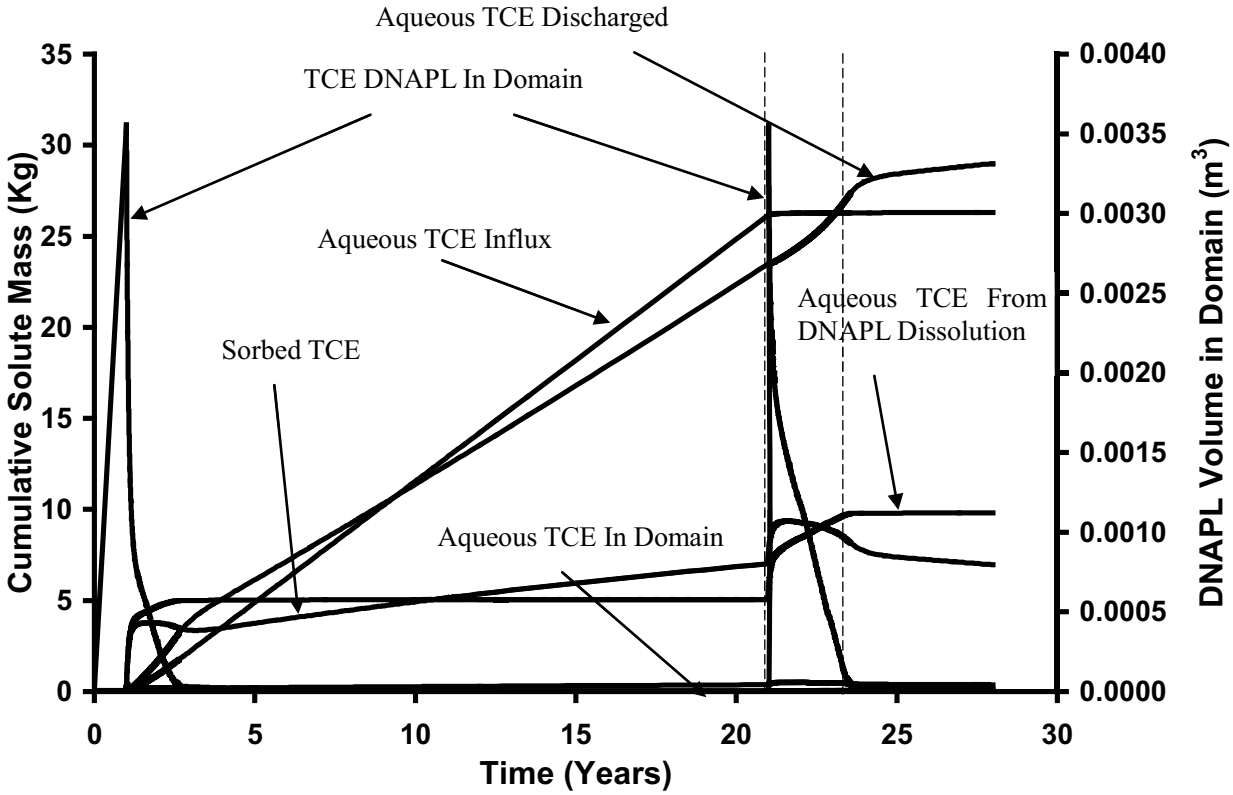

Figure C2: Cumulative aqueous and sorbed TCE from all sinks and sources for No Surfactant Simulation.

(a)

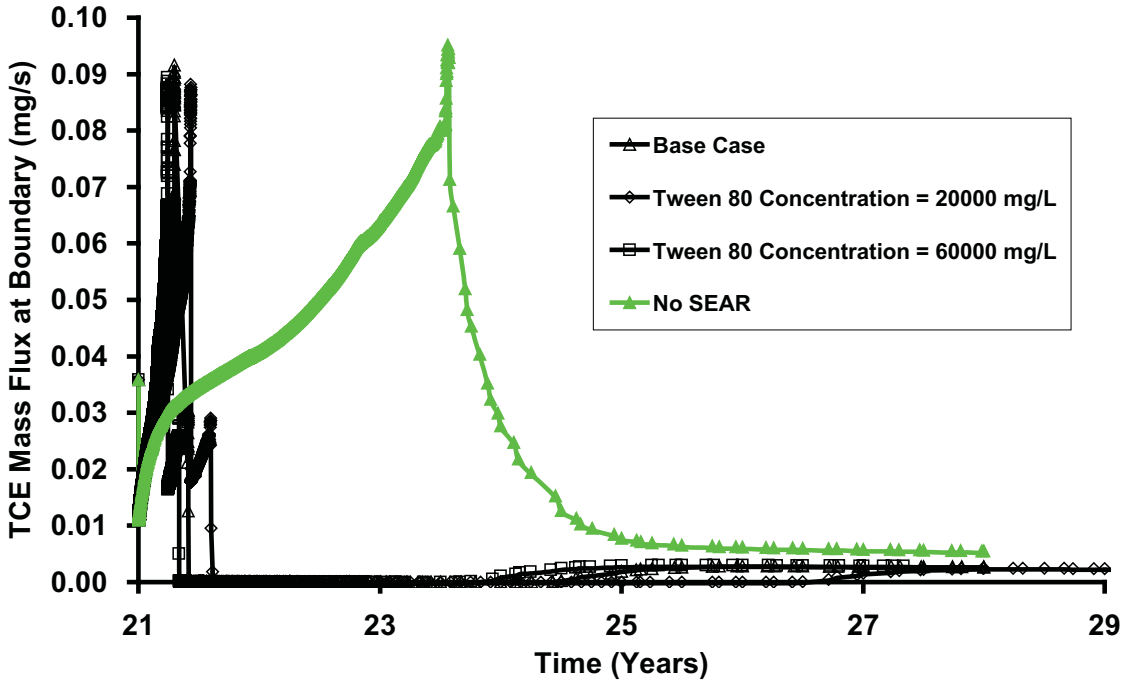

(b)

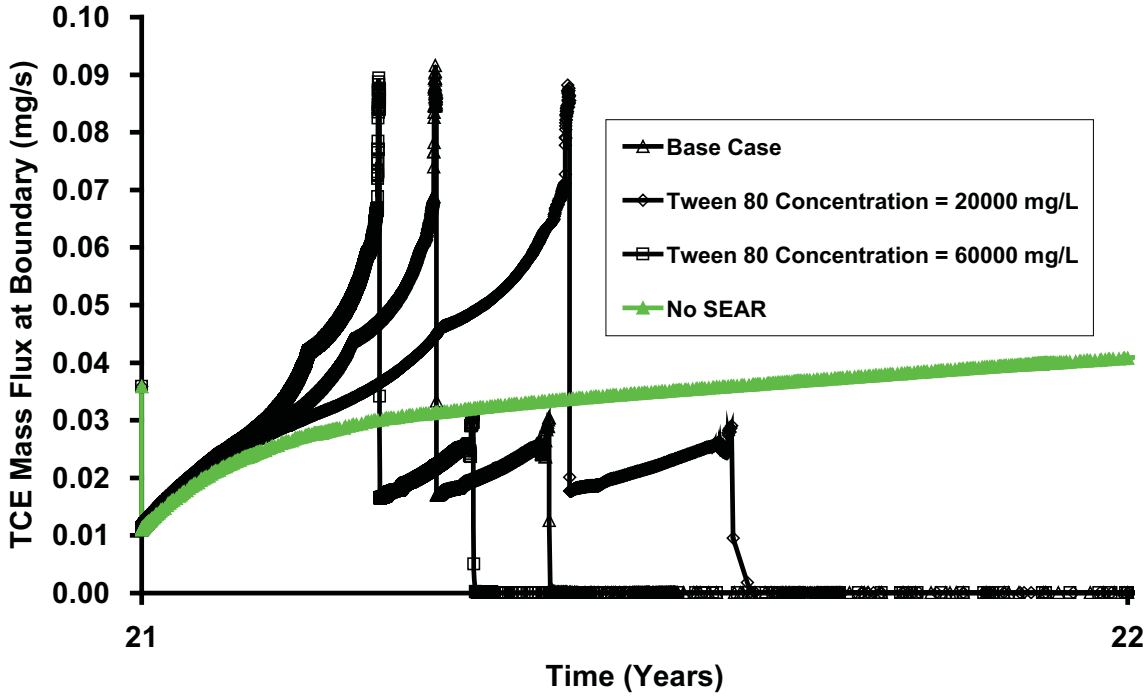

Figure C3: Comparison of total boundary mass discharge (TCE) for base case with (a) various Tween-80 concentration (b) zoom in of results.

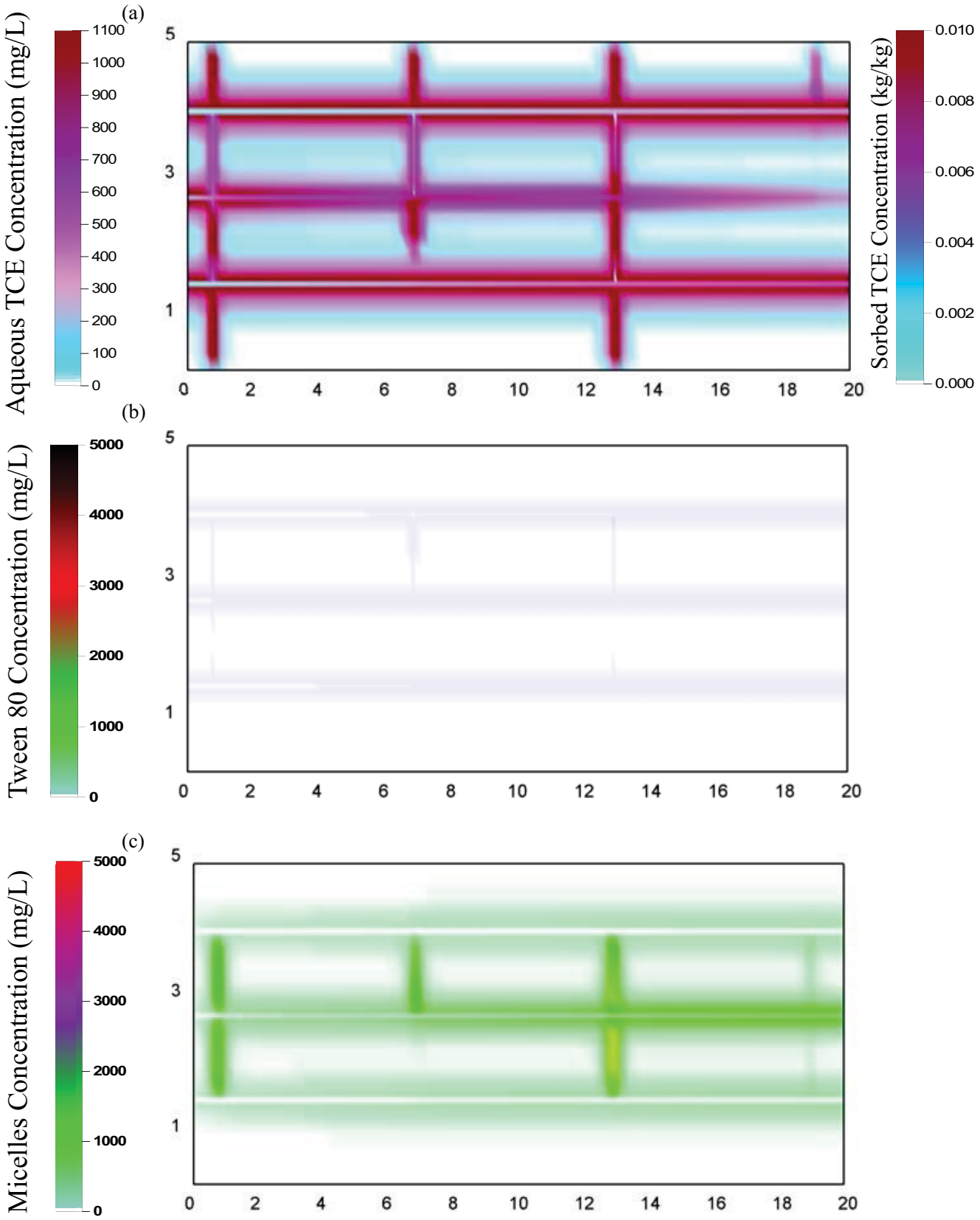

Figure C4: Distribution of (a) Aqueous TCE; (b) Tween-80; (c) TCE occupied micelles, 5 years after injecting 20000mg/L of Tween-80.

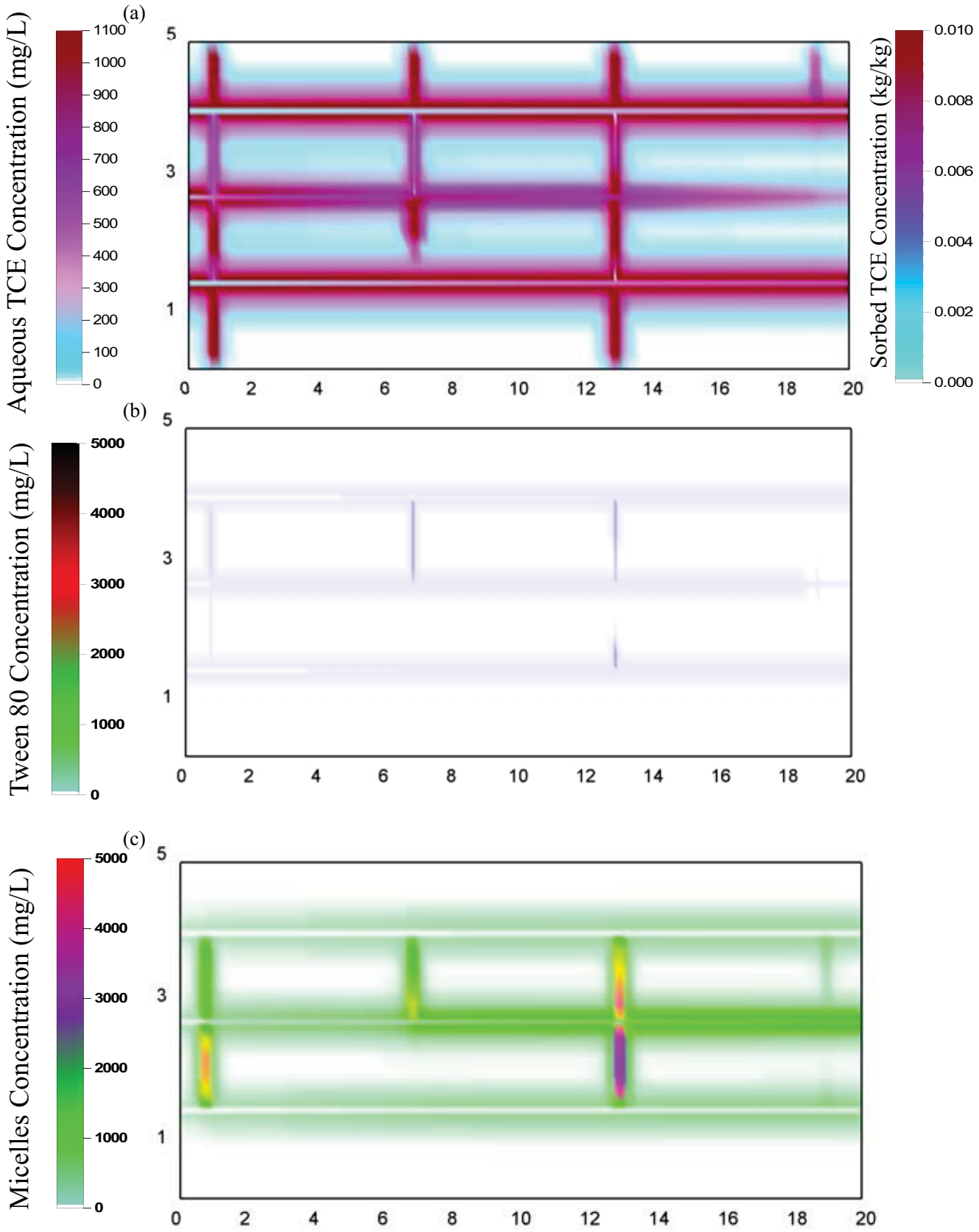

Figure C5: Distribution of (a) Aqueous TCE; (b) Tween-80; (c) TCE occupied micelles, 5 years after injecting 60000mg/L of Tween-80.

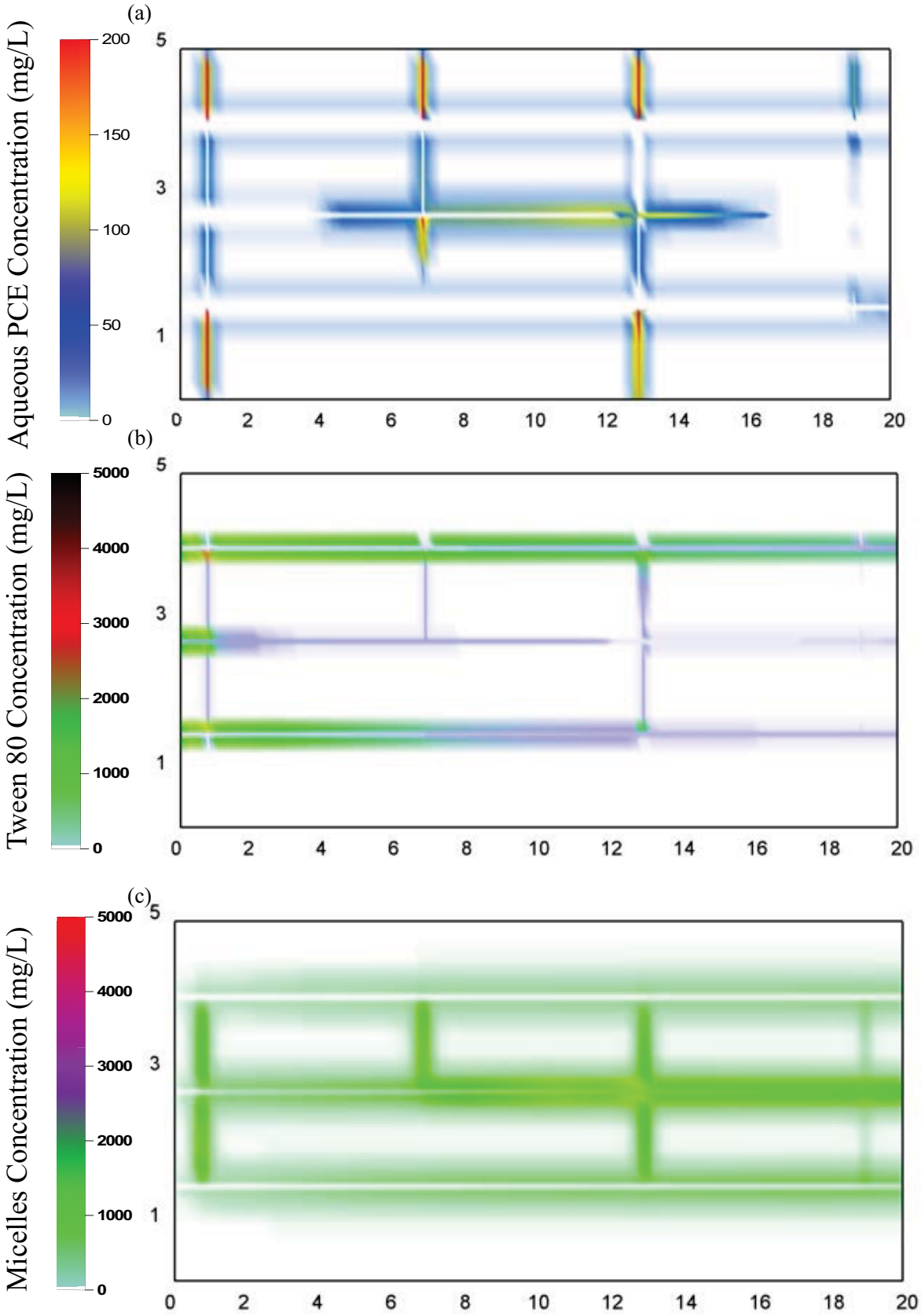

Figure C6: Distribution of (a) Aqueous PCE; (b) Tween-80; (c) PCE occupied micelles, 5 years after surfactant injection for a domain inhibited with PCE.

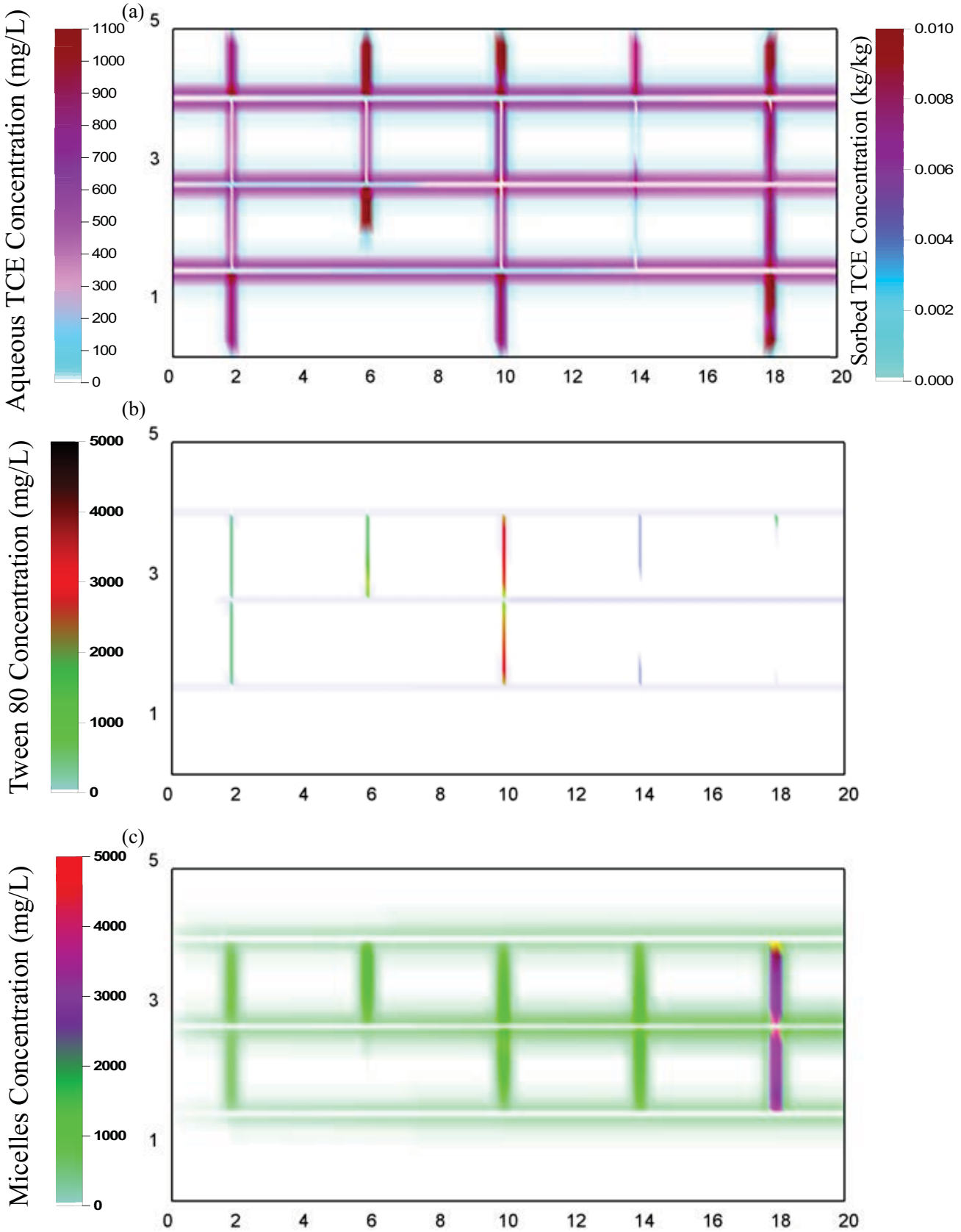

Figure C7: Distribution of (a) Aqueous TCE; (b) Tween-80; (c) TCE occupied micelles, 5 years after surfactant injection for Shale.

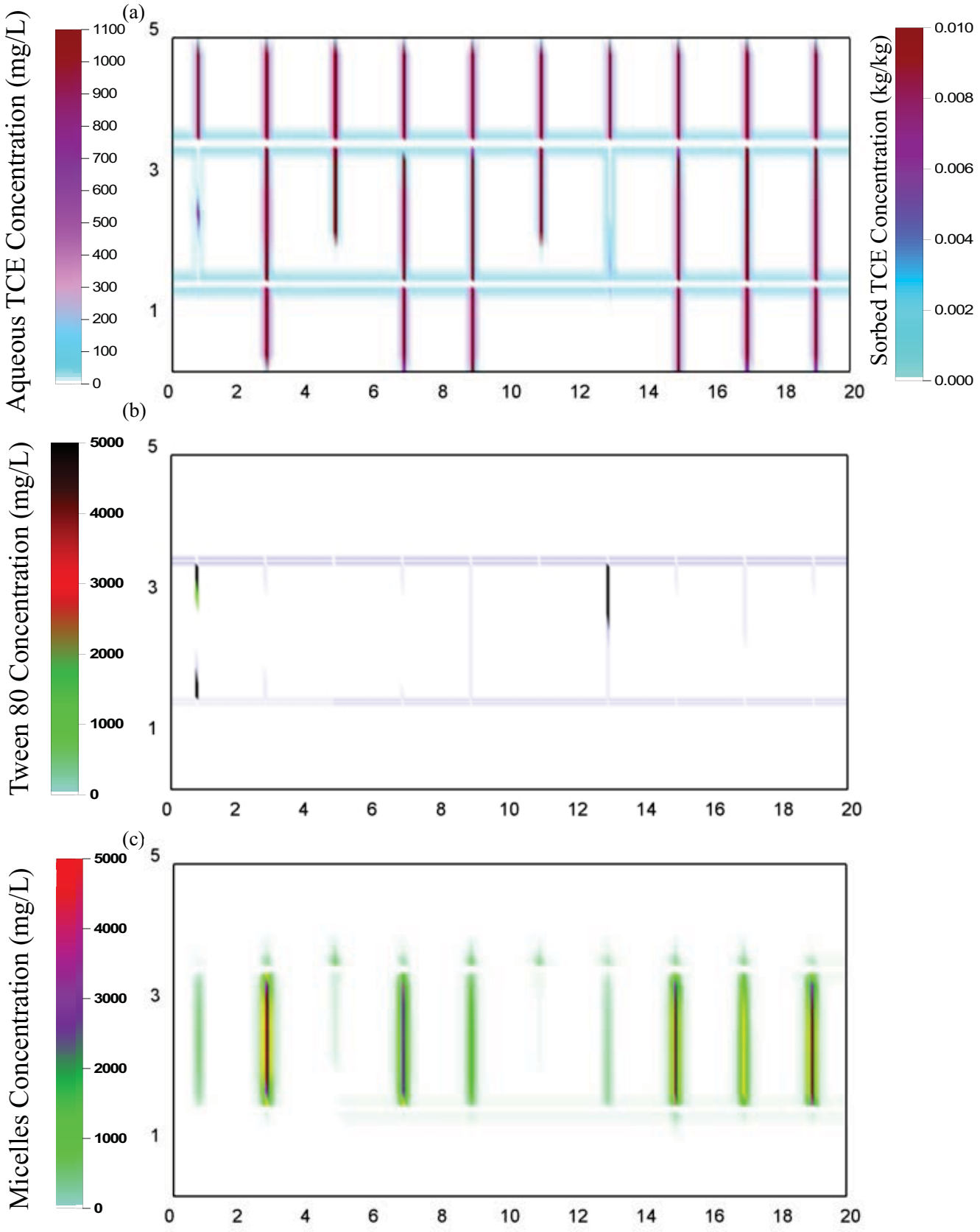

Figure C8: Distribution of (a) Aqueous TCE; (b) Tween-80; (c) TCE occupied micelles, 5 years after surfactant injection for Granite.

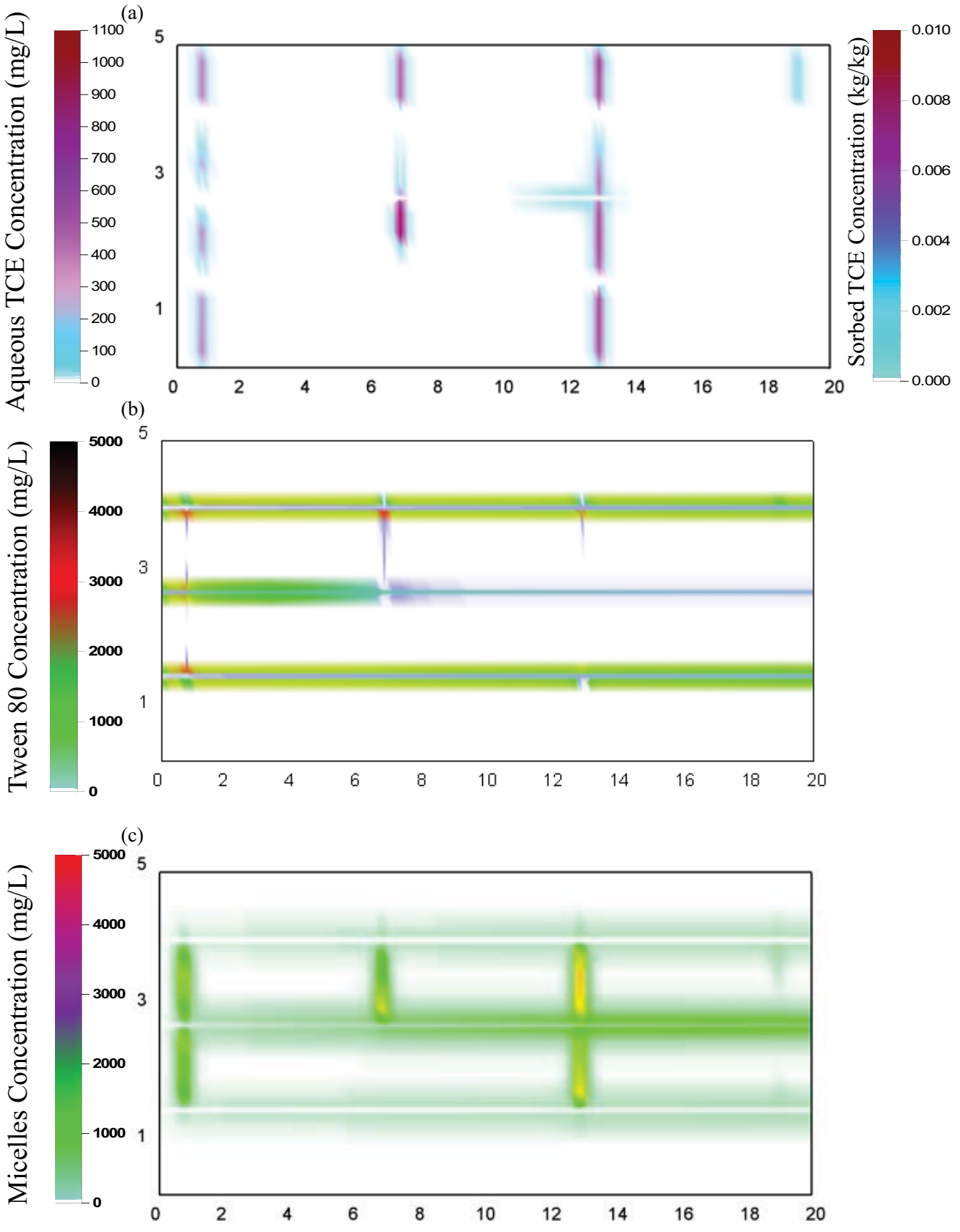

Figure C9: Distribution of (a) Aqueous TCE; (b) Tween-80; (c) TCE occupied micelles, 5 years after Tween-80 injection for a 0-year 'aged' site.

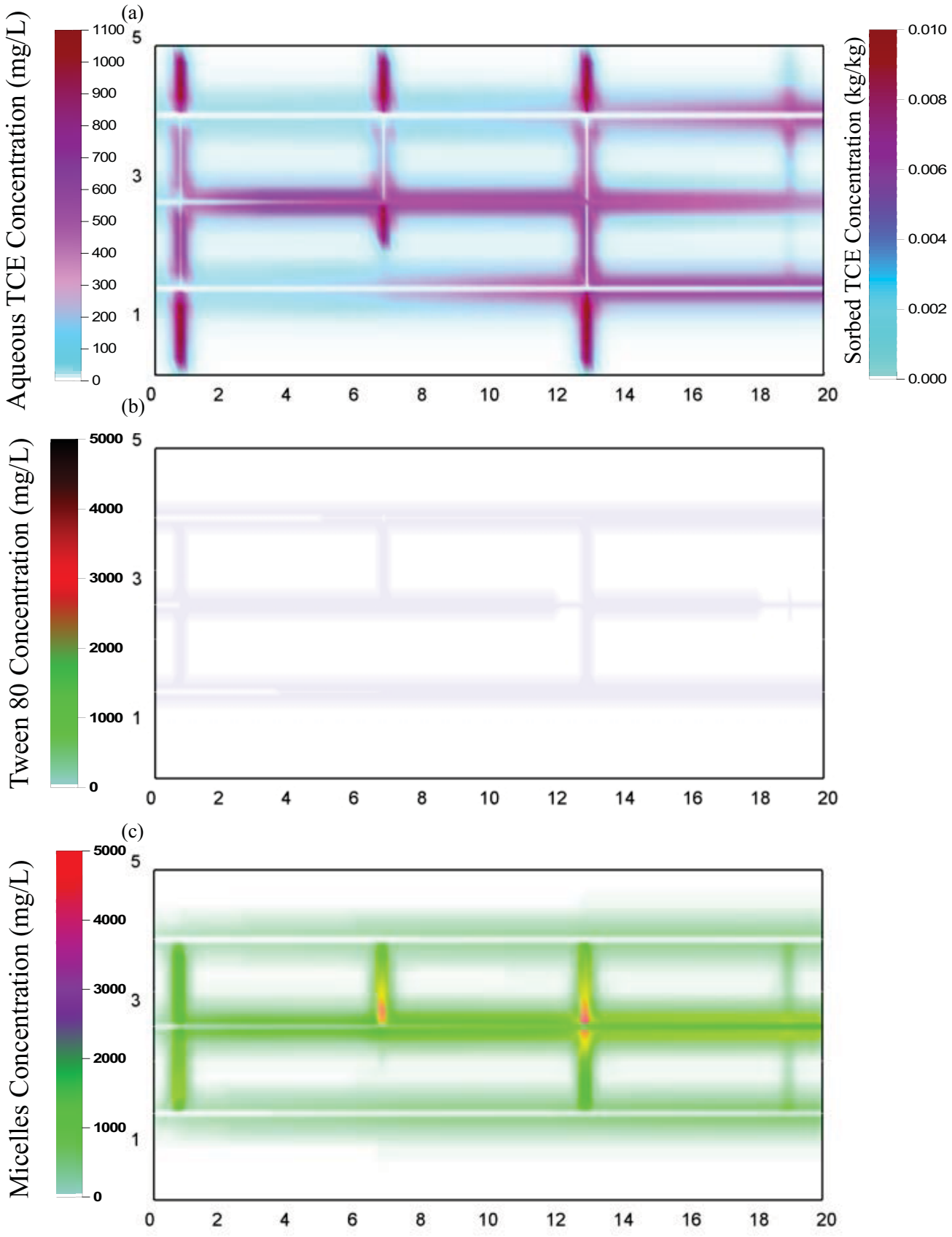

Figure C10: Distribution of (a) Aqueous TCE; (b) Tween-80; (c) TCE occupied micelles, 5 years after Tween-80 injection for a 5-years 'aged' site.

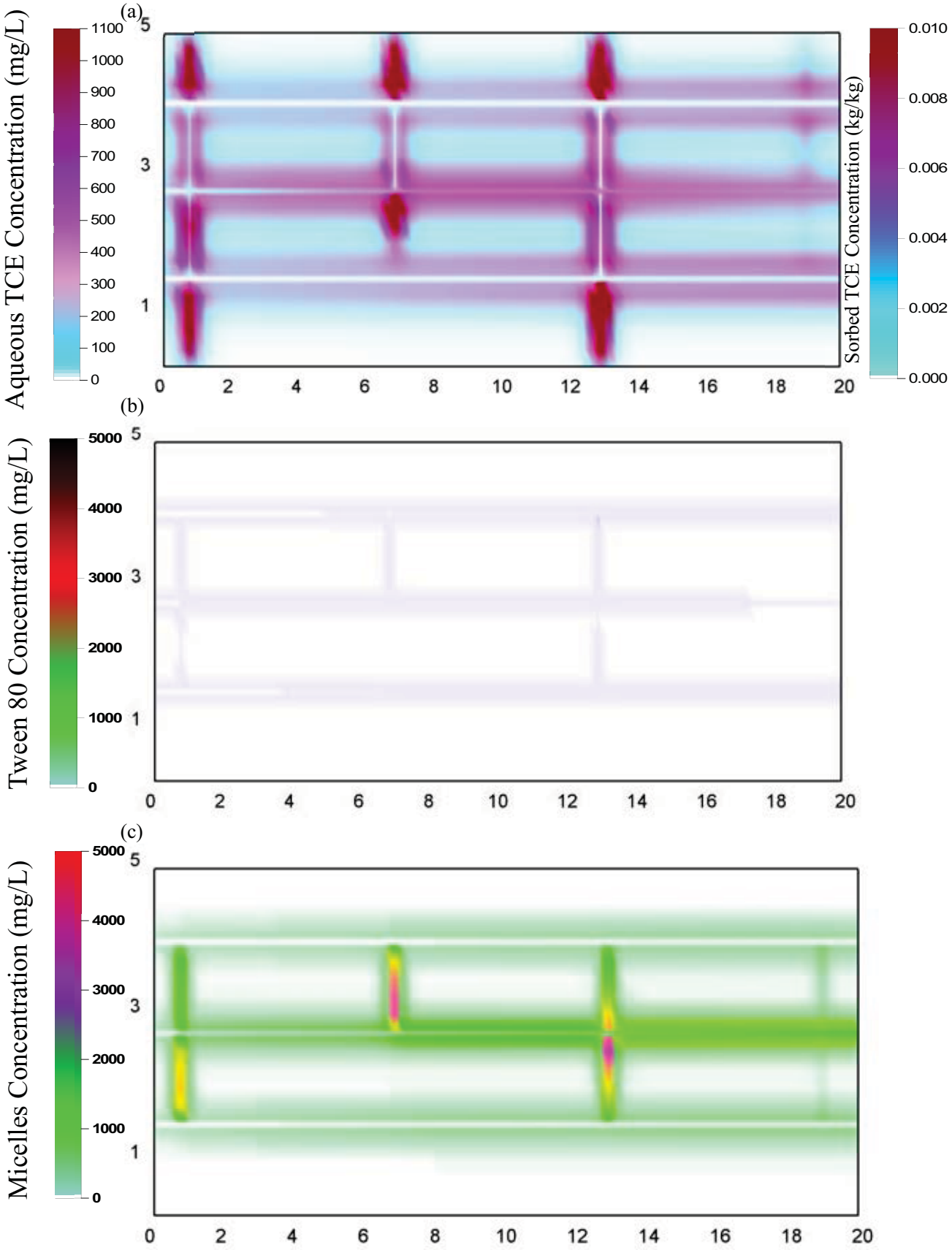

Figure C11: Distribution of (a) Aqueous TCE; (b) Tween-80; (c) TCE occupied micelles, 5 years after Tween-80 injection for a 10-years 'aged' site.

Figure 4.1: Verification of DNAPL3D-RX

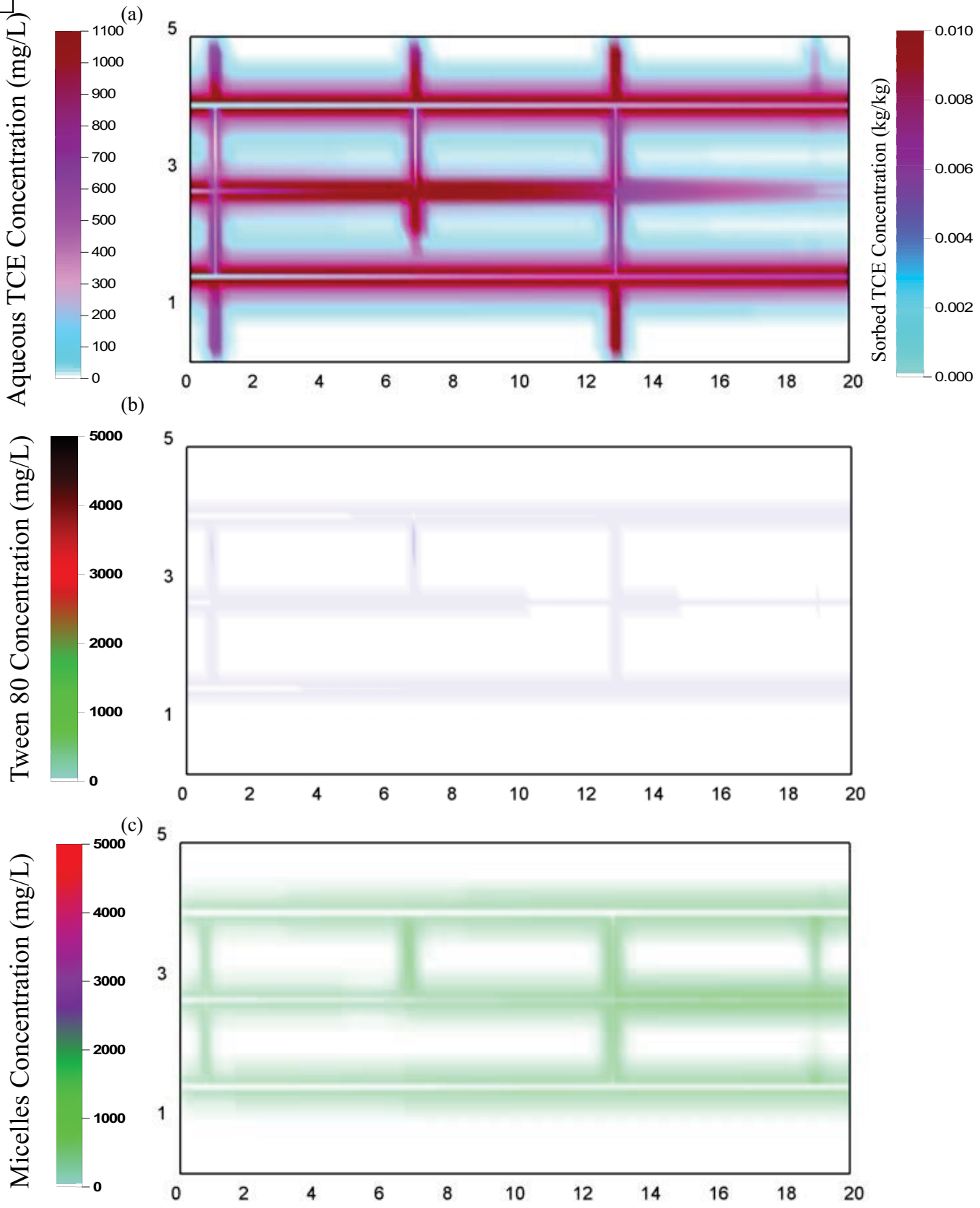

Figure C12: Distribution of (a) Aqueous TCE; (b) Tween-80; (c) TCE occupied micelles, 5 years after surfactant injection for rate-limited mass transfer model.

APPENDIX D.6

NOTATION AND REFRENCES FOR FRACTURED ROCK NUMERICAL SIMULATIONS STUDIES

NOTATION AND DEFINITION OF TERMS

Typical units are presented in brackets. [-] denotes a dimensionless parameter.

a^n specific interfacial area between DNAPL and groundwater for a REV [L^2L^{-3}]

a_0 specific contact area between the NAPL and the aqueous phase and is defined as the ratio of the NAPL/aqueous phase contact area per unit volume [L^{-1}]

α adsorption constant related to the binding energy in a Langmuir Isotherm (L^3M^{-1})

β maximum amount of solute that can be adsorbed by the solids (MM^{-1}) in a Langmuir Isotherm

B either the fracture spacing for slabs or the sphere radius [L]

C solute concentration in the bulk aqueous phase [M/L^3]

C_{eq} concentration at equilibrium (solubility) [M/L^3]

C_f average concentration in the fracture plane [M/L^3]

C_i concentration in the surrounding aqueous phase in the fracture [M/L^3]

C_M concentration in the matrix [M/L^3]

C_s concentration of sorbed aqueous phase [M/M]

C_{sw} concentration at the fracture surface boundary and is equal to the aqueous solubility of the chemical [M/L^3].

C_w concentration of solute in the aqueous phase [M/L^3]

C_{cmc}^{CE} concentration of chlorinated ethene DNAPL at CMC

C_{eq}^{CE} equilibrium chlorinated ethene solute concentration in the presence of a given surfactant concentration greater than the CMC

CMC critical micellar concentration

C^{Surf} surfactant concentration

C_{cmc}^{Surf} surfactant CMC

C_{TCE}^{EX} equilibrium extramicellular mass fraction of TCE at a given surfactant concentration

$\partial C_w / \partial x_i$ chemical concentration gradient defined in the opposite direction of the flux[M/L^3/L]

d_m mean particle diameter [L]

dh/dx magnitude of hydraulic gradient applied across the fracture plane [-]

D_e effective diffusion coefficient [L^2/T]

D^0, D^* free solution diffusion coefficient [L^2/T]

D^*_{im} matrix effective molecular diffusion coefficient [L^2/T]

D_{ij} hydrodynamic dispersion tensor [L^2/T]

D_m molecular diffusion coefficient for the soluble constituent [L^2 /T]

D_M effective diffusion coefficient in the matrix [L^2/T]

e fracture aperture [L]

e_h hydraulic aperture [L]

e_f frictional loss aperture [L]

e_{mb} mass balance aperture [L]

erfc complementary error function [-]

f_{oc} fraction of organic carbon [-]

g gravity [L/T^2]

J solute mass flux from the DNAPL to the aqueous phase [M/L^{3}T]

J_D diffusive flux [M/L^{3}T]

K mass transfer coefficient [L/T]

K_d distribution coefficient of the compound of interest [L^3/M].

Koc organic carbon partition coefficient [L^3/M]

k_e effective mass transfer coefficient [L/T]

k_i intrinsic mass transfer coefficient [L/T]

k_{la} average mass transfer coefficient for the DNAPL-water interface [L/T]

k permeability of the fracture [L^2]

kr_w relative permeabilities to the wetting phases [-]

kr_{NW} relative permeabilities to the non-wetting phases [-]

L_i matrix block length in each of the principle directions [L]

M_m maximum chemical mass storage capacity in the matrix

M_f mass storage capacity in the fractures

M_t total mass diffused into the matrix per unit area of fracture face

MSR molar solubilization ratio [mol/mol]

nw water-imbibition fitting exponent

P_e entry pressure of the fracture [Pa]

P_w wetting phase pressure [Pa]

P_{NW} nonwetting phase pressure [Pa]

P_i a function of the dimensionless time variable [$D_e t/RL_i^2$] [-]

Q volumetric flow rate [L^3/T]

q_M mass flux exchange between the matrix and the fracture [$M/L^2/T$]

q_d aqueous phase source due to dissolution from the presence of NAPL in the fracture plane [$M/L^3/T$]

Re Reynold's number

R contaminant retardation factor [-]

Sh Sherwood number [-]

Solub solubility of DNAPL

Sn*(t) normalized DNAPL saturation

Sn(t)	DNAPL saturation
$Sn_{8\%}$	DNAPL saturation when 8% of initial mass is removed
S_w	degree of water saturation [-]
S_{wb}	water breakthrough saturation [-]
T	tortuosity of the matrix [-]
T_f^r	aqueous-phase relative transmissivity [L^2/T]
Y_{H2}	Hydrogen yield coefficient [-]
t	time [T]
x	distance in the x-direction [L]
w	fracture width perpendicular to flow [L]
t_D	disappearance time [T]
υ	magnitude of the average aqueous phase velocity in the fracture [L/T]
υ_i	average aqueous phase velocity in the fracture plane [M/T]
α_L	longitudinal dispersivities [L]
α_T	transverse dispersivities [L]
δ	aperture ratio [-]
δ_{ij}	Kroneker delta function [-]
μ	fluid viscosity [P.T]
μ_w	viscosity of wetting phase [P.T]
μ_{NW}	viscosities of nonwetting phases [P.T]
ρ	density of the flowing fluid [M/L^3]
ρ_W	density of the wetting phases [M/L^3]
ρ_{NW}	density of the nonwetting phases [M/L^3]

ρ_b dry bulk density [M/L^3]

σ interfacial tension between the fluids [M/L]

θ porosity of the porous medium [-]

λ first-order decay constant [T^{-1}]

$\emptyset_b$ bulk porosity [-]

$\emptyset_m$ matrix porosity [-]

$\emptyset_f$ fracture porosity [-]

REFERENCES

Abdul, A.S., Gibson, T.L., Rai, D.N. 1990, Selection of surfactants for the removal of petroleum products from shallow sandy aquifers, *Ground Water* 28 (6), 920.

Abriola, L. M., Dekker, T. J., and Pennell, K. D. 1993, Surfactant-enhanced solubilisation of residual dodecane in soil columns. 2. Mathematical modelling, *Environmental Science & Technology*, 27 (12), 2341-2351.

Abriola, L. M., Drummond, C. D., Hahn, E. J., Hayes, K. F., Kibbey, T. C. G., Lemke, L.D., Pennell, K. D., Petrovskis, E. A., Ramsburg, C. A., and Rathfelder, K. M. 2005, Pilot-Scale Demonstration of Surfactant-Enhanced PCE Solubilization at the Bachman Road Site. 1. Site Characterization and Test Design, *Environmental Science & Technology*, 39 (6), 1778-1790.

Abriola. L. and Pinder, G. 1985a, A multiphase approach to the modelling of porous media contamination by organic compounds. 1. Equation development. *Water Resour. Res.* 21(1): 11-18.

Abriola. L. and Pinder, G. 1985b, A multiphase approach to the modelling of porous media contamination by organic liquids. 2. Numerical simulation. *Water Resour. Res.,* 21(1): 19-26.

Adamson D.T, McDade J.M, Hughes JB. 2003, Inoculation of a DNAPL source zone to initiate reductive dechlorination of PCE. *Environ Sci Technol* 37(11):2525-33.

Adamson D.A, Lyon D.Y, Hughes J.B. 2004, Flux and product distribution during biological treatment of tetrachloroethene dense non-aqueous-phase liquid. *Environ Sci Technol* 38(7):2021-8.

Allen, D.J., Bloomfield, J.P., Gibbs, B.R. and Wagstaff, S.J., 1998. Fracturing and the hydrogeology of the Permo-Triassic Sandstones in England and Wales. Technical Report of the British Geological Survey WD/98/1.

Amidon, G. E., Higuchi, W. I., and Ho, N. F. H. 1982, Theoretical and experimental studies of transport of micelle-solubilised solutes. *J. Pharm. Sci.*, 71(1), 77–84.

Amos B.K, Christ J.A, Abriola L.M, Pennell K.D, Loeffler F.E. 2007, Experimental evaluation and mathematical modelling of microbially enhanced tetrachloroethene (PCE) dissolution. *Environ Sci Technol* 41(3):963-70

Anderson. M.R.. Johnson, R.L. and Pankow. J.F. 1992a, Dissolution of dense chlorinated solvent into ground water. 1. Dissolution from a well-defined source. *Ground Water.* 30(2): 250-256.

Anderson. M.R.. Johnson, R.L. and Pankow. J.F. 1992b, Dissolution of dense chlorinated solvent into ground water. 2. Modelling contaminant plumes from fingers and pools of solvents. *Environ. Sci. Technol.,* 26(5): 901-908.

Anderson, S.E., Thomson, N.R. 1999, Two-phase flow in a variable aperture fracture: laboratory validation of a two-dimensional numerical model. *Proceedings from Dynamics of Fluids in Fractured Rocks*: Concepts and Recent Advances, Berkeley, CA, 30–34.

Andrews S.D., Mahaffey W, Barlock, V., and Santangelo-Dreiling, T. 2002, Methane-Enhanced In Situ Biological Degradation Of Chlorinated Hydrocarbons – A Case Study, *Proceedings of the Third International Conference on Remediation of Chlorinated and Recalcitrant Compounds Part B*, Paper 2B-55.

Amarante, D. 2000, *Applying In Situ Chemical Oxidation,* Pollution Engineering, February.

Attwood D. and Florence A. T. 1983, In Surfactant Systems: Their Chemistry, Pharmacy and Biology.Chapman & Hall, New York.

Babadagli, T. 2003, Selection of proper enhanced oil recovery fluid for efficient matrix recovery in fractured oil reservoirs, *Colloids and surfaces A-Physicochemical and Engineering aspects*, 223 (1-3): 157-175, AUG 21.

Baehr, A.L. and Corapcioglu, M.Y. 1987, A compositional multiphase model for groundwater contamination by petroleum products, 2. Numerical simulation. *Water Resour. Res.,* 23(l): 201-203.

Bailey J.E, Ollis D.F. 1986, Biochemical engineering fundamentals. 2nd edition. McGraw-Hill, New-York.

Baraka-Lokmane, S. 2002, Hydraulic versus pneumatic measurements of fractured sandstone permeability, *Journal of Petroleum Science and Engineering*, 36, pp.183– 192.

Battelle. 2001, Chemical Oxidation of a DNAPL Source Zone at Launch Complex 34 in Cape Canaveral Air Station, Draft Final Technology Evaluation Report, 101 pp.

Baveye, P., P. Vandevivere, B. L. Hoyle, P. C. DeLeo, and D. Sanchez de Lozada. 1998, Environmental Impact and Mechanisms of the Biological Clogging of Saturated Soils and Aquifer Materials, *Critical Reviews in Environmental Science and Technology*. 28(2): 123-191.

Bear. J. 1972, Dynamics of Fluids in Porous Media. 764 pp., Dover, Mineola, N.Y.

Bear, J., C. F. Tsang, and G. de Marsily, (Eds.) 1993, Flow and Contaminated Transport in Fractured Rock, *Academic,* San Diego, Calif.

Becker, M.W., Metge, D.W., Collins, S.A., Shapiro, A.M., and Harvey, R.W., 2003 Bacterial transport experiments in fractured crystalline Bedrock. *Ground Water,* 41(5), 682-689.

Becker, M.W., Shapiro, A.M. 2000, Tracer transport in fractured crystalline rock: evidence of nondiffusive breakthrough tailing. *Water Resour.* 36, 1677–1686.

Bekins, B. A., Godsy, E. M., and Warren, E. 1999, Distribution of Microbial Physiologic Types in an Aquifer Contaminated by Crude Oil, *Microbial Ecology*, 37 (4), 263-275.

Birkhölzer, J., Rubin, H., Daniels, H., and Rouvè, G.. 1993a, Contaminant transport in fractured permeable formation. 1. Parametric evaluation and analytical solution, *J. Hydrol.,* 144, 1–33.

Bloomfield, J.P., Gooddy, D.C., Bright, M.I., Williams, P.J., 2001. Pore-throat size distributions in sandstones and some implications for contaminant hydrogeology. *Hydrogeology Journal,* 9 (3), 219–230.

Brandon, B., Marajh-Whittemore, P., McTigue, D., Chaffin, D. 2002, Regulatory perspective: In situ chemical oxidation pilot test in fractured granite, *Proceedings of the Third International Conference on Remediation of Chlorinated and Recalcitrant Compounds ,* 1447-1458.

Brooks R H and A.T. Corey 1966, Properties of porous media affecting fluid flow. *Journal of the Irrigation and Drainage Division, Proceedings of the American Society of Civil Engineers*, pages 61-88, 1966.

Brusseau, M.L. 1992, Rate-limited mass transfer and transport of organic solutes in porous media that contain immobile immiscible organic liquid. *Water Resour. Res.,* 28(l): 33-45.

Busch, A., Alles, S., Gensterblum, Y., Prinz, D., Dewhurst, D.N., Raven, M.D., Stanjek, H., B.M., Krooss. 2008, Carbon dioxide potential of shale, *International Journal of Greenhouse Gas Control*, pp. 297 – 308.

Carr, C.S., and Hughes, J.B. 1998, Enrichment of High-Rate PCE Dechlorination and Comparative Study of Lactate, Methanol, and Hydrogen as Electron Donors To Sustain Activity, *Environmental Science & Technology*, 32 (12), 1817-1824.

Carr C.S., Garg S., Hughes J.B. 2000, Effect of dechlorinating bacteria on the longevity and composition of PCE-containing nonaqueous phase liquids under equilibrium dissolution conditions. *Environ Sci Technol* 34(6):1088-94.

Castellanos, M.R., Peel, T.A., McMaster M.L., Adkisson, J., Dworatzek. S. 2002, Laboratory Evaluation of Enhanced Bioremediation of Chlorinated Ethenes in Groundwater at the MLP/VAB Area, *Proceedings of the Third International Conference on Remediation of Chlorinated and Recalcitrant Compounds* , 1405-1411, Paper 2B-30.

Chaki, S., Takarli, M., Agbodjan, W.P. 2008, Influence of thermal damage on physical properties of a granite rock: Porosity, permeability and ultrasonic wave evolutions, *Construction and Building Materials,* 22, pp. 1456–1461.

Chapelle FH. 1996, Identifying redox conditions that favor natural attenuation of chlorinated solvents in contaminated ground-water systems. *In: Proceedings of the Symposium on Natural Attenuation of Chlorinated Organics in Ground Water, Dallas, Texas.*

Charbonneau, A., Novakowski, K., and Ross, N. 2006, The effect of a biofilm on solute diffusion in fractured porous media, *Journal of Contaminant Hydrology*, 85 (3-4), 212- 228.

Chen, Z. 1995, Large Scale Averaging Analysis of Multiphase Flow in Fractured Reservoirs, *Tran. Por. Media,* 21, pp 269- 295.

Cherry, J.A. 1989, Hydrogeologic contaminant behaviour in fractured and unfractured clayey deposits in Canada. In: H.E. Kobus and W. Kinzelbach (Editors), *Contaminant Transport in Groundwater.* A.A. Balkema, Rotterdam, pp. 11-20.

Christ J.A., Ramsburg C.A., Abriola L.M., Pennell K.D., Löffler F.E. 2005, Coupling aggressive mass removal with microbial reductive chlorination for remediation of DNAPL source zones: A review and assessment. *Environ Health Perspect* 113(4):465-74.

Christ, J. A., and Abriola, L. M. 2007, Modelling metabolic reductive dechlorination in dense non-aqueous phase liquid source-zones, *Advances in Water Resources*, 30 (6-7), 1547-1561.

Cho, H. J., Fiacco, R. J. and M. H. Daly. 2002, Soil vapor extraction and chemical oxidation to remediate chlorinated solvents in fractured crystalline rock. *Remediation Journal,* in press.

Chown, J.C., Kueper, B.H., McWhorter, D.B. 1997, The use of upward hydraulic gradients to arrest downward DNAPL migration in rock fractures, *Ground Water* Volume 35, Issue 3, Pages 483-491.

Chu M., Kitanidis P.K., McCarty P.L. 2003, Effects of biomass accumulation on microbially enhanced dissolution of a PCE pool: A numerical simulation. *J Contam Hydrol* 65(1-2):79-100.

Chu M, Kitanidis P.K., McCarty P.L. 2004, Possible factors controlling the effectiveness of bioenhanced dissolution of non-aqueous phase tetrachloroethene. *Adv Water Resour* 27(6):601-615.

Clement, T. P. 1997, RT3D - A Modular Computer Code for Simulating Reactive Multispecies Transport in 3-Dimensional Groundwater Systems (Version 1.0), 59 pp, Pacific Northwest National Laboratory, Richland, Washington 99352.

Clement, T. P., Sun, Y., Hooker, B. S., and Petersen, J. N. 1998, Modelling Multispecies Reactive Transport in Ground Water, *Ground Water Monitoring & Remediation*, 18 (2), 79-92.

Colwell, F.S., Stormberg, G.J., Phelps, T.J., Birnbaum, S.A., McKinley, J., Rawson, S.A., Veverka, C., Goodwin, S., Long, P.E., Russell, B.F., Garland, T., Thompson, D., Skinner,

Conrad, M.E., DePaolo, D.J., Kennedy, B.M., Miller, E.C. 1997b, Carbon isotope evidence for degradation of mixed contaminants in the vadose zone, *Geol. Soc. Am.*, Abstr. Prog. 26 (6), A186.

Conrad, S.H., Glass, R.J., Peplinski, W.J. 2002, Bench-scale visualization of DNAPL remediation processes in analog heterogeneous aquifers: surfactant floods and in situ oxidation using permanganate. *J. Contam. Hydrol.* 58, 13– 49.

Cornuet, T. S., Sandefur, C., Eliason, W. M., Johnson, S. E., and Serna, C. 2000, Aerobic and Anaerobic Bioremediation of cis-1,2-Dichloroetene and Vinyl Chloride, In Accelerated Bioremediation of Chlorinated compounds in Groundwater. Editors: Koenigsberg, S. S. and Ward, C. H., *Regenesis Bioremediation Products*, pp. 41-49.

Cope N, Hughes J.B. 2001, Biologically-enhanced removal of PCE from NAPL source zone. *Environ Sci Technol*;35(10):2014-21.

Crow C.W, 1968. New Treating Technique to Remove Bacterial Residues From Water-Injection Wells, Journal of Petroleum Technology, Vol 20, No.5, pp 475-478.

Cumbie, D.H. and MacKay, L.D. 1999. Influence of diameter on particle transport in a fractured shale saprolite. *Journal of Contaminant Hydrology*, 37, 139-157.

Cupples A.M., Spormann A.M., McCarty P.L. 2004a, Vinyl chloride and cis-dichloroethene dechlorination kinetics and microorganism growth under substrate limiting conditions. *Environ Sci Technol,* 38(6):1102-7.

Cupples A.M., Spormann A.M., McCarty P.L. 2004b Comparative evaluation of chloroethene dechlorination to ethene by *dehalococcoides*-like microorganisms. *Environ Sci Technol*, 38(18):4768-74.

Dana, E. and Skoczylas, F. 2002, Experimental study of two-phase flow in three sandstones. II. Capillary pressure curve measurement and relative permeability pore space capillary models, *International Journal of Multiphase Flow*, 28, 1965–1981.

Dayan, H., Abrajano, T., Sturchio, N.C. and Winsor, L. 1999, Carbon isotopic fractionation during reductive dehalogenation of chlorinated ethenes by metallic iron, *Org. Geochem.*, 30: 755-763.

de Beer, D., Stoodley, P., and Lewandowski, Z. 1997, Measurement of local diffusion coefficients in biofilms by microinjection and confocal microscopy, *Biotechnology and Bioengineering*, 53 (2), 151-158.

de Lima, O.A.L. and Niwas S. 2000, Estimation of hydraulic parameters of shaly sandstone aquifers from geoelectrical measurements, *Journal of Hydrology*, 235, pp.12–26.

Dennis, F., Andrews, N.J., Parker, A., Poole, J., Wolf, M. 1997, Isotopic and noble gas study of Chalk groundwater in the London Basin, England, *Applied Geochemistry*, Vol. 12, pp. 763-773.

Dickson, S.E., Thomson, N.R. 2003, Dissolution of entrapped DNAPLs in variable aperture

fractures: experimental data and empirical model, *Environ. Sci. Technol.* 37, 4128-4137, Paper 1D-01.

Domenico, P.A and Schwartz F.W. Physical and chemical hydrogeology. John Wiley & Sons, Inc, 1990.

Driese, S.G., and MacKay, L.D., 2004. Epi-fluorescence micromorphology of saprolite reveals evidence for colloid retention in microscale pore systems. *Geoderma* 121, 143-152.

Dullien, F.A.L. 1992, Porous Media: Fluid Transport and Pore Structure, *2nd ed. Academic Press*, Inc., San Diego, CA. 574 pp.

Dutton S.P. and Loucks R.G. 2010, Diagenetic controls on evolution of porosity and permeability in lower Tertiary Wilcox sandstones from shallow to ultradeep (200–6700 m) burial, Gulf of Mexico Basin, U.S.A., *Marine and Petroleum Geology,* 27, 69–81.

Edwards, D. A., Luthy, R. G., and Liu, Z. 1991, Solubilization of polycyclic aromatic hydrocarbons in micellar nonionic surfactant solutions, *Environmental Science & Technology*, 25 (1), 127-133.

Eikemo B., Lie K., Eigestad G.T.,Dahle H.K., 2009, Discontinuous Galerkin methods for advective transport in single-continuum models of fractured media. *Advances in Water Resources*, 32 (2009) 493–506.

Ellis D.E., Lutz E.J., Odom J.M., Buchanan Jr R.J., Bartlett C.L., Lee M.D., Harkness M.R., Deweerd K.A. 2000, Bioaugmentation for accelerated in situ anaerobic bioremediation. *Environ Sci Technol*,34(11):2254-60.

Ellis, W.D., Morgan, D.R., Ranjithan, S.R. 1986, Treatment of contaminated soils with aqueous surfactants, EPA/600/2-85/129, *Hazardous Waste Engineering Research Laboratory*.

Environmental Protection Agency (EPA). 2001, The State-of-the Practice of Characterization and Remediation of Contaminated Ground Water at Fractured Rock Sites. EPA542-R-01-010.

Esposito S. J. and Thomson N. R. 1999, Two-phase flow and transport in a single fracture-porous medium system, *Journal of Contaminant Hydrology* Volume 37, Issues 3-4 , Pages 319-341.

Feenstra, S. 1992, Geochemical evaluation of polychlorinated biphenyls (PCBs) in groundwater. In: S. Lesage and R.E. Jackson (Editors), Groundwater Contamination and Analysis at Hazardous Waste Sites. Marcel Dekker, New York, NY, 545 pp.

Feenstra, S., Mackay, D.M., Cherry, J.A. 1991, Presence of residual NAPL based on organic chemical concentrations in soil samples. *Ground Water Monit.* Rev. 11 (2), 128– 136.

Fennell, D. E., Gossett, J. M., and Zinder, S. H. 1997, Comparison of Butyric Acid, Ethanol, Lactic Acid, and Propionic Acid as Hydrogen Donors for the Reductive Dechlorination of

Tetrachloroethene, *Environmental Science & Technology*, 31 (3), 918-926.

Fennell D.E., Gossett J.M. 1998, Modelling the production of and competition for hydrogen in a dechlorinating culture. *Environ Sci Technol,* 32(16):2450-60.

Fetter, C.W. 1993, Contaminant Hydrogeology, *Macmillan Publishing Company,* New York. pp. 458

Forsyth, P.A. 1991, A control volume finite element approach to NAPL groundwater contamination. SIAM (Sot. Ind. Appl. Math.) *J. Sci. Stat. Comput.*, 12(5): 1029-1057.

Forsyth, P.A., Shao, B.Y. 1991, Numerical Simulation of Gas Venting for NAPL Site Remediation; *University of Waterloo*, Ontario, Res. Rep. CS-91-06.

Fountain, J.C., Starr, R.C., Middleton, T., Beikirch, M., Taylor, C., Hodge, D. 1996, A controlled field test of surfactant-enhanced aquifer remediation, *Ground Water* 35 (5), 910–916.

Freeze, R.A., Cherry, J.A. 1979, *Groundwater*, Prentice-Hall, Englewood Cliffs, NJ.

Freeze, R.A., McWhorter, D.B. 1997, A framework for assessing risk reduction due to DNAPL mass removal from low-permeability soils, *Ground Water* Volume 35, Issue 1, Pages 111-123.
Fried, J.J., Muntzer, P. and Zilloix, L. 1979, Groundwater pollution by transfer of oil hydrocarbons. *Ground Water,* 17(6): 586-594.

Frind, E.O., J.W. Molsen, and M. Schirmer. 1999, Dissolution and mass transfer of multiple organics under field conditions: The Borden emplaced source, *Water Resources Research,* 35(3), 683-694.

Gabrovsek, F. , Romanov, D. , Dreybrodt, W. 2004, Early karstification in a dual-fracture aquifer: The role of exchange flow between prominent fractures and a dense net of fissures, Journal of Hydrology Volume 299, Issue 1-2, Pages 45-66.

Gandhi, R.K., G.D. Hopkins, M.N. Goltz, S.M. Gorelick, and P.L. McCarty, 2002, Fullscale demonstration of in situ cometabolic biodegradation of trichloroethylene in groundwater, 1: Dynamics of a recirculating well system, *Water Resources Research*, awaiting print.

Gandhi, S., Oh, B., Schnoor J.L., Alvarez P. J. 2002, Degradation of TCE, Cr(VI), sulfate, and nitrate mixtures by granular iron in flow-through columns under different microbial conditions. *Water Research* 36(8), 1973-1982

Gannon, O.K., Bribing, P., Raney, K., Ward, A., Wilson, J., Underwood, J.L., Deblak, K.A. 1992, Soil clean up by in situ surfactant flushing: III. Laboratory results, *Journal of Science Technology*, September, pp.1073–1094.

Garavito, A.M., Kooi, H., Neuzil, C.E. 2006, Numerical modeling of a long-term in situ chemical osmosis experiment in the Pierre Shale, South Dakota, *Advances in Water Resources*, 29, pp. 481–492.

Geller, J.T. and Hunt, J.R. 1993, Mass transfer from non aqueous-phase organic liquids in water saturated porous media, *Water Resour. Res.*, 29(4): 833-845.

Geosyntec Consultants. 2004, Accessing the feasibility of DNAPL source zone remediation: Review of case studies, April.

Geosyntec Consultants. – Private communications with Geosyntec Consultants 2007

Gerhard, J. I., Kueper, B. H., and Hecox, G. R. 1998, The Influence of Waterflood Design on the Recovery of Mobile DNAPLs, *Ground Water*, 36 (2), 283-292.

Gerhard, J. I., Kueper, B. H., Hecox, G. R., and Schwarz, E. J. 2001, Site-Specific Design for Dual Phase Recovery and Stabilization of Pooled DNAPL, *Ground Water Monitoring & Remediation*, 21 (2), 71-88.

Gerhard, J. I., and Kueper, B. H. 2003a, Capillary pressure characteristics necessary for simulating DNAPL infiltration, redistribution, and immobilization in saturated porous media, *Water Resources Research*, 39 (8).
Gerhard, J. I., and Kueper, B. H. 2003b, Influence of constitutive model parameters on the predicted migration of DNAPL in heterogeneous porous media, *Water Resources Research*, 39 (10), 1279.

Gerhard, J. I., and Kueper, B. H. 2003c, Relative permeability characteristics necessary for simulating DNAPL infiltration, redistribution, and immobilization in saturated porous media, *Water Resources Research*, 39 (8), 1213.

Gerhard, J. I., Pang, T.W. and Kueper, B. H. 2007, Time scales of DNAPL migration in sandy aquifers examined via numerical simulation, *Ground Water* Vol. 45 (2) pp 147–157.

Glass R.J. and M.J. Nicholl, 1995, Quantitative visualization of entrapped phase dissolution within a horizontal flowing fracture. *Geophysical Research Letters*, 22:1413-1416.

Godsy, E. M., Goerlitz, D. F., and Grbic-Galic, D. 1992, Methanogenic Biodégradation of Creosote Contaminants in Natural and Simulated Ground- Water Ecosystems, *Ground Water*, 30 (2), 232-242.

Gonullu, T., Farquhar, G.J. 1989, Oxidation to Remove TCE from Soil, Internal Report Department of Civil Engineering, Univ. of Waterloo. Available at http://www.civil.uwaterloo.ca/groundwater/oxlitrev.html.

Gooddy, D.C., Bloomfield, J.P., Harrold, G., Leharne, S.A. 2002, Towards a better understanding of tetrachloroethene entry pressure in the matrix of Permo-Triassic sandstones, *Journal of Contaminant Hydrology*, 59, pp. 247– 265.

Grant, G. P. 2005, The Evolution of Complex DNAPL Releases: Rates of Migration and Dissolution, Ph.D. thesis, 431 pp, The University of Edinburgh, Edinburgh, Scotland, United Kingdom.

Grant, G. P., and Gerhard, J. I. 2004, Sensitivity of Predicted DNAPL Source Zone Longevity to Mass Transfer Correlation Model, Geoenvironmental Engineering: Integrated Management of Groundwater and Contaminated Land, *Telford Publishing, London*, 59-67.

Grant, G. P., and Gerhard, J. I. 2007a, Simulating the dissolution of a complex dense nonaqueous phase liquid source zone: 1. Model to predict interfacial area, *Water Resources Research*, 43 (12).

Grant, G. P., and Gerhard, J. I. 2007b, Simulating the dissolution of a complex dense nonaqueous phase liquid source zone: 2. Experimental validation of an interfacial areabased mass transfer model, *Water Resources Research*, 43 (12).

Grant, G. P., Gerhard, J. I., and Kueper, B. H. 2007，Multidimensional validation of a numerical model for simulating a DNAPL release in heterogeneous porous media Journal of Contaminant Hydrology 92 109–128

Grant, G. P., Gerhard, J. I., and Kueper, B. H. 2007a, Field scale impacts of spatially correlated relative permeability in heterogeneous multiphase systems, *Advances in WaterResources*, 30 (5), 1144-1159.

Grisak, G.E., Pickens, J.F. 1981, An analytical solution for solute transport through fractured media with matrix diffusion, *J. Hydrol.* 52, 47–57.

Gutierrez, M., Øino, L.E., Nygard, R. 2000, Stress-dependent permeability of a de-mineralised fracture in shale, *Marine and Petroleum Geology,* 17, pp. 895–907.

Gwo, J.P., Jardine, P.M., Sanford, W.E. 2005, Modelling field-scale multiple tracer injection at a low-level waste disposal site in fractured rocks: Effect of multiscale heterogeneity and source term uncertainty on conceptual understanding of mass transfer processes, Journal of Contaminant Hydrology Volume 77, Issue 1-2, Pages 91-118.

Gwo, J.P., Mayes, M.A., Jardine, P.M. 2007, Quantifying the physical and chemical mass transfer processes for the fate and transport of Co(II)EDTA in a partially-weathered limestone–shale saprolite, *Journal of Contaminant Hydrology*, 90, pp. 184–202.

Haghighi, M., Xu, B, and Y.C. Yortsos. 1994, Visualization and Simulation of Immiscible Displacement in Fractured Systems Using Micromodels: 1. Drainage, *J. Coll. Int. Sci.,* 166, pp 168-179.

Harrison, B., E.A. Sudicky, and J.A. Cherry 1992, Numerical analysis of solute migration through fractured clayey deposits into underlying aquifers. *Water Resources Research*, 28:515-526.

Hanson, J.R., C.R. Ackerman, and K.M. Scow. 1999, Biodegradation of Methyl tertbutyl ether by a bacterial pure culture, *Appl. Environ. Microbiol*. 65:4788-4792.

Haston Z.C., McCarty P.L.1999, Chlorinated ethene half-velocity coefficients (Ks) for reductive dehalogenation. *Environ Sci Technol*, 33(2):223-6.

Hazen, T., Jiménez, L., López de Victoria, G., and Fliermans, C. 1991, Comparison of bacteria from deep subsurface sediment and adjacent groundwater, *Microbial Ecology*, 22 (1), 293-304.

Hirasaki, G.J., Miller, C.A., Szafranski, R., Lawson, J.B., Akiya, N. 1997, Surfactant foam process for aquifer remediation. SPE paper 37257. *SPE International Symposium on Oil Field Chemistry*, Houston, TX.

Hitchmough, A.M., Riley, M.S., Herbert, A.W., Tellam, J.H. 2007, Estimating the hydraulic properties of the fracture network in a sandstone aquifer, *Journal of Contaminant Hydrology*, 93, pp. 38–57.

Hood, E., Major, D., Driedger, G. 2007, The effect of concentrated electron donors on the solubility of Trichloroethene, *Ground Water Monitoring & Remediation*, 27(4) 93-98.

Hood, E.D., and Thomson, N.R. 2000, Numerical simulation of in situ chemical oxidation, In *Chemical Oxidation and Reactive Barriers; International Conference on Remediation of Chlorinated and Recalcitrant Compounds*. Battelle Press.

Hood, E.D., Thomson, N.R., Grosse, D. and Farquhar, G.J. 2002. Experimental determination of the kinetic rate law for the oxidationd of perchloroethylene by potassium permanganate. *Chemosphere*, 40:1383-1388.

Hu, Q.H. and Mori, A. 2008, Radionuclide transport in fractured granite interface zones, *Physics and Chemistry of the Earth*, 33, pp.1042–1049.

Hunt, J.R., Sitar, N. and Udell, K.S. 1988a, Non aqueous-phase liquid transport and cleanup, 1. Analysis of mechanisms. *Water Resour. Res.,* 24(8): 1247- 1258.

Hunt, J.R., Sitar. N. and Udell, K.S. 1988b, Non-aqueous-phase liquid transport and cleanup, 2. Experimental studies. *Water Resour. Res*., 24(8): 1259- 1269.

Hunter, K.S., Wang, Y., Van Cappellen, P. 1998, Kinetic modelling of microbially-driven redox chemistry of subsurface environments: coupling transport, microbial metabolism and geochemistry, *Journal of Hydrology,* 209, pp. 53-80.

Interstate Technology and Regulatory Cooperation Work Group (ITRC). 2001, Technical and Regulatory Guidance for In Situ Chemical Oxidation of Contaminated Soil and Groundwater. *Prepared by the In Situ Chemical Oxidation Work Group.*

Imhoff, P.T., P.R. Jaffé and G.F. Pinder. 1993, An experimental study of complete dissolution of a nonaqueous phase liquid in saturated porous media, *Water Resour. Res.,* 30(2): 307-320.

Imhoff, P.T., S.N. Gleyzer, J.F. McBride, L.A. Vancho, I. Okuda, and C.T. Miller, 1995, Cosolvent-enhanced remediation of residual dense nonaqueous phase liquids: experimental investigation, *Environmental Science and Technology* 29(8): 1966-1976.

Jafvert, C.T., Van Hoof, P.L., and Chu, W. 1995, The Phase Distribution of Polychlorobiphenyl Congeners in Surfactant-Amended Sediment Slurries, *War. Res.* Vol. 29, No. 10, pp. 2387-2397.

James, G. and R. Hiebert. 2001, Biofilm barriers for groundwater containment, *The Sixth International In Situ and On-Site Bioremediation Symposium*, pp. 79-85, San Diego, CA, 2001.

Jardine, P.M., Brooks, S.C., Wilson, G.V. and W.E. Sanford. 2000, Basic research strategies for resolving remediation needs in contaminated fractured media, In B. Faybishenko, P.A. Witherspoon, and S.M. Benson (Eds.), Dynamics of Fluids in Fracture Rock, pp. 389-400. American Geophysical Union, Washington, DC.

Jardine, P.M., Mehlhorn, T.L., Larsen, I.L., Bailey, W.B., Brooks, S.C., Roh, Y., Gwo, J.P. 2002, Influence of hydrological and geochemical processes on the transport of chelated metals and chromate in fractured shale bedrock, *Journal of Contaminant Hydrology*, 55, pp.137– 159.

Jardine, P.M., Sanford, W.E., Gwo, J.P., Reedy, O.C., Hicks, D.S., Riggs, J.S., Bailey, W.B. 1999, Quantifying diffusive mass transfer in fractured shale bedrock. *Water Resour. Res.* 35 (7), 2015–2030.

Jardine, P.M., Weber, N., McCarthy, J., 1989. Mechanisms of dissolved organic carbon adsorption on soil. Soil Sci. Soc. Am. 53, pp.1378– 1385.

Johnson, R.L. and Pankow, J.F. 1992, Dissolution of dense chlorinated solvents into groundwater, 2. Source functions for pools of solvent. *Environ. Sci. Technol.,* 26(5): 896-901.

Kalish, P. J., Stewart, J. E., Rogers, W. F., and Bennett., E. O. 1964, The Effect of Bacteria on Sandstone Permeability, *Journal of Petroleum Technology*, 805- 814.

Kaluarachchi. J.J. and Parker, J.C. 1990, Modelling multicomponent organic chemical transport in three-fluid phase porous media. *J. Contam. Hydrol.,* 5(4): 349-374.

Kalyuzhnyi S, de Leon Fragaso C, Rodriguez Martinez J. 1997, Biological sulphate reduction in an UASB reactor fed with ethanol as electron donor. Mikrobiologiya 66(5):562-7.

Karickhoff, S.W., Brown, D.S., and Scott, T.A. 1979, Sorption of Hydrophobic Pollutants on Natural Sediments, *Water Research* v.13, pp. 241-248.

Karickhoff, S.W. 1981, Semi-empirical Estimation of Sorption of Hydrophobic Pollutants on Natural Sediments and Soils, *Chemosphere*. v. 10, pp. 833-846.

Karickhoff, S.W. 1984, Organic Pollutants Sorption in Aquatic Systems, *Journal of Hydraulic Engineering,* v. 110, pp. 707-735.

Kauffman, M.D., LaChance, J.C., Traviglia, A.M., Krivansky, M.E., Leipert, M.W. 2002, In situ chemical oxidation of CVOCs in fractured bedrock, *Proceedings of the Third International Conference on Remediation of Chlorinated and Recalcitrant Compounds* , 1405-1411, Paper 2C-40.

Kean, J.A., Graves, D., Bishop K., Mott-Smith, E. and Lodato, M. 2002, Obstacles to Complete PCE Degradation During Reductive Dechlorination, *Proceedings of the Third International Conference on Remediation of Chlorinated and Recalcitrant Compounds*, Part C, Paper 2B-48.

Keller, A.A. 1998, Steam injection to displace DNAPLs from fractured media, *IAHS-AISH Publication* Issue 250, Pages 105-110.

Kim, K.S., Kwon, T.S., Yang, J.S., and Yang, J.W. 2007, Simultaneous removal of chlorinated contaminants by pervaporation for the reuse of a surfactant, *Desalination*, 205, 87–96.

Klutz. Tony, Andrew Baird, George Maalouf, and Daniel McDonnell, Craig Sandefur. 2002, Accelerated Bioremediation of Trichloroethylene: A comparison between saprolite and crystalline bedrock aquifers, *Proceedings of the Third International Conference on Remediation of Chlorinated and Recalcitrant Compounds,* Part C, Paper 2C-46.

Koenigsberg, S.S., Farone, W. The Use of Hydrogen Release Compound (HRCTM) for CAH Bioremediation, In: Leeson, A., Alleman, B.C. (eds.). 1999, Engineered Approaches for In Situ Bioremediation of Chlorinated Solvent Contamination, pp. 67-72, *Battelle Press*, Columbus, OH.

Koenigsberg, S.S., C. Sandefur and K. Lapus. 2001, Time-Release Electron Donor Technology: Results of Forty-Two Field Applications, In: Magar, V.S., Fennell, D.E., Morse, J. J., B.C. Alleman and A. Leeson (Eds.), Anaerobic Degradation of Chlorinated Solvents, pp. 257-264. *Battelle Press,* Columbus, OH.

Kölbel-Boelke, J., Anders, E. M., and Nehrkorn, A. 1988, Microbial communities in the saturated groundwater environment II: Diversity of bacterial communities in a Pleistocene sand aquifer and their in vitro activities, *Microbial Ecology*, 16 (1), 31-48.

Konzuk, J.S., Kueper, B.H. 2004, Evaluation of cubic law based models describing single-phase flow through a rough-walled fracture, Water Resources Research Volume 40, Issue 2, December 2004, W024021-W02402117.

Kostarelos K., Pope G. A., Rouse B. A. and Shook G. M. 1998, A new concept: the use of neutrally-buoyant microemulsions for DNAPL remediation, *Journal of Contaminant Hydrology* Volume 34, Issue 4 , Pages 383-397.

Kozar, M. S., McIlvaine, C.L., Duffy, B.E., Street, W.M. 2002, Enhanced degradation of chlorinated solvents in fractured rock ground water using subsurface injection of HRC, *Proceedings of the Third International Conference on Remediation of Chlorinated and Recalcitrant Compounds,* Pages 2441-2447, Paper 2C-42.

Kueper, B.H. and E.O. Frind. 1991a, Two-phase flow in heterogeneous porous media: 2. Model development. *Water Res. Res.* 27 (6), 1049–1057.

Kueper, B.H., and E.O. Frind. 1991b, Two phase flow in heterogeneous porous media: 2. Model application, *Water Resources Research*, 27(6), 1059-1070.

Kueper, B.H., and E.O. Frind 1992, Numerical modelling of multiphase / multicomponent flow and transport in porous media: An overview, in: *Proceedings of the International Conference on Subsurface Contamination by Immiscible Fluids,* Calgary, Canada, April 18-20.

Kueper, B.H., Haase, C.S., King, H.L. 1992, Leakage of dense, nonaqueous phase liquids from waste impoundments constructed in fractured rock and clay—theory and case-history. *Canadian Geotechnical Journal,* 29, 234–244.

Kueper, B.H., McWhorter, David B. 1991, Behavior of dense, nonaqueous phase liquids in fractured clay and rock, *Ground Water* Volume 29, Issue 5, Pages 716-728.

Kueper, B.H.; McWhorter, D. B. 1996, In Dense Chlorinated Solvents and Other DNAPLs in Groundwater; Pankow, J. K., Cherry, J. A., Eds.; Waterloo Press: Portland, OR, pp 337-353.

Kueper, B.H., Mcwhorter, D.B. 1998, DNAPL pool mobilization in fractured rock, *IAHS-AISH Publication* Issue 250, Pages 149-155.

Kueper, B.H., Wealthall G.P., Smith, J.W.N., Leharne, S.A. and Lerner, D.N. 2003, An illustrated handbook of DNAPL transport and fate in the subsurface. ISBN: 1844320669, Environment Agency, UK.

Le Thiez, P.A., Ducreux, J., 1994. A 3-D numerical model for analyzing hydrocarbon migration into soils and aquifers. In: Siriwardane, Zaman (Eds.), Computer Methods and Advances in Geomechanics. Balkema, Rotterdam, pp. 1165–1170.

Lee I.S., Bae J-H, Yang Y., McCarty P.L. 2004, Simulated and experimental evaluation of factors affecting the rate and extent of reductive dehalogenation of chloroethenes with glucose. *J Contam Hydrol* 74(1-4):313-31.

Lee Y.J., Miyahara T., Noike T. 2002, Effect of pH on microbial hydrogen fermentation. *J Chem Technol Biotechnol*, 77(6):694-8.

Lee, M.D., J.M. Odom, and R.J. Buchanan Jr. 1998, New Perspectives on Microbial Dehalogenation of Chlorinated Solvents: Insights from the Field, *Annual Review of Microbiology* 52: 423-452.

Leech, Kennedy, Gevaert, 1984. Sondierbohrung Böttstein: hydrological testing of cristaline rocks. National Cooperative for the Disposal of Radioactive Waste (NAGRA), Baden, Switzerland.

Lerman, A. 1979, Geochemical Processes: Water and Sediment Environments, John Wiley and Sons, Inc., New York, 481 pp.

Lerner D.N., Wealthall, G.P., Steele, A. 2002, Assessing risk from DNAPLs in fractured aquifers. *Agricultural Sciences*, 7(2):47-52

Lever, D.A. and Bradbury, M.H. 1985, Rock-matrix diffusion and its implications for radionuclide migration, *Mineral Mag.* 49, 245-254.

Lide, D. R. 2004, *CRC Handbook of Chemistry and Physics*, 85th ed., Chemical Rubber Company, Cleveland, Ohio, USA

Lipson, D.S., Kueper, B.H. and Gefell, M.J. 2005, Matrix Diffusion-Derived Plume Attenuation in Fractured Bedrock, *Ground Water*, 43 (1), 30-39.

Liu, Z., Edwards, D.A., Luthy, R.G., 1992. Sorption of non-ionic surfactants onto soil. *Water Res.* 26 (10), 1337–1345.
Lomize, G. M. 1951, Flow in Fractured Rocks (in Russian), 127 pp., *Gosenergoizdat,* Moscow.

Long C.M. and Border R.C. 2006, Enhanced Reductive Dehlorination in Columns Treated with Edible Oil Emulsion, *Journal of Contaminant Hydrology*, 87, 54-72.

Longino, B.L., Kueper, B.H. 1999, Nonwetting phase retention and mobilization in rock fractures, *Water Resources Research,* Volume 35, Issue 7, Pages 2085-2093.

Longino, B.L., Kueper, B.H. 1999, Effects of capillary pressure and use of polymer solutions on dense, non-aqueous-phase liquid retention and mobilization in a rough-walled fracture, *Environ. Sci. Technol.* Vol. 33, 2447-2455.

Louis, C., A study of groundwater flow in jointed rock and its influence on the stability of rock masses, *Rock Mech. Res. Rep.* 10, 90 pp., Imp. Coll. London, 1969.

Lowe SE, Jain MK, Zeikus JG. 1993, Biology, ecology, and biotechnical applications of anaerobic bacteria adapted to environmental stresses in temperature, pH, salinity, or substrates. Microbiol Rev 57:451-509.

Lunati, I., Kinzelbach, W. 2004, Water-soluble gases as partitioning tracers to investigate the pore volume-transmissivity correlation in a fracture, Journal of Contaminant Hydrology Volume 75, Issue 1-2, Pages 31-54.

Lunn, S.R.D. and B.H. Kueper. 1997, Removal of Pooled Dense, Nonaqueous Phase Liquid from Saturated Porous Media Using Upward Gradient Alcohol Floods, *Water Resour. Res*. 33(10):2207-2219.

Lunn, S.R.D., Kueper, B.H. 1999, Risk reduction during chemical flooding: Preconditioning DNAPL density in situ prior to recovery by miscible displacement, *Environmental Science and Technology* Volume 33, Issue 10, Pages 1703-1708.

Macbeth, T.W., Cummings, D.E., Spring, S., Petzke, L.M., Sorenson, K.S. Jr, 2004, Molecular Characterization of a Dechlorinating Community Resulting from In Situ Biostimulation in a Trichloroethene-Contaminated Deep, Fractured Basalt Aquifer and Comparison to a Derivative Laboratory Culture, *Applied and Environmental Microbiology,* 70 (12) p. 7329–7341.

Mackay, D.M., Cherry, J.A. 1989, Groundwater Contamination: Pump-and-treat remediation, *Environ. Sci. Technol.* Vol.23, No. 6, Pages 630-636.

Mackay, D.M., Shiu, W.Y., Maijanen, A. and Feenstra, S.1991, Dissolution of non-aqueous phase fluids in groundwater, *J. Contam. Hydrol.,* 8(l): 23-42.

MacKinnon, L.K., Cox, E.E., Hood, E.D., Mumford, K.G., Thomson, N.R. 2002, Evaluation of oxidation and bioremediation for CVOCs in fractured bedrock, *Proceedings of the Third International Conference on Remediation of Chlorinated and Recalcitrant Compounds* , 2467-2474, Paper 2H-58.

MacKinnon, L.K., Thomson, N.R. 2002, Laboratory-scale in situ chemical oxidation of a perchloroethylene pool using permanganate, *J. Contam. Hydrol.* 56 (1– 2), 49–74.

Mahani, H., 2005. Upscaling and Optimal coarse grid Generation for the Numerical Simulation of Two-Phase Flow in Porous Media. PhD thesis, Department of Earth Science and Engineering. London, Imperial College London.

Major D.W., McMaster M.L., Cox E.E., Edwards E.A., Dworatzek S.M., Hendrickson E.R., Starr M.G., Payne J.A., Buonamici L.W. 2002, Field demonstration of successful bioaugmentation to achieve dechlorination of tetrachloroethene to ethene. *Environ Sci Technol*, 36(23):5106-16.

Maloszewski, P., Zuber. 1991, A, Influence of matrix diffusion and exchange reactions on radiocarbon ages in fissured carbonate aquifers. *Water Resour. Res.* 27, 1937– 1945.

Maloszewski, P., Zuber, A. 1993, Tracer experiments in fractured rocks: matrix diffusion and the validity of models. *Water Resour. Res.* 29, 2723–2735.

Manger, G.E. 1963, Porosity and bulk density of sedimentary rocks, U.S. Geological Survey Bull. 1144-E.

Martel, R., Gelinas, P.J. 1996, Surfactant solutions developed for NAPL recovery in contaminated aquifers. *Ground Water* 34 (1), 143–154.

Mason, A. R., and Kueper, B. H. 1996, Numerical Simulation of Surfactant-Enhanced Solubilization of Pooled DNAPL, Environmental Science & Technology, 30 (11), 3205-3215.

Mayes, M.A., Jardine, P.M., Mehlhorn, T.L., Bjornstad, B.N., Ladd, J.L., Zachara, J.M., 2003. Transport of multiple tracers in variably saturated humid region structured soils and semi-arid region laminated sediments. *J. Hydrol.* 275, 141–161.

Maymó-Gatell, X., Chien, Y., Gossett, J. M., Zinder, S. H. (1997). Isolation of a Bacterium That Reductively Dechlorinates Tetrachloroethene to Ethene. *Science* 276: 1568-1571.

McCarty, P.L., Goltz, M.N., Hopkins, G.D., Dolan, M.W., Allan, J.P., Kawakami, B.T., Carrothers, T.J. 1998, Full scale evaluation of in situ cometabolic degradation of trichloroethylene in groundwater through toluene injection. *Environ. Sci. Technol.* 32, 88–100.

McWhorter, D. B., and D. K. Sunada 1990, Exact intergral solutions for two-phase flow*, Water Resour. Res.,* 26, 399-413.

Mejías, M., Renard, P., Glenz, D. *2009,* Hydraulic testing of low-permeability formations: A case study in the granite of Cadalso de los Vidrios, Spain, *Engineering Geology*, 107, pp.88–97.

Mendoza, C.A. 1992, Capillary Pressure and Relative Transmissivity Relationships Describing Two-phase Flow through Rough-walled Fractures in Geologic Materials, PhD thesis, University of Waterloo, Waterloo, Ontario.

Mercer, J. W., and R. M. Cohen. 1990, A review of immiscible fluids in the subsurface: Properties, models, characterization and remediation, *J. Contam. Hydrol*., 6, 107–163.

Mercer, J.W., and R.M. Cohen. 1993, DNAPL Site Evaluation, 6, pp. 107-163, C.K.Smoley. CRC Press, Inc. 200 Corporate Boulevard, NW., Boca Raton, Florida 33431., Boca Raton.

Michael Basel, Leo Lehmicke. 2002, Natural attenuation of Freons and TCE in fractured rock, *Proceedings of the Third International Conference on Remediation of Chlorinated and Recalcitrant Compounds,* Part D, Paper 2D-15.

Miller, C.T., M.M. Poirier-McNeill and A.S. Mayer. 1990, Dissolution of trapped nonaqueous phase liquids: mass transfer characteristics, *Water Resour. Res.*, 26(11): 2783-2796, 1990.

Miller, C.T., Christakos, G., Imhoff, P.T., McBride, J.F., Pedit, J.A. 1998, Multiphase flow and transport modelling in heterogeneous porous media: challenges and approaches, *Adv. Water*

Resour. 21 (2), 77– 120.

Miller, C.T., E.H. Hill III, and M. Moutier. 2000, Remediation of DNAPL-Contaminated Subsurface Systems Using Density Motivated Mobilization, *Environ. Sci. Technol.* 34(4):719-724.

Millington, R.J. and J.P. 1961, Quirk, Permeability of Porous Solids. *Trans. Faraday Society.* v.57, pp. 1200-1207.

Mohamedzein, Y.E-A., Al-Rawas, A.A., Al-Aghbari, M.Y., Qatan, A., Al-Rawas, A.H. 2005, Assessment of crushed shales for use as compacted landfill liners, *Engineering Geology*, 80, pp. 271–281.

Mohnke, O. and Yaramanci, U. 2008, Pore size distributions and hydraulic conductivities of rocks derived from Magnetic Resonance Sounding relaxation data using multi-exponential decay time inversion, *Journal of Applied Geophysics,* 66, pp.73–81.

Moreno, L., Y. W. Tsang, C. F. Tsang, F. V. Hale, and I. Neretnieks. 1988, Flow and tracer transport in a single fracture: A stochastic model and its relation to some field observations, *Water Resour. Res.*, 24(12), 2033–2048.

Morris, D.A. and A.I. Johnson, 1967. Summary of hydrologic and physical properties of rock and soil materials as analyzed by the Hydrologic Laboratory of the U.S. Geological Survey, U.S. *Geol. Surv. Water-Supply* Paper 1839-1842p.

Mumford, K. G., Thomson, N. R., and Allen-King, R. M. 2005, Bench-Scale Investigation of Permanganate Natural Oxidant Demand Kinetics, *Environmental Science & Technology*, 39 (8), 2835-2840.

Mundle, K., Reynolds, D. A., West, M. R., and Kueper, B. H. 2007, Concentration Rebound Following In Situ Chemical Oxidation in Fractured Clay, *Ground Water*, 45 (6), 692-702.

Murphy, J.R., Thomson, N.R. 1993, Two-phase flow in a variable aperture fracture, *Water Res. Res.* 29 (10), 3453–3476.

Mutch, R. D., Scott, J. I., and Wilson, D. J. 1993, Cleanup of fractured rock aquifers: Implications of matrix diffusion, Environmental Monitoring and Assessment, 24 (1), 45-70.

Nakashima M, Wu X, Okada, R. and Nishigaki M. 2002, Enhanced Bioremediation of a Site in Japan Contaminated with Chlorinated Solvents using HRC Injection, *Proceedings of the Third International Conference on Remediation of Chlorinated and Recalcitrant Compounds*, Paper 2B-42.

Nambi, I.M., and S.E. Powers. 2003, Mass transfer correlations for nonaqueous phase liquid dissolution from regions with high initial saturations, *Water Resources Research,* 39(2), SBH41-SBH411.

National Research Council, 1984 . Groundwater Contamination, National Academy Press, pp 61.

National Research Council (NRC). 1994, Alternatives for groundwater cleanup. National Academy Press, Washington, DC.

National research Council. 1996, Rock Fractures and Fluid Flow, Natl. Acad. Press, Washington, D.C.

Newell, C. J., Cowie, I., McGuire, T. M., and Walt W. McNab, J. 2006, Multiyear Temporal Changes in Chlorinated Solvent Concentrations at 23 Monitored Natural Attenuation Sites, *Journal of Environmental Engineering*, 132 (6), 653-663.

Novakowski, K.S. 1992, The analysis of tracer experiments conducted in divergent radial flow fields. *Water Resour. Res.* 28(12), 3215–3225.

Nyer, E., Lenzo, F.L., Burdick, J. S. 1998, In Situ Reactive Zones: Dehalogenation of Chlorinated Hydrocarbons, *Groundwater Monitoring Review*, Spring.

Ogata, A., and Banks, R. B. 1961, A Solution of the Differential Equation of Longitudinal Dispersion in Porous Media, USGS, Reston, Virginia, USGS Prof. Paper No. 411-A

Pakdel, H., Couture, G., Roy, C., Masson, A., Locat, .I., Gelinas, P. and Lesage, S. 1992, Developing methods for the analysis of toxic chemicals in soil and groundwater: The case of Ville Mercier, Quebec, Canada. In: S. Lesage and R.E. Jackson (Editors), *Groundwater Contamination and Analysis at Hazardous Waste Sites.* Marcel Dekker, New York, NY, 545 pp.

Palumbo, A.V., McCarthy, J.F., Parker, A., Pfiffner, S., Colwell, F.S., Phelps, T.J. 1994, Potential for microbial growth in arid subsurface sediments, *Appl. Biochem. Biotechnol.* 45-46, 823–834.

Pankow, J. F. and Cherry, J. A. 1996, Dense Chlorinated Solvents and Other DNAPLs in Groundwater: *History, Behaviour, and Remediation*, *Waterloo Press* pp.1-46, pp129-143, pp508, pp522.

Pape, H., Tillich, J.E., Holz, M. 2006, Pore geometry of sandstone derived from pulsed field gradient NMR, *Journal of Applied Geophysics,* 58, pp. 232–252.

Parker, B.L. 1996, Effects of molecular diffusion on the persistence of dense, immiscible phase organic liquids in fractured porous geologic media. PhD Thesis, Univ. of Waterloo.

Parker, B L., Gillham, Robert W., Cherry, John A. 1994, Diffusive disappearance of immiscible-phase organic liquids in fractured geologic media, *Ground Water,* Volume 32, Issue 5, Pages 805-819.

Parker, B.L., McWhorter, D.B., Cherry, J.A. 1997, Diffusive loss of non-aqueous phase organic solvents from idealized fracture networks in geologic media, *Ground Water*, Volume 35, Issue 6,

Pages 1077-1088.

Parker, J. C., and Park, E. 2004, Modelling field-scale dense nonaqueous phase liquid dissolution kinetics in heterogeneous aquifers, *Water Resources Research*, 40 (W05109), 1-12.

Pedersen, K., and S. Ekendahl. 1990. Distribution and activity of bacteria in deep granitic groundwaters of southeastern Sweden. *Microb. Ecol.* 20:37–52.

Pennell, K.D., Jin, M., Abriola, L.M., Pope, G.A. 1994, Surfactant enhanced remediation of soil columns contaminated by residual tetrachloroethylene. *J. Contaminant Hydrology* 16 (1), 35.

Pennell, K. D., Pope, G. A., and Abriola, L. M. 1996, Influence of Viscous and Buoyancy Forces on the Mobilization of Residual Tetrachloroethylene during Surfactant Flushing, *Environmental Science & Technology*, 30 (4), 1328-1335.

Persoff, P. and K. Pruess. 1995, Two Phase flow Visualization and relative Permeability Measurement in Natural Rough-Walled Rock Fractures, *Water Res. Res.*, 31(5), pp 1175-1186.

Pettijohn, F. J., Potter, P. E., and Siever, R. 1987, Sand and sandstone, Springer, New York.

Pitkänen, Snellman, Leino-Forsman, Front, 1992. Groundwater chemistry and water–rock interaction at Olkiluoto: Report YJT-92-02. *Nuclear Waste Commission of Finnish Power Companies*, Helsinki, Finland, pp. 321.

Pope, G.A., Wade, W.H. 1995, Lessons from enhanced oil recovery research for surfactant enhanced aquifer remediation. In: Sabatini, D.A., Knox, R.C., Harwell, J.H.Eds, Surfacant-enhanced subsurface remediation: emerging technologies, ACS symposium series No. 594. *American Chemical Society,* Washington, DC, pp. 142–160.

Powers, S.E., Loureiro, C.O., Abriola, L.M. and Weber, Jr., W.J. 1991, Theoretical study of the significance of non equilibrium dissolution of non-aqueous-phase liquids in subsurface systems, *Water Resour. Res.*, 27(4): 463-477.

Powers, S. E., Abriola, L. M., and Weber Jr., W. J. 1992, An experimental investigation of nonaqueous phase liquid dissolution in saturated subsurface systems: Steady state mass transfer rates, *Water Resour. Res.*, 28(10), 2691–2706.

Pruess, K., Tsang, Y.W. 1990, On two-phase relative permeability and capillary pressure of rough-walled rock fractures. *Water Resour. Res*. 26 (9), 1915–1926.

Pyrak-Nolte, L.J. 1991, Multiphase flow in a fracture. *Proceedings of the 1991 Coalbed Methane Symposium*, University of AlabamarTuscaloosa, pp. 433–442.

Ramsburg, C. A., and K. D. Pennell. 2002, Density-modified displacement for DNAPL source zone remediation: Density conversion and recovery in heterogeneous aquifer cells, *Environ. Sci. Technol.,* 36, 3176 – 3187.

Ramsburg, C. A., Pennell, K. D., Abriola, L. M., Daniels, G., Drummond, C. D., Gamache, M., Hsu, H. L., Petrovskis, E. A., Rathfelder, K. M., Ryder, J. L., and Yavaraski, T. P. 2005, Pilot-Scale Demonstration of Surfactant-Enhanced PCE Solubilization at the Bachman Road Site. 2. System Operation and Evaluation, *Environmental Science & Technology*, 39 (6), 1791-1801.

Rangel-German, E., Akin, S., Castanier, L., 2006, Multiphase-flow properties of fractured porous media, *Journal of Petroleum Science and Engineering*, 51(3-4), pp 197-213.

Rathfelder, K. M., Abriola, L. M., Taylor, T. P., and Pennell, K. D. 2001, Surfactant enhanced recovery of tetrachloroethylene from a porous medium containing low permeability lenses: 2. Numerical simulation, *Journal of Contaminant Hydrology*, 48 (3-4), 351-374.

Reitsma, S. 1992, Laboratory measurement of capillary pressure – saturation relationships in natural rock fractures, M.Sc. Thesis, University of Waterloo, Waterloo, Ontariom Canada, 152pgs.

Reitsma, S., Kueper, B.H. 1994, Laboratory measurement of capillary pressure – saturation relationships in a rock fracture. *Water Resour. Res*. 30(4), 865-878.

Reynolds, D.A. 2001, Multiphase Flow and Transport in Fractured Geologic Environments, PhD thesis, University of Kingston, Ontario, Canada.

Reynolds, D.A., Kueper, B.H. 2001, Multiphase flow and transport in fractured clay/sand sequences, *J. Contam. Hydrol.* 51 (1–2), 41– 62.

Reynolds, D.A., Kueper, B.H. 2004, Multiphase flow and transport through fractured heterogeneous porous medium, *J. Contam. Hydrol*. 71, 89– 110.

Robinson, C., Barry, D.A., McCarty, P.L., Gerhard, J.I. and Kouznetsova I. 2009, pH Control for Enhanced Reductive Bioremediation of Chlorinated Solvent Source Zones. *Science of the Total Environment,* 407, 4560-4573.

Ross, B., Lu, N. 1999, Dynamics of DNAPL penetration into fractured porous media, *Ground Water* Volume 37, Issue 1, Pages 140-147.

Ross, N., Kennedy, C., Voralek, J., Lesage, S., Novakowski K., Samson, R. 2002, Biofilm development in a large-scale planar fracture, *Proceedings of the Third International Conference on Remediation of Chlorinated and Recalcitrant Compounds,* Pages 2441-2447, Paper 2C-41.

Saba, T., and T.H. Illangasekare. 2000, Effect of groundwater flow dimensionality on mass transfer from entrapped nonaqueous phase liquid contaminants, *Water Resources Research*, 36(4), 971-979.

Sardin, M., Dridl-Dhaouadi, S., Maunier, C. and Simonnot, M.O. 1998, Transient Transport of

Surfactant in a Calcaeous and Clayey Sand, *Physics and Chemistry of the Earth*, 23(2) , pp. 221-227.

Sausse, J. 2002, Hydromechanical properties and alteration of natural fracture surfaces in the Soultz granite (Bas-Rhin, France), *Tectonophysics,* 348, pp.169– 185.

Sausse, J., Fourar, M., Genter, A. 2006, Permeability and alteration within the Soultz granite inferred from geophysical and flow log analysis, *Geothermics,* 35, pp. 544–560.

Schnarr, M., Truax, C., Farquhar, G., Hood, E., Gonullu, T., Stickney, B. 1998, Laboratory and controlled field experiments using potassium permanganate to remediate trichloroethylene and perchloroethylene DNAPLs in porous media, *J. Contam. Hydrol.* 29 (3), 205– 224.

Schroth, M.H., Oostrom, M., Wietsma, T.W., Istok, J.D. 2001, In-situ oxidation of trichloroethene by permanganate: effects on porous medium hydraulic properties, *J. Contam. Hydrol.* 50, 79–98.

Schwartz, F.W., Cherry. J.A. and Roberts, J.A. 1982, A case study of chemical spill polychlorinated biphenyls, 2: Hydrogeological conditions and contaminant migration, *Water Resour. Res,* 18(3): 535-545.

Schwarzenbach, R.P. and Westhall J. 1981, Transport of nonpolar organic compounds from surface water to groundwater: Laboratory Studies, *Environmental Science and Technology,* v. 15, pp. 1360-1367.

Schwarzenbach, R.P., Gschwend, P. M., and Imboden, D.M. 1993, *Environmental Organic Chemistry,* John Wiley and Sons, Toronto, pp. 681.

Schwille, F. 1988, Dense chlorinated solvents in porous and fractured media; Model experiments. Translated by J.F. Pankow. Lewis Publishers.

Seagren E.A., Rittmann B.E., Valocchi A.J. 1994, Quantitative evaluation of the enhancement of NAPL-pool dissolution by flushing and biodegradation. *Environ Sci Technol*, 28(5):833-9.

Sehayek, L., Vandell, T.D., Sleep, B.E., Lee, M.D., Chien, C. 1999, Investigation and remediation of a 1,2-dichloroethane spill: Part I: Short and long-term remediation strategies, *Ground Water Monitoring and Remediation Volume* 19, Issue 3, Pages 71-81.

Seol, Y., Zhang, H., and Schwartz, F.W. 2003, A review of In Situ Chemical Oxidation and Heterogeneity, *Environment & Engineering Geoscience,* 9(1), February, pp. 37-49.
Shapiro, A.M. 2001, Effective matrix diffusion in kilometer-scale transport in fractured crystalline rock. *Water Resour.* 37, 37507–37522.

SERDP. 2001, SERDP/ESTCP Expert Panel Workshop on Research and Development Needs for Cleanup of Chlorinated Solvent Sites.

Shiau, B., Rouse, J.D., Sabatini, D.A., Harwell, J.H. 1995, Surfactant selection for optimizing surfactant-enhanced subsurface remediation. In: Sabatini, D.A., Knox, R.C., Harwell, J.H.(Eds), Surfacant-enhanced subsurface remediation: emerging technologies, ACS symposium series No. 594. American Chemical Society, Washington, DC, pp. 65–79.

Siegrist, R. L., Urynowicz, M. A., West, O. R., Crimi, M. L., and Lowe, K. S. 2001, Principles and Practices of in Situ Chemical Oxidation Using Permanganate, 348 pp., *Battelle Press,* Columbus, Ohio, USA

Sleep B.E., Sykes J.F. 1993, Compositional simulation of groundwater contamination by organic compounds. 1, Model development and verification. *Water Resour Res,* 29(6):1697-1708.

Slough, K.J., Sudicky, E.A., Forsyth, E.A. 1999a, Numerical Simulation of Multiphase Flow and Phase Partitioning in Discretely Fractured Geologic Media, *J. Cont. Hyd.,* 40, p 107-136.

Slough, K.J., Sudicky, E.A., Forsyth, E.A. 1999b, Grid refinement for modelling multiphase flow discretely fractured porous media, *Advances in Water Resources* 23, pp 261-269.

Smith, L. and F.W. Schwartz. 1984, An Analysis of the Influence of Fracture Geometry on Mass Transport in Fractured Media. *Water Resour. Res.* 20, 1241-1252.
Sorenson, K. S. 2002. Enhanced bioremediation for treatment of chlorinated solvent residual source areas. *ACS Symp.* Ser. 837:119–131.

Sousa, L.M.O. 2007, Granite fracture index to check suitability of granite outcrops for quarrying, *Engineering Geology*, 92, pp.146–159.

Streltsova, T.D. 1976a, Advances and uncertainties in the study of groundwater flow in fissyred rocks, *Adv. Groundwater Hydrol*., pp. 48-56.

Steele A. and Lerner D.N. 2001, Predictive modelling of NAPL injection tests in variable aperture spatially correlated fractures, *Journal of Conyaminant Hydrology,* 49 (3-4): 287-310.
Suarez, M.P., and Rifai, H.S., 1999. Biodegradation rates for fuel hydrocarbons and chlorinated solvents in groundwater, CRC Press LLC, 337-362.

Suchomel, E. J., Ramsburg, C. A., and Pennell, K. D. 2007, Evaluation of trichloroethene recovery processes in heterogeneous aquifer cells flushed with biodegradable surfactants, *Journal of Contaminant Hydrology*, 94 (3-4), 195-214.

Sudicky, E.A., Frind, E.O. 1982, Contaminant transport in fractured porous media: analytical solutions for a system of parallel fractures. *Water Resour. Res.* 18, 1634–1642.

Sudicky, E.A., Slough, K.J. 1998, Forsyth, P.A., DNAPL migration in fractured porous rock media: Parameter sensitivity, prediction uncertainty and implications for remediation, IAHS-AISH Publication Issue 250, Pages 157-165.

Sung, Y., K. M. Ritalahti, R. A. Sanford, J. W. Urbance, S. J. Flynn, J. M. Tiedje, and F. E.

Lo¨ffler. 2003. Characterization of two tetrachloroethene-reducing, acetate-oxidizing anaerobic bacteria and their description as *Desulfuromonas michiganensis* sp. nov. Appl. Environ. Microbiol. 69:2964–2974.

Suthersan, S and F. Payne. 2005. *In Situ* Remediation Engineering. Boca Raton: CRC Press.

Swanson, S.K., Bahr, J.M., Bradbury, K.R., Anderson, K.M. 2006, Evidence for preferential flow through sandstone aquifers in Southern Wisconsin*, Sedimentary Geology*, 184, pp. 331–342.

Tang, D.H., Frind, E.O., and Sudicky, E.A. 1981, Contaminant Transport in Fractured Porous Media: Analytical Solution for a Single Fracture, *Water Resources Research*, 17 (3), 555-564.

Taylor, T. P., Pennell, K. D., Abriola, L. M., and Dane, J. H. 2001, Surfactant enhanced recovery of tetrachloroethylene from a porous medium containing low permeability lenses 1. Experimental studies, *Journal of Contaminant Hydrology*, 48 (3-4), 325-350.

Taylor, T. P., Rathfelder, K. M., Pennell, K. D., and Abriola, L. M. 2004, Effects of ethanol addition on micellar solubilization and plume migration during surfactant enhanced recovery of tetrachloroethene, *Journal of Contaminant Hydrology*, 69 (1-2), 73-99.

Thomson, N.R., Fraser, M.J., Lamarche, C., Barker, J.F.,Forsey S.P., 2008, Rebound of a coal tar creosote plume following partial source zone treatment with permanganate, *Journal of Contaminant Hydrology,* 102, 154–171.

Tomlin, A., Berzins, M., Ware, J., Smith, J. and Pilling M.J., 1997, On the use of adaptive gridding methods for modelling chemical transport from multi-scale sources, *Atmospheric Environment*, 31(18), Pages 2945-2959.

Trivedi, J.J., Babadli, T. 2008, Experimental and numerical modelling of the mass transfer between rock matrix and fracture, Chemical Engineering Journal, In-Press.

Tsang, Y.W., Tsang, C.F. 1987, Channel model of flow through fractured media, *Water Resour. Res.* 23, 467– 479.

Tsang, Y.W. 1992, Usage of "equivalent apertures" for rock fractures as derived from hydraulic and tracer tests, *Water Resours. Res.*, 28(5): 1451-1455.

Tunnicliffe B. S. and Thomson N. R. 2004, Mass removal of chlorinated ethenes from rough-walled fractures using permanganate, *Journal of Contaminant Hydrology* Volume 75, Issues 1-2 , Pages 91-114.

Uhlman, K, Barner, W. 1998, Contaminant transport mechanisms in karst terranes, *IAHS-AISH Publication Issue* 253, Pages 327-335.

Unger, A.J.A., Sudicky, E.A. and Forsyth, P.A. 1995, Mechanisms controlling vacuum extraction

coupled with air sparging for remediation of heterogeneous formations contaminated with dense non-aqueous-phase liquids, *Water Resour. Res.,* 31(8): 1913-1925.

USEPA, 2001. The State-of-the Practice of Characterization and Remediation of Contaminated Ground Water at Fractured Rock Sites EPA 542-R-01-010.

USEPA, 2003b. Chemical Oxidation Site Profiles. Available at http://www.clu-in.org/products/chemox/search/chem_search.cfm

Urynowicz, M.A., and Siegrist, R.L. 2005. Interphase mass transfer during chemical oxidation of tce dnapl in an aqueous system. *Journal of Contaminant Hydrology*, 80:93-106.

VanderKwaak, J.E., Sudicky, E.A.1996, Dissolution of non-aqueous-phase liquids and aqueous-phase contaminant transport in discretely-fractured porous media, *Journal of Contaminant Hydrology* 23, Pages 45-68.

Vasconcelos, G., Lourenco, P.B., Alves, C.A.S., Pamplona, J. 2008, Ultrasonic evaluation of the physical and mechanical properties of granites, *Ultrasonics,* 48, pp. 453–466.

Vella, P.A., and Veronda, B. 1992, Oxidation of trichloroethylene: Comparison of potassium permanganate and fenton's reagent, chemical oxidation technologies for the nineties. *Technical report,* Technomin, Lancaster, PA, USA.

Vella, P.A. and B. Veronda. 1994, Oxidation of Trichloroethylene: A comparison of potassium permanganate and Fenton's reagent. *3rd Intern. Symposium on Chemical Oxidation. In: In Situ Chemical Oxidation for the Nineties.* Vol. 3. Technomic Publishing Co., Inc. Lancaster, PA. pp.62-73.

Vilks P., Cramer, J.J., Jensen, M., Miller, N.H., Miller, H.G., Stanchell, F.W. 2003*,* In situ diffusion experiment in granite: Phase I, *Journal of Contaminant Hydrology,* 61, 191– 202.

Villaume, J.F. 1985, Investigations at sites contaminated with dense, non-aqueous-phase liquids (NAPLs), *Ground Water Monit. Rev.*, 5(2): 60-75.

Walker, Rhén, Gurban, 1997. Summary of hydrogeological conditions at Aberg, Beberg and Ceberg. *Technical Report,* TR 97-23, SKB SKB Stockholm, Sweden.

Walter, G.R., G.M. Thompson. 1982, A repeated pulse technique for determining the hydraulic properties of tight formations, *Ground Water* 20, 186-193.

Water Science and Technology Board (WSTB). 2004, Contaminants in the Subsurface: Source Zone Assessment and Remediation, National Research Council of the National Academies, *The National Academies Press,* Washington D.C.

Watkins, 2003. Determining a representative hydraulic conductivity of the Carnmenellis granite of Cornwall, UK, based on a range of sources of information. *Paper presented at the IHP*

International Hydrological Program, Bratislava, Slovak Rep.

Wealthall, G.P., Lerner, D.N. 2002, Fractured rock mass characterisation to predict DNAPL source zones, *Proceedings of the Third International Conference on Remediation of Chlorinated and Recalcitrant Compounds*, Pages 239-246, Paper 1D-07.

Wealthall, G.P., Steele, A., Bloomfield, J.P., Moss, R.H. and Lerner, D.N. 2001, Sediment filled fractures in the Permo-Triassic sandstones of the Cheshire Basin: observations and implications for pollutant transport, *Journal of Contaminant Hydrology* 50, 41-51.
Wealthall, G.P., S.F. Thornton, and D.N. Lerner. 2001. Assessing the trasport and fate of MTBE-amended petroleum hydrocarbones in the UK Chalk aquifer. Paper presented at Groundwater Quality 2001, Third International Conference on Groundwater Quality, June 18-21, 2001, in University of Sheffield, United Kingdom.

Werner, P.G.. 2002, Chemical oxidation of Tetrachloroethene (PCE) contamination in a fractured saprolitic bedrock aquifer, *Proceedings of the Third International Conference on Remediation of Chlorinated and Recalcitrant Compounds*, Part C, Paper 2C-44.

West M.R. 2009, Mathematical Modelling of DNAPL Source Zone Remediation, PhD Thesis, Queens University, Kingston, Ontario.

West, M. R., Grant, G. P., Gerhard, J. I., and Kueper, B. H. 2008, The influence of precipitate formation on the chemical oxidation of TCE DNAPL with potassium permanganate, *Advances in Water Resources*, 31 (2), 324-338.

West, C.C. and Harwell, J.H. 1992, Surfactants and Subsurface Remediation, *Environ. Sci. Technol.*, Vol. 26, No. 12.

Wice, R.B., Vogeding, J.R., Walters, G., Ficklen, H.D. 2002, Enhanced DNAPL recovery from fractured limestone AFP4, Fort Worth, Texas, *Proceedings of the Third International Conference on Remediation of Chlorinated and Recalcitrant Compounds*, Pages 2441-2447, Paper 2H-55.

Widdowson M.A. 2004, Modelling natural attenuation of chlorinated ethenes under spatially varying redox conditions. *Biodegradation*, 15(6):435-51.

Williams, C.L., Spiers C.A. 2002, Degradation of Trichloroethene (TCE) in a fractured bedrock aquifer using Sodium Permanganate, *Proceedings of the Third International Conference on Remediation of Chlorinated and Recalcitrant Compounds,* Pages 2441-2447, Paper 2C-43.

Wilke, C. R., and Chang, P. 1955, Correlation of diffusion coefficients in dilute solutions, *AIChE Journal*, 1 (2), 264-270.

Witherspoon, P. A., J. S. Y. Wang, K. Iwai, and J. E., Gale. 1980, Validity of cubic law for fluid flow in a deformable rock fracture, *Water Resour. Res.*, 16(6), 1016– 1024.

Wood, B.D., Ginn, T.R., and Dawson, C.N. 1995, Effects of Microbial Metabolic Lag in

Contaminant Transport and Biodegradation Modelling, *Water Resources Research*, 31 (3), pp. 553-563.

Wu, W.-M., Nye, J., Jain, M. K., and Hickey, R. F. 1998, Anaerobic dechlorination of trichloroethylene (TCE) to ethylene using complex organic materials, *Water Research*, 32 (5), 1445-1454.

Wu, X., Alshawabkeh, A.N., Gent, D.B., Larson, S. L. and Davis J. L., 2007, Lactate transport in soil by DC Fields, *J. Geotech and Geoenvir. Eng.*, 133(12), 1587-1596.

Wulff, A.M., Raab, S., Huenges, E. 2000, Alteration of Seismic Wave Properties and Fluid Permeability in Sandstones due to Microfracturing, *Phys. Chem. Earth (A),* Vol. 25, No. 2, pp. 141-147.

Yager, R. M., S. E. Bilotta, C. L. Mann, and E. L. Madsen. 1997. Metabolic adaptation and in situ attenuation of chlorinated ethenes by naturally occurring microorganisms in a fractured dolomite aquifer near Niagara Falls, New York. Environ. Sci. Technol. 31:3138–3147.

Yang, Y., and McCarty, P.L. 1998, Competition for Hydrogen Within a Chlorinated Solvent Dehalogenating Anaerobic Mixed Culture, *Environmental Science and Technology*. 32(22):3591-3597.

Yang, Y., and McCarty, P. L. 2000a, Biomass, Oleate, and Other Possible Substrates for Chloroethene Reductive Dehalogenation, *Bioremediation Journal*, 4 (2), 125 - 133.

Yang Y., McCarty .PL. 2002, Comparison between donor substrates for biologically enhanced tetrachloroethene DNAPL dissolution. *Environ Sci Technol*,36(15):3400-4.

Yan, Y.E. and Schwartz, F.W. 1996, Oxidation of chlorinated solvents by permanganate. Proc. Intern. Conf. On Remediation of Chlorinated and Recalcitrant Compounds, Ohio: *Battelle Press.* pp. 403-408.

Yan, Y.E., and Schwartz, F.W. 1999, Oxidative degradation and kinetics of chlorinated ethylenes by potassium permanganate, *Journal of Contaminant Hydrology*, 37 (3-4), 343-365.

Yan, Y.E., and Schwartz, F.W. 2000, Kinetics and Mechanisms for TCE Oxidation by Permanganate, *Environmental Science & Technology*, 34 (12), 2535-2541.

Yeo, I.W., Ji, S.-H., Lee, K.-K. 2003, Density-surfactant-motivated removal of DNAPL trapped in dead-end fractures, *Geophysical Research Letters* Volume 30, Issue 9, Pages 24-1.

Yu, J., and Pinder, K. L. 1994, Effective diffusivities of volatile fatty acids in methanogenic biofilms, *Bioresource Technology*, 48 (2), 155-161.

Yu S., Semprini L. 2004, Kinetics and modelling of reductive dechlorination at high PCE and TCE concentrations. *Biotechnol Bioeng*, 88(4):451-64.

Zekri, AY; Almehaideb, R. 2003 Microbial and waterflooding of fractured carbonate rocks: An experimental approach, *Petroleum Science and Technology,* 21 (1-2): 315-331.

Zhang, X., Sanderson, D.J., Harkness, R.M., and N.C. Last. 1996, Evaluation of the 2-D Permeability Tensor of Fractured Rock, *Int. J. Rock Mech. Min. Sci.*, 33, p 17-37.

Zhang, X., Sanderson, D.J. 1999, Scale up of Two-dimensional Conductivity Tensor for Heterogeneous Fracture Networks, Eng. Geol., 53, p 83-99.

Zhang, H., and Schwartz, F. W. 2000, Simulating the in Situ Oxidative Treatment of Chlorinated Ethylenes by Potassium Permanganate, *Water Resources Research*, 36 (10), 3031-3042.

Zhong, LR; Mayer, A; Glass, RJ. 2001, Visualization of surfactant-enhanced nonaqueous phase liquid mobilization and solubilization in a two-dimensional micromodel, *Water resources research,* 37 (3): 523-537.

Zhong, L., Mayer, A. S., and Pope, G. A. 2003, The effects of surfactant formulation on nonequilibrium NAPL solubilization, *Journal of Contaminant Hydrology*, 60 (1-2), 55-75.

Zhuang P., Pavlostathis S.G. 1995, Effect of temperature, pH and electron donor on the microbial reductive dechlorination of chloroalkes. *Chemosphere,* 31(6):3537-48.

APPENDIX E

DQR CALCULATIONS

Criteria A: Quality of the Information Source

The reputability of the information source was rated according to the criteria outlined in **Table E.4**. Records that were peer-reviewed by a third party of technical experts were given the highest ratings. For case studies for which information was compiled from multiple records, the highest rating of the individual records was used.

Table E.1: Criteria for quality of the information source.

Information Source	**Rating out of 3**
Peer-reviewed journal article or report U.S. Department of Energy Innovative Technology Summary Report (ITSR) ESTCP Final Technical Report U.S. EPA Superfund Innovative Technology Evaluation (SITE Report)	3
Graduate student thesis Other government document (*i.e.*, compilation of case studies) Conference proceedings paper	2
Unpublished academic sources Technology vendor fact sheets Other	1

Criteria B: Age of the Study

Each application of a remedial technology should, in theory, incorporate the lessons learned from previous applications. Thus, data from older studies may not provide as accurate an indication of the performance of future technology applications as would a relatively recent study. A review of the case study records input to the database suggests that most of the principal technologies studied in this project were first applied to chlorinated solvent DNAPL sites in the mid-to-late 1990s. In the late 1990s and early 2000s, several important guidance documents and case study compilations were published to advance these technologies. Hence, the age of the study was rated as shown in **Table E.2**. The cutoff years may be revised in subsequent versions of DNAPL TEST.

Table E.2. Criteria for age of the study.

Year in which Treatment Began	**Rating out of 3**
2002 or more recent	3
1998 to 2001	2
1997 or earlier	1

If the year in which treatment began was not provided, the publication year of the information source was substituted. This may bias the rating higher as most records become available 1-2 years after the completion of remedial treatment.

Criteria C: Quality of DNAPL Assessment Methods

Several quantitative and qualitative methods may be used to assess the presence and distribution of DNAPL. In general, high quality data sources describe in detail the methods used to characterize the DNAPL, including the number of sampling points used. The quality rating for DNAPL assessment methods was based primarily on the accuracy of the method used as shown in **Table E.3**. Known DNAPL spills were considered to be a good indicator of DNAPL presence, given the typical lifespan and low solubility of the majority of the chlorinated solvent DNAPLs. Sites for which DNAPL presence was determined by indirect means (*i.e*, soil or groundwater concentrations) but were sampled at a relatively high density ($\geq$ 1 sample per 20 m^3 of target soil volume) received a one point increase in their rating for this criterion. This sampling density threshold was selected so that approximately 5% of case studies would be eligible for the rating increase. For case studies where several different methods were used to assess DNAPL, the method producing the highest rating was used.

Table E.3. Criteria for DNAPL assessment method.

DNAPL Assessment Method	Rating out of 3
Known spill Direct visual observation, including use of dyes DNAPL extracted from monitoring well Partitioning tracer test Interface probe Ribbon sampler DNAPL accumulation in well	3
Inferred from groundwater concentrations Inferred from soil concentrations Direct olfactory observation Direct observation through PID readings	2*
Known use on site Other	1*

* Ratings were increased by one if the site was sampled at least once per 20 m^3 of target soil volume.

Criteria D: Quality of Pre-Treatment Characterization

The rating for the quality of pre-treatment characterization was based primarily on the amount of hydrogeological and DNAPL characterization information provided in the record. Case studies that provided information on the size of the site, groundwater flow, and DNAPL distribution (*e.g.*, pooled, residual, or sorbed) received the highest rating. Lower ratings were assigned to case studies with less comprehensive data sets as listed in **Table E.4**. Matrix porosity was

considered to be a key indicator of the quality of pre-treatment characterization for fractured bedrock sites. Hence, sites for which the majority of the treatment volume was consolidated received a low rating if matrix porosity was not specified.

Table E.4. Criteria for pre-treatment data provided for each case study.

Pre-Treatment Characterization Data Provided	**Rating out of 3**
All of the following: • Description of DNAPL distribution • Hydraulic conductivity, groundwater velocity, and/or sustainable well yield • Hydraulic gradient • Treatment area and/or volume • Matrix porosity (only if treatment volume > 50% consolidated)	3
All of the following: • Description of DNAPL distribution • Hydraulic conductivity, groundwater velocity, and/or sustainable well yield • Matrix porosity (only if treatment volume > 50% consolidated)	2
Insufficient data to meet the above criteria	1

Criteria E: Quality of Post-Treatment Characterization

DNAPL remediation technology performance is typically evaluated by the following four categories of performance metrics: *i*) treatment cost; *ii*) contaminant mass removed; *iii*) reduction in soil and/or groundwater concentrations; and *iv*) plume impact (*i.e.*, plume stability, mass flux, and mass discharge). Scientifically rigorous reports of field case studies often provide data on multiple performance metrics and include the results of post-treatment monitoring for an extended period of time to assess concentration rebound. In contrast, laboratory and modeling studies tend to focus on only one or two performance metrics, but the data is gathered with greater resolution and precision than is typically possible in the field. Thus, the quality rating for post-treatment characterization was designed to accommodate both approaches by incorporating the number of performance criteria evaluated, the duration of post-treatment monitoring, and the ability to calculate a mass balance on the contaminant using the data provided. The data requirements for each quality rating are described in **Table E.5**.

Table E.5. Criteria for post-treatment characterization data provided for each case study.

Post-Treatment Characterization Data Provided	**Rating out of 3**
Data on at least three out of the following five metrics: Treatment cost Contaminant mass removal Post-treatment concentrations Monitoring data for at least one year after treatment Plume stability, mass flux, or mass discharge	3
Data on at least two of the following four metrics: Treatment cost Contaminant mass removal Post-treatment concentrations Monitoring data for at least one year after treatment OR Data on at least two of the following four metrics: Contaminant mass prior to treatment Contaminant mass remaining after treatment Contaminant mass removed during treatment Percent mass removed/remaining	2
Insufficient data to meet the above criteria	1

APPENDIX F

STATISTICAL ANALYSIS

APPENDIX F: STATISTICAL CORRELATIONAL ANALYSIS

Statistical techniques were used to evaluate the relationship between site parameters and performance metrics and to quantify the extent to which the variability in the performance metric may be explained by the site parameter. The analysis was completed using the statistical software package SPSS version 15.0 (SPSS, 2006). SPSS 15.0 is a comprehensive software package for analyzing data and is capable of generating tabulated reports, charts, and plots of distribution and trends, descriptive statistics (mean, variance, etc.) and complex statistical analysis (SPSS, 2006).

The site parameters evaluated in the statistical analysis included the following:

- Physical site characteristics:
  - Depth to groundwater and depth to the top of aquifer;
  - Horizontal hydraulic conductivity and horizontal hydraulic gradient;
  - Groundwater velocity;
  - The saturated thickness of the aquifer; and
  - Soil porosity.
- DNAPL source zone characteristics:
  - Areal extent, thickness, maximum depth, and volume of the DNAPL source zone;
  - Pre-remediation DNAPL mass;
  - Number of wells; and
- Technology specific parameters:
  - Total number of oxidant injections, oxidant application duration, and oxidant concentration (ISCO);
  - Total mass of oxidant rejected (ISCO);
  - Number of electrodes and electrode spacing, the maximum aquifer temperature achieved during treatment, time to maximum temperature and target temperature (Thermal);
  - Surfactant injection rate and total duration of amendment (SEAR);
  - Mass of electron donor injected and electron donor well spacing (EISB); and
  - Monitoring duration (all technologies).

The performance metrics used in the statistical analysis included the following:

- Percent reduction in groundwater and soil concentrations, and groundwater mass flux;
- Removal of DNAPL mass;
- Duration of active treatment implementation; and
- Unit cost (per treatment volume) of implementation.

Prior to beginning the analysis, the dataset of performance metric – site parameter pairs was reviewed and appropriateness for inclusion in the analysis was assessed as follows:

i) ***Quality Assurance/Quality Control:*** All pairs were plotted on scatter plots to validate the linearity assumption and to identify potential outliers in the data set. Both original data sets and log-transformed data sets were plotted for comparative purposes. Log transformations are performed in order to improve linearity and to stabilize the variability in the data. Extreme data points were identified and those believed to be an artifact of a systematic error (*i.e.,* data entry errors, etc.) were corrected where possible or were flagged as outliers and removed from the data set. If there was no evidence to suggest that the outliers were errors, they were retained for the analysis.

ii) ***Appropriateness for Statistical Evaluation:*** Datasets were checked to ensure that they contained sufficient (*i.e.,* >5 data points within each pair) and unique (*i.e.,* the site parameter values within each pair dataset could not all be the same) datasets to ensure that the dataset contained a random and representative sample of the true population. Any pairs with less than 5 data points or with only one value for the site parameter were excluded from the analysis.

The process for evaluating correlations between site parameters and performance metrics was conducted in two parts:

i) A series of correlation tests were conducted to identify linear associations between a given site parameter and a given technology performance metric. A 5% level of significance was used as the criteria for statistically significant linear correlations; and

ii) Site parameter – performance metric pairs that showed a statistically significant correlation were analyzed using simple linear regression methods. Regression quantifies the sensitivity of the technology performance to each site parameter, and was also used to calculate a range of site parameters values given a particular technology performance value *via* a 95% confidence interval.

In recognition of the differences in technology performance anticipated for each technology, the performance metric – site parameter datasets were broken down into separate technology groupings and sub-grouping (*e.g.,* ISCO sites were further broken down into sub categories for the various oxidants including permanganate, Fenton's reagent and ozone). To account for any potential difference between field studies and modeling studies, separate analyses were completed with just field studies in the datasets and with both field and modeling studies retained

in the datasets. Similarly, to evaluate differences in technology performance between geologic environments (*i.e.,* unconsolidated soil environments *versus* consolidated media such as fractured rock or clay where contaminant storage within a hydraulically inaccessible matrix could have a significant influence on technology performance), the datasets were again split up into both media, unconsolidated media only and consolidated media only.

Table F.1 lists each technology, broken down by sub-technology where applicable, and the corresponding data subsets that were evaluated. Only chemical oxidation and SEAR could be analyzed for all subsets of field, modeling and media type, due to lack of data for the other technologies. Due to limited datasets in the technology sub-groupings, parent technologies were also grouped together and used for the regression analysis in an attempt to increase the size of the dataset. A summary of the results of the correlation test, including calculated Pearson correlation coefficients, associated p-values and sample sizes, for the pairwise combinations are provided in **Tables F.2 to F.5**.

The final pairs analyzed by regression methods were selected based on the results of the correlation tests. Due to the often limited datasets available for the correlation analysis, professional judgment was also used in evaluating whether statistical significance of the correlation test accurately represented a true correlation. Any pair that produced a statistically significant correlation and had a lower coefficient of determination value (R^2; indicating a weak correlation) or few data points and the relationship suggested by the correlation analysis was counterintuitive, were not considered for the analysis. Significant correlations (shown in bold font in **Tables F.2 to F.5**) were also cross-referenced with the scatterplots and only those pairs that appeared to have a dataset representative of the true population were considered for the regression analysis (i.e., datasets that contained a cluster of similar values and one outlier were not considered representative datasets).

Table F.1 provides a summary of the datasets that were used in the linear regression analyses (highlighted technologies and datasets). No correlations were observed in any of the chemical oxidation datasets for any performance metric – site parameter pairs and these were thus not included in the regression analysis. Insufficient data was available for aerobic EISB, and while the conductive thermal dataset theoretically had sufficient data (5 case studies), the dataset was still too limited to define correlations if any existed. For the anaerobic EISB dataset, insufficient data was available for consolidated sites, and the analysis was therefore limited to unconsolidated sites. For SEAR, significant correlations were observed for both media types and separately for each media; therefore, the combined dataset was retained for the regression analysis.

Table F.1. Summary of datasets that were evaluated in the correlation analysis.

Technology	Field - Both Media	Combined Field and Modeling Case Studies		
		Consolidated	Unconsolidated	Both
Chemical Oxidation – Fenton's Reagent or Hydrogen Peroxide [1]	X	NM	NM	X
Chemical Oxidation – Permanganate [1]	X	X	X	X
Chemical Oxidation – All [1]	X	X	X	X
EISB – Anaerobic	X	NM	X	NA
EISB – Aerobic	ID	ID	ID	ID
SEAR	X	X	X	X
Thermal – conductive heating [2]	X	NM	NM	NM
Thermal – resistive heating	X	NM	NM	NM
Thermal – steam heating	X	NM	NM	NM
Thermal – All	X	NM	NM	NM

Notes:

Grey highlight indicates the technologies and datasets that were considered in the regression analysis.

[1] No significant correlations were observed; therefore, regression analysis was not performed.

[2] Data set was very limited; no significant correlations were observed.

Acronyms:

ID - insufficient data

NM - no modeling case study data; therefore, results were no different from field case studies and there was no need to differentiate.

NA - not applicable due to lack of consolidated media data.

X - sufficient data available for analysis

Table F.6 provides a listing of the performance metric – site parameter pairs for which significant correlations were observed and were retained for the linear regression analysis. A total of nine pairs for all technologies were analyzed *via* regression techniques. As seen in **Table F.6**, the only two performance metrics that had a significant correlation with site parameters were reduction in DNAPL mass and treatment duration. Five site parameters, specifically areal extent of the DNAPL zone, electrode spacing, hydraulic conductivity, pre-remediation DNAPL mass, and volume of the DNAPL zone were correlated with these two performance metrics.

Two alternate regression models were fit to the data pairs outlined above, including:

i) Performance metric as the dependent variable and site parameter as the independent variable (regression analysis 1). This model determines the amount of variation in the performance metric that can be explained by the site parameter (*i.e.,* it quantifies the sensitivity of technology performance to changes in the site parameter).

ii) Site parameter as dependent variable and performance metric as independent variable (regression analysis 2). This model was used to quantify 95% confidence intervals for site parameters. These confidence intervals were used in DNAPL TEST in the site specific analysis case study selection protocol to select case studies that are anticipated to have statistically similar technology performance to the site of interest to the user.

Results for these two regression analyses can be found in **Tables F.6 and F.7**, respectively. These include estimates of the model parameters (*i.e.,* regression coefficients), their associated standard errors, the coefficient of determination (also called R^2) which measures how well the model fits the data, and the 95% confidence intervals for the mean/median of the dependent variable. As seen in **Table F.6**, the R^2 values for the first regression analysis range from 0.44 to 0.99 indicating a relatively good fit to an almost perfect fit, respectively. Similarly, the R^2 values for the second regression analysis range from 0.51 to 0.99 indicating a relatively good fit to an almost perfect fit, respectively (**Table F.**7).

Estimates of the slope parameters are indicative of the type of correlation that exists (*i.e.,* a negative sign indicates a negative correlation and a positive sign indicates a positive correlation). The slope also quantifies the relative influence that the independent variable (being the site parameter and the performance metric for the first and second regression analyses respectively) has on the dependent variable (*i.e.,* a larger slope indicates that the site parameter exerts a greater influence on the technology performance). The 95% confidence interval is indicative of the reliability of the estimate of the mean provided by the regression model, since it is an observed interval calculated from the dataset. For example, for the first regression analysis, the 95% confidence interval indicates that for a given site parameter value, the technology performance is anticipated to lie within a range quantified by the mean performance predicted by the model +/- the confidence interval specified in **Table F.6**. For the second regression analysis, the 95% confidence interval indicates that for a given value of technology performance (e.g., 50% DNAPL mass removal), the values of the correlated site parameter that is anticipated to result in this degree of performance will lie within a range quantified by the mean site parameter value predicted by the model +/- the confidence interval specified in **Table F.7**.

For models that consist of log-transformed data sets, the impact of the site parameter becomes multiplicative, rather than additive, and the relative change is in terms of the median performance metric (i.e., the 95% confidence interval is calculated by multiplying or dividing the median performance metric by a factor, instead of adding as is done with untransformed data).

Table F.2 Correlations with field case studies - all media

PERFORMANCE METRIC	TECHNOLOGY	DATA TRANSFORMATION	STATISTICS	Areal Extent of DNAPL Source	Depth to Groundwater	Depth to Top of Aquifer	Hydraulic Conductivity	Horizontal Hydraulic Gradient	Groundwater Velocity	Maximum Depth of the DNAPL Zone	Preremediation DNAPL Mass	Saturated Aquifer Thickness	Thickness of DNAPL Zone	Total Number of Oxidant Injections	Volume of DNAPL Zone	Soil Porosity	Total Mass of Oxidant Injected	Oxidant Application Duration
Decrease in Groundwater Concentrations	Chemical Oxidation - Fenton's Reagent or Hydrogen Peroxide	N	r	0.073	0.233	0.299	0.406	0.557	--	0.135	--	0.194	0.310	0.332	0.461	--	--	-0.021
			p	0.908	0.422	0.345	0.425	0.251	--	0.799	--	0.754	0.611	0.246	0.434	--	--	0.957
			n	5	14	12	6	6	--	6	--	5	5	14	5	--	--	9
Decrease in Groundwater Concentrations	Chemical Oxidation - Fenton's Reagent or Hydrogen Peroxide	LN	r	0.199	-0.103	0.132	0.800	0.335	--	-0.093	--	-0.155	0.386	0.025	0.669	--	--	-0.033
			p	0.748	0.726	0.682	0.056	0.517	--	0.860	--	0.804	0.521	0.933	0.217	--	--	0.933
			n	5	14	12	6	6	--	6	--	5	5	14	5	--	--	9
Decrease in Groundwater Concentrations	Chemical Oxidation - Permanganate	N	r	0.397	-0.107	0.154	0.653	--	--	-0.524	--	-0.123	0.580	-0.082	-0.232	0.549	0.131	-0.230
			p	0.378	0.728	0.651	0.160	--	--	0.098	--	0.816	0.132	0.811	0.658	0.338	0.641	0.473
			n	7	13	11	6	--	--	11	--	6	8	11	6	5	15	12
Decrease in Groundwater Concentrations	Chemical Oxidation - Permanganate	LN	r	0.570	-0.094	-0.009	0.173	--	--	-0.491	--	-0.353	0.618	-0.423	0.577	0.753	-0.129	-0.257
			p	0.182	0.760	0.979	0.744	--	--	0.125	--	0.493	0.102	0.195	0.231	0.142	0.647	0.420
			n	7	13	11	6	--	--	11	--	6	8	11	6	5	15	12
Decrease in Groundwater Concentrations	Chemical Oxidation - All	N	r	0.279	0.092	0.230	0.395	0.394	--	-0.394	0.007	0.024	0.358	0.043	0.046	0.549	0.055	-0.055
			p	0.379	0.641	0.280	0.181	0.260	--	0.117	0.987	0.943	0.229	0.840	0.894	0.338	0.834	0.814
			n	12	28	24	13	10	--	17	8	11	13	25	11	5	17	21
Decrease in Groundwater Concentrations	Chemical Oxidation - All	LN	r	0.543	-0.081	0.196	0.313	0.221	--	-0.391	0.753	-0.264	0.408	-0.001	0.003	0.073	-0.093	0.006
			p	0.068	0.683	0.359	0.297	0.539	--	0.121	0.142	0.432	0.166	0.994	0.992	0.863	0.723	0.979
			n	12	28	24	13	10	--	17	5	11	13	25	11	8	17	21
Decrease in Groundwater Concentrations	Enhanced Bioremediation - Anaerobic	N	r	0.132	0.147	0.152	0.008	-0.241	0.460	0.137	--	0.181	0.129	--	--	--	--	--
			p	0.682	0.535	0.511	0.983	0.503	0.252	0.587	--	0.616	0.782	--	--	--	--	--
			n	12	20	21	10	10	8	18	--	10	7	--	--	--	--	--
Decrease in Groundwater Concentrations	Enhanced Bioremediation - Anaerobic	LN	r	-0.136	0.157	-0.085	**0.725**	-0.390	**0.754**	0.111	--	-0.017	-0.102	--	--	--	--	--
			p	0.674	0.509	0.714	0.018	0.265	0.031	0.662	--	0.964	0.828	--	--	--	--	--
			n	12	20	21	10	10	8	18	--	10	7	--	--	--	--	--
Decrease in Groundwater Concentrations	Thermal - Resistive Heating	N	r	0.254	0.209	0.175	0.137	--	--	-0.125	-0.144	-0.265	0.140	--	0.395	--	--	--
			p	0.403	0.473	0.549	0.706	--	--	0.684	0.786	0.526	0.740	--	0.230	--	--	--
			n	13	14	14	10	--	--	13	6	8	8	--	11	--	--	--
Decrease in Groundwater Concentrations	Thermal - Resistive Heating	LN	r	0.134	0.184	0.063	-0.163	--	--	-0.180	-0.296	-0.293	0.019	--	0.359	--	--	--
			p	0.662	0.529	0.830	0.652	--	--	0.556	0.568	0.481	0.963	--	0.278	--	--	--
			n	13	14	14	10	--	--	13	6	8	8	--	11	--	--	--
Decrease in Groundwater Concentrations	Thermal - Steam Flushing	N	r	-0.104	-0.321	-0.403	--	--	--	--	--	--	--	--	--	--	--	--
			p	0.867	0.599	0.501	--	--	--	--	--	--	--	--	--	--	--	--
			n	5	5	5	--	--	--	--	--	--	--	--	--	--	--	--
Decrease in Groundwater Concentrations	Thermal - Steam Flushing	LN	r	-0.118	-0.384	-0.427	--	--	--	--	--	--	--	--	--	--	--	--
			p	0.850	0.524	0.474	--	--	--	--	--	--	--	--	--	--	--	--
			n	5	5	5	--	--	--	--	--	--	--	--	--	--	--	--
Decrease in Groundwater Concentrations	Thermal - All	N	r	-0.062	0.075	-0.091	0.051	--	--	-0.372	-0.205	-0.259	-0.542	--	0.036	--	--	--
			p	0.808	0.755	0.710	0.857	--	--	0.156	0.627	0.442	0.085	--	0.904	--	--	--
			n	18	20	19	15	--	--	16	8	11	11	--	14	--	--	--
Decrease in Groundwater Concentrations	Thermal - All	LN	r	-0.652	-0.006	-0.127	-0.445	--	--	0.110	-0.366	-0.571	-0.086	--	-0.559	--	--	--
			p	0.057	0.986	0.710	0.317	--	--	0.749	0.333	0.236	0.855	--	0.150	--	--	--
			n	9	11	11	7	--	--	11	9	6	7	--	8	--	--	--
Decrease in Soil Concentrations	Chemical Oxidation - Fenton's Reagent or Hydrogen Peroxide	N	r	--	0.426	0.423	--	--	--	--	0.436	--	--	0.061	--	--	--	0.343
			p	--	0.399	0.478	--	--	--	--	0.463	--	--	0.923	--	--	--	0.572
			n	--	6	5	--	--	--	--	5	--	--	5	--	--	--	5
Decrease in Soil Concentrations	Chemical Oxidation - Fenton's Reagent or Hydrogen Peroxide	LN	r	--	0.143	0.406	--	--	--	--	0.227	--	--	0.076	--	--	--	0.141
			p	--	0.786	0.498	--	--	--	--	0.714	--	--	0.903	--	--	--	0.822
			n	--	6	5	--	--	--	--	5	--	--	5	--	--	--	5

Table F.2 Correlations with field case studies - all media

PERFORMANCE METRIC	TECHNOLOGY	DATA TRANSFORMATION	STATISTICS	Oxidant Concentration	Mass of Electron Donor Injected	Electron Donor Well Spacing	Duration of Monitoring	Maximum Temperature	Number of Electrodes	Number of Wells	Electrode Spacing	Target Temperature	Time to Maximum Temperature	InjectionRate	Total Duration of Amendment
Decrease in Groundwater Concentrations	Chemical Oxidation - Fenton's Reagent or Hydrogen Peroxide	N	r	0.513	--	--	--	--	--	--	--	--	--	--	--
			p	0.130	--	--	--	--	--	--	--	--	--	--	--
			n	10	--	--	--	--	--	--	--	--	--	--	--
Decrease in Groundwater Concentrations	Chemical Oxidation - Fenton's Reagent or Hydrogen Peroxide	LN	r	0.341	--	--	--	--	--	--	--	--	--	--	--
			p	0.335	--	--	--	--	--	--	--	--	--	--	--
			n	10	--	--	--	--	--	--	--	--	--	--	--
Decrease in Groundwater Concentrations	Chemical Oxidation - Permanganate	N	r	**-0.729**	--	--	--	--	--	--	--	--	--	--	--
			p	0.003	--	--	--	--	--	--	--	--	--	--	--
			n	14	--	--	--	--	--	--	--	--	--	--	--
Decrease in Groundwater Concentrations	Chemical Oxidation - Permanganate	LN	r	**-0.681**	--	--	--	--	--	--	--	--	--	--	--
			p	0.007	--	--	--	--	--	--	--	--	--	--	--
			n	14	--	--	--	--	--	--	--	--	--	--	--
Decrease in Groundwater Concentrations	Chemical Oxidation - All	N	r	-0.105	--	--	--	--	--	--	--	--	--	--	--
			p	0.626	--	--	--	--	--	--	--	--	--	--	--
			n	24	--	--	--	--	--	--	--	--	--	--	--
Decrease in Groundwater Concentrations	Chemical Oxidation - All	LN	r	-0.266	--	--	--	--	--	--	--	--	--	--	--
			p	0.208	--	--	--	--	--	--	--	--	--	--	--
			n	24	--	--	--	--	--	--	--	--	--	--	--
Decrease in Groundwater Concentrations	Enhanced Bioremediation - Anaerobic	N	r	--	-0.213	-0.309	--	--	--	--	--	--	--	--	--
			p	--	0.353	0.199	--	--	--	--	--	--	--	--	--
			n	--	21	19	--	--	--	--	--	--	--	--	--
Decrease in Groundwater Concentrations	Enhanced Bioremediation - Anaerobic	LN	r	--	-0.241	-0.442	--	--	--	--	--	--	--	--	--
			p	--	0.293	0.058	--	--	--	--	--	--	--	--	--
			n	--	21	19	--	--	--	--	--	--	--	--	--
Decrease in Groundwater Concentrations	Thermal - Resistive Heating	N	r	--	--	--	--	-0.561	0.231	--	0.178	-0.468	0.232	--	--
			p	--	--	--	--	0.073	0.427	--	0.623	0.242	0.519	--	--
			n	--	--	--	--	11	14	--	10	8	10	--	--
Decrease in Groundwater Concentrations	Thermal - Resistive Heating	LN	r	--	--	--	--	-0.483	0.229	--	0.136	-0.455	0.061	--	--
			p	--	--	--	--	0.132	0.430	--	0.708	0.257	0.866	--	--
			n	--	--	--	--	11	14	--	10	8	10	--	--
Decrease in Groundwater Concentrations	Thermal - Steam Flushing	N	r	--	--	--	--	--	0.275	--	--	--	--	--	--
			p	--	--	--	--	--	0.655	--	--	--	--	--	--
			n	--	--	--	--	--	5	--	--	--	--	--	--
Decrease in Groundwater Concentrations	Thermal - Steam Flushing	LN	r	--	--	--	--	--	--	--	--	--	--	--	--
			p	--	--	--	--	--	--	--	--	--	--	--	--
			n	--	--	--	--	--	--	--	--	--	--	--	--
Decrease in Groundwater Concentrations	Thermal - All	N	r	--	--	--	--	0.046	0.233	--	0.054	-0.439	-0.042	--	--
			p	--	--	--	--	0.875	0.323	--	0.869	0.177	0.887	--	--
			n	--	--	--	--	14	20	--	12	11	14	--	--
Decrease in Groundwater Concentrations	Thermal - All	LN	r	--	--	--	--	0.068	-0.603	--	0.277	-0.337	-0.133	--	--
			p	--	--	--	--	0.872	0.114	--	0.547	0.579	0.775	--	--
			n	--	--	--	--	8	8	--	7	5	7	--	--
Decrease in Soil Concentrations	Chemical Oxidation - Fenton's Reagent or Hydrogen Peroxide	N	r	--	--	--	--	--	--	--	--	--	--	--	--
			p	--	--	--	--	--	--	--	--	--	--	--	--
			n	--	--	--	--	--	--	--	--	--	--	--	--
Decrease in Soil Concentrations	Chemical Oxidation - Fenton's Reagent or Hydrogen Peroxide	LN	r	--	--	--	--	--	--	--	--	--	--	--	--
			p	--	--	--	--	--	--	--	--	--	--	--	--
			n	--	--	--	--	--	--	--	--	--	--	--	--

Table F.2 Correlations with field case studies - all media

PERFORMANCE METRIC	TECHNOLOGY	DATA TRANSFORMATION	STATISTICS	Areal Extent of DNAPL Source	Depth to Groundwater	Depth to Top of Aquifer	Hydraulic Conductivity	Horizontal Hydraulic Gradient	Groundwater Velocity	Maximum Depth of the DNAPL Zone	Preremediation DNAPL Mass	Saturated Aquifer Thickness	Thickness of DNAPL Zone	Total Number of Oxidant Injections	Volume of DNAPL Zone	Soil Porosity	Total Mass of Oxidant Injected	Oxidant Application Duration
Decrease in Soil Concentrations	Chemical Oxidation - Permanganate	N	r	--	0.230	--	--	--	--	--	--	--	--	--	--	--	-0.155	-0.090
			p	--	0.710	--	--	--	--	--	--	--	--	--	--	--	0.804	0.886
			n	--	5	--	--	--	--	--	--	--	--	--	--	--	5	5
Decrease in Soil Concentrations	Chemical Oxidation - Permanganate	LN	r	--	0.356	--	--	--	--	--	--	--	--	.	.	--	-0.118	0.225
			p	--	0.556	--	--	--	--	--	--	--	--	.	.	--	0.851	0.716
			n	--	5	--	--	--	--	--	--	--	--	3	1	--	5	5
Decrease in Soil Concentrations	Chemical Oxidation - All	N	r	0.168	0.311	0.343	0.382	--	--	0.711	0.406	-0.411	0.370	-0.033	0.596	--	-0.245	0.166
			p	0.787	0.352	0.405	0.526	--	--	0.113	0.366	0.492	0.539	0.938	0.288	--	0.596	0.646
			n	5	11	8	5	--	--	6	7	5	5	8	5	--	7	10
Decrease in Soil Concentrations	Chemical Oxidation - All	LN	r	0.162	0.030	0.441	0.162	--	--	0.559	--	-0.450	0.209	0.027	0.805	0.255	0.013	0.105
			p	0.794	0.930	0.274	0.795	--	--	0.248	--	0.447	0.735	0.950	0.100	0.581	0.979	0.773
			n	5	11	8	5	--	--	6	--	5	5	8	5	7	7	10
Decrease in Soil Concentrations	Thermal - Conductive Heating	N	r	--	-0.468	--	--	--	--	-0.029	--	--	--	--	--	--	--	--
			p	--	0.427	--	--	--	--	0.963	--	--	--	--	--	--	--	--
			n	--	5	--	--	--	--	5	--	--	--	--	--	--	--	--
Decrease in Soil Concentrations	Thermal - Conductive Heating	LN	r	--	-0.350	--	--	--	--	-0.104	--	--	--	--	--	--	--	--
			p	--	0.563	--	--	--	--	0.868	--	--	--	--	--	--	--	--
			n	--	5	--	--	--	--	5	--	--	--	--	--	--	--	--
Decrease in Soil Concentrations	Thermal - Resistive Heating	N	r	-0.157	0.012	0.044	0.141	--	--	0.406	--	0.073	--	--	-0.025	--	--	--
			p	0.710	0.975	0.917	0.790	--	--	0.278	--	0.908	--	--	0.957	--	--	--
			n	8	9	8	6	--	--	9	--	5	--	--	7	--	--	--
Decrease in Soil Concentrations	Thermal - Resistive Heating	LN	r	-0.137	-0.078	-0.066	-0.047	--	--	0.365	--	-0.005	--	--	-0.202	--	--	--
			p	0.747	0.841	0.877	0.930	--	--	0.335	--	0.993	--	--	0.664	--	--	--
			n	8	9	8	6	--	--	9	--	5	--	--	7	--	--	--
Decrease in Soil Concentrations	Thermal - Steam Flushing	N	r	--	-0.586	-0.133	--	--	--	--	--	--	--	--	--	--	--	--
			p	--	0.299	0.802	--	--	--	--	--	--	--	--	--	--	--	--
			n	--	5	6	--	--	--	--	--	--	--	--	--	--	--	--
Decrease in Soil Concentrations	Thermal - Steam Flushing	LN	r	--	-0.618	0.019	--	--	--	--	--	--	--	--	--	--	--	--
			p	--	0.266	0.972	--	--	--	--	--	--	--	--	--	--	--	--
			n	--	5	6	--	--	--	--	--	--	--	--	--	--	--	--
Decrease in Soil Concentrations	Thermal - All	N	r	0.023	-0.222	-0.213	0.019	--	--	-0.143	0.076	0.156	0.513	--	0.192	--	--	--
			p	0.935	0.361	0.446	0.951	--	--	0.611	0.886	0.648	0.239	--	0.572	--	--	--
			n	15	19	15	13	--	--	15	6	11	7	--	11	--	--	--
Decrease in Soil Concentrations	Thermal - All	LN	r	-0.220	-0.266	-0.156	-0.068	--	--	-0.193	0.202	-0.017	**0.852**	--	0.023	--	--	--
			p	0.432	0.271	0.579	0.826	--	--	0.490	0.702	0.961	0.015	--	0.947	--	--	--
			n	15	19	15	13	--	--	15	6	11	7	--	11	--	--	--
Removal of DNAPL Mass	Chemical Oxidation - Fenton's Reagent or Hydrogen Peroxide	N	r	--	0.464	--	--	--	--	--	--	--	--	-0.025	--	--	--	--
			p	--	0.431	--	--	--	--	--	--	--	--	0.969	--	--	--	--
			n	--	5	--	--	--	--	--	--	--	--	5	--	--	--	--
Removal of DNAPL Mass	Chemical Oxidation - Fenton's Reagent or Hydrogen Peroxide	LN	r	--	0.099	--	--	--	--	--	--	--	--	-0.064	--	--	--	--
			p	--	0.874	--	--	--	--	--	--	--	--	0.919	--	--	--	--
			n	--	5	--	--	--	--	--	--	--	--	5	--	--	--	--
Removal of DNAPL Mass	Chemical Oxidation - All	N	r	-0.253	0.246	0.280	0.736	--	--	0.130	--	0.391	-0.266	-0.135	-0.055	0.197	-0.226	0.335
			p	0.628	0.558	0.542	0.156	--	--	0.806	--	0.515	0.610	0.750	0.906	0.640	0.714	0.417
			n	6	8	7	5	--	--	6	--	5	6	8	7	8	5	8
Removal of DNAPL Mass	Chemical Oxidation - All	LN	r	-0.372	-0.087	0.502	0.835	--	--	-0.106	--	0.121	-0.335	-0.137	-0.096	0.087	-0.034	0.077
			p	0.468	0.837	0.251	0.079	--	--	0.841	--	0.847	0.517	0.747	0.838	0.838	0.957	0.857
			n	6	8	7	5	--	--	6	--	5	6	8	7	8	5	8

Table F.2 Correlations with field case studies - all media

PERFORMANCE METRIC	TECHNOLOGY	DATA TRANSFORMATION	STATISTICS	Oxidant Concentration	Mass of Electron Donor Injected	Electron Donor Well Spacing	Duration of Monitoring	Maximum Temperature	Number of Electrodes	Number of Wells	Electrode Spacing	Target Temperature	Time to Maximum Temperature	InjectionRate	Total Duration of Amendment
Decrease in Soil Concentrations	Chemical Oxidation - Permanganate	N	r	0.564	--	--	--	--	--	--	--	--	--	--	--
			p	0.322	--	--	--	--	--	--	--	--	--	--	--
			n	5	--	--	--	--	--	--	--	--	--	--	--
Decrease in Soil Concentrations	Chemical Oxidation - Permanganate	LN	r	0.281	--	--	--	--	--	--	--	--	--	--	--
			p	0.647	--	--	--	--	--	--	--	--	--	--	--
			n	5	--	--	--	--	--	--	--	--	--	--	--
Decrease in Soil Concentrations	Chemical Oxidation - All	N	r	0.314	--	--	--	--	--	--	--	--	--	--	--
			p	0.410	--	--	--	--	--	--	--	--	--	--	--
			n	9	--	--	--	--	--	--	--	--	--	--	--
Decrease in Soil Concentrations	Chemical Oxidation - All	LN	r	-0.114	--	--	--	--	--	--	--	--	--	--	--
			p	0.771	--	--	--	--	--	--	--	--	--	--	--
			n	9	--	--	--	--	--	--	--	--	--	--	--
Decrease in Soil Concentrations	Thermal - Conductive Heating	N	r	--	--	--	--	--	0.786	-0.389	--	--	--	--	--
			p	--	--	--	--	--	0.115	0.517	--	--	--	--	--
			n	--	--	--	--	--	5	5	--	--	--	--	--
Decrease in Soil Concentrations	Thermal - Conductive Heating	LN	r	--	--	--	--	--	0.734	-0.068	--	--	--	--	--
			p	--	--	--	--	--	0.158	0.913	--	--	--	--	--
			n	--	--	--	--	--	5	5	--	--	--	--	--
Decrease in Soil Concentrations	Thermal - Resistive Heating	N	r	--	--	--	--	-0.038	-0.106	--	0.068	-0.579	-0.045	--	--
			p	--	--	--	--	0.929	0.785	--	0.886	0.173	0.933	--	--
			n	--	--	--	--	8	9	--	7	7	6	--	--
Decrease in Soil Concentrations	Thermal - Resistive Heating	LN	r	--	--	--	--	-0.053	-0.196	--	-0.034	-0.565	-0.147	--	--
			p	--	--	--	--	0.902	0.614	--	0.942	0.187	0.781	--	--
			n	--	--	--	--	8	9	--	7	7	6	--	--
Decrease in Soil Concentrations	Thermal - Steam Flushing	N	r	--	--	--	--	--	--	--	--	--	--	--	--
			p	--	--	--	--	--	--	--	--	--	--	--	--
			n	--	--	--	--	--	--	--	--	--	--	--	--
Decrease in Soil Concentrations	Thermal - Steam Flushing	LN	r	--	--	--	--	--	--	--	--	--	--	--	--
			p	--	--	--	--	--	--	--	--	--	--	--	--
			n	--	--	--	--	--	--	--	--	--	--	--	--
Decrease in Soil Concentrations	Thermal - All	N	r	--	--	--	--	0.159	0.229	--	0.243	-0.430	0.344	--	--
			p	--	--	--	--	0.557	0.361	--	0.447	0.110	0.228	--	--
			n	--	--	--	--	16	18	--	12	15	14	--	--
Decrease in Soil Concentrations	Thermal - All	LN	r	--	--	--	--	0.147	0.184	--	0.391	-0.411	**0.538**	--	--
			p	--	--	--	--	0.588	0.465	--	0.209	0.128	0.047	--	--
			n	--	--	--	--	16	18	--	12	15	14	--	--
Removal of DNAPL Mass	Chemical Oxidation - Fenton's Reagent or Hydrogen Peroxide	N	r	--	--	--	--	--	--	--	--	--	--	--	--
			p	--	--	--	--	--	--	--	--	--	--	--	--
			n	--	--	--	--	--	--	--	--	--	--	--	--
Removal of DNAPL Mass	Chemical Oxidation - Fenton's Reagent or Hydrogen Peroxide	LN	r	--	--	--	--	--	--	--	--	--	--	--	--
			p	--	--	--	--	--	--	--	--	--	--	--	--
			n	--	--	--	--	--	--	--	--	--	--	--	--
Removal of DNAPL Mass	Chemical Oxidation - All	N	r	0.299	--	--	--	--	--	--	--	--	--	--	--
			p	0.516	--	--	--	--	--	--	--	--	--	--	--
			n	7	--	--	--	--	--	--	--	--	--	--	--
Removal of DNAPL Mass	Chemical Oxidation - All	LN	r	-0.163	--	--	--	--	--	--	--	--	--	--	--
			p	0.727	--	--	--	--	--	--	--	--	--	--	--
			n	7	--	--	--	--	--	--	--	--	--	--	--

Table F.2 Correlations with field case studies - all media

PERFORMANCE METRIC	TECHNOLOGY	DATA TRANSFORMATION	STATISTICS	Areal Extent of DNAPL Source	Depth to Groundwater	Depth to Top of Aquifer	Hydraulic Conductivity	Horizontal Hydraulic Gradient	Groundwater Velocity	Maximum Depth of the DNAPL Zone	Preremediation DNAPL Mass	Saturated Aquifer Thickness	Thickness of DNAPL Zone	Total Number of Oxidant Injections	Volume of DNAPL Zone	Soil Porosity	Total Mass of Oxidant Injected	Oxidant Application Duration
Removal of DNAPL Mass	Surfactant Flushing	N	r	--	--	--	0.002	--	--	**0.945**	-0.517	--	0.283	--	--	--	--	--
			p	--	--	--	0.998	--	--	0.015	0.372	--	0.645	--	--	--	--	--
			n	--	--	--	5	--	--	5	5	--	5	--	--	--	--	--
Removal of DNAPL Mass	Surfactant Flushing	LN	r	--	--	--	0.437	--	--	0.827	-0.633	--	0.032	--	--	--	--	--
			p	--	--	--	0.461	--	--	0.084	0.252	--	0.959	--	--	--	--	--
			n	--	--	--	5	--	--	5	5	--	5	--	--	--	--	--
Removal of DNAPL Mass	Thermal - Resistive Heating	N	r	**-0.923**	**-0.885**	**-0.836**	--	--	--	-0.076	-0.200	--	--	--	**-0.951**	--	--	--
			p	0.009	0.019	0.038	--	--	--	0.886	0.704	--	--	--	0.013	--	--	--
			n	6	6	6	--	--	--	6	6	--	--	--	5	--	--	--
Removal of DNAPL Mass	Thermal - Resistive Heating	LN	r	-0.798	-0.777	-0.545	--	--	--	-0.195	-0.417	--	--	--	-0.824	--	--	--
			p	0.057	0.069	0.264	--	--	--	0.711	0.410	--	--	--	0.086	--	--	--
			n	6	6	6	--	--	--	6	6	--	--	--	5	--	--	--
Removal of DNAPL Mass	Thermal - Steam Flushing	N	r	--	0.133	0.133	--	--	--	0.203	--	--	--	--	--	--	--	--
			p	--	0.831	0.831	--	--	--	0.744	--	--	--	--	--	--	--	--
			n	--	5	5	--	--	--	5	--	--	--	--	--	--	--	--
Removal of DNAPL Mass	Thermal - Steam Flushing	LN	r	--	-0.066	-0.067	--	--	--	0.266	--	--	--	--	--	--	--	--
			p	--	0.916	0.915	--	--	--	0.666	--	--	--	--	--	--	--	--
			n	--	5	5	--	--	--	5	--	--	--	--	--	--	--	--
Removal of DNAPL Mass	Thermal - All	N	r	**-0.907**	0.153	0.124	-0.012	--	--	0.165	-0.232	-0.612	0.176	--	-0.580	--	--	--
			p	0.001	0.653	0.716	0.980	--	--	0.628	0.549	0.197	0.706	--	0.132	--	--	--
			n	9	11	11	7	--	--	11	9	6	7	--	8	--	--	--
Removal of DNAPL Mass	Thermal - All	LN	r	-0.652	-0.006	-0.127	-0.445	--	--	0.110	-0.366	-0.571	-0.086	--	-0.559	--	--	--
			p	0.057	0.986	0.710	0.317	--	--	0.749	0.333	0.236	0.855	--	0.150	--	--	--
			n	9	11	11	7	--	--	11	9	6	7	--	8	--	--	--
Treatment Duration	Chemical Oxidation - Fenton's Reagent or Hydrogen Peroxide	N	r	0.810	0.316	-0.422	-0.425	-0.319	--	0.637	--	--	--	0.019	-0.341	--	--	0.347
			p	0.097	0.317	0.196	0.401	0.600	--	0.248	--	--	--	0.956	0.574	--	--	0.400
			n	5	12	11	6	5	--	5	--	--	--	11	5	--	--	8
Treatment Duration	Chemical Oxidation - Fenton's Reagent or Hydrogen Peroxide	LN	r	0.530	0.360	-0.511	-0.377	-0.023	--	0.566	--	--	--	0.233	-0.198	--	--	0.549
			p	0.358	0.250	0.108	0.461	0.971	--	0.320	--	--	--	0.491	0.749	--	--	0.159
			n	5	12	11	6	5	--	5	--	--	--	11	5	--	--	8
Treatment Duration	Chemical Oxidation - Permanganate	N	r	0.388	-0.281	-0.394	-0.317	--	--	-0.255	--	--	-0.377	0.696	-0.493	--	0.378	**1.000**
			p	0.447	0.463	0.294	0.603	--	--	0.508	--	--	0.404	0.083	0.399	--	0.281	0.000
			n	6	9	9	5	--	--	9	--	--	7	7	5	--	10	10
Treatment Duration	Chemical Oxidation - Permanganate	LN	r	-0.118	-0.201	-0.269	-0.461	--	--	-0.310	--	--	-0.267	0.677	-0.747	--	0.482	**1.000**
			p	0.824	0.604	0.484	0.434	--	--	0.416	--	--	0.563	0.095	0.147	--	0.158	0.000
			n	6	9	9	5	--	--	9	--	--	7	7	5	--	10	10
Treatment Duration	Chemical Oxidation - All	N	r	0.422	-0.120	-0.373	-0.394	-0.236	--	-0.137	-0.176	-0.131	-0.135	0.003	-0.344	--	0.488	**0.562**
			p	0.196	0.594	0.095	0.205	0.542	--	0.640	0.705	0.758	0.692	0.990	0.330	--	0.128	0.015
			n	11	22	21	12	9	--	14	7	8	11	18	10	--	11	18
Treatment Duration	Chemical Oxidation - All	LN	r	-0.088	0.002	-0.354	-0.392	0.072	--	-0.091	-0.130	0.197	0.066	0.287	-0.430	--	0.569	**0.662**
			p	0.797	0.991	0.115	0.208	0.854	--	0.756	0.781	0.640	0.848	0.249	0.214	--	0.068	0.003
			n	11	22	21	12	9	--	14	7	8	11	18	10	--	11	18
Treatment Duration	Enhanced Bioremediation - Anaerobic	N	r	-0.042	-0.127	-0.065	-0.045	0.453	-0.384	-0.009	--	-0.323	-0.106	--	--	--	--	--
			p	0.896	0.626	0.793	0.902	0.307	0.452	0.975	--	0.363	0.802	--	--	--	--	--
			n	12	17	19	10	7	6	14	--	10	8	--	--	--	--	--
Treatment Duration	Enhanced Bioremediation - Anaerobic	LN	r	0.188	-0.278	0.074	0.089	0.184	-0.672	0.214	--	-0.159	-0.005	--	--	--	--	--
			p	0.558	0.279	0.763	0.808	0.693	0.144	0.462	--	0.661	0.990	--	--	--	--	--
			n	12	17	19	10	7	6	14	--	10	8	--	--	--	--	--

Table F.2 Correlations with field case studies - all media

PERFORMANCE METRIC	TECHNOLOGY	DATA TRANSFORMATION	STATISTICS	Oxidant Concentration	Mass of Electron Donor Injected	Electron Donor Well Spacing	Duration of Monitoring	Maximum Temperature	Number of Electrodes	Number of Wells	Electrode Spacing	Target Temperature	Time to Maximum Temperature	InjectionRate	Total Duration of Amendment
Removal of DNAPL Mass	Surfactant Flushing	N	r	--	--	--	--	--	--	--	--	--	--	--	--
			p	--	--	--	--	--	--	--	--	--	--	--	--
			n	--	--	--	--	--	--	--	--	--	--	--	--
Removal of DNAPL Mass	Surfactant Flushing	LN	r	--	--	--	--	--	--	--	--	--	--	--	--
			p	--	--	--	--	--	--	--	--	--	--	--	--
			n	--	--	--	--	--	--	--	--	--	--	--	--
Removal of DNAPL Mass	Thermal - Resistive Heating	N	r	--	--	--	--	--	-0.781	--	-0.688	--	--	--	--
			p	--	--	--	--	--	0.119	--	0.199	--	--	--	--
			n	--	--	--	--	--	5	--	5	--	--	--	--
Removal of DNAPL Mass	Thermal - Resistive Heating	LN	r	--	--	--	--	--	-0.685	--	-0.589	--	--	--	--
			p	--	--	--	--	--	0.201	--	0.296	--	--	--	--
			n	--	--	--	--	--	5	--	5	--	--	--	--
Removal of DNAPL Mass	Thermal - Steam Flushing	N	r	--	--	--	--	--	--	--	--	--	--	--	--
			p	--	--	--	--	--	--	--	--	--	--	--	--
			n	--	--	--	--	--	--	--	--	--	--	--	--
Removal of DNAPL Mass	Thermal - Steam Flushing	LN	r	--	--	--	--	--	--	--	--	--	--	--	--
			p	--	--	--	--	--	--	--	--	--	--	--	--
			n	--	--	--	--	--	--	--	--	--	--	--	--
Removal of DNAPL Mass	Thermal - All	N	r	--	--	--	--	0.075	**-0.779**	--	0.302	-0.402	-0.256	--	--
			p	--	--	--	--	0.860	0.023	--	0.511	0.503	0.579	--	--
			n	--	--	--	--	8	8	--	7	5	7	--	--
Removal of DNAPL Mass	Thermal - All	LN	r	--	--	--	--	0.068	-0.603	--	0.277	-0.337	-0.133	--	--
			p	--	--	--	--	0.872	0.114	--	0.547	0.579	0.775	--	--
			n	--	--	--	--	8	8	--	7	5	7	--	--
Treatment Duration	Chemical Oxidation - Fenton's Reagent or Hydrogen Peroxide	N	r	-0.363	--	--	--	--	--	--	--	--	--	--	--
			p	0.377	--	--	--	--	--	--	--	--	--	--	--
			n	8	--	--	--	--	--	--	--	--	--	--	--
Treatment Duration	Chemical Oxidation - Fenton's Reagent or Hydrogen Peroxide	LN	r	-0.439	--	--	--	--	--	--	--	--	--	--	--
			p	0.276	--	--	--	--	--	--	--	--	--	--	--
			n	8	--	--	--	--	--	--	--	--	--	--	--
Treatment Duration	Chemical Oxidation - Permanganate	N	r	-0.068	--	--	--	--	--	--	--	--	--	--	--
			p	0.842	--	--	--	--	--	--	--	--	--	--	--
			n	11	--	--	--	--	--	--	--	--	--	--	--
Treatment Duration	Chemical Oxidation - Permanganate	LN	r	-0.365	--	--	--	--	--	--	--	--	--	--	--
			p	0.270	--	--	--	--	--	--	--	--	--	--	--
			n	11	--	--	--	--	--	--	--	--	--	--	--
Treatment Duration	Chemical Oxidation - All	N	r	-0.101	--	--	--	--	--	--	--	--	--	--	--
			p	0.682	--	--	--	--	--	--	--	--	--	--	--
			n	19	--	--	--	--	--	--	--	--	--	--	--
Treatment Duration	Chemical Oxidation - All	LN	r	-0.091	--	--	--	--	--	--	--	--	--	--	--
			p	0.710	--	--	--	--	--	--	--	--	--	--	--
			n	19	--	--	--	--	--	--	--	--	--	--	--
Treatment Duration	Enhanced Bioremediation - Anaerobic	N	r	--	0.267	0.332	--	--	--	--	--	--	--	--	--
			p	--	0.356	0.227	--	--	--	--	--	--	--	--	--
			n	--	14	15	--	--	--	--	--	--	--	--	--
Treatment Duration	Enhanced Bioremediation - Anaerobic	LN	r	--	0.253	0.417	--	--	--	--	--	--	--	--	--
			p	--	0.382	0.122	--	--	--	--	--	--	--	--	--
			n	--	14	15	--	--	--	--	--	--	--	--	--

Table F.2 Correlations with field case studies - all media

PERFORMANCE METRIC	TECHNOLOGY	DATA TRANSFORMATION	STATISTICS	Areal Extent of DNAPL Source	Depth to Groundwater	Depth to Top of Aquifer	Hydraulic Conductivity	Horizontal Hydraulic Gradient	Groundwater Velocity	Maximum Depth of the DNAPL Zone	Preremediation DNAPL Mass	Saturated Aquifer Thickness	Thickness of DNAPL Zone	Total Number of Oxidant Injections	Volume of DNAPL Zone	Soil Porosity	Total Mass of Oxidant Injected	Oxidant Application Duration
Treatment Duration	Surfactant Flushing	N	r	--	--	--	0.366	--	--	0.292	--	0.115	--	--	--	--	--	--
			p	--	--	--	0.545	--	--	0.575	--	0.854	--	--	--	--	--	--
			n	--	--	--	5	--	--	6	--	5	--	--	--	--	--	--
Treatment Duration	Surfactant Flushing	LN	r	--	--	--	0.063	--	--	0.251	--	-0.078	--	--	--	--	--	--
			p	--	--	--	0.920	--	--	0.631	--	0.901	--	--	--	--	--	--
			n	--	--	--	5	--	--	6	--	5	--	--	--	--	--	--
Treatment Duration	Thermal - Conductive Heating	N	r	--	0.810	--	--	--	--	-0.381	--	--	--	--	--	--	--	--
			p	--	0.096	--	--	--	--	0.527	--	--	--	--	--	--	--	--
			n	--	5	--	--	--	--	5	--	--	--	--	--	--	--	--
Treatment Duration	Thermal - Conductive Heating	LN	r	--	0.549	--	--	--	--	-0.503	--	--	--	--	--	--	--	--
			p	--	0.338	--	--	--	--	0.387	--	--	--	--	--	--	--	--
			n	--	5	--	--	--	--	5	--	--	--	--	--	--	--	--
Treatment Duration	Thermal - Resistive Heating	N	r	0.321	-0.208	-0.147	-0.280	--	--	0.039	0.740	0.641	-0.176	--	**0.538**	--	--	--
			p	0.225	0.422	0.586	0.404	--	--	0.887	0.093	0.063	0.651	--	0.047	--	--	--
			n	16	17	16	11	--	--	16	6	9	9	--	14	--	--	--
Treatment Duration	Thermal - Resistive Heating	LN	r	0.472	-0.179	-0.085	0.100	--	--	-0.117	**0.950**	0.609	-0.305	--	**0.591**	--	--	--
			p	0.065	0.491	0.753	0.770	--	--	0.666	0.004	0.082	0.425	--	0.026	--	--	--
			n	16	17	16	11	--	--	16	6	9	9	--	14	--	--	--
Treatment Duration	Thermal - Steam Flushing	N	r	**0.982**	0.177	0.195	-0.069	--	--	**0.765**	--	--	--	--	**0.995**	--	--	--
			p	0.000	0.648	0.589	0.896	--	--	0.045	--	--	--	--	0.000	--	--	--
			n	7	9	10	6	--	--	7	--	--	--	--	5	--	--	--
Treatment Duration	Thermal - Steam Flushing	LN	r	0.749	0.185	0.478	-0.694	--	--	0.442	--	--	--	--	**0.902**	--	--	--
			p	0.053	0.634	0.162	0.126	--	--	0.321	--	--	--	--	0.036	--	--	--
			n	7	9	10	6	--	--	7	--	--	--	--	5	--	--	--
Treatment Duration	Thermal - All	N	r	**0.74**	0.245	0.208	-0.083	--	--	0.109	**0.704**	0.095	0.316	--	**0.741**	--	--	--
			p	0.000	0.185	0.299	0.721	--	--	0.604	0.023	0.727	0.251	--	0.000	--	--	--
			n	26	31	27	21	--	--	25	10	16	15	--	21	--	--	--
Treatment Duration	Thermal - All	LN	r	**0.524**	0.261	0.160	0.011	--	--	-0.032	**0.820**	0.291	0.327	--	**0.661**	--	--	--
			p	0.006	0.157	0.424	0.964	--	--	0.878	0.004	0.274	0.234	--	0.001	--	--	--
			n	26	31	27	21	--	--	25	10	16	15	--	21	--	--	--
Unit Cost (by volume) of Source Zone Treatment	Chemical Oxidation - Permanganate	N	r	--	--	-0.468	0.507	--	--	--	--	--	--	--	--	--	-0.311	--
			p	--	--	0.426	0.383	--	--	--	--	--	--	--	--	--	0.611	--
			n	--	--	5	5	--	--	--	--	--	--	--	--	--	5	--
Unit Cost (by volume) of Source Zone Treatment	Chemical Oxidation - Permanganate	LN	r	--	--	-0.770	0.638	--	--	--	--	--	--	--	--	--	-0.426	--
			p	--	--	0.128	0.247	--	--	--	--	--	--	--	--	--	0.474	--
			n	--	--	5	5	--	--	--	--	--	--	--	--	--	5	--
Unit Cost (by volume) of Source Zone Treatment	Chemical Oxidation - All	N	r	-0.312	-0.138	-0.179	-0.095	-0.230	--	-0.330	--	**0.968**	-0.388	-0.212	-0.520	--	-0.312	**0.988**
			p	0.496	0.744	0.644	0.839	0.709	--	0.424	--	0.007	0.390	0.615	0.231	--	0.547	0.000
			n	7	8	9	7	5	--	8	--	5	7	8	7	--	6	6
Unit Cost (by volume) of Source Zone Treatment	Chemical Oxidation - All	LN	r	**-0.945**	-0.147	-0.389	0.471	-0.150	--	-0.293	--	**0.931**	-0.206	-0.299	**-0.984**	--	-0.442	0.760
			p	0.001	0.729	0.301	0.286	0.809	--	0.481	--	0.022	0.658	0.472	0.000	--	0.380	0.080
			n	7	8	9	7	5	--	8	--	5	7	8	7	--	6	6
Unit Cost (by volume) of Source Zone Treatment	Enhanced Bioremediation - Anaerobic	N	r	--	--	--	--	--	--	--	--	--	--	--	--	--	--	--
			p	--	--	--	--	--	--	--	--	--	--	--	--	--	--	--
			n	--	--	--	--	--	--	--	--	--	--	--	--	--	--	--
Unit Cost (by volume) of Source Zone Treatment	Enhanced Bioremediation - Anaerobic	LN	r	--	--	--	--	--	--	--	--	--	--	--	--	--	--	--
			p	--	--	--	--	--	--	--	--	--	--	--	--	--	--	--
			n	--	--	--	--	--	--	--	--	--	--	--	--	--	--	--

Table F.2 Correlations with field case studies - all media

PERFORMANCE METRIC	TECHNOLOGY	DATA TRANSFORMATION	STATISTICS	Oxidant Concentration	Mass of Electron Donor Injected	Electron Donor Well Spacing	Duration of Monitoring	Maximum Temperature	Number of Electrodes	Number of Wells	Electrode Spacing	Target Temperature	Time to Maximum Temperature	InjectionRate	Total Duration of Amendment
Treatment Duration	Surfactant Flushing	N	r	--	--	--	--	--	--	--	--	--	--	0.219	0.747
			p	--	--	--	--	--	--	--	--	--	--	0.724	0.147
			n	--	--	--	--	--	--	--	--	--	--	5	5
Treatment Duration	Surfactant Flushing	LN	r	--	--	--	--	--	--	--	--	--	--	0.215	0.870
			p	--	--	--	--	--	--	--	--	--	--	0.728	0.055
			n	--	--	--	--	--	--	--	--	--	--	5	5
Treatment Duration	Thermal - Conductive Heating	N	r	--	--	--	--	--	**-0.917**	-0.393	--	--	--	--	--
			p	--	--	--	--	--	0.028	0.513	--	--	--	--	--
			n	--	--	--	--	--	5	5	--	--	--	--	--
Treatment Duration	Thermal - Conductive Heating	LN	r	--	--	--	--	--	**-0.943**	-0.694	--	--	--	--	--
			p	--	--	--	--	--	0.016	0.193	--	--	--	--	--
			n	--	--	--	--	--	5	5	--	--	--	--	--
Treatment Duration	Thermal - Resistive Heating	N	r	--	--	--	--	0.047	0.199	--	**0.788**	-0.005	0.343	--	--
			p	--	--	--	--	0.874	0.429	--	0.001	0.988	0.251	--	--
			n	--	--	--	--	14	18	--	13	11	13	--	--
Treatment Duration	Thermal - Resistive Heating	LN	r	--	--	--	--	0.130	0.236	--	**0.613**	0.279	0.408	--	--
			p	--	--	--	--	0.657	0.346	--	0.026	0.405	0.166	--	--
			n	--	--	--	--	14	18	--	13	11	13	--	--
Treatment Duration	Thermal - Steam Flushing	N	r	--	--	--	--	0.071	0.669	--	0.049	-0.120	0.344	--	--
			p	--	--	--	--	0.894	0.070	--	0.937	0.847	0.504	--	--
			n	--	--	--	--	6	8	--	5	5	6	--	--
Treatment Duration	Thermal - Steam Flushing	LN	r	--	--	--	--	0.035	0.274	--	0.713	-0.321	**0.876**	--	--
			p	--	--	--	--	0.948	0.512	--	0.176	0.598	0.022	--	--
			n	--	--	--	--	6	8	--	5	5	6	--	--
Treatment Duration	Thermal - All	N	r	--	--	--	--	-0.053	-0.099	--	0.307	0.162	0.033	--	--
			p	--	--	--	--	0.802	0.596	--	0.176	0.494	0.880	--	--
			n	--	--	--	--	25	31	--	21	20	23	--	--
Treatment Duration	Thermal - All	LN	r	--	--	--	--	-0.091	0.096	--	**0.661**	0.129	0.396	--	--
			p	--	--	--	--	0.664	0.608	--	0.001	0.588	0.061	--	--
			n	--	--	--	--	25	31	--	21	20	23	--	--
Unit Cost (by volume) of Source Zone Treatment	Chemical Oxidation - Permanganate	N	r	--	--	--	--	--	--	--	--	--	--	--	--
			p	--	--	--	--	--	--	--	--	--	--	--	--
			n	--	--	--	--	--	--	--	--	--	--	--	--
Unit Cost (by volume) of Source Zone Treatment	Chemical Oxidation - Permanganate	LN	r	--	--	--	--	--	--	--	--	--	--	--	--
			p	--	--	--	--	--	--	--	--	--	--	--	--
			n	--	--	--	--	--	--	--	--	--	--	--	--
Unit Cost (by volume) of Source Zone Treatment	Chemical Oxidation - All	N	r	-0.303	--	--	--	--	--	--	--	--	--	--	--
			p	0.508	--	--	--	--	--	--	--	--	--	--	--
			n	7	--	--	--	--	--	--	--	--	--	--	--
Unit Cost (by volume) of Source Zone Treatment	Chemical Oxidation - All	LN	r	-0.401	--	--	--	--	--	--	--	--	--	--	--
			p	0.373	--	--	--	--	--	--	--	--	--	--	--
			n	7	--	--	--	--	--	--	--	--	--	--	--
Unit Cost (by volume) of Source Zone Treatment	Enhanced Bioremediation - Anaerobic	N	r	--	--	--	--	--	--	--	--	--	--	--	--
			p	--	--	--	--	--	--	--	--	--	--	--	--
			n	--	--	--	--	--	--	--	--	--	--	--	--
Unit Cost (by volume) of Source Zone Treatment	Enhanced Bioremediation - Anaerobic	LN	r	--	--	--	--	--	--	--	--	--	--	--	--
			p	--	--	--	--	--	--	--	--	--	--	--	--
			n	--	--	--	--	--	--	--	--	--	--	--	--

Table F.2 Correlations with field case studies - all media

PERFORMANCE METRIC	TECHNOLOGY	DATA TRANSFORMATION	STATISTICS	Areal Extent of DNAPL Source	Depth to Groundwater	Depth to Top of Aquifer	Hydraulic Conductivity	Horizontal Hydraulic Gradient	Groundwater Velocity	Maximum Depth of the DNAPL Zone	Preremediation DNAPL Mass	Saturated Aquifer Thickness	Thickness of DNAPL Zone	Total Number of Oxidant Injections	Volume of DNAPL Zone	Soil Porosity	Total Mass of Oxidant Injected	Oxidant Application Duration
Unit Cost (by volume) of Source Zone Treatment	Thermal - Resistive Heating	N	r	0.323	-0.420	-0.333	-0.378	--	--	-0.517	--	0.135	--	--	-0.662	--	--	--
			p	0.397	0.300	0.382	0.404	--	--	0.154	--	0.829	--	--	0.105	--	--	--
			n	9	8	9	7	--	--	9	--	5	--	--	7	--	--	--
Unit Cost (by volume) of Source Zone Treatment	Thermal - Resistive Heating	LN	r	0.592	-0.389	-0.320	-0.602	--	--	-0.348	--	0.264	--	--	-0.622	--	--	--
			p	0.093	0.340	0.402	0.153	--	--	0.359	--	0.668	--	--	0.136	--	--	--
			n	9	8	9	7	--	--	9	--	5	--	--	7	--	--	--
Unit Cost (by volume) of Source Zone Treatment	Thermal - All	N	r	-0.365	-0.464	-0.403	-0.370	--	--	-0.498	--	0.442	-0.498	--	-0.507	--	--	--
			p	0.199	0.094	0.153	0.237	--	--	0.083	--	0.273	0.255	--	0.112	--	--	--
			n	14	14	14	12	--	--	13	--	8	7	--	11	--	--	--
Unit Cost (by volume) of Source Zone Treatment	Thermal - All	LN	r	-0.266	**-0.615**	-0.520	-0.218	--	--	**-0.571**	--	0.351	-0.329	--	**-0.848**	--	--	--
			p	0.358	0.019	0.056	0.497	--	--	0.042	--	0.393	0.471	--	0.001	--	--	--
			n	14	14	14	12	--	--	13	--	8	7	--	11	--	--	--

Table F.2 Correlations with field case studies - all media

PERFORMANCE METRIC	TECHNOLOGY	DATA TRANSFORMATION	STATISTICS	Oxidant Concentration	Mass of Electron Donor Injected	Electron Donor Well Spacing	Duration of Monitoring	Maximum Temperature	Number of Electrodes	Number of Wells	Electrode Spacing	Target Temperature	Time to Maximum Temperature	InjectionRate	Total Duration of Amendment
Unit Cost (by volume) of Source Zone Treatment	Thermal - Resistive Heating	N	r	--	--	--	--	-0.007	-0.074	--	0.457	0.093	0.416	--	--
			p	--	--	--	--	0.986	0.839	--	0.255	0.843	0.412	--	--
			n	--	--	--	--	8	10	--	8	7	6	--	--
Unit Cost (by volume) of Source Zone Treatment	Thermal - Resistive Heating	LN	r	--	--	--	--	0.197	-0.028	--	0.312	-0.031	0.572	--	--
			p	--	--	--	--	0.641	0.939	--	0.452	0.947	0.235	--	--
			n	--	--	--	--	8	10	--	8	7	6	--	--
Unit Cost (by volume) of Source Zone Treatment	Thermal - All	N	r	--	--	--	--	0.192	-0.013	--	-0.245	-0.117	0.126	--	--
			p	--	--	--	--	0.551	0.963	--	0.468	0.731	0.766	--	--
			n	--	--	--	--	12	15	--	11	11	8	--	--
Unit Cost (by volume) of Source Zone Treatment	Thermal - All	LN	r	--	--	--	--	0.288	0.131	--	-0.388	-0.202	0.446	--	--
			p	--	--	--	--	0.364	0.642	--	0.239	0.551	0.267	--	--
			n	--	--	--	--	12	15	--	11	11	8	--	--

Notes

All tests conducted using Pearson Correlations at the 5% level of significance. Null hypothesis for the test states that there is no correlation; whereas, the alternative hypothesis states that a correlation does exist.
Bold indicates a significant correlation as determined by the test (p-value < 0.05).
Regressions were performed with the Input Fields that showed a correation to the given Metric Field, however, in the case of a multivariate regression, there were not enough observations to create a sufficient enough data set. Therefore only simple linear regressions were performed.
-- - insufficient data for analysis (<5 observations)
. - insufficient amount of unique independent data values to compute a correlation coefficient
LN - lognormal data transformation
n - sample size
N - no data transformation
r -correlation coefficient
p - p-value. The p-value is calculated as the probability of observing a correlation coefficent at least as extreme as the one observed, given the null hypothesis is true.

Table F.3 Correlations with field and modeling case studies combined - consolidated data sets

PERFORMANCE METRIC	TECHNOLOGY	DATA TRANSFORMATION	STATISTICS	Areal Extent of DNAPL Source	Depth to Groundwater	Depth to Top of Aquifer	Hydraulic Conductivity	Horizontal Hydraulic Gradient	Groundwater Velocity	Maximum Depth of the DNAPL Zone	Preremediation DNAPL Mass	Saturated Aquifer Thickness	Thickness of DNAPL Zone	Total Number of Oxidant Injections	Volume of DNAPL Zone	Soil Porosity	Total Mass of Oxidant Injected	Oxidant Application Duration
Decrease in Groundwater Concentrations	Chemical Oxidation - Permanganate	N	r	.	0.442	0.442	**-0.967**	**-0.967**	**-0.967**	0.048	--	**-0.967**	**0.970**	-0.433	.	--	-0.304	-0.192
			p	.	0.273	0.273	0.000	0.000	0.000	0.911	--	0.000	0.000	0.244	.	--	0.393	0.648
			n	6	8	8	7	7	7	8	--	7	7	9	6	--	10	8
Decrease in Groundwater Concentrations	Chemical Oxidation - Permanganate	LN	r	.	--	--	**-0.905**	**-0.905**	**-0.905**	-0.196	--	**-0.905**	**0.911**	-0.468	.	--	-0.330	-0.220
			p	.	--	--	0.005	0.005	0.005	0.642	--	0.005	0.004	0.204	.	--	0.351	0.601
			n	6	--	--	7	7	7	8	--	7	7	9	6	--	10	8
Decrease in Groundwater Concentrations	Chemical Oxidation - All	N	r	**0.945**	0.107	0.066	-0.315	-0.051	-0.215	0.048	--	**-0.967**	**0.804**	-0.218	**0.945**	--	-0.304	-0.088
			p	0.001	0.728	0.837	0.448	0.897	0.609	0.911	--	0.000	0.016	0.455	0.001	--	0.393	0.775
			n	7	13	12	8	9	8	8	--	7	8	14	7	--	10	13
Decrease in Groundwater Concentrations	Chemical Oxidation - All	LN	r	**0.873**	0.423	0.453	0.275	0.303	0.572	-0.196	--	**-0.905**	**0.772**	-0.252	**0.873**	--	-0.330	-0.047
			p	0.010	0.403	0.443	0.509	0.428	0.138	0.642	--	0.005	0.025	0.407	0.010	--	0.351	0.884
			n	7	6	5	8	9	8	8	--	7	8	13	7	--	10	12
Decrease in Groundwater Concentrations	Surfactant Flushing	N	r	.	.	.	.	.	.	.	.	.	.	--	.	--	--	--
			p	.	.	.	.	.	.	.	.	.	.	--	.	--	--	--
			n	7	7	7	7	7	7	7	7	7	7	--	7	--	--	--
Decrease in Groundwater Concentrations	Surfactant Flushing	LN	r	.	--	--	.	.	.	.	.	.	.	--	.	--	--	--
			p	.	--	--	.	.	.	.	.	.	.	--	.	--	--	--
			n	7	--	--	7	7	7	7	7	7	7	--	7	--	--	--
Removal of DNAPL Mass	Chemical Oxidation - All	N	r	--	--	--	--	--	--	--	--	--	--	--	--	--	--	--
			p	--	--	--	--	--	--	--	--	--	--	--	--	--	--	--
			n	--	--	--	--	--	--	--	--	--	--	--	--	--	--	--
Removal of DNAPL Mass	Chemical Oxidation - All	LN	r	--	--	--	--	--	--	--	--	--	--	--	--	--	--	--
			p	--	--	--	--	--	--	--	--	--	--	--	--	--	--	--
			n	--	--	--	--	--	--	--	--	--	--	--	--	--	--	--
Removal of DNAPL Mass	Surfactant Flushing	N	r	.	.	.	**-0.941**	.	**-0.941**	.	**-0.936**	.	.	--	.	--	--	--
			p	.	.	.	0.000	.	0.000	.	0.000	.	.	--	.	--	--	--
			n	10	10	10	10	10	10	10	10	10	10	--	10	--	--	--
Removal of DNAPL Mass	Surfactant Flushing	LN	r	.	--	--	**-0.942**	.	**-0.942**	.	**-0.928**	.	.	--	.	--	--	--
			p	.	--	--	0.000	.	0.000	.	0.000	.	.	--	.	--	--	--
			n	10	--	--	10	10	10	10	10	10	10	--	10	--	--	--
Treatment Duration	Chemical Oxidation - Permanganate	N	r	.	**-0.692**	**-0.692**	-0.018	0.606	-0.038	**-0.639**	--	0.606	-0.576	0.173	.	--	**-0.601**	**1.000**
			p	.	0.018	0.018	0.960	0.063	0.918	0.034	--	0.063	0.081	0.612	.	--	0.039	0.000
			n	9	11	11	10	10	10	11	--	10	10	11	9	--	12	11
Treatment Duration	Chemical Oxidation - Permanganate	LN	r	.	--	--	**0.850**	**0.939**	**0.639**	**-0.856**	--	**0.939**	**-0.845**	-0.203	.	--	**-0.772**	**1.000**
			p	.	--	--	0.002	0.000	0.047	0.001	--	0.000	0.002	0.549	.	--	0.003	0.000
			n	9	--	--	10	10	10	11	--	10	10	11	9	--	12	11
Treatment Duration	Chemical Oxidation - All	N	r	-0.578	**-0.736**	**-0.725**	0.110	0.518	0.096	**-0.639**	--	0.606	-0.495	0.147	-0.578	--	**-0.601**	**1.000**
			p	0.080	0.001	0.002	0.748	0.084	0.780	0.034	--	0.063	0.121	0.588	0.080	--	0.039	0.000
			n	10	16	15	11	12	11	11	--	10	11	16	10	--	12	16
Treatment Duration	Chemical Oxidation - All	LN	r	**-0.849**	0.471	0.520	**0.891**	0.508	**0.755**	**-0.856**	--	**0.939**	**-0.689**	0.017	**-0.849**	--	**-0.772**	**0.934**
			p	0.002	0.285	0.290	0.000	0.092	0.007	0.001	--	0.000	0.019	0.950	0.002	--	0.003	0.000
			n	10	7	6	11	12	11	11	--	10	11	16	10	--	12	16

Table F.3 Correlations with field and modeling case studies combined - consolidated data sets

PERFORMANCE METRIC	TECHNOLOGY	DATA TRANSFORMATION	STATISTICS	Oxidant Concentration	Mass of Electron Donor Injected	Electron Donor Well Spacing	Duration of Monitoring	Maximum Temperature	Number of Electrodes	Number of Wells	Electrode Spacing	Target Temperature	Time to Maximum Temperature	InjectionRate	TotalDurationOfAmendment
Decrease in Groundwater Concentrations	Chemical Oxidation - Permanganate	N	r	-0.361	--	--	-0.578	--	--	--	--	--	--	--	--
			p	0.305	--	--	0.103	--	--	--	--	--	--	--	--
			n	10	--	--	9	--	--	--	--	--	--	--	--
Decrease in Groundwater Concentrations	Chemical Oxidation - Permanganate	LN	r	-0.392	--	--	-0.311	--	--	--	--	--	--	--	--
			p	0.263	--	--	0.415	--	--	--	--	--	--	--	--
			n	10	--	--	9	--	--	--	--	--	--	--	--
Decrease in Groundwater Concentrations	Chemical Oxidation - All	N	r	-0.049	--	--	-0.115	--	--	--	--	--	--	--	--
			p	0.869	--	--	0.708	--	--	--	--	--	--	--	--
			n	14	--	--	13	--	--	--	--	--	--	--	--
Decrease in Groundwater Concentrations	Chemical Oxidation - All	LN	r	-0.194	--	--	-0.529	--	--	--	--	--	--	--	--
			p	0.525	--	--	0.095	--	--	--	--	--	--	--	--
			n	13	--	--	11	--	--	--	--	--	--	--	--
Decrease in Groundwater Concentrations	Surfactant Flushing	N	r	--	--	--	.	--	--	.	--	--	--	.	.
			p	--	--	--	.	--	--	.	--	--	--	.	.
			n	--	--	--	7	--	--	7	--	--	--	7	7
Decrease in Groundwater Concentrations	Surfactant Flushing	LN	r	--	--	--	.	--	--	.	--	--	--	.	.
			p	--	--	--	.	--	--	.	--	--	--	.	.
			n	--	--	--	7	--	--	7	--	--	--	7	7
Removal of DNAPL Mass	Chemical Oxidation - All	N	r	--	--	--	--	--	--	--	--	--	--	--	--
			p	--	--	--	--	--	--	--	--	--	--	--	--
			n	--	--	--	--	--	--	--	--	--	--	--	--
Removal of DNAPL Mass	Chemical Oxidation - All	LN	r	--	--	--	--	--	--	--	--	--	--	--	--
			p	--	--	--	--	--	--	--	--	--	--	--	--
			n	--	--	--	--	--	--	--	--	--	--	--	--
Removal of DNAPL Mass	Surfactant Flushing	N	r	--	--	--	.	--	--	.	--	--	--	.	.
			p	--	--	--	.	--	--	.	--	--	--	.	.
			n	--	--	--	10	--	--	10	--	--	--	10	10
Removal of DNAPL Mass	Surfactant Flushing	LN	r	--	--	--	.	--	--	.	--	--	--	.	.
			p	--	--	--	.	--	--	.	--	--	--	.	.
			n	--	--	--	10	--	--	10	--	--	--	10	10
Treatment Duration	Chemical Oxidation - Permanganate	N	r	-0.481	--	--	0.041	--	--	--	--	--	--	--	--
			p	0.113	--	--	0.904	--	--	--	--	--	--	--	--
			n	12	--	--	11	--	--	--	--	--	--	--	--
Treatment Duration	Chemical Oxidation - Permanganate	LN	r	**-0.832**	--	--	0.580	--	--	--	--	--	--	--	--
			p	0.001	--	--	0.061	--	--	--	--	--	--	--	--
			n	12	--	--	11	--	--	--	--	--	--	--	--
Treatment Duration	Chemical Oxidation - All	N	r	**-0.594**	--	--	**0.562**	--	--	--	--	--	--	--	--
			p	0.015	--	--	0.029	--	--	--	--	--	--	--	--
			n	16	--	--	15	--	--	--	--	--	--	--	--
Treatment Duration	Chemical Oxidation - All	LN	r	**-0.899**	--	--	**0.589**	--	--	--	--	--	--	--	--
			p	0.000	--	--	0.027	--	--	--	--	--	--	--	--
			n	16	--	--	14	--	--	--	--	--	--	--	--

Table F.3 Correlations with field and modeling case studies combined - consolidated data sets

PERFORMANCE METRIC	TECHNOLOGY	DATA TRANSFORMATION	STATISTICS	Areal Extent of DNAPL Source	Depth to Groundwater	Depth to Top of Aquifer	Hydraulic Conductivity	Horizontal Hydraulic Gradient	Groundwater Velocity	Maximum Depth of the DNAPL Zone	Preremediation DNAPL Mass	Saturated Aquifer Thickness	Thickness of DNAPL Zone	Total Number of Oxidant Injections	Volume of DNAPL Zone	Soil Porosity	Total Mass of Oxidant Injected	Oxidant Application Duration
Treatment Duration	Surfactant Flushing	N	r	--	--	--	-0.170	--	--	.	-0.216	.	.	--	--	--	--	--
			p	--	--	--	0.639	--	--	.	0.548	.	.	--	--	--	--	--
			n	--	--	--	10	--	--	10	10	10	10	--	--	--	--	--
Treatment Duration	Surfactant Flushing	LN	r	.	.	.	-0.170	.	-0.170	.	-0.216	.	.	--	.	--	--	--
			p	.	.	.	0.639	.	0.639	.	0.548	.	.	--	.	--	--	--
			n	10	10	10	10	10	10	10	10	10	10	--	10	--	--	--
Actual Mass Flux	Chemical Oxidation - All	N	r	.	.	.	0.633	.	0.633	.	--	.	.	0.386	.	--	0.659	0.363
			p	.	.	.	0.092	.	0.092	.	--	.	.	0.345	.	--	0.075	0.376
			n	8	8	8	8	8	8	8	--	8	8	8	8	--	8	8
Actual Mass Flux	Chemical Oxidation - All	LN	r	.	--	--	0.506	.	0.506	.	--	.	.	0.469	.	--	0.554	0.404
			p	.	--	--	0.201	.	0.201	.	--	.	.	0.241	.	--	0.154	0.321
			n	8	--	--	8	8	8	8	--	8	8	8	8	--	8	8
Actual Mass Flux	Chemical Oxidation - Permanganate	N	r	.	.	.	0.633	.	0.633	.	--	.	.	0.386	.	--	0.659	0.363
			p	.	.	.	0.092	.	0.092	.	--	.	.	0.345	.	--	0.075	0.376
			n	8	8	8	8	8	8	8	--	8	8	8	8	--	8	8
Actual Mass Flux	Chemical Oxidation - Permanganate	LN	r	.	--	--	0.506	.	0.506	.	--	.	.	0.469	.	--	0.554	0.404
			p	.	--	--	0.201	.	0.201	.	--	.	.	0.241	.	--	0.154	0.321
			n	8	--	--	8	8	8	8	--	8	8	8	8	--	8	8

Table F.3 Correlations with field and modeling case studies combined - consolidated data sets

PERFORMANCE METRIC	TECHNOLOGY	DATA TRANSFORMATION	STATISTICS	Oxidant Concentration	Mass of Electron Donor Injected	Electron Donor Well Spacing	Duration of Monitoring	Maximum Temperature	Number of Electrodes	Number of Wells	Electrode Spacing	Target Temperature	Time to Maximum Temperature	InjectionRate	TotalDurationOfAmendment
Treatment Duration	Surfactant Flushing	N	r	--	--	--	--	--	--	--	--	--	--	.	.
			p	--	--	--	--	--	--	--	--	--	--	.	.
			n	--	--	--	--	--	--	--	--	--	--	10	10
Treatment Duration	Surfactant Flushing	LN	r	--	--	--	.	--	--	.	--	--	--	.	.
			p	--	--	--	.	--	--	.	--	--	--	.	.
			n	--	--	--	10	--	--	10	--	--	--	10	10
Actual Mass Flux	Chemical Oxidation - All	N	r	-0.166	--	--	.	--	--	--	--	--	--	--	--
			p	0.694	--	--	.	--	--	--	--	--	--	--	--
			n	8	--	--	8	--	--	--	--	--	--	--	--
Actual Mass Flux	Chemical Oxidation - All	LN	r	-0.086	--	--	.	--	--	--	--	--	--	--	--
			p	0.839	--	--	.	--	--	--	--	--	--	--	--
			n	8	--	--	8	--	--	--	--	--	--	--	--
Actual Mass Flux	Chemical Oxidation - Permanganate	N	r	-0.166	--	--	.	--	--	--	--	--	--	--	--
			p	0.694	--	--	.	--	--	--	--	--	--	--	--
			n	8	--	--	8	--	--	--	--	--	--	--	--
Actual Mass Flux	Chemical Oxidation - Permanganate	LN	r	-0.086	--	--	.	--	--	--	--	--	--	--	--
			p	0.839	--	--	.	--	--	--	--	--	--	--	--
			n	8	--	--	8	--	--	--	--	--	--	--	--

Notes

All tests conducted using Pearson Correlations at the 5% level of significance. Null hypothesis for the test states that there is no

Bold indicates a significant correlation as determined by the test (p-value < 0.05).

Regressions were performed with the Input Fields that showed a correation to the given Metric Field, however, in the case of a

-- - insufficient data for analysis (<5 observations)

. - insufficient amount of unique independent data values to compute a correlation coefficient

LN - lognormal data transformation

n - sample size

N - no data transformation

r -correlation coefficient

p - p-value. The p-value is calculated as the probability of observing a correlation coefficent at least as extreme as the one observed,

Table F.4 Correlations with field and modeling case studies combined - unconsolidated data sets

PERFORMANCE METRIC	TECHNOLOGY	DATA TRANSFORMATION	STATISTICS	Areal Extent of DNAPL Source	Depth to Groundwater	Depth to Top of Aquifer	Hydraulic Conductivity	Horizontal Hydraulic Gradient	Groundwater Velocity	Maximum Depth of the DNAPL Zone	Preremediation DNAPL Mass	Saturated Aquifer Thickness	Thickness of DNAPL Zone	Total Number of Oxidant Injections	Volume of DNAPL Zone	Soil Porosity	Total Mass of Oxidant Injected	Oxidant Application Duration	Oxidant Concentration	Mass of Electron Donor Injected	Electron Donor Well Spacing	Duration of Monitoring	Maximum Temperature
Decrease in Groundwater Concentrations	Chemical Oxidation - Permanganate	N	r	0.130	0.075	0.210	0.096	0.048	**0.598**	0.193	**-0.531**	0.072	0.245	0.161	-0.202	0.045	0.117	0.161	0.287	--	--	**-0.392**	--
			p	0.400	0.612	0.162	0.543	0.773	0.001	0.200	0.000	0.650	0.249	0.290	0.194	0.781	0.430	0.279	0.051	--	--	0.006	--
			n	44	48	46	42	39	28	46	41	42	24	45	43	41	48	47	47	--	--	48	--
Decrease in Groundwater Concentrations	Chemical Oxidation - Permanganate	LN	r	-0.024	-0.175	0.336	0.185	-0.024	0.071	0.129	-0.318	-0.032	-0.015	0.160	-0.068	0.011	0.065	-0.029	0.268	--	--	-0.224	--
			p	0.889	0.607	0.377	0.295	0.898	0.761	0.442	0.072	0.859	0.957	0.343	0.699	0.951	0.692	0.860	0.099	--	--	0.170	--
			n	36	11	9	34	31	21	38	33	34	16	37	35	33	40	39	39	--	--	39	--
Decrease in Groundwater Concentrations	Chemical Oxidation - All	N	r	0.135	0.132	0.195	0.142	0.051	**0.562**	0.210	**-0.488**	0.134	0.109	0.153	-0.142	0.045	0.102	0.147	0.184	--	--	**-0.353**	--
			p	0.362	0.324	0.154	0.336	0.745	0.001	0.134	0.001	0.368	0.582	0.271	0.343	0.781	0.483	0.302	0.186	--	--	0.008	--
			n	48	58	55	48	44	30	52	44	47	28	54	47	41	50	51	53	--	--	56	--
Decrease in Groundwater Concentrations	Chemical Oxidation - All	LN	r	0.014	-0.059	0.274	0.199	-0.050	0.070	0.146	-0.301	-0.012	-0.106	0.182	-0.039	0.011	0.069	-0.071	0.233	--	--	-0.237	--
			p	0.930	0.805	0.343	0.225	0.774	0.752	0.345	0.079	0.941	0.656	0.233	0.818	0.951	0.664	0.657	0.128	--	--	0.112	--
			n	40	20	14	39	36	23	44	35	39	20	45	38	33	42	42	44	--	--	46	--
Decrease in Groundwater Concentrations	Surfactant Flushing	N	r	-0.296	0.225	0.144	0.290	-0.180	--	0.065	-0.274	-0.273	0.006	--	-0.263	-0.150	--	--	--	--	--	-0.219	--
			p	0.327	0.460	0.639	0.336	0.596	--	0.824	0.366	0.366	0.983	--	0.409	0.641	--	--	--	--	--	0.494	--
			n	13	13	13	13	11	--	14	13	13	13	--	12	12	--	--	--	--	--	12	--
Decrease in Groundwater Concentrations	Surfactant Flushing	LN	r	-0.505	--	--	0.184	--	--	-0.246	-0.534	-0.590	-0.342	--	--	--	--	--	--	--	--	--	--
			p	0.385	--	--	0.767	--	--	0.638	0.354	0.295	0.574	--	--	--	--	--	--	--	--	--	--
			n	5	--	--	5	--	--	6	5	5	5	--	--	--	--	--	--	--	--	--	--
Decrease in Soil Concentrations	Chemical Oxidation - Permanganate	N	r	--	--	--	--	--	--	--	--	--	--	--	--	--	--	--	--	--	--	--	--
			p	--	--	--	--	--	--	--	--	--	--	--	--	--	--	--	--	--	--	--	--
			n	--	--	--	--	--	--	--	--	--	--	--	--	--	--	--	--	--	--	--	--
Decrease in Soil Concentrations	Chemical Oxidation - Permanganate	LN	r	--	--	--	--	--	--	--	--	--	--	--	--	--	--	--	--	--	--	--	--
			p	--	--	--	--	--	--	--	--	--	--	--	--	--	--	--	--	--	--	--	--
			n	--	--	--	--	--	--	--	--	--	--	--	--	--	--	--	--	--	--	--	--
Decrease in Soil Concentrations	Chemical Oxidation - All	N	r	--	0.317	0.371	--	--	--	0.711	0.368	--	--	0.280	--	--	-0.087	0.206	0.352	--	--	0.389	--
			p	--	0.406	0.413	--	--	--	0.113	0.473	--	--	0.591	--	--	0.869	0.625	0.393	--	--	0.388	--
			n	--	9	7	--	--	--	6	6	--	--	6	--	--	6	8	8	--	--	7	--
Decrease in Soil Concentrations	Chemical Oxidation - All	LN	r	--	0.578	--	--	--	--	0.559	0.467	--	--	0.657	--	--	0.128	-0.126	0.634	--	--	0.304	--
			p	--	0.133	--	--	--	--	0.248	0.427	--	--	0.229	--	--	0.810	0.788	0.126	--	--	0.558	--
			n	--	8	--	--	--	--	6	5	--	--	5	--	--	6	7	7	--	--	6	--
Removal of DNAPL Mass	Chemical Oxidation - Permanganate	N	r	**0.368**	**0.682**	**0.452**	0.054	**-0.556**	-0.053	**0.535**	0.224	0.268	-0.042	0.227	**0.436**	**-0.393**	**0.580**	0.167	**0.474**	--	--	**-0.519**	--
			p	0.018	0.000	0.003	0.740	0.000	0.785	0.000	0.154	0.095	0.856	0.158	0.004	0.012	0.000	0.292	0.002	--	--	0.000	--
			n	41	41	41	41	40	29	42	42	40	21	40	41	40	41	42	42	--	--	42	--
Removal of DNAPL Mass	Chemical Oxidation - Permanganate	LN	r	-0.042	--	--	0.022	**-0.461**	-0.254	**0.426**	**0.376**	0.062	-0.228	0.205	-0.090	-0.291	**0.381**	-0.283	0.260	--	--	**-0.505**	--
			p	0.802	--	--	0.892	0.004	0.202	0.006	0.017	0.710	0.347	0.217	0.587	0.077	0.017	0.077	0.106	--	--	0.001	--
			n	39	--	--	39	38	27	40	40	38	19	38	39	38	39	40	40	--	--	38	--
Removal of DNAPL Mass	Chemical Oxidation - All	N	r	**0.370**	**0.411**	**0.434**	0.127	**-0.556**	-0.053	**0.543**	0.174	**0.571**	-0.018	**0.330**	**0.458**	**-0.393**	**0.576**	0.069	**0.500**	--	--	**-0.523**	--
			p	0.015	0.005	0.003	0.418	0.000	0.785	0.000	0.252	0.000	0.936	0.029	0.002	0.012	0.000	0.652	0.000	--	--	0.000	--
			n	43	45	45	43	40	29	44	45	43	23	44	44	40	42	45	45	--	--	46	--
Removal of DNAPL Mass	Chemical Oxidation - All	LN	r	0.033	-0.035	-0.093	0.072	**-0.461**	-0.254	**0.495**	**0.360**	**0.343**	-0.191	**0.320**	-0.019	-0.291	**0.415**	**-0.415**	**0.427**	--	--	**-0.598**	--
			p	0.839	0.948	0.881	0.658	0.004	0.202	0.001	0.019	0.028	0.406	0.042	0.907	0.077	0.008	0.006	0.005	--	--	0.000	--
			n	41	6	5	40	38	27	42	42	41	21	41	41	38	40	42	42	--	--	41	--
Removal of DNAPL Mass	Surfactant Flushing	N	r	**-0.663**	**0.729**	0.496	0.360	**-0.982**	--	0.381	**-0.564**	**-0.593**	-0.258	--	**-0.961**	-0.377	--	--	--	--	--	**-0.984**	--
			p	0.007	0.001	0.071	0.171	0.000	--	0.131	0.023	0.015	0.334	--	0.000	0.184	--	--	--	--	--	0.000	--
			n	15	16	14	16	12	--	17	16	16	16	--	13	14	--	--	--	--	--	13	--
Removal of DNAPL Mass	Surfactant Flushing	LN	r	**-0.708**	0.674	--	0.193	**-0.852**	--	-0.056	**-0.542**	**-0.544**	-0.469	--	**-0.844**	-0.399	--	--	--	--	--	**-0.719**	--
			p	0.005	0.212	--	0.490	0.001	--	0.836	0.037	0.036	0.078	--	0.001	0.177	--	--	--	--	--	0.008	--
			n	14	5	--	15	11	--	16	15	15	15	--	12	13	--	--	--	--	--	12	--
Treatment Duration	Chemical Oxidation - Permanganate	N	r	-0.122	-0.180	-0.274	-0.208	0.174	0.308	-0.268	0.074	-0.145	-0.107	-0.125	-0.149	0.040	**0.292**	**0.997**	**-0.292**	--	--	-0.163	--
			p	0.432	0.221	0.062	0.181	0.282	0.105	0.072	0.641	0.359	0.618	0.419	0.341	0.805	0.046	0.000	0.046	--	--	0.267	--
			n	44	48	47	43	40	29	46	42	42	24	44	43	41	47	48	47	--	--	48	--
Treatment Duration	Chemical Oxidation - Permanganate	LN	r	-0.107	-0.114	-0.327	**0.340**	**0.392**	0.233	**-0.710**	-0.302	0.059	-0.057	**-0.346**	-0.122	-0.017	**0.359**	**0.999**	**-0.641**	--	--	**0.628**	--
			p	0.490	0.754	0.391	0.026	0.012	0.224	0.000	0.052	0.711	0.792	0.021	0.435	0.914	0.013	0.000	0.000	--	--	0.000	--
			n	44	10	9	43	40	29	46	42	42	24	44	43	41	47	48	47	--	--	45	--

Table F.4 Correlations with field and modeling case studies combined - unconsolidated data sets

PERFORMANCE METRIC	TECHNOLOGY	DATA TRANSFORMATION	STATISTICS	Number of Electrodes	Number of Wells	Electrode Spacing	Target Temperature	Time to Maximum Temperature	InjectionRate	TotalDurationOfAmendment
Decrease in Groundwater Concentrations	Chemical Oxidation - Permanganate	N	r	--	--	--	--	--	--	--
			p	--	--	--	--	--	--	--
			n	--	--	--	--	--	--	--
Decrease in Groundwater Concentrations	Chemical Oxidation - Permanganate	LN	r	--	--	--	--	--	--	--
			p	--	--	--	--	--	--	--
			n	--	--	--	--	--	--	--
Decrease in Groundwater Concentrations	Chemical Oxidation - All	N	r	--	--	--	--	--	--	--
			p	--	--	--	--	--	--	--
			n	--	--	--	--	--	--	--
Decrease in Groundwater Concentrations	Chemical Oxidation - All	LN	r	--	--	--	--	--	--	--
			p	--	--	--	--	--	--	--
			n	--	--	--	--	--	--	--
Decrease in Groundwater Concentrations	Surfactant Flushing	N	r	--	0.208	--	--	--	--	**-0.930**
			p	--	0.475	--	--	--	--	0.000
			n	--	14	--	--	--	--	14
Decrease in Groundwater Concentrations	Surfactant Flushing	LN	r	--	0.365	--	--	--	--	-0.214
			p	--	0.476	--	--	--	--	0.683
			n	--	6	--	--	--	--	6
Decrease in Soil Concentrations	Chemical Oxidation - Permanganate	N	r	--	--	--	--	--	--	--
			p	--	--	--	--	--	--	--
			n	--	--	--	--	--	--	--
Decrease in Soil Concentrations	Chemical Oxidation - Permanganate	LN	r	--	--	--	--	--	--	--
			p	--	--	--	--	--	--	--
			n	--	--	--	--	--	--	--
Decrease in Soil Concentrations	Chemical Oxidation - All	N	r	--	--	--	--	--	--	--
			p	--	--	--	--	--	--	--
			n	--	--	--	--	--	--	--
Decrease in Soil Concentrations	Chemical Oxidation - All	LN	r	--	--	--	--	--	--	--
			p	--	--	--	--	--	--	--
			n	--	--	--	--	--	--	--
Removal of DNAPL Mass	Chemical Oxidation - Permanganate	N	r	--	--	--	--	--	--	--
			p	--	--	--	--	--	--	--
			n	--	--	--	--	--	--	--
Removal of DNAPL Mass	Chemical Oxidation - Permanganate	LN	r	--	--	--	--	--	--	--
			p	--	--	--	--	--	--	--
			n	--	--	--	--	--	--	--
Removal of DNAPL Mass	Chemical Oxidation - All	N	r	--	--	--	--	--	--	--
			p	--	--	--	--	--	--	--
			n	--	--	--	--	--	--	--
Removal of DNAPL Mass	Chemical Oxidation - All	LN	r	--	--	--	--	--	--	--
			p	--	--	--	--	--	--	--
			n	--	--	--	--	--	--	--
Removal of DNAPL Mass	Surfactant Flushing	N	r	--	**0.613**	--	--	--	**0.926**	-0.048
			p	--	0.009	--	--	--	0.024	0.866
			n	--	17	--	--	--	5	15
Removal of DNAPL Mass	Surfactant Flushing	LN	r	--	**0.676**	--	--	--	0.485	0.194
			p	--	0.004	--	--	--	0.407	0.506
			n	--	16	--	--	--	5	14
Treatment Duration	Chemical Oxidation - Permanganate	N	r	--	--	--	--	--	--	--
			p	--	--	--	--	--	--	--
			n	--	--	--	--	--	--	--
Treatment Duration	Chemical Oxidation - Permanganate	LN	r	--	--	--	--	--	--	--
			p	--	--	--	--	--	--	--
			n	--	--	--	--	--	--	--

Table F.4 Correlations with field and modeling case studies combined - unconsolidated data sets

PERFORMANCE METRIC	TECHNOLOGY	DATA TRANSFORMATION	STATISTICS	Areal Extent of DNAPL Source	Depth to Groundwater	Depth to Top of Aquifer	Hydraulic Conductivity	Horizontal Hydraulic Gradient	Groundwater Velocity	Maximum Depth of the DNAPL Zone	Preremediation DNAPL Mass	Saturated Aquifer Thickness	Thickness of DNAPL Zone	Total Number of Oxidant Injections	Volume of DNAPL Zone	Soil Porosity	Total Mass of Oxidant Injected	Oxidant Application Duration	Oxidant Concentration	Mass of Electron Donor Injected	Electron Donor Well Spacing	Duration of Monitoring	Maximum Temperature
Treatment Duration	Chemical Oxidation - All	N	r	-0.155	-0.214	-0.190	-0.227	0.130	**0.360**	-0.267	-0.065	-0.203	-0.108	-0.114	-0.213	0.040	0.236	**0.995**	-0.228	--	--	-0.043	--
			p	0.289	0.106	0.157	0.117	0.393	0.046	0.056	0.669	0.171	0.583	0.420	0.146	0.805	0.103	0.000	0.101	--	--	0.754	--
			n	49	58	57	49	45	31	52	46	47	28	52	48	41	49	53	53	--	--	55	--
Treatment Duration	Chemical Oxidation - All	LN	r	-0.234	-0.135	-0.278	0.236	**0.369**	0.290	**-0.664**	-0.286	-0.081	0.025	**-0.414**	-0.235	-0.017	**0.286**	**0.970**	**-0.600**	--	--	**0.626**	--
			p	0.106	0.571	0.337	0.102	0.013	0.114	0.000	0.054	0.589	0.900	0.002	0.107	0.914	0.047	0.000	0.000	--	--	0.000	--
			n	49	20	14	49	45	31	52	46	47	28	52	48	41	49	53	53	--	--	51	--
Treatment Duration	Surfactant Flushing	N	r	-0.213	0.400	-0.029	0.028	-0.040	--	0.338	-0.036	0.074	-0.053	--	-0.365	-0.096	--	--	--	--	--	-0.083	--
			p	0.464	0.140	0.921	0.921	0.906	--	0.184	0.900	0.785	0.851	--	0.243	0.755	--	--	--	--	--	0.778	--
			n	14	15	14	15	11	--	17	15	16	15	--	12	13	--	--	--	--	--	14	--
Treatment Duration	Surfactant Flushing	LN	r	-0.347	--	--	-0.411	-0.237	--	**0.579**	0.298	0.340	0.330	--	-0.484	-0.215	--	--	--	--	--	0.258	--
			p	0.224	--	--	0.128	0.483	--	0.015	0.280	0.198	0.230	--	0.111	0.480	--	--	--	--	--	0.373	--
			n	14	--	--	15	11	--	17	15	16	15	--	12	13	--	--	--	--	--	14	--
Unit Cost (by volume) of Source Zone Treatment	Chemical Oxidation - Permanganate	N	r	--	--	--	--	--	--	--	--	--	--	--	--	--	--	--	--	--	--	--	--
			p	--	--	--	--	--	--	--	--	--	--	--	--	--	--	--	--	--	--	--	--
			n	--	--	--	--	--	--	--	--	--	--	--	--	--	--	--	--	--	--	--	--
Unit Cost (by volume) of Source Zone Treatment	Chemical Oxidation - Permanganate	LN	r	--	--	--	--	--	--	--	--	--	--	--	--	--	--	--	--	--	--	--	--
			p	--	--	--	--	--	--	--	--	--	--	--	--	--	--	--	--	--	--	--	--
			n	--	--	--	--	--	--	--	--	--	--	--	--	--	--	--	--	--	--	--	--
Unit Cost (by volume) of Source Zone Treatment	Chemical Oxidation - All	N	r	-0.438	-0.162	-0.175	-0.123	--	--	-0.199	--	**0.968**	0.106	-0.212	-0.745	--	-0.299	0.082	-0.030	--	--	-0.582	--
			p	0.386	0.729	0.679	0.817	--	--	0.669	--	0.007	0.841	0.615	0.089	--	0.625	0.895	0.955	--	--	0.304	--
			n	6	7	8	6	--	--	7	--	5	6	8	6	--	5	5	6	--	--	5	--
Unit Cost (by volume) of Source Zone Treatment	Chemical Oxidation - All	LN	r	-0.708	-0.154	-0.076	0.686	--	--	0.287	--	**0.931**	0.575	-0.299	**-0.872**	--	-0.187	0.717	-0.043	--	--	-0.579	--
			p	0.115	0.742	0.871	0.132	--	--	0.533	--	0.022	0.233	0.472	0.024	--	0.763	0.173	0.936	--	--	0.306	--
			n	6	7	7	6	--	--	7	--	5	6	8	6	--	5	5	6	--	--	5	--
Actual Mass Flux	Chemical Oxidation - Permanganate	N	r	.	.	.	0.301	.	0.276	.	0.207	.	.	.	.	.	0.455	0.101	.	--	--	0.264	--
			p	.	.	.	0.240	.	0.549	.	0.426	.	.	.	.	.	0.066	0.701	.	--	--	0.305	--
			n	17	17	17	17	17	7	17	17	17	17	17	17	17	17	17	17	--	--	17	--
Actual Mass Flux	Chemical Oxidation - Permanganate	LN	r	.	--	--	0.449	.	0.082	.	0.491	.	.	.	.	.	0.529	0.138	.	--	--	-0.366	--
			p	.	--	--	0.107	.	0.896	.	0.075	.	.	.	.	.	0.052	0.639	.	--	--	0.242	--
			n	14	--	--	14	14	5	14	14	14	14	14	14	14	14	14	14	--	--	12	--
Actual Mass Flux	Chemical Oxidation - All	N	r	.	.	.	0.301	.	0.276	.	0.207	.	.	.	.	.	0.455	0.101	.	--	--	0.264	--
			p	.	.	.	0.240	.	0.549	.	0.426	.	.	.	.	.	0.066	0.701	.	--	--	0.305	--
			n	17	17	17	17	17	7	17	17	17	17	17	17	17	17	17	17	--	--	17	--
Actual Mass Flux	Chemical Oxidation - All	LN	r	.	--	--	0.449	.	0.082	.	0.491	.	.	.	.	.	0.529	0.138	.	--	--	-0.366	--
			p	.	--	--	0.107	.	0.896	.	0.075	.	.	.	.	.	0.052	0.639	.	--	--	0.242	--
			n	14	--	--	14	14	5	14	14	14	14	14	14	14	14	14	14	--	--	12	--
Actual Mass Flux	Surfactant Flushing	N	r	.	.	.	0.332	.	--	.	0.316	.	.	--	.	.	--	--	--	--	--	0.494	--
			p	.	.	.	0.349	.	--	.	0.374	.	.	--	.	.	--	--	--	--	--	0.147	--
			n	10	10	10	10	10	--	10	10	10	10	--	10	10	--	--	--	--	--	10	--
Actual Mass Flux	Surfactant Flushing	LN	r	.	--	--	**0.751**	.	--	.	0.094	.	.	--	.	.	--	--	--	--	--	**0.908**	--
			p	.	--	--	0.020	.	--	.	0.809	.	.	--	.	.	--	--	--	--	--	0.001	--
			n	9	--	--	9	9	--	9	9	9	9	--	9	9	--	--	--	--	--	9	--

Table F.4 Correlations with field and modeling case studies combined - unconsolidated data sets

PERFORMANCE METRIC	TECHNOLOGY	DATA TRANSFORMATION	STATISTICS	Number of Electrodes	Number of Wells	Electrode Spacing	Target Temperature	Time to Maximum Temperature	InjectionRate	TotalDurationOfAmendment
Treatment Duration	Chemical Oxidation - All	N	r	--	--	--	--	--	--	--
			p	--	--	--	--	--	--	--
			n	--	--	--	--	--	--	--
Treatment Duration	Chemical Oxidation - All	LN	r	--	--	--	--	--	--	--
			p	--	--	--	--	--	--	--
			n	--	--	--	--	--	--	--
Treatment Duration	Surfactant Flushing	N	r	--	0.206	--	--	--	0.418	**0.935**
			p	--	0.428	--	--	--	0.410	0.000
			n	--	17	--	--	--	6	16
Treatment Duration	Surfactant Flushing	LN	r	--	0.470	--	--	--	**0.871**	**0.973**
			p	--	0.057	--	--	--	0.024	0.000
			n	--	17	--	--	--	6	16
Unit Cost (by volume) of Source Zone Treatment	Chemical Oxidation - Permanganate	N	r	--	--	--	--	--	--	--
			p	--	--	--	--	--	--	--
			n	--	--	--	--	--	--	--
Unit Cost (by volume) of Source Zone Treatment	Chemical Oxidation - Permanganate	LN	r	--	--	--	--	--	--	--
			p	--	--	--	--	--	--	--
			n	--	--	--	--	--	--	--
Unit Cost (by volume) of Source Zone Treatment	Chemical Oxidation - All	N	r	--	--	--	--	--	--	--
			p	--	--	--	--	--	--	--
			n	--	--	--	--	--	--	--
Unit Cost (by volume) of Source Zone Treatment	Chemical Oxidation - All	LN	r	--	--	--	--	--	--	--
			p	--	--	--	--	--	--	--
			n	--	--	--	--	--	--	--
Actual Mass Flux	Chemical Oxidation - Permanganate	N	r	--	--	--	--	--	--	--
			p	--	--	--	--	--	--	--
			n	--	--	--	--	--	--	--
Actual Mass Flux	Chemical Oxidation - Permanganate	LN	r	--	--	--	--	--	--	--
			p	--	--	--	--	--	--	--
			n	--	--	--	--	--	--	--
Actual Mass Flux	Chemical Oxidation - All	N	r	--	--	--	--	--	--	--
			p	--	--	--	--	--	--	--
			n	--	--	--	--	--	--	--
Actual Mass Flux	Chemical Oxidation - All	LN	r	--	--	--	--	--	--	--
			p	--	--	--	--	--	--	--
			n	--	--	--	--	--	--	--
Actual Mass Flux	Surfactant Flushing	N	r	--	.	--	--	--	--	-0.494
			p	--	.	--	--	--	--	0.147
			n	--	10	--	--	--	--	10
Actual Mass Flux	Surfactant Flushing	LN	r	--	.	--	--	--	--	-0.560
			p	--	.	--	--	--	--	0.117
			n	--	9	--	--	--	--	9

Notes

All tests conducted using Pearson Correlations at the 5% level of significance. Null hypothesis for the test states that there is no correlation; whereas, the alternative hypothesis states that a correlation does exist.

Bold indicates a significant correlation as determined by the test (p-value < 0.05).

Regressions were performed with the Input Fields that showed a correation to the given Metric Field, however, in the case of a multivariate regression, there were not enough observations to create a sufficient enough data set. Therefore only simple linear regressions were performed.

-- - insufficient data for analysis (<5 observations)

. - insufficient amount of unique independent data values to compute a correlation coefficient

LN - lognormal data transformation

n - sample size

N - no data transformation

r -correlation coefficient

p - p-value. The p-value is calculated as the probability of observing a correlation coefficent at least as extreme as the one observed, given the null hypothesis is true.

Table F.5 Correlations with field case studies and modeling studies - all media

PERFORMANCE METRIC	TECHNOLOGY	DATA TRANSFORMATION	STATISTICS	Areal Extent of DNAPL Source	Depth to Groundwater	Depth to Top of Aquifer	Hydraulic Conductivity	Horizontal Hydraulic Gradient	Groundwater Velocity	Maximum Depth of the DNAPL Zone	Preremediation DNAPL Mass	Saturated Aquifer Thickness	Thickness of DNAPL Zone	Total Number of Oxidant Injections	Volume of DNAPL Zone	Soil Porosity	Total Mass of Oxidant Injected	Oxidant Application Duration	Oxidant Concentration
Actual Mass Flux	Chemical Oxidation - Permanganate	N	r	**-0.468**	.	.	0.374	**-0.468**	0.473	.	-0.018	.	.	0.257	**-0.468**	.	0.192	0.035	0.036
			p	0.018	.	.	0.066	0.018	0.075	.	0.943	.	.	0.214	0.018	.	0.358	0.869	0.865
			n	25	25	25	25	25	15	25	19	25	25	25	25	17	25	25	25
Actual Mass Flux	Chemical Oxidation - Permanganate	LN	r	**-0.432**	--	--	**0.529**	**-0.432**	**0.609**	.	-0.138	.	.	0.249	**-0.432**	.	-0.253	0.209	-0.009
			p	0.045	--	--	0.011	0.045	0.027	.	0.611	.	.	0.265	0.045	.	0.255	0.351	0.970
			n	22	--	--	22	22	13	22	16	22	22	22	22	14	22	22	22
Actual Mass Flux	Chemical Oxidation - All	N	r	**-0.468**	.	.	0.374	**-0.468**	0.473	.	-0.018	.	.	0.257	**-0.468**	.	0.192	0.035	0.036
			p	0.018	.	.	0.066	0.018	0.075	.	0.943	.	.	0.214	0.018	.	0.358	0.869	0.865
			n	25	25	25	25	25	15	25	19	25	25	25	25	17	25	25	25
Actual Mass Flux	Chemical Oxidation - All	LN	r	**-0.432**	--	--	**0.529**	**-0.432**	**0.609**	.	-0.138	.	.	0.249	**-0.432**	.	-0.253	0.209	-0.009
			p	0.045	--	--	0.011	0.045	0.027	.	0.611	.	.	0.265	0.045	.	0.255	0.351	0.970
			n	22	--	--	22	22	13	22	16	22	22	22	22	14	22	22	22
Actual Mass Flux	Enhanced Bioremediation - Anaerobic	N	r	.	.	.	0.407	.	--	.	-0.238	.	.	--	.	.	--	--	--
			p	.	.	.	0.189	.	--	.	0.457	.	.	--	.	.	--	--	--
			n	12	12	12	12	12	--	12	12	12	12	--	12	12	--	--	--
Actual Mass Flux	Enhanced Bioremediation - Anaerobic	LN	r	.	--	--	**0.769**	.	--	.	-0.163	.	.	--	.	.	--	--	--
			p	.	--	--	0.003	.	--	.	0.612	.	.	--	.	.	--	--	--
			n	12	--	--	12	12	--	12	12	12	12	--	12	12	--	--	--
Actual Mass Flux	Surfactant Flushing	N	r	**-0.495**	.	.	0.292	**-0.495**	.	.	-0.222	.	.	--	**-0.495**	.	--	--	--
			p	0.031	.	.	0.226	0.031	0	.	0.361	.	.	--	0.031	.	--	--	--
			n	19	19	19	19	19	9	19	19	19	19	--	19	10	--	--	--
Actual Mass Flux	Surfactant Flushing	LN	r	-0.371	--	--	**0.519**	-0.371	-0.595	.	-0.352	.	.	--	-0.371	.	--	--	--
			p	0.129	--	--	0.027	0.129	0.091	.	0.152	.	.	--	0.129	.	--	--	--
			n	18	--	--	18	18	9	18	18	18	18	--	18	9	--	--	--
Decrease in Groundwater Concentrations	Chemical Oxidation - Fenton's Reagent or Hydrogen Peroxide	N	r	0.073	0.203	0.252	0.406	0.557	--	0.135	--	0.194	0.310	0.303	0.461	--	--	0.016	0.486
			p	0.908	0.487	0.429	0.425	0.251	--	0.799	--	0.754	0.611	0.292	0.434	--	--	0.966	0.154
			n	5	14	12	6	6	--	6	--	5	5	14	5	--	--	9	10
Decrease in Groundwater Concentrations	Chemical Oxidation - Fenton's Reagent or Hydrogen Peroxide	LN	r	0.199	-0.103	0.132	0.800	0.335	--	-0.093	--	-0.155	0.386	0.025	0.669	--	--	-0.033	0.341
			p	0.748	0.726	0.682	0.056	0.517	--	0.860	--	0.804	0.521	0.933	0.217	--	--	0.933	0.335
			n	5	14	12	6	6	--	6	--	5	5	14	5	--	--	9	10
Decrease in Groundwater Concentrations	Chemical Oxidation - Permanganate	N	r	0.146	0.089	0.208	-0.203	0.114	**0.573**	-0.009	**-0.531**	0.052	**0.388**	0.078	-0.117	0.026	0.135	0.165	-0.145
			p	0.312	0.515	0.130	0.162	0.453	0.000	0.951	0.000	0.724	0.031	0.576	0.425	0.869	0.312	0.228	0.281
			n	50	56	54	49	46	35	54	41	49	31	54	49	42	58	55	57
Decrease in Groundwater Concentrations	Chemical Oxidation - Permanganate	LN	r	0.056	-0.094	-0.009	-0.049	0.037	0.050	-0.023	-0.318	-0.069	0.072	-0.027	0.012	0.010	0.112	-0.044	-0.016
			p	0.726	0.760	0.979	0.760	0.824	0.801	0.879	0.072	0.669	0.743	0.861	0.942	0.954	0.437	0.770	0.912
			n	42	13	11	41	38	28	46	33	41	23	46	41	34	50	47	49
Decrease in Groundwater Concentrations	Chemical Oxidation - All	N	r	0.153	0.128	0.171	-0.188	0.127	**0.552**	0.062	**-0.493**	0.126	0.243	0.074	-0.017	0.026	0.125	0.155	0.032
			p	0.266	0.286	0.167	0.165	0.363	0.000	0.637	0.001	0.364	0.153	0.547	0.902	0.869	0.343	0.220	0.794
			n	55	71	67	56	53	38	60	45	54	36	68	54	42	60	64	67
Decrease in Groundwater Concentrations	Chemical Oxidation - All	LN	r	0.105	0.096	0.215	-0.037	0.058	0.144	0.033	-0.303	-0.035	-0.040	0.024	0.057	0.010	0.121	-0.029	0.035
			p	0.484	0.640	0.377	0.806	0.704	0.439	0.818	0.073	0.820	0.839	0.858	0.709	0.954	0.393	0.833	0.795
			n	47	26	19	47	45	31	52	36	46	28	58	45	34	52	54	57
Decrease in Groundwater Concentrations	Enhanced Bioremediation - Anaerobic	N	r	0.156	0.132	0.132	0.151	-0.163	0.460	0.133	-0.405	0.170	0.118	--	0.229	-0.213	--	--	--
			p	0.466	0.458	0.458	0.501	0.470	0.252	0.477	0.151	0.449	0.631	--	0.412	0.427	--	--	--
			n	24	34	34	22	22	8	31	14	22	19	--	15	16	--	--	--
Decrease in Groundwater Concentrations	Enhanced Bioremediation - Anaerobic	LN	r	-0.011	0.213	0.256	0.289	-0.193	**0.754**	0.059	-0.304	0.155	0.102	--	-0.129	-0.184	--	--	--
			p	0.959	0.368	0.305	0.193	0.402	0.031	0.762	0.291	0.502	0.688	--	0.646	0.495	--	--	--
			n	23	20	18	22	21	8	29	14	21	18	--	15	16	--	--	--
Decrease in Groundwater Concentrations	Thermal - Resistive Heating	N	r	0.254	0.209	0.175	0.137	--	--	-0.125	-0.144	-0.265	0.140	--	0.395	--	--	--	--
			p	0.403	0.473	0.549	0.706	--	--	0.684	0.786	0.526	0.740	--	0.230	--	--	--	--
			n	13	14	14	10	--	--	13	6	8	8	--	11	--	--	--	--

Table F.5 Correlations with field case studies and modeling studies - all media

PERFORMANCE METRIC	TECHNOLOGY	DATA TRANSFORMATION	STATISTICS	Mass of Electron Donor Injected	Electron Donor Well Spacing	Duration of Monitoring	Maximum Temperature	Number of Electrodes	Number of Wells	Electrode Spacing	Target Temperature	Time to Maximum Temperature	InjectionRate	TotalDurationOfAmendment
Actual Mass Flux	Chemical Oxidation - Permanganate	N	r	--	--	0.086	--	--	--	--	--	--	--	--
			p	--	--	0.682	--	--	--	--	--	--	--	--
			n	--	--	25	--	--	--	--	--	--	--	--
Actual Mass Flux	Chemical Oxidation - Permanganate	LN	r	--	--	**-0.563**	--	--	--	--	--	--	--	--
			p	--	--	0.010	--	--	--	--	--	--	--	--
			n	--	--	20	--	--	--	--	--	--	--	--
Actual Mass Flux	Chemical Oxidation - All	N	r	--	--	0.086	--	--	--	--	--	--	--	--
			p	--	--	0.682	--	--	--	--	--	--	--	--
			n	--	--	25	--	--	--	--	--	--	--	--
Actual Mass Flux	Chemical Oxidation - All	LN	r	--	--	**-0.563**	--	--	--	--	--	--	--	--
			p	--	--	0.010	--	--	--	--	--	--	--	--
			n	--	--	20	--	--	--	--	--	--	--	--
Actual Mass Flux	Enhanced Bioremediation - Anaerobic	N	r	0.575	--	-0.455	--	--	--	--	--	--	--	--
			p	0.064	--	0.137	--	--	--	--	--	--	--	--
			n	11	--	12	--	--	--	--	--	--	--	--
Actual Mass Flux	Enhanced Bioremediation - Anaerobic	LN	r	**0.688**	--	.	--	--	--	--	--	--	--	--
			p	0.019	--	.	--	--	--	--	--	--	--	--
			n	11	--	10	--	--	--	--	--	--	--	--
Actual Mass Flux	Surfactant Flushing	N	r	--	--	**-0.473**	--	--	.	--	--	--	.	0.435
			p	--	--	0.041	--	--	.	--	--	--	.	0.063
			n	--	--	19	--	--	19	--	--	--	9	19
Actual Mass Flux	Surfactant Flushing	LN	r	--	--	-0.339	--	--	.	--	--	--	.	0.096
			p	--	--	0.169	--	--	.	--	--	--	.	0.705
			n	--	--	18	--	--	18	--	--	--	9	18
Decrease in Groundwater Concentrations	Chemical Oxidation - Fenton's Reagent or Hydrogen Peroxide	N	r	--	--	--	--	--	--	--	--	--	--	--
			p	--	--	--	--	--	--	--	--	--	--	--
			n	--	--	--	--	--	--	--	--	--	--	--
Decrease in Groundwater Concentrations	Chemical Oxidation - Fenton's Reagent or Hydrogen Peroxide	LN	r	--	--	--	--	--	--	--	--	--	--	--
			p	--	--	--	--	--	--	--	--	--	--	--
			n	--	--	--	--	--	--	--	--	--	--	--
Decrease in Groundwater Concentrations	Chemical Oxidation - Permanganate	N	r	--	--	**-0.390**	--	--	--	--	--	--	--	--
			p	--	--	0.003	--	--	--	--	--	--	--	--
			n	--	--	57	--	--	--	--	--	--	--	--
Decrease in Groundwater Concentrations	Chemical Oxidation - Permanganate	LN	r	--	--	-0.255	--	--	--	--	--	--	--	--
			p	--	--	0.081	--	--	--	--	--	--	--	--
			n	--	--	48	--	--	--	--	--	--	--	--
Decrease in Groundwater Concentrations	Chemical Oxidation - All	N	r	--	--	**-0.279**	--	--	--	--	--	--	--	--
			p	--	--	0.020	--	--	--	--	--	--	--	--
			n	--	--	69	--	--	--	--	--	--	--	--
Decrease in Groundwater Concentrations	Chemical Oxidation - All	LN	r	--	--	**-0.291**	--	--	--	--	--	--	--	--
			p	--	--	0.028	--	--	--	--	--	--	--	--
			n	--	--	57	--	--	--	--	--	--	--	--
Decrease in Groundwater Concentrations	Enhanced Bioremediation - Anaerobic	N	r	0.163	-0.309	-0.065	--	--	--	--	--	--	--	--
			p	0.374	0.199	0.682	--	--	--	--	--	--	--	--
			n	32	19	42	--	--	--	--	--	--	--	--
Decrease in Groundwater Concentrations	Enhanced Bioremediation - Anaerobic	LN	r	-0.084	0.084	-0.299	--	--	--	--	--	--	--	--
			p	0.648	0.747	0.081	--	--	--	--	--	--	--	--
			n	32	17	35	--	--	--	--	--	--	--	--
Decrease in Groundwater Concentrations	Thermal - Resistive Heating	N	r	--	--	--	-0.561	0.231	--	0.178	-0.468	0.232	--	--
			p	--	--	--	0.073	0.427	--	0.623	0.242	0.519	--	--
			n	--	--	--	11	14	--	10	8	10	--	--

Table F.5 Correlations with field case studies and modeling studies - all media

PERFORMANCE METRIC	TECHNOLOGY	DATA TRANSFORMATION	STATISTICS	Areal Extent of DNAPL Source	Depth to Groundwater	Depth to Top of Aquifer	Hydraulic Conductivity	Horizontal Hydraulic Gradient	Groundwater Velocity	Maximum Depth of the DNAPL Zone	Preremediation DNAPL Mass	Saturated Aquifer Thickness	Thickness of DNAPL Zone	Total Number of Oxidant Injections	Volume of DNAPL Zone	Soil Porosity	Total Mass of Oxidant Injected	Oxidant Application Duration	Oxidant Concentration
Decrease in Groundwater Concentrations	Thermal - Resistive Heating	LN	r	0.134	0.184	0.063	-0.163	--	--	-0.180	-0.296	-0.293	0.019	--	0.359	--	--	--	--
			p	0.662	0.529	0.830	0.652	--	--	0.556	0.568	0.481	0.963	--	0.278	--	--	--	--
			n	13	14	14	10	--	--	13	6	8	8	--	11	--	--	--	--
Decrease in Groundwater Concentrations	Thermal - Steam Flushing	N	r	-0.104	-0.321	-0.403	--	--	--	--	--	--	--	--	--	--	--	--	--
			p	0.867	0.599	0.501	--	--	--	--	--	--	--	--	--	--	--	--	--
			n	5	5	5	--	--	--	--	--	--	--	--	--	--	--	--	--
Decrease in Groundwater Concentrations	Thermal - Steam Flushing	LN	r	-0.118	-0.384	-0.427	--	--	--	--	--	--	--	--	--	--	--	--	--
			p	0.850	0.524	0.474	--	--	--	--	--	--	--	--	--	--	--	--	--
			n	5	5	5	--	--	--	--	--	--	--	--	--	--	--	--	--
Decrease in Groundwater Concentrations	Thermal - All	N	r	-0.062	0.075	-0.091	0.051	--	--	-0.372	-0.205	-0.259	-0.542	--	0.036	--	--	--	--
			p	0.808	0.755	0.710	0.857	--	--	0.156	0.627	0.442	0.085	--	0.904	--	--	--	--
			n	18	20	19	15	--	--	16	8	11	11	--	14	--	--	--	--
Decrease in Groundwater Concentrations	Thermal - All	LN	r	0.042	0.042	-0.076	-0.115	--	--	-0.308	-0.300	-0.255	-0.493	--	-0.077	--	--	--	--
			p	0.867	0.862	0.758	0.682	--	--	0.246	0.470	0.450	0.124	--	0.794	--	--	--	--
			n	18	20	19	15	--	--	16	8	11	11	--	14	--	--	--	--
Decrease in Soil Concentrations	Chemical Oxidation - Fenton's Reagent or Hydrogen Peroxide	N	r	--	0.426	0.423	--	--	--	--	0.436	--	--	0.061	--	--	--	0.343	--
			p	--	0.400	0.478	--	--	--	--	0.463	--	--	0.922	--	--	--	0.572	--
			n	--	6	5	--	--	--	--	5	--	--	5	--	--	--	5	--
Decrease in Soil Concentrations	Chemical Oxidation - Fenton's Reagent or Hydrogen Peroxide	LN	r	--	0.143	0.406	--	--	--	--	0.227	--	--	0.076	--	--	--	0.141	--
			p	--	0.786	0.498	--	--	--	--	0.714	--	--	0.903	--	--	--	0.822	--
			n	--	6	5	--	--	--	--	5	--	--	5	--	--	--	5	--
Decrease in Soil Concentrations	Chemical Oxidation - Permanganate	N	r	--	0.230	--	--	--	--	--	--	--	--	--	--	--	-0.155	-0.090	0.564
			p	--	0.710	--	--	--	--	--	--	--	--	--	--	--	0.804	0.886	0.322
			n	--	5	--	--	--	--	--	--	--	--	--	--	--	5	5	5
Decrease in Soil Concentrations	Chemical Oxidation - Permanganate	LN	r	--	0.356	--	--	--	--	--	--	--	--	--	--	--	-0.118	0.225	0.281
			p	--	0.556	--	--	--	--	--	--	--	--	--	--	--	0.851	0.716	0.647
			n	--	5	--	--	--	--	--	--	--	--	--	--	--	5	5	5
Decrease in Soil Concentrations	Chemical Oxidation - All	N	r	0.168	0.311	0.344	0.382	--	--	0.711	0.406	-0.411	0.370	-0.033	0.597	--	-0.245	0.166	0.314
			p	0.787	0.352	0.403	0.526	--	--	0.113	0.366	0.492	0.539	0.938	0.288	--	0.596	0.646	0.411
			n	5	11	8	5	--	--	6	7	5	5	8	5	--	7	10	9
Decrease in Soil Concentrations	Chemical Oxidation - All	LN	r	0.162	0.370	0.776	--	--	--	0.559	0.552	-0.450	0.209	-0.349	--	--	0.013	-0.157	0.631
			p	0.794	0.293	0.123	--	--	--	0.248	0.256	0.447	0.735	0.443	--	--	0.979	0.687	0.093
			n	5	10	5	--	--	--	6	6	5	5	7	--	--	7	9	8
Decrease in Soil Concentrations	Thermal - Conductive Heating	N	r	--	-0.468	--	--	--	--	-0.029	--	--	--	--	--	--	--	--	--
			p	--	0.427	--	--	--	--	0.963	--	--	--	--	--	--	--	--	--
			n	--	5	--	--	--	--	5	--	--	--	--	--	--	--	--	--
Decrease in Soil Concentrations	Thermal - Conductive Heating	LN	r	--	-0.350	--	--	--	--	-0.104	--	--	--	--	--	--	--	--	--
			p	--	0.563	--	--	--	--	0.868	--	--	--	--	--	--	--	--	--
			n	--	5	--	--	--	--	5	--	--	--	--	--	--	--	--	--
Decrease in Soil Concentrations	Thermal - Resistive Heating	N	r	-0.157	0.012	0.044	0.141	--	--	0.406	--	0.073	--	--	-0.025	--	--	--	--
			p	0.710	0.975	0.917	0.790	--	--	0.278	--	0.908	--	--	0.957	--	--	--	--
			n	8	9	8	6	--	--	9	--	5	--	--	7	--	--	--	--
Decrease in Soil Concentrations	Thermal - Resistive Heating	LN	r	-0.137	-0.078	-0.066	-0.047	--	--	0.365	--	-0.005	--	--	-0.202	--	--	--	--
			p	0.747	0.841	0.877	0.930	--	--	0.335	--	0.993	--	--	0.664	--	--	--	--
			n	8	9	8	6	--	--	9	--	5	--	--	7	--	--	--	--
Decrease in Soil Concentrations	Thermal - Steam Flushing	N	r	--	-0.586	-0.133	--	--	--	--	--	--	--	--	--	--	--	--	--
			p	--	0.299	0.802	--	--	--	--	--	--	--	--	--	--	--	--	--
			n	--	5	6	--	--	--	--	--	--	--	--	--	--	--	--	--
Decrease in Soil Concentrations	Thermal - Steam Flushing	LN	r	--	-0.618	0.019	--	--	--	--	--	--	--	--	--	--	--	--	--
			p	--	0.266	0.972	--	--	--	--	--	--	--	--	--	--	--	--	--
			n	--	5	6	--	--	--	--	--	--	--	--	--	--	--	--	--

Table F.5 Correlations with field case studies and modeling studies - all media

PERFORMANCE METRIC	TECHNOLOGY	DATA TRANSFORMATION	STATISTICS	Mass of Electron Donor Injected	Electron Donor Well Spacing	Duration of Monitoring	Maximum Temperature	Number of Electrodes	Number of Wells	Electrode Spacing	Target Temperature	Time to Maximum Temperature	InjectionRate	TotalDurationOfAmendment
Decrease in Groundwater Concentrations	Thermal - Resistive Heating	LN	r	--	--	--	-0.483	0.229	--	0.136	-0.455	0.061	--	--
			p	--	--	--	0.132	0.430	--	0.708	0.257	0.866	--	--
			n	--	--	--	11	14	--	10	8	10	--	--
Decrease in Groundwater Concentrations	Thermal - Steam Flushing	N	r	--	--	--	--	--	--	--	--	--	--	--
			p	--	--	--	--	--	--	--	--	--	--	--
			n	--	--	--	--	--	--	--	--	--	--	--
Decrease in Groundwater Concentrations	Thermal - Steam Flushing	LN	r	--	--	--	--	--	--	--	--	--	--	--
			p	--	--	--	--	--	--	--	--	--	--	--
			n	--	--	--	--	--	--	--	--	--	--	--
Decrease in Groundwater Concentrations	Thermal - All	N	r	--	--	--	0.046	0.233	--	0.054	-0.439	-0.042	--	--
			p	--	--	--	0.875	0.323	--	0.869	0.177	0.887	--	--
			n	--	--	--	14	20	--	12	11	14	--	--
Decrease in Groundwater Concentrations	Thermal - All	LN	r	--	--	--	0.111	0.356	--	0.088	-0.418	-0.138	--	--
			p	--	--	--	0.707	0.123	--	0.785	0.201	0.639	--	--
			n	--	--	--	14	20	--	12	11	14	--	--
Decrease in Soil Concentrations	Chemical Oxidation - Fenton's Reagent or Hydrogen Peroxide	N	r	--	--	--	--	--	--	--	--	--	--	--
			p	--	--	--	--	--	--	--	--	--	--	--
			n	--	--	--	--	--	--	--	--	--	--	--
Decrease in Soil Concentrations	Chemical Oxidation - Fenton's Reagent or Hydrogen Peroxide	LN	r	--	--	--	--	--	--	--	--	--	--	--
			p	--	--	--	--	--	--	--	--	--	--	--
			n	--	--	--	--	--	--	--	--	--	--	--
Decrease in Soil Concentrations	Chemical Oxidation - Permanganate	N	r	--	--	--	--	--	--	--	--	--	--	--
			p	--	--	--	--	--	--	--	--	--	--	--
			n	--	--	--	--	--	--	--	--	--	--	--
Decrease in Soil Concentrations	Chemical Oxidation - Permanganate	LN	r	--	--	--	--	--	--	--	--	--	--	--
			p	--	--	--	--	--	--	--	--	--	--	--
			n	--	--	--	--	--	--	--	--	--	--	--
Decrease in Soil Concentrations	Chemical Oxidation - All	N	r	--	--	0.454	--	--	--	--	--	--	--	--
			p	--	--	0.258	--	--	--	--	--	--	--	--
			n	--	--	8	--	--	--	--	--	--	--	--
Decrease in Soil Concentrations	Chemical Oxidation - All	LN	r	--	--	0.470	--	--	--	--	--	--	--	--
			p	--	--	0.287	--	--	--	--	--	--	--	--
			n	--	--	7	--	--	--	--	--	--	--	--
Decrease in Soil Concentrations	Thermal - Conductive Heating	N	r	--	--	--	--	0.786	-0.389	--	--	--	--	--
			p	--	--	--	--	0.115	0.517	--	--	--	--	--
			n	--	--	--	--	5	5	--	--	--	--	--
Decrease in Soil Concentrations	Thermal - Conductive Heating	LN	r	--	--	--	--	0.734	-0.068	--	--	--	--	--
			p	--	--	--	--	0.158	0.913	--	--	--	--	--
			n	--	--	--	--	5	5	--	--	--	--	--
Decrease in Soil Concentrations	Thermal - Resistive Heating	N	r	--	--	--	-0.038	-0.106	--	0.068	-0.579	-0.045	--	--
			p	--	--	--	0.929	0.785	--	0.886	0.173	0.933	--	--
			n	--	--	--	8	9	--	7	7	6	--	--
Decrease in Soil Concentrations	Thermal - Resistive Heating	LN	r	--	--	--	-0.053	-0.196	--	-0.034	-0.565	-0.147	--	--
			p	--	--	--	0.902	0.614	--	0.942	0.187	0.781	--	--
			n	--	--	--	8	9	--	7	7	6	--	--
Decrease in Soil Concentrations	Thermal - Steam Flushing	N	r	--	--	--	--	--	--	--	--	--	--	--
			p	--	--	--	--	--	--	--	--	--	--	--
			n	--	--	--	--	--	--	--	--	--	--	--
Decrease in Soil Concentrations	Thermal - Steam Flushing	LN	r	--	--	--	--	--	--	--	--	--	--	--
			p	--	--	--	--	--	--	--	--	--	--	--
			n	--	--	--	--	--	--	--	--	--	--	--

Table F.5 Correlations with field case studies and modeling studies - all media

PERFORMANCE METRIC	TECHNOLOGY	DATA TRANSFORMATION	STATISTICS	Areal Extent of DNAPL Source	Depth to Groundwater	Depth to Top of Aquifer	Hydraulic Conductivity	Horizontal Hydraulic Gradient	Groundwater Velocity	Maximum Depth of the DNAPL Zone	Preremediation DNAPL Mass	Saturated Aquifer Thickness	Thickness of DNAPL Zone	Total Number of Oxidant Injections	Volume of DNAPL Zone	Soil Porosity	Total Mass of Oxidant Injected	Oxidant Application Duration	Oxidant Concentration
Decrease in Soil Concentrations	Thermal - All	N	r	0.023	-0.222	-0.213	0.019	--	--	-0.143	0.076	0.156	0.513	--	0.192	--	--	--	--
			p	0.935	0.361	0.446	0.951	--	--	0.611	0.886	0.648	0.239	--	0.572	--	--	--	--
			n	15	19	15	13	--	--	15	6	11	7	--	11	--	--	--	--
Decrease in Soil Concentrations	Thermal - All	LN	r	-0.220	-0.266	-0.156	-0.068	--	--	-0.193	0.202	-0.017	**0.852**	--	0.023	--	--	--	--
			p	0.432	0.271	0.579	0.826	--	--	0.490	0.702	0.961	0.015	--	0.947	--	--	--	--
			n	15	19	15	13	--	--	15	6	11	7	--	11	--	--	--	--
Removal of DNAPL Mass	Chemical Oxidation - Fenton's Reagent or Hydrogen Peroxide	N	r	--	0.446	--	--	--	--	--	--	--	--	-0.004	--	--	--	--	--
			p	--	0.452	--	--	--	--	--	--	--	--	0.995	--	--	--	--	--
			n	--	5	--	--	--	--	--	--	--	--	5	--	--	--	--	--
Removal of DNAPL Mass	Chemical Oxidation - Fenton's Reagent or Hydrogen Peroxide	LN	r	--	0.099	--	--	--	--	--	--	--	--	-0.064	--	--	--	--	--
			p	--	0.874	--	--	--	--	--	--	--	--	0.919	--	--	--	--	--
			n	--	5	--	--	--	--	--	--	--	--	5	--	--	--	--	--
Removal of DNAPL Mass	Chemical Oxidation - Permanganate	N	r	0.295	**0.592**	**0.393**	-0.032	**-0.517**	-0.108	**0.468**	0.165	0.221	-0.040	0.183	**0.328**	**-0.393**	**0.489**	0.129	**0.402**
			p	0.052	0.000	0.008	0.837	0.000	0.556	0.001	0.278	0.154	0.854	0.240	0.030	0.012	0.001	0.398	0.006
			n	44	44	44	44	43	32	45	45	43	24	43	44	40	44	45	45
Removal of DNAPL Mass	Chemical Oxidation - Permanganate	LN	r	-0.031	--	--	-0.041	**-0.353**	-0.233	**0.383**	0.220	0.055	-0.186	0.182	-0.073	-0.291	0.174	-0.254	0.230
			p	0.845	--	--	0.799	0.024	0.215	0.011	0.156	0.732	0.407	0.256	0.648	0.077	0.271	0.100	0.137
			n	42	--	--	42	41	30	43	43	41	22	41	42	38	42	43	43
Removal of DNAPL Mass	Chemical Oxidation - All	N	r	**0.319**	**0.373**	**0.394**	-0.034	**-0.517**	-0.108	**0.495**	0.125	**0.509**	-0.018	0.273	**0.360**	**-0.393**	**0.498**	0.045	**0.455**
			p	0.029	0.008	0.006	0.822	0.000	0.556	0.000	0.391	0.000	0.929	0.060	0.012	0.012	0.001	0.757	0.001
			n	47	49	48	46	43	32	47	49	46	27	48	48	40	45	49	48
Removal of DNAPL Mass	Chemical Oxidation - All	LN	r	0.058	0.064	-0.093	-0.030	**-0.353**	-0.233	**0.451**	0.214	**0.310**	-0.153	**0.304**	0.016	-0.291	0.210	**-0.389**	**0.388**
			p	0.704	0.891	0.881	0.847	0.024	0.215	0.002	0.153	0.041	0.465	0.042	0.919	0.077	0.177	0.008	0.008
			n	45	7	5	43	41	30	45	46	44	25	45	45	38	43	46	45
Removal of DNAPL Mass	Enhanced Bioremediation - Anaerobic	N	r	0.135	0.097	0.343	0.388	.	--	-0.248	-0.157	-0.135	-0.135	--	0.135	.	--	--	--
			p	0.660	0.731	0.230	0.190	.	--	0.373	0.575	0.660	0.660	--	0.660	.	--	--	--
			n	13	15	14	13	12	--	15	15	13	13	--	13	13	--	--	--
Removal of DNAPL Mass	Enhanced Bioremediation - Anaerobic	LN	r	0.051	0.109	0.235	**0.696**	.	--	-0.165	-0.076	-0.051	-0.051	--	0.051	.	--	--	--
			p	0.868	0.699	0.419	0.008	.	--	0.557	0.789	0.868	0.868	--	0.868	.	--	--	--
			n	13	15	14	13	12	--	15	15	13	13	--	13	13	--	--	--
Removal of DNAPL Mass	Surfactant Flushing	N	r	**-0.838**	0.277	0.197	0.317	**-0.981**	-0.082	0.191	**-0.731**	-0.162	-0.066	--	**-0.964**	-0.377	--	--	--
			p	0.000	0.170	0.357	0.115	0.000	0.790	0.340	0.000	0.428	0.750	--	0.000	0.184	--	--	--
			n	25	26	24	26	22	13	27	26	26	26	--	23	14	--	--	--
Removal of DNAPL Mass	Surfactant Flushing	LN	r	**-0.847**	0.674	--	**0.622**	**-0.939**	0.001	-0.018	**-0.744**	-0.222	-0.199	--	**-0.908**	-0.399	--	--	--
			p	0.000	0.212	--	0.001	0.000	0.997	0.932	0.000	0.285	0.341	--	0.000	0.177	--	--	--
			n	24	5	--	25	21	13	26	25	25	25	--	22	13	--	--	--
Removal of DNAPL Mass	Thermal - Resistive Heating	N	r	**-0.923**	**-0.885**	**-0.836**	--	--	--	-0.076	-0.200	--	--	--	**-0.951**	--	--	--	--
			p	0.009	0.019	0.038	--	--	--	0.886	0.704	--	--	--	0.013	--	--	--	--
			n	6	6	6	--	--	--	6	6	--	--	--	5	--	--	--	--
Removal of DNAPL Mass	Thermal - Resistive Heating	LN	r	-0.798	-0.777	-0.545	--	--	--	-0.195	-0.417	--	--	--	-0.824	--	--	--	--
			p	0.057	0.069	0.264	--	--	--	0.711	0.410	--	--	--	0.086	--	--	--	--
			n	6	6	6	--	--	--	6	6	--	--	--	5	--	--	--	--
Removal of DNAPL Mass	Thermal - Steam Flushing	N	r	--	0.133	0.133	--	--	--	0.203	--	--	--	--	--	--	--	--	--
			p	--	0.831	0.831	--	--	--	0.744	--	--	--	--	--	--	--	--	--
			n	--	5	5	--	--	--	5	--	--	--	--	--	--	--	--	--
Removal of DNAPL Mass	Thermal - Steam Flushing	LN	r	--	-0.066	-0.067	--	--	--	0.266	--	--	--	--	--	--	--	--	--
			p	--	0.916	0.915	--	--	--	0.666	--	--	--	--	--	--	--	--	--
			n	--	5	5	--	--	--	5	--	--	--	--	--	--	--	--	--
Removal of DNAPL Mass	Thermal - All	N	r	**-0.907**	0.153	0.124	-0.012	--	--	0.165	-0.232	-0.612	0.176	--	-0.580	--	--	--	--
			p	0.001	0.653	0.716	0.980	--	--	0.628	0.549	0.197	0.706	--	0.132	--	--	--	--
			n	9	11	11	7	--	--	11	9	6	7	--	8	--	--	--	--

Table F.5 Correlations with field case studies and modeling studies - all media

PERFORMANCE METRIC	TECHNOLOGY	DATA TRANSFORMATION	STATISTICS	Mass of Electron Donor Injected	Electron Donor Well Spacing	Duration of Monitoring	Maximum Temperature	Number of Electrodes	Number of Wells	Electrode Spacing	Target Temperature	Time to Maximum Temperature	InjectionRate	TotalDurationOfAmendment
Decrease in Soil Concentrations	Thermal - All	N	r	--	--	--	0.159	0.229	--	0.243	-0.430	0.344	--	--
			p	--	--	--	0.557	0.361	--	0.447	0.110	0.228	--	--
			n	--	--	--	16	18	--	12	15	14	--	--
Decrease in Soil Concentrations	Thermal - All	LN	r	--	--	--	0.147	0.184	--	0.391	-0.411	**0.538**	--	--
			p	--	--	--	0.588	0.465	--	0.209	0.128	0.047	--	--
			n	--	--	--	16	18	--	12	15	14	--	--
Removal of DNAPL Mass	Chemical Oxidation - Fenton's Reagent or Hydrogen Peroxide	N	r	--	--	--	--	--	--	--	--	--	--	--
			p	--	--	--	--	--	--	--	--	--	--	--
			n	--	--	--	--	--	--	--	--	--	--	--
Removal of DNAPL Mass	Chemical Oxidation - Fenton's Reagent or Hydrogen Peroxide	LN	r	--	--	--	--	--	--	--	--	--	--	--
			p	--	--	--	--	--	--	--	--	--	--	--
			n	--	--	--	--	--	--	--	--	--	--	--
Removal of DNAPL Mass	Chemical Oxidation - Permanganate	N	r	--	--	**-0.473**	--	--	--	--	--	--	--	--
			p	--	--	0.001	--	--	--	--	--	--	--	--
			n	--	--	45	--	--	--	--	--	--	--	--
Removal of DNAPL Mass	Chemical Oxidation - Permanganate	LN	r	--	--	**-0.450**	--	--	--	--	--	--	--	--
			p	--	--	0.003	--	--	--	--	--	--	--	--
			n	--	--	41	--	--	--	--	--	--	--	--
Removal of DNAPL Mass	Chemical Oxidation - All	N	r	--	--	--	--	--	--	--	--	--	--	--
			p	--	--	--	--	--	--	--	--	--	--	--
			n	--	--	--	--	--	--	--	--	--	--	--
Removal of DNAPL Mass	Chemical Oxidation - All	LN	r	--	--	--	--	--	--	--	--	--	--	--
			p	--	--	--	--	--	--	--	--	--	--	--
			n	--	--	--	--	--	--	--	--	--	--	--
Removal of DNAPL Mass	Enhanced Bioremediation - Anaerobic	N	r	**0.673**	--	-0.416	--	--	--	--	--	--	--	--
			p	0.016	--	0.109	--	--	--	--	--	--	--	--
			n	12	--	16	--	--	--	--	--	--	--	--
Removal of DNAPL Mass	Enhanced Bioremediation - Anaerobic	LN	r	0.520	--	-0.328	--	--	--	--	--	--	--	--
			p	0.083	--	0.215	--	--	--	--	--	--	--	--
			n	12	--	16	--	--	--	--	--	--	--	--
Removal of DNAPL Mass	Surfactant Flushing	N	r	--	--	**-0.839**	--	--	0.246	--	--	--	**0.610**	**0.724**
			p	--	--	0.000	--	--	0.217	--	--	--	0.016	0.000
			n	--	--	23	--	--	27	--	--	--	15	25
Removal of DNAPL Mass	Surfactant Flushing	LN	r	--	--	**-0.438**	--	--	0.305	--	--	--	0.445	**0.644**
			p	--	--	0.042	--	--	0.130	--	--	--	0.096	0.001
			n	--	--	22	--	--	26	--	--	--	15	24
Removal of DNAPL Mass	Thermal - Resistive Heating	N	r	--	--	--	--	-0.781	--	-0.688	--	--	--	--
			p	--	--	--	--	0.119	--	0.199	--	--	--	--
			n	--	--	--	--	5	--	5	--	--	--	--
Removal of DNAPL Mass	Thermal - Resistive Heating	LN	r	--	--	--	--	-0.685	--	-0.589	--	--	--	--
			p	--	--	--	--	0.201	--	0.296	--	--	--	--
			n	--	--	--	--	5	--	5	--	--	--	--
Removal of DNAPL Mass	Thermal - Steam Flushing	N	r	--	--	--	--	--	--	--	--	--	--	--
			p	--	--	--	--	--	--	--	--	--	--	--
			n	--	--	--	--	--	--	--	--	--	--	--
Removal of DNAPL Mass	Thermal - Steam Flushing	LN	r	--	--	--	--	--	--	--	--	--	--	--
			p	--	--	--	--	--	--	--	--	--	--	--
			n	--	--	--	--	--	--	--	--	--	--	--
Removal of DNAPL Mass	Thermal - All	N	r	--	--	--	0.075	**-0.779**	--	0.302	-0.402	-0.256	--	--
			p	--	--	--	0.860	0.023	--	0.511	0.503	0.579	--	--
			n	--	--	--	8	8	--	7	5	7	--	--

Table F.5 Correlations with field case studies and modeling studies - all media

PERFORMANCE METRIC	TECHNOLOGY	DATA TRANSFORMATION	STATISTICS	Areal Extent of DNAPL Source	Depth to Groundwater	Depth to Top of Aquifer	Hydraulic Conductivity	Horizontal Hydraulic Gradient	Groundwater Velocity	Maximum Depth of the DNAPL Zone	Preremediation DNAPL Mass	Saturated Aquifer Thickness	Thickness of DNAPL Zone	Total Number of Oxidant Injections	Volume of DNAPL Zone	Soil Porosity	Total Mass of Oxidant Injected	Oxidant Application Duration	Oxidant Concentration
Removal of DNAPL Mass	Thermal - All	LN	r	-0.652	-0.006	-0.127	-0.445	--	--	0.110	-0.366	-0.571	-0.086	--	-0.559	--	--	--	--
			p	0.057	0.986	0.710	0.317	--	--	0.749	0.333	0.236	0.855	--	0.150	--	--	--	--
			n	9	11	11	7	--	--	11	9	6	7	--	8	--	--	--	--
Treatment Duration	Chemical Oxidation - Fenton's Reagent or Hydrogen Peroxide	N	r	0.810	0.316	-0.422	-0.425	-0.319	--	0.637	--	--	--	0.019	-0.341	--	--	0.347	-0.363
			p	0.097	0.317	0.196	0.401	0.600	--	0.248	--	--	--	0.956	0.574	--	--	0.400	0.377
			n	5	12	11	6	5	--	5	--	--	--	11	5	--	--	8	8
Treatment Duration	Chemical Oxidation - Fenton's Reagent or Hydrogen Peroxide	LN	r	0.530	0.360	-0.511	-0.377	-0.023	--	0.566	--	--	--	0.233	-0.198	--	--	0.549	-0.439
			p	0.358	0.250	0.108	0.461	0.971	--	0.320	--	--	--	0.491	0.749	--	--	0.159	0.276
			n	5	12	11	6	5	--	5	--	--	--	11	5	--	--	8	8
Treatment Duration	Chemical Oxidation - Permanganate	N	r	-0.107	-0.182	**-0.290**	-0.098	0.249	0.251	-0.210	0.096	-0.108	-0.136	-0.114	-0.087	0.055	**0.309**	**0.997**	-0.165
			p	0.448	0.169	0.027	0.485	0.081	0.124	0.116	0.532	0.444	0.442	0.406	0.540	0.729	0.017	0.000	0.212
			n	53	59	58	53	50	39	57	45	52	34	55	52	42	59	59	59
Treatment Duration	Chemical Oxidation - Permanganate	LN	r	-0.110	-0.101	-0.281	0.170	**0.383**	0.175	**-0.582**	-0.253	0.197	-0.133	**-0.321**	-0.120	-0.012	0.144	**0.999**	**-0.628**
			p	0.434	0.756	0.402	0.223	0.006	0.287	0.000	0.093	0.162	0.454	0.017	0.398	0.938	0.276	0.000	0.000
			n	53	12	11	53	50	39	57	45	52	34	55	52	42	59	59	59
Treatment Duration	Chemical Oxidation - All	N	r	-0.142	-0.214	-0.201	-0.070	0.220	**0.312**	**-0.251**	-0.047	-0.172	-0.131	-0.101	-0.191	0.055	**0.254**	**0.996**	**-0.271**
			p	0.282	0.067	0.090	0.595	0.100	0.044	0.047	0.747	0.200	0.426	0.415	0.152	0.729	0.048	0.000	0.024
			n	59	74	72	60	57	42	63	50	57	39	68	58	42	61	69	69
Treatment Duration	Chemical Oxidation - All	LN	r	**-0.268**	-0.083	-0.193	0.177	**0.403**	0.302	**-0.613**	-0.243	0.010	-0.029	**-0.344**	**-0.270**	-0.012	0.096	**0.959**	**-0.690**
			p	0.040	0.679	0.414	0.176	0.002	0.052	0.000	0.089	0.943	0.862	0.004	0.040	0.938	0.462	0.000	0.000
			n	59	27	20	60	57	42	63	50	57	39	68	58	42	61	69	69
Treatment Duration	Enhanced Bioremediation - Anaerobic	N	r	-0.133	-0.133	-0.274	0.045	0.340	0.344	-0.170	0.215	-0.175	-0.132	--	-0.108	0.086	--	--	--
			p	0.525	0.467	0.123	0.837	0.121	0.404	0.378	0.460	0.424	0.580	--	0.689	0.750	--	--	--
			n	25	32	33	23	22	8	29	14	23	20	--	16	16	--	--	--
Treatment Duration	Enhanced Bioremediation - Anaerobic	LN	r	0.227	-0.099	0.122	**0.767**	0.281	**0.730**	-0.292	**0.817**	-0.155	-0.173	--	0.444	0.018	--	--	--
			p	0.276	0.678	0.618	0.000	0.205	0.040	0.124	0.000	0.481	0.465	--	0.085	0.948	--	--	--
			n	25	20	19	23	22	8	29	14	23	20	--	16	16	--	--	--
Treatment Duration	Surfactant Flushing	N	r	**-0.744**	-0.226	-0.166	**0.523**	**-0.827**	-0.534	-0.146	**-0.533**	0.277	0.104	--	**-0.797**	-0.096	--	--	--
			p	0.000	0.278	0.437	0.007	0.000	0.074	0.466	0.006	0.171	0.621	--	0.000	0.755	--	--	--
			n	24	25	24	25	21	12	27	25	26	25	--	22	13	--	--	--
Treatment Duration	Surfactant Flushing	LN	r	**-0.814**	--	--	**0.743**	**-0.784**	0.225	0.293	**-0.498**	0.381	0.364	--	**-0.861**	-0.215	--	--	--
			p	0.000	--	--	0.000	0.000	0.481	0.138	0.011	0.055	0.074	--	0.000	0.480	--	--	--
			n	24	--	--	25	21	12	27	25	26	25	--	22	13	--	--	--
Treatment Duration	Thermal - Conductive Heating	N	r	--	--	--	-0.832	--	--	0.546	--	--	--	--	--	--	--	--	--
			p	--	--	--	0.081	--	--	0.341	--	--	--	--	--	--	--	--	--
			n	--	--	--	5	--	--	5	--	--	--	--	--	--	--	--	--
Treatment Duration	Thermal - Conductive Heating	LN	r	--	0.317	--	--	--	--	-0.748	--	--	--	--	--	--	--	--	--
			p	--	0.604	--	--	--	--	0.146	--	--	--	--	--	--	--	--	--
			n	--	5	--	--	--	--	5	--	--	--	--	--	--	--	--	--
Treatment Duration	Thermal - Resistive Heating	N	r	0.321	-0.208	-0.147	-0.280	--	--	0.039	0.740	0.641	-0.176	--	**0.538**	--	--	--	--
			p	0.225	0.422	0.586	0.404	--	--	0.887	0.093	0.063	0.651	--	0.047	--	--	--	--
			n	16	17	16	11	--	--	16	6	9	9	--	14	--	--	--	--
Treatment Duration	Thermal - Resistive Heating	LN	r	0.472	-0.179	-0.085	0.100	--	--	-0.117	**0.950**	0.609	-0.305	--	**0.591**	--	--	--	--
			p	0.065	0.491	0.753	0.770	--	--	0.666	0.004	0.082	0.425	--	0.026	--	--	--	--
			n	16	17	16	11	--	--	16	6	9	9	--	14	--	--	--	--
Treatment Duration	Thermal - Steam Flushing	N	r	**0.982**	0.177	0.195	-0.069	--	--	**0.765**	--	--	--	--	**0.995**	--	--	--	--
			p	0.000	0.648	0.589	0.896	--	--	0.045	--	--	--	--	0.000	--	--	--	--
			n	7	9	10	6	--	--	7	--	--	--	--	5	--	--	--	--
Treatment Duration	Thermal - Steam Flushing	LN	r	0.749	0.185	0.478	-0.694	--	--	0.442	--	--	--	--	**0.902**	--	--	--	--
			p	0.053	0.634	0.162	0.126	--	--	0.321	--	--	--	--	0.036	--	--	--	--
			n	7	9	10	6	--	--	7	--	--	--	--	5	--	--	--	--

Table F.5 Correlations with field case studies and modeling studies - all media

PERFORMANCE METRIC	TECHNOLOGY	DATA TRANSFORMATION	STATISTICS	Mass of Electron Donor Injected	Electron Donor Well Spacing	Duration of Monitoring	Maximum Temperature	Number of Electrodes	Number of Wells	Electrode Spacing	Target Temperature	Time to Maximum Temperature	InjectionRate	TotalDurationOfAmendment
Removal of DNAPL Mass	Thermal - All	LN	r	--	--	--	0.068	-0.603	--	0.277	-0.337	-0.133	--	--
			p	--	--	--	0.872	0.114	--	0.547	0.579	0.775	--	--
			n	--	--	--	8	8	--	7	5	7	--	--
Treatment Duration	Chemical Oxidation - Fenton's Reagent or Hydrogen Peroxide	N	r	--	--	--	--	--	--	--	--	--	--	--
			p	--	--	--	--	--	--	--	--	--	--	--
			n	--	--	--	--	--	--	--	--	--	--	--
Treatment Duration	Chemical Oxidation - Fenton's Reagent or Hydrogen Peroxide	LN	r	--	--	--	--	--	--	--	--	--	--	--
			p	--	--	--	--	--	--	--	--	--	--	--
			n	--	--	--	--	--	--	--	--	--	--	--
Treatment Duration	Chemical Oxidation - Permanganate	N	r	--	--	-0.160	--	--	--	--	--	--	--	--
			p	--	--	0.225	--	--	--	--	--	--	--	--
			n	--	--	59	--	--	--	--	--	--	--	--
Treatment Duration	Chemical Oxidation - Permanganate	LN	r	--	--	**0.617**	--	--	--	--	--	--	--	--
			p	--	--	0.000	--	--	--	--	--	--	--	--
			n	--	--	56	--	--	--	--	--	--	--	--
Treatment Duration	Chemical Oxidation - All	N	r	--	--	0.004	--	--	--	--	--	--	--	--
			p	--	--	0.972	--	--	--	--	--	--	--	--
			n	--	--	70	--	--	--	--	--	--	--	--
Treatment Duration	Chemical Oxidation - All	LN	r	--	--	**0.619**	--	--	--	--	--	--	--	--
			p	--	--	0.000	--	--	--	--	--	--	--	--
			n	--	--	65	--	--	--	--	--	--	--	--
Treatment Duration	Enhanced Bioremediation - Anaerobic	N	r	**0.493**	0.330	-0.023	--	--	--	--	--	--	--	--
			p	0.008	0.196	0.890	--	--	--	--	--	--	--	--
			n	28	17	38	--	--	--	--	--	--	--	--
Treatment Duration	Enhanced Bioremediation - Anaerobic	LN	r	**0.630**	0.266	**0.410**	--	--	--	--	--	--	--	--
			p	0.000	0.302	0.020	--	--	--	--	--	--	--	--
			n	28	17	32	--	--	--	--	--	--	--	--
Treatment Duration	Surfactant Flushing	N	r	--	--	-0.343	--	--	-0.270	--	--	--	0.211	**0.936**
			p	--	--	0.101	--	--	0.173	--	--	--	0.432	0.000
			n	--	--	24	--	--	27	--	--	--	16	26
Treatment Duration	Surfactant Flushing	LN	r	--	--	0.224	--	--	-0.086	--	--	--	**0.756**	**0.990**
			p	--	--	0.292	--	--	0.669	--	--	--	0.001	0.000
			n	--	--	24	--	--	27	--	--	--	16	26
Treatment Duration	Thermal - Conductive Heating	N	r	--	--	--	--	-0.215	-0.321	--	--	--	--	--
			p	--	--	--	--	0.728	0.599	--	--	--	--	--
			n	--	--	--	--	5	5	--	--	--	--	--
Treatment Duration	Thermal - Conductive Heating	LN	r	--	--	--	--	0.029	-0.540	--	--	--	--	--
			p	--	--	--	--	0.963	0.347	--	--	--	--	--
			n	--	--	--	--	5	5	--	--	--	--	--
Treatment Duration	Thermal - Resistive Heating	N	r	--	--	--	0.047	0.199	--	**0.788**	-0.005	0.343	--	--
			p	--	--	--	0.874	0.429	--	0.001	0.988	0.251	--	--
			n	--	--	--	14	18	--	13	11	13	--	--
Treatment Duration	Thermal - Resistive Heating	LN	r	--	--	--	0.130	0.236	--	**0.613**	0.279	0.408	--	--
			p	--	--	--	0.657	0.346	--	0.026	0.405	0.166	--	--
			n	--	--	--	14	18	--	13	11	13	--	--
Treatment Duration	Thermal - Steam Flushing	N	r	--	--	--	0.071	0.669	--	0.049	-0.120	0.344	--	--
			p	--	--	--	0.894	0.070	--	0.937	0.847	0.504	--	--
			n	--	--	--	6	8	--	5	5	6	--	--
Treatment Duration	Thermal - Steam Flushing	LN	r	--	--	--	0.035	0.274	--	0.713	-0.321	**0.876**	--	--
			p	--	--	--	0.948	0.512	--	0.176	0.598	0.022	--	--
			n	--	--	--	6	8	--	5	5	6	--	--

Table F.5 Correlations with field case studies and modeling studies - all media

PERFORMANCE METRIC	TECHNOLOGY	DATA TRANSFORMATION	STATISTICS	Areal Extent of DNAPL Source	Depth to Groundwater	Depth to Top of Aquifer	Hydraulic Conductivity	Horizontal Hydraulic Gradient	Groundwater Velocity	Maximum Depth of the DNAPL Zone	Preremediation DNAPL Mass	Saturated Aquifer Thickness	Thickness of DNAPL Zone	Total Number of Oxidant Injections	Volume of DNAPL Zone	Soil Porosity	Total Mass of Oxidant Injected	Oxidant Application Duration	Oxidant Concentration
Treatment Duration	Thermal - All	N	r	**0.740**	0.186	0.208	0.020	--	--	0.109	**0.704**	0.369	0.157	--	**0.741**	--	--	--	--
			p	0.000	0.317	0.299	0.931	--	--	0.604	0.023	0.160	0.576	--	0.000	--	--	--	--
			n	26	31	27	21	--	--	25	10	16	15	--	21	--	--	--	--
Treatment Duration	Thermal - All	LN	r	**0.524**	0.053	0.160	0.137	--	--	-0.032	**0.820**	0.364	0.120	--	**0.661**	--	--	--	--
			p	0.006	0.778	0.424	0.553	--	--	0.878	0.004	0.165	0.670	--	0.001	--	--	--	--
			n	26	31	27	21	--	--	25	10	16	15	--	21	--	--	--	--
Unit Cost (by volume) of Source Zone Treatment	Chemical Oxidation - Permanganate	N	r	--	--	--	--	--	--	--	--	--	--	--	--	--	--	--	--
			p	--	--	--	--	--	--	--	--	--	--	--	--	--	--	--	--
			n	--	--	--	--	--	--	--	--	--	--	--	--	--	--	--	--
Unit Cost (by volume) of Source Zone Treatment	Chemical Oxidation - Permanganate	LN	r	--	--	--	--	--	--	--	--	--	--	--	--	--	--	--	--
			p	--	--	--	--	--	--	--	--	--	--	--	--	--	--	--	--
			n	--	--	--	--	--	--	--	--	--	--	--	--	--	--	--	--
Unit Cost (by volume) of Source Zone Treatment	Chemical Oxidation - All	N	r	-0.438	-0.162	-0.175	-0.123	--	--	-0.199	--	**0.968**	0.106	-0.212	-0.745	--	-0.299	0.082	-0.030
			p	0.386	0.729	0.679	0.817	--	--	0.669	--	0.007	0.841	0.615	0.089	--	0.625	0.895	0.955
			n	6	7	8	6	--	--	7	--	5	6	8	6	--	5	5	6
Unit Cost (by volume) of Source Zone Treatment	Chemical Oxidation - All	LN	r	-0.708	-0.154	-0.076	0.686	--	--	0.287	--	**0.931**	0.575	-0.299	**-0.872**	--	-0.187	0.717	-0.043
			p	0.115	0.742	0.871	0.132	--	--	0.533	--	0.022	0.233	0.472	0.024	--	0.763	0.173	0.936
			n	6	7	7	6	--	--	7	--	5	6	8	6	--	5	5	6
Unit Cost (by volume) of Source Zone Treatment	Thermal - Resistive Heating	N	r	0.323	-0.420	-0.333	-0.378	--	--	-0.517	--	0.135	--	--	-0.662	--	--	--	--
			p	0.397	0.300	0.382	0.404	--	--	0.154	--	0.829	--	--	0.105	--	--	--	--
			n	9	8	9	7	--	--	9	--	5	--	--	7	--	--	--	--
Unit Cost (by volume) of Source Zone Treatment	Thermal - Resistive Heating	LN	r	0.592	-0.389	-0.320	-0.602	--	--	-0.348	--	0.264	--	--	-0.622	--	--	--	--
			p	0.093	0.340	0.402	0.153	--	--	0.359	--	0.668	--	--	0.136	--	--	--	--
			n	9	8	9	7	--	--	9	--	5	--	--	7	--	--	--	--
Unit Cost (by volume) of Source Zone Treatment	Enhanced Bioremediation - Anaerobic	N	r	--	--	--	--	--	--	--	--	--	--	--	--	--	--	--	--
			p	--	--	--	--	--	--	--	--	--	--	--	--	--	--	--	--
			n	--	--	--	--	--	--	--	--	--	--	--	--	--	--	--	--
Unit Cost (by volume) of Source Zone Treatment	Enhanced Bioremediation - Anaerobic	LN	r	--	--	--	--	--	--	--	--	--	--	--	--	--	--	--	--
			p	--	--	--	--	--	--	--	--	--	--	--	--	--	--	--	--
			n	--	--	--	--	--	--	--	--	--	--	--	--	--	--	--	--
Unit Cost (by volume) of Source Zone Treatment	Thermal - All	N	r	-0.365	-0.464	-0.403	-0.370	--	--	-0.498	--	0.442	-0.498	--	-0.507	--	--	--	--
			p	0.199	0.094	0.153	0.237	--	--	0.083	--	0.273	0.255	--	0.112	--	--	--	--
			n	14	14	14	12	--	--	13	--	8	7	--	11	--	--	--	--
Unit Cost (by volume) of Source Zone Treatment	Thermal - All	LN	r	-0.266	**-0.615**	-0.520	-0.218	--	--	**-0.571**	--	0.351	-0.329	--	**-0.848**	--	--	--	--
			p	0.358	0.019	0.056	0.497	--	--	0.042	--	0.393	0.471	--	0.001	--	--	--	--
			n	14	14	14	12	--	--	13	--	8	7	--	11	--	--	--	--

Table F.5 Correlations with field case studies and modeling studies - all media

PERFORMANCE METRIC	TECHNOLOGY	DATA TRANSFORMATION	STATISTICS	Mass of Electron Donor Injected	Electron Donor Well Spacing	Duration of Monitoring	Maximum Temperature	Number of Electrodes	Number of Wells	Electrode Spacing	Target Temperature	Time to Maximum Temperature	InjectionRate	TotalDurationOfAmendment
Treatment Duration	Thermal - All	N	r	--	--	--	-0.162	0.041	--	0.307	-0.079	0.301	--	--
			p	--	--	--	0.439	0.835	--	0.176	0.739	0.163	--	--
			n	--	--	--	25	31	--	21	20	23	--	--
Treatment Duration	Thermal - All	LN	r	--	--	--	-0.116	0.146	--	**0.661**	-0.012	**0.614**	--	--
			p	--	--	--	0.579	0.434	--	0.001	0.960	0.002	--	--
			n	--	--	--	25	31	--	21	20	23	--	--
Unit Cost (by volume) of Source Zone Treatment	Chemical Oxidation - Permanganate	N	r	--	--	--	--	--	--	--	--	--	--	--
			p	--	--	--	--	--	--	--	--	--	--	--
			n	--	--	--	--	--	--	--	--	--	--	--
Unit Cost (by volume) of Source Zone Treatment	Chemical Oxidation - Permanganate	LN	r	--	--	--	--	--	--	--	--	--	--	--
			p	--	--	--	--	--	--	--	--	--	--	--
			n	--	--	--	--	--	--	--	--	--	--	--
Unit Cost (by volume) of Source Zone Treatment	Chemical Oxidation - All	N	r	--	--	--	0.582	--	--	--	--	--	--	--
			p	--	--	--	0.304	--	--	--	--	--	--	--
			n	--	--	--	5	--	--	--	--	--	--	--
Unit Cost (by volume) of Source Zone Treatment	Chemical Oxidation - All	LN	r	--	--	--	-0.579	--	--	--	--	--	--	--
			p	--	--	--	0.306	--	--	--	--	--	--	--
			n	--	--	--	5	--	--	--	--	--	--	--
Unit Cost (by volume) of Source Zone Treatment	Thermal - Resistive Heating	N	r	--	--	--	-0.007	-0.074	--	0.457	0.093	0.416	--	--
			p	--	--	--	0.986	0.839	--	0.255	0.843	0.412	--	--
			n	--	--	--	8	10	--	8	7	6	--	--
Unit Cost (by volume) of Source Zone Treatment	Thermal - Resistive Heating	LN	r	--	--	--	0.197	-0.028	--	0.312	-0.031	0.572	--	--
			p	--	--	--	0.641	0.939	--	0.452	0.947	0.235	--	--
			n	--	--	--	8	10	--	8	7	6	--	--
Unit Cost (by volume) of Source Zone Treatment	Enhanced Bioremediation - Anaerobic	N	r	--	--	--	--	--	--	--	--	--	--	--
			p	--	--	--	--	--	--	--	--	--	--	--
			n	--	--	--	--	--	--	--	--	--	--	--
Unit Cost (by volume) of Source Zone Treatment	Enhanced Bioremediation - Anaerobic	LN	r	--	--	--	--	--	--	--	--	--	--	--
			p	--	--	--	--	--	--	--	--	--	--	--
			n	--	--	--	--	--	--	--	--	--	--	--
Unit Cost (by volume) of Source Zone Treatment	Thermal - All	N	r	--	--	--	0.192	-0.013	--	-0.245	-0.117	0.126	--	--
			p	--	--	--	0.551	0.963	--	0.468	0.731	0.766	--	--
			n	--	--	--	12	15	--	11	11	8	--	--
Unit Cost (by volume) of Source Zone Treatment	Thermal - All	LN	r	--	--	--	0.288	0.131	--	-0.388	-0.202	0.446	--	--
			p	--	--	--	0.364	0.642	--	0.239	0.551	0.267	--	--
			n	--	--	--	12	15	--	11	11	8	--	--

Notes

All tests conducted using Pearson Correlations at the 5% level of significance. Null hypothesis for the test states that there is no

Bold indicates a significant correlation as determined by the test (p-value < 0.05).

Regressions were performed with the Input Fields that showed a correation to the given Metric Field, however, in the case of a

-- - insufficient data for analysis (<5 observations)

. - insufficient amount of unique independent data values to compute a correlation coefficient

LN - lognormal data transformation

n - sample size

N - no data transformation

r -correlation coefficient

p - p-value. The p-value is calculated as the probability of observing a correlation coefficent at least as extreme as the one observed,

Table F.6 Summary of Regression Analysis 1

Technology	Media Type	Performance Metric (Dependent Variable)	Input Parameter (Independent Variable)	Regression Coefficients		R^2	95% Confidence Interval [2]	Units
				Intercept	Slope [1]			
EISB	Unconsolidated	Reduction in DNAPL mass	Hydraulic conductivity	6.23 (0.72)	0.4 (0.12)	0.44	*/÷ 1.3 [3]	kg
SEAR	Both	Reduction in DNAPL mass	Areal extent of DNAPL zone	94.2 (7.3)	-0.38 (0.05)	0.69	+/- 10.1	kg
SEAR	Both	Reduction in DNAPL mass	Pre-remediation DNAPL mass	78.2 (7.36)	-0.02 (0.003)	0.51	+/- 12.2	kg
SEAR	Both	Reduction in DNAPL mass	Volume of DNAPL zone	97.8 (3.74)	-0.09 (0.006)	0.93	+/- 5.25	kg
Thermal - resistive	Both	Reduction in DNAPL mass	Areal extent of DNAPL zone	101 (9.73)	-0.02 (0.004)	0.82	+/- 20.0	kg
Thermal - resistive	Both	Reduction in DNAPL mass	Volume of DNAPL zone	102 (9.97)	-0.002 (0.0005)	0.87	+/- 22.0	kg
Thermal - resistive	Both	Treatment Duration	Pre-remediation DNAPL mass	1.06 (0.36)	0.26 (0.04)	0.88	*/÷ 0.22 [3]	wks
Thermal - resistive	Both	Treatment Duration	Electrode spacing	-7.36 (10.6)	7.26 (1.71)	0.59	+/- 9.81	wks
Thermal - steam	Both	Treatment Duration	Volume of DNAPL zone	16.1 (5.29)	0.0006 (0.00003)	0.99	+/- 14.4	wks

Notes:

[1] All estimates of the slope parameter were statistically significant at the 5% level of significance (i.e., p-value < 0.05).

[2] 95% confidence intervals give the range of the expected upper and lower limits for a performance metric, given a specific input parameter value.

[3] Log-transformed data was used to fit the model; therefore, the effect of the independent variable is multiplicative rather than additive.

Acronyms:

R^2 - coefficient of determination
SE - standard error
kg - kilograms
wks - weeks

Table F.7 Summary of Regression Analysis 2

Technology	Media Type	Performance Metric (Independent Variable)	Input Parameter (Dependent Variable)	Regression Coefficients		R^2	95% Confidence Interval	Units
				Intercept (SE)	Slope (SE)			
EISB	Unconsolidated	Reduction in DNAPL mass	Hydraulic conductivity	-10.5 (1.51)	1.22 (0.38)	0.98	*/÷ 1.58 [3]	cm/s
SEAR	Both	Reduction in DNAPL mass	Areal extent of DNAPL zone	206 (17.5)	-1.86 (0.25)	0.69	+/- 22	m^2
SEAR	Both	Reduction in DNAPL mass	Preremediation DNAPL mass	3,260 (439)	-33.1 (6.32)	0.51	+/- 553	kg
SEAR	Both	Reduction in DNAPL mass	Volume of DNAPL zone	1,000 (40.1)	-9.89 (0.59)	0.93	+/- 54	m^3
Thermal - resistive	Both	Reduction in DNAPL mass	Areal extent of DNAPL zone	4,370 (675)	-41.1 (8.55)	0.81	+/- 889	m^2
Thermal - resistive	Both	Reduction in DNAPL mass	Volume of DNAPL zone	38,600 (5,090)	-363 (68.0)	0.87	+/- 8,380	m^3
Thermal - resistive	Both	Treatment Duration	Electrode spacing	2.75 (0.83)	0.09 (0.02)	0.59	*/÷ 2.17 [3]	kg
Thermal - resistive	Both	Treatment Duration	Preremediation DNAPL mass	-2.83 (1.83)	3.42 (0.56)	0.68	+/- 1.06	m
Thermal - steam	Both	Treatment Duration	Volume of DNAPL zone	-27,500 (10,300)	1,760 (104)	0.99	+/- 25,200	m^3

Notes:

[1] All estimates of the slope parameter were statistically significant at the 5% level of significance (i.e., p-value < 0.05).

[2] 95% confidence intervals give the range of the expected upper and lower limits for a performance metric, given a specific input parameter value.

[3] Log-transformed data was used to fit the model; therefore, the effect of the independent variable is multiplicative rather than additive.

Acronyms:

R^2 - coefficient of determination
SE - standard error
kg - kilograms
m- meters
m^2 - squared meters
m^3 - cubic meters
cm/s - centimeters per second

APPENDIX G

PROTOCOL VALIDATION

APPENDIX G: DNAPL TEST SITE SELECTION PROTOCOL VALIDATION

As part of the quality control process, several scenarios were run using DNAPL test and the results were verified against actual case study data to confirm that all filters are functioning properly. Three verification scenarios are presented here:

- Verification of the General Analysis;
- Verification of the Site Specific Analysis when no statistical filters are applied; and
- Verification of the Site Specific Analysis when statistical filters are applied.

Table G.1 shows the results of the verification of the General Analysis. This verification was conducted by running a General Analysis and selecting filtering criteria randomly. The first column in the table shows the input criteria available in the General Analysis and the second column shows the criteria selected for the analysis. The next several columns show all of the case studies identified in the output reports, and the specific values for each case study for each of the input criteria. Finally, the ”Verified?” column (last column) indicates whether the case studies included in the output met the specified criteria (indicated by a check). As seen in **Table G.1**, verification of the General Analysis was successful and all case studies included in the output were appropriate.

Table G.2 shows the results of the verification of the Site Specific Analysis for a scenario where statistical filters are not relevant. This verification scenario is similar to that of the General Analysis and confirms that the direct filtering criteria programmed into the Site Specific Analysis are performing correctly. The bottom eight rows of this table also provide validation of the data generated in the summary reports for each performance metric. The first column lists all of the output reports, and the second column indicates the value for key metrics in each output report. The next three columns provide the individual values for each case study (or “NR” if the value wasn’t reported). Finally, the verification step for the individual reports involved checking the values in the summary report to confirm they were calculated correctly. As seen in **Table G.2**, verification of the Site Specific Analysis non-statistical filters was successful and all case studies included in the output were appropriate.

Table G.3 shows the results of the verification of the site specific analysis when statistical filters are relevant. The top portion of this table is similar to the other verifications, and contains columns that show the criteria, the value entered into the tool for both statistical and non-statistical filters, and the actual values for each criterion for each case study included in the analysis. The second and third sections of the table show verification of the “Reduction in DNAPL Mass Report”, which includes statistical filters

for the technologies provided in this example, and for the "Treatment Duration Report", for which there are no statistical filters for the technologies provided.

As shown in **Table G.3**, for SEAR and anaerobic EISB, the technologies included in this verification scenario, the following statistical correlations exist:

- For anaerobic EISB, reduction in DNAPL mass is correlated to hydraulic conductivity in unconsolidated media; and

- For SEAR, reduction in DNAPL mass is correlated with areal extent, volume, and pre-remediation DNAPL mass.

For the Reduction in DNAPL Mass Report, user specified inputs that are not statistically correlated for these technologies with the removal in DNAPL mass performance metric, verification that each case study should be included was conducted by confirming that the actual value for the case study matched the scenario input values. Input parameters that are statistically correlated were validated as follows:

For parameters source treatment area, pre-remediation DNAPL mass and volume of impacted soils: these inputs are only correlated to in the removal of DNAPL mass performance for the SEAR technology. The SEAR case studies were therefore verified by confirming the values for each SEAR study fell within the range of the value input for the statistical filter plus/minus the value shown in **Table G.3** for each correlation.

For site parameter hydraulic conductivity: this input is only correlated to the removal of DNAPL mass performance metric for anaerobic EISB in unconsolidated media. The EISB case studies were verified by confirming the values for each EISB study fell within the range of the value input for the statistical filter plus/minus the value shown in **Table G.3** for each correlation.

Note that if multiple statistical filters exist for one performance metric, case studies will be included if *any* of the statistical filter criteria are met (*i.e.,* there is an OR criterion for case study selection). For example, in Case Study 1, the actual values for the source treatment area and volume are not within the statistical filter range for these inputs, but the case study is included because the value for pre-remediation DNAPL mass is within the statistical filter range.

Verification of the treatment duration report, because there are no statistical filters, involved confirming that the actual values for each criteria were consistent with *all* of the input criteria (*i.e.,* there is an AND criterion for case study selection). This check also confirmed that Sites that were included in the analysis, but did not meet the non-statistical criteria ranges specified (*e.g.* Case Study 2), were not included in the treatment duration output report.

Table G.1. Summary of the General Analysis Verification.

	Entered into Tool (GA Verification Scenario 1)	Case Studies Output From Tool														Verified?
		Case Study 1	Case Study 2	Case Study 3	Case Study 4	Case Study 5	Case Study 6	Case Study 7	Case Study 8	Case Study 9	Case Study 10	Case Study 11	Case Study 12	Case Study 13	Case Study 14	
Study Identifier	-	**45**	**75**	**77**	**78**	**136**	**145**	**147**	**156**	**158**	**209**	**214**	**143**	**207**	**220**	
Technology	ISCO-Permanganate; ISCO-Fentons or Peroxide; EISB-Anaerobic; SEAR; Thermal-Conductive	EISB-An	EISB-An	EISB-An	EISB-An	EISB-An	EISB-An	EISB-An	EISB-An	EISB-An	EISB-An	ISCO-FP	ISCO-MnO4	ISCO-MnO4	Th-Conductive	✓
Data Quality Ranking	All DQRs	1.65	1.5	1.5	2.4	2.2	1.6	2	1.6	1.65	1.85	1.4	1.65	2.15	2.1	✓
Study Type	Full Scale Field; Modeling Studies	Field Application - Full Scale Pilot	Field Application - Full Scale Pilot	Field Application - Full Scale Pilot	Field Application - Full Scale Pilot	Field Application - Full Scale Pilot	Field Application - Full Scale Pilot	Field Application - Full Scale Pilot	Field Application - Full Scale Pilot	Field Application - Full Scale Pilot	Field Application - Full Scale Pilot	Field Application - Full Scale Pilot	Field Application - Full Scale Pilot	Field Application - Full Scale Pilot	Field Application - Full Scale Pilot	✓
Source Treatment Area	<50 m^2 (<538ft^2); >500m^2 (>5382ft^2); Unknown	Unknown	Unknown	Unknown	Unknown	Unknown	37,161 m^2	900 m^2	Unknown	Unknown	Unknown	1457 m^2	9308 m^2	Unknown	Unknown	✓
Geology	Unconsolidated: Gravel; Sand; Silt; Clay. Consolidated: Igneous; Other Consolidated	Unconsolidated (Sand)	Unconsolidated (Gravel)	Unconsolidated (Sand)	Unconsolidated (Sand)	Unconsolidated (Clay)	Unconsolidated (Sand)	Unconsolidated (Silt)	Unconsolidated (Clay)	Unconsolidated (Sand)	Unconsolidated (Clay)	Unconsolidated (Clay)	Unconsolidated (Sand)	Consolidated (Igneous)	Consolidated (Other Consolidated)	✓
Degree of Heterogeneity	Low heterogeneity (<3 orders of magnitude variation in hydraulic conductivity…); Medium heterogeneity (3 to 5 orders of magnitude variation in hydraulic conductivity); Unspecified	unknown	unknown	unknown	unknown	Low heterogeneity (<3 orders of magnitude variation in hydraulic conductivity…)	Low heterogeneity (<3 orders of magnitude variation in hydraulic conductivity…)	Low heterogeneity (<3 orders of magnitude variation in hydraulic conductivity…)	Low heterogeneity (<3 orders of magnitude variation in hydraulic conductivity…)	Medium heterogeneity (3 to 5 orders of magnitude variation in hydraulic conductivity)	Medium heterogeneity (3 to 5 orders of magnitude variation in hydraulic conductivity)	Medium heterogeneity (3 to 5 orders of magnitude variation in hydraulic conductivity)	Low heterogeneity (<3 orders of magnitude variation in hydraulic conductivity).	not applicable	not applicable	✓
Hydraulic Conductivity (cm/s)	1.0E-6 to 1.0E-4 cm/s (3.28E-8 to 3.28E-6 6 cm/s); >1.0 cm/s (>3.28E-2 cm/s); Unspecified	8.12E-05	Unspecified	Unspecified	Unspecified	2.82E-05	Unspecified	Unspecified	Unspecified	Unspecified	Unspecified	Unspecified	Unspecified	Unspecified	9.88E-06	✓
Pre-remediation Mass	100 to 1000 kg (220 - 2205 lbs); Unspecified	Unspecified	Unspecified	Unspecified	Unspecified	Unspecified	Unspecified	Unspecified	Unspecified	Unspecified	Unspecified	Unspecified	Unspecified	Unspecified	Unspecified	✓
Case Study Chemistry	Chlorinated Ethenes (e.g., PCE, TCE); Chlorinated Benzenes (e.g., 1,2,4-TCB)	PCE	PCE, TCE, cDCE	TCE, cDCE	PCE, TCE, 111TCA	PCE	PCE, TCE, cDCE, tDCE, VC	PCE, TCE, cDCE, VC	PCE, TCE	PCE	PCE	PCE	PCE, TCE, cDCE, tDCE, VC	PCE, cDCE	TCE	✓

Acronyms

1,2,4-TCB - 1,2,4-trichlorobenzene
111TCA - 1,1,1-trichloroethane
An - Anaerobic
cDCE - cis-1,2-dichloroethene
cDCE - trans-1,2-dichloroethene
cm/s - centimeters per second
DNAPL - dense non-aqueous phase liquids
EISB - enhanced *in situ* bioremediation
FP Fentons/Peroxide
ft/sec - feet per second
ft^2 - square feet
GA - General Analysis
ISCO - *in situ* chemical oxidation
kg - kilograms
lbs - pounds
m^2 - square meters
MnO4 - Permanganate
PCE - tetrachloroethene
SEAR - surfactant enhanced aquifer remediation
TCE - trichloroethene
Th - Thermal
VC - vinyl chloride

Table G.2. Summary of the Site Specific Analysis Verification for Non-Statistical Filters

	Entered into Tool (Verification Scenario 1) [1]	Case Studies Output From Tool			Verification
		Case Study 1	Case Study 2	Case Study 3	Correct Case Studies Included?
Study Identifier	50	26	50	53	n/a
Study Type	Field - Full Scale, Field - Pilot Scale	Field - Pilot Scale	Field - Pilot Scale	Field - Pilot Scale	✓
Technology	ISCO - $KMnO_4$	ISCO - $KMnO_4$	ISCO - $KMnO_4$	ISCO - $KMnO_4$	✓
DNAPL Constituents	TCE	TCE	TCE	TCE	✓
Geology	Unconsolidated	Unconsolidated	Unconsolidated	Unconsolidated	✓
Degree of Heterogeneity	High	High	High	High	✓
Bioaugmented	sites with and without	n/a - ISCO	n/a - ISCO	n/a - ISCO	n/a
Source Treatment Area - Range for Non-statistical filters	not entered [2]	1839 m^2	348 m^2	not provided	✓
Source Treatment Area - Value for Statistical Filters	3750 ft^2	1839 m^2	348 m^2	not provided	n/a
Hydraulic Conductivity - Range for Non-statistical filters	not entered [2]	0.00706 cm/s	0.0012355 cm/s	0.00001 cm/s	✓
Hydraulic Conductivity - Value for Statistical Filters	3.4 ft/d	0.00706 cm/s	0.0012355 cm/s	0.00001 cm/s	n/a
Volume of Impacted Soils - Range for Non-statistical filters	not entered [2]	3364 m^3	4247 m^3	not provided	✓
Volume of Impacted Soils Value for Statistical Filters	150,000 ft^3	3364 m^3	4247 m^3	not provided	n/a
Pre-Remediation DNAPL Mass - Range for Non-statistical filters	not entered [2]	124 kg	5,039 kg	not provided	✓
Pre-Remediation DNAPL Mass - Value for Statistical Filters	7,110 kg	124 kg	5,039 kg	not provided	n/a
Correct Values for Performance Metrics in Reports?	**Summary Output**	**Individual**			**Summary Output Verified?**
DNAPL Mass Removal Report	average: 77% min: 77% max: 77%	77%	77%	NR	✓
Groundwater Concentration Decrease Report	average: 77% min: 77% max: 77%	77%	NR	NR	✓
Soil Concentration Decrease Report	No Report	NR	NR	NR	✓
Achievement of MCLs Report	100% of studies reported achieved MCLs	NR	Yes	NR	✓
Rebound Report	50% of studies reported observed rebound	Yes	No	NR	✓
Treatment Duration Report	average: 6 weeks min: 0.01 weeks max: 12 weeks	5 weeks	12 weeks	0.014 weeks	✓
Unit Cost of Source Zone Treatment Report	average: \$150/m^3 min: \$35/m^3 max: \$240/m^3	\$170/m^3	\$240/m^3	\$35/m^3	✓

Notes

1 - There are no statistical correlations for ISCO, therefore this Verification Scenario evaluates only non-statistical filters

2 - When values are not entered to specify ranges in site characteristics to include in the analyses (in 'Step 4 - Input Non-Statistical Filters', all case studies are included, with the exception of cases where statistical correlations are present (in which case the value input on 'Step 5 - Input Statistical Filters' will be used)

Acronyms

cm/s - centimeters per second
ft/day - feet per day
ISCO - in situ chemical oxidation
kg - kilograms
$KMnO_4$ - permanganate
m^2 - square meters
m^3 - cubic meters
MCLs - maximum contaminant levels
n/a - not applicable
NR - not reported
TCE - trichloroethene

Table G.3. Summary of the Verification of the Site Specific Analysis Site Selection Protocol for Statistical Filters

	Entered into Tool (Verification Scenario 2) [1]		Case Studies Output From Tool			
	Statistical Filters	**Non-Statistical Filters**	**Case Study 1**	**Case Study 2**	**Case Study 3**	**Case Study 4**
Study Identifier	148		16	18	132	148
Study Type	n/a	All	Field - Pilot Scale	Field - Pilot Scale	Field - Pilot Scale	Field - Pilot Scale
Technology	n/a	EISB-An, EISB-A, SEAR, Thermal - ERH	SEAR	SEAR	SEAR	EISB - An
DNAPL Constituents	n/a	PCE, TCE, cDCE, tDCE, VC	PCE	PCE, TCE, 111TCA,	TCE, cDCE, 111TCA,	PCE, TCE, cDCE
Geology	n/a	Consolidated/ Unconsolidated	Unconsolidated	Unconsolidated	Unconsolidated	Unconsolidated
Degree of Heterogeneity	n/a	All	Low	Low	High	Low
Bioaugmented	n/a	With and Without	n/a	n/a	n/a	With
Source Treatment Area	512 ft^2 (47.6 m^2)	100 - 1,000 ft^2 (9.3 m^2 - 93 m^2)	13.8 m^2	not reported	37.2 m^2	47.6 m^2
Hydraulic Conductivity	0.007 cm/s	0.0007 - 0.07 cm/s	0.01	0.04	0.004	0.007
Volume of Impacted Soils - Range for Non-statistical filters	12,810 ft^3 (363 m^3)	4,000 - 20,000 ft^3 (113 - 566 m^3)	165.3 m^3	not reported	119 m^3	362 m^3
Pre-Remediation DNAPL Mass - Range for Non-statistical filters	163 kg	50-400 kg	80 kg	181 kg	not reported	162 kg
Verification	**Filter**	**Range (Filter Type)**	**Case Study Matches Criteria?**			
Reduction in DNAPL Mass Report	Study Type	All studies (non-statistical)	✓	✓	✓	✓
	Technology	EISB-An, EISB-A, SEAR, Thermal - ERH	✓	✓	✓	✓
	DNAPL Constituents	PCE, TCE, cDCE, tDCE, VC	✓	✓	✓	✓
	Geology	Consolidated/ Unconsolidated	✓	✓	✓	✓
	Degree of Heterogeneity	All	✓	✓	✓	✓
	Bioaugmentation	With and Without	✓	✓	✓	✓
	Source Treatment Area	100 - 1,000 ft^2 (non-statistical)	n/a	n/a	n/a	✓
		47.6 ± 22 m^2 (statistical; SEAR only)	✗ (2)	✗ (2)	✓	n/a
	Pre-Remediation DNAPL Mass	163 ± 553 kg (statistical, SEAR only)	✓	✓	✓	n/a
		50-400 kg (non-statistical)	n/a	n/a	n/a	✓
	Volume of Impacted Soils	363 ± 54 m^3	✗ (2)	✓	✗ (2)	
		113-566 m^3	n/a	n/a	n/a	✓
	Hydraulic Conductivity	0.007/1.58 to 0.007*1.58 (statistical; Unconsolidated EISB-An only)	n/a	n/a	n/a	✓
		0.0007 - 0.07 cm/s (non-statistical)	✓	✓	✓	✓
Statistical Filter Verification - Include In DNAPL Mass Report?			✓	✓	✓	✓

	Entered into Tool (Verification Scenario 2) [1]		Case Studies Output From Tool			
	Statistical Filters	**Non-Statistical Filters**	**Case Study 1**	**Case Study 2**	**Case Study 3**	**Case Study 4**
Treatment Duration Report	**Study Type**	All	✓	✓	✓	✓
	Technology	EISB-An, EISB-A, SEAR, Thermal - ERH	✓	✓	✓	✓
	DNAPL Constituents	PCE, TCE, cDCE, tDCE, VC	✓	✓	✓	✓
	Geology	Consolidated/ Unconsolidated	✓	✓	✓	✓
	Degree of Heterogeneity	All	✓	✓	✓	✓
	Bioaugmented	With and Without	n/a	n/a	n/a	✓
	Source Treatment Area	100 - 1,000 ft^2 (9.3 m^2 - 93 m^2)	✓	✗	✓	✓
	Hydraulic Conductivity	0.0007 - 0.07 cm/s	✓	✓	✓	✓
	Volume of Impacted Soils - Range for Non-statistical filters	4,000 - 20,000 ft^3 (113 - 566 m^3)	✓	✓	✓	✓
	Pre-Remediation DNAPL Mass - Range for Non-statistical filters	50-400 kg	✓	✓	✗	✓
	Data Reported for this Metric?	n/a	✓	✓	✓	✓
	Site In Treatment Duration Report?	n/a	✓	✗	✗	✓
Non-statistical Filter Verification - Treatment Duration Report?			✓	✓	✓	✓

Notes

1 - Verification Scenario 2 is based on Lebron et al. (2007) and involves verification of both statistical and non-statistical filters.

2 - Where more than one statistical filter exists for the same performance metric and technology combination, if any one of the statistical filters match, they will be included in the analysis. Case Study 1 is therefore included because pre-remediation DNAPL mass falls within the criteria, and Case Study 3 is included because source treatment area and pre-remediation DNAPL mass fall within the criteria.

Acronyms

111TCA - 1,1,1-trichlorethene
cDCE - cis-1,2-dichloroethene
cm/s - centimeters per second
DNAPL - dense non-aqueous phase liquid
EISB-A - aerobic enhanced in-situ bioremediation
EISB-An - anaerobic enhanced in-situ bioremediation
ft/day - feet per day
ISCO - in situ chemical oxidation
kg - kilograms
KMnO4 - permanganate
m2 - square meters
m3 - cubic meters
n/a - not applicable
PCE - tetrachloroethene
SEAR - surfactant enhanced aquifer remediation
TCE - trichloroethene
tDCE - trans-1,2-dichloroethene
VC - vinyl chloride